HELLENIC SOCIETY OF
BRIDGES STUDY

HELLENIC SOCIETY FOR
EARTHQUAKE ENGINEERING

Proceedings of the

INTERNATIONAL CONFERENCE IBSBI 2011

"Innovations on Bridges and Soil-Bridge Interaction"

October 13-15, 2011
Athens, Greece

Editors
George T. Michaltsos
George Gazetas

EUGENIDES FOUNDATION
GOLD MEDAL AWARD
OF THE ATHENS ACADEMY

ATHENS 2011

Proceeding of the

INTERNATIONAL CONFERENCE

IBSBI 2011

HELLENIC SOCIETY OF
BRIDGES STUDY

HELLENIC SOCIETY FOR
EARTHQUAKE ENGINEERING

Proceeding of the

INTERNATIONAL CONFERENCE IBSBI 2011

“Innovations on Bridges and Soil-Bridge Interaction”

October 13-15, 2011
Athens, Greece

Editors
George T. Michaltsos – George Gazetas

EUGENIDES FOUNDATION
GOLD MEDAL AWARD
OF THE ATHENS ACADEMY

ATHENS 2011

MAIN SPONSOR

ΧΡΥΣΟΥΝ ΜΕΤΑΛΛΙΟΝ
ΑΚΑΔΗΜΙΑΣ ΑΘΗΝΩΝ

SPONSORS

IBSBI 2011
"Innovations on Bridges and Soil-Bridge Interaction"
Proceedings of the Conference

Published by Eugenides Foundation

ISBN 978-960-337-106-9

Cover photos:
The Rion-Antirion Bridge "Charilaos Trikoupis".
The old stone bridge at Vlychos, Hydra Island, Greece.

FOREWORD

The First International Conference on "Innovations on Bridges and Soil-Bridge Interaction" (IBSBI 2011) was held 13-15 October 2011 in Athens, Greece. IBSBI 2011 conference aims to bring together engineers and researchers with interests in the area of Bridge Design and Construction and in Soil-Bridge Interaction in order to promote the exchange of ideas and experiences among participants for consolidation of recent developments in this important area.

IBSBI 2011 Conference covers a board spectrum of topics related to Bridge Design and Construction and Soil-Bridge interaction, 72 quality papers including 8 keynote lectures have been selected from more than 160 submitted abstracts and presented in 14 technical sessions by experts from many countries around the world during the three day Conference.

The "Hellenic Society of Bridges Study" (HSBS) and the "Hellenic Society for Earthquake Engineering" (HSEE) who organized this International Conference are two non-profit scientific associations with members from all around Greece, while their purpose is the promotion of the theoretical and applied research on the design and construction of Bridge Structures and Soil-Bridge Interaction.

We have the ambition to consecrate this International Conference as a permanent institution, which will take place every three years.

The financial support provided by the "Eugenides Foundation" is gratefully acknowledged, especially in this difficult economic period for Greece.

We would like also to acknowledge the companies TITAN SA and VINCI CONCESSIONS SA for their kind sponsoring.

Finally, we would like to extend our appreciation to the members of the Local Organizing Committee, and the International Scientific Committee for their time and also the Conference Secretariat for their hard work in preparing the Conference.

Athens September 2011

George T. Michaltsos
George Gazetas

ORGANIZING COMMITTEE
Bazeos Nikitas
Gazetas George
Kolias Vassilios
Konstantakopoulos Theodore
Michaltsos George
Pitilakis Kyriazis
Raftoyiannis Ioannis
Sigalas Ioannis
Voudiklaris Theodore

HONORARY COMMITTEE
Hajdin Nikola
Kounadis Anthony
Simopoulos Simos

KEYNOTE SPEAKERS
Bruno Domenico
Calvi Michele
Constantinou Michael
Hajdin Nikola
Kawashima Kazuhiko
Papanikolas Panagiotis
Pecker Alain
Saiidi Saiid M.

SCIENTIFIC COMMITTEE
Michaltsos George, Chairman
Gazetas George, Co-Chairman
Avraam Tassos
Baniotopoulos Charalampos
Bazeos Nikitas
Beskos Dimitrios
Bousias Efstathios
Bruno Domenico
Calvi Michele
Constantinou Michael
Hajdin Nikola
Kappos Andreas
Kawashima Kazuhiko
Kotsovos Michalis
Liolios Asterios
Makris Nikolaos
Malakatas Nikolaos
Marinos Pavlos
Panagiotakos Telemachos
Papanikolas Panagiotis
Priestley Nigel
Pecker Alain
Raftoyiannis Ioannis
Sophianopoulos Dimitrios
Spiliopoulos Konstantinos
Stavridis Leonidas
Tsiknias Tilemachos
Tsopelas Panagiotis

CONTENTS

TOPIC 2

TOPIC 3

TOPIC 4

TOPIC 5

TOPIC 6

KEYNOTE LECTURES

IBSBI 2011, October 13-15, 2011, Athens, Greece

STRUCTURAL MODELLING IN LONG SPAN CABLE STAYED BRIDGES

Domenico Bruno

Department of Structural Engineering, University of Calabria, Cosenza, Italy
e-mail: d.bruno@unical.it

ABSTRACT: The aim of the paper is to provide some qualitative evaluations of the static and dynamical behaviour of long span cable stayed bridges.
The fan-shaped cable-stayed bridge scheme is examined by using both an analytical and a numerical model of the bridge.

The analytical developments refer to a continuous model of the bridge, which is founded on the assumption of diffused distribution of stays along the girder and of the prevailing truss behaviour of the bridge. The analytical treatment of the relevant governing equations is based on the assumption that for long spans the bending stiffness of the girder is negligible if compared to the global flexural stiffness of the bridge. Simple approximate analytical solutions that are capable of giving a synthetic understanding of the main bridge behaviour characteristics are obtained.

Agreeing analytical and numerical results which are able to capture the essential features of the static and dynamic behaviour of the bridge are given. Some results showing the importance of the static deformability and of the aerodynamic instability in long spans are also given.

KEY WORDS: long spans; static deformability; aerodynamic stability.

1 INTRODUCTION

Cable supported bridges have been of great interest in recent years, particularly with respect to the fan-shaped cable stayed scheme and the suspension one for long spans [1].

As concerns long-span bridges, one of the most important problem is related to the deformability under live loads. In the case of long span bridges, carrying both road and railway traffic, the design and the feasibility of the structure can be seriously affected. In addition, increasing the span length makes the aerodynamic behaviour of the bridge the feasibility key problem.

Como *et al.* [2] analyzed the static behaviour of long span cable stayed bridges. Bruno and Grimaldi [3] investigated the nonlinear static behaviour of cable-stayed bridges using both a continuous and a discrete model of the bridge and showed the strong influence of nonlinearities for long spans.

Moreover, the dynamic behaviour of cable-stayed bridges has been investigated by Bruno *et al.* [4] who analyzed the effects of moving loads and by Bruno and Leonardi [5], Bruno *et al.* [6] and Como [7] who analyzed aerodynamic instability problems.

In the abovementioned studies the fan-shaped cable-stayed bridges have been studied using both a continuous and a discrete model of the bridge, and the dominant truss behaviour of the bridge was found. In particular, as far as the continuous model is concerned, it was shown how, through a perturbative solution technique, it is possible to obtain solutions, which are approximate but capable to give simple and synthetic evaluations of the main bridge behaviour characteristics.

Recently, many projects with central span exceeding largely the longest existing suspension and cable stayed bridges have been proposed. Studies of new bridges propose central spans larger than 3500 mts. for suspension solutions, and 1500 mts. for cable stayed solutions. The main technical aspects limiting the effective feasibility of so long bridges are strictly related to their deformability and aerodynamic stability.

In this paper, some qualitative evaluations concerning deformability and aerodynamic stability of long span cable stayed bridges are given by using continuous models of the bridges and comparisons with finite element numerical models. Simple analytical results focus the most relevant technical parameters that influence the bridge behaviour in long spans.

Some applications and examples of long span bridges are given. In particular, the geometric aspect ratios between the main span length and the tower height, the loads ratio p/g between live and dead loads, the relative flexural stiffness between girder and cables, are taken into account.

2 THE CABLE STAYED BRIDGE MODEL

The fan shaped self-anchored cable stayed bridge scheme shown in Fig.1 is examined.

The longitudinal vertical plane *yz* is assumed to be a symmetrical one; in addition, the bridge is also symmetrical with respect to the midspan cross plane.

The girder is simply supported at its ends and is hung to the tops of H-shaped towers by means of two stays curtains.

Developments refer to H-shaped towers typology; however, the formulation can be easily adapted for "*A*" shaped pylons, starting from the "*H*" ones and introducing slight modifications to the main governing equations. In both cases, the cable system is arranged symmetrically with respect to both midspan and longitudinal *yz* planes.

The fan shaped cable stayed system of fig.1 is analyzed by means of a continuum approach, in which the stays are assumed to be uniformly distributed along the deck.

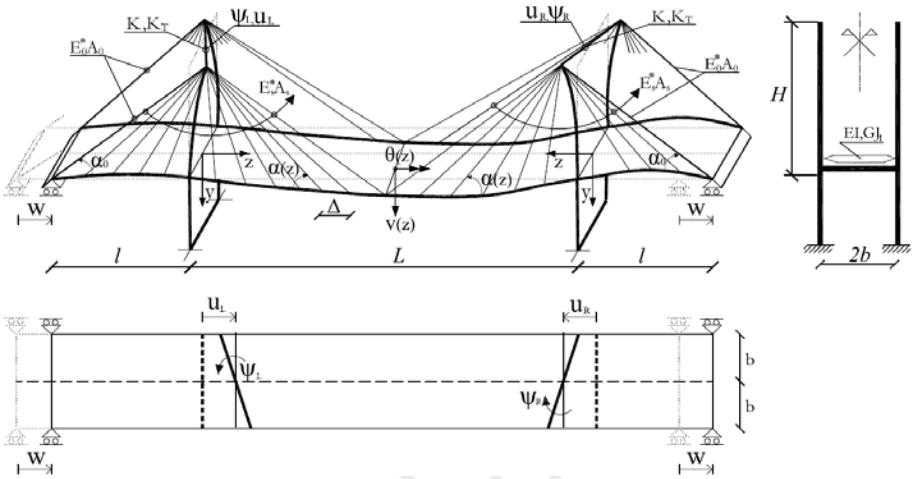

Figure 1. Cable stayed bridge scheme: bridge kinematics and stiffness parameters.

In particular, the stay spacing is quite small in comparison with the bridge central span (i.e. $\Delta/L<<1$). As a result, the self-weigh loads produce negligible bending moments on the girder with respect to that raised by the live loads. The initial stress distribution, at the “zero configuration”, i.e. under dead load only, is supposed to be produced by a correct erection process which yields tension in the stays and compression in both girder and pylons. Moreover, under dead loads, the girder is arranged with an initial straight profile, which is practically free from bending moments for reduced values of the stays spacing. In particular, the erection procedure is based on the free cantilevered method, which is able to control the initial tension distribution in the cable system to a value practically constant in each stay. This assumption has been verified for long span cable stayed bridges, in view of the prevailing truss behavior of the structure. Therefore, the live loads modify the initial configuration and, consequently, produce additional stress and deformation states. It is worth noting that for long span bridges, the initial stress state produced by the dead loading needs to be accounted mainly in the cable stayed system, in which the initial tension strongly affects the stays behaviour due to Dischinger effects.

The geometry and stiffness characteristics of the bridges are selected with respect to typical ranges suggested by practical design rules. In particular, the cross sectional stay areas are designed so that the dead loads g produce constant stress over all the distributed elements, which are assumed equal to a fixed design value, namely σ_g. As a result, cross sectional area A_s of the stays varies along the girder, but the safety factors are practically constant for each element of the cable system. Moreover, for the anchor stays, the cross sectional geometric area A_0, is designed so that the allowable stress is obtained in the static case, for live loads applied to the central span only. Therefore, the geometric measurement for the cables system can be expressed by the following equations:

$$A_s = \frac{g\Delta}{\sigma_g \sin\alpha}, \quad A_0 = \frac{gl}{2\sigma_g}[1+(\frac{l}{H})^2]^{1/2}[(\frac{L}{2l})^2 - 1], \tag{1}$$

where α is the slope of a generic stay element with respect to the reference system, *(L,l,H)* are representative geometric lengths of the bridge structure, and Δ is the stay spacing step, (for more details see Fig.1). The bridge analysis is based on the following assumptions:

- the stress increments in the stays are proportional to the live loads, p;
- the long span fan shaped bridge is characterized by a dominant truss behavior.

In this framework, the tension σ_g and σ_{go} for distributed and anchor stays, respectively, can be expressed by the following relations:

$$\sigma_g = \sigma_a g/(p+g), \quad \sigma_{g0} = \sigma_a \{1+(p/g)[1-(2L/l)^2]^{-1}\}^{-1} \tag{2}$$

It is worth noting that the allowable stay stress, σ_a, represents a known variable of the cable system in terms of which the design tension under dead loading can be determined by the use of Eqs. (2). Since it is assumed that for dead loads only the bridge structure remains in the undeformed configuration, the application of live loads leads to additional stress and deformation increments with respect to the self-weight loading condition. In particular, as reported in Fig.1 with respect to the reference system with the origin fixed at the midspan girder cross section, the bridge kinematic, for the "*H*" shaped tower typology, is described by following displacement variables:

- vertical girder displacements $v(z)$,
- horizontal girder displacement w;
- left and right horizontal pylon top displacements $[u_L, u_R]$,
- girder torsional rotation $\theta(z)$,
- left and right pylon top torsional rotations $[\psi_L, \psi_R]$,

In particular, bridge deformations related to flexure and torsion for girder and pylons and axial deformations for stays have been taken into account, whereas pylon and girder axial deformability has been neglected. Consistently with the bridge configuration reported in Fig.1, the bridge scheme is constrained with respect to both vertical and torsional displacements at boundary cross sections of the bridge and at girder/pylon connections.

The stays are modeled as bar elements and the non-linear behavior is evaluated consistently with the Dischinger formulation, which takes into account geometric nonlinearities of the inclined stays introducing a fictitious elastic modulus for an equivalent straight member, as shown in the following equation:

$$E_s^* = \frac{E}{1+\left(\frac{\gamma^2 l_0{}^2 E}{12\sigma_0^3}\right)\left(\frac{1+\beta}{2\beta^2}\right)}, \quad \text{with } \beta = \frac{\sigma}{\sigma_0}, \tag{3}$$

where E_s^* is known as the secant Dischinger modulus, E is the Young modulus of the cable material, γ is the specific weight, l_0 the horizontal projection of the stay length and σ_o and σ are the initial and actual tension values of the stay, respectively, i.e. $\sigma_o = \sigma_g$ for the double layer of stays and $\sigma_o = \sigma_{go}$ for the anchor stays. Moreover, the tangent value of the Dischinger modulus can be obtained from Eq.(3) by putting β=1. As far as the secant modulus is concerned, its value depends on cable stress states under self-weight and live loading conditions. Sufficient accuracy in the actual stress state might even be achieved by assuming β as proportional to the ratio between live and self-weight loads, i.e. $\beta = \sigma_a/\sigma_g = (p+g)/g$ for the double layer of distributed stays and $\beta = \sigma_a/\sigma_g = (1+p/g)(L/2l)^2/[(L/2l)^2-1]$ for the anchor stays.

The axial deformation increments of a stay, generic for the left (L) and right (R) pylons produced by live loads, depend on both kinematic and geometric variables, as in the following relationships:

$$\Delta\varepsilon_L = \frac{1}{H}\left[(v \pm \theta b)\sin^2\alpha - (u_L \pm \psi_L b - w)\sin\alpha\cos\alpha\right], \tag{4}$$

$$\Delta\varepsilon_R = \frac{1}{H}\left[(v \pm \theta b)\sin^2\alpha - (u_R \pm \psi_R b + w)\sin\alpha\cos\alpha\right], \tag{5}$$

where (+/-) refers, in Eq.s (4)-(5) and in the following ones, to the right (+) and left (-) distributed stays with respect to the longitudinal girder geometric axis. Similarly, for the left and right pylon anchor stays, the incremental axial deformations are described as:

$$\Delta\varepsilon_{L0} = \frac{1}{H}\left[(u_L \pm \psi_L b - w)\sin\alpha_0\cos\alpha_0\right], \tag{6}$$

$$\Delta\varepsilon_{R0} = \frac{1}{H}\left[(u_R \pm \psi_R b + w)\sin\alpha_0\cos\alpha_0\right], \tag{7}$$

where α_0 is the girder/anchor stay orientation angle.

The increment of stay stress $\Delta N_s = E_s^* \Delta\varepsilon_s$ due to live load may thus be evaluated from eqs. (3÷7).

According to the assumption of uniform stay distribution, the following interaction forces per unit length between bridge components is given (Fig.2):

$$q_{vL(R)} = \frac{E_S^* A_S}{H\Delta}\left[v\sin^3\alpha - \left(u_{L(R)} - (+)w\right)\sin^2\alpha\cos\alpha\right], \tag{8a}$$

$$q_{oL(R)} = -\frac{E_S^* A_S}{H\Delta}\left[(-)v\sin^2\alpha\cos\alpha - \left((-)u_{L(R)} - w\right)\cos^2\alpha\sin\alpha\right], \tag{8b}$$

$$m_{\theta L(R)} = \frac{E_S^* A_S b^2}{H\Delta}\left(-\theta \sin^3 \alpha + \psi_{L(R)} \cos\alpha \sin^2 \alpha\right), \tag{8c}$$

$$m_{\psi_{L(R)}} = \frac{E_S^* A_S b^2}{H\Delta}\left(-\theta \sin^2 \alpha \cos\alpha + \psi_{L(R)} \cos^2 \alpha \sin\alpha\right). \tag{8d}$$

$$S^0_{L(R)} = \frac{E_0^* A_0}{H}\left((-)u_{L(R)} - w\right)\cos^2 \alpha_0 \sin\alpha_0, \; M^0_{L(R)} = \frac{E_0^* A_0 b^2}{H}\psi_{L(R)} \cos^2 \alpha_0 \sin\alpha_0 \tag{9}$$

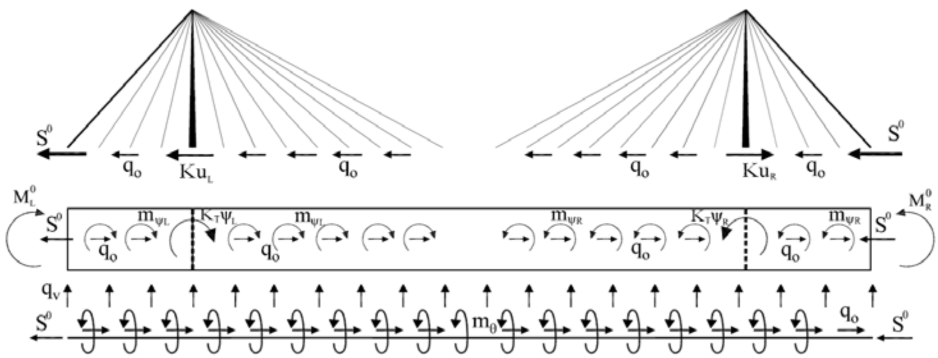

Figure 2. Interaction forces between bridge components.

3 STATIC ANALYSIS

In this section an analysis of long span cable stayed bridges static behaviour is made by assuming the already mentioned typical characteristics, namely:

- diffused stay arrangement along the deck($\Delta/L<<1$);
- truss-like scheme.

These conditions enable to develop an analytical model described by a convenient set of integro-differential equations. An approximate solution of these equations is given which reflects the above conditions, namely that of the state of axial forces prevailing over the flexural one. Some simple analytical results are obtained which, though approximated, grasps main qualitative and quantitative aspects.

At first the *yz* in-plane flexural analysis of the bridge under vertical live loads is examined; then, torsional effects due to load eccentricities are investigated.

3.1 In-plane flexure

Here we consider the bridge subject to live vertical load *p* symmetrically placed with respect to its longitudinal axis *yz*.

In this case no torsion occurs and the displacement field is characterized by: $u_L = u_R = u$; $\theta(z) = \psi_L = \psi_R = 0$.

The equilibrium equations of the bridge are:

$$\underline{\text{GIRDER}} \qquad\qquad \underline{\text{LEFT PYLON'S TOP}} \qquad\qquad \underline{\text{RIGHT PYLON'S TOP}}$$

$$EIv^{IV} + q_v = p, \qquad S_L^0 + \int_L q_{oL} dz + Ku = 0, \qquad S_R^0 + \int_R q_{oR} dz - Ku = 0 \tag{10}$$

where EI is flexural girder stiffness, K is the pylon's top flexural stiffness and the integration is extended to the stays curtain respectively belonging to the bridge's left (L) or right (R) side.

In order to develop a generalized formulation, the equilibrium equations are proposed in dimensionless form, introducing the following quantities:

$$\xi = \frac{z}{H}; \qquad V(\xi) = \frac{v(z)}{H}; \qquad U = \frac{u}{H}; \qquad W = \frac{w}{H}$$

$$a = \frac{\gamma^2 H^2 E}{12\sigma_g^3}; \quad \frac{\varepsilon^4}{4} = \frac{I\sigma_g}{H^3 g}; \quad \varphi(\xi) = \frac{1}{(1+a\xi^2)(1+\xi^2)}; \quad P = \frac{p\sigma_g}{Eg}; \tag{11}$$

$$\chi = \frac{K\sigma_g}{Eg}; \quad \chi_0 = \frac{E_0^* A_0}{E}\frac{\sigma_g}{gH}\sin\alpha_0 \cos^2\alpha_0; \quad \rho = \int_L \frac{\cos^2\alpha}{1+a\xi^2} d\xi + \chi_0$$

Equilibrium equations (10) can be put in the following dimensionless form:

$$\frac{\varepsilon^4}{4} V^{IV} + \varphi V - \xi\varphi U \pm \xi\varphi W = P \tag{12a}$$

$$(\rho+\chi)U - \rho W - \int_L \xi\varphi V d\xi = 0; \qquad (\rho+\chi)U + \rho W - \int_R \xi\varphi V d\xi = 0 \tag{12b}$$

The exact solution of equations (12) is quite difficult to find. An approximate solution can be found observing that the value of parameter ε is small; in fact, it represents the ratio between the girder bending stiffness and the stay axial stiffness, which is small in long span bridges (usually about ε=0.1÷0.3). This implies that the bridge's statical behaviour is characterized by a truss-like effect which usually prevails over the girder's bending.

An approximate solution of eqs. (12) can be obtained by using a perturbative technique [2-3]: the general solution U, V, W is expressed as it follows:

$$U = U_0 + U_1; \qquad V = V_0 + V_1; \qquad W = W_0 + W_1; \tag{13}$$

where U_0, V_0, W_0 is a particular approximate solution obtained from eqs. (12) by putting $\varepsilon=0$ and U_1, V_1, W_1 is the general approximate solution of the homogeneous equilibrium equations obtained from eqs. (12) by putting $P=0$.

After some manipulation the following expression of the truss dominant solution U_0, V_0, W_0 is obtained:

$$W_0 = \frac{1}{2\chi_0}\left[-\int_L \xi P d\xi + \int_R \xi P d\xi\right]$$

$$U_0 = \frac{1}{2(\chi + \chi_0)} \left[\int_L \xi P d\xi + \int_R \xi P d\xi \right], \tag{14}$$

$$V_0 = (U_0 \mp W_0)\xi + \frac{P(\xi)}{\varphi(\xi)}$$

An approximate solution of the homogeneous system is given by:

$$U_1 = 0; \; W_1 = 0 \;\; ;$$

$$V_1 = c_1 e^{-f(\xi)} \sin f(\xi) + c_2 e^{-f(\xi)} \cos f(\xi) + c_3 e^{f(\xi)} \sin f(\xi) + c_4 e^{f(\xi)} \cos f(\xi) \tag{15}$$

with $$f(\xi) = \frac{1}{\varepsilon} \int_0^{\xi} \varphi^{1/4} d\xi;$$

The approximate solution given by (14) and (15) reflects the truss-like behaviour of the bridge scheme: in fact, the displacements U_0, V_0, W_0 given by eqn. (14) involve the whole structure and correspond to $\varepsilon = 0$, i.e. to the bridge scheme with hinged connections of the stays to the girder, and subject to live load P; while displacements U_1, V_1, W_1, which are of local nature and strictly depend on the parameter ε, represent the additional displacements required to re-establish the flexural compatibility uncomplied with by the truss displacements U_0, V_0, W_0.

3.2 Torsion

We now examine torsional effects due to load eccentricities. The girder is assumed to be symmetric with respect to the *yz* vertical plane.

It must be observed that the elastic response of stays to positive or negative stress increments is different (eqn. (3)) and consequently torsion and vertical bending of the girder are coupled in a nonlinear analysis. However, if the initial stress state of stays in the starting configuration corresponding to dead load action is reasonably high, the Dischinger tangent response of stays can be reasonably accepted, i.e. β=1 and $\sigma_o = \sigma_g$ in eqn. (3), then flexural and torsional effects due to load eccentricities can be examined separately.

On the base of these assumptions, it is easy to show that the the displacement field is characterized by: $u_L = u_R = w = 0$; $v(z) = 0$.

The equilibrium equations of the bridge are:

GIRDER — LEFT PYLON'S TOP — RIGHT PYLON'S TOP

$$GJ_t \theta^{II} + m_\theta + m = 0, \quad K_T \psi_L + \int_L m_{\psi_L} dz + M_L^0 = 0, \quad K_T \psi_R + \int_R m_{\psi_L} dz + M_R^0 = 0 \tag{16}$$

where GJ_t is the torsional girder stiffness, K_T is the torsional top pylon stiffness and m is the torsional load.

Also in this case, in order to develop a generalized formulation, the equilibrium equations are written in dimensionless form, introducing the following quantities:

$$\tau = \left(\frac{GJ_t \sigma_g}{Eb^2 Hg} \right)^{1/2}, \qquad \mu(\xi) = \frac{H\sigma_g}{Egb^2} m(\xi) \qquad \chi = \frac{K\sigma_g}{Eg}, \tag{17}$$

with $K=K_T/b^2$.

Equilibrium equations (16) can be put in the following dimensionless form:

$$\tau^2 \theta^{II} - \varphi(\xi)\theta + \frac{\xi\varphi(\xi)}{(\chi+\rho)} \int_{L,R} \xi\varphi(\xi)\theta(\xi)d\xi = \mu(\xi) \tag{18a}$$

$$\Psi_L = \frac{1}{(\chi+\rho)} \int_L \xi\varphi(\xi)\theta(\xi)d\xi, \qquad \Psi_R = \frac{1}{(\chi+\rho)} \int_R \xi\varphi(\xi)\theta(\xi)d\xi \tag{18b}$$

Also in this case, a perturbative approach can be used to obtain an approximate solution of eqs. (18) because the value of the relative girder's torsional stiffness parameter τ is small (usually about 0.05÷0.2).

An approximate solution of eqs. (18) can be put in the following form:

$$\theta(\xi) = \theta_0(\xi) + \theta_1(\xi); \qquad \Psi_L = \Psi_L^0 + \Psi_L^1; \qquad \Psi_R = \Psi_R^0 + \Psi_R^1; \tag{19}$$

where $\theta_0(\xi), \Psi_L^0, \Psi_R^0$ is a particular approximate solution obtained from eqs. (18) by putting $\tau=0$ and $\theta_1(\xi), \Psi_L^1, \Psi_R^1$ is the general approximate solution of the homogeneous equilibrium equations obtained from eqs. (18) by putting $\mu=0$.

After some manipulation the following expression of the particular solution is obtained:

$$\theta_0(\xi) = \frac{\mu(\xi)}{\varphi(\xi)} + \frac{\xi}{(\chi+\chi_0)} + \int_{L,R} \xi\mu(\xi)d\xi \tag{20a}$$

$$\Psi_{L,R}^0(\xi) = \frac{1}{(\chi+\rho)} + \int_{L,R} \xi\theta_0(\xi)\varphi(\xi)d\xi \tag{20b}$$

An approximate solution of the homogeneous system is given by:

$$\Psi_L^1 = \Psi_R^1 = 0 \tag{21a}$$

$$\theta_1(\xi) = c_1 e^{-f(\xi)} + c_2 e^{-f(\xi)}, \text{ with } f(\xi) = \frac{1}{\tau}\int_0^\xi \varphi^{1/2} d\xi; \tag{21b}$$

In Fig.3 some results relative to the deformation of the cable-stayed bridge scheme are given, where both an analytical continuous model and a FEM discrete one of the bridge are employed.

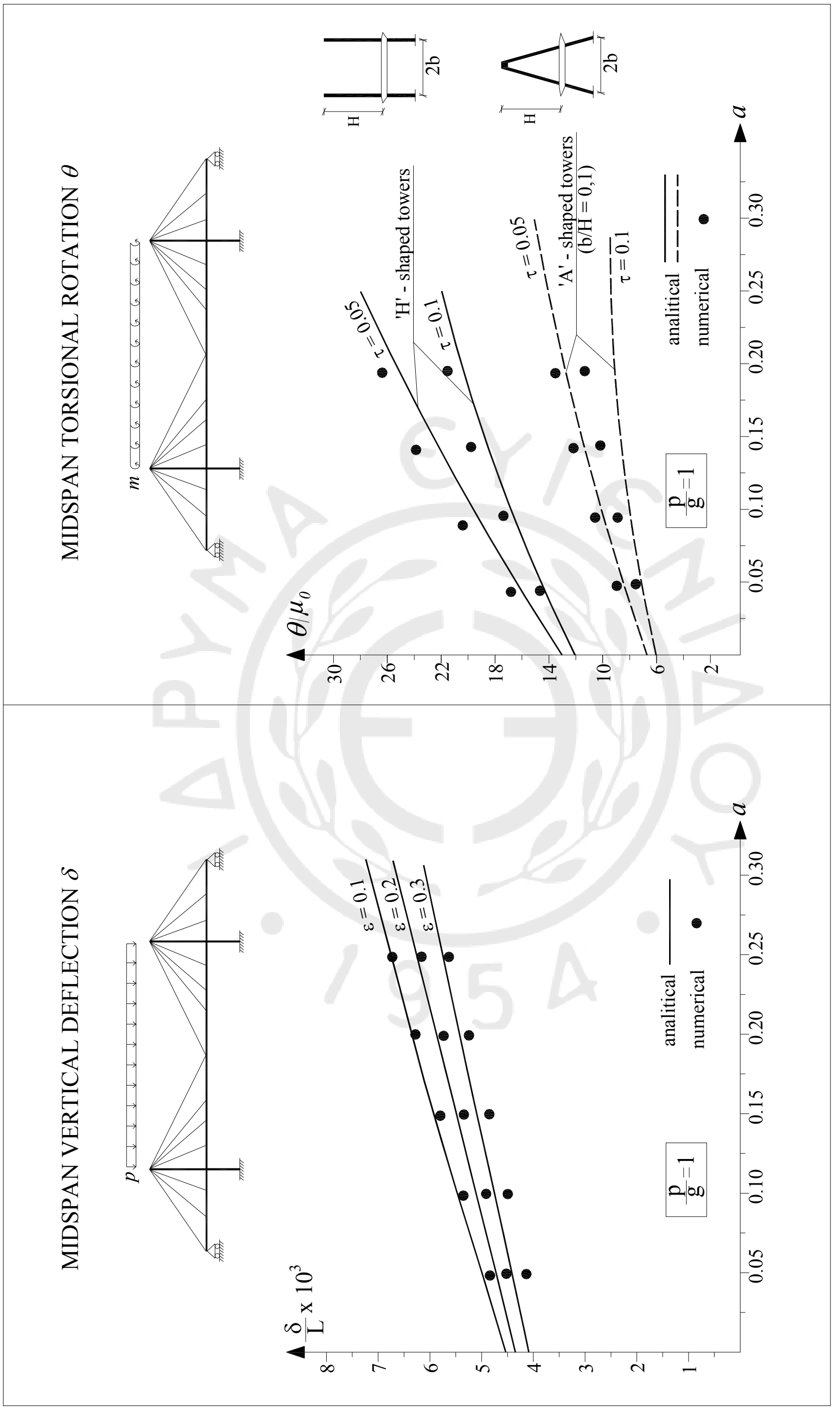

Figure 3. **Cable stayed bridge scheme**
Statical analysis: Flexural and Torsional deformations.

It can be observed that for given material stays and load ratio *p/g*, parameter *a* given by eqn.(11) can assume the meaning of bridge span parameter.

The results refer to the following geometrical and material parameters of the bridge: r_1=L/H=2.5; r_2=L/*l*=5/3; E/σ_a=2.1x10^6/7200; K/g=50.

In this figure the case of high live loads (*p/g=1*), like that railway bridges, is considered.

In particular, as far as the flexural deformation analysis is concerned, the live load *p* acting on the central span is considered to give the maximum midspan transverse deflection δ of the bridge. The ratio δ/L between the vertical midspan deflection and the central span length is plotted versus the bridge span parameter *a*, and some realistic values of the relative girder's tity δ/L linearly depends both on *a* and ε. Moreover, it appears that the influflexural stiffness parameter ε are considered. It can be observed that the quanence of ε is not relevant and therefore it can be concluded that the midspan deflection linearly grows with L^3.

In the same figure some results relative to the torsional effects due to a uniform torsional couple *m* acting on the whole central span are given. Here the maximum midspan torsional rotation θ is plotted versus the bridge span parameter *a,* for some values of the girder's torsional stiffness τ. The results are given in dimensionless form, where the quantity μ_0 represents the nodimensional torsional couple $\mu_0=H\sigma_g m/Egb^2$.

It can be observed that whereas the transverse deflection of long span bridges is practically unaffected by the tower shape and the girder's flexural relative stiffness ε, on the contrary, the torsional deformation is strongly influenced by the tower shape and the girder's torsional stiffness parameter τ.

4 DYNAMIC ANALYSIS

One of the most important topics related to long-span bridges is the analysis of dynamic behaviour. The influence of moving loads, seismic forces, and aerodynamic effects must be carefully examined; in fact, the more dangerous effects are related to these external actions, in particular, aerodynamic instability.

4.1 Free vibrations

Here we give some results about free vibrations of the fan shaped cable stayed bridge scheme of Fig.1, according to the continuous model and to the truss assumption examined in previous sections.

A more exhaustive discussion about free vibrations of long span cable stayed bridges can be found in [8].

Firstly, the symmetric oscillations of the bridge are discussed. The displacement parameters that characterize symmetric oscillations are (Fig. 4):

the vertical deflection of the girder *v(z,t)* and the tower tops horizontal displacement *u(t)*.

The dynamical equilibrium equations governing symmetric vertical oscillations of the bridge can be written in the following dimensionless form:

GIRDER *PYLON'S TOP*

$$\frac{\varepsilon^4}{4}V^{IV} + \varphi V - \xi\varphi U = -M\frac{\partial^2 V}{\partial t^2}; \qquad (\rho+\chi)U - \int_{-l/H}^{L/2H}\xi\varphi V d\xi = 0 \tag{22}$$

where $M=\mu H\sigma_g/Eg$, and μ is the mass per unit length of the girder.

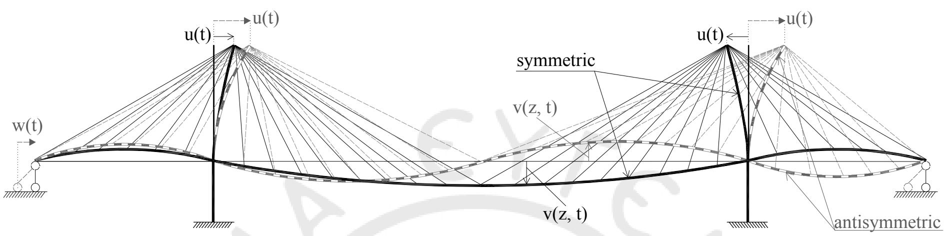

Figure 4. Symmetric and antisymmetric vertical oscillations.

We now refer to the truss scheme discussed in section 2.1, by putting ε=0 in eqn.(22). assuming a stationary solution of the Moreover, type:

$$V(\xi,t) = \bar{V}(\xi)\sin\omega_0 t; \qquad U(t) = \bar{U}\sin\omega_0 t, \tag{23}$$

the following frequency equation is derived from eqs. (22):

$$-(\rho+\chi) + \int_{-l/H}^{L/2H}\frac{\xi^2\varphi^2}{\varphi - M\omega_0^2}d\xi = 0 \tag{24}$$

An approximate solution of eqn. (24) can be obtained by using a linear Taylor expansion of the integral on the left-hand side. After some manipulation the following expression of the frequency equation is given:

$$-(\chi+\chi_0) + \nu M\omega_0^2 = 0 \tag{25}$$

where $\nu=[(l/H)^3+(L/2H)^3]/3$.

From eqn. (25) we obtain the frequency ω_0 and the period T_{1V}^{s} of the symmetric vertical oscillations:

$$\omega_0 = \sqrt{(\chi+\chi_0)/\nu M}; \qquad T_{1V}^{S} = 2\pi\sqrt{\nu M/(\chi+\chi_0)} \tag{26}$$

We now consider antisymmetric vertical oscillations. The involved displacement parameters are (Fig. 4): the horizontal translation of the girder *w(t),* the vertical deflection of the girder *v*(*z*,*t*) and the horizontal displacement of the tower tops *u(t).*

Assuming also the dominant truss behavior of the bridge ($\varepsilon\rightarrow 0$), the dynamical equilibrium equations in dimensionless form, corresponding to antisymmetric oscillations, can be written as:

$$\varphi V - \xi\varphi\left(U - W\right) = -M\frac{\partial^2 V}{\partial t^2}; \qquad \int_{-l/H}^{L/2H} \xi\varphi V d\xi - \rho\left(U - W\right) + \lambda M\frac{\partial^2 W}{\partial t^2} = 0 \tag{27}$$

$$\rho W - (\rho + \chi)U + \int_{-l/H}^{L/2H} \xi\varphi V d\xi = 0 \tag{28}$$

where $\lambda = l/H + L/2H$.

Also in this case a stationary solution of (27), (28) of the type given by eqn. (22) is assumed. Moreover, the approximation technique already employed in the case of symmetric oscillations is also used. Then, the following linear approximation of the fundamental periods of antisymmetric oscillations is derived:

$$T_V^A = 2\pi\sqrt{2\nu M}\left(\left[\chi\left(1+\nu/\lambda\right)+\chi_0\right] \pm \left\{\left[\chi\left(1+\nu/\lambda\right)-\chi_0\right]^2 + 4\chi\chi_0\right\}^{1/2}\right)^{-1/2} \tag{29}$$

In the case of long span bridges, the tower stiffness can be neglected with respect to that of the anchor stays (i.e. χ=0 in eqn. (29)); this implies that the first antisymmetric oscillation degenerates into a rigid translation of the girder, while the period of second antisymmetric oscillation goes to overlap the period of the fundamental symmetrical vertical oscillations of the bridge.

Finally, we examine the torsional oscillations of the bridge. In this case also the analysis of the continuous model is based on the assumption of dominant truss behavior of the bridge.

For torsional oscillations, the involved displacement parameters are: the torsional rotation $\theta(z,t)$ of the girder; and the torsional rotation $\psi(t)$ of the tower tops.

The dynamical equilibrium equations governing torsional oscillations of the bridge are [8]:

$$\tau^2\frac{\partial^2\theta}{\partial\xi^2} - \varphi\theta + \frac{\xi\varphi}{\chi+\rho}\int_{-l/H}^{L/2H}\xi\varphi\theta d\xi = J_0\frac{\partial^2\theta}{\partial t^2}; \qquad \psi = \frac{1}{\chi+\rho}\int_{-l/H}^{L/2H}\xi\varphi\theta d\xi \tag{30}$$

where $J_0 = I_0 H\sigma_g / Egb^2$ and I_0 is the polar moment of inertia of mass of the girder cross section.

Assuming the truss behavior of the bridge (i.e. $\tau \to 0$) and a stationary solution of the type

$$\theta\left(\xi,t\right) = \bar{\theta}\left(\xi\right)\sin\omega_0 t; \qquad \psi\left(t\right) = \bar{\psi}\sin\omega_0 t, \tag{31}$$

The linear approximation of the frequency equation is

$$-(\chi + \chi_0) + \nu J_0 \omega_0^2 = 0 \tag{32}$$

From (32) we derive the fundamental period of torsional oscillations

$$T_{1\theta}^S = 2\pi\sqrt{\nu J_0 / \left(\chi + \chi_0\right)} \tag{33}$$

both for the symmetric and antisymmetric case.

4.2 Aerodynamic stability

As it is well known, among the numerous problems involving the behaviour of long span bridges, aerodynamic instability is the most complex and relevant one because of its strong influence on the feasibility aspects. In particular, the flutter instability can represent the most dangerous phenomenon in long spans. Moreover, this phenomenon is strongly related to the dynamic properties of the bridge, like that free oscillations in still air. In particular, the ratio $\phi=T_V/T_\theta$ between vertical and torsional natural periods is the key parameter with respect to flutter instability.

Now the air forces acting on the bridge are considered. It is widely accepted that the nonstationary formulation is the most adequate one for predicting the aeroelastic behaviour of the girder with good accuracy. Moreover, to obtain simple formulas we refer to the simple thin airfoil theory.

According to these assumptions, the aerodynamic lift l and torque m per unit length, acting on the cross section of the bridge in a laminar approaching flow with zero mean angle of attack, can be expressed by:

$$l = \rho V_0^2 (2c)[kH_1^* \dot{v}/V_0 + kH_2^* c\dot{\theta}/V_0 + k^2 H_3^* \theta]/2 \tag{34a}$$

$$m = \rho V_0^2 (2c^2)[kA_1^* \dot{v}/V_0 + kA_2^* c\dot{\theta}/V_0 + k^2 A_3^* \theta]/2 \tag{34b}$$

where V_0 is the approaching wind speed; ρ is the air density; $k=c\omega/V_0$ is the reduced frequency, ω is the frequency of the oscillating bridge deck and c is the half-width of the girder cross section.

Moreover, H_i^*, A_i^* are the nondimensional Theodorsen aerodynamic coefficients, given in real notation, according to Scanlan, by:

$$\begin{cases} kH_1^* = -2\pi F \\ kH_2^* = -\pi(1 + F + 2G/k) \\ k^2 H_3^* = -2\pi(F - kG/2) \end{cases} \qquad \begin{cases} kA_1^* = \pi F \\ kA_2^* = -\pi(1 - F - 2G/k)/2 \\ k^2 A_3^* = \pi(F - kG/2) \end{cases} \tag{35}$$

where F(k) and G(k) are the real and imaginary parts of the Theodorsen functions.

Now a continuous model, founded on the prevailing truss behaviour of the bridge (i.e. $\varepsilon=\tau=0$), is employed to obtain simple formulas able to capture the main features of the bridge behaviour. In this case, for symmetrical motions with respect to midspan, the deformation of the girder is described by the flexural $v(z)$ and torsional $\theta(z)$ displacement functions, respectively, together with the scalar displacement parameters $u_L= u_R= u$, $\psi_L= \psi_R= \psi$, with $w=0$.

On these assumptions, the dynamic equilibrium equations for the continuous model are:

$$\varphi V - \xi\varphi U = -M\ddot{V} + Q_1\theta + Q_2\dot{\theta} + Q_3\dot{V}\,; \quad -(\rho+\chi)U + \int_L \xi\varphi V d\xi = 0 \tag{36a}$$

$$-\varphi\theta + \xi\varphi\psi = J_0\ddot{\theta} - \mu_1\theta - \mu_2\dot{\theta} - \mu_3\dot{V}\,; \qquad \psi = \frac{1}{\rho+\chi}\int_L \xi\varphi\theta d\xi \tag{36b}$$

where Q_1, Q_2, Q_3 and μ_1, μ_2, μ_3 are the nondimensional aerodynamic forces.

The aerodynamic instability and the corresponding critical wind speed can be obtained by putting the solution of eqn (36) in the form:

$$V(\xi,t)=\overline{V}(\xi)e^{st};U(t)=\overline{U}e^{st};\theta(\xi,t)=\overline{\theta}(\xi)e^{st};\psi(t)=\overline{\psi}e^{st} \tag{37}$$

where a purely immaginary value of $s=\alpha+i\omega$ corresponds to flutter.

Substituting eqn (37) in (36), a linear homogeneous system, with time-independent displacement variables introduced in (37) is obtained; putting its determinant equal to zero and disregarding less relevant terms, the following frequency equation is obtained:

$$\begin{aligned}\sigma^4+\sigma^3\beta\Omega\pi(2F+\gamma G_1)/k+\sigma^2(1+\varphi^2-\beta\gamma\Omega^2G_2+\beta^2\gamma\Omega^2G_3)+\\+\sigma\beta\Omega\pi(2\varphi^2F+\gamma G_1)/k+(\varphi^2-\beta\gamma\Omega^2G_2)=0\end{aligned} \tag{38}$$

with

$$\beta=\frac{\rho c^2}{\mu};\quad \gamma=\frac{\mu c^2}{I_0};\quad \phi=\frac{\omega_{0\theta}}{\omega_{0v}};\quad \Omega=\frac{\omega}{\omega_{0v}};\quad \sigma=\frac{s}{\omega_{0v}} \tag{39}$$

$$G_1(k)=(1-F-2G/k)/2\,;\quad G_2(k)=\pi(F-kG/2)/k^2;\quad G_3(k)=2\pi^2F/k^2; \tag{40}$$

where ω_{0v} and $\omega_{0\theta}$ denote the flexural and torsional free oscillation frequencies in still air.

The flutter condition is formulated by putting $\sigma=i\Omega_c$ in eqn (38). We obtain:

$$\Omega_c^4(-G_1+2F\beta G_2-2F\beta^2G_3)+\Omega_c^2(2G_1-2F\beta G_2)-G_1=0 \tag{41a}$$

$$\Phi^2=\left(\Omega_c^2(2F+\gamma G_1)-\gamma G_1\right)/2F\,, \tag{41b}$$

and the critical wind speed is given by the relation: $V_c/c\omega_{ov}=\Omega_c/k_c$.

In Fig.5a the flutter critical wind speed V_c is plotted versus the frequency ratio parameter ϕ, for some values of the mass parameters β and γ; it can be observed that for $\phi=\omega_{0\theta}/\omega_{OV}\rightarrow 1$, any wind speed is critical. In addition, a very high sensitivity of the bridge aerodynamic behaviour emerges with respect to variations of ϕ. Moreover, a numerical investigation based on a FEM analysis already developed in [5] is made to give useful comparisons between analytical and numerical results. This comparison is established in Fig. 5b where agreeing analytical and numerical results are given, referring to the following bridge parameters: r_1=2.5; r_2=5/3; L=750 m; l=250m; H=150 m; Δ=25 m; b= 17m; c=19.50 m; I=11.69 m^4; I_0=918,378 t_mm; K=2350 t/m; μ=4.8 t_m/m; g=47 t/m; p=28t/m; E=21x10^6t/m^2; σ_a=72x10^3t/m^2; ε=0.3; τ=0.05; 0.1; 0.15; 0.2; 0.25; 0.3.

5 CONCLUSIONS

In this paper an analysis of the static deformability and of the aerodynamic stability of long span cable stayed bridges is developed. Simple qualitative evaluations of the main static deformation and dynamic characteristics parameters are given. Both continuous and discrete models of the bridge schemes are used to establish useful agreeing comparisons between the obtained results. The standard assumption of diffused arrangement of stays along the girder is made to give analytical developments for the continuous model, while a FEM analysis accounting for the actual stays spacing is used.

Some applications and examples of long span bridges are given showing the influence of the main geometric aspect ratios, the relative stiffness between girder and cables, and mass properties.

Simple analytical results point out the most relevant technical parameters that influence the static and dynamic behaviour of long span cable stayed bridges.

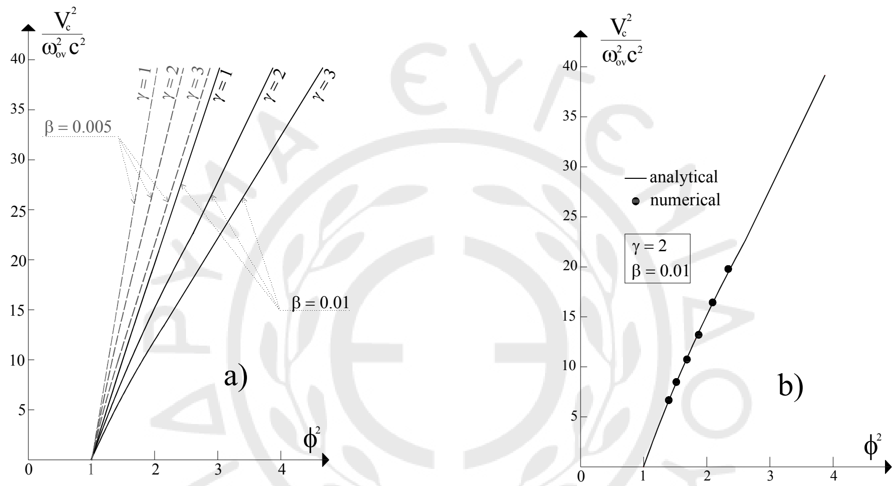

Figure 5. Critical wind speed V_C versus flutter parameter ϕ.

REFERENCES

[1] Gimsing N.J. (1997).“Cable-Supported Bridges”, John Wiley & Sons, New York,(USA).

[2] Como, M., Grimaldi, A., Maceri, F. (1985). "Statical Behaviour of Long-Span Cable-Stayed Bridges". *Int. J. Solids and Struct.,* 21(8), 831-850.

[3] Bruno, D., Grimaldi, A. (1985). "Nonlinear Behaviour of Long-Span Cable-Stayed Bridges". *Meccanica*, Vol. 20, N. 4, 303-313.

[4] D. Bruno, F. Greco, P. Lonetti (2008). "Dynamic impact analysis of long span cable-stayed bridges under moving loads". *Engineering Structures*, vol.4, pp. 1160-1177, 2008.

[5] Bruno D., Leonardi A. (1998). "Aerodynamic Instability of Long Span Cable-Stayed Bridges". IABSE Symposium, Kobe, Japan.

[6] Bruno D., Como M., Grimaldi A., Leonardi A. (2001). " Deformability and Aerodynamic Stability as Limits in Long Span Bridges". IABSE Symposium, Seoul, Korea.

[7] Como M. (2000). “Stabilità Aerodinamica dei ponti di grande luce”, Ingegneria delle Strutture, Ed. da Elio Giangreco, Edizioni UTET 2000.

[8] Bruno D., Leonardi A. (1997).“Natural Periods of Long-Span Cable-Stayed Bridges”, Journal of Bridge Engineering-Asce, Vol.2, N.3.

IBSBI 2011, October 13-15, 2011, Athens, Greece

CONCEPTUAL SEISMIC DESIGN OF CABLE-STAYED BRIDGES

Gian Michele Calvi[1], Timothy John Sullivan[2] and Antonio Villani[3]

[1] Istituto Universitario di Studi Superiori, Pavia, Italy
[2] Università degli Studi di Pavia, Pavia, Italy
[3] EQCO s.r.l., Pavia, Italy
e-mail: gm.calvi@iusspavia.it, timothy.sullivan@unipv.it, antonio.villani@eqco.it

ABSTRACT: This article reviews and discusses some of the important conceptual design considerations for cable-stayed bridges, first for gravity loads and then for seismic excitation. The advantages and disadvantages of different cable-stayed bridge solutions are highlighted, with review of deck sections, tower con-figurations in both the longitudinal and transverse direction, deck-to-pier connections, and cable arrangements, amongst other things. After reviewing the important conceptual design considerations for cable-stayed bridges, a simple preliminary sizing procedure is proposed. The preliminary sizing procedure is intended to offer designers a quick but rational means of identifying reasonable member sizes for cable-stayed bridges that should then be verified through advanced analyses in the developed and detailed design stages of the project.

1 INTRODUCTION

As demands for improved infrastructure increase around the world, civil engineers continue to be challenged to develop large bridges that must perform well even under extreme loading. An effective means of bridging large distances in both seismic and non seismic regions is through the use of cable-stayed bridges. The decks of a cable-stayed bridge are supported using cables that climb diagonally to strong stiff towers, which act as the main load-bearing elements for the bridge. The orientation and construction methodology adopted for the bridges is such that under uniform loading the static horizontal forces imposed by the cables on the decks are typically balanced. Consequently, the towers will be designed to resist the vertical component of the gravity load and additional lateral loads associated with live loads, wind and seismic actions, impact from colliding objects, drag from water flow, and possibly others.

2 PERFORMANCE OBJECTIVES AND DESIGN LOADS

Performance-based seismic design (PBD) is a framework for seismic design that has continued to increase in popularity since the early nineties. The aim of

PBD is essentially to offer engineers an effective means of controlling the risk posed by earthquakes. As part of a PBD process, engineers ensure that certain performance levels (or damage states) are satisfied for different design ground motion intensities. With knowledge of the probability of exceedence of different ground motion intensities, the engineer can control the risk posed by an earthquake, if they can successfully limit the structural response under a given ground motion to prescribed performance limits.

Important performance states typically considered for the performance-based seismic design of bridge structures include:

- Serviceability limit state (Performance Level 1) in which no elements suffer notable damage and the bridge continues to function normally following the earthquake without any need for repairs.
- Repairable damage (Performance Level 2) in which inelastic response may develop in pre-selected and adequately detailed plastic hinge zones. The plastic mechanism should be carefully selected such that eventual repairs do not require closure of the bridge. The cover concrete in the plastic hinge zones may spall and the longitudinal reinforcement may yield but strains are limited to moderate values (without risk of re-bar buckling). Joints in the deck may be damaged but must remain traversable by emergency services and should be easily repaired.
- Collapse prevention (Performance Level 3) in which significant damage may develop in pre-selected and adequately detailed plastic hinge zones, and minor localized damage may occur in other parts of the bridge. The damage may require closure of the bridge to repair, but collapse of the bridge is avoided. Deformations in plastic hinge regions could result in significant concrete spalling and longitudinal re-bar strains may be close to critical values for the onset of re-bar buckling. Joints in the deck may be damaged but should remain traversable by emergency services.

Selection of an appropriate nonlinear mechanism (typically referred to as an inelastic mechanism, but may also involve nonlinear elastic response) is key for the adequate performance of the bridge. In order to ensure functionality, the bridge deck, cables, and connections are usually always designed to respond elastically or with minor amounts of inelasticity (e.g., partial yielding of a steel beam section or small inelastic demands on a limited number of reinforcing bars at the perimeter of a large concrete section). For the collapse prevention limit state, some design strategies will permit individual cables to exceed the yield strength, provided that there is still adequate protection against collapse through redistribution of loads to adjacent cables. This approach is similar to an impact loading scenario in which it might be assumed that due to vehicle collision, one or more cables fail and the bridge must be verified to sustain the likely gravity loads in its damaged state. In light of these considerations, a desirable mechanism for the lateral response of a cable-stayed bridge under extreme loads will typically involve formation of a flexural-plastic hinge in the main piers and fuses at connections between the deck and piers. Another alternative, that could also be incorporated into the pier-yielding mechanism, is to design and detail foundation systems at the base of the towers that limit seismic forces; this option will be discussed further in later sections. Joints at the deck-abutment connections will usually be detailed to sustain large displacements without offering resistance.

A design seismic intensity is assigned for each of the important performance levels. The acceptable probability of exceeding a given performance state for important structures is lower than for normal structures. Note that the probability of exceedence for a certain period of time can be directly correlated to an equivalent earthquake return period using Eq. (1).

$$p = 1 - e^{-LN} \tag{1}$$

where N is the inverse of the return period (Tr = 1/N), p is the probability of exceedence, and L is the design life considered. As such, a design intensity event having 10% probability of exceedence in 50 years is equivalent to what is commonly referred to as a 475-year return period event, and a design intensity having 2% probability of exceedence in 50 years is equivalent to a 2,475-year return period event. Cable-stayed bridges are typically classified as important structures, however, minimum design intensities for cablestayed bridges do not yet appear to have been set with designers typically consulting with clients in order to set suitable probabilities of exceedence for design.

Care should be taken not to lose sight of the potential that performance-based design offers for the control of risk. PBD should not simply be considered a framework that requires performance criteria to be checked for a number of different earthquake intensities. If it were, one could argue that performance-based design has been going on since the 1970s, from the time that either gravity, wind, or earthquake loads were checked for both serviceability and ultimate limit states. Seismic risk can be defined as the convolution of seismic hazard and the vulnerability:

$$\text{Seismic Risk} = \text{Hazard x Vulnerability} \tag{2}$$

There are also alternative, expanded definitions of seismic risk in the literature, which introduces Exposure and Cost, but this basic definition is sufficient to introduce the concepts of risk here. The hazard considers the probability of different levels of seismic intensity at a site, whereas the vulnerability indicates the susceptibility of a building to sustain losses due to ground shaking. If the risk due to natural hazards is to be insured, then it would appear that the acceptable seismic risk in a region of low wind demands (for example) should be greater than that of a region of high wind demands. Nonetheless, it appears that current design tools do not yet permit practicing engineers to rationally control the risk posed by natural hazards in such a refined manner. This may be due to the difficulty in quantifying losses for a given performance level. As a result, current practice is to undertake the performance-based design of bridges without the explicit calculation of the seismic risk.

Design and verification of a bridge for a range of performance levels requires different representations of the seismic loads and this is typically done through reference to response spectra. For cable-stayed bridge structures it is important that the seismic hazard assessment used to set the design spectrum is applicable out to long periods, as noted in *Fig. 2*, since the flexible structures are often characterized by fundamental periods in excess of 7.0 s.

Of particular significance to the seismic demands on large cable-stayed bridges will be the peak spectral displacement demand, T_D, and the spectral displacement corner period, T_D, both of which are indicated in Fig. 1.

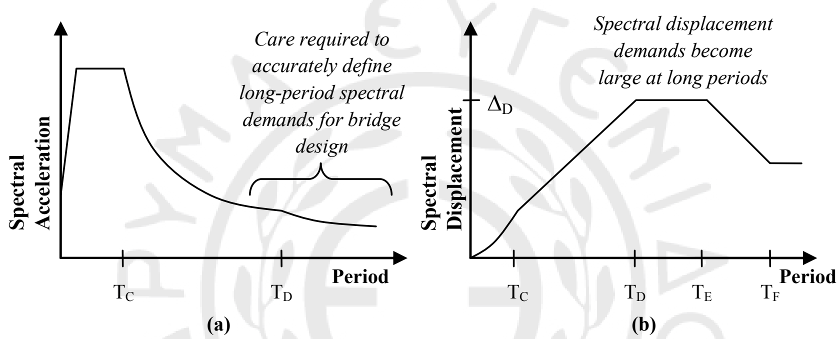

Figure 1. Typical shape of (a) design acceleration spectrum, (b) design displacement spectrum (note that the long period portion of the displacement spectrum has been condensed to fit within the page as the T_D to T_E period range is often several times greater than the T_C to T_D period range)

It should be noted that as the bridge structure will evolve in different stages, it will not usually be necessary to consider the whole construction period in identifying the design return period, but rather the maximum likely period for each construction phase. Consequently, seismic loads are reduced and the seismic design intensity for a 6-month construction stage may be around 20% of the collapse-prevention seismic intensity of the finished bridge. While the seismic demands considered for each of the different construction phases may be rather low, the seismic capacity of the unfinished bridge can also be rather low, depending on the construction methodology. As the construction will typically involve cantilever decks from either side of a central tower pier, either lateral propping of the deck or a rigid connection to the tower may be required to avoid in-plan torsion problems until the adjacent spans are connected. Temporary propping of the pier legs may also be necessary and some reflection should be given as to the appropriate design loads for temporary works structures.

3 DESIGN CONSIDERATIONS FOR NON-SEISMIC LOADS

There are different ways in which the requirements of non seismic load cases can affect the seismic design solution. Gravity loading on the bridge will have a strong influence on the peak compression forces that develop in the longitudinal axis of the deck. Therefore, one might consider a strong heavy deck to resist the compression but of course the gravity loads themselves are a function of the weight of the deck. In addition, while a heavy deck may not be problematic for wind loading, it would certainly be an issue for seismic loading. As such, the ideal deck section is a strong but lightweight deck.

One might also consider the benefits of a flexurally stiff deck for non seismic loads. Extensive parametric studies showed that for static loads the use of a stiff deck section is not ideal for cable-stayed bridges, since it attracts significant bending moments at three critical zones: deck-to-pier, abutments, and mid spans. However, this observation comes from static considerations, and a stiff deck can instead be quite beneficial when dynamic wind and earthquake loads are considered. Also note that vertical displacements of the deck may be most significantly affected by the stiffness of the cable-pier system. This can be appreciated simply considering the typical span-to-depth ratios of decks in cable-stayed bridges, which tend to be in the range of 100–200, well above normal ratios used to control deformations associated with beam flexure. As such, the deck stiffness will be more relevant for local deformations between cable support points and for dynamic vibrations associated with wind and seismic response. The use of composite construction has been shown to provide an economical solution for cable-stayed bridges with spans running from 350 to around 600–700 m.

The spacing of cables should be set with due regard to construction lifting and transport requirements for the main beams, in addition to limiting static flexural demands on the main beams. The transverse beams are required to transmit gravity loads to the main beams, but can also be an effective means of stabilizing the main beams against lateral torsional buckling. Longitudinal and transverse stiffeners may often be necessary for the longitudinal beams but do add cost to the construction and therefore one might consider the use of stockier sections in order to avoid the need for a large number of stiffeners.

The gravity loads are also likely to impose the greatest axial loads on the piers and foundations. However, as both the piers and foundations of cable-stayed bridges tend to be massive structures in order to provide adequate lateral stiffness for wind, earthquake, and eccentric gravity loading, the vertical loading for these elements is not usually critical. Eccentricity in vertical loads along the length of the deck requires the following considerations to be made:

- Deck continuity: The deck should be continuous in order to permit redistribution of loads to different bridge segments and piers, and to aid overall stability.

- Decompression of cables: The sagging of one bridge deck segment could cause the adjacent segment to go into hogging, with a resulting reduction in cable tension force.
- Horizontal deck restraint: For single pier bridges the unbalanced compression forces in the deck imply that an external reaction is required. This could either be provided through a horizontal restraint at the deck-pier interface, or with a connection at the abutments. However, the deck-pier connection is preferred for temperature effects and differential vertical movements of nearby cables relative to the abutments.
- Flexural response of towers: The eccentric load on the deck will typically imply that the piers are subject to bending and shear. For this reason, gravity load considerations imply that the piers should possess high lateral stiffness.
- Deck vertical displacements: The eccentric load on the deck can produce large deck displacements and is another motivation for a stiff tower and a limited cable spacing. Note that for relatively common three span bridges the "back stay effect" can help control the displacements without needing very high tower stiffness.

Wind loading can prove to be a critical non seismic load case in the transverse direction. Important characteristics of the bridge will be the deck stiffness (lateral, vertical, and torsional) as well as the shape of the deck section itself, with sharp angled sections (such as box-girders) being more likely to evoke instability effects such as vortex shedding. For a general text on wind effects on structures.

The ideal pier configuration deserves some consideration. Ideally, the pier head will be positioned centrally above the deck so that under gravity-only loads the cables do not induce bending in the piers. As most bridges have single decks, then common pylon shapes are as shown in *Fig. 2a–d*. Centrally located piers are also possible, as in the case of the Millau Viaduct, France, which has a configuration similar to that in *Fig. 2e*. Note that for decks supported by a single central line of cables such as that of *Fig. 2e*, increased torsional stiffness of the deck section may be necessary and pre-cast box sections are sometimes used for this purpose. When two decks are desired, or a very wide deck solution is desired, there is also the possibility of using a centrally located pier with angled arms tied at their top, as shown in *Fig. 2f*.

Longitudinally, there are also different options available for the tower configuration, although the variation in typical configurations is reduced. *Fig. 3* shows some typical configurations in the longitudinal direction.

From a gravity load point of view, stiffer pier configurations are advantageous since vertical displacements of the deck due to eccentric gravity loads will be greatly affected by the lateral stiffness of the piers. Such considerations may motivate designers to use inclined piers, and by coupling piers designers can also maximise the lateral stiffness. With this in mind, one could argue that the configurations shown in *Figs. 2a*, *c*, and *d*, as well as those in *Figs. 3b* and *c*, are desirable solutions for gravity load requirements. However, as will be explained and discussed in the next section, such configurations may not always be an optimum solution for seismic design.

4 DESIGN CONSIDERATIONS FOR SEISMIC LOADS

In order to develop an optimal seismic design solution the engineer must be aware of the ideal structural characteristics for non gravity load cases identified in the previous section. There are several important issues to be dealt with in developing the seismic design. It may appear that compromises are required at times, since the ideal characteristics for seismic load may be completely different to those for non-seismic loads. However, through good engineering and with the help of special structural elements, optimal characteristics can be identified for both seismic and non seismic load cases, as explained in the following paragraphs.

4.1 Deck to pier connection

An important decision in the concept design of a cable-stayed bridge will be whether to connect the bridge deck(s) to the pier(s), as illustrated in *Fig. 4*.

There are essentially three options available to the engineer: (i) provide no connection; (ii) provide a strong stiff connection; or (iii) provide an intermediate solution with limited transfer force and intermediate stiffness. If no connection is provided between the deck and the piers, the deck will exhibit a pendulum-type response with little lateral stiffness. Given that the majority of the bridge mass is distributed along the deck, this response mode will be characterized by a very long period of vibration. Note that the period of a pure pendulum can be obtained from:

$$T_p = 2\pi\sqrt{\frac{H}{g}} \tag{3}$$

where H is the pendulum length which could be considered equivalent to the pier height, and g is the acceleration due to gravity.

As a reasonable pier height could be assumed to be the deck span, L_{span}, divided by four, the pendulum period could be estimated to be:

$$T_p = \sqrt{L_{span}} \tag{4}$$

In reality however, considerable longitudinal stiffness is also provided by the cables and piers, and this will reduce the longitudinal period from that given by Eq. (4). The exact period will therefore depend on the pier configuration adopted, but from experience, one should expect a longitudinal period in the order of Tp/2.

With reference to the shape of typical response spectra shown *Fig. 1*, it is clear that as the period of a structure increases, the acceleration demands decrease and the displacement demands increase. The benefits of avoiding a deck-to-pier connection are therefore that the seismic design forces are low and the drawback is that the bridge has to be detailed to be able to sustain very large relative displacements between the deck and piers and the deck and abutments.

In addition, without a deck-to-pier connection, the low lateral stiffness may imply that the response under eccentric live loading and wind loading is unacceptable.

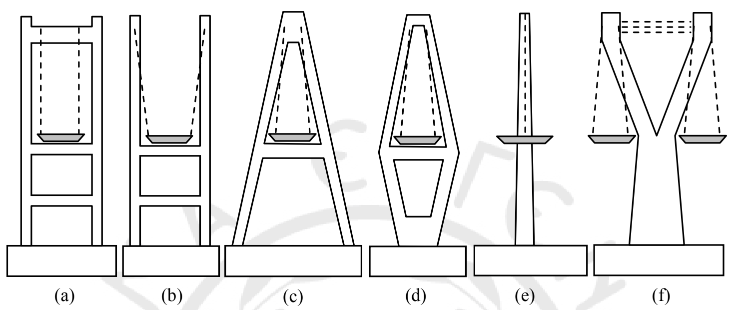

Figure 2. Transverse view of tower pier configurations for cable-stayed bridges.

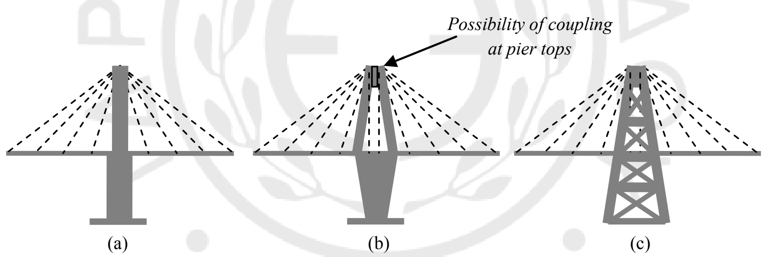

Figure 3. Longitudinal view of tower pier configurations for cable-stayed bridges.

If a stiff, strong deck-to-pier connection is provided, the period of the system reduces, the acceleration demands increase and therefore the force demands also increase rather dramatically. While the connection itself can be sized to transmit such forces, the large demands will be particularly problematic for the piers and possibly for the composite deck in the region of the connection.

The third alternative is to provide an intermediate solution for the deck-to-pier connection which could be achieved through the use of fuses, springs or dampers. The connection should be designed to ensure adequate stiffness and strength under non-seismic loading, but with good flexibility, displacement capacity and energy dissipation characteristics under seismic loading. The Rion-Antirion bridge adopts such a connection strategy for the transverse response direction, using a stiff metallic fuse device sized to transfer wind and static loads to the pier, in parallel to a number of viscous dampers that dissipate large amounts of energy after the fuses yield during an intense earthquake event.

It is likely that an intermediate solution will offer the best solution for cable-stayed bridges in seismic regions.

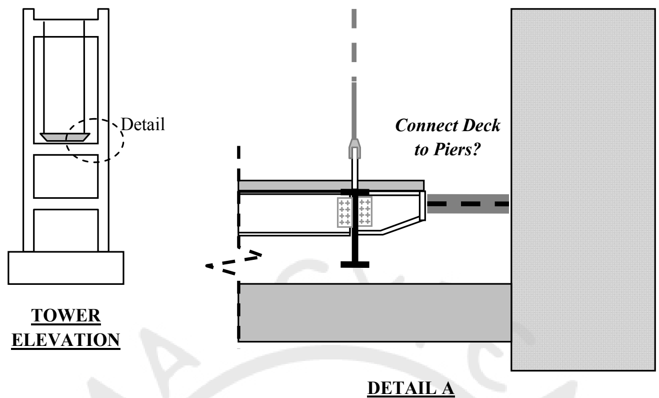

Figure 4. Deck-to-pier connection consideration.

The design of a pier-to-deck connection should consider the control of both longitudinal and transverse response. The critical response direction will depend on the relative magnitude of seismic and eccentric gravity loads, as well as displacement limits for the different response directions. For standard cable-stayed bridge configurations, the connection in the longitudinal direction will need good stiffness to limit deck displacements due to eccentric gravity loads. However, if eccentric gravity loads in the longitudinal direction do not cause excessive displacements even when the deck-to-pier connection is omitted, then provided that the earthquake displacements can be sustained, the deck-to-pier connection in the longitudinal direction can be freed. This was the solution adopted in the Rion bridge that is characterized by very stiff towers and a slightly arched deck that meant that eccentric gravity loads are not problematic.

In the transverse direction, the displacements should be limited to avoid pounding between the deck and piers, and the characteristics of the deck-to-pier connection should be set with this objective in mind. If the displacements at the deck-to-pier connection are relatively limited in the transverse direction, it is clear that the longitudinal response may engage more of the deck mass. However, identification of a critical response direction is not necessarily straightforward since longitudinal resistance is provided by both the cable-pier system in addition to the deck-to-pier connection. In contrast, the cables provide little restraint to the deck movements in the transverse direction and therefore practically the full Conceptual Seismic Design of Cable-Stayed Bridges proportion of the deck mass excited in the transverse direction must be transferred at the deck-to-pier connection.

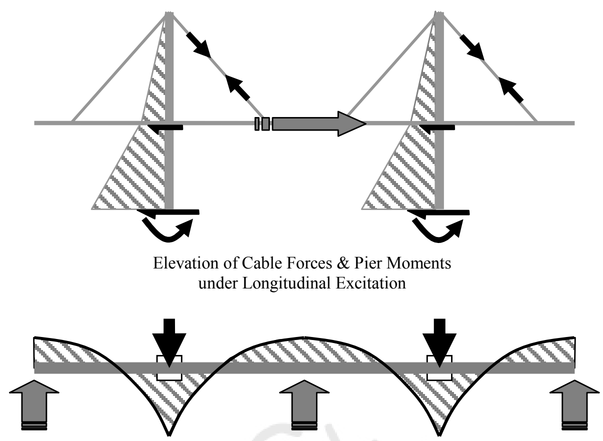

Figure 5. Force distributions for longitudinal and transverse response.

In line with the above considerations, assuming that either a rigid or an intermediate deck-to-pier connection is adopted, large longitudinal and transverse shears should be expected in the pier. The magnitude of these forces suggests that large tower bases will be necessary, but this is typically acceptable given the large stiffness that the towers should possess in order to limit deformations of the deck under eccentric gravity loads and the benefits that large tower bases have on distributing loads onto the foundations. Note that in addition to large shears, the deck-to-pier connection may also induce potentially significant torsional moments, depending on the pier configuration and the response direction being considered. If single pier towers are adopted, with deck segments either side of each tower, then torsional moments due to the deck-to-pier connection should be relatively small. However, for two-pier tower options, such as those shown in *Figs. 2a–d*, the longitudinal response will require that the piers resist torsion and this should be considered together with the shear requirements in verifying the pier sections. Note also that in addition to providing lateral stiffness and strength, the transverse beams that link typical two-pier tower configurations immediately below the deck level can be an effective means of reducing the torsion component below the deck level.

The deck-to-pier connections may involve construction of inclined structural members, providing some vertical restraint to the deck. This has the practical advantages of offering good space for the installation of the devices up under the deck, and also has aesthetic advantages in that the connection devices are likely to be relatively hidden. The structural benefits of the vertical restraint offered by the deck-to-pier connection can also be considered as by inclining the connection devices, some vertical restraint and energy dissipation can be expected. The vertical response of the deck is principally associated with longitudinal seismic excitation (with flexure of piers resulting in vertical displacements of deck) and not the vertical excitation component of the ground motion.

4.2 Tower pier design

Important decisions for the design of the tower piers should be whether to utilize one, two, or four legs and whether to connect the cables up the height of the piers or only at the pier tops. Regarding the number of legs in the tower, one should consider the different lateral load resisting mechanisms that could be expected to develop as well as the stiffness provided. Coupled tower piers are relatively stiff and therefore offer an effective means of limiting deformations under eccentric gravity loads. This consideration supports the use of four-leg towers, such as the towers realized in the Rion Antirion bridge.

As shown in *Fig. 9a*, a multiple leg configuration in which the piers are connected by transverse beams will be expected to develop significant coupling forces. The coupling action subjects the piers to varying axial loads and this implies that changes in the pier flexural resistance and stiffness should be expected during the seismic response. The piers will be subject to very high axial forces due to gravity loads alone, and the additional axial load due to seismic response should be carefully evaluated as it may lead to an earlier onset of concrete crushing in critical piers. This is considered particularly relevant for the capacity design of four-leg towers in which, under diagonal attack, three of the four legs could go into tension, imposing very large axial loads on a single pier. As such, doubts should be raised about the reliability of a coupled mechanism for the bridge piers, and some account for the uncertainties in capacity should be made in the design. One possibility for controlling the axial force due to coupling is to design the coupling beams to fuse, thereby limiting the axial loads that can be transferred to the piers as part of a capacity design approach.

The uncoupled pier configuration, shown in *Fig. 6b*, appears to be advantageous from a seismic viewpoint, therefore, since the lateral loading does not alter the axial loads in the piers and this implies that the flexural resistance, stiffness and ductility capacity of the pier can be more reliably estimated. However, despite the simple cantilever form, the axial load in the piers may still vary significantly due to vertical earthquake excitation components. The performance of a concrete pier and in particular its shear resistance, can be significantly affected by the vertical component of excitation. Given the fundamental importance of the piers to the overall performance of the bridge structures, the seismic design should therefore account for axial load variation on the seismic response. In practice, this can be done by first sizing the elements without account for vertical excitation effects, and then verifying the response of the structure when subject to three ground motion excitation components through nonlinear time-history analyses. However, additional research is also required to ensure that shear resistance models adequately account for axial load variation effects.

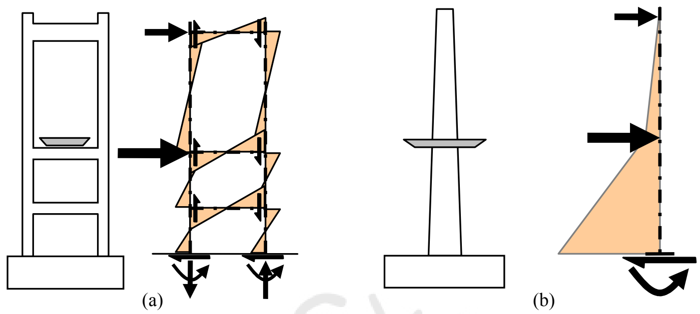

Figure 6. Effect of number of tower legs on likely load resisting mechanisms in towers: (a) coupled multiple leg tower elevation and bending moment diagram; (b) single leg tower elevation and bending moment diagram.

In the longitudinal direction of the bridge, the designer could choose to connect cables to a single pier or to multiple coupled and or inclined piers, as indicated in *Fig. 6*. Coupled piers may again be prone to some of the uncertainties in resistance due to axial load variations. However, there are some practical advantages to a coupled pier solution in the longitudinal direction as, in contrast to the transverse direction, piers can be positioned relatively close to each other and therefore vertical piers can be coupled by relatively short devices up the full height of the piers, as indicated in *Fig. 7c*.

As pointed out earlier, another important decision to make in developing the structural scheme is whether to connect the cables in a distributed fashion up the height of the piers or only at the pier tops in a fan-type arrangement, as indicated in *Fig. 8*. The option of fixing the cables at different levels up the height of the pier may at first seem desirable since it avoids congestion of cables at a single point on the pier, easing construction needs, requires a shorter total length of cables and is arguably more aesthetically pleasing than the single connection alternative. However, in seismic regions the fan arrangement might be preferred owing to the increased deformation capacity it offers the bridge. This can be appreciated by considering the strains that develop in the cables for the two configurations shown in *Fig. 8* when the deck is displaced longitudinally an amount Δ_x. The cables of the single connection point solution are all relatively long in comparison to the multiple connection point solution, in which the cables close to the base of the piers are short. As such, a uniform longitudinal displacement of the deck imposes much larger strains on the short cables, which implies that the longitudinal displacement capacity of the bridge is much lower than an identical bridge with a fan-type cable arrangement.

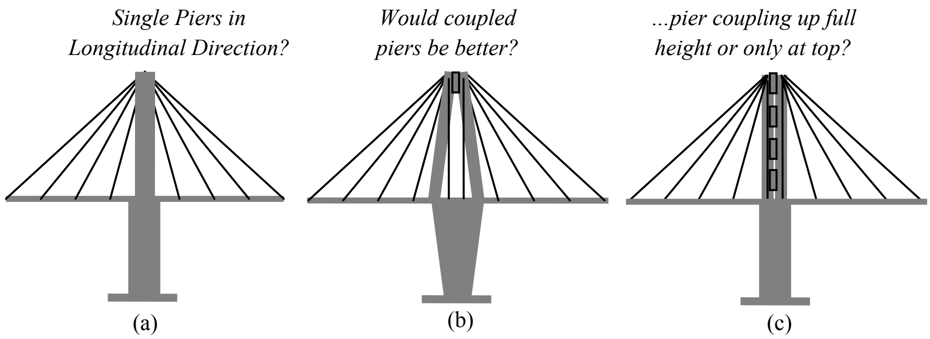

Figure 7. Tower leg configuration possibilities for longitudinal response: (a) single tower pier; (b) inclined piers coupled at top; (c) straight piers coupled up height.

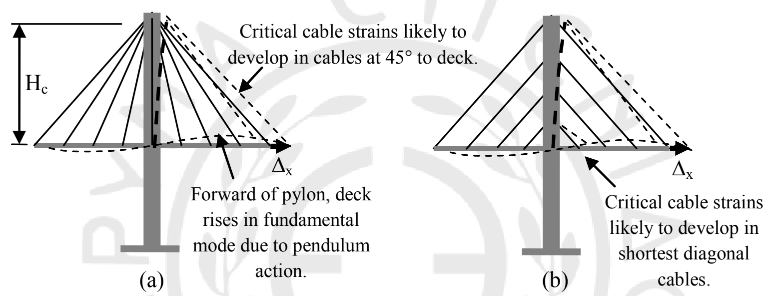

Figure 8. Two alternative strategies for the connection of cables to piers: (a) cables connect to top of piers in a fan-type arrangement; (b) cable are connected up the height of the piers.

While the increased displacement capacity offered by the fan-arrangement of *Fig. 8a* may be attractive, there are also reasons for which the distributed cable arrangement of *Fig. 8b* may be preferred. For example, the shorter cables will provide a stiffer solution, which may be particularly useful in limiting the lateral displacement of the deck, thereby limiting demands on dampers and expansion joints. Greater damping could be expected in the longitudinal mode when a distributed cable arrangement is adopted. As such, in deciding on a cable arrangement, the designer should weigh the benefits of reducing deformation demands on dampers and joints against the increased cable diameters that are likely to be required to sustain the larger design forces associated with the stiffer system. In order to assess the critical cable position for fan-type arrangements, consider that the change in cable length, δ_{cable}, due to a longitudinal displacement of the deck can be approximated by Eq. (5).

$$\delta_{cable} = (\Delta_x - \Delta_p)\cos\alpha \tag{5}$$

where Δ_x is the longitudinal displacement of the deck (see *Fig. 8*), Δ_p is the lateral displacement of the pier at the cable connection point, and α is the angle

of the cable relative to the deck.
In addition, note that the length of each cable, L_{cable}, is given by:

$$L_{cable} = \frac{H_c}{\sin\alpha} \quad (6)$$

where H_c is the height of the cable-to-pier connection point above the deck, as indicated in *Fig. 8a*.

Consequently, the cable strain due to the longitudinal displacement of the deck can be obtained through the division of Eq. (5) by Eq. (6), to give:

$$\varepsilon_{cable} = \frac{(\Delta_x - \Delta_p)}{2H_c} \sin 2\alpha \quad (7)$$

There are of course other aspects of the response that will affect the strains, such as deck vertical deformations, but Eq. (7) is of interest since it suggests that for bridges with fantype cable arrangements (in which H_c and Δ_p are approximately the same for all the cables), the critical cable strains due to longitudinal seismic response are likely to develop in the cables inclined at an angle of 45°.

4.3 Tower base design

The tower base sections, below the deck level, are subject to very large forces, with large forces transferred from the deck-to-pier connection and from the cables at the top of the towers adding to the seismic excitation of the towers themselves. Continuity in bending resistance must be ensured from the tower piers to the tower base. This implies that the base section should be at least as large as the upper sections, and in order to resist the additional bending that develops due to the large deck-level shears, the pier sections are often combined to form a large single section for the tower base. For bridges in deep water this has practical advantages for construction in which the tower base is initially constructed in a dry dock, then floated in a wet dock, and positioned as a single unit in place for the superstructure above. By having only a single pier base to manoeuvre into position and connect to typically underwater foundations, the construction challenges are restricted to a single installation event for each tower. This was the construction method and pylon base solution adopted for the Rion Antirion bridge. When towers are not located in deep water, it is likely that the pier base will be constructed directly in the final position, after the installation of a working platform at each tower location.

4.4 Foundation design and soil-structure-interaction

As with most civil engineering structures, the foundations for cable-stayed bridges require careful consideration. Suitable foundation solutions will clearly made regarding cable-stayed bridge foundations and some seismic design issues should be highlighted.

Given the magnitude of the design forces, the foundation area will typically need to be large and some soil improvement measures may be required. Improvement measures might include the use of driven piles to reinforce the soil as was done for the Rion Antirion bridge.

Construction possibilities may also influence the choice of foundation system and the choice between drilled, driven, or specialty piles will depend on the water level, soil properties, and site conditions.

Predictions of the foundation stiffness should then consider eventual uncertainties in the site characteristics and pile group effects. Uncertainties in foundation stiffness will make it difficult to analytically predict the differential displacements of adjacent towers and as such, a construction methodology should be developed that permits suitable adjustment of the adjoining deck sections.

Soil-structure interaction effects (also now referred to as soil-foundation structure interaction effects) can considerably affect the seismic response of structures. While this is true, it is considered that proper evaluation of soil structure interaction effects need not be undertaken until a developed or detailed design stage. Typically, initial conceptual design considerations should instead aim to mitigate the influence of the foundations on the seismic response by providing strong, rigid foundations. An interesting alternative concept, however is to develop foundation systems that fuse as part of a capacity design approach. Such a concept was incorporated into the design of the Rion-Antirion bridge, where circular tower footings sit atop a 2.8 m thick gravel layer in order to enable sliding in the event of extreme shear forces at the footing-gravel interface. Not only does this mechanism help to limit the forces imposed on the foundations, it also dissipates an important amount of energy, thereby helping to reduce the bridge response above.

5 PRELIMINARY SIZING IN SEISMIC REGIONS

The intention of the expressions presented in the following sub-sections is not to accurately establish member sizes, but instead, to illustrate how reasonable member sizes can be quickly set for the purposes of initial feasibility studies, costing exercises, and initial structural modeling. The member sizes obtained from the procedure should clearly be refined as the design develops, following the application of accurate, albeit time-consuming, analysis techniques.

Preliminary sizing should start by setting the spacing of the towers. This may depend on the ground conditions and general characteristics of the site in question. Typically, cable stayed bridges should be competitive for spans of between 50–500 m, although longer cable-stayed bridges have also been constructed, suggesting they are also effective for longer spans. For bridges with multiple towers the spacing should be regular so as to ensure balanced gravity loads.

Once the distance between the towers, L_{span}, has been established, the height of the towers, H_{tower}, can be found as:

$$H_{tower} = H_{deck} + L_{span}/4 \quad (8)$$

where H_{deck} is the height from the tower foundations to the level of the deck, as indicated in *Fig. 9*, and is usually dictated by a given navigation clearance.

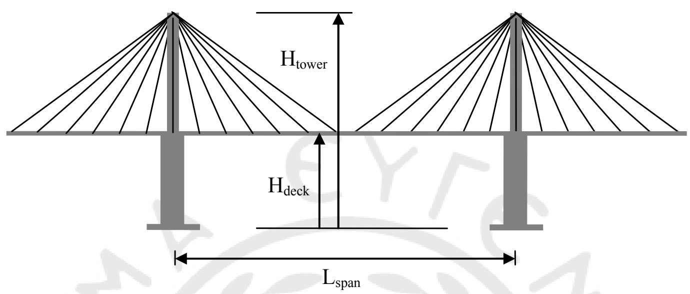

Figure 9. Elevation of a typical cable-stayed bridge.

The basis of Eq. (8) is simply to provide an average cable inclination of 45°. An average cable angle of 45° implies that the deck compression due to gravity loading only is equal to the total gravity load acting on the deck.

5.1 Preliminary member sizing for gravity loads

Having established the bridge span and tower heights, an initial sizing of the deck can be made with knowledge of the intended deck width and proposed use. The dead load will very much depend on the type of deck solution adopted and more accurate estimates of the live load could be obtained directly from the design brief. The expected axial force in the deck under gravity loading only is then given by:

$$N_{deck} = w_{deck} \cdot L_{span}/2 \quad (9)$$

where w_{deck} is the factored deck gravity loading (units of force per m length of deck) and L_{span} is again the distance between bridge towers.

The deck axial load obtained from Eq. (9) can then be used to estimate the required section area of the longitudinal steel beams (*Fig. 2*) from:

$$A_{beams} = \frac{N_{deck} - t_{slab} . b_{eff} . 0.85 f'_c}{F_{y,d}} \quad (10)$$

Where A_{beams}, is the total area of longitudinal beams (to be divided by number of beams to obtain required section area of a single beam), $F_{y,d}$ is the design resistance of the steel to be specified for the beams, t_{slab} is the thickness of the reinforced concrete slab deck possessing effective width b_{eff}, f'_c is the concrete compressive strength, and N_{deck} is taken from Eq. 9. Note that the approach proposed here assumes that transverse beams will be used to brace the main longitudinal beams at sufficiently short centres to ensure that reductions in axial resistance due to instability are not required. A reasonable spacing for transverse beams might be one-third to one-half the cable spacing and the concrete deck thickness can be initially sized to provide sufficient strength and stiffness under gravity loadings to span between the transverse beams. A typical cable spacing will be between 5m and 10m, and in setting the cable spacing, one should consider the construction methodology as this may require main beams to cantilever unsupported prior to the cable connection and may also dictate transport and lifting sizes for main beams.

An average size for the cables can be set as a function of gravity loads using the expression:

$$A_{cable} = \frac{w_{deck} . s}{F_{y,d} \sqrt{2}} \tag{11}$$

where A_{cable} is the average area required of the cables, $F_{y,d}$ is the design strength (stress) of the cables, s is the spacing between cables (assumed constant), and w_{deck} is again the factored ultimate gravity load of the deck (force per unit length). Note that the value of A_{cable} given by Eq. (11) assumes that two lines of cable would be provided to each deck.

The area required by Eq. (11) is the average area necessary to resist standard gravity loads. Seismic loading could also influence the necessary cable sizes, and accurate checks should be undertaken following nonlinear time-history analyses. A capacity-design estimate of the required cable area for seismic loads can be made considering that the maximum longitudinal force that be applied to the deck is that which exceeds the restoring force caused by the self weight, as indicated in *Fig. 10*. As such, the maximum longitudinal force that will be transferred through the cables if the deck is not held down, can be given by:

$$A_{cable} = \sqrt{2} \frac{w_{deck,EQ} . s}{F_{y,d}} \tag{12}$$

$w_{deck,EQ}$ is the gravity load of the deck expected to be present at the time of the maximum design intensity earthquake event and the other symbols are as for Eq. (11). While Eq. (12) might be useful as a capacity design estimate, if limited inelastic deformations are permitted in the cables this will add considerable deformation capacity and the preliminary cable design may be based only on the requirements of Eq. (11).

After only a few quick calculations, therefore, the overall geometry is set and preliminary sizes for the deck elements and cables are established. The remaining preliminary design tasks are to size the main tower section, the deck-to-pier connection and the foundations. As discussed earlier in the article, an important function that the tower piers have is to resist out-of-balance forces due to eccentric gravity loading. As such, preliminary sizing of the piers should first be based on the eccentric gravity loads expected. In the longitudinal direction, one assumes that live loads could act on one side of the towers only, thereby providing the out-of-balance moment acting on the system. For multiple tower bridges and for cable-stayed bridges with vertical restraint at abutments, this out-of-balance moment is resisted not only by the tower piers, but also by the deck in bending. However, it has been found that by making the simplifying analogy shown in *Fig. 11*, one can quickly gauge the approximate section size required for the piers.

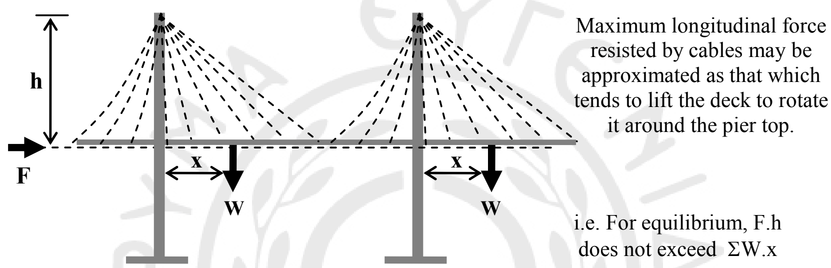

Figure 10. Partial elevation of typical tower base section.

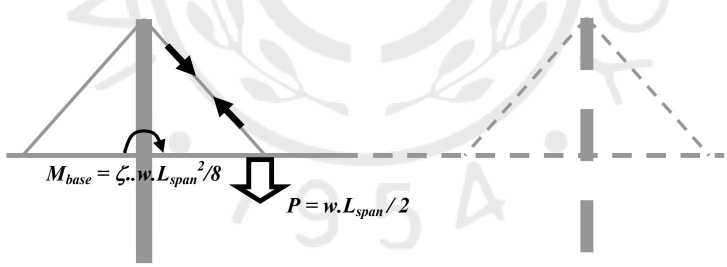

Figure 11. Idealization of eccentric gravity loading for preliminary sizing of towers.

The approach illustrated in *Fig. 11* is to assume that the eccentric gravity loading imposes a moment on the tower base, M_{base}, given by:

$$M_{base} = \zeta.w\frac{L_{spam}^{2}}{8} \tag{13}$$

where w is the eccentric gravity loading on the deck (units of kN/m), L_{span} is the deck span between towers, and ζ is a continuity coefficient intended to take account of the flexural resistance offered by the continuous deck. The continuity coefficient will clearly depend on the relative stiffness of the deck the relative stiffness of the deck versus the tower-cable system and designers could select a value considering the bridge in question. For preliminary sizing purposes a value of 0.5 may be reasonable.

In the transverse direction the importance of eccentric gravity load will depend on the selected pier configuration. For pier configurations in which the piers are positioned either side of the deck, eccentric loading in the transverse direction will not cause significant bending in the piers and instead will result in different pier axial loads. For a single pier solution, however, the full moment due to eccentric gravity loading in the transverse direction will need to be resisted by the pier sections. This consideration also provides a simple means of setting initial pier section dimensions as a design moment can be taken as:

$$M_{pier} = w_{deck} . L_{span} . x \tag{14}$$

where x is the eccentricity of the gravity loads with respect to the pier centreline, and the other symbols are as defined earlier. Another important consideration for the tower pier design is the lateral stiffness required to control vertical displacements of the deck. It is clear that if the tower piers do not possess high stiffness in the longitudinal direction, the vertical displacements of the deck can be rather large.

With this in mind, one can select a vertical displacement limit (such as deck span on 500) and, accounting for cable elongation under the eccentric gravity loading, identify the necessary pier lateral stiffness. It is also noted, however, that for spans close to abutments, a back-stay effect offered by the vertical restrain of the abutment can provide an effective means of controlling the deck displacements without relying on the stiffness of the pylons. Considering this, one may choose to do some initial elastic analyses under static loads to check the displacements and modify the tower pier sizes required by Eq. (14). In addition, the pier stiffness could also be important in order to control the vertical dynamic response of the deck when subject to wind and traffic loadings. While this does introduce additional uncertainty as to the required lateral stiffness, it can be expected that if vertical displacements are relatively limited under eccentric gravity loading then the vertical frequencies should be relatively high.

5.2 Preliminary seismic design in the longitudinal direction

After using gravity load considerations to set the bridge geometry and main member sizes, suitable characteristics for the deck-to-pier connections should be established with consideration of the seismic loads. In addition, for highly seismic regions, the tower pier sizing procedure outlined in the previous section may be not provide sufficient stiffness and strength to control the vertical response of the deck under seismic actions.

The vertical response of the deck becomes relevant for the longitudinal seismic response because, as illustrated earlier in *Fig. 6* and also in *Fig. 13*, as the deck displaces longitudinally, the pendulum nature of the response causes portions of the deck to either sag or lift. This in turn excites the vertical modes of vibration of the deck. The fundamental longitudinal mode will typically see the deck segments forward of the pier rise due to the pendulum nature of the response. However, an important higher mode in the longitudinal response is that in which the deck displaces the tops of the towers, with the deck segments located forward accelerating downwards, and deck segments behind the towers accelerating upwards. Such a longitudinal seismic response can impose significant eccentric forces on the towers.

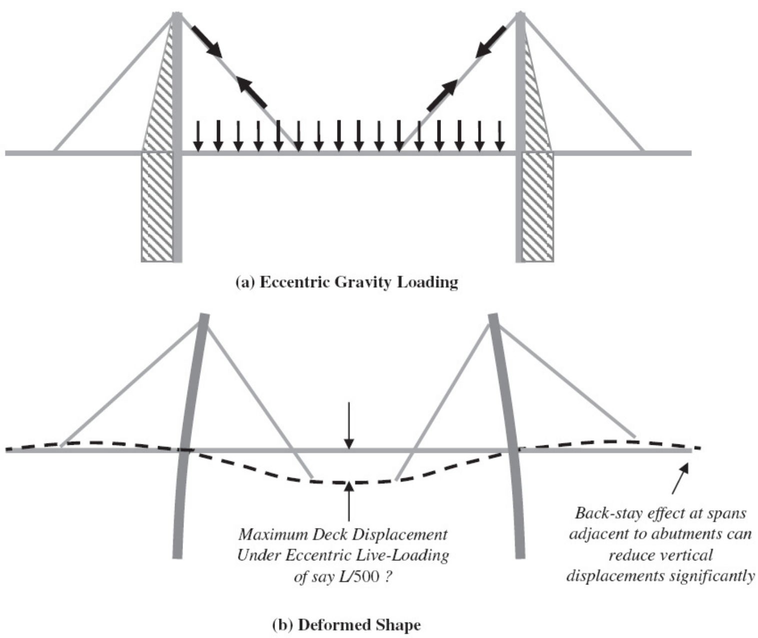

Figure 12. Eccentric gravity loading affects on (a) internal forces and (b) deformed shape.

The actual eccentric load that must be carried by the tower piers will depend on the vertical acceleration of the deck. As this will depend on the deck frequencies and damping, a quick means of calculating the vertical accelerations is not available. However, in order to conservatively size the tower pier sections at the conceptual design stage with allowance for vertical deck response, one can consider the extreme scenario (illustrated in *Fig. 13*) in which the rising side of the deck slackens the cables completely, such that the cable loads associated with the sagging portion of the deck must be carried by the tower piers.

Accordingly, the conceptual design force considered to act at the top of the tower piers is given by:

$$F_{pier,long} = \zeta \frac{w_{deck,EQ} \cdot L_{span}}{2} \tag{15}$$

where $w_{deck,EQ}$ is the gravity load of the deck expected to be present at the time of the maximum design intensity earthquake event, L_{span} is the deck span between towers, and ζ is a continuity coefficient intended to take account of the flexural resistance offered by the continuous deck. The continuity coefficient will clearly depend on the relative stiffness of the deck vs. the tower-cable system and designers could select a value considering the bridge in question. For preliminary sizing purposes a value of 0.5 may be reasonable.

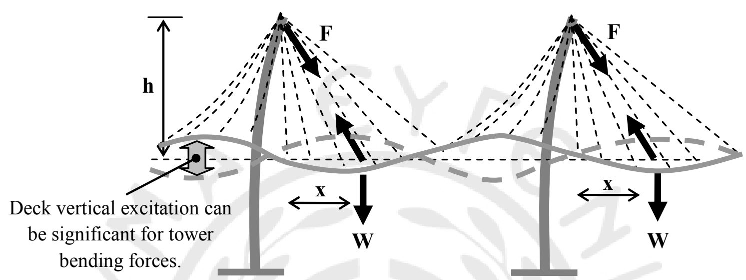

Figure 13. Deformed shape of bridge under longitudinal seismic excitation.

For the deck-to-pier connections, reasonable characteristics can be set in order to suitably limit the seismic response of the deck. Important criteria for the seismic design in the longitudinal direction may include requirements to:

- Limit the longitudinal displacements of the deck in order to ease joint requirements. The displacement capacity of movement joints is dependent on manufacturer capabilities. However, a typical movement joint may have a limit of up to 0.5 m, whereas specialist movement joints can be manufactured to sustain over a metre of movement.
- Limit the vertical displacements of the deck by controlling the lateral displacements at the top of the tower piers.
- Limit the curvature demands in the tower piers.

As satisfaction of the last two of these criteria will depend on the excitation of the tower itself in addition to the longitudinal movements of the deck, they are difficult to control via the deck-to-pier connection alone. However, it is argued that the first design requirement can be effectively controlled through good selection of the deck-to-pier connections. In order to do this, one can use a direct displacement-based design procedure.

5.3 Seismic design considerations for the transverse direction

While the transverse seismic response of a cable-stayed bridge incorporating a full-isolation concept may at first appear rather straightforward, there are a number of factors that make aspects of this response difficult to predict, as will be discussed subsequently. However, it will also be argued that for what concerns the preliminary conceptual design, the transverse response direction will not typically be critical for member sizing.

In the transverse direction it may be assumed that the cables and therefore piers provide little lateral restraint to the deck. As such, if the deck is isolated from the piers at the deck level, the period of vibration in the transverse direction should correspond to that predicted by the period expression for a classic pendulum, presented earlier in Eq. (3). This transverse period will of course be significantly reduced if a connection is provided that has an elastic, displacement-dependent force component. However, in the case that the bridge does not have elastic restrainers, and instead incorporates linear or nonlinear viscous dampers, as in the case of the South Crossing of Guayaquil, then a long period of vibration could be expected. Considering the spectral displacement demands in the long period range, one would estimate that the peak displacement in the transverse direction would be equal to the peak ground displacement, or at most the peak spectral displacement (from periods TD to TE in *Fig. 1*). Consequently, if such a displacement demand can be accommodated through provision of a sufficient gap between the deck and the piers, then one could argue that the transverse response should be fine.

However, the pendulum-type dynamic response of the deck is likely to be influenced by the response of the tower piers with considerable interaction with the higher modes of vibration of the tower itself. Such interaction could be due to both the transverse and vertical excitation of the tower piers. Furthermore, the higher modes of vibration of the deck are likely to have long periods in the transverse direction, with significant mass participation. Such higher modes may also be excited through interaction of the transverse and longitudinal response of the deck-to-pier connections. In the Guayaquil bridge the longitudinal response is limited through incorporation of nonlinear viscous dampers between the deck and the piers. In order to allow for transverse movements of the deck, and to provide some damping in the transverse direction, the dampers are oriented at 45° to the line of the deck. As such, as the longitudinal response develops, the dampers develop forces which will also act to resist the transverse response of the deck. The balanced configuration of the dampers implies that the longitudinal excitation is not expected to excite the transverse response, but it may still permit transverse excitation of the pier to be imposed onto the deck when the dampers are moving at a high velocity due to the longitudinal response. Note that the dampers may well even tend to filter the imposed action in the transverse direction to that associated with the frequencies of vibration in the longitudinal direction.

Evidently, therefore, the seismic response in the transverse direction is rather difficult to accurately predict without nonlinear dynamic analyses. However, this should not impact too greatly on the preliminary conceptual design requirements. As outlined in Sec. 5.1, preliminary sizing for the tower piers and tower bases in the transverse direction can be made through consideration of eccentric gravity loads. The cables should not be affected by transverse seismic response and nor should the deck section. Finally, while the dampers will assist in limiting the response in the transverse direction, it is suggested that their preliminary sizing be based on the longitudinal seismic response direction.

In regions of very high seismicity the pier sections could also be sized considering that the vertical modes of vibration of the deck could also impose large moments on the tower piers in the transverse direction in a similar manner to that described for the longitudinal direction. For the case of two-deck bridges, such as the South Crossing bridge in Guayaquil, one deck could move vertically out of phase with respect to the other (see *Fig. 14*). Again, for sizing the piers one could consider that the rising deck slackens the cables completely, such that the weight of the sagging portion of the deck must be carried by the Tower piers.

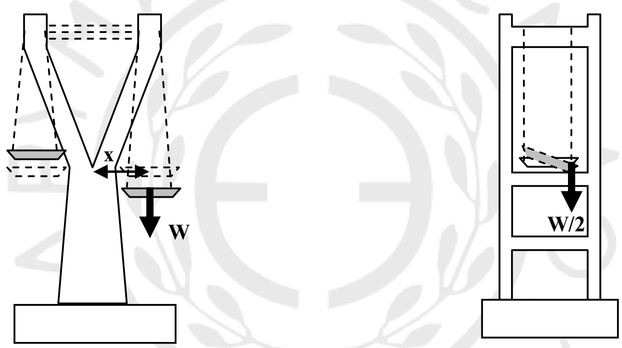

Figure 14. Eccentric loads to be carried by tower piers due to vertical

In line with this, the design overturning for the tower piers in the transverse direction is given by:

$$M_{\text{piers,trans}} = \zeta . w_{\text{deck,EQ}} . L_{\text{span}} . x \tag{16}$$

Where $w_{deck,EQ}$ is the gravity load expected on the deck at the time of the design earthquake, L_{span} is the tower-to-tower span of the deck, and x is the eccentricity as indicated in *Fig. 14(a)* below. Note that for single-deck bridges one can also use a similar analogy considering that the vertical excitation will also excite torsional modes of vibration in the deck, potentially lifting one edge of the deck and sagging the other, as indicated in *Fig. 14(b)*.

Some consideration should also be directed towards the ends of the bridge where the transverse response may be more critical for what regards the joint design. The dampers at the ends of the deck should be sized to control the displacement demands on the joints, and while this could be achieved using a

DBD approach such as that proposed for the longitudinal direction, the participating mass and equivalent SDOF characteristics are more difficult to establish, suggesting that one might resort to a more trial-and-error approach using advanced analyses.

6 CONCLUSIONS

This article has reviewed and discussed some of the important conceptual design considerations for cable-stayed bridges, first for gravity loads and then for seismic excitation. The advantages and disadvantages of different cable-stayed bridge solutions have been highlighted, with review of deck sections, tower configurations in both the longitudinal and transverse directions, deck-to-pier connections, and cable arrangements. It has been argued that the use of intermediate-type deck-to-pier connections is likely to provide the best control of seismic response, as they can limit the actions imposed onto the bridge towers which should be stiff in order to limit deck displacements under both gravity and seismic loads. Reference has been made to a number of real cable-stayed bridge solutions.

In addition to identifying important conceptual design issues, a preliminary sizing procedure has been proposed. In addition to a series of simple design expressions for member sizes and bridge proportions, a novel formulation of the direct displacement-based design procedure has been proposed for identification of suitable deck-to-pier connection characteristics.

ACKNOWLEDGEMENTS AND REFERENCES

This paper is derived from the paper with same title and authors published on the Journal of Earthquake Engineering, Vol. 14, ISS8, 2010, pp. 1139-1171.
Interested readers are therefore invited to see the original paper for a more comprehensive presentation, a design example and a thorough literature review.

UNIFIED LRFD-BASED PROCEDURES FOR ANALYSIS AND DESIGN OF BRIDGE BEARINGS AND SEISMIC ISOLATORS

Michael C. Constantinou

University at Buffalo, State University of New York, Department of Civil, Structural and Environmental Engineering, Buffalo, NY 14260, USA
e-mail: constan1@buffalo.edu

ABSTRACT: This paper presents a brief introduction to the lecture "Unified LRFD-based Procedures for Analysis and Design of Bridge Bearings and Seismic Isolators", conclusions, references and acknowledgements, and the actual presentation of the lecture at ISBSBI, Athens, Greece, 2011.

KEY WORDS: Seismic isolation, bridges, elastomeric bearings, sliding bearings, Load Resistance Factor Design

1 INTRODUCTION

Current design procedures for bridge bearings and seismic isolators are based on different and conflicting procedures. Furthermore, these design procedures are not based on contemporary LRFD framework-a situation that may result in inconsistency, difficulty and confusion in design applications. The presentation appended to this paper highlights the results of a recently completed project on the development of analysis and design procedures for bridge bearings, seismic isolators and related hardware that:

(a) Are based on the LRFD framework,
(b) Are based on similar fundamental principles, which include the latest developments and understanding of behavior,
(c) Are applicable through the same procedures regardless of whether the application is for seismic-isolated or conventional bridges, and
(d) Consider service, design earthquake and maximum earthquake effects.

Furthermore, the presentation briefly discusses the topic of modeling the behavior of seismic isolators with due consideration for the effects of heating and the implications in the testing of isolators.

2 PRESENTATION

Appended to this paper is the presentation of the lecture "Unified LRFD-based

Procedures for Analysis and Design of Bridge Bearings and Seismic Isolators". The interested reader may find more details of the information presented in this lecture in the publications listed in the References.

3 CONCLUSIONS

The presentation appended to this paper presents detailed analysis and design specifications for bridge bearings, seismic isolators and related hardware that are based on the LRFD framework, are based on similar fundamental principles, and are applicable through the same procedures regardless of whether the application is for seismic-isolated or conventional bridges. The procedures are cast in a form that allows the user to understand the margin of safety inherent in the design. Moreover, a report provided in the references ("LRFD-Based Analysis and Design Procedures for Bridge Bearings and Seismic Isolators") presents the background theory on which the analysis and design procedures are based.

The presentation also presents a number of analysis and design examples. Detailed presentation of these examples is found in the aforementioned report. The examples include several cases of design of bridge elastomeric bearings, a case of design of a multidirectional spherical sliding bearing, and three cases of analysis and design of an isolation system for an example bridge. The three cases are one for a triple FP isolation system, one for a single FP isolation system and one for a lead-rubber isolation system.

The design procedures utilize different acceptable limits for service, design earthquake and maximum earthquake conditions. For service conditions, the design procedures parallel those of the latest AASHTO LRFD Bridge Specifications (AASHTO, 2010) except that equations are cast into simpler form. The maximum earthquake effects are defined as those of the design earthquake multiplied by a factor. The value of this factor is dependent on the site of the bridge and on the properties of the seismic isolation system so that a single value cannot be representative of all cases. It is believed that the value of 1.5 for this factor is conservative for California.

ACKNOWLEDGMENTS

Financial support for this project was provided by:

1) The Pacific Earthquake Engineering Research Center (PEER) through a contract with the California Department of Transportation (Caltrans).
2) MCEER, University at Buffalo, State University of New York through a contract with the Federal Highway Administration, Project 020, Title V.

REFERENCES

[1] American Association of State Highway and Transportation Officials (2010), AASHTO LRFD Bridge Design Specifications", Washington, D.C.

[2] American Association of State Highway and Transportation Officials (2010), "Guide Specifications for Seismic Isolation Design", Washington, D.C.

[3] Constantinou, M.C., Whittaker, A.S., Kalpakidis, Y., Fenz, D.M. and Warn, G.P. (2007), "Performance of Seismic Isolation Hardware under Service and Seismic Loading," *Report No. MCEER-07-0012*, Multidisciplinary Center for Earthquake Engineering Research, Buffalo, NY.

[4] Constantinou, M.C., Kalpakidis, I., Filliatrault, A. and Ecker Lay, R.A. (2011),"LRFD-Based Analysis and Design Procedures for Bridge Bearings and Seismic Isolators", PEER/MCEER Report, to be published.

[5] Kalpakidis I.V. and Constantinou, M.C. (2008), "Effects of Heating and Load History on the Behavior of Lead-rubber Bearings," Report No. MCEER-08-0027, Multidisciplinary Center for Earthquake Engineering Research, Buffalo, NY.

[6] Kalpakidis, I.V. and Constantinou, M.C. (2009), "Effects of Heating on the Behavior of Lead-rubber Bearings. I: Theory," ASCE, J. Structural Engineering, Vol. 135, No.12, 1440-1449.

[7] Kalpakidis, I.V. and Constantinou, M.C. (2009), "Effects of Heating on the Behavior of Lead-rubber Bearings. II: Verification of Theory," ASCE, J. Structural Engineering, Vol. 135, No.12, 1450-1461.

[8] Kalpakidis, I.V., Constantinou, M.C. and Whittaker, A.S. (2010), "Modeling Strength Degradation in Lead-rubber Bearings under Earthquake Shaking," Earthquake Engineering and Structural Dynamics, Vol. 39, No. 13, 1533-1549.

[9] Kalpakidis, I.V. and Constantinou, M.C. (2010), "Principles of Scaling and Similarity for Testing of Lead-rubber Bearings," Earthquake Engineering and Structural Dynamics, Vol. 39, No. 13, 2010, 1551-1568.

[10] Konstantinidis, D., Kelly, J.M. and Makris, N. (2008), "Experimental Investigation on the Seismic Response of Bridge Bearings," Report EERC 2008-02, Earthquake Engineering Research Center, University of California, Berkeley.

[11] Stanton, J.F., Roeder, C.W., Mackenzie-Helnwein, P., White, C., Kuester, C. and Craig, B. (2008), "Rotation Limits for Elastomeric Bearings," NCHRP Report 596, Transportation Research Board, National Research Council, Washington, D.C.

Unified LRFD-based Analysis and Design Procedures for Bridge Bearings and Seismic Isolators

Michael C. Constantinou
Professor
Department of Civil, Structural, and Environmental Engineering
University at Buffalo, State University of New York

IBSBI 2011, October 13-15, Athens, Greece   Civil, Structural & Environmental Eng. , University at Buffalo

SCOPE OF PRESENTATION

- Present a general description of project to develop unified LRFD-based procedures for bridge bearings and seismic isolators.
- Present details of the approach followed in the development of LRFD-based analysis and design procedures for elastomeric isolators and elastomeric bearings.
- Present a summary of approach followed in the design of sliding bearings.
- Present summary results on effects of hysteretic and frictional heating on isolator behavior.

IBSBI 2011, October 13-15, Athens, Greece   Civil, Structural & Environmental Eng. , University at Buffalo

ACKNOWLEDGEMENTS

This work has been supported by

- Pacific Earthquake Engineering Research Center (PEER) through a contract with the California Department of Transportation.
- MCEER, University at Buffalo, State University of New York through a contract with the Federal Highway Administration, Project 020, Title V.
- Professor A. Filiatrault and Dr. Y. Kalpakidis participated in the LRFD project.
- Reviewers for the LRFD project were Dr. T. Delis, Dr. A. Kartoum and Mr. T. Shantz on behalf of Caltrans and Professors J. Kelly and S. Mahin and Dr. F. Naeim on behalf of PEER.
- Dr. E. D. Wolff, Dr. D. M. Fenz and Dr. I. Kalpakidis participated in the work on hysteretic and frictional heating.

IBSBI 2011, October 13-15, Athens, Greece   Civil, Structural & Environmental Eng. , University at Buffalo

LRFD PROJECT OBJECTIVES

- Develop analysis and design specifications for bridge bearings and seismic isolators
  - Based on LRFD framework.
  - Based on the same fundamental principles, which include the latest developments and understanding of behavior.
  - Applied by the same principles regardless of whether the application is for seismic-isolated or conventional bridges.
  - Consider service, design earthquake and maximum earthquake effects.

IBSBI 2011, October 13-15, Athens, Greece   Civil, Structural & Environmental Eng. , University at Buffalo

REFERENCES

- "*Guide Specifications for Seismic Isolation Design*", AASHTO, 1999 and recent 2010 revision.
- "Design of Structures for Earthquake Resistance. Part 2: Bridges," Eurocode 8, EN1998-2, 2005.
- "*LRFD Bridge Design Specifications*", AASHTO, 4th Edition, 2007 and recent 2010 5th Edition.
- "*Rotation Limits for Elastomeric Bearings*", Report 12-68, University of Washington, 2006 (published as report NCHRP 596, 2008).
- "*Performance of Seismic Isolation Hardware under Service and Seismic Loading*", Report MCEER-07-0012, 2007.
- "*Experimental Investigation on the Seismic Response of Bridge Bearings*", Univ. of California, Berkeley, EERC-2008-02, 2008.
- "LRFD-based Analysis and Design Procedures for Bridge Bearings and Seismic Isolators", Joint PEER-MCEER report, final draft, March 12, 2011.

IBSBI 2011, October 13-15, Athens, Greece   Civil, Structural & Environmental Eng. , University at Buffalo

SUMMARY OF WORK

- Concentration on sliding and elastomeric bearings.
- Sliding bearings are either flat or spherically shaped. Key characteristic is that they have spherical rotational part (flat or Friction Pendulum). Pot bearings and disc bearings are not considered (and not used in California).
- Elastomeric bearings are rectangular, square, circular, hollow circular (central hole) and circular with one central core of lead. Shape factors are in the range of 5 to 30. Bearings are bolted or kept by keeper plates. Regular bridge bearings may be kept by friction. Only steel reinforced bearings are considered.

IBSBI 2011, October 13-15, Athens, Greece   Civil, Structural & Environmental Eng. , University at Buffalo

LOADINGS FOR ANALYSIS AND DESIGN OF SEISMICALLY ISOLATED BRIDGES

- Service loadings per AASHTO LRFD Specifications, 2010.
- Design earthquake (DE) per AASHTO LRFD Specifications, 2010 (probabilistic response spectrum having 7% probability of being exceeded in 75 years-return period ~1000years)
  - Design earthquake in California based on Caltrans ARS Website. Defined as the largest of (a) probabilistic response spectrum having 5% probability of being exceeded in 50 years-return period 1000years, and (b) deterministic median spectrum calculated based on the NGA project of PEER.
- Maximum earthquake not explicitly defined.
  - For isolators, the effects of maximum earthquake defined as those of the DE multiplied by a factor. For California the factor on isolator displacement is 1.5. The factor for force to be determined by analysis-range of 1.0 to 1.5. Use 1.5 default value.
  - For elastomeric bridge bearings, the effects of maximum earthquake are not considered. Bearings may overturn but sufficient bearing seat width is provided (1.5 times the DE displacement).
  - For spherical sliding bridge bearings, the maximum earthquake effects are defined as those of the DE multiplied by factor 1.5.

IBSBI 2011, October 13-15, Athens, Greece   Civil, Structural & Environmental Eng. , University at Buffalo

SLIDING BEARINGS

- Review of knowledge on spherical bearings

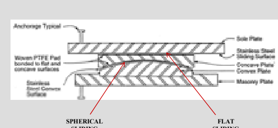

IBSBI 2011, October 13-15, Athens, Greece   Civil, Structural & Environmental Eng. , University at Buffalo

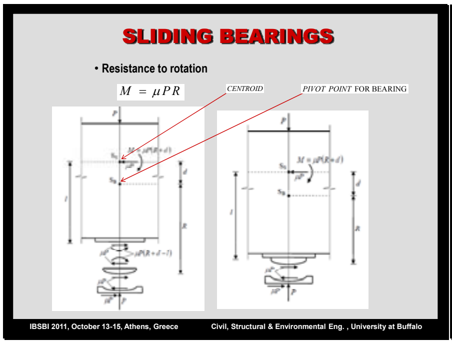
SLIDING BEARINGS
• Resistance to rotation
$M = \mu P R$
CENTROID
PIVOT POINT FOR BEARING
IBSBI 2011, October 13-15, Athens, Greece
Civil, Structural & Environmental Eng. , University at Buffalo

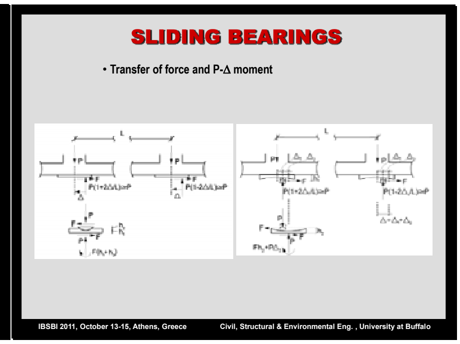
SLIDING BEARINGS
• Transfer of force and P-Δ moment
IBSBI 2011, October 13-15, Athens, Greece
Civil, Structural & Environmental Eng. , University at Buffalo

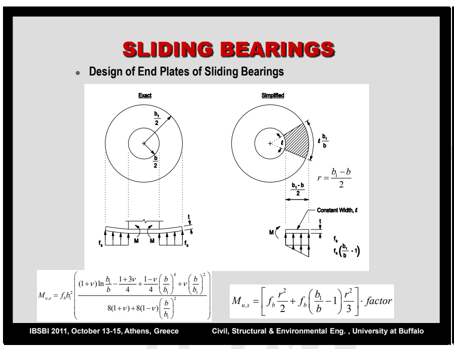
SLIDING BEARINGS
Design of End Plates of Sliding Bearings
Exact
Simplified
Constant Width, ℓ
IBSBI 2011, October 13-15, Athens, Greece
Civil, Structural & Environmental Eng. , University at Buffalo

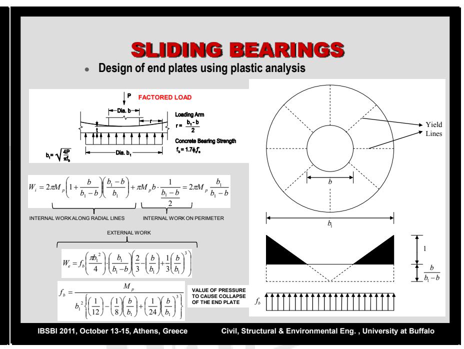
SLIDING BEARINGS
Design of end plates using plastic analysis
FACTORED LOAD
Loading Arm
Concrete Bearing Strength
Yield Lines
INTERNAL WORK ALONG RADIAL LINES
INTERNAL WORK ON PERIMETER
EXTERNAL WORK
VALUE OF PRESSURE TO CAUSE COLLAPSE OF THE END PLATE
IBSBI 2011, October 13-15, Athens, Greece
Civil, Structural & Environmental Eng. , University at Buffalo

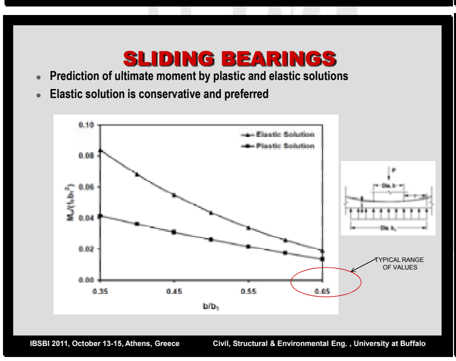
SLIDING BEARINGS
Prediction of ultimate moment by plastic and elastic solutions
Elastic solution is conservative and preferred
Elastic Solution
Plastic Solution
TYPICAL RANGE OF VALUES
b/b1
IBSBI 2011, October 13-15, Athens, Greece
Civil, Structural & Environmental Eng. , University at Buffalo

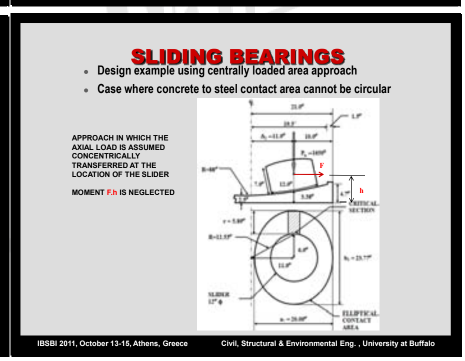
SLIDING BEARINGS
Design example using centrally loaded area approach
Case where concrete to steel contact area cannot be circular
APPROACH IN WHICH THE AXIAL LOAD IS ASSUMED CONCENTRICALLY TRANSFERRED AT THE LOCATION OF THE SLIDER
MOMENT F.h IS NEGLECTED
CRITICAL SECTION
SLIDER
ELLIPTICAL CONTACT AREA
IBSBI 2011, October 13-15, Athens, Greece
Civil, Structural & Environmental Eng. , University at Buffalo

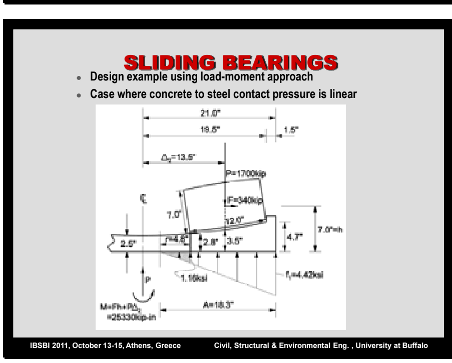
SLIDING BEARINGS
Design example using load-moment approach
Case where concrete to steel contact pressure is linear
21.0"
19.5"
1.5"
P=1700kip
F=340kip
7.0"
12.0"
7.0"=h
2.5"
2.8"
3.5"
4.7"
1.16ksi
f1=4.42ksi
A=18.3"
M=Fh+PΔ2
=25330kip-in
IBSBI 2011, October 13-15, Athens, Greece
Civil, Structural & Environmental Eng. , University at Buffalo

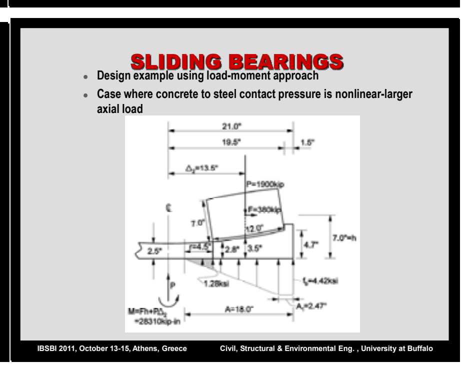
SLIDING BEARINGS
Design example using load-moment approach
Case where concrete to steel contact pressure is nonlinear-larger axial load
21.0"
19.5"
1.5"
P=1900kip
F=380kip
7.0"
12.0"
7.0"=h
2.5"
2.8"
3.5"
4.7"
1.28ksi
f1=4.42ksi
A=18.0"
M=Fh+PΔ2
=28310kip-in
IBSBI 2011, October 13-15, Athens, Greece
Civil, Structural & Environmental Eng. , University at Buffalo

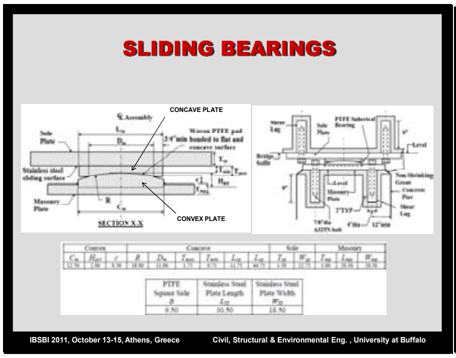

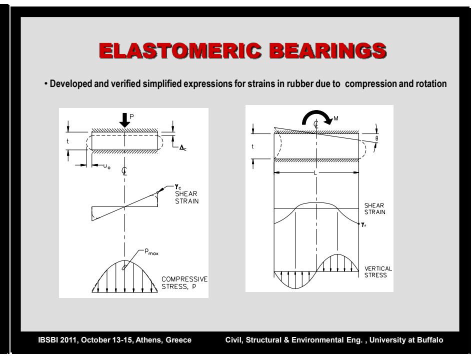

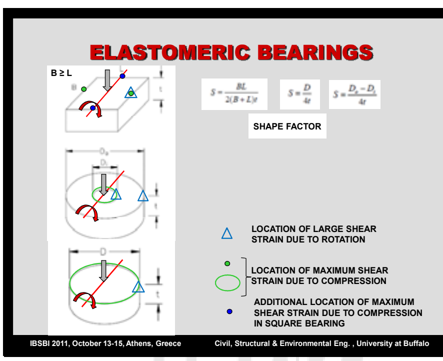

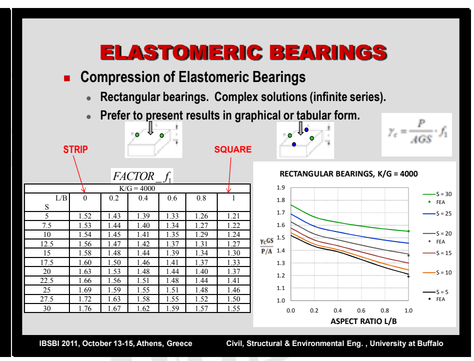

K/G = 4000						
L/B S	0	0.2	0.4	0.6	0.8	1
5	1.52	1.43	1.39	1.33	1.26	1.21
7.5	1.53	1.44	1.40	1.34	1.27	1.22
10	1.54	1.45	1.41	1.35	1.29	1.24
12.5	1.56	1.47	1.42	1.37	1.31	1.27
15	1.58	1.48	1.44	1.39	1.34	1.30
17.5	1.60	1.50	1.46	1.41	1.37	1.33
20	1.63	1.53	1.48	1.44	1.40	1.37
22.5	1.66	1.56	1.51	1.48	1.44	1.41
25	1.69	1.59	1.55	1.51	1.48	1.46
27.5	1.72	1.63	1.58	1.55	1.52	1.50
30	1.76	1.67	1.62	1.59	1.57	1.55

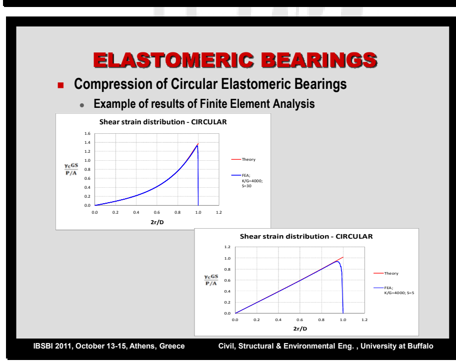

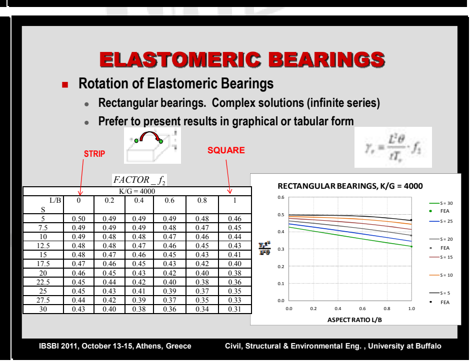

K/G = 4000						
L/B S	0	0.2	0.4	0.6	0.8	1
5	0.50	0.49	0.49	0.49	0.48	0.46
7.5	0.49	0.49	0.49	0.48	0.47	0.45
10	0.49	0.48	0.48	0.47	0.46	0.44
12.5	0.48	0.48	0.47	0.46	0.45	0.43
15	0.48	0.47	0.46	0.45	0.43	0.41
17.5	0.47	0.46	0.45	0.43	0.42	0.40
20	0.46	0.45	0.43	0.42	0.40	0.38
22.5	0.45	0.44	0.42	0.40	0.38	0.36
25	0.45	0.43	0.41	0.39	0.37	0.35
27.5	0.44	0.42	0.39	0.37	0.35	0.33
30	0.43	0.40	0.38	0.36	0.34	0.31

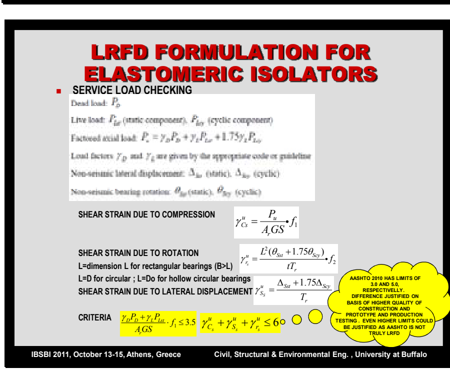

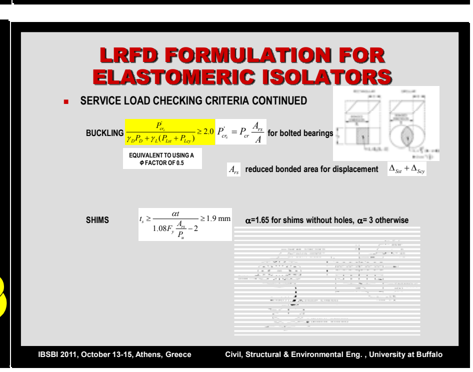

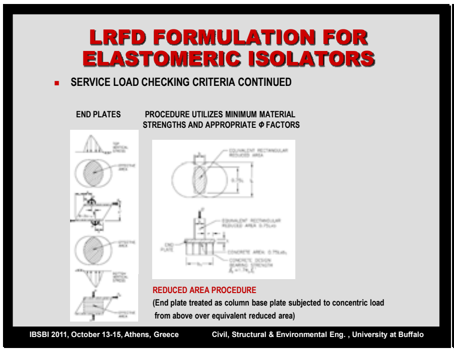
LRFD FORMULATION FOR ELASTOMERIC ISOLATORS
SERVICE LOAD CHECKING CRITERIA CONTINUED
END PLATES
PROCEDURE UTILIZES MINIMUM MATERIAL STRENGTHS AND APPROPRIATE Φ FACTORS
REDUCED AREA PROCEDURE
(End plate treated as column base plate subjected to concentric load from above over equivalent reduced area)
IBSBI 2011, October 13-15, Athens, Greece
Civil, Structural & Environmental Eng. , University at Buffalo

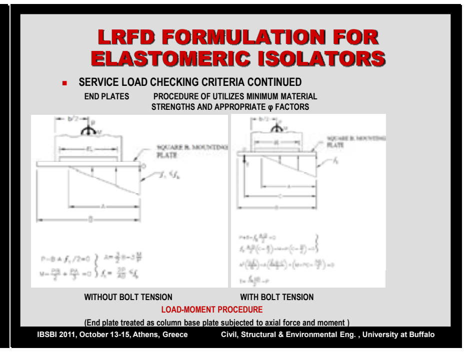
LRFD FORMULATION FOR ELASTOMERIC ISOLATORS
SERVICE LOAD CHECKING CRITERIA CONTINUED
END PLATES
PROCEDURE OF UTILIZES MINIMUM MATERIAL STRENGTHS AND APPROPRIATE φ FACTORS
WITHOUT BOLT TENSION
WITH BOLT TENSION
LOAD-MOMENT PROCEDURE
(End plate treated as column base plate subjected to axial force and moment)
IBSBI 2011, October 13-15, Athens, Greece
Civil, Structural & Environmental Eng. , University at Buffalo

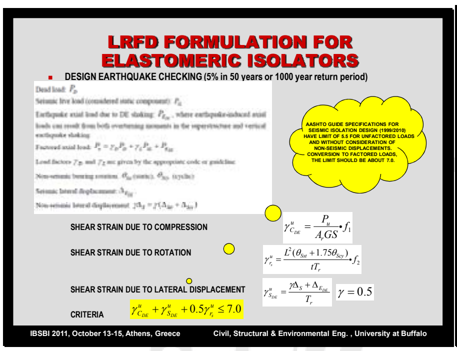
LRFD FORMULATION FOR ELASTOMERIC ISOLATORS
DESIGN EARTHQUAKE CHECKING (5% in 50 years or 1000 year return period)
AASHTO GUIDE SPECIFICATIONS FOR SEISMIC ISOLATION DESIGN (1999/2010) HAVE LIMIT OF 5.5 FOR UNFACTORED LOADS AND WITHOUT CONSIDERATION OF NON-SEISMIC DISPLACEMENTS. CONVERSION TO FACTORED LOADS, THE LIMIT SHOULD BE ABOUT 7.0.
SHEAR STRAIN DUE TO COMPRESSION
SHEAR STRAIN DUE TO ROTATION
SHEAR STRAIN DUE TO LATERAL DISPLACEMENT
CRITERIA
IBSBI 2011, October 13-15, Athens, Greece
Civil, Structural & Environmental Eng. , University at Buffalo

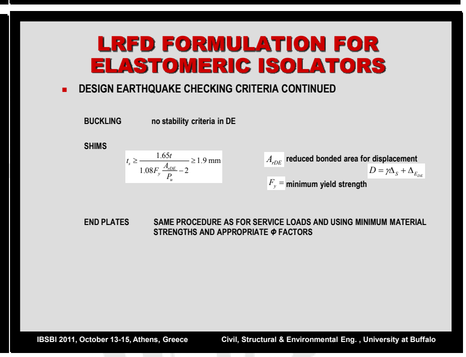
LRFD FORMULATION FOR ELASTOMERIC ISOLATORS
DESIGN EARTHQUAKE CHECKING CRITERIA CONTINUED
BUCKLING
no stability criteria in DE
SHIMS
reduced bonded area for displacement
minimum yield strength
END PLATES
SAME PROCEDURE AS FOR SERVICE LOADS AND USING MINIMUM MATERIAL STRENGTHS AND APPROPRIATE Φ FACTORS
IBSBI 2011, October 13-15, Athens, Greece
Civil, Structural & Environmental Eng. , University at Buffalo

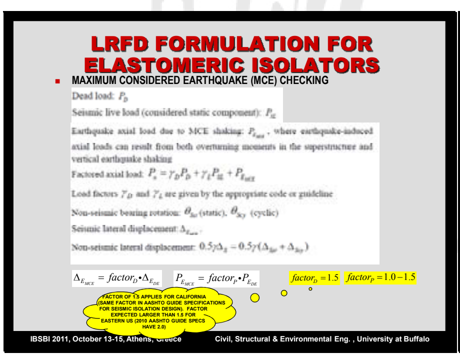
LRFD FORMULATION FOR ELASTOMERIC ISOLATORS
MAXIMUM CONSIDERED EARTHQUAKE (MCE) CHECKING
FACTOR OF 1.5 APPLIES FOR CALIFORNIA (SAME FACTOR IN AASHTO GUIDE SPECIFICATIONS FOR SEISMIC ISOLATION DESIGN). FACTOR EXPECTED LARGER THAN 1.5 FOR EASTERN US (2010 AASHTO GUIDE SPECS HAVE 2.0)
IBSBI 2011, October 13-15, Athens, Greece
Civil, Structural & Environmental Eng. , University at Buffalo

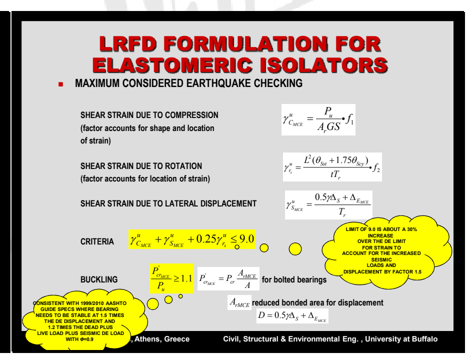
LRFD FORMULATION FOR ELASTOMERIC ISOLATORS
MAXIMUM CONSIDERED EARTHQUAKE CHECKING
SHEAR STRAIN DUE TO COMPRESSION
(factor accounts for shape and location of strain)
SHEAR STRAIN DUE TO ROTATION
(factor accounts for location of strain)
SHEAR STRAIN DUE TO LATERAL DISPLACEMENT
CRITERIA
LIMIT OF 9.0 IS ABOUT A 30% INCREASE OVER THE DE LIMIT FOR STRAIN TO ACCOUNT FOR THE INCREASED SEISMIC LOADS AND DISPLACEMENT BY FACTOR 1.5
BUCKLING
for bolted bearings
reduced bonded area for displacement
CONSISTENT WITH 1999/2010 AASHTO GUIDE SPECS WHERE BEARING NEEDS TO BE STABLE AT 1.5 TIMES THE DE DISPLACEMENT AND 1.2 TIMES THE DEAD PLUS LIVE LOAD PLUS SEISMIC DE LOAD WITH Φ=0.9
Athens, Greece
Civil, Structural & Environmental Eng. , University at Buffalo

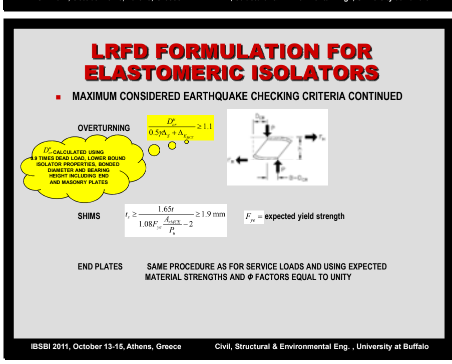
LRFD FORMULATION FOR ELASTOMERIC ISOLATORS
MAXIMUM CONSIDERED EARTHQUAKE CHECKING CRITERIA CONTINUED
OVERTURNING
CALCULATED USING 0.9 TIMES DEAD LOAD, LOWER BOUND ISOLATOR PROPERTIES, BONDED DIAMETER AND BEARING HEIGHT INCLUDING END AND MASONRY PLATES
SHIMS
expected yield strength
END PLATES
SAME PROCEDURE AS FOR SERVICE LOADS AND USING EXPECTED MATERIAL STRENGTHS AND Φ FACTORS EQUAL TO UNITY
IBSBI 2011, October 13-15, Athens, Greece
Civil, Structural & Environmental Eng. , University at Buffalo

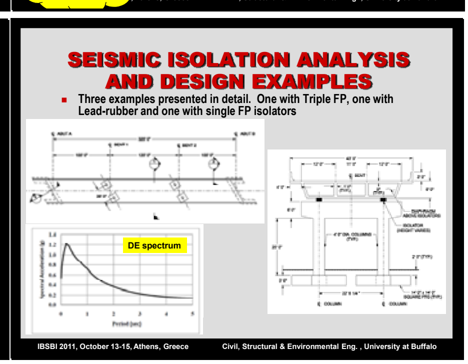
SEISMIC ISOLATION ANALYSIS AND DESIGN EXAMPLES
Three examples presented in detail. One with Triple FP, one with Lead-rubber and one with single FP isolators
DE spectrum
IBSBI 2011, October 13-15, Athens, Greece
Civil, Structural & Environmental Eng. , University at Buffalo

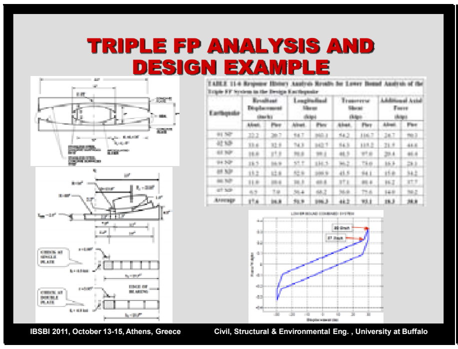
TRIPLE FP ANALYSIS AND DESIGN EXAMPLE
IBSBI 2011, October 13-15, Athens, Greece
Civil, Structural & Environmental Eng. , University at Buffalo

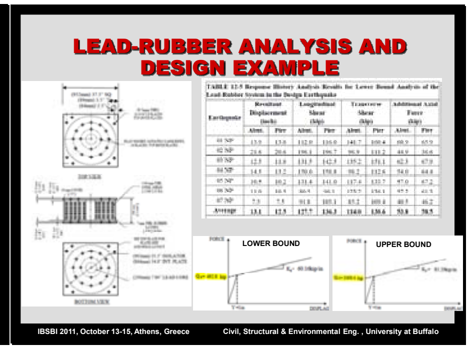
LEAD-RUBBER ANALYSIS AND DESIGN EXAMPLE
LOWER BOUND
UPPER BOUND
IBSBI 2011, October 13-15, Athens, Greece
Civil, Structural & Environmental Eng. , University at Buffalo

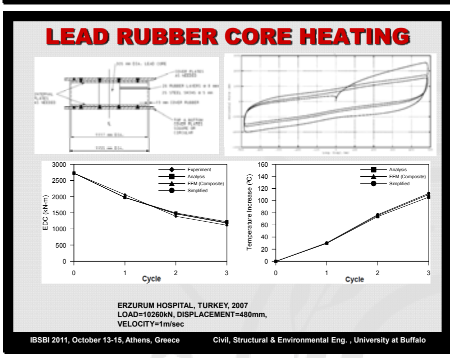
LEAD RUBBER CORE HEATING
EDC (kN-m)
Cycle
Temperature Increase (°C)
Cycle
ERZURUM HOSPITAL, TURKEY, 2007
LOAD=10260kN, DISPLACEMENT=480mm,
VELOCITY=1m/sec
IBSBI 2011, October 13-15, Athens, Greece
Civil, Structural & Environmental Eng. , University at Buffalo

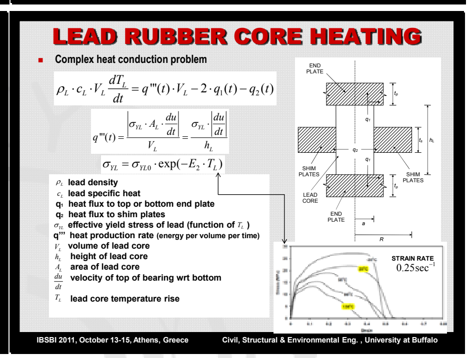
LEAD RUBBER CORE HEATING
Complex heat conduction problem
$\rho_L \cdot c_L \cdot V_L \frac{dT_L}{dt} = q'''(t) \cdot V_L - 2 \cdot q_1(t) - q_2(t)$
$\sigma_{YL} = \sigma_{YL0} \cdot \exp(-E_2 \cdot T_L)$
ρ_L lead density
c_L lead specific heat
q_1 heat flux to top or bottom end plate
q_2 heat flux to shim plates
σ_{YL} effective yield stress of lead (function of T_L)
q''' heat production rate (energy per volume per time)
V_L volume of lead core
h_L height of lead core
A_L area of lead core
$\frac{du}{dt}$ velocity of top of bearing wrt bottom
T_L lead core temperature rise
END PLATE
SHIM PLATES
LEAD CORE
STRAIN RATE
IBSBI 2011, October 13-15, Athens, Greece
Civil, Structural & Environmental Eng. , University at Buffalo

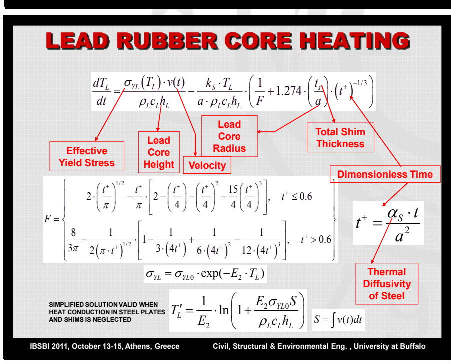
LEAD RUBBER CORE HEATING
Effective Yield Stress
Lead Core Height
Velocity
Lead Core Radius
Total Shim Thickness
Dimensionless Time
Thermal Diffusivity of Steel
$\sigma_{YL} = \sigma_{YL0} \cdot \exp(-E_2 \cdot T_L)$
SIMPLIFIED SOLUTION VALID WHEN HEAT CONDUCTION IN STEEL PLATES AND SHIMS IS NEGLECTED
$S = \int v(t)dt$
IBSBI 2011, October 13-15, Athens, Greece
Civil, Structural & Environmental Eng. , University at Buffalo

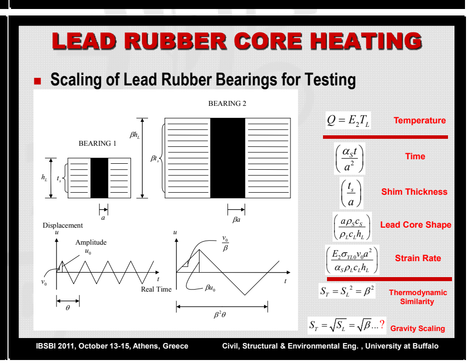
LEAD RUBBER CORE HEATING
Scaling of Lead Rubber Bearings for Testing
BEARING 2
BEARING 1
Displacement
Amplitude
Real Time
Temperature
Time
Shim Thickness
Lead Core Shape
Strain Rate
Thermodynamic Similarity
Gravity Scaling
IBSBI 2011, October 13-15, Athens, Greece
Civil, Structural & Environmental Eng. , University at Buffalo

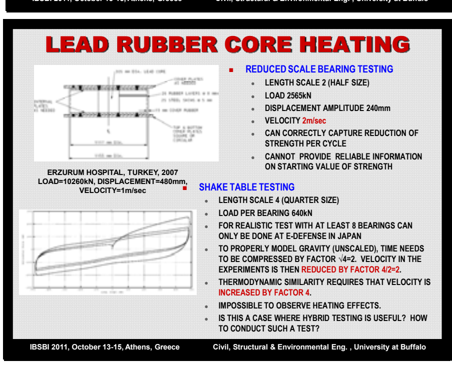
LEAD RUBBER CORE HEATING
ERZURUM HOSPITAL, TURKEY, 2007
LOAD=10260kN, DISPLACEMENT=480mm,
VELOCITY=1m/sec
REDUCED SCALE BEARING TESTING
LENGTH SCALE 2 (HALF SIZE)
LOAD 2565kN
DISPLACEMENT AMPLITUDE 240mm
VELOCITY 2m/sec
CAN CORRECTLY CAPTURE REDUCTION OF STRENGTH PER CYCLE
CANNOT PROVIDE RELIABLE INFORMATION ON STARTING VALUE OF STRENGTH
SHAKE TABLE TESTING
LENGTH SCALE 4 (QUARTER SIZE)
LOAD PER BEARING 640kN
FOR REALISTIC TEST WITH AT LEAST 8 BEARINGS CAN ONLY BE DONE AT E-DEFENSE IN JAPAN
TO PROPERLY MODEL GRAVITY (UNSCALED), TIME NEEDS TO BE COMPRESSED BY FACTOR √4=2. VELOCITY IN THE EXPERIMENTS IS THEN REDUCED BY FACTOR 4/2=2.
THERMODYNAMIC SIMILARITY REQUIRES THAT VELOCITY IS INCREASED BY FACTOR 4.
IMPOSSIBLE TO OBSERVE HEATING EFFECTS.
IS THIS A CASE WHERE HYBRID TESTING IS USEFUL? HOW TO CONDUCT SUCH A TEST?
IBSBI 2011, October 13-15, Athens, Greece
Civil, Structural & Environmental Eng. , University at Buffalo

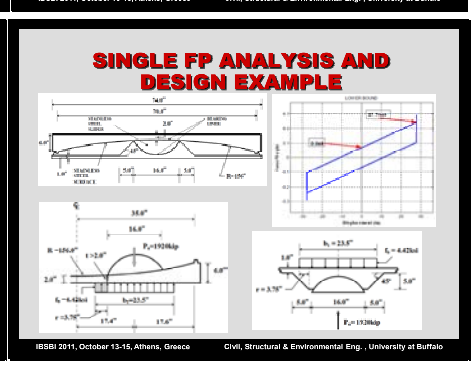
SINGLE FP ANALYSIS AND DESIGN EXAMPLE
IBSBI 2011, October 13-15, Athens, Greece
Civil, Structural & Environmental Eng. , University at Buffalo

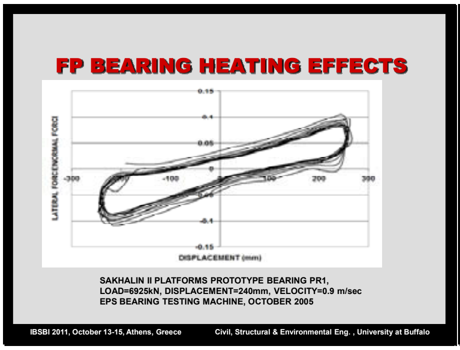
FP BEARING HEATING EFFECTS
LATERAL FORCE/NORMAL FORCE
DISPLACEMENT (mm)
SAKHALIN II PLATFORMS PROTOTYPE BEARING PR1,
LOAD=6925kN, DISPLACEMENT=240mm, VELOCITY=0.9 m/sec
EPS BEARING TESTING MACHINE, OCTOBER 2005
IBSBI 2011, October 13-15, Athens, Greece
Civil, Structural & Environmental Eng. , University at Buffalo

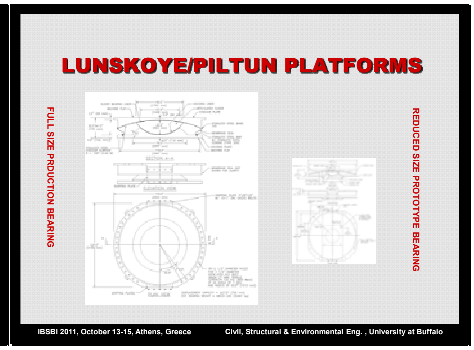
LUNSKOYE/PILTUN PLATFORMS
FULL SIZE PRODUCTION BEARING
REDUCED SIZE PROTOTYPE BEARING
IBSBI 2011, October 13-15, Athens, Greece
Civil, Structural & Environmental Eng. , University at Buffalo

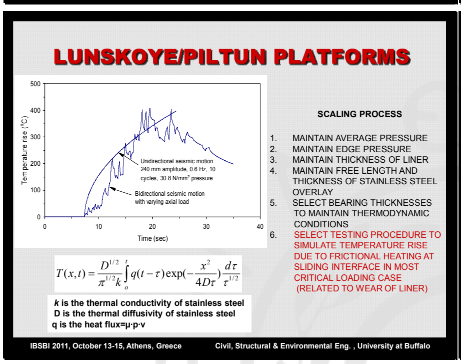
LUNSKOYE/PILTUN PLATFORMS
Temperature rise (°C)
Time (sec)
Unidirectional seismic motion 240 mm amplitude, 0.6 Hz, 10 cycles, 30.8 N/mm² pressure
Bidirectional seismic motion with varying axial load
SCALING PROCESS
1. MAINTAIN AVERAGE PRESSURE
2. MAINTAIN EDGE PRESSURE
3. MAINTAIN THICKNESS OF LINER
4. MAINTAIN FREE LENGTH AND THICKNESS OF STAINLESS STEEL OVERLAY
5. SELECT BEARING THICKNESSES TO MAINTAIN THERMODYNAMIC CONDITIONS
6. SELECT TESTING PROCEDURE TO SIMULATE TEMPERATURE RISE DUE TO FRICTIONAL HEATING AT SLIDING INTERFACE IN MOST CRITICAL LOADING CASE (RELATED TO WEAR OF LINER)
$T(x,t)=\frac{D^{1/2}}{\pi^{1/2}k}\int_o^t q(t-\tau)\exp(-\frac{x^2}{4D\tau})\frac{d\tau}{\tau^{1/2}}$
k is the thermal conductivity of stainless steel
D is the thermal diffusivity of stainless steel
q is the heat flux=μ·p·v
IBSBI 2011, October 13-15, Athens, Greece
Civil, Structural & Environmental Eng. , University at Buffalo

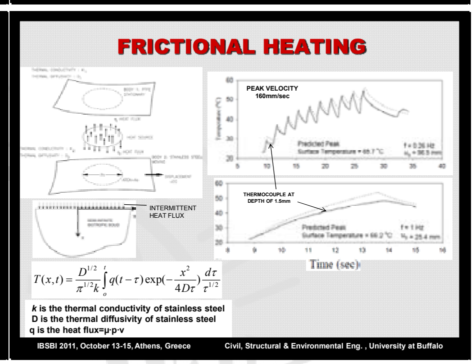
FRICTIONAL HEATING
PEAK VELOCITY 160mm/sec
THERMOCOUPLE AT DEPTH OF 1.5mm
INTERMITTENT HEAT FLUX
Time (sec)
$T(x,t)=\frac{D^{1/2}}{\pi^{1/2}k}\int_o^t q(t-\tau)\exp(-\frac{x^2}{4D\tau})\frac{d\tau}{\tau^{1/2}}$
k is the thermal conductivity of stainless steel
D is the thermal diffusivity of stainless steel
q is the heat flux=μ·p·v
IBSBI 2011, October 13-15, Athens, Greece
Civil, Structural & Environmental Eng. , University at Buffalo

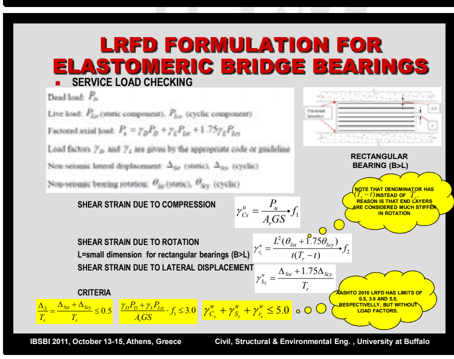
LRFD FORMULATION FOR ELASTOMERIC BRIDGE BEARINGS
SERVICE LOAD CHECKING
Dead load: P_D
Live load: P_{Lst} (static component), P_{Lcy} (cyclic component)
Factored axial load: $P_u=\gamma_D P_D+\gamma_L P_{Lst}+1.75\gamma_L P_{Lcy}$
Load factors γ_D and γ_L are given by the appropriate code or guideline
Non-seismic lateral displacement: Δ_{Sst} (static), Δ_{Scy} (cyclic)
Non-seismic bearing rotation: θ_{Sst} (static), θ_{Scy} (cyclic)
RECTANGULAR BEARING (B>L)
NOTE THAT DENOMINATOR HAS $(T_r - t)$ INSTEAD OF T_r. REASON IS THAT END LAYERS ARE CONSIDERED MUCH STIFFER IN ROTATION
SHEAR STRAIN DUE TO COMPRESSION $\gamma^u_{Cs}=\frac{P_u}{A_r GS}\bullet f_1$
SHEAR STRAIN DUE TO ROTATION $\gamma^u_{r_s}=\frac{L^2(\theta_{Sst}+1.75\theta_{Scy})}{t(T_r-t)}\bullet f_2$
L=small dimension for rectangular bearings (B>L)
SHEAR STRAIN DUE TO LATERAL DISPLACEMENT $\gamma^u_{S_S}=\frac{\Delta_{Sst}+1.75\Delta_{Scy}}{T_r}$
CRITERIA
$\frac{\Delta_S}{T_r}=\frac{\Delta_{Sst}+\Delta_{Scy}}{T_r}\le 0.5$
$\frac{\gamma_D P_D+\gamma_L P_{Lst}}{A_r GS}\cdot f_1\le 3.0$
$\gamma^u_{C_s}+\gamma^u_{S_s}+\gamma^u_{r_s}\le 5.0$
AASHTO 2010 LRFD HAS LIMITS OF 0.5, 3.0 AND 5.0, RESPECTIVELLY, BUT WITHOUT LOAD FACTORS.
IBSBI 2011, October 13-15, Athens, Greece
Civil, Structural & Environmental Eng. , University at Buffalo

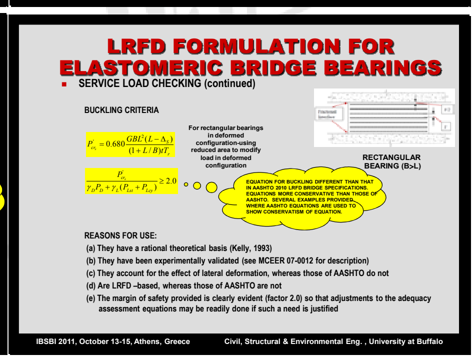
LRFD FORMULATION FOR ELASTOMERIC BRIDGE BEARINGS
SERVICE LOAD CHECKING (continued)
BUCKLING CRITERIA
$P'_{cr_s}=0.680\frac{GBL^2(L-\Delta_S)}{(1+L/B)tT_r}$
For rectangular bearings in deformed configuration-using reduced area to modify load in deformed configuration
$\frac{P'_{cr_s}}{\gamma_D P_D+\gamma_L(P_{Lst}+P_{Lcy})}\ge 2.0$
RECTANGULAR BEARING (B>L)
EQUATION FOR BUCKLING DIFFERENT THAN THAT IN AASHTO 2010 LRFD BRIDGE SPECIFICATIONS. EQUATIONS MORE CONSERVATIVE THAN THOSE OF AASHTO. SEVERAL EXAMPLES PROVIDED WHERE AASHTO EQUATIONS ARE USED TO SHOW CONSERVATISM OF EQUATION.
REASONS FOR USE:
(a) They have a rational theoretical basis (Kelly, 1993)
(b) They have been experimentally validated (see MCEER 07-0012 for description)
(c) They account for the effect of lateral deformation, whereas those of AASHTO do not
(d) Are LRFD –based, whereas those of AASHTO are not
(e) The margin of safety provided is clearly evident (factor 2.0) so that adjustments to the adequacy assessment equations may be readily done if such a need is justified
IBSBI 2011, October 13-15, Athens, Greece
Civil, Structural & Environmental Eng. , University at Buffalo

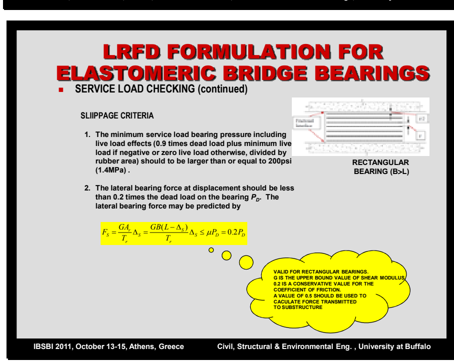
LRFD FORMULATION FOR ELASTOMERIC BRIDGE BEARINGS
SERVICE LOAD CHECKING (continued)
SLIIPPAGE CRITERIA
1. The minimum service load bearing pressure including live load effects (0.9 times dead load plus minimum live load if negative or zero live load otherwise, divided by rubber area) should to be larger than or equal to 200psi (1.4MPa) .
2. The lateral bearing force at displacement should be less than 0.2 times the dead load on the bearing P_D. The lateral bearing force may be predicted by
$F_S=\frac{GA_r}{T_r}\Delta_S=\frac{GB(L-\Delta_S)}{T_r}\Delta_S\le\mu P_D=0.2P_D$
RECTANGULAR BEARING (B>L)
VALID FOR RECTANGULAR BEARINGS.
G IS THE UPPER BOUND VALUE OF SHEAR MODULUS
0.2 IS A CONSERVATIVE VALUE FOR THE COEFFICIENT OF FRICTION.
A VALUE OF 0.5 SHOULD BE USED TO CACULATE FORCE TRANSMITTED TO SUBSTRUCTURE
IBSBI 2011, October 13-15, Athens, Greece
Civil, Structural & Environmental Eng. , University at Buffalo

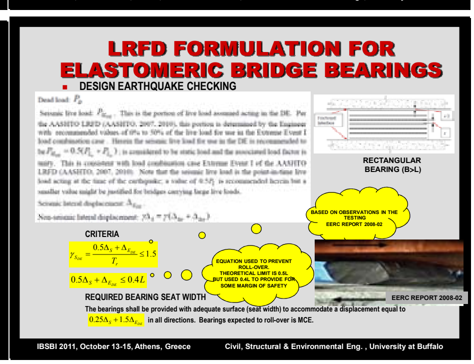
LRFD FORMULATION FOR ELASTOMERIC BRIDGE BEARINGS
DESIGN EARTHQUAKE CHECKING
Dead load: P_D
RECTANGULAR BEARING (B>L)
BASED ON OBSERVATIONS IN THE TESTING EERC REPORT 2008-02
CRITERIA
$\gamma_{S_{eq}}=\frac{0.5\Delta_S+\Delta_{E_{eq}}}{T_r}\le 1.5$
$0.5\Delta_S+\Delta_{E_{eq}}\le 0.4L$
EQUATION USED TO PREVENT ROLL-OVER. THEORETICAL LIMIT IS 0.5L BUT USED 0.4L TO PROVIDE FOR SOME MARGIN OF SAFETY
EERC REPORT 2008-02
REQUIRED BEARING SEAT WIDTH
The bearings shall be provided with adequate surface (seat width) to accommodate a displacement equal to $0.25\Delta_S+1.5\Delta_{E_{eq}}$ in all directions. Bearings expected to roll-over is MCE.
IBSBI 2011, October 13-15, Athens, Greece
Civil, Structural & Environmental Eng. , University at Buffalo

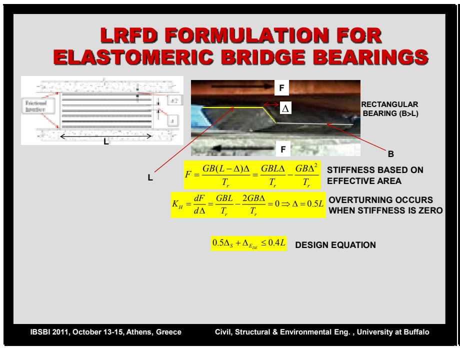
LRFD FORMULATION FOR
ELASTOMERIC BRIDGE BEARINGS
F
Δ
F
L
RECTANGULAR BEARING (B>L)
L
B
$F = \frac{GB(L-\Delta)\Delta}{T_r} = \frac{GBL\Delta}{T_r} - \frac{GB\Delta^2}{T_r}$
STIFFNESS BASED ON EFFECTIVE AREA
$K_H = \frac{dF}{d\Delta} = \frac{GBL}{T_r} - \frac{2GB\Delta}{T_r} = 0 \Rightarrow \Delta = 0.5L$
OVERTURNING OCCURS WHEN STIFFNESS IS ZERO
$0.5\Delta_S + \Delta_{E_{DE}} \leq 0.4L$
DESIGN EQUATION
IBSBI 2011, October 13-15, Athens, Greece
Civil, Structural & Environmental Eng. , University at Buffalo

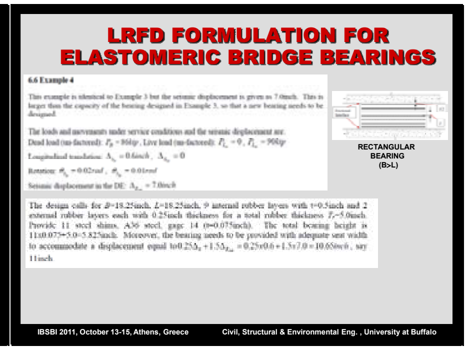
LRFD FORMULATION FOR
ELASTOMERIC BRIDGE BEARINGS
6.6 Example 4
Seismic displacement in the DE: $\Delta_{E_{DE}} = 7.0inch$
The design calls for B=18.25inch, L=18.25inch, 9 internal rubber layers with t=0.5inch and 2 external rubber layers each with 0.25inch thickness for a total rubber thickness T_r=5.0inch. Provide 11 steel shims, A36 steel, gage 14 (t=0.075inch). The total bearing height is 11x0.075+5.0=5.825inch. Moreover, the bearing needs to be provided with adequate seat width to accommodate a displacement equal to $0.25\Delta_S + 1.5\Delta_{E_{DE}} = 0.25x0.6 + 1.5x7.0 = 10.65inch$, say 11inch.
RECTANGULAR BEARING (B>L)
IBSBI 2011, October 13-15, Athens, Greece
Civil, Structural & Environmental Eng. , University at Buffalo

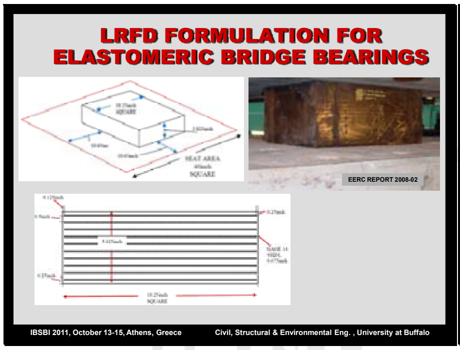
LRFD FORMULATION FOR
ELASTOMERIC BRIDGE BEARINGS
SEAT AREA
SQUARE
EERC REPORT 2008-02
IBSBI 2011, October 13-15, Athens, Greece
Civil, Structural & Environmental Eng. , University at Buffalo

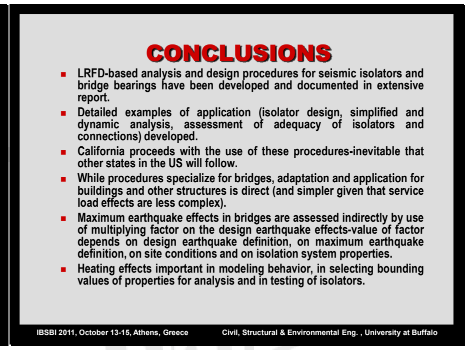
CONCLUSIONS
LRFD-based analysis and design procedures for seismic isolators and bridge bearings have been developed and documented in extensive report.
Detailed examples of application (isolator design, simplified and dynamic analysis, assessment of adequacy of isolators and connections) developed.
California proceeds with the use of these procedures-inevitable that other states in the US will follow.
While procedures specialize for bridges, adaptation and application for buildings and other structures is direct (and simpler given that service load effects are less complex).
Maximum earthquake effects in bridges are assessed indirectly by use of multiplying factor on the design earthquake effects-value of factor depends on design earthquake definition, on maximum earthquake definition, on site conditions and on isolation system properties.
Heating effects important in modeling behavior, in selecting bounding values of properties for analysis and in testing of isolators.
IBSBI 2011, October 13-15, Athens, Greece
Civil, Structural & Environmental Eng. , University at Buffalo

ON BELGRADE BRIDGES OVER THE SAVA RIVER

Nikola Hajdin

Serbian Academy of Sciences and Arts, Department of Technical Sciences, Serbia
e-mail: hajdin@eunet.rs, nikola.hajdin@sanu.ac.rs

ABSTRACT: The object of this presentation are bridges over the Sava River, their characteristics, position and level compared to the contemporary view bridges in Europe and the world at large of those times.

KEY WORDS: Bridge; Cable-stayed system

1 INTRODUCTION

King Alexander Bridge. This bridge was modern for the times in which it had been built, which were 1930'. The suspension bridge system as this one had been, was not as some think, conservative for those days because its technical level also enabled that system to exist in those times, i.e. the suspension bridge or the arch-shaped bridge with tie-beam of 260 m represented major progress in the bridge-building of Yugoslavia of those times.
What characterises this bridge and why it sets an important precedent for all the future bridges was a wise decision to construct it without pillars in the river, i.e. from one bank to the other.

Branko's bridge. As a result of the development of the theory, construction materials and construction technology time had come to achieve the 260 m span with one continuous girder.
We should immediately note that this had been the greatest span of a continuous girder in the world. This was well-known and important achievement in the bridge-building in regard to Belgrade.

Gazela. This bridge represents a final breakthrough of our designers and constructors when it comes to the Sava bridges in Belgrade. Already then, when this bridge was being constructed, our country had an extremely powerful high-ranking designer and execution capability. On the whole, the bridge provided proof of our country's high scientific and technological level of the times.

Railway Bridge. New, important step in bridge-building are cable stayed bridges, making a lasting impact on the construction of modern bridges. Designed and constructed at the pioneer days of this technology, it represents the first attempt in the world at using this system for railway traffic.

It was not only the first railway traffic bridge in this system, but at the same time, also carried the largest span (254 m) for railway traffic, in general.
The bridge has a number of interesting characteristics, both as regards the design and construction, such as the use of ballast for railway traffic on such a long span, etc.

New bridge across the Sava River. In order to reduce traffic congestion in Belgrade city and increase the capacity of the network, it is under construction new bridge across Sava River, passing over the lower tip of Ada Ciganlija Island. As a part of the future Inner City Semi-Ring Road, the Sava Bridge serves for the distribution of traffic flows between diametric peripheral city zones, and operationally connected to the city highway, it shall allow diversions of highway flows to the Inner City Semi-Ring Road and vice versa.
The Sava Bridge with its communications, shall contribute to the Belgrade look as a proper European metropolis. This is the largest bridge project currently under construction in Europe.

2 KING ALEXANDER BRIDGE

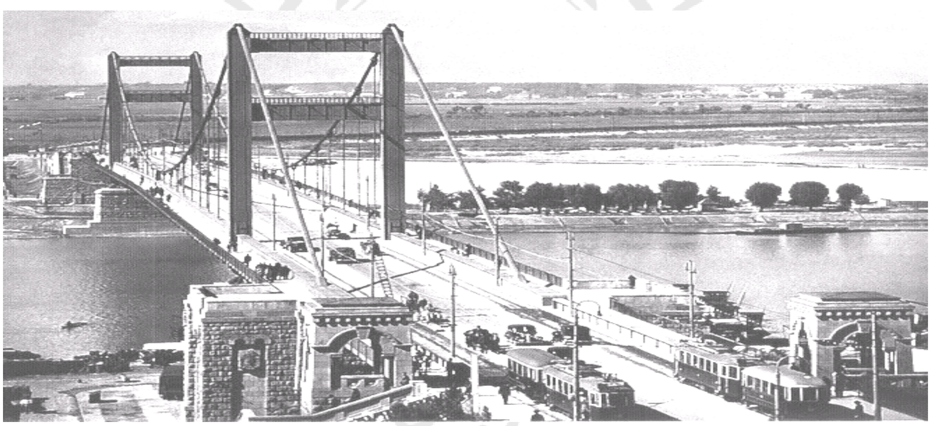

Photo 1. King Alexander Bridge

This bridge was modern for the times in which it had been built, i.e. 1930's. That type of suspension bridge system was not as some think conservative for those times, since the technical level of that age made this system possible, i.e. a suspension bridge or arch bridge with 260 m span, represented significant progress in the bridge-building of Yugoslavia of those times.

What is characteristic of this bridge and makes it an important precedent is a wise decision to build it without laying pillars in the river, i.e. from bank to bank. Having in mind the traffic on the Sava River in that part of Belgrade, this can be considered to constitute a visionary move that should apply to all bridges built after it. For greater part that was exactly the case.

Negative features of this bridge include a combination of a relatively modern steel construction with Byzantine-Serbian style support, which was obsolete already at that time. Bridges done in that period no longer had either “horses or riders nor saints and dragons”, but were clean constructions which expressed their construction strength.

3 THE BRANKO’S BRIDGE

Photo 2. The Branko’s Bridge

As a result of the development of the theory, construction materials and construction technology the moment was ripe so that it became possible to achieve the 260 m span with a continuous girder.

Allow us to observe right away that this had been the greatest span of a continuous girder in the world. This was a famous and significant accomplishment in the bridge-building when it comes to Belgrade.

Apart from that, the orthotropic deck, as a major achievement in the bridge-building technology, was then used for the first time in Yugoslavia.

At this time, an important novelty with regard to this bridge was the design and construction of steel girders with much larger number of the so called plates in the lower belt, which in itself partially made it possible such progress in the bridge building. It should be noted that at that time German regulations limited the number of plates and their thickness thus restricting larger spans.

Later on this bridge was reconstructed by the addition of another girder with closed cross-section, according to the design of engineer Dragojevic. This is an interesting example of two concepts set over ten years apart, used at the same place.

4 BRIDGE GAZELA

This bridge represents a final advancement of our designers and constructors with regard to the Sava bridges in Belgrade. Already in those days, when this bridge was being constructed, our country ranked very high with its extremely powerful designer and execution capability, which was quite strange when compared to our country's other technology branches and development.

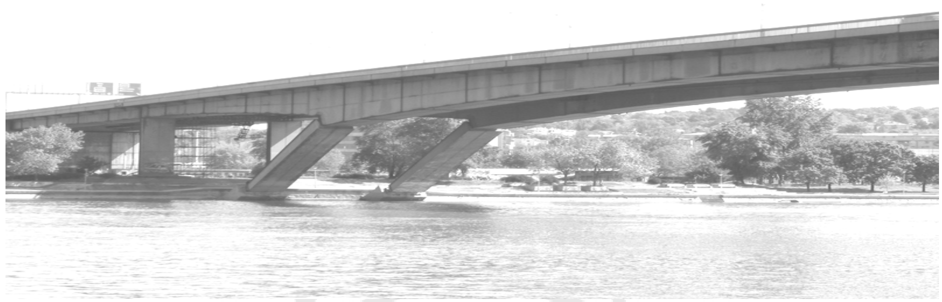

Photo 3. Bridge Gazela

This bridge of Professor Djuric represents an original solution, which, instead of the arch that would visually greatly burden the surroundings, was adopted with a shallow configuration strut. It was so reliably designed and constructed that it has been in service for over 40 years without any repairs, carrying the traffic that is three times larger in volume from the one for which it had been originally designed.

All in all, the bridge provided proof of the high level of our science and technology of those times.

5 RAILWAY BRIDGE

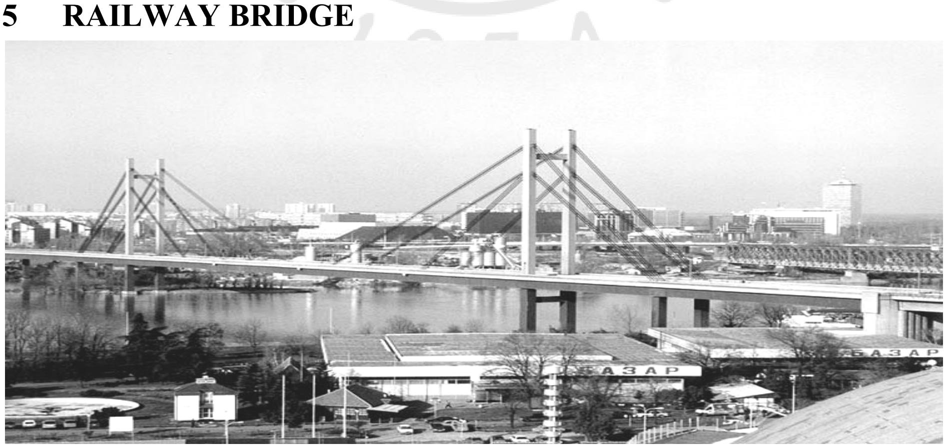

Photo 4. Railway Bridge

New, important step in bridge-building was the appearance of cable-stayed bridges that made a long-term influence on the construction of modern bridges. Designed and constructed at the pioneer days of this technology, it represents the first attempt in the world at using this system for railway traffic. It was not only the first railway traffic bridge in this system, but at the same time, also the largest span (254 m) for railway traffic, in general.

The bridge had a number of new features for those times, such as high-strength wire cables in polyethylene pipes, which were applied here for the first time in Europe.

The bridge has a whole series of interesting qualities as regards design, as well as construction, such as the use of ballast for railway traffic on such a large span and similar.

What is characteristic for all these bridges is the fact that despite retrograde trends, this community was able to achieve a progress which does credit to both Belgrade and Serbia.

This bridge represent an important achievement in the sense that is has have no pillars in the river, which had become rule for all the possible future bridges on the River Sava.

The Gazela and the Railway Bridge are altogether a product of our intellect, both in designing and construction. Unfortunately, 1900's meant a major fall that brought us into a situation in which we can build large bridges only with foreign assistance, primarily financial, as well as professional. We hope that this period will soon be behind us and that we will start creating our own bridge future in the years to come.

6 NEW BELGRADE BRIDGE ACROSS SAVA RIVER IN THE SCOPE OF THE INNER SEMI-RING ROAD

Photo 5. New bridge across the Sava River (preliminary design)

Almost three decades have passed since the times of the first bridges with cable-stayed system in our country. This construction fully reflects the technological advance.

The Bridge has a continuous deck over entire length of 967 m, supported by 6 piers. The main bridge part is an asymmetric cable-stayed structure, with a steel main span of 376 m and a concrete back span of 200 m, elastically supported, each by 20 pairs of cable stays that are anchored in one pylon (concrete).

The cable-stayed bridge (376+200m) is prolonged in a continuous beam structure by 338m length side spans (70+108+80+80m) and 50 m end span. The unique single pylon in the form of sharp cone is 200 m high. The stays of fan-type configuration are in two quasi-middle planes.

The bridge deck, having width of 45 m, carries 2x3 lanes of vehicular traffic, 2 rail tracks of LRT and 2 lanes of pedestrian / cycle way. The aesthetics plays a major role in bridge design. The Bridge is the largest bridge currently under construction in Europe.

The general design, with the previous feasibility study of Inner City Semi-Ring Road, was made in 2003. The international competition for concept design proposal was lounched in 2004 by client - City of Belgrade i.e. Belgrade Land Development Public Agency.

The awarded concept designer Ponting Maribor (with DDC Ljubljana & CPV Novi Sad) finalized preliminary design in 2006.

As the overall bridge deck is integral structure with pylon, the expansion joints are placed only at the bridge ends, i.e. at pier axis 1 and 8.

The cable system is VT BBR HiAm CONA type, with bundle of galvanized mono-strands (41 to 88).

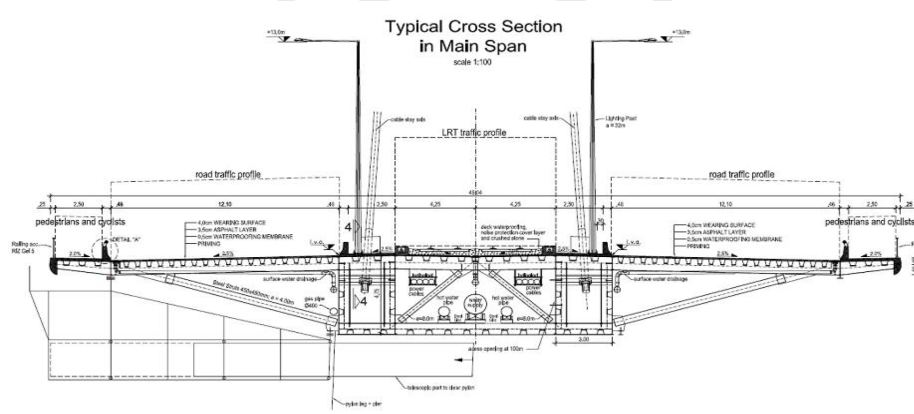

Figure 1. Bridge cross-section in main span (steel deck) – final design

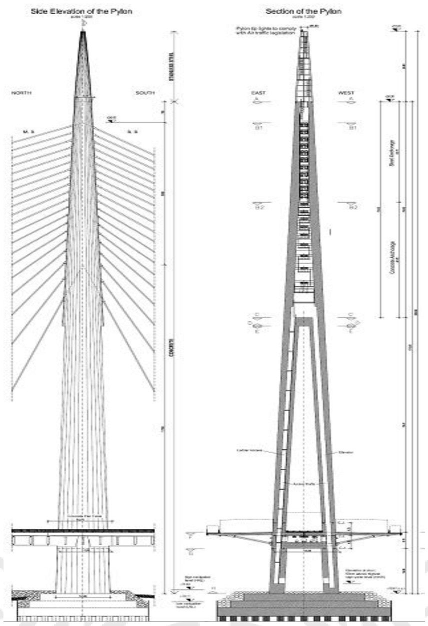

Figure 2. Pylon – final design

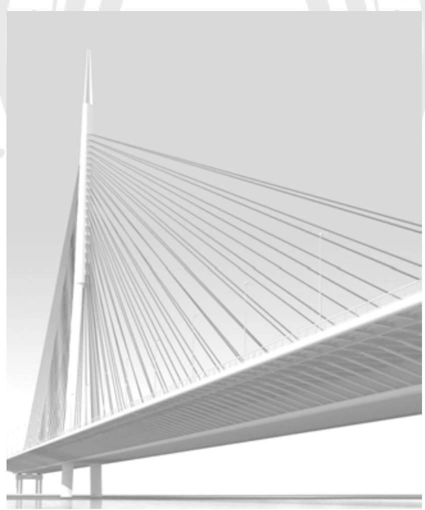

*Photo 6***.** Photo visualization from water table

7 CONCLUSIONS

The paper gives a general review of the bridges over the Sava river in Belgrade. It shows the major tendency in the design and construction in the long period of about 80 years. All bridges described in this paper represent a progress in bridge design and construction not only in Belgrade but also the main tendency in Europe.

The special attention is given to the cable stayed bridges showing the development of this technology in the last 40 years.

REFERENCES

[1] Hajdin N, „Vergleich zwischen den Paralleldrahsteilen und Vershlossenen Seilen am Beispiel der Eisenbahnschrägseilbrücke über die Save in Belgrad“, *Dixième congrès de l'Association internationale des ponts et charpentes*, September 6-11, 1976, Tokyo, rapport préliminaire, Zürich : Secrétariat de l' AIPC, 1976. p. 471-475.

[2] Hajdin N, Jevtović Lj, Cvetković S, Matić V, “Novi železnički most preko Save u Beogradu”- “New Railway Bridge over Sava River in Belgrade, *VI kongres Jugoslovenskog društva građevinskih konstruktora*, Bled 26-29. 9. 1978. Beograd : JDGK, 1978. Knj. Mostovi-M, str. 81-100. M 9

[3] Hajdin N, Jevtović Lj, Cvetković S, Matić V, The Railway Cable-stayed Bridge over River Sava in Belgrade IABSE Periodica 4 (1979): IABSE Structures C - 10 /79 - Bridges I. p. 30.

[4] Hajdin N, Stipanic B, “Project of New Roadway Bridge across Sava River in Belgrade”, *Proceedings of 6th International Conference on Bridges across the Danube - Bridges in Danube Basin*, Muegyetmi Kiado Budapest, 2007.

[5] Stipanic B, Hajdin N, “On Belgrade bridges on the Sava River”, *7th International Conference on Bridges across the Danube 2010* – “Theory and Practice in Bridge Engineering”, Sofia, Bulgaria, October 14-15.2010.

EFFECTIVENESS OF POLYPROPYLENE FIBER REINFORCED CEMENT COMPOSITES FOR ENHANCING THE SEISMIC PERFORMANCE OF BRIDGE COLUMNS

K. Kawashima[1] , R. Zafra[2], T. Sasaki[3], K. Kajiwara[4], M. Nakayama[5]

[1,2] Department of Civil Engineering, Tokyo Institute of Technology, O-okayama, Meguro, Tokyo, Japan
[3,4,5] Hyogo Earthquake Engineering Research Center, National Research Institute for Earth Science and Disaster Prevention, Miki, Hyogo, Japan

ABSTRACT: This study investigates the effect of polypropylene fiber reinforced cement composites (PFRC) for enhancing the damage control and ductility capacity of a 7.5 m tall, 1.8 m by 1.8 m square bridge column subjected to 80% of the original intensity of the near-field ground motion recorded at the JR Takatori station during the 1995 Kobe, Japan earthquake using the E-Defense shake table. PFRC is a mixture of cement mortar and short discontinuous polypropylene fibers. Compared to the brittle failure of concrete in tension, PFRC exhibits ductile failure due to the formation of closely spaced micro cracks and the bridging action of fibers. The use of PFRC at the plastic hinge region mitigated cover and core concrete damage, local buckling of longitudinal bars and deformation of ties even after six times of repeated excitation. The damage sustained was much less than the normal damage of regular reinforced concrete columns.

1 INTRODUCTION

A large scale bridge experimental program was conducted in 2007-2010 by the National Research Institute for Earth Science and Disaster Prevention (NIED), Japan (Nakashima et al. 2008). In the program, shake table experiments were conducted for two typical reinforced concrete columns which failed during the 1995 Kobe, Japan earthquake (C1-1 and C1-2 experiments), a typical reinforced concrete column designed in accordance with the 2002 Japan design code (JRA 2002) (C1-5 experiment) and a new generation column using polypropylene fiber reinforced cement composites for enhancing the damage control and ductility (C1-6 experiment). The experiments were conducted using the E-Defense shake table where the table is 20 m by 15 m and has a payload of 1200 tf (12 MN). The maximum stroke of the table is 1 m and 0.5 m in the lateral and vertical directions, respectively. It was designed so that the ground motions during the 1995 Kobe earthquake can be generated.

C1-5 experiment was conducted using the E-Defense shake table with a ground motion 80% of the original intensity of the near-field ground motion recorded at the JR Takatori station during the 1995 Kobe earthquake. This is referred herein as the E-Takatori ground motion. The column performed satisfactorily under this ground motion. However, when the excitations were repeated under much stronger intensity and longer duration near-field ground motion, the column suffered extensive damage with blocks of crushed core concrete spilling out like explosion from the steel cage (Kawashima et al. 2010). Such failure was never seen in past quasi-static cyclic or hybrid loading experiments. Therefore, it is expected to develop columns which contribute to construct damage free bridges using materials that mitigate such damage under severe seismic loading.

Prior to the C1-6 experiment, a series of cyclic loading experiments were conducted on 1.68 m high, 0.4 m by 0.4 m square cantilever regular high strength concrete column and a column each using steel fiber reinforced concrete and polypropylene fiber reinforced cement composite at the plastic hinge region and the footing for deciding the material of C1-6 column (Kawashima et al. 2011). The polypropylene fiber reinforced cement composite column had superior performance in mitigating cover and core concrete damage, longitudinal bar buckling and deformation of tie bars at the plastic hinge region resulting from the crack control capability of polypropylene fiber reinforced cement composite. As a result, C1-6 column was built using polypropylene fiber reinforced cement composite at the plastic hinge region and a part of the footing.

High performance fiber reinforced cement composites (HPFRCC) are materials that exhibit multiple fine cracks upon loading in tension which leads to improvement in toughness, fatigue resistance and deformation capacity (Matsumoto & Mihashi 2002). Engineered cementitious composites (ECC) is an HPRCC that has tensile strain capacity of about 0.03 to 0.05 resulting from the formation of closely spaced micro cracks due to the bridging action of fibers (Li & Leung, 1992). It has low elastic stiffness compared to concrete, and larger strain at peak compressive strength, due to the absence of course aggregates (Li et al. 1995). Polypropylene fiber reinforced cement composites, referred herein as PFRC, belongs to the class of ECC.

Previous investigations have shown the positive effects of using HPFRCC for structural members subjected to seismic loads. Kosa et al. (2007) examined the use of this material with polyvynil alcohol (PVA) fibers for the seismic strengthening of scaled bridge piers similar to concrete jacketing. They found that a pier using PVA-HPFRCC on the cover concrete can provide confinement effect as much as the pier whose entire cross section was constructed of this material. Furthermore, the deformation capacity and the energy absorption capacity were also significantly improved compared with a pier constructed of ordinary concrete.

Saiidi et al. (2009) investigated the effect of incorporating ECC with polyvynil alcohol (PVA) fibers and shape-memory alloys (SMA) on model columns subjected to cyclic loading. Use of PVA-ECC substantially reduced damage in the plastic hinge. Furthermore, the combination of PVA-ECC and SMA led to larger drift capacity compared to the conventional steel reinforced concrete column.

This study aims to investigate the effectiveness of PFRC for enhancing the damage control and ductility capacity of a full-size bridge column subjected to a strong near-field ground motion using the E-Defense shake table. This column is called herein as C1-6 column. The information obtained from the shake table experiments can provide reliable data for verification of structure performance and can provide an insight on the response of such structures subjected to real earthquake conditions.

2 E-DEFENSE SHAKE-TABLE EXCITATIONS

2.1 Column configuration and properties

C1-6 column is a 7.5 m tall, 1.8 m by 1.8 m square, cantilever column shown in Figure 1. It was designed based on the 2002 Japan design code assuming moderate soil condition under the Type II design ground motion (near-field ground motion). PFRC was used at a part of the footing with a depth of 0.60 m below the column base and a depth of 2.7 m above the column base to minimize the cost. The 2.7 m depth of PFRC is three times the code specified plastic hinge length of one-half the column width (0.90 m). This height was set to avoid failure at the PFRC-concrete interface. The 0.60 m depth of PFRC at the footing was provided to minimize damage. Regular concrete with design compressive strength of 30 MPa was used in the other parts of the column. The actual 28-day cylinder compressive strength of concrete was 41 MPa.

The design compressive strength of PFRC was 40 MPa. PFRC was made by combining cement mortar, fine aggregates with maximum grain size of 0.30 mm, water and 3% volume of polypropylene fibers. Monofilament polypropylene fibers with diameter of 42.6 μm, length of 12 mm, tensile strength of 482 MPa, Young's modulus of 5 GPa and density of 0.91 kg/m^3 were used (Hirata et al. 2009). Superplasticizers were added to improve the workability of the mix. The actual 28-day cylinder compressive strength of PFRC was 36 MPa with a strain at peak of 0.47%.

Eighty-35 mm diameter deformed longitudinal bars were provided in two layers. The corresponding reinforcement ratio ρ_l was 2.47%. The nominal yield strength of longitudinal bars was 345 MPa (SD345) and the actual yield strength was 386 MPa at 0.2% strain. Deformed 22 mm diameter ties with 135 degree bent hooks lap-spliced with 40 times the bar diameter were provided. The outer ties were spaced at 150 mm and the inner ties were spaced at 300 mm throughout the column height. Cross-ties with 180 degree hooks at 150 mm spacing were provided as shown in Figure 1 to increase confinement of the square ties. Volumetric tie reinforcement ratio ρ_s within a height of 2.7 m from the column base was 1.72%. The nominal yield strength of ties was 345 MPa (SD345) and the actual yield strength was 396 MPa at 0.2% strain. Concrete cover of 150 mm was provided.

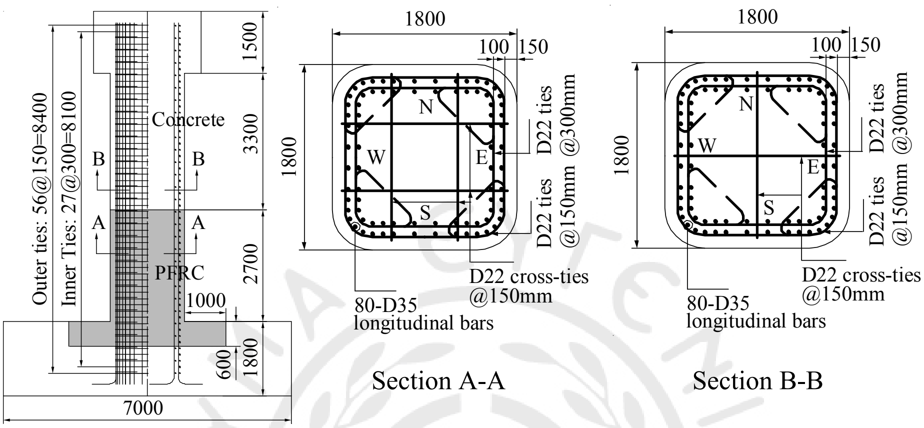

Figure 1. C1-6 column configuration and dimensions (mm)

2.2 Experiment set-up and shake-table excitations

Photo 1 shows the experiment set-up using the E-Defense shake table. Four mass blocks were set on the column through two simply supported decks. Note that the decks were not designed to idealize the stiffness and strength of real decks. Each deck was supported by the column on one side and by the steel end support on the other side. Tributary mass to the column by two decks including four weights was 307 tf (3011 kN) and 215 tf (2109 kN) in the longitudinal and transverse directions, respectively. The column was excited using the E-Takatori ground motion with the EW, NS and UD components, shown in Figure 2, applied in the longitudinal, transverse and vertical directions of the column, respectively. This ground motion is referred herein as the 100% E-Takatori ground motion.

Shake table excitations were conducted six times. Excitations were repeated to clarify column performance when subjected to much stronger and longer duration near-field ground motion. The column was excited twice with 100% E-Takatori ground motion (1-100%(1) and 1-100%(2) excitations). After the mass in the longitudinal direction was increased by 21% from 307 tf (3011 kN) to 372 tf (3649 kN), excitations were conducted with 100% E-Takatori ground motion once (2-100% excitation) and 125% E-Takatori ground motion three times (2-125%(1), 2-125%(2) and 2-125%(3) excitations).

Photo 1. Experiment set-up using E-Defense shake table

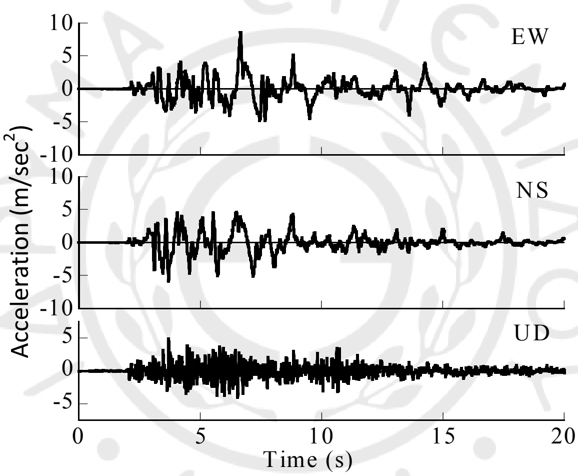

Figure 2. E-Takatori ground motion

3 EFFECT OF POLYPROPYLENE FIBER REINFORCED CEMENT COMPOSITE ON COLUMN SEISMIC PERFORMANCE

3.1 Progress of failure

Photos 2 to 4 show the damage progress within 1.2 m from the column base at the SW and NE corner during 1-100%(1), 2-100% and 2-125%(3) excitations at the instance of peak response displacement where the SW corner was subjected to compression while the NE corner was subjected to tension. As shown in Photo 2, during 1-100%(1) excitation, only micro cracks were observed around the column. During 1-100%(2) excitation, very thin flexural cracks as wide as 0.1 - 0.2 mm occurred within 1.6 m from the base all around the column.

During 2-100% excitation, with the mass increased by 21%, damage progressed as shown in Photo 3. Flexural cracks propagated and a crack 0.6 m from the column base at the NE corner opened about 8 mm at the peak response displacement. After the excitation, the maximum residual crack at the above location was 1 - 2 mm wide. Although only flexural cracks occurred all around the column with the cover concrete remaining as a whole shell due to the bridging action of fibers, vertical hairline cracks started to occur at the NE and SW corners within 0.6 m from the column base due to the large strut action of cover concrete shell resulting from the footing reaction when the column was laterally displaced.

During 2-125%(1) excitation, in which the seismic excitation intensity was increased by 25%, at the peak response displacement, the crack 0.6 m from the base opened to 14 mm at the NE corner which was subjected to tension while a vertical crack opened to 9 mm at the opposite SW corner subjected to compression. As the loading progressed, at the SW corner subjected to tension, a crack 1.2 m from the base opened to 9 mm and vertical cracks started to widen at the opposite NE corner.

Succeeding excitations resulted to further propagation of flexural cracks within 2 m from the base around the column and the widening of the vertical crack at the SW corner. As shown in Photo 4, the damage progressed during 2-125%(3) excitation wherein at the peak response displacement, the crack 0.6 m from the base at the NE corner opened to 20 mm and the vertical crack at the SW corner opened to 15 mm. Note that at the NW corner, cover concrete spalled within 200 mm from the column base when it was subjected to compression while flexural cracks opened to 13 mm at the opposite SE corner subjected to tension. After the excitation, the cracks which opened to over 10 mm during the excitation almost closed with widths of only 5 - 8 mm in flexural cracks and 7 - 12 mm in vertical cracks. Moreover, majority of other small cracks closed to hairline cracks after the excitations due to the fiber bridging action of fibers. Cover concrete spalling was much restricted and there were no exposed longitudinal bars and ties in C1-6 column after 2-125%(3) excitation.

To investigate how the damage progressed in the core and in the longitudinal bars at the NE corner after 2-125%(3) excitation, the column was opened at the area shown in Photo 5. Note that removal of cover concrete in the fiber mixed concrete was very difficult because of its solid nature compared to that of regular reinforced concrete.

In Photo 5, only the outer and inner longitudinal bars and inner ties can be seen because outer ties and a part of the PFRC cover concrete were removed. Maximum lateral offset among three outer longitudinal bars from their original vertical axis was 8 mm. On the other hand, the inner longitudinal bars did not buckle because they were constrained by the undamaged concrete between the outer and inner longitudinal bars. At the SW corner which was subjected to the largest compression during the peak response displacement, the maximum lateral offset of the outer longitudinal bars due to local buckling was 5 mm which was much less than the buckling of bars at the NE corner. In general, local bar buckling was limited.

(a) SW corner (b) NE corner

Photo 2. Column damage during 1-100%(1) excitation

(a) SW corner (b) NE corner

Photo 3. Column damage during 2-100% excitation

(a) SW corner (b) NE corner

Photo 4. Column damage during 2-125%(3) excitation

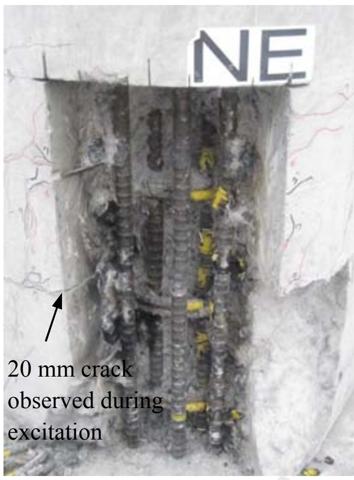

(a) Opened section at NE corner

(b) Longitudinal bar buckling

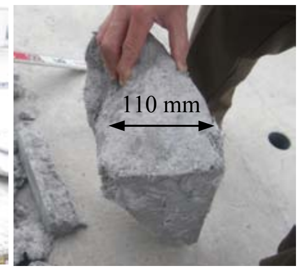

(c) PFRC cover concrete block

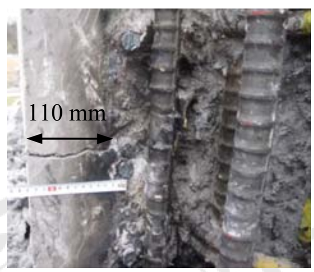

(d) Crack on PFRC cover concrete

Photo 5. Damage of PFRC cover concrete and buckling of longitudinal bars at the NE corner after 2-125%(3) excitation

At the location where crack opening of 20 mm was observed, it was found that the crack occurred only in the PFRC cover concrete with a depth of 110 mm and did not propagate into the core concrete. Also shown is the block of cover concrete that was removed at the bottom right portion where the presence of fibers held the cover concrete together preventing the disintegration of cover concrete. Hence, it is worthy to note that even after six times of excitation, the damage sustained by C1-6 column was much less than the damage of regular reinforced concrete columns.

3.2 Response acceleration and displacement

The principal response angle θ_P is defined to identify the principal response direction when the maximum column response displacement occurs. It is given by

$$\theta_P = \tan^{-1}\left(\frac{u_{TR}}{u_{LG}}\right) \tag{1}$$

where u_{LG} and u_{TR} are the response displacements in the longitudinal and transverse directions, respectively.

Figure 3 shows the acceleration and displacement at the top of column in the principal response direction and Table 1 summarizes the peak acceleration, displacement, residual displacement and moment at each excitation. The principal response angle θ_P varied from 194 to 205 degrees during the six excitations which was almost at the NE-SW direction. The measured peak response acceleration during the series of excitations varied from 13-20 m/s^2.

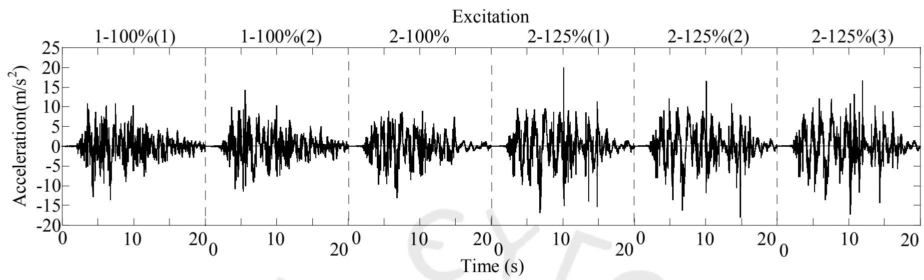

(a) Response acceleration

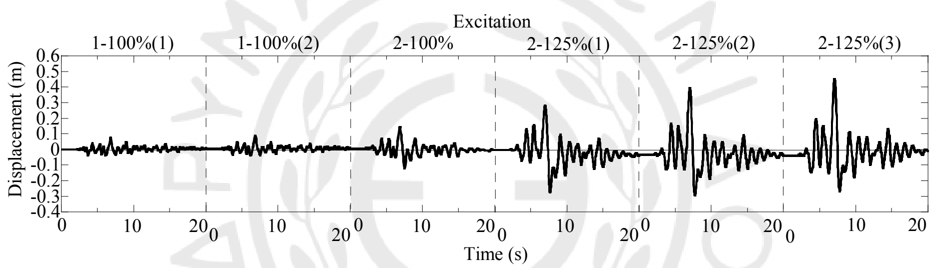

(b) Response displacement

Figure 3. Column response acceleration and displacement in the principal direction

Due to the high acceleration pulse in the input ground motion, the column experienced high amplitude displacement during each excitation. The peak response displacement was equal to 0.078 m (1% drift) during 1-100%(1) excitation and increased to 0.45 m (6% drift) during 2-125%(3) excitation. As the excitation progressed with increasing intensity of ground motion, the response displacements increased due to column stiffness deterioration resulting from the damage. The residual displacement was only -0.004 m (0.05% drift) after 2-100% excitation, increased to -0.037 m (0.49% drift) after 2-125%(2) excitation then decreased to -0.013 m (0.13% drift) after the last excitation. Since the allowable residual drift for a cantilever column based on the 2002 JRA code is 1%, the residual drift of the column was still smaller than the allowable limit. It is important to note that residual displacement not only increases but also decreases during seismic excitations because it is more affected by the ratio of post elastic stiffness to elastic stiffness as well as the instantaneous structure period (MacRae & Kawashima 1997).

Table 1. Column response in the principal direction

Excitation	θ_P (Degrees)	$\ddot{u}_P$ (m/s^2)	u_P (m)	u_P Drift (%)	Residual displacement (m)	M_P (MNm)
1-100%(1)	201.9	-13.4	0.078	1.0	0.005	20.5
1-100%(2)	193.5	14.2	0.089	1.2	0.007	21.8
2-100%	196.0	-13.0	0.144	1.9	-0.004	24.0
2-125%(1)	201.1	19.9	0.280	3.7	-0.035	24.3
2-125%(2)	204.8	-17.9	0.392	5.2	-0.037	25.3
2-125%(3)	204.6	-17.1	0.450	6.0	-0.013	24.9

3.3 Moment and ductility capacity

The bending moment at the column base was evaluated as

$$M_k = M_{Bk} + M_{Ck} \tag{2}$$

where M_{Bk} and M_{Ck} represent the moment based on measured load cell forces and based on pier and column mass accelerations, respectively, and are given by

$$M_{Bk} = \sum_{i=1}^{N} \{F_{Lki} h_{Li} - V_{Li}(x_{ki} + u_k)\} \tag{3}$$

$$M_{Ck} = \int_0^{h_B} m_C \ddot{u}_{Ck} dz + \int_{h_B}^{h} m_B \ddot{u}_{Bk} dz \tag{4}$$

where F_{Lki} is the inertia force measured by the i-th load cell in the k direction ($k =$ LG and TR corresponding to the longitudinal and transverse directions, respectively); V_{Li} is the vertical force measured by the i-th load cell in the k direction; h_{Li} is the height from the base to the i-th load cell; x_{ki} is the load cell coordinate in the k direction from the column center; u_k is the response displacement at top of column in the k direction; N is the load cell number ($N = 32$); z is the coordinate of the column from the base upward; m_C and m_B are the mass per unit length of the column and pier cap, respectively; $\ddot{u}_{Ck}$ is the column acceleration response; $\ddot{u}_{Bk}$ is the pier cap acceleration response; h_B is the height from base to the bottom of the pier cap and h is the height from base to the top of pier cap.

Figure 4 shows the hysteresis of moment at the base vs. displacement at the top of the column in the principal response direction. The hysteresis during the entire six times of excitation is stable with sufficient energy dissipation. As summarized in Table 1, the peak moment gradually increased as the excitation progressed. A maximum capacity of 25.3 MNm at 5.2% drift was developed during 2-125%(2) excitation. During this excitation, flexural cracks further propagated all around the column and the vertical cracks at the SW corner widened as described in 3.1. During the subsequent 2-125%(3) excitation, the peak drift increased to 6% while the peak moment slightly deteriorated by 2%. It should be noted that even during the 2-125%(3) excitation, the moment vs. lateral displacement hysteresis was still very stable.

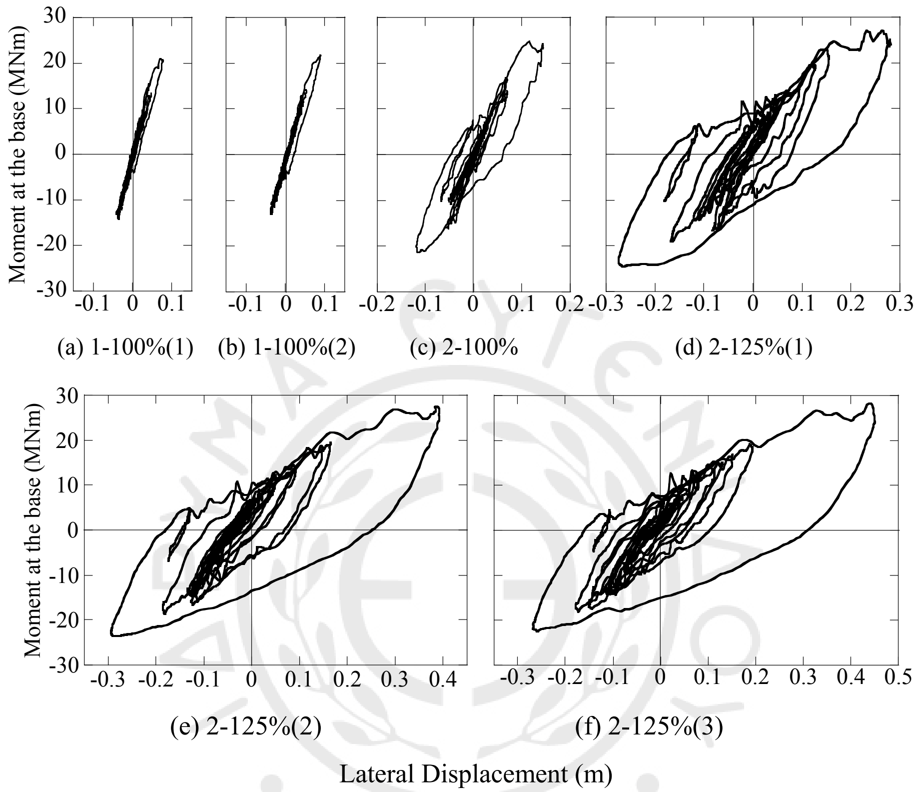

Figure 4. Hysteresis of moment at the base vs. displacement at the top of column in the principal direction

3.4 Strains of longitudinal and tie bars

Figure 5 shows strains of longitudinal and tie bars of C1-6 column at the plastic hinge zone (300-400 mm from the base) at the SW corner where the most extensive damage occurred. Only strains during 1-100%(1), 2-100%, 2-125%(1) and 2-125%(3) excitations are shown due to space limitation. Because longitudinal bars were set in two layers, strains of both the outer and inner longitudinal bars and tie bars are shown here. Noting that the yield strain of both longitudinal and tie bars was nearly 2,000 μ , the longitudinal bars started to yield in tension during 1-100%(1) while tie bars started to yield in tension during 2-125%(1) excitation. The outer and inner longitudinal bars and tie bars exhibited similar response however the amplitude of strains were generally larger in the outer longitudinal and tie bars than the respective inner longitudinal and tie bars. The difference of strain amplitude between outer and inner tie bars is particularly large during and after 2-125%(1) excitation resulting from local buckling of longitudinal bars, which will be described later.

An interesting point in Figure 5 is that the compression strains of the outer and inner longitudinal bars were nearly the same with tension strains during the early excitations. For example, the compression strain of the outer longitudinal bar was 1,800 μ while the tension strain was 1,400 μ during 1-100%(1) excitation. This obviously resulted from the low elastic modulus of PFRC. Resulting from further softening and failure of core concrete, the compression strains of the outer and inner longitudinal bars progressed during 2-125%(1) excitation. Thus, compression strain of the outer longitudinal bar reached 19,000 μ while tension strain reached 18,000 μ during 2-125%(1) excitation. The large compression strain must have caused the outer longitudinal bar to buckle. Note however that in spite of the bar buckling as described in 3.1, spalling of cover concrete did not occur indicating that the presence of fibers made the cover concrete remain as a whole shell.

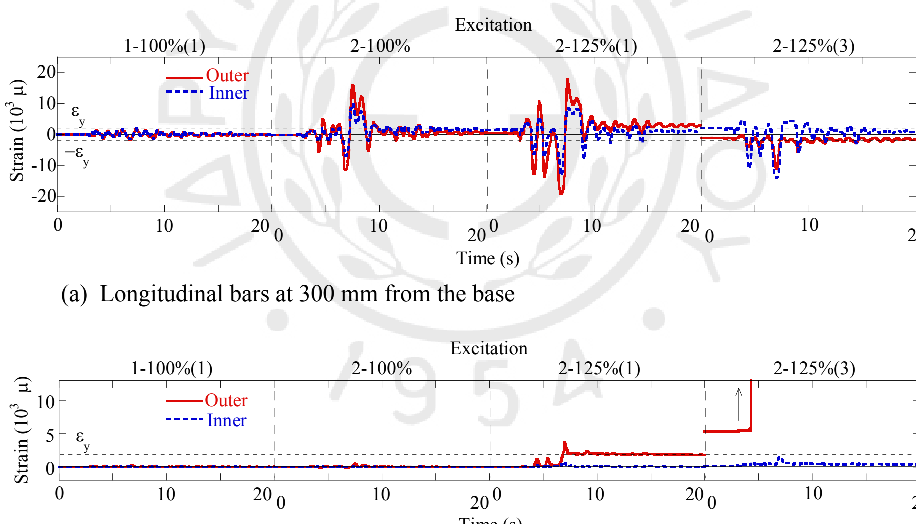

Figure 5. Strains of longitudinal bars and tie bars at the SW corner during 1-100%(1), 2-100%, 2-125%(1) and 2-125%(3) excitations

On the other hand, the tie bar was still elastic during 1-100%(1) until 2-100% excitations. At the instance when compression strain of the outer longitudinal bar sharply increased during 2-125%(1) excitation, the outer tie strain started to increase to 3,700 μ, indicating that the tie resisted the longitudinal bar buckling. Compression strain of the inner longitudinal bar also sharply increased at the same time, however, the inner tie strain did not increase indicating that the inner longitudinal bar did not buckle. This was because confinement for bar buckling was larger at the inner longitudinal bar than the outer longitudinal bar due to the resistance of core concrete between outer and inner ties which was still intact as shown in Photo 5.

Figure 6 further shows the interaction of a longitudinal bar with a tie bar for outer and inner bars. The tie strains during 2-125%(3) excitation were larger than 5,000 μ and only reliable data are shown here. A sharp increase of the outer tie strain resulting from restraining local buckling of the outer longitudinal bar under high compression strain is clearly seen during and after 2-125%(1) excitation while the inner tie strain remained below 2,000 μ because inner longitudinal bars did not yet buckle.

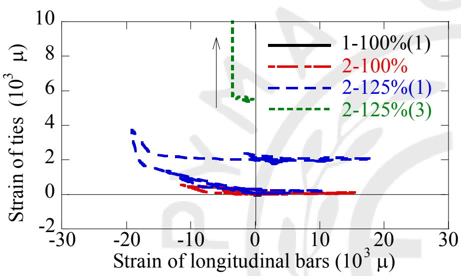

(a) Outer bars

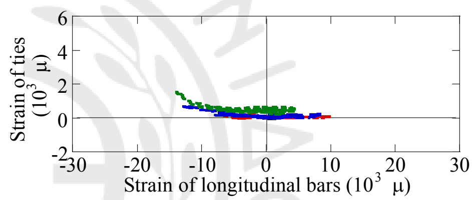

(b) Inner bars

Figure 6. Strain of a tie at 400 mm from the base vs. strain of a longitudinal bar at 300 mm from the base at the SW corner of C1-6 column

4 CONCLUSIONS

A series of shake table experiments of a full-size bridge column using polypropylene fiber reinforced cement composites (PFRC) at the potential plastic hinge and part of the footing, referred herein as C1-6 column, were conducted. Based on the results presented, the following conclusions were deduced:

1. PFRC did not have the brittle compression failure of regular reinforced concrete under repeated large inelastic deformation due to the bridging mechanism of fibers. This prevented the brittle crushing of cover and core concrete.
2. As a consequence of a), the use of PFRC reduced buckling of longitudinal bars and deformation of tie bars thus mitigating the damage of C1-6 column even after six times of strong excitations.
3. As a result of the damage mitigation properties of PFRC, the column had a stable flexural capacity and enhanced ductility reaching until 6% drift.

REFERENCES

[1] Japan Road Association 2002. *Specifications for Highway Bridges*. Maruzen: Tokyo.

[2] Hirata, T., Kawanishi, T., Okano, M. & Watanabe, S. 2009. Study on material properties and structural performance of high-performance cement composites using polypropylene fiber. *Proc. Japan Concrete Institute* 31(1): 295-300.

[3] Kawashima, K., Sasaki, T., Ukon, H., Kajiwara, K., Unjoh, S., Sakai, J., Kosa, K., Takahashi, Y., Yabe, M. & Matsuzaki, H. 2010. Evaluation of seismic performance of a circular reinforced concrete bridge column designed in accordance with the current design code based on e-defense excitation. *Journal of Japan Society of Civil Engineers* 65(2): 324-343.

[4] Kawashima, K., Zafra, R., Sasaki, T., Kajiwara, K. & Nakayama, M. 2011. Effect of polypropylene fiber reinforced cement composite and steel fiber reinforced concrete for enhancing the seismic performance of bridge columns. *Journal of Earthquake Engineering* (accepted for publication).

[5] Kosa, K., Wakita, K., Goda, H. & Ogawa, A. 2007. Seismic strengthening of piers with partial use of high ductility cement. In C. U. Grosse (ed.), *Advances in construction materials*: 269-277. Springer: Berlin Heidelberg.

[6] Li, V. & Leung, C. 1992. Steady-state and multiple cracking of short random fiber composites. *Journal of Engineering Mechanics*, *ASCE* 118(11): 2246-2264.

[7] Li, V., Mishra, D. & Wu, H. 1995. Matrix design for pseudo-strain-hardening fibre reinforced cementitious composites. *Materials and Structures* 28: 586-595.

[8] MacRae, G. & Kawashima, K. 1997. Post-earthquake residual displacements of bilinear oscillators. *Earthquake Engineering and Structural Dynamics* 26: 701-716.

[9] Matsumoto, T. & Mihashi, H. 2002. JCI-DFRCC summary report on dfrcc terminologies and application concepts *JCI International Workshop on Ductile Fiber Reinforced Cementitious Composites – Application and Evaluation*. Takayama: Japan.

[10] Nakashima, M., Kawashima, K., Ukon, H. & Kajiwara, K. 2008. Shake table experimental project on the seismic performance of bridges using E-Defense. *14th World Conference on Earthquake Engineering*. Paper S17-02-010 (CD-ROM). Beijing: China.

[11] Saiidi, M., O'Brien, M. & Sadrossadat-Zadeh, M. 2009. Cyclic response of concrete bridge columns using superelastic nitinol and bendable concrete. *ACI Structural Journal* 106(1): 69-77.

IBSBI 2011, October 13-15, 2011, Athens, Greece

WIND INDUCED CABLE VIBRATION
OF RION ANTIRION BRIDGE "CHARILAOS TRIKOUPIS"

Panagiotis Papanikolas[1], Aris Stathopoulos-Vlamis[2], Akis Panagis[3], Gerard Grillaud[4] and Olivier Flamand[5]

[1,2,3] GEFYRA S.A. – Concession Company for the Rion-Antirion Bridge, Greece
[4,5] Centre Scientifique et Technique du Batiment (CSTB), France
e-mail: ppapanikolas@gefyra.gr, gsastructural@gefyralitourgia.gr, panagis.akis@gmail.com, gerard.grillaud@cstb.fr, olivier.flamand@cstb.fr

ABSTRACT: The wind induced cable vibration was thoroughly investigated during design in order to provide suitable alleviation measures. The structural response analysis, as recorded by the monitoring system, concluded to the most appropriate technical improvement. Dampers installation improved the response of the stays, as indicated by commissioning tests and actual recordings.

KEY WORDS: External dampers; Intrinsic Structural Damping; Rion Antirion Bridge; Stay Cable Vibrations; Structural Health Monitoring.

1 INTRODUCTION

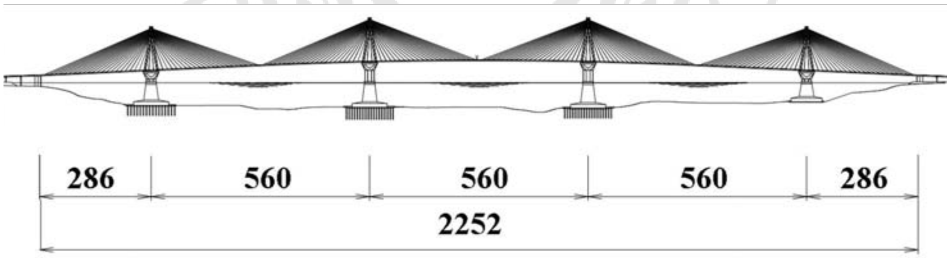

Figure 1. Rion Antirion Bridge elevation

Rion Antirion "Charilaos Trikoupis" bridge is a 5 span cable-stayed bridge joining Continental Greece with Peloponnese. The continuous composite deck has total length of 2252 m with three main spans of 560 m and side spans of 286 m. It is suspended by 4 concrete pylons with total height of 189 up to 227 m through 368 cables with total length from 79 up to 295 m. At each far end of the deck, a steel rotating frame (RF) supports the structure allowing longitudinal movement that is accommodated by special designed expansion joint. Furthermore, at pylon and RF location, the deck is transversally restrained through a fusing steel element that releases the deck when the transverse load, on each element, exceeds ±10.500/±3.400 kN (pylon/abutment). Their capacity is based on wind ultimate design loads. In case of moderate/strong earthquakes, the deck is released and the induced energy is dissipated through viscous dampers located close to fuse elements.

The detailed design of the superstructure against wind induced vibration was very important in order to anticipate possible aerodynamic phenomena that could lead to instability of both deck and cables. Especially, the design of cables where aerodynamic problems can occur due to the very low intrinsic structural damping resulting from high tension, which is a common feature of cable stayed bridges. The theoretical studies needed to be complemented by actual measurements and observations (especially the first years of operation) that were provided by the Structural Health Monitoring system and visual inspections respectively. The analysis of actual strong wind events gave significant insight of structural behaviour allowing a better assessment of the possible risk that had to be compensated.

2 CABLE DESIGN AGAINST WIND INDUCED VIBRATION

Rion Antirion Bridge includes a large number of different cable stays. Basic dynamic properties are presented for 4 characteristic cables. The effects of various aerodynamic phenomena on the cable response as well as the necessary actions that need to be taken for mitigation of expected vibration are reviewed.

2.1 Cable dynamics

The modes in the horizontal (transverse) plane are sinusoidal with frequency related to the tension load T, the linear mass m and length L according to the approximate classical Eq.(1), [1]:

$$n_k = \frac{k}{2L}\sqrt{\frac{T}{m}} \tag{1}$$

Due to sag effect, the first mode in vertical plane is close to sinusoidal around the equilibrium shape with frequency equal to Eq.(2):

$$n_1 = \frac{1}{2L}\sqrt{\frac{T\left(1+\frac{EA}{T}\frac{\pi^2 s^2}{2L^2}\right)}{m}} \tag{2}$$

where: E is the Young modulus
A is the cross section area
s is the vertical sag of the cable.

The sag close to mid span is given by eq. (3):

$$s = \frac{4mgL^2 \cos\alpha}{\pi^2 T} \tag{3}$$

where: g is the gravity acceleration
α is the mean cable inclination

The characteristics of the 4 representative cables are presented to the next table.

Table 1. Main characteristics of representative cables

Cable	No of Strands	Length (m)	Area (cm^2)	Mass (kg/m)	Tension (kN)	Inclination (deg)	1st Vertical Frequency (Hz)	1st Horizontal Frequency (Hz)
C3S23	70	286.2	105.0	97.1	6023	20.5	0.532	0.435
C3S19	59	239.4	88.5	81.4	5316	23.0	0.605	0.533
C3S14	47	182.5	70.5	65.2	4063	28.5	0.741	0.684
C3S04	43	87.0	64.5	59.8	1980	70.0	1.066	1.046

A comparison between the expected frequencies of the deck (for various modes) and the expected 1st natural frequency of the cables are illustrated in *Fig.2*, where it is clear that longer cables have common frequency range with higher deck modes.

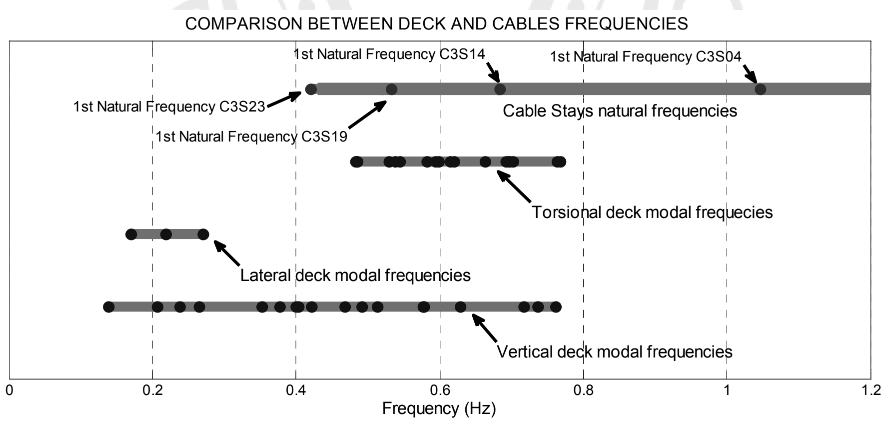

Figure 2. Comparison of deck with 1st cable stay frequencies

An important fact regarding cable stays is the very low structural damping ξ_s. For the Rion Antirion Bridge it was estimated that ξ_s varies for long to short cables according the Eq.(4):

$$\xi_s = -6 \cdot 10^{-4} \cdot L + 0.24 \tag{4}$$

leading to ξ_s=0.068% (longer) up to ξ_s=0.193% (shorter).

However, along with the structural damping it should be introduced the high wind speed aerodynamic damping ξ_α that is proportional to the wind velocity U (when specific aerodynamic phenomena are absent) and is calculated through Eq.(5.1) for modes parallel and Eq.(5.2) for modes perpendicular to wind direction.

$$\xi_\alpha = \frac{\rho U D C_d}{4\pi m n_k} \tag{5.1}$$

$$\xi_\alpha = \frac{\rho U D C_d}{8\pi m n_k} \tag{5.2}$$

where: ρ is the air density
D is the cable diameter
C_d is the drag coefficient

For high wind speed (above 15 m/sec) it's worth mentioning that the aerodynamic damping is prevailing and in particular for 30 m/sec the ξ_α is 5 to 12 times the ξ_s.

2.2 Parametric excitation and buffeting

This is one of the most important phenomena for stay cable vibrations in Rion Antirion Bridge since for a wide number of cases the 1st natural frequency of the cables is in the same range with higher deck mode frequencies, as already illustrated in *Fig.2*.

For the estimation of the vibration amplitude of the cables, it is important to calculate the response of the deck and the pylons (where the cables are anchored), for different cases of wind speed. This was performed after deck buffeting analysis that included 15 wind cases. From these, only five cases were studied, regarding the excitation of the cables, plus the extreme wind speed case:

- No1 U(m/s)=5.90 (corresponding to the lowest damping of mode 1)
- No3 U(m/s)=10.0 (corresponding to the lowest damping of mode 5)
- No6 U(m/s)=15.9 (corresponding to the lowest damping of mode 9)
- No10 U(m/s)=19.7 (corresponding to the lowest damp. of mode 13)
- No15 U(m/s)=21.7 (corresponding to the lowest damp. of mode 18)
- Max U(m/s)=50.0 (corresponding to extreme wind speed)

Furthermore, the direct impact of wind buffeting to the cables was calculated in order to estimate the overall amplitude. The configuration is illustrated in *Fig.3*.

The analysis of the response subjected to deck excitation and buffeting indicated that the vibration amplitude, even for moderate winds (15.9 m/s) was quite high (more than 800 mm) especially for long cables (#16 and above). This is mainly due to parametric excitation, while buffeting influence can be neglected. The addition of structural damping (reaching δ=3%) through dampers significantly limits the vibration amplitude in about 300 mm. Even if dampers significantly improve the cable performance, it should be mentioned that only the shifting of cables modal frequency using cross-ties would be fully efficient.

The above results were incorporated to the cable configuration with the necessary adaptations in order to make feasible the installation of External Hydraulic Dampers (EHD) for cables #11 to #23 and/or Internal Hydraulic Dampers (IHD) for cables #1 to#10 and cross ties, if necessary. The installation of aforementioned dampers would be implemented if the actual behavior of the cables to strong winds would not be satisfactory. However, the suitable provisions such as anchors points on deck and cables had been taken into consideration during design/construction. The detailed design of the improvements should be reviewed and finalized by incorporating the data recorded from the Structural Health Monitoring system.

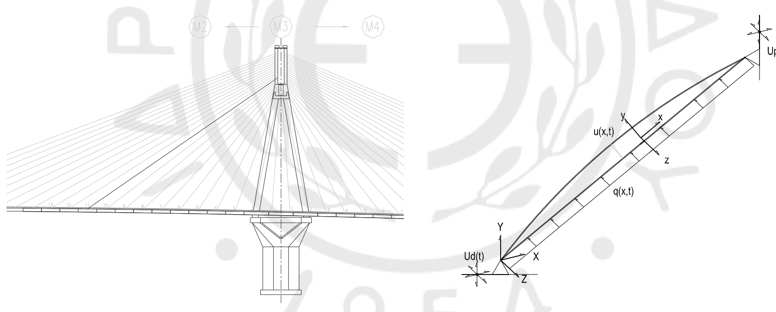

Figure 3. Configuration model for cable response calculation

2.3 Galloping

This kind of instability, usually perpendicular to the wind, is well known for slender structure whose cross section presents a strong negative slope for the lift coefficient C_L for some wind directions α. However, for the circular sections, selected for Rion Antirion Bridge stay cables, the Den Hartog criterion Eq.(6)

$$\frac{dC_L}{d\alpha} + C_D < 0 \qquad (6)$$

is not fulfilled and thus galloping cannot occur.

However, this might not be the case for specific conditions, for instance ice accretion which modify the symmetric cross section of the cables.

2.4 Rain Wind induced vibrations

Rain-wind induced vibration is one of the most usual stability problems of inclined cables [2]. For moderate rain conditions and wind velocities (8 up to 15 m/sec), large amplitude vibrations can occur for different combinations of cable inclination and wind directions. The presence of two water rivulets with the upper one oscillating circumferentially, synchronously with the cable's motion, is one of the key points of this instability [3]. The water acts as a trigger for an instability called "dry cable vibration" making it stronger and more stable.

The most efficient and common alleviation method is the disorganization of the transition through critical Reynolds number with helical thread on the protective ducts. However, since the diameter of the duct used in Rion Antirion Bridge is larger than the previously experimentally studied ones, it was proposed a series of tests in order to verify the effectiveness on current situation in the Jules Verne climatic wind tunnel in Nantes.

The test was consisting in reproduction of instability for smooth High Density Polyethylene (HDPE) ducts, on a sectional model of Rion Antirion Bridge by examining various combinations of wind speed and cable inclination, and then evaluation of the cable response covered with helical threaded HDPE duct for the same parameter combination.

The good performance of the helical threaded HDPE was verified for all the cases examined and thus the risk of rain-wind induced vibrations for Rion Antirion Bridge cable stays was eliminated.

3 MONITORING SYSTEM

The Rion Antirion Bridge is equipped with a Structural Health Monitoring system that is oriented to provide useful information regarding the response of the structure to various environmental loads such as earthquakes and strong winds.

In particular for the evaluation of the cable stays response four different types of sensors are used:

- 13 3D Accelerometers on cables (at 10 m height from deck)
- 12 3D and 3 1D Accelerometers on deck (located close to mid spans)
- 16 Load cells on cable strands (at top anchorage)
- 2 Anemometers (M1-M2 and M3-M4, 6 m above deck)

The location of each instrument is presented in *Fig.4*.

Two main categories of data files are created:

- History files (0.5 sec averaged values recorded every 30sec, except wind speed and direction that are 2' & 10' average after February 2008)
- Dynamic files (High sampling frequency at 100 Hz with 60 sec duration)

The History files are created continuously, while the Dynamic files are recorded every 2 hours (Automatic) or when particular threshold is over passed (Alert).

All types of files (History/Automatic/Alert) are very useful in order to understand the actual bridge response and evaluate the effect of potential improvements.

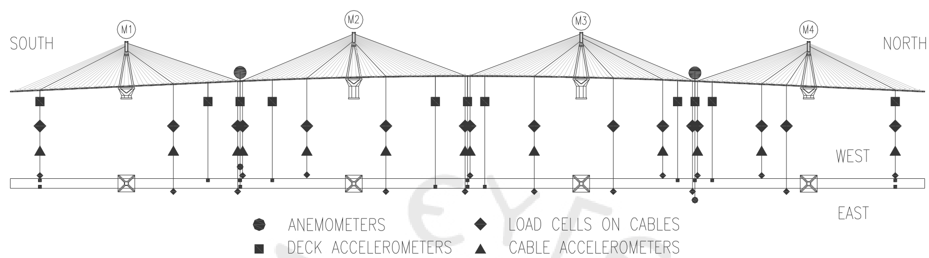

Figure 4. Location of structural monitoring sensors (cable relevant)

4 23RD OF JANUARY 2006 STRONG WIND EVENT

On 23rd of January 2006 a strong storm occurred in the vicinity of Rion Antirion Bridge. The main characteristics of the storm were the particularly eastern (120° clockwise from Bridge axis) strong winds (31.2 and 28.3 m/sec 2' average on M1M2 and M3M4 meteo stations) and the particularly low temperature (1.2°C). In *Fig.5* the 2' average wind speed and direction are provided.

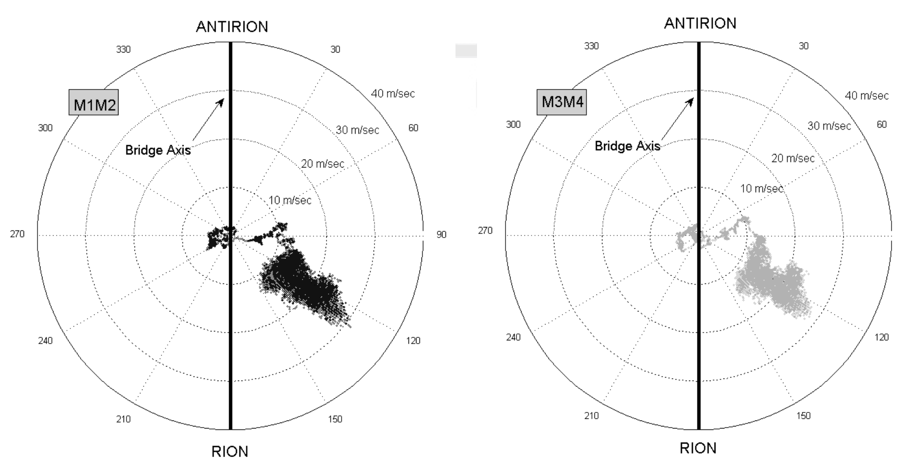

Figure 5. 2' average wind speed and direction graphs

During this event significant vibrations of the cables were observed, especially for intermediate and long cable stays (#16 and upper) the amplitude of which was exceeding ±2.0 m. Also due to low temperatures, ice formation was observed on several cables. The recorded response was calculated thanks to Alert files and is presented in the next paragraphs.

The large cable vibration enabled further analyses of the recorded data in order to optimize the design of the dampers for preventing similar vibration incidents in the future.

4.1 Deck vibration

In order to calculate the maximum displacement amplitude from acceleration time histories contained in Alert files, the following processing was applied:

- Mean removal
- band pass filtering "8th order Butterworth with corner frequencies 0.1 and 5 Hz"

The maximum vertical displacement amplitude at each sensor's location is presented in the next table, and in *Fig.6*.

Table 2. Maximum vertical displacement amplitude at sensor location

Position	Accelerometer channel	Amplitude (cm)	Position	Accelerometer channel	Amplitude (cm)
M1S18E	E3 Z axis	10.23	M2M3W	D17 Z axis	15.62
M1S18W	E4 Z axis	9.26	M3S20W	E19 Z axis	14.01
M1N17E	E7 Z axis	10.21	M3N20E	E24 Z axis	14.32
M1M2W	E9 Z axis	11.62	M3M4E	D26 Z axis	15.51
M1M2E	D9 Z axis	13.75	M4S20E	E28 Z axis	11.94
M2S17E	E11 Z axis	16.03	M4N18W	E32 Z axis	10.65
M2N14W	E15 Z axis	13.44	M4N18E	E33 Z axis	10.66
M2M3E	E17 Z axis	15.21	-	-	-

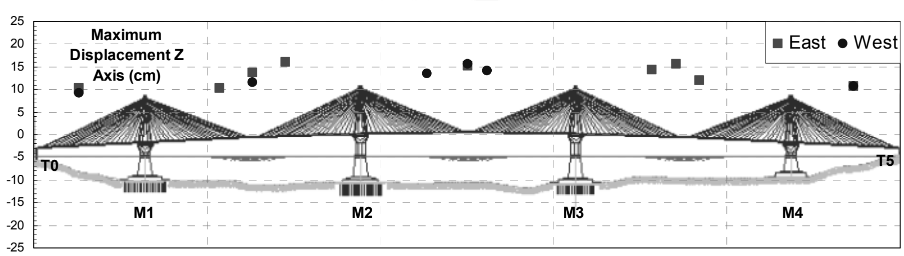

Figure 6. Maximum vertical displacement amplitude at sensors location

The frequency analysis of the acceleration time histories indicate that a large number of deck modes were participating to vibration but only few of them had significant displacement amplitude. In *Fig.7* the average normalized power spectral density [4] for acceleration and displacement time histories of all the deck sensors are presented and compared with the frequency band on the 1^{st} natural mode of the cables.

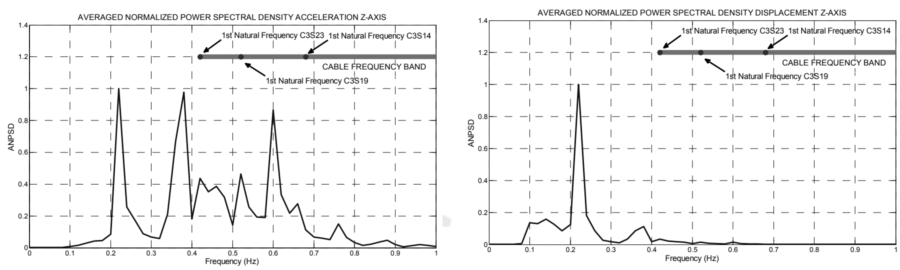

Figure 7. ANPSD for acceleration and displacement based on 02:00 24/01/2006 dynamic file

4.2 Cable vibration

In order to calculate the maximum displacement amplitude from acceleration time histories contained in the Alert files, the following processing was applied:

- Mean removal of Y and Z axis
- Frequency analysis of both Y and Z axis for identification of participating modes.
- Calculation of displacement time history (for both Y and Z axis) and decomposition into participating mode time histories $u_i(t)$ at accelerometer location L_a, $u_i(L_a,t)$, based on frequency content.
- Calculation of each modal coordinate response $q_i(t)$ based on Eq.(7), since $u_i(L_a,t)$ is known and $\Phi_i(L_a)$ is also known for cables and is described in Eq.(8).
- Calculation of maximum displacement for each location as an orthogonal composition of Y and Z displacement time histories for all participating modes according Eq.(9).

$$u_i(x,t) = \Phi_i(x) \cdot q_i(t) \tag{7}$$

$$\Phi_i(x) = \mathrm{Sin}\left(i\pi \frac{x}{L}\right) \tag{8}$$

$$u_m(x) = \max\left(\sqrt{\sum_{i=k}^{n} u^2{}_{y,i}(x,t) + u^2{}_{z,i}(x,t)}\right) \tag{9}$$

The maximum amplitude of vibration U_m=max(u_m(x)) for all cables calculated for all Alert files are presented to Table 3 and *Fig.8*.

Table 3. Maximum vertical displacement amplitude

Position	Accelerometer channel	Amplitude (cm)	Position	Accelerometer channel	Amplitude (cm)
C1S18W	J4 Y and Z	227.4	C3S23W	J18 Y and Z	263.6
C1N10E	J6 Y and Z	168.4	C3S10E	J20 Y and Z	36.9
C1N23E	J8 Y and Z	241.9	C3N17W	J23 Y and Z	257.1
C2S23W	J10 Y and Z	207.1	C4S23W	J27 Y and Z	317.1
C2S10W	J12 Y and Z	91.3	C4S10W	J29 Y and Z	19.6
C2N07E	J14 Y and Z	57.3	C4N18W	J32 Y and Z	249.96
C2N23E	J16 Y and Z	255.5	-	-	-

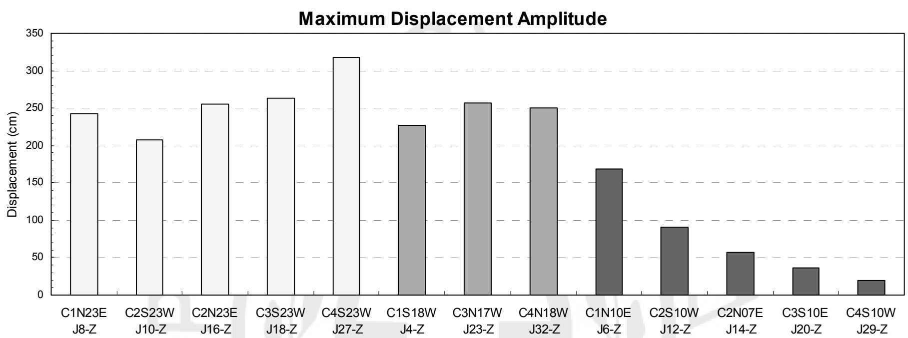

Figure 8. Maximum displacement amplitude of cable stays sorted per length

Despite the large amplitude of cable vibration, the respective loads were within SLS (50% of F_{GUTS}=265.5 kN) as presented hereunder.

Table 4. Maximum cable load

Position	Sensor	Maximum load (kN)	Percentage of F_{GUTS} (%)	Position	Sensor	Maximum load (kN)	Percentage of F_{GUTS} (%)
C1S18W	K4	103.9	39.1	C3S10E	K20	83.6	31.5
C1N10E	K6	94.7	35.7	C2N07E	K22	69.5	26.2
C1N23E	K8	104.8	39.5	C3N17W	K23	100.6	37.9
C2S23W	K10	95.8	36.1	C3N23E	K25	90.9	34.2
C2S10W	K12	91.3	34.4	C4S23W	K27	104.0	39.2
C2N07E	K14	71.1	26.8	C4S10W	K29	91.7	34.5
C2N23E	K16	103.5	39.0	C4N05E	K30	66.7	25.1
C3S23W	K18	102.6	38.6	C4N18W	K32	112.4	42.3

5 DESIGN AND IMPLEMENTATION OF TECHNICAL IMPROVEMENT

The data recorded from the monitoring system, and particularly the dynamic records were further processed in order to optimize the design of the required technical improvement for the mitigation of cable vibrations. Two possible solutions were available, dampers EHD and/or IHD and cross-ties, with the first being the most favorable one, since the implementation of cross-ties in RA Bridge do not shift all cable frequencies beyond higher deck modes frequencies.

5.1 Design parameters

During design phase, it was investigated if the EHD system is efficient enough to mitigate the cable vibrations as they were observed and recorded by the monitoring system of Rion Antirion Bridge. Thus the main question was how much damping is required to be added for minimizing the cable vibration.
Three different excitation scenarios were investigated:

- Resonance and parametric excitation
- Iced cable galloping
- Dry inclined cable galloping

Initially it was investigated the damping ratio that is required in order to avoid resonance and parametric excitation. The damping was calculated for different length of cables with basic criterion the limitation of the vibration amplitude to one diameter, when input excitation was described by an envelope frequency function Eq.(10) that was calculated from 23rd of January 2006 wind event.
The results are presented to *Fig.9* and indicate that ξ=1% of total structural damping is required from cables with length between 100 and 250 m and ξ=1.5 % for longer cables. No additional damping was required for short cables with length less than 100m.

$$\mathrm{V}(f) = 1 + \frac{3}{f^2} \text{ (mm)} \tag{10}$$

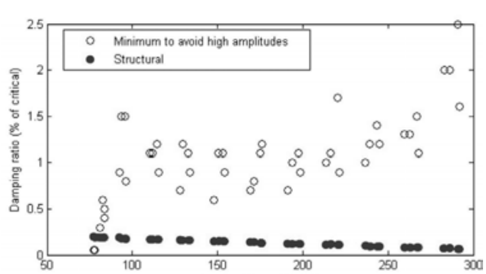

Figure 9. Required damping ratio for vibration mitigation

For the selected damping ratio (1.0%/1.5% for intermediate/long, and no additional damping for short cables L<100m) the critical wind velocity was calculated for both ice [5] and dry inclined galloping. *Fig.10* summarizes these results.

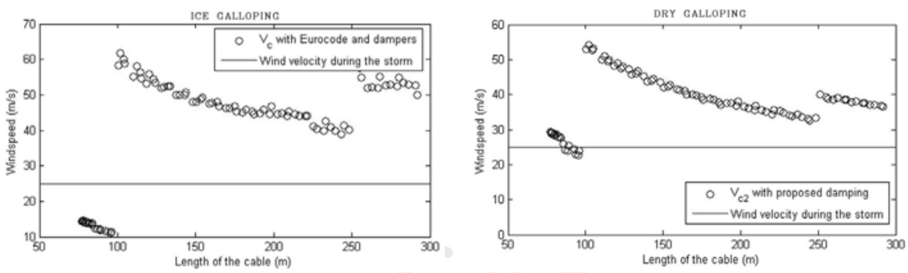

Figure 10. Critical wind speed for ice and dry galloping

The required damping ratio includes the aerodynamic damping and thus the required structural damping ratio is significantly lower. The selected damping system was designed in order to guarantee 4% logarithmic decrement for all cables above #11. The general arrangement is illustrated to *Fig.11*.

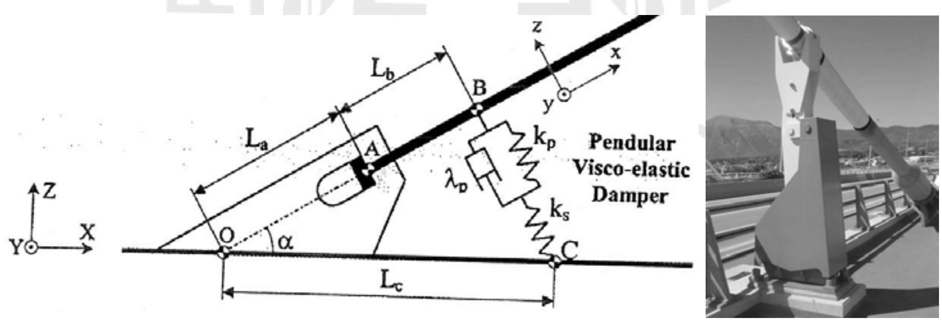

Figure 11. General arrangement of dampers for cables #11 and above and actual implementation (C4N23E)

5.2 Installation and commissioning test

The installation of 208 dampers was performed in the first semester of 2007. In order to verify the proper functioning of damper commissioning tests were performed on 6 different cables. The aim was to excite the 1st natural mode of each cable and calculate the logarithmic decrement from measured acceleration time histories, before and after damper installation. For the tests a mobile temporary acquisition system was used. The results of the commissioning tests are summarized in Table 5.

Table 5. Commissioning test results

Position	Logarithmic decrement w/o damper	Logarithmic decrement with damper	Position	Logarithmic decrement w/o damper	Logarithmic decrement with damper
C2S11W	1.79 %	6.42 %	C2S16W	1.58 %	4.99 %
C2S12W	2.06 %	6.15 %	C2S19W	1.08 %	6.01 %
C2S14W	1.53 %	5.31 %	C2S22W	1.82 %	5.35 %

The commissioning tests led to the acceptance of the installed EHD dampers as an efficient tool for cable stay vibration mitigation.

6 8TH OF MARCH 2010 STRONG WIND EVENT

Three years after the installation of external dampers, the most severe wind storm during Bridge operation period occurred. This event provided an excellent opportunity to verify the overall behaviour of the cable stays equipped with dampers.

The main characteristics of the storm were eastern (100° clockwise from Bridge axis) strong winds (35.4 and 30.7 m/sec 10’ average on M1M2 and M3M4 meteo stations) and low temperature (6.5°C). In *Fig.12*, the 10’ average wind speed and direction are presented.

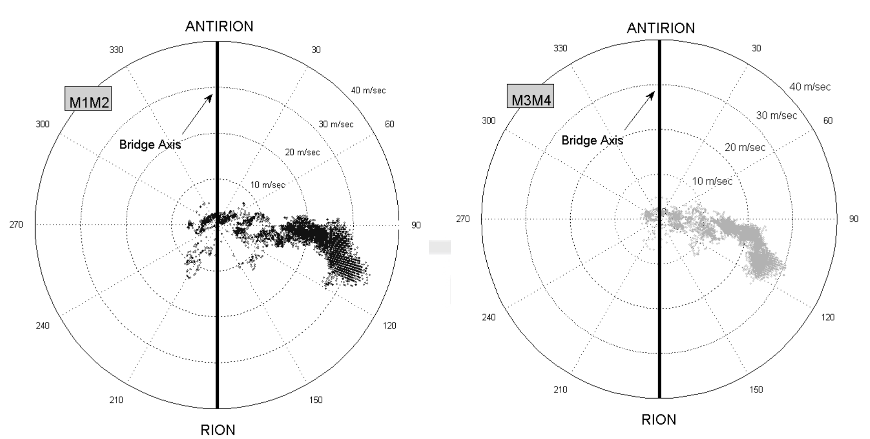

Figure 12. 10’ average wind speed and direction graphs

During this event no significant vibrations of the cables were observed. The response of the deck had similar frequency content but higher vibration amplitudes compared with 2006 event, as expected. No ice formation was observed during 2010 event. For comparison with 2006 event, the same treatment of data (deck/cable accelerometers and load on cables) was performed and the results are presented hereunder.

6.1 Deck vibration

The maximum vertical displacement amplitude at each sensor's location is presented in the Table 6, and in *Fig.13*.

Table 6. Maximum vertical displacement amplitude at sensor location

Position	Accelerometer channel	Amplitude (cm)	Position	Accelerometer channel	Amplitude (cm)
M1S18E	E3 Z axis	14.75	M2M3W	D17 Z axis	18.59
M1S18W	E4 Z axis	14.45	M3S20W	E19 Z axis	18.76
M1N17E	E7 Z axis	14.60	M3N20E	E24 Z axis	17.78
M1M2W	E9 Z axis	18.47	M3M4E	D26 Z axis	14.40
M1M2E	D9 Z axis	18.79	M4S20E	E28 Z axis	14.10
M2S17E	E11 Z axis	16.79	M4N18W	E32 Z axis	12.48
M2N14W	E15 Z axis	15.00	M4N18E	E33 Z axis	12.99
M2M3E	E17 Z axis	19.75	-	-	-

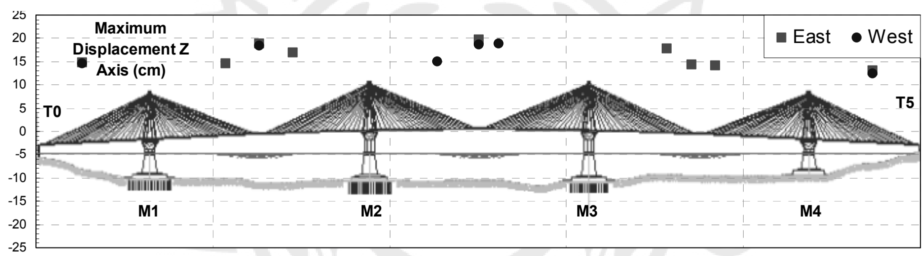

Figure 13. Maximum vertical displacement amplitude at sensor location

In *Fig.14* the average normalized power spectra density for acceleration and displacement time histories of all the deck sensors are presented and compared with the frequency band on the 1st natural mode of the cables.

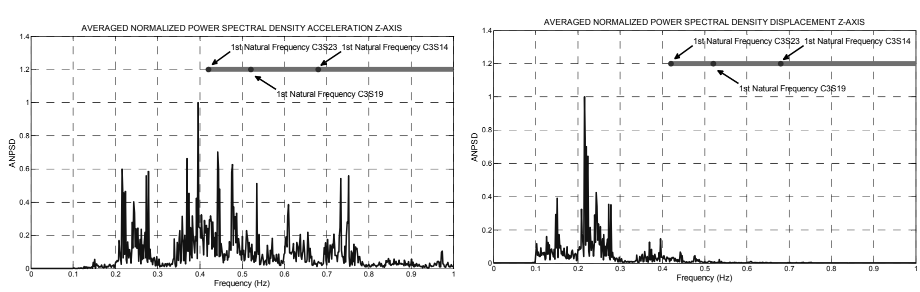

Figure 14. ANPSD for acceleration and displacement based on 07:15 08/03/2010 Alert file

6.2 Cable vibration

The maximum amplitude of vibration $U_m = \max(u_m(t))$ for all cables calculated for all Alert files are presented to Table 7 and *Fig.15*.

Table 7. Maximum vertical displacement amplitude

Position	Accelerometer channel	Amplitude (cm)	Position	Accelerometer channel	Amplitude (cm)
C1S18W	J4 Y and Z	29.5	C3S23W	J18 Y and Z	23.5
C1N10E	J6 Y and Z	15.5	C3S10E	J20 Y and Z	20.8
C1N23E	J8 Y and Z	33.3	C3N17W	J23 Y and Z	30.2
C2S23W	J10 Y and Z	40.4	C4S23W	J27 Y and Z	25.5
C2S10W	J12 Y and Z	22.1	C4S10W	J29 Y and Z	12.5
C2N07E	J14 Y and Z	14.6	C4N18W	J32 Y and Z	27.3
C2N23E	J16 Y and Z	24.5	-	-	-

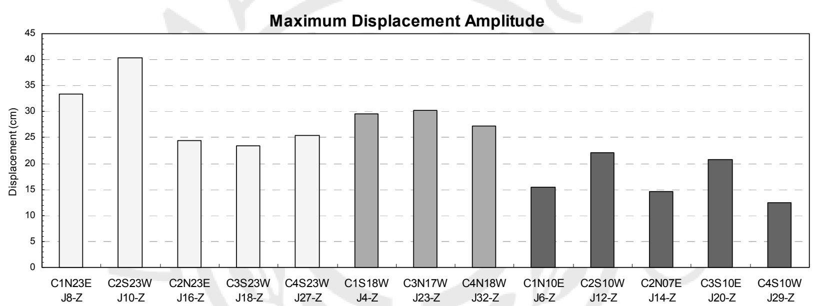

Figure 15. Maximum displacement amplitude of cable stays sorted per length

The maximum load of the cables was within SLS (50% of F_{GUTS}=265.5 kN) as presented hereunder.

Table 8. Maximum cable load

Position	Sensor	Maximum load (kN)	Percentage of F_{GUTS} (%)	Position	Sensor	Maximum load (kN)	Percentage of F_{GUTS} (%)
C1S18W	K4	96.0	36.2	C3S10E	K20	77.6	29.2
C1N10E	K6	86.4	32.5	C2N07E	K22	64.6	24.3
C1N23E	K8	91.8	34.6	C3N17W	K23	87.0	32.8
C2S23W	K10	85.8	32.3	C3N23E	K25	77.8	29.3
C2S10W	K12	84.7	31.9	C4S23W	K27	87.8	33.1
C2N07E	K14	64.5	24.3	C4S10W	K29	89.2	33.6
C2N23E	K16	88.6	33.4	C4N05E	K30	60.8	22.9
C3S23W	K18	87.0	32.8	C4N18W	K32	101.2	38.1

7 CONCLUSIONS

The design against wind induced vibrations of slender structures, such as cable-stays, is a high importance issue regarding safety and user comfort, especially for important infrastructures such as the Rion Antirion Bridge. Several studies (theoretical and experimental) were performed during design phase in order to minimize uncertainties regarding cable stay vibration. Additionally, proper adaptations on the deck and cables were performed during design/construction phase for easy implementation of potential mitigation measures. The analysis of the actual structural response recorded through the Monitoring system of the Bridge due to a strong wind event in 2006 gave the opportunity to optimize the required technical improvement, in this case external dampers on the intermediate and long cables. The efficiency of adopted improvement was verified through commissioning tests. Three years after the implementation the most severe wind storm stroke the Rion Antirion Bridge. Nevertheless, the response of the cable stays to that excitation was limited, even though the deck vibration was more intense than in 2006, as expected.

ACKNOWLEDGEMENTS

The design, supply and installation of EHDs were performed by Freyssinet.

REFERENCES

[1] Blevins R.D, "Formulas for natural frequency and mode shape" Robert E. Krieger Publishing Company, Malabar, Florida.
[2] Flamand O, "Rain-Wind induced vibrations of cables", International Conference A.I.D.C.-F.I.P., Deauville, October 12-15, 1994
[3] Wang Z.J, Zhou Y,Huang J.F, Xu Y.L, "Fluid dynamics around an inclined cylinder with running water rivulets", Journal of fluid and structures 21, Vol. 21, pp. 49-60, 2005
[4] H.Wenzel D.Pichler, "Ambient Vibration Monitoring", WILEY publications
[5] AFNOR, Eurocode 1, "Actions du vent et de la neige sur les structures", ENV 1991-2-4: 1995,2002.

INFLUENCE OF NON LINEAR SOIL STRUCTURE INTERACTION ON THE SEISMIC DEMAND IN BRIDGES

Alain Pecker[1]

[1] Géodynamique et Structure, Bagneux, France
e-mail: alain.pecker@geodynamique.com

ABSTRACT: Examination of the seismic behavior of bridge foundations during earthquake points out that even at low shaking level permanent displacements, i.e. nonlinear soil structure interaction, takes place. Nonlinear soil structure interaction is usually not considered in design although it may have a beneficial effect as illustrated in this paper. Results of incremental dynamic analyses (IDA) of a simple structural bridge pier for a fixed base system or the same system with consideration of linear and nonlinear soil structure interaction, including uplift and soil plasticity, are presented. The results highlight the beneficial role of foundation nonlinearities in decreasing the ductility demand in the superstructure but point out the need to carefully assess the variability of the response when non linearity is allowed at the foundation design.

KEY WORDS: Soil structure interaction, nonlinearity, ductility demand, incremental dynamic analyses.

1 INTRODUCTION

The topic of soil structure interaction (SSI) has long been recognized as a major factor controlling the design of the structure. During an earthquake, the soil deforms under the influence of incident seismic waves and imposes its motions to the foundation and to the supported structure. In turn, the induced motion of the foundation creates inertial forces in the superstructure that are transmitted back to the foundation and to the underlying soil. Therefore, the induced deformations create additional waves that emanate from the soil-foundation interface. Both phenomena occur simultaneously and therefore are closely linked and dependent on one another. SSI increases in significance as the supporting soil becomes softer. Although recognized by recent building codes, like Eurocode 8, [1], which requires to take into consideration SSI for massive structures founded on soft deposits, most building codes ignore the effect of SSI: “For the majority of usual building structures, the effects of SSI tend to be beneficial, since they reduce the bending moments and shear forces acting in the various members of the super-structure”, [1]. As pointed in [2] this statement may hold for a large class of structures but may be misleading for others and mainly relies on the smooth shape of normalized code spectra. To the best, SSI is considered in the dynamic analysis assuming a linear behavior of the soil foundation interface. Even though, the results obtained by various authors on the beneficial or detrimental effect of SSI are controversial. Within the framework of performance based design, the question becomes essential to know how nonlinear soil structure interaction may affect the seismic demand in the superstructure. With the advance of efficient numerical tools to model the nonlinear behavior of foundations, it becomes possible to investigate this effect through the concept of incremental dynamic analysis (IDA) as defined by Vamvatsikos & Cornell, [3].

The paper presents one example of observed nonlinear soil structure interaction on the foundations of the Rion Antirion Bridge during a moderate earthquake, highlighting the fact that, although such a phenomenon is not usually considered in design, it may exist. Furthermore, preliminary results obtained through IDA show that this effect may be beneficial for protecting the superstructure by reducing the ductility demand in the pier and suggest alternatives for the seismic design of foundations. For that purpose, the studied structure is a reinforced concrete bridge pylon founded on the surface of a homogeneous cohesive soil by means of a circular footing.

2 ILLUSTRATION OF NONLINEAR SOIL STRUCTURE INTERACTION

The Rion Antirion bridge, a five-span cable stay bridge (286m+560m+560m+560m+286m), has been designed to withstand earthquakes with p.g.a. of 0.48g and tectonic movements up to 2m between consecutive pylons. The soil profile consists of deep alluvial deposits with poor mechanical characteristics. The piers are founded on shallow foundations resting on reinforced soil, [4], and were designed taking into account nonlinear soils structure interaction for the extreme (2000 year return period) design earthquake; this implies that uplift, sliding and even partial soil yielding would occur for that event. However, for moderate earthquakes, with return periods typically of the order of 100 to 500 years, linear soil structure interaction was considered.

The bridge was hit by the Achaia-Ilia earthquake that took place on June 08, 2008. The epicenter of this earthquake with moment magnitude Mw = 6.5 was located at a distance of approximately 36km SW from the bridge and its focal depth was estimated to around 30km (Figure 1). Examination of available seismological data recorded during the main shock and the aftershocks indicated that the earthquake occurred on a dextral strike slip fault. The peak ground acceleration recorded on site (Rion shore) was 0.127g, significantly smaller that the design earthquake. This was the first major earthquake event experienced by the bridge initiating full scale inspection in order to identify potential damages of the structure. Given that tectonic movements might take place at this site, a geometrical survey was conducted to monitor permanent movements due to the event.

Figure 1. Epicenter and bridge site

Interpretation of the measured values of the ground motion parameters (p.g.a, Arias Intensity and Cumulative Absolute Velocity) leads to the conclusion that the return period of the earthquake is in-between 80 to 135 years. This observation complies with the calculated spectra at the banks and the feet of the bridge pylons that were shown to be in the range of or slightly smaller than the 120 year period design earthquake. For such a small event nonlinear soil structure interaction would never been considered in design. Nevertheless, monitoring of the foundations permanent movements after the earthquake clearly show that permanent movement (settlements) of the foundation took place, an evidence of nonlinear foundation behaviour.

After the earthquake a complete geometrical monitoring was conducted in order to check if tectonic movements or settlements had occurred during the earthquake, [5]. It is important to mention that just before the earthquake the scheduled geometrical monitoring campaign had been completed for planimetric and leveling measurements on Rion and Antirion shores. The comparison of measurements before and after the earthquake does not show significant movements. Relative altitudes on both shores remain very consistent with their pre- earthquake values. The maximum earthquake induced settlement was measured at M1 pier and is 21 mm. At the other piers the settlements range between 0mm and 16mm. In plane no important displacements that can be attributed to the earthquake have been observed. The settlements, although small and representing less than 10% of the total settlements experienced since the beginning of construction, are however large enough to draw attention on the nonlinear foundation behaviour.

The lesson drawn from these observations is that even if engineers would attempt to prevent nonlinear foundation behavior and request, following usual practice, that they remain essentially elastic during earthquake, nonlinearities will nevertheless occur. The obvious question, to which the remaining of the paper will attempt to bring partial answers, is to know whether they are beneficial or detrimental.

3 SOIL STRUCTURE INTERACTION

Despite the fact that SSI is not very often considered in building codes, it has a long history which started back in 1936 with the work of Reissner. Since then, several improvements have been achieved and the present state of the art is well developed and understood.

3.1 Linear soil structure interaction

Several modeling techniques are available to account for SSI in the dynamic analysis. The most sophisticated ones are based on finite element analyses in which the supporting medium is explicitly modeled as a continuum. This technique is very demanding, both in computer time and manpower, and is not very efficient at early design stages of a project. Therefore, a substructure approach is often preferred in which all the degrees of freedom of the supporting medium are lumped at the soil-foundation interface in the form of dynamic impedances that can be viewed as frequency-dependent springs and dashpots, [6]. If those impedances are assumed frequency-independent or if simple rheological models are used the analysis is rendered very attractive and efficient. Such simple models can therefore be implemented to analyze the impact of linear soil structure interaction on the seismic response of structures.

A recent very comprehensive study, [7], has investigated the effects of soil-shallow foundation-structure interaction on the seismic response of structures using Monte Carlo simulations. The structure was modeled as a nonlinear one degree of freedom system and SSI was taken into account with conventional springs and dashpots; in other words, SSI was treated as a linear phenomenon. The authors concluded that SSI effects on the median response of a structure exhibiting a nonlinear behavior is relatively small; however there is a 30-50% probability for an increase in the total structural displacement of more than 10% due to SSI. Therefore, based on these results, SSI does not seem to be a major issue, at least in terms of median response. However, one may wonder how much these conclusions are influenced by the initial modeling assumptions regarding SSI.

3.2 Nonlinear soil structure interaction

More than 30 years ago the earthquake engineering community realized that the increase of strength of a structural system does not necessarily enhance its safety. This recognition has led to the development of new design principles, aiming at rationally controlling seismic damage and rendering the structure “fail-safe”. This concept is embedded in the capacity design philosophy which is widely implemented in structural design, but is given less attention in geotechnical engineering. Even when foundation compliance is taken into account, little care is given to the nonlinearity of soil and foundation. Such an approach may lead to non-conservative oversimplifications, especially in the case of strong geometric nonlinearities, such as foundation uplifting and sliding. Most importantly, neglecting such phenomena prohibits the exploitation of strongly non-linear energy dissipating mechanisms in case of occurrence of ground motions larger than design. Today, a growing body of evidence suggests that soil-foundation plastic yielding under seismic excitation is not only unavoidable, but may even be beneficial, [8] to [13]. Such evidences has even led some authors to make the proposal of totally reversing the foundation design philosophy by allowing significant yielding in the foundation to protect the structure, [8].

However, implementation of a design philosophy in which, even partial, yielding is allowed at the foundation level requires that efficient and reliable tools be available for design. Nonlinear structural analyses are very sensitive to small changes in the structural properties and in the input motion. Obviously, the situation is even worse in foundation engineering where the properties of the soil are never known with a great accuracy. A safe design will therefore require a large amount of analyses to be run and this can hardly be efficiently achieved with heavy, although rigorous, numerical models such as finite element models. The concept of dynamic macroelements, developed over the last decade, offers a unique opportunity to evaluate the effect of nonlinear soil structure interaction on the response of a yielding structure.

Advantage of macroelement modelling is used in this paper, to examine the effect of nonlinear soil structure interaction on the response of a yielding structure. This is performed with a series of Incremental Dynamic Analyses (IDA). The results are further compared to analyses with linear SSI and without SSI (fixed-base structure) to highlight the changes in behaviour of the structure when SSI is accounted for either with a linear assumption or with a nonlinear one.

4 ILLUSTRATIVE EXAMPLE

4.1 Description of physical model

The studied structure is depicted in Figure 2; it represents a typical highway bridge pier under seismic excitation. The deck of mass md is monolithically connected to the reinforced concrete circular column of diameter d and height h. The pier is founded on a relatively stiff homogeneous clay stratum by means of a shallow circular foundation of height h_f and diameter D. Separation (uplift) and no sliding are allowed along the soil-footing interface. The system is subjected to seismic loading only along the transverse (with respect to the bridge axis) horizontal direction.

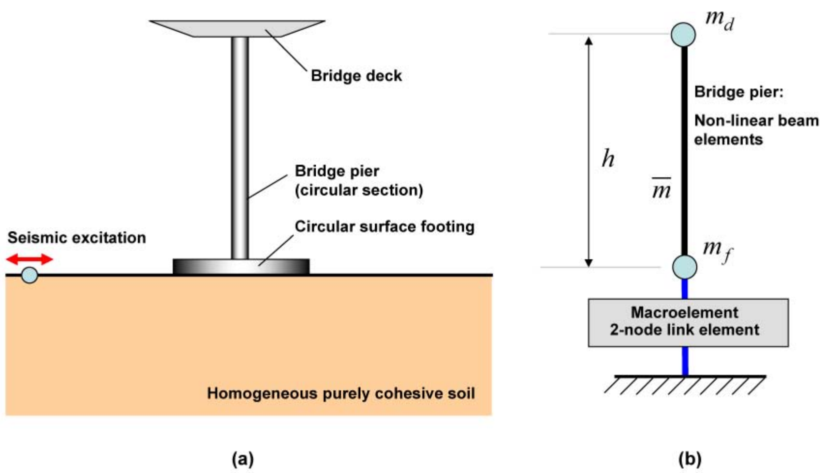

Figure 2. Soil-foundation-structure system (a) physical, (b) model

A direct displacement-based design procedure (DDBD), [14], appropriately modified to take into account soil-structure interaction effects, has been implemented for the pier design. The procedure is detailed in [15]. The design of the bridge pylon has been performed considering a seismic input represented by the Eurocode 8 design spectrum, Type 1, with firm soil conditions and a peak ground acceleration $a_g = 0.5g$. The following design performance criteria have been defined:

- System drift limit $\Delta_d = 0.03h$.
- Maximum foundation rotation $\theta_{lim} = 0.01$.
- Maximum structure ductility demand $\mu_{lim} = 3.2$.

The bridge pier is modeled with non-linear beam elements. The foundation and the soil are replaced by one unique 2-node link element, which is the non-linear dynamic macroelement for shallow foundations as developed in [16] and [17]. The first node of the macroelement is attached to the superstructure. The mass of the foundation is lumped at this node; the input motion is applied at the second node. The constitutive behavior of the macroelement reproduces the non-linear phenomena arising at the soil-footing interface: elastoplastic soil behavior leading to irreversible foundation displacements, possibility for the

footing to get detached from the soil (foundation uplift). Additionally, the macroelement is coupled with a viscous dashpot reproducing radiation damping.
The numerical parameters defining the problem are given in Table 1.

Table 1. Properties of the soil-structure system

Physical quantity	**Symbol**	**Unit**	**Value**
Mass of deck	m_d	kt	0.973
Column height	h	m	20.
Column diameter	d	m	2.5
Column mass	m_c	kt	0.245
Concrete compression strength	f_c	MPa	30.
Steel yield strength	f_y	MPa	400.
Number of longitudinal rebar	n	-	100
Diameter of longitudinal rebar	d_{long}	mm	26
Diameter of transverse rebar	d_{trans}	mm	12
Spacing of transverse rebar	s	mm	70
Foundation diameter	D	m	7.5
Foundation height	h_f	m	2.0
Foundation mass	m_f	kt	0.221
Total weight of structure	W_{tot}	MN	14.12
Soil undrained shear strength	c_u	MPa	0.15
Soil shear modulus	G_s	MPa	104.
Soil shear wave velocity	V_s	m/s	255.
Static bearing capacity factor	FS	-	2.84
Fixed base period of structure	T_0	s	1.379
Period for structure with SSI	T_{SSI}	s	1.650

4.2 Summary description of the macroelement

Several macroelement models have been developed during the last decade to account for nonlinear soil structure interaction. A comprehensive review of the existing models is presented in [18]. The model used in the present study is detailed in [16] and [17]. Only the main features are recalled hereafter.

The model comprises three non-linear mechanisms: a) a mechanism of sliding at the soil-footing interface, b) a mechanism of soil yielding in the vicinity of the footing and c) a mechanism of uplift as the footing may get detached from the soil. The first two are irreversible and dissipative and are combined within a multi-mechanism plastic formulation, [19]. The third mechanism is reversible and non-dissipative. It is reproduced with a phenomenological non-linear elastic model. Each non-linear mechanism participating in the global response of the system is modeled independently and the surface of ultimate loads is retrieved as the combined result of all active mechanisms. This allows formulating each mechanism by respecting its particular characteristics and offers the possibility of activating, modifying or deactivating each mechanism, an option that will be used in this paper.

4.3 Model parameters

The model parameters are listed in Table 2. Derivation of those parameters is briefly commented below.

4.3.1 Viscoelastic parameters

They are determined using the classical impedance functions for a circular footing on a halfspace, [20].

4.3.2 Bounding surface parameters

The ultimate vertical force for a centred load is given by the ultimate bearing capacity of a circular footing on a cohesive soil $N_{\max} = 6.05c_uA$ where c_u is the soil undrained shear strength and A the footing area. The parameters ψ and ξ are given by $\psi = V_{\max}/N_{\max}$ and $\xi = M_{\max}/DN_{\max}$. The ultimate shear force and overturning moment for a perfectly bonded footing are given by $V_{\max} = c_uA$ and $M_{\max} = 0.67c_uAD$.

4.3.3 Plasticity model parameters

These are the only parameters (h_0, p, p_g) that require a calibration from a 3D static finite element model. The numerical parameters h_0, p are chosen to reproduce the soil hardening behavior in diagrams of vertical force versus vertical displacement and diagrams of horizontal force versus horizontal displacement. The numerical parameter p_g is calibrated to fit the accumulated vertical settlement during the loading phase under the horizontal force.

Table 2. Model parameters

Parameter description	**Symbol**	**Unit**	**Value**
Footing diameter	D	m	7.50
Ultimate vertical force	$N_{\max}$	MN	40.09
Ultimate horizontal force	$V_{\max}$	MN	6.63
Ultimate moment	$M_{\max}$	MN.m	33.30
Bounding surface parameter	ψ	-	0.17
Bounding surface parameter	ξ	-	0.11
Vertical elastic stiffness	K_{NN}	MN/m	2225
Horizontal elastic stiffness	K_{VV}	MN/m	1833
Rocking elastic stiffness	K_{MM}	MN.m	20862
Vertical dashpot coefficient	C_{NN}	MN.s/m	27.8
Horizontal dashpot coefficient	C_{VV}	MN.s/m	18.0

Rocking dashpot coefficient	C_{NN}	MN.m.s	4.8
Plastic parameter (initial loading)	h_0/K_{NN}	-	4.0
Plastic parameter (reloading)	p	-	0.5
Non-associative parameter	p_g	-	5.0
Uplift initiation parameter	α	-	6.0
Uplift parameter	γ	-	2.0
Uplift parameter	δ	-	0.5
Uplift parameter	ε	-	0.2
Uplift plasticity coupling parameter	ζ	-	1.5

4.4 Superstructure model

The bridge pier is modeled using small-displacement/small-rotation Timoshenko beam elements with an elastoplastic constitutive law. For simplicity, an elastoplastic bilinear model is adopted in the analyses. The moment-curvature diagram for the examined concrete column has been calculated in [15]. The parameters used for the definition of the bilinear moment-curvature diagram are the yield moment M_y and the post yield stiffness of the beam in pure tension. The elastic stiffness of the beam elements is calculated from the geometric characteristics of the cross section and the elastic properties of reinforced concrete. The numerical parameters used for the definition of the bilinear model for the beam elements are presented in Table 3.

Table 3. Structural model parameters

Parameter	**Symbol**	**Unit**	**Value**
Yield moment for elastoplastic beam element	M_y	MN.m	37.5
Yield curvature	κ_y	-	$6.52\ 10^{-4}$
Post-yield stiffness for beam elements under traction	K_{post}	MPa	5.0

5 INCREMENTAL DYNAMIC ANALYSES

An incremental dynamic analysis (IDA) consists in performing a series of non-linear time-history analyses, using as input motion the same acceleration record scaled to increasing amplitudes, and keeping track of some characteristic quantities of the response of the structure. Using the terminology introduced in [3], we refer to *intensity measures* (IMs), characterizing the severity of the input motion and to *damage measures* (DMs), characterizing the response of the structure. The output of an IDA is an *IDA curve*, *i.e.* a plot of a selected IM versus a selected DM. Similarly, an *IDA curve set* is a collection of IDA curves of the same structural model under different records that have been parameterized on the same IM and DM.

Different options are available for the IM to be used in the IDA curves (PGA, CAV, spectral acceleration at some specific frequency…). In the following, we choose the cumulative absolute velocity (CAV), guided by its cumulative character which may be a better proxy for the residual response parameters of the structure.

Several quantities may also be considered for the DMs: drift, residual displacements (rotations), etc… We choose the maximum structural ductility demand in the concrete column, μ_d related to the maximum curvature κ and yield curvature (tab. 3) through:

$$\mu_d = \frac{\max\{\kappa\}}{\kappa_y} \tag{1}$$

A set of 30 acceleration records has been chosen for the incremental dynamic analyses. The compilation of the suite of records has been given in [3]. The selected acceleration records are from relatively large-magnitude earthquakes (M = 6.5-6.9) with moderate distances and exhibiting no marks of directivity. Additionally, they have all been recorded on firm soil conditions. They represent a realistic earthquake scenario for the examined soil-structure system. Figure 3 presents the 5% damped response spectra of the suite of records.

The incremental dynamic analyses have been performed for every possible combination of the IMs and DMs. Each IDA analysis is made of 30 curves corresponding to the 30 time histories. A common feature to all IDA analyses is that some curves exhibit instabilities, [3], possibly followed by regain at higher levels, while other do not show any sign of instability, at least up to the highest tested IM. These kinds of curves are instructive because they clearly evidence the variability of the response as a function of the individual records, although all records are deemed to represent an almost unique earthquake scenario. The content of an IDA set is more compact and meaningful if, instead of individual curves, the median and some fractiles, for instance 16% and 84% fractiles, are presented, which can be further incorporated in a PBEE framework, [3]. IDA curves have been constructed for the three cases involving (or not) soil-structure interaction, namely:

- Nonlinear fixed-base structure
- Nonlinear structure with linear soil-structure interaction
- Nonlinear structure with nonlinear soil-structure interaction

As mentioned previously, it is anticipated that IMs that reflect the cumulative damaging effect of the earthquake are good proxies for correlation with a DM related to residual states (permanent settlement, permanent foundation rotation). Therefore ductility demand and permanent settlements have been related to CAV. On the other hand, DMs related to peak responses, like the maximum deck displacement, should be better correlated to the spectral acceleration at the fundamental period of the system.

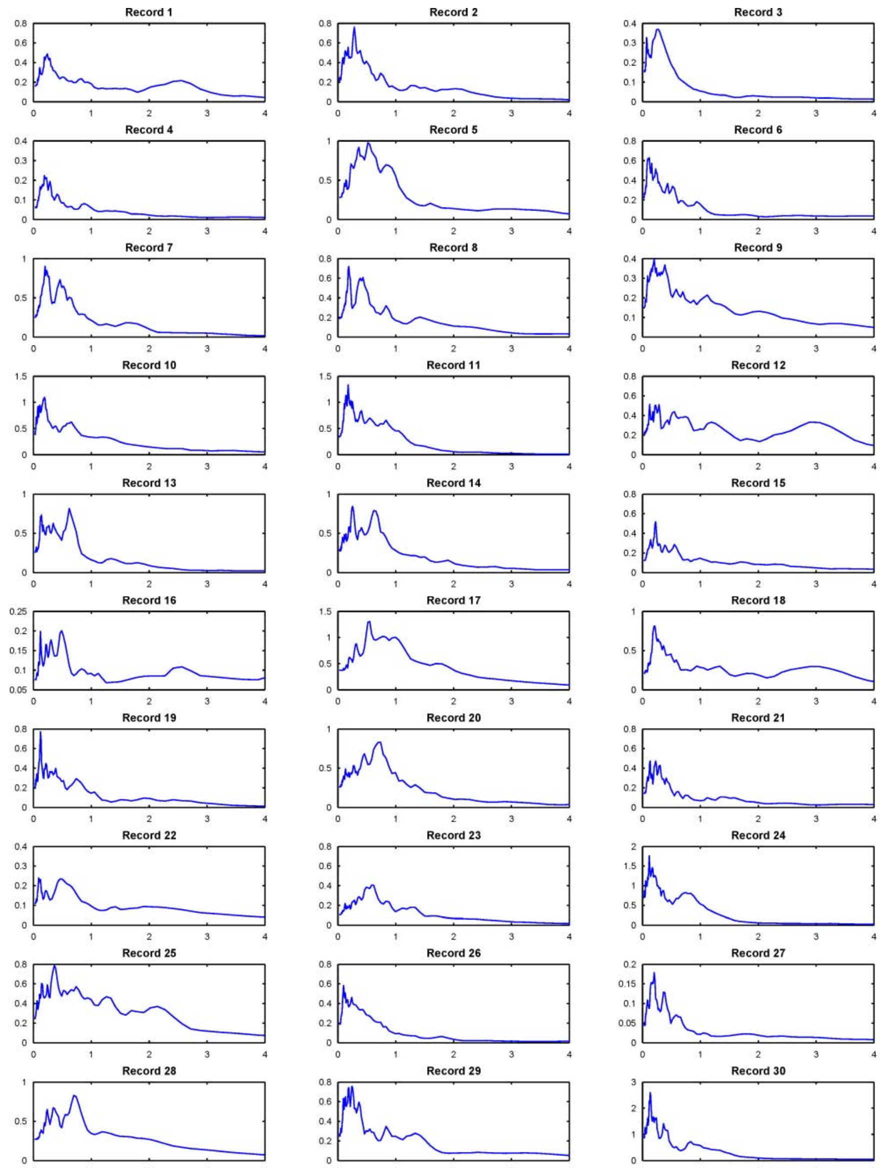

Figure 3. Acceleration response spectra of the suite of unscaled records

5.1 Typical results of an IDA analysis

A typical dynamic response produced with the macroelement is depicted in Figure 4 showing the variation during excitation of typical quantities: pier curvature versus bending moment, horizontal displacement and deck drift versus time, foundation rotation versus rocking moment and foundation settlement versus rotation.

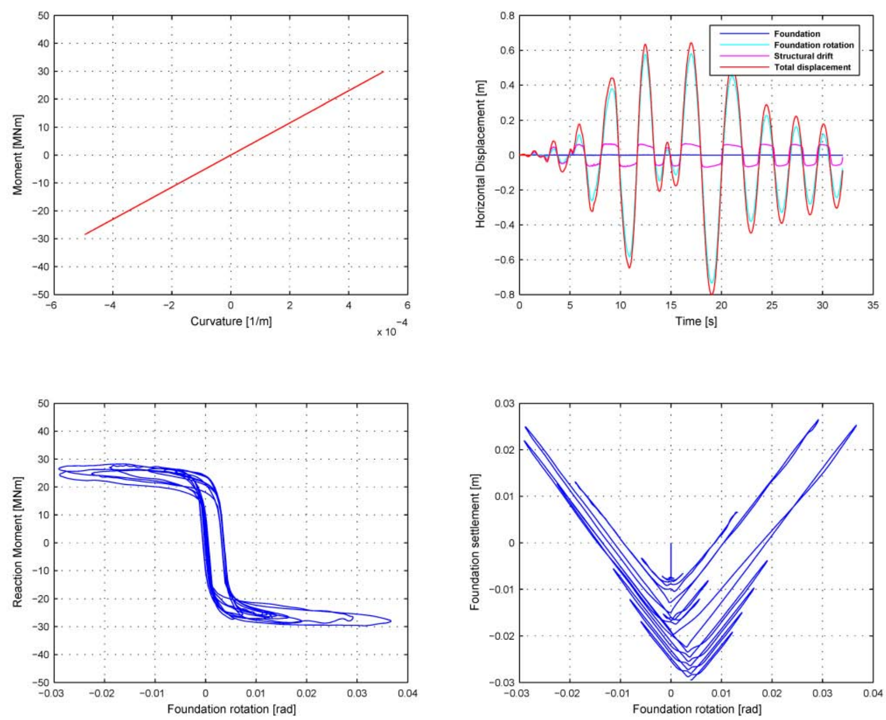

Figure 4. Example of a dynamic analysis with the macroelement; non-linear foundation, record 1, PGA=0.5g

This figure illustrates the capability of the macroelement to produce permanent settlement under horizontal excitation and uplift of the foundation, evidenced by the S-shaped of the moment-rotation diagram. The deck develops significant horizontal displacements almost entirely due to foundation rotation. However, the structure remains elastic as revealed by the moment-structural curvature diagram: it is clear that uplift acts as an isolation mechanism for the superstructure.

5.2 Statistical results

For each of the IDA set of curves, similar to those of Figure 4, statistical values corresponding to the median and to the 16% and 84% fractiles are computed. Comparisons are made in terms of structural behavior for the three possible assumptions for the foundation behavior: fixed-base structure, elastic linear foundation (linear SSI) and nonlinear behavior. All results are obtained with the macroelement model, with the proper options activated, and the nonlinear structural model for the structure. Due to space limitations, only few significant results are presented. They correspond to the ductility demand in the bridge pier, the permanent foundation settlement (for the nonlinear foundation). As mentioned previously the ductility demand and the residual settlements are related to the CAV.

Figures 5 to 8 present the statistical curves for the ductility demand for the three cases of foundation behavior. The overall behavior is not so different between the fixed-base structure and the linear elastic foundation: beyond a CAV of the order of 20, the ductility demand increases at a very rapid rate, denoting the onset of instability. It is interesting to note that up to a CAV of 10m/s, both systems produce the same median curve; for larger CAV, the ductility demand is slightly larger, for a given IM value, for the linear elastic SSI system indicating that SSI may not be favorable. This result is in line with the more extensive study of [7]. For the non linear foundation system, the behavior is strikingly totally different: up to a CAV of 35m/s, the ductility demand remains limited, of the order of 1.0, with no evidence so far of instability in the bridge pier.

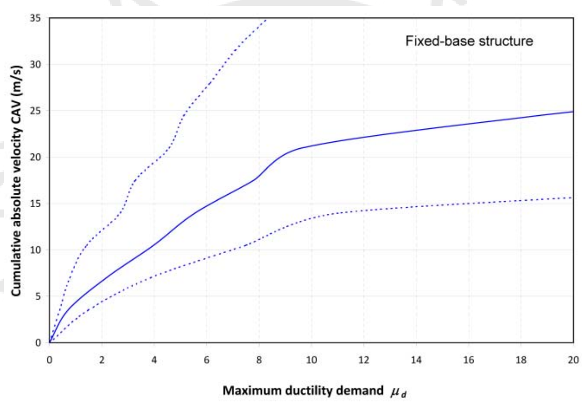

Figure 5. IDA curves for ductility demand versus CAV for the fixed-base structure. Thick curve: median, dotted curves: 16% and 84% fractiles

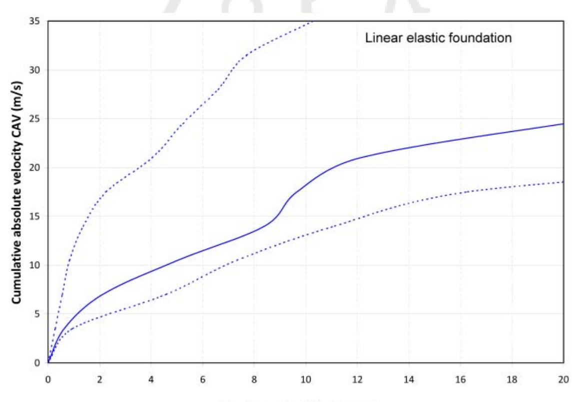

Figure 6. IDA curves for linear elastic foundation

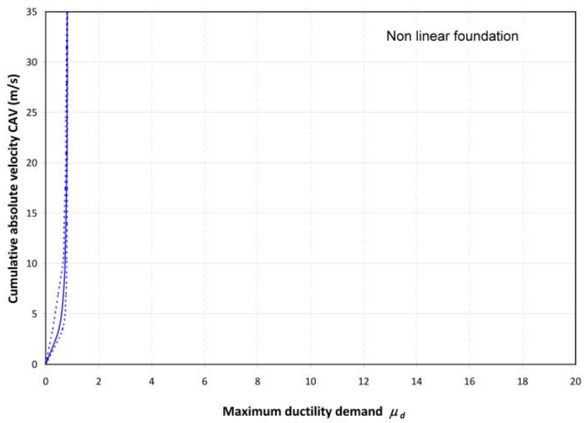

Figure 7. IDA curves for nonlinear foundation

The explanation for such a different behavior lies in the yielding of the foundation that protects the structure, as pointed out in [8]; the structure is prevented from yielding but permanent settlement and rotation are developed at the foundation. This is evidenced in Figure 8 showing the residual foundation displacement; obviously for the fixed-base structure and the linear SSI system no such values exist. The median maximum displacement remains limited but the variability increases drastically as the CAV increases; at the maximum CAV value the 84% fractile is 2.5 times the median. Therefore, foundation settlement may become highly unpredictable and can easily go from an acceptable quantity to an unacceptable one depending on the probability of exceedance the designer is ready to accept. This factor requires in depth consideration before accepting significant foundation yielding.

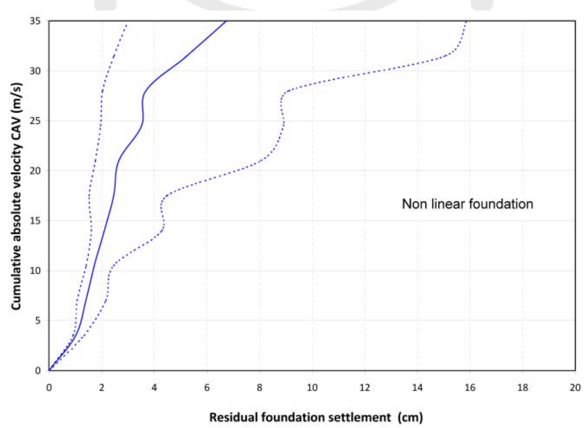

Figure 8. Residual foundation settlements versus CAV for non-linear foundation

Other results not shown herein exhibit the same trend: yielding of the foundation “protects” the structure but the price to pay is an increase of the maximum or permanent displacements and rotations of the foundation; more importantly, the variability in the computed response becomes large for the nonlinear SSI system when the IM is approaching the value for which the fixed-base structure or the linear SSI system show instabilities.

6 CONCLUSIONS

The development of a dynamic macroelement renders possible the use of extensive time history analyses to analyze the effect of foundation compliance and nonlinearity on the structural response of a nonlinear structure. The approach followed in this paper is based on the concept of incremental dynamic analyses which allows the derivation of statistical properties of the response. A simple bridge pier modeled either as a fixed-base structure, or founded on a foundation, for which linear or nonlinear soil structure interaction is considered, has served to illustrate the most salient features of the response. On a whole, consideration of nonlinear soil structure interaction appears beneficial to drastically reduce the ductility demand in the structure; however, this positive effect is counterbalanced by larger displacements and rotations at the foundation which may become unacceptable. Furthermore, it has been noticed that the variability in the response becomes large as more demand is placed on the foundation. Therefore, care must be exercised before accepting to transfer the ductility demand from the structure to the foundation. This implies a careful definition of acceptable criteria for the foundation displacement and rotation, and a thorough investigation of the variability of the response. As demonstrated in the paper the variability is conveniently handled with incremental dynamic analyses, which can be further incorporated in a performance based design approach. Nevertheless, this concept of allowing nonlinearities to develop in the foundation shows some promise as already pointed out in [2]. A final interesting finding of this study is that, as already shown in [7], consideration of linear soil structure interaction may not be always as beneficial as considered in practice.

ACKNOWLEDGMENTS

The work presented in this study has been carried out within the framework of the 7th framework European Research Project SERIES "Seismic Engineering Research Infrastructures for European Synergies" (Project No. 227887) and the research project DARE, which is funded through the European Research Council in Support of Frontier Research–Advanced (Grant, ERC–2–9–AdG228254–DARE). The financial support of the European Commission is gratefully acknowledged.

REFERENCES

[1] EC8 (2000) Design provisions for earthquake resistance of structures, part 5: foundations, retaining structures and geotechnical aspects, EN, 1998–5. European Committee for Standardization, Brussels, 2000.

[2] Gazetas, G, "Seismic design of foundations and soil–structure interaction". *Proc. 1st Eur Conf on Earthq Eng and Seismology*, Geneva, 2006

[3] Vamvatsikos, C, Cornell, C.A "Incremental Dynamic Analysis". Earthq Eng Str D Vol. 31, No. 3, pp491–514, 2002.

[4] Pecker, A, "Aseismic foundation design process, lessons learned from two major projects: the Vasco de Gama and the Rion Antirion bridges". *ACI Int Conf Seismic Bridge Design and Retrofit*, University of California at San Diego, La Jolla, USA, 2003.

[5] Papanikolas, P, Stathopoulos-Vlamis, A, Panagis, A, Pecker, A, Infanti, S, "The behavior of Rion – Antirion Bridge during the earthquake of "Achaia-Ilia" on june 8, 2008", *3rd Fib Intern. Congress,* 2010.

[6] Kausel, E, Roësset, JM, "Soil structure interaction problems for nuclear containment structures". *Proc. ASCE Power Division Conference*, Boulder, Colorado, 1974.

[7] Moghaddasi Kuchaksarai, M, Cubrinovki, M, Chase, J, Pampanin, S, Carr, A, "A Probabilistic Evaluation of Soil-Foundation-Structure Interaction Effects on Seismic Structural Response" Earthq Eng Str Dyn., Vol. 40, No. 2, pp135-154, 2011.

[8] Anastasopoulos, I, Gazetas, G, Loli, M, Apostolou, M, Gerolymos, N, "Soil failure can be used for seismic protection of structures". Bull Earthq Eng. Vol. 8, No. 2., pp 309-326, 2010.

[9] Paolucci, R, "Simplified evaluation of earthquake-induced permanent displacement of shallow foundations. J Earthq Eng, Vol. 1, No.3, pp563–579, 1997.

[10] Pecker, A, "Capacity design principles for shallow foundations in seismic areas". *Proc. 11th Eur Conf Earthq Eng*, 1998

[11] Martin, GR, Lam, IP, "Earthquake resistant design of foundations: retrofit of existing foundations". *Proc. GeoEng 2000 Conf*, Melbourne, 2000.

[12] Gazetas, G, Apostolou, M, Anastasopoulos, I, "Seismic uplifting of foundations on soft soil, with examples from Adapazari (Izmit 1999, Earthquake)". *BGA Int Conf on Found Innov, Observations, Design & Practice*, Univ. of Dundee, Scotland, pp 37–50, 2003.

[13] Gajan, S, Kutter, BL, "Capacity, settlement, and energy dissipation of shallow footings subjected to rocking". J Geotech Geoenviron Eng ASCE Vol. 134, No. 8, pp1129–1141, 2008.

[14] Priestley, MJN, Calvi, GM, Kowalski, MJ, *Displacement-based seismic design of structures*, IUSS Press Pavia, 2007.

[15] Figini, R, "Nonlinear dynamic soil-structure interaction: Application to seismic analysis and design of structures on shallow foundations". PhD thesis, Politecnico di Milano, 2010.

[16] Chatzigogos, CT, Pecker, A, Salençon, J, "Macroelement modeling of shallow foundations". Soil Dyn Earthq Eng, Vol. 29, No. 6, pp765–781, 2009.

[17] Chatzigogos, CT, Figini, R, Pecker, A, Salençon, J, "A macroelement formulation for shallow foundations on cohesive and frictional soils. Int J Numer Anal Meth Geomech., doi 10.1002/nag.934, 2010.

[18] Chatzigogos, CT, "Comportement sismique des fondations superficielles: vers la prise en compte d'un critère de performance dans la conception". PhD thesis, Ecole Polytechnique, 2007

[19] Dafalias, YF, Hermann, LR, "Bounding surface formulation of soil plasticity". In: Pande GN, Zienkiewicz OC (eds) *Soil Mechanics – transient and cyclic loading*, Wiley, 1982.

[20] Gazetas, G, Foundation Vibrations. In: Fang HY (ed) *Foundation Engineering Handbook*, 2nd edn. Van Reinhold Rostrand, 1991.

[21] Chatzigogos, CT, Pecker, A, Salençon, J, "Seismic bearing capacity of a circular footing on a heterogeneous cohesive soil". Soils Found, Vol. 47, No. 4, pp783-797, 2007.

INNOVATIVE EARTHQUAKE-RESISTANT BRIDGES
Repair, Connections, and Materials

M. Saiid Saiidi[1], A. Vosooghi[2], A. Zaghi[3], S. Motaref[4], and C. Cruz[5]

[1,2,4] University of Nevada at Reno (UNR), Dept. of Civil Engineering, USA
[3] University of Connecticut, Dept. of Civil Engineering, USA
[5] Carleton University, Dept. of Civil Engineering, Canada
e-mail: saiidi@unr.edu, ashkan@unr.edu, zaghi@engr.uconn.edu, s.motaref@gmail.com, cruznogu@gmail.com

ABSTRACT: This paper presents the highlights of several studies on seismic performance of bridges. The results showed that novel repair methods using fiber-reinforced polymer jackets, pipe pin connections, superelastic shape memory alloys, fiber-reinforced grouts, and built-in elastomeric pads successfully resisted earthquake forces while substantially reducing damage.

KEY WORDS: Bridge; Elastomeric pads; Fiber-reinforced concrete; Pipe pins; Shape memory alloys.

1 INTRODUCTION
The driving force behind innovation may be merely curiosity or search for a solution to a known problem. Whereas innovation in science is often is instigated by curiosity, innovation in engineering is linked to potentially practical solutions to problems that are either clearly or vaguely defined. The purpose of this paper it to briefly describe several innovative approaches related to the seismic performance of bridges. The paper presents the highlights of several research projects focused on repair and detailing of highway bridges using novel concepts or advanced materials such as fiber-reinforced polymer (FRP) materials, elastomeric plastic hinges, shape memory alloys, and high-performance fiber-reinforced cementitious materials.

2 REPAIR OF EARTHQUAKE-DAMAGED COLUMNS
2.1 Background
Standard modern reinforced concrete bridge columns are designed to resist earthquake demand through nonlinear action associated with yielding of reinforcement and damage to concrete. The performance objective in these columns under strong earthquakes is to undergo several cycles of nonlinear deformations, yet continue to carry vertical loads, thus preventing bridge

collapse. Appropriate design and detailing methods have been developed for columns to achieve this objective. However, until recently, little attention was given to the post-earthquake function of the bridge and means to restore service. Considering the potential tremendous impact that out-of-commission bridges could have on the community and emergency response traffic, there is a need for rapid repair of earthquake damaged columns and, at least, a temporary restoration of service. The purpose of this study was to determine the feasibility of repairing earthquake damaged bridge columns within a week using carbon fiber reinforced polymer (CFRP) sheets. Details of the study are presented in reference [1].

2.2 Repair Strategy

The column damage can vary depending on the intensity of the earthquake and the force and deformation demand placed on the column. Different damage levels warrant different repairs. Because the focus of the project was on rapid repair, it was felt that evaluation of the damage should be based the visual appearance of the damaged column rather than specialized non-destructive testing, which is time consuming. An extensive data base of past shake table tests of bridge columns was compiled that correlated the apparent damage to various response parameters. Five damage states were identified ranging from flexural cracks to start of core damage. For example, Fig. 1 shows damage state 4 defined as when the reinforcing bars are exposed. Damage associated with fractured bars were excluded because it was felt that these columns cannot be generally repaired rapidly. Therefore, the repair needed to restore only the shear capacity and confinement of the column, both of which are accomplished by FRP jackets with horizontal fibers. Only CFRP was considered because previous studies have indicated that it is as effective as other jackets while being durable.

2.3 Test Models and Repair

Five large-scale models were tested on a shake table under simulated earthquakes of successively increasing amplitude until the columns reached the highest repairable damage state. The original columns were not tested to failure. Three of the models represented columns designed based on current codes and two represented substandard columns. Both low-shear and high-shear columns were included in each group. Following the testing of the original columns, they were repaired and retested using the same loading protocol as that of the original column. However, additional earthquakes with higher intensities were applied on the repaired models until failure.

The repair work consisted of straightening the models to less than 1% drift, removing lose concrete, injecting the cracks with high pressure epoxy, applying high-strength grout, applying CFRP jackets, curing the jacket under high temperature for 24 hours, and curing the jacket for another 24 hours under the laboratory temperature before testing. Fig. 2 shows curing of one of the test models under elevated temperature. The jacket thickness was designed using seismic retrofit guidelines in the initial test models. However, the requirements were reduced because the measured data indicated that existing spirals and concrete even in damaged columns significantly contribute to the column capacity. The complete repair work was done in four days. Both the original and repaired models were heavily instrumented to determine the response.

2.4 Results

Elasto-plastic idealized envelopes of the measured hysteretic force-displacement relationships were used to estimate the strength and stiffness of the column models. Figure 3 shows force-displacement relationship of one of the high shear standard bridge column models. The measured lateral load strength of the original column was 90.5 k (402.5 kN) and that of the repaired column was 90.3 k (401.6 kN). Since the original column model was not tested to failure, its drift capacity was extrapolated using a relationship developed in previous studies [2]. The estimated drift capacity of the original column was 9.0 %. The measured drift capacity of the repaired column was 13.1%. The initial stiffness of the original and the repaired columns were 71.6 k/in. (12.5 kN/mm) and 27.2 k/in. (4.76 kN/mm), respectively. These results along with those of the other column models indicated that the strength and ductility of the standard columns were successfully restored and those of sub-standard columns were upgraded to the current seismic standards after the repair. However, the initial stiffness was not restored due to material degradation during the original column tests.

Based on the results from the experimental and analytical studies, repair design recommendations were developed and design charts were prepared to aid bridge engineers in quickly designing the number of layers of CFRP fabrics based on the apparent damage and basic information about the column fixity, size, and reinforcement.

3 PIPE PIN HINGES

3.1 Background

Reinforced concrete bridge columns are often detailed to act as a hinge either at the top or bottom connection to minimize or eliminate moment transfer to either the cap beam or the footing. The common reinforced concrete hinge detail consists of a group of longitudinal bars placed near the center of a reduced column section with a gap that is filled with construction materials. This detail inevitably transfers some moment. Furthermore, under moderate and strong earthquakes the hinge may be damaged, but is difficult to inspect or repair the hinge due to a lack of access to the reduced section. A new column hinge detail utilizing steel pipes has been developed and used is several bridges in earthquake prone regions of California (Fig. 4). In this connection, a steel pipe is embedded in the column with the top part protruding out of the column. The hollow pipe at the center of the column in Fig. 4 is the pipe pin. The plastic pipe on the left is to pass electric wires and is non-structural. A steel can in the superstructure accommodates the protruded pipe (Fig. 5). Column shear is transmitted through the pipe and vertical load is transmitted through the hinge throat shown in Fig. 5. The purpose of the study was to determine the shear resisting mechanism of pipe-pin connections and to develop a design procedure under seismic loading. More details about the study are presented by Zaghi and Saiidi [3, 4].

3.2 Experimental and Analytical Studies

The preliminary procedure used to design pipe pins in existing bridges considered only the pure shear failure of pipe. To investigate the performance of pipe-pin connections, three sets of test models were designed to determine (a) the behavior of pipe pins embedded in concrete members representing the column and pier cap through single column and push test models, (b) behavior of in-filled steel pipes under pure shear, and (c) performance of pipe pins designed using a method developed as part of this study through shake table testing of a two-column pier model. Extensive analytical studies were also conducted using different computer programs of different sophistication to understand the behavior of the models and to conduct parametric studies of all the factors that were not included in the tests. Figure 6 shows one of the push test models. The segment in the right was connected to the segment on the left through a concrete filled steel pipe. The analytical studies consisted of global analysis of pinned column response using SAP 2000, detailed finite element analysis of column and push models using ABAQUS, and global analysis of the pier model using OpenSEES. Upon successful modeling of the push specimens, ABAQUS was used for extensive parametric studies, and the effect of all the important factors was determined. A modified pipe-pin hinge detail was devised and a practical design method was developed incorporating the results of the tests and parametric studies. The new method was used to design pipe pins at column pier cap connection of a two-column pier model subjected to several simulated earthquake records of increasing amplitude on a shake table.

3.3 Results

Fig. 7 shows the measured and calculated lateral load-displacement response of single hinged column test model. It is evident that all the essential features of the measured response were captured by the analytical model. Evaluation of the test and parametric results led to identification of three failure mechanisms for pipe-pin hinges as shown in Fig. 8. Mode “a” engages concrete at the diagonal crack, the spiral around the pipe (Fig. 5), and the column spiral. Mode “b” is controlled by the bearing failure of concrete against the edge of the pipe. The bearing strength was determined based the push test results of this study. Mode “c” was the only failure mode assumed in the tentative design procedure. However, a new equation was developed for this mode based on the results of the concrete filled steel pipe tests conducted in this study. The design recommendations from this study included provisions for pipe diameter, embedment length and protruded length, the hinge throat diameter and thickness, pipe pin spiral, and column spiral. Furthermore, it was recommended that no pipe studs (Fig. 5) be used. The shake table test results showed that the seismic performance pipe pins designed based on the new method was satisfactory as shown in Fig. 9.

4 COLUMNS WITH ADVANCED MATERIALS

4.1 Background

As stated in Sec. 2.1, modern bridge columns in standard bridges are expected to become nonlinear due to yielding of steel and spalling of concrete during strong earthquakes but should be able to carry vertical loads. Yielding of steel and damage to concrete are often associated with permanent drift largely because of residual strain of the steel. While collapse prevention saves lives, it does not address serviceability of the bridge following an earthquake. Damaged bridges are taken out of commission after the earthquakes severely jeopardizing disaster recovery operation and affecting the economic well being of the community, often impacting the region and beyond. Performance-based design may be used for conventional construction to address the serviceability of the bridge after strong earthquakes. An alternative approach is to use advanced materials to reduce residual drift and damage. Several studies have been undertaken at the University of Nevada, Reno (UNR) to address these issues in bridge columns. Superelastic shape memory alloy (SMA) reinforcement, elastomeric plastic hinges, and engineered cementitious composite (ECC) have been used in various studies to determine their effectiveness in minimizing permanent lateral drift and damage in critical regions of reinforced concrete columns. The highlights of some of these studies are presented in this section.

4.2 Shape Memory Alloy

Shape memory alloys are able to fully recover deformations even after yielding through application of external heat or removal of stress. The latter group, known as superelastic materials, was the subject of the UNR studies. The focus of the study has been on Nickel-Titanium SMA or Nitinol (NiTi). The yield stress of NiTi can be approximately the same as that of 400 MPa steel, but its modulus of elasticity is approximately one-third of the steel modulus. A typical stress-strain relationship for superelastic NiTi is shown in Fig. 10. Upon yielding slight strain hardening is observed. At a strain of six percent major strain hardening occurs. When the stress is released, the stress-strain curve relationship follows a path that leads to a flag-shaped response. The area within the curve presents the dissipated energy. SMA is hence able to dissipate the earthquake energy, but with no residual strain once the stress is removed. The effectiveness of deformation recovery of SMA bars used as reinforcement in concrete members was investigated. Details of the studies are presented in [5, 6, 7, and 8].

4.3 Engineered Cementitious Composites (ECC)

The low tensile strength of concrete is responsible for its cracking and spalling. Various fiber types have been added to concrete mixes to address this issue. Among these fibers is a polyvinyl fiber with special coating that allows for partial slippage and formation of microcracks but hardens and prevents widening of the crack. As a result new microcracks are formed. The relatively large number of microcracks enables the material to maintain tensile stresses up to strains of 3 to 5%, which is substantially higher than the tensile strain capacity of conventional concrete. A cement-based grout incorporating polyvinyl fibers by 2% volume, known as ECC, was studied in several bridge columns under earthquake loading to determine the effectiveness of ECC in reducing column damage under large deformations. Details of the study are presented in [5, 7, 8, and 9].

4.4 Elastomeric Plastic Hinges

Because of their low modulus of elasticity, elastomeric materials can undergo large deformations without damage. They have been used in seismic isolators for several decades, in which they help soften the structure through their shear deformation, thus elongating the vibration period and reducing seismic forces. A new application of elastomeric pads was explored in Ref [10] by replacing part of the concrete in the plastic hinge of columns with rubber. Unlike seismic isolation, elastomeric pads acted mainly in flexure in this application. The column reinforcement was passed through the pad, and the pad was post-tensioned. The detail was successful in that there was no damage in the elastomeric pad under cyclic loads. However, at drift ratio of 3% the longitudinal column bars began to buckle and failed under low-cycle fatigue. The pad did not provide sufficient lateral restraint against buckling of the longitudinal reinforcement. A modified version of the pad was developed at UNR by incorporating steel shims in the pad while increasing the thickness to approximately one-half the column diameter. To eliminate shear deformation an unbounded central steel pipe was included (Fig. 11). Studs were welded to the end plates of the pad to anchor it to the concrete above and below the pad. Similar to the pad in Ref. [10] the longitudinal column bars passed through the pad and the columns were post tensioned. More details about the design and properties of the pad are provided in [8 and 9].

4.5 Experimental and Analytical Studies

The initial studies of SMA-reinforced beams consisted of testing a series of simply-supported reinforced concrete beams subjected to symmetric two-point loading with SMA or steel reinforcement in the constant moment region. The objective of the study of the beams was to determine the deflection recovery characteristics of SMA-reinforced concrete members. Because of promising results the study was extended to cantilever reinforced concrete columns with longitudinal SMA reinforcement in the plastic hinge zones. Superelastic SMA bars were used to reduce permanent drift of the columns under lateral cyclic loads. To minimize earthquake damage, the effectiveness of ECC in the plastic hinge was also explored both in original and repaired column models. Some of the column models were subjected to slow cyclic loading and others were tested on a shake table under simulated earthquakes. The study of combined SMA/ECC columns was extended to the bottom plastic hinges in one of the piers of a 33-m long, four-span bridge model tested on shake tables. The bridge model was subjected to bi-directional motions simulating one of the 1994 Northridge earthquake records. The top plastic hinges in the same columns were constructed of conventional reinforced concrete.

The damage resistance of ECC to dynamic excitations was also evaluated in two other shake table studies, one involving segmental columns and the other a precast reinforced concrete column in which concrete in the plastic hinge was replaced by ECC. Steel reinforcement was used in these models. In both cases similar models made with conventional concrete had been tested and hence benchmark data existed. The lateral reinforcement in all cases was made of steel and met current seismic code requirements.

The performance of elastomeric plastic hinges was investigated in two studies one on segmental columns and the other in the bottom plastic hinges of one of the piers of the aforementioned four-span bridge model. The details of the elastomeric element were the same on both cases (Fig. 11).

In all studies OpenSEES computer program was used for extensive analytical modeling and parametric studies of the of the test models prior to finalizing the design and loading of the test models and after the completion of the tests.

4.6 Results

A sample measured lateral load-drift hysteretic behavior of a column with SMA/ECC at the plastic hinge is shown in Fig. 12. It is evident that loading performance of the column is what is normally expected of conventional reinforced concrete columns. The initial parts of the unloading curves are also similar to those of steel-reinforced concrete columns. However, as the unloading curves approach the horizontal axis they bend towards the origin, thus leading to a very small permanent drift as they cross the axis. This feature is drastically different than that of conventional RC members, which exhibit relatively large drifts at zero force. The damage in the upper and lower plastic hinges of the columns with SMA/ECC at the bottom plastic hinges at the conclusion of testing the four-span bridge is shown in Fig. 13. It can be seen that there was substantial spalling in the conventional construction at the top of the column exposing longitudinal and transverse reinforcement. Furthermore a large number of other flexural cracks turning to shear cracks formed as can be seen in the left photo in Fig. 13. In contrast the damage in the SMA/ECC plastic hinge was minimal with minor cracking and spalling (the right photo in Fig. 13).

The contrast between the performance of ordinary concrete and ECC can also be seen in damage in Fig. 14 and in the envelopes of the measured force-displacement relationships in Fig. 15. The damage was initiated at the junction of the base segment and the adjacent segment due to the compressive failure of the concrete or ECC. It is clear in Fig. 14 that concrete damage was substantially more extensive in terms of the surface area and depth of damage than the damage in ECC. Figure 15 shows the degradation of the lateral load capacity in SC-2 (with concrete) starting at approximately 80 mm lateral displacement. It can be seen that SE-2 (with ECC) was able to maintain its strength up to 170 mm and degradation after this displacement was at a much lower rate.

No damage was observed in elastomeric plastic hinges in testing of the 4-span bridge model or the cantilever segmental column. Testing of the 4-span bridge was terminated due fracture of steel reinforcement in the top plastic hinges constructed with conventional RC. The bottom plastic hinges that were constructed with built-in elastomeric pads experienced no damage in the rubber and only minor cracks in the adjacent concrete (Fig. 16).

5 CONCLUSIONS

Rapid restoration of earthquake-damaged bridges was found to be possible using fiber-reinforced polymer fabrics with accelerated curing. The summary results presented in this article also demonstrated that a new paradigm of damage-free bridges is feasible in earthquake-resistant design of bridges by using advanced materials and details. Through innovation in detailing and materials it is possible to eliminate or substantially reduce earthquake damage while accomplishing satisfactory performance under strong earthquakes. Specifically, pipe-pin hinges were found to be satisfactory alternative for two-way hinge construction in bridge column ends. Furthermore, a superelastic Nickel-Titanium alloy showed that it could replace reinforcement steel in plastic hinges and help the structure recover lateral deformation. The fiber-reinforced grout, or the ECC, experienced substantially less damage during demanding shake table tests discussed in this paper and its strength degradation was minor. Finally, built-in elastomeric pads in column plastic hinges were found to remain completely free from damage even under large rotational demand.

ACKNOWLEDGMENTS

The studies presented in this article were funded by the National Science Foundation (Grants CMS-0420347, CMMI-0650935, and CMS-0402490) and various grants from the California Department of Transportation.

REFERENCES

[1] Vosooghi, A. and M., Saiidi, “Post-Earthquake Evaluation and Emergency Repair of Damaged RC Bridge Columns Using CFRP Materials,” Report No. CCEER-10-05, Center for Civil Engineering Earthquake Research, Dept. of Civil Eng., Univ. of Nevada, Reno, September 2010.

[2] Vosooghi, A. and M., Saiidi, “Seismic Damage States and Response Parameters for Bridge Columns,” ACI Special Publications, Series SP-271, Structural Concrete in Performance-Based Seismic Design of Bridges, SP-271-2, pp. 29-46, May 2010.

[3] Zaghi, A., and M. Saiidi, “Seismic Performance of Pipe-Pin Two-Way Hinges in Concrete Bridge Columns,” Journal of Earthquake Engineering, Vol. 14, No. 8, pp. 1253-1302, December 2010.[4] Zaghi, A., and M. Saiidi, “Bearing and Shear Failure of Pipe-Pin Hinges Subjected to Earthquakes,” Journal of Bridge Engineering, ASCE, Vol. 16, No. 3, pp. 340-350, May/June 2011.

[5] Saiidi, M., and H. Wang, “An Exploratory Study of Seismic Response of Concrete Columns with Shape Memory Alloys Reinforcement,” American Concrete Institute, ACI Structural Journal, Vol. 103, No. 3, May-June 2006, pp. 436-443, May-June 2006.

[6] Saiidi, M., M. Zadeh, C. Ayoub, and A. Itani, “A Pilot Study of Behavior of Concrete Beams Reinforced with Shape Memory Alloys,” Journal of Materials in Civil Engineering, ASCE, Vol. 19, No. 6, June 2007, pp. 454-461.

[7] Saiidi, M., M. O’Brien, and M. Zadeh, “Cyclic Response of Concrete Bridge Columns Using Superelastic Nitinol and Bendable Concrete,” American Concrete Institute, ACI Structural Journal, Vol. 106, No. 1, January-February 2009, pp. 69-77.

[8] Cruz, C., and M. Saiidi, “Shake Table Studies of a 4-Span Bridge Model with Advanced Materials,” In press, Journal of Structural Engineering, ASCE.

[9] Motaref, S., M. Saiidi, and D. Sanders, “Seismic Response of Precast Bridge Columnswith Energy Dissipating Joints,” Center for Civil Engineering Earthquake Research, Department of Civil and Environmental Engineering, University of Nevada, Reno, Nevada, Report No. CCEER-11-1, May 2011, 760 pp.

[10] Kawashima, K. and Watanabe, G. [2006]. “Seismic Performance of Unbonded Columns and Isolator Built-in Columns based on Cyclic Loading Tests,” Proceedings, International Association of Bridge Management and Safety (IABMAS), Porto, Portugal.

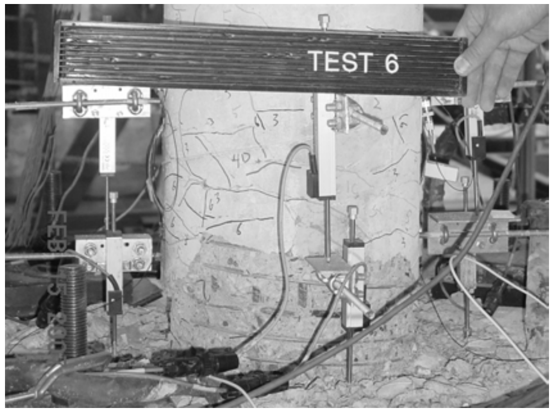

Figure 1. Exposed steel reinforcement (damage state 4)

Figure 2. Accelerated curing of CFRP jacket

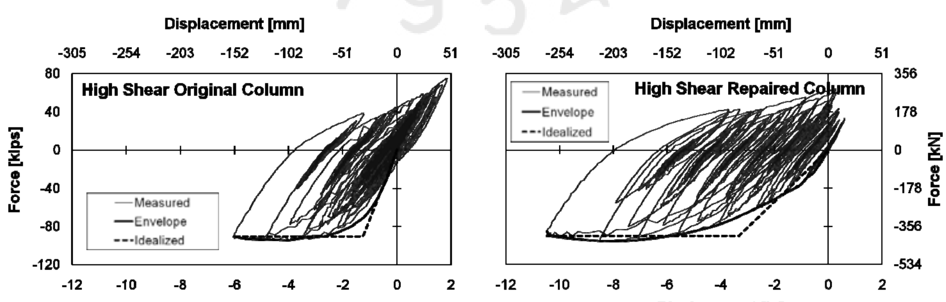

Figure 3. Force-displacement relationships for a high shear standard column

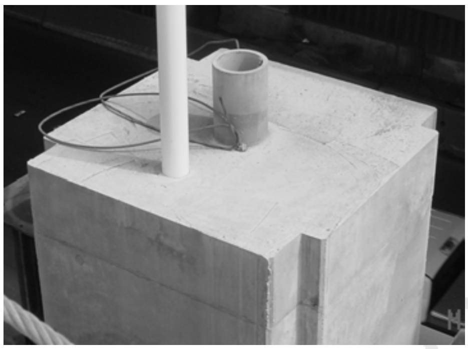

Figure 4. Pipe pin at top of a bridge column in San Francisco

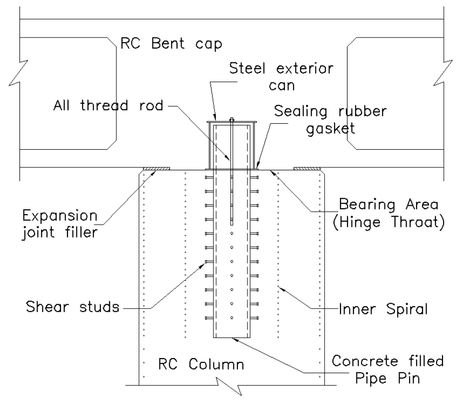

Figure 5. Detail of original pipe-pin connection

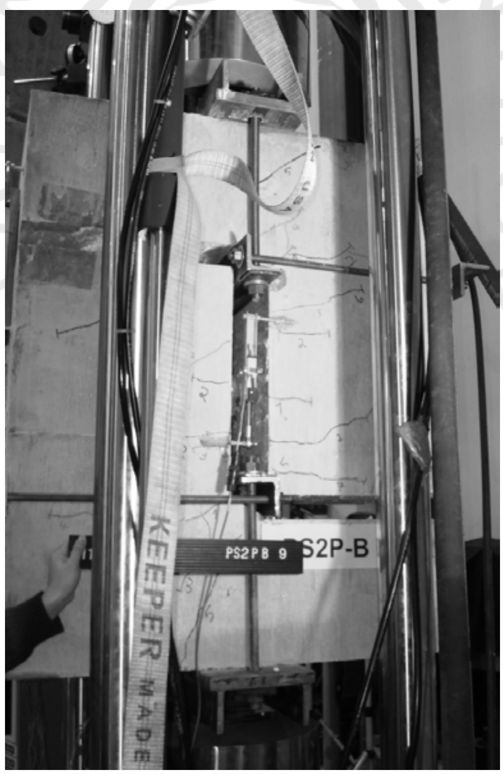

Figure 6. A sample push specimen

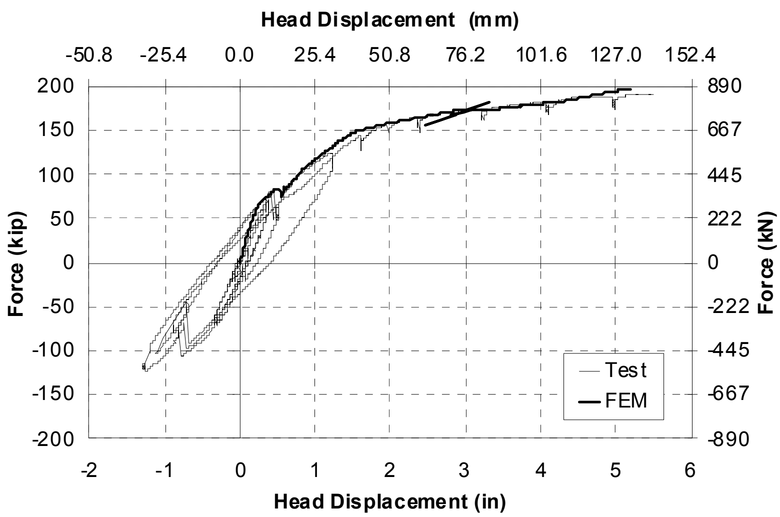

Figure 7. Measured and calculated response of single pinned column

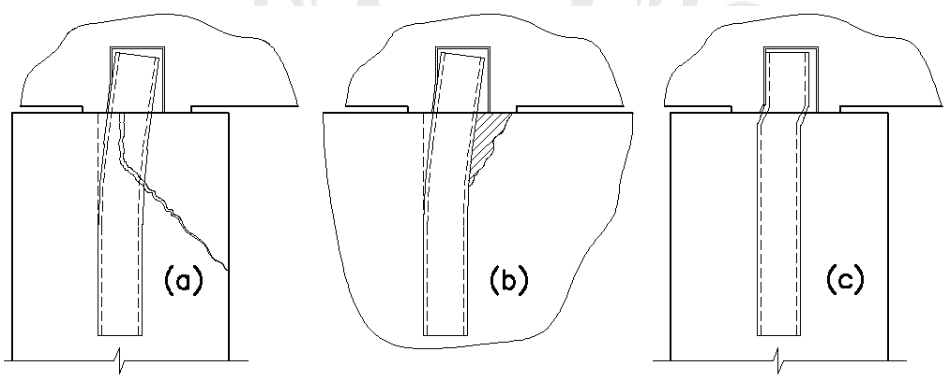

Figure 8. Failure modes of pipe-pin Hinges: (a) Diagonal tension (b) Bearing, and (c) Pure shear

Figure 9. Pipe-pin connection at conclusion of pier test

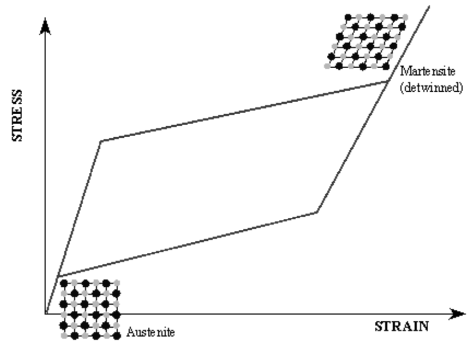

Figure 10. Superelastic behavior

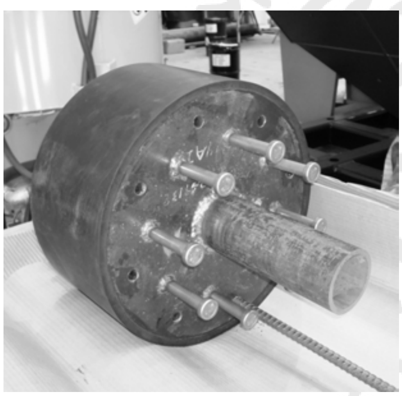

Figure 11. UNR elastomeric plastic hinge

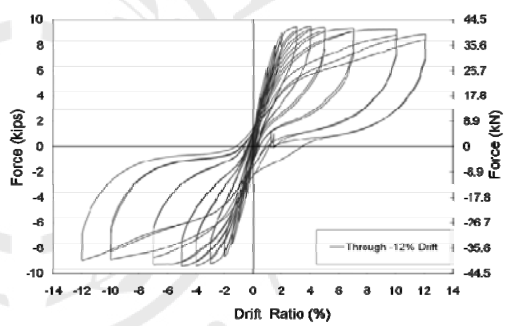

Figure 12. Performance of column with SMA/ECC plastic hinge

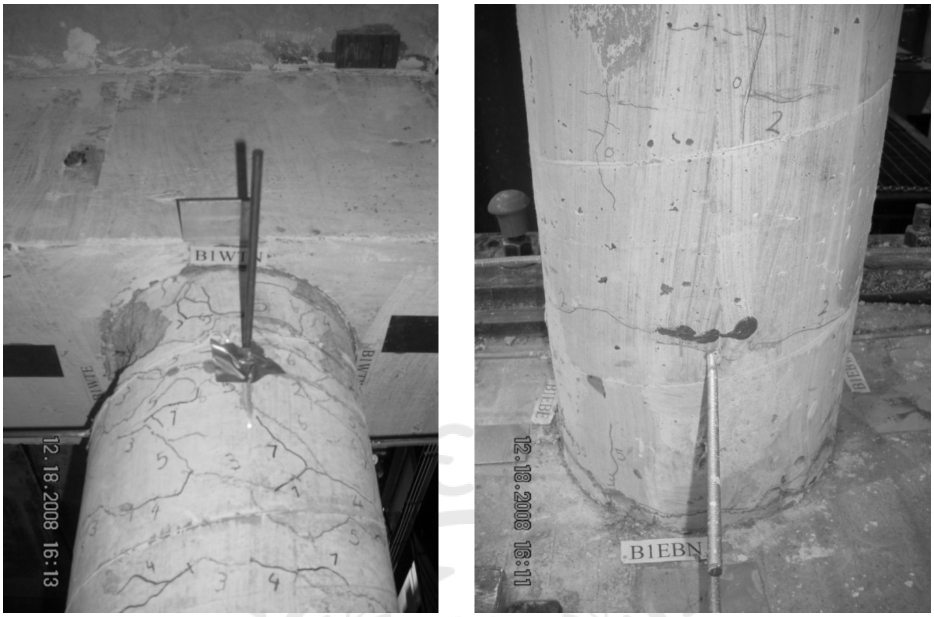

Figure 13. Damage at RC (left) and ECC (right) plastic hinges in 4-span bridge column

Figure 14. Damage at RC (left) and ECC (right) plastic hinges of segmental columns

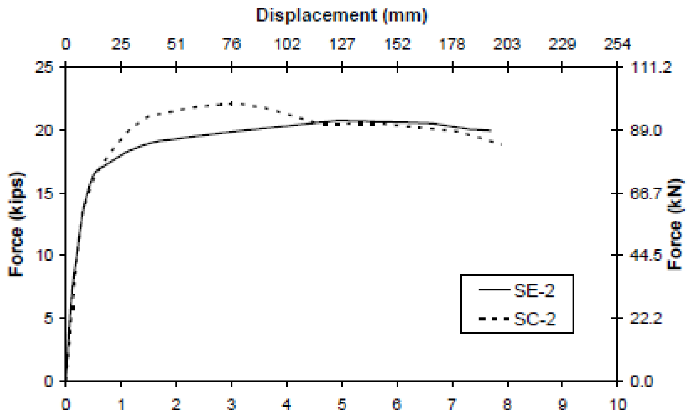

Figure 15. Measured response envelopes of RC (SC-2) and ECC (SE-2)

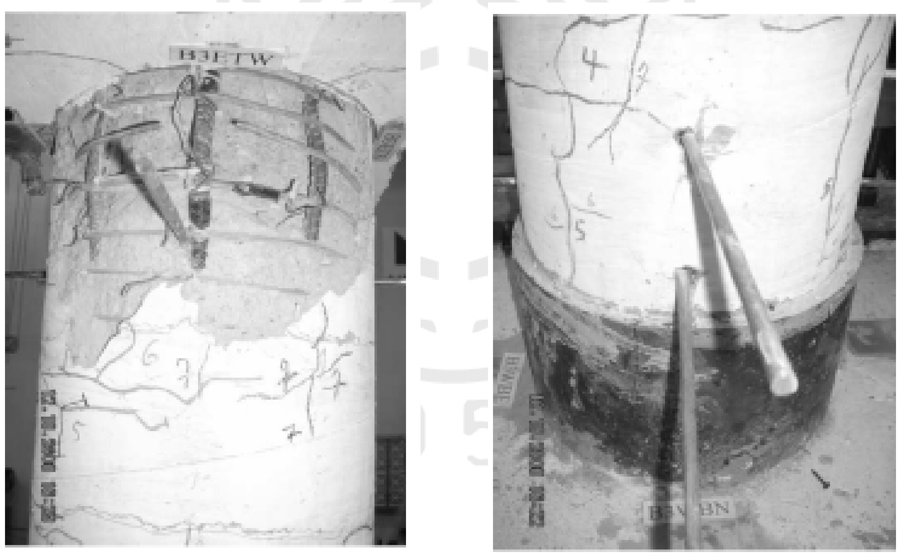

Figure 16. Damage at RC (left) and rubber (right) plastic hinges of 4-span bridge

TOPIC 1

Seismic Behaviour

Isolation and Damping Systems

"COMPLETE SIMILARITIES" IN THE RESPONSE OF SEISMIC ISOLATED BRIDGES

Nicos Makris[1] and Michalis F. Vassiliou[2]

[1,2] Dept. of Civil Engineering, University of Patras, Greece, GR26500
nmakris@upatras.gr, mfvassiliou@gmail.com

ABSTRACT: In this paper the seismic response of isolated bridge decks supported on bearings with trilinear behavior is revisited in an effort to better understand the relative significance of the involving various parameters. For the case of trilinear behavior the paper shows that the presence of the intermediate slope is immaterial to the peak response of most isolated structures–a finding that shows that the response of the trilinear oscillator exhibits a complete similarity in the difference between the coefficients of friction along the two sliding surfaces as well as in the ratio of the intermediate to the final slope. This finding implies that even with different coefficient of friction, the response of the structures for most practical configurations can be computed by replacing the double concave spherical bearings with single spherical bearings with effective radius of curvature and coefficient of friction.

KEY WORDS: Seismic Protection, Bridges, Dimensional Analysis, Earthquake Engineering, Spherical Sliding Bearings

1 INTRODUCTION

During the last three decades, seismic isolation enjoyed substantial growth, major improvements in its performance and an increasing worldwide acceptance (Kelly 1998[1]). Several design documents are now available guidelines on design structures with this new seismic protection technology (FEMA[2], AASHTO 1999[3], ICB 2000[4]. The most widely used isolation bearings are the lead rubber bearings (Kelly 1998 [1]) and the spherical sliding bearings (Constantinou et al. 1998[5]). Until the early years of this decade most spherical sliding bearings used involved only a single concave sliding surface, and the bilinear model was sufficient to approximate the behavior of both lead rubber and sliding spherical bearings. The rapid growth of seismic isolation generated the need for more compact size, long period bearings. These are served with the double concave spherical sliding bearing–see Figure 1 (Tsai et al. 2005[6], Fenz and Constantinou 2006[7], Tsai et al. 2006[8]). When the double concave spherical bearing has sliding surfaces with the same coefficient of friction, μ, (no need for same radii of curvature) it becomes like a traditional single concave spherical bearing with isolation period $T_b = 2\pi\sqrt{\frac{R_1 + R_2 - h_1 - h_2}{g}}$ and coefficient of friction μ. When the coefficients of friction are different, the behavior of the DCSS bearing is trilinear and it can be modeled using two traditional SCSS bearings acting on series together with a point mass representing the articulated slider. With this mathematical model one can capture the shaved portions of the hysteretic loops at the initiation and at the reversal of motion when, initially, the sliding surface with the lower coefficient of friction is mobilized. Nevertheless, the implementation of two spring–slider elements in series may challenge the convergence of commercially available software, used by practitioner engineers. In this paper it is shown that when trilinear behavior prevails the presence of the intermediates slope, k_{tr}, and the shaving of the loops when the motion reverses, is immaterial to the response of the isolated superstructure for most practical values of the coefficients of friction used in seismic isolation. In more rigorous mathematical terms this finding shows that the response of the trilinear oscillator exhibits a complete similarity in the difference of the coefficient of friction along the two sliding surfaces as well as in the ratio of the intermediate to the final slope. This finding implies that under strong shaking an isolated bridge exhibits the same maximum displacement regardless whether it is supported on a double concave (R_1-h_1, R_2-h_2, μ_1, μ_2) or single concave (R_e,μ_e) spherical sliding bearing provided that

$$\frac{1}{R_e} = \frac{1}{R_1 + R_2 - h_1 - h_2} \quad \text{and} \quad \mu_e = \frac{\mu_1(R_1 - h_1) + \mu_2(R_2 - h_2)}{R_1 + R_2 - h_1 - h_2} \tag{1}$$

The existence of this complete similarity has practical significance since it eliminates the need of implementing two spring-slider elements in series and the analysis may be performed for all practical purposes with an equivalent single concave spherical sliding bearing. The permanent displacement that results from the equivalent single spherical bearings can be either smaller or larger than that resulting from the double spherical bearings, depending on the ground motion.

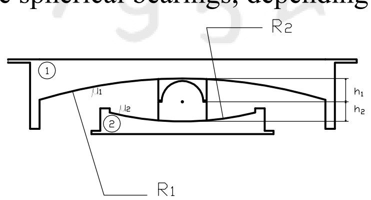

Figure 1. Crossection of a double concave spherical sliding bearing with different radii of curvature

2 PARAMETERS OF THE TRILINEAR SDOF OSCILLATOR

Our study proceeds with the dimensional analysis of the dynamic response of the trilinear SDOF oscillator. The DCSS is shown in Figure 1. The top and bottom concave surfaces have radii of curvature R_1 and R_2. The coefficients of friction are μ_1 and μ_2. An articulated slider faced with a non-metallic sliding material separates the two surfaces. The principal benefit of the DCSS bearing is its capacity to accommodate larger displacement demands compared to the single concave spherical sliding (SCSS) bearing.

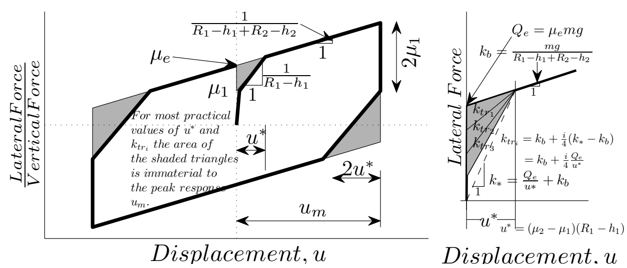

Figure 2. Left: Generic force-displacement loop of the DCSS bearing (heavy line) Right: Values of the transition slope, ktr, used in this parametric study.

Using different values of coefficients of friction, the force-displacement loop of the DCSS bearing is not bilinear–as is for the SCSS bearing, but rather trilinear given that at the initiation and at the reversal of motion, the bilinear loop looses the corner triangles (Figure 2) when the sliding surface with the lower coefficient of friction is mobilized. The purpose of this section is to show that the loss of the corner triangles is immaterial in the response of the isolated superstructure for most practical values of the coefficients of friction used. In mathematical terms, the paper shows that the trilinear oscillator exhibits a complete similarity in the difference between the coefficients of friction along the two sliding surfaces as well as in the ratio of the intermediate to the final slope.

The trilinear force – displacement loop is uniquely defined with the isolation frequency offered by the bearings, $\omega_b = \sqrt{g/(R_1 - h_1 + R_2 - h_2)}$, the characteristic strength, $Q_e = mg\dfrac{\mu_1(R_1 - h_1) + \mu_2(R_2 - h_2)}{R_1 - h_1 + R_2 - h_2}$, the yield displacement of the equivalent bilinear system $u_{ye} \approx 0.25$mm, which according to the previous analysis we expect to have marginal effect, the transition displacement from the second to the last slope, $u^* = (\mu_2 - \mu_1)(R_1 - h_1)$ and the transition frequency associated with the second slope, $\omega_b = \sqrt{g/(R_1 - h_1)}$. In this study, while the analysis focuses on the DCSS bearings the formulation is presented for the general trilinear oscillator ($u_{ye} \neq 0$) and the result that the normalized maximum displacement exhibits a complete similarity in the normalized yield displacement is re-established.

3 DIMENSIONAL ANALYSIS OF THE TRILINEAR OSCILLATOR

Consider a trilinear oscillator that is described with the five parameters ω_b, Q_e,

u_{ye}, u^* and ω_{tr} which is subjected to a pulse-type strong ground motion having a predominant acceleration pulse with duration T_p and amplitude a_p. The maximum inelastic displacement of the triliear SDOF oscillator is a function of seven variables

$$u_{max} = F(\omega_b, Q_e/m, u_{ve}, u^*, \omega_{vr}, a_p, \omega_p) \qquad (2)$$

The eight variables appearing in equation (2) involve only two reference dimensions; that of length [L] and time [T]. According to Buckingham's Π-theorem, the number of dimensionless products (Π-terms)=[number of variables in Eq. (2) = 8 – number of reference dimensions = 2]; therefore, for the trilinear SDOF oscillator we have 8 - 2 = 6 Π-terms. These are defined as:

$$\Pi_m = \frac{u_{max}\omega_p^2}{\alpha_p}, \Pi_\omega = \frac{\omega_b}{\omega_p}, \Pi_Q = \frac{Q_e}{m\alpha_p}, \Pi_y = \frac{u_{ye}\omega_p^2}{\alpha_p} \neq 0, \Pi_* = \frac{u^*\omega_p^2}{\alpha_p}, \Pi_{tr} = \frac{\omega_{tr}}{\omega_p} \qquad (3)$$

We selected as repeating variables the characteristics of the pulse excitation, a_p and $\omega_p = 2\pi / T_p$. With the six Π-terms given by equation (3), the relation of the eight variables appearing in equation (2) is reduced to a relation of six variables

$$\frac{u_{max}\omega_p^2}{\alpha_p} = \varphi(\frac{\omega_b}{\omega_p}, \frac{Q_e}{m\alpha_p}, \frac{u_{ye}\omega_p^2}{\alpha_p}, \frac{u^*\omega_p^2}{\alpha_p}, \frac{\omega_{tr}}{\omega_p}) \qquad (4)$$

<u>*Range of interest of the Π-terms*</u>

- $\Pi_\omega = \omega_b/\omega_p$

Given that the majority of isolation periods used are larger than 1.5 sec ($T_p >$ 1.5sec) and that energetic pulses from near source records can be as large as 3 sec, the range of interest for $\frac{\omega_b}{\omega_p}$ is $0 < \frac{\omega_b}{\omega_p} = \frac{T_p}{T_b} = \frac{3\,\text{sec}}{1.5\,\text{sec}} = 2$. Beyond the value of $\Pi_\omega = \omega_b/\omega_p = 2$ the phenomenon of complete similarity that we intend to show becomes even stronger.

- $\Pi_Q = Q_e/ma_p$

Even for ground motions which are approximated with low amplitude acceleration pulse say a_p=0.25g and for an equivalent coefficient of friction as high as μ_e=0.05 the dimensionless product $\Pi_Q = \frac{Q_e}{ma_p} = \frac{\mu g}{a_p}$ as high as 0.2.

- $\Pi_y = u_{ye}\omega_p^2/a_p$

Given that the yield displacement of the Teflon coat before sliding along the stainless steel surface is u_y=0.2m and that u_{ye} is of the same order of magnitude, the range of interest of $\Pi_y = \frac{u_{ye}\omega_p^2}{a_p}$ is $0.0001 < \Pi_y < 0.01$

- $\Pi^* = u^*\omega_p^2/a_p$

For the persistent near fault ground motions Π* is well below one. However for few relative short duration pulse type ground motions such as the OTE record from the 1995 Aigion Greece earthquake and relative large values of μ_2-μ_1, Π* may reach the value of one. Accordingly $0.1 < \Pi^* < 1.0$.

- $\Pi_{tr} = \omega_{tr}/\omega_p$

With reference to Figure 2 (bottom) the transition slopes k_{tr} is bounded by $k_b < k_{tr} < \frac{Q_e}{u^*} + k_b = k^*$. Accordingly, in terms of frequencies $\omega_b < \omega_{tr} < \sqrt{\frac{Q_e}{mu^*} + \omega_b^2}$.

Recognizing that $\frac{Q_e}{mu^*} = \frac{\Pi_Q}{\Pi^*}\omega_p^2$, after dividing with ω_p^2 it is $\Pi_\omega < \Pi_{tr} < \sqrt{\frac{\Pi_Q}{\Pi^*} + \Pi_\omega^2}$.

The limiting value of $\Pi_{tr} = \sqrt{\frac{\Pi_Q}{\Pi^*} + \Pi_\omega^2}$ corresponds to the unrealistic event that the coefficient of friction along one sliding surface is zero (say μ_1=0). In our parametric study we consider that the low end value of the coefficient of friction is as low as 1/4 of the high value; therefore ,

$$\Pi_\omega^2 < \Pi_{tr}^2 < \Pi_\omega^2 + \frac{3}{4}\frac{\Pi_Q}{\Pi^*} \Rightarrow \quad \Pi_\omega < \Pi_{tr} < \sqrt{\Pi_\omega^2 + \frac{3}{4}\frac{\Pi_Q}{\Pi^*}} \tag{5}$$

Complete similarity on the dimensional yield displacement

Figure 4 plots the dimensionless value of the solution of equation (4), $\Pi_m = u_{\max}\omega_p^2 / a_p$ as a function of $\Pi_\omega=\omega_b/\omega_p$ when Π^*=0.5 and $\Pi_{tr} = \sqrt{\Pi_\omega^2 + \frac{1}{2}\frac{\Pi_Q}{\Pi^*}}$, for three different values $\Pi_Q=Q_e/ma_p$ and different values of $\Pi_{ye}=u_{ey}\omega_p^2/a_p$ when the trilinear oscillator (rigid deck supported on DCSS bearings) is excited by an antisymmetric Ricker wavelet. Figure 3 shows that the solution for the dimensionless maximum displacement, Π_m, is nearly indifferent even when the dimensionless yield displacement of the backbone curve Π_{ye} is varied by two orders of magnitude (Π_{ye}=0.0001 – 0.01). This result indicates that the response of the trilinear oscillator exhibits a complete similarity in the dimensionless product Π_{ye}; and therefore the dimensionless product Π_{ye} drops out of consideration. Accordingly, equation (4) reduces to

$$\frac{u_{\max}\omega_p^2}{a_p} = \varphi\left(\frac{\omega_b}{\omega_b}, \frac{Q_e}{ma_p}, \frac{u^*\omega_p^2}{a_p}, \frac{\omega_{tr}}{\omega_p}\right) \tag{6}$$

It is worth mentioning that the work of Constantinou (2004)[9] and subsequently the work of Fenz and Constantinou 2006[7] silently use the result of equation (6) – that the response is insensitive to the value of the yield displacement and throughout their study they adopted that $u_{ye} = 0$

Interpretation of the Response Analysis of the DCSS

Figure 4 plots dimensionless response spectra of the trilinear oscillator for three values of the normalized strength $\Pi_Q = \frac{Q_e}{ma_p} = \frac{\mu_e g}{a_p} = 0.05, 0.1 \text{ and } 0.2$ when subjected to a symmetric Ricker wavelet. The heavy black line plots the response of the rigid deck when supported on equivalent single concave spherical sliding bearings (backbone curve) while the other curves plot the response of the rigid deck supported on various DCSS bearings (Π*=0.1, 0.5, 1.0) and $\Pi_{tr} = \sqrt{\Pi_\omega^2 + j\frac{\Pi_Q}{\Pi^*}}$, $j = \frac{1}{4}, \frac{1}{2}, \frac{3}{4}$, a total of 9 combinations). The combination of Π* = 1.0 and $\Pi_{tr} = \sqrt{\Pi_\omega^2 + \frac{3}{4}\frac{\Pi_Q}{\Pi^*}}$ corresponds to the triangles with the larger area (larger departure from the backbone loop-see Figure 2). Figure 4 indicates that the backbone heavy black line (deck on equivalent SCSS bearings) is invariably below all curves (smaller peak bearing displacements). For the case of Π_Q = 0.05 and Π_Q =0.1 (which is the majority of practical situations), the peak bearing displacements from all configurations are practically the same (complete similarity) for Π_ω<0.5 and Π_ω>1 while within the range 0.5< Π_ω<1 the response curves exhibit a mild amplification as the size of the gray triangles in Figure 2 increases. The right plot shown in Figure 4 which is for the high-end values of the dimensionless strength $\Pi_Q = \frac{Q_e}{ma_p} = \frac{\mu_e g}{a_p} = 0.2$, indicates that the complete similarity appears in the range of interest (Π_ω<1.5) only when Π*<0.5 and $\Pi_{tr} < \sqrt{\Pi_\omega^2 + \frac{1}{2}\frac{\Pi_Q}{\Pi^*}}$. Figure 5 plots dimensionless response spectra of the trilinear oscillator when subjected to an antisymmetric Ricker wavelet. The response spectra in Figure 5 exhibit remarkable order and the phenomenon of complete similarity becomes most apparent in particular for the values of Π_Q<0.1. Also note that the curves which depart the most from the heavy black backbone line are those with the stars (*) which correspond to very high values of the transition slope. The result of the dimensional analysis presented herein concludes that for values of Π_Q≤0.1 and values of $\Pi_{tr} < \sqrt{\Pi_\omega^2 + \frac{1}{2}\frac{\Pi_Q}{\Pi^*}}$ the dimensionless products Π* and Π_{tr} drop out of consideration; and therefore equation (6) further reduces to

$$\frac{u_{\max}\omega_p^2}{a_p} = \varphi\left(\frac{\omega_b}{\omega_b}, \frac{Q_e}{ma_p}, 0, any\right) \Rightarrow \frac{u_{\max}\omega_p^2}{a_p} = \varphi\left(\frac{\omega_b}{\omega_b}, \frac{Q_e}{ma_p}\right) \tag{7}$$

The finding that the response of the trilinear oscillator exhibits a complete similarity in the normalized yield displacement, Π_{ye}, in the difference between the coefficient of friction, Π*, and the ratio of the transition to the final slope, Π_{tr}, is what is of most interest to the designer. For instance, in some cases DCSS are viable alternatives due to space limitation; however, the coefficient of friction may be different due to various imperfections. The analysis presented in this paper shows that these imperfections are immaterial to the response and one can use with confidence the equivalent values of the SCSS bearings. Furthermore, because of the existence of the three complete similarities as expressed by equations (6) and (7) the number of arguments in the function φ( ) appearing in equation (4) are reduced by three (3).

4 CONCLUSIONS

In this paper the seismic response of isolated structures supported on bearings with bilinear and trilinear behavior is revisited with dimensional analysis.

The paper introduces the concept of complete similarity by showing the dimensionless maximum response of trilinear systems exhibit a complete similarity in the dimensionless yield displacement. Given that the double concave spherical sliding bearings may be viable alternatives due to installation limitations, the paper proceeds with a wide parametric analysis on the response of decks isolated on double concave spherical sliding bearings and concludes that for values of the dimensionless strength $\Pi_Q = \frac{Q_e \omega_p^2}{a_p} < 0.1$ and values of the dimensionless transition slope $\Pi_{tr} = \frac{\omega_{tr}}{\omega_p} < \sqrt{\Pi_\omega^2 + \frac{1}{2}\frac{\Pi_Q}{\Pi^*}}$ the response of the trilinear system exhibits a complete similarity in the difference between the coefficients of friction along the sliding surface as well as in the ratio of the transition (intermediate) to the final slope. The finding that for most practical configurations and design ground motions the response of the trilinear oscillator exhibits a complete similarity in (a) the normalized (transition) yield displacement, (b) the difference between the coefficient of friction and (c) the ratio of the intermediate to the final slope is of great interest to the design engineer since the response of a structure isolated with DCSS bearings can be computed with confidence by using the equivalent properties of the SCSS bearings.

5 ACKNOWLEDGEMENTS

Partial financial support has been provided by the EU research project "DARE" ("Soil-Foundation-Structure Systems Beyond Conventional Seismic Failure Thresholds"), funded through the 7th Framework Programme "Ideas", Support for Frontier Research – Advanced Grant, with number ERC-2—9-AdG 228254-DARE to Professor G. Gazetas. Partial financial support for this study has been provided to the second author by the Alexander S. Onassis Foundation.

6 REFERENCES

[1] Kelly JM. Earthquake Resistant Design with Rubber. Springer: London, 1997.
[2] Federal Emergency Management Agency (FEMA). Prestandard and commentary for the seismic rehabilitation of buildings. Report No. FEMA-356, Washington, DC, 2000.
[3] AASHTO. Guide Speci:cations for Seismic Isolation Design. American Associate of State Highway and Transportation Officials, Washington, DC, 1999.
[4] International Code Council (ICC), International Building Code 2000
[5] Constantinou MC, Soong TT, Dargush GF (eds), Passive Energy Dissipation Systems for Structural Design and Retrofit, Monograph Series-1, Multidisciplinary Center for Earthquake Engineering Research, Buffalo, New York, 1998.
[6] Tsai CS, Chiang TC, Chen BJ. Experimental evaluation piecewise exact solution for predicting seismic responses of spherical sliding type isolated structures. Earthquake

Engineering and Structural Dynamics 2005; 34(9): 1027–1046.
[7] Fenz DM, Constantinou MC. Behaviour of the double concave Friction Pendulum bearing. Earthquake Engineering and Structural Dynamics. 2006; 35:1403–1424
[8] Tsai CS, Chen WS, Chiang TC, Chen BJ. Component and shaking table tests for full-scale multiple Friction Pendulum system. Earthquake Engineering and Structural Dynamics 2006; 35(11):1653–1675.
[9] Constantinou M. Friction Pendulum Double Concave Bearing, Technical Report, available at: http://nees.buffalo.edu/docs/dec304/FP-DC%20Report-DEMO.pdf, 2004.

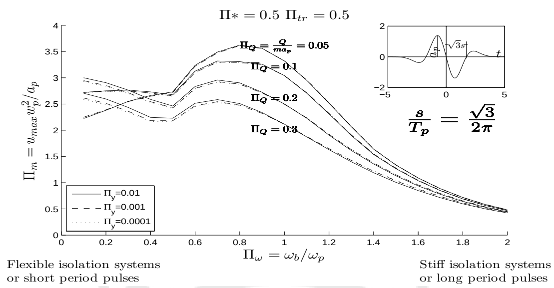

Figure 3. Dimensionless maximum displacement spectra of a trilinear oscillator (Π*=0.5, Πtr=0.5) subjected to an antisymmetric Ricker wavelet. For a given dimensionless strength ΠQ the response is practically indifferent to two orders of magnitude variation of the dimensionless yield displacement Πye.

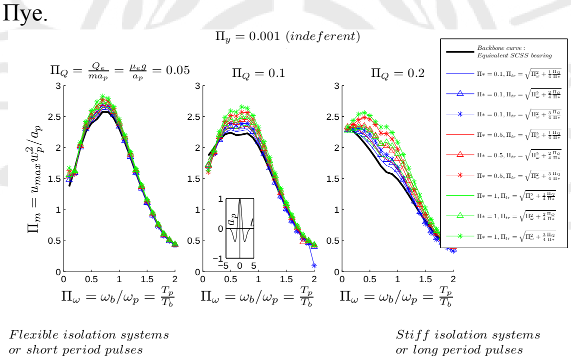

Figure 4. Dimensionless maximum inelastic displacement of a rigid deck supported on DCSS bearings with a wide range of parameters when subjected to a symmetric Ricker pulse.

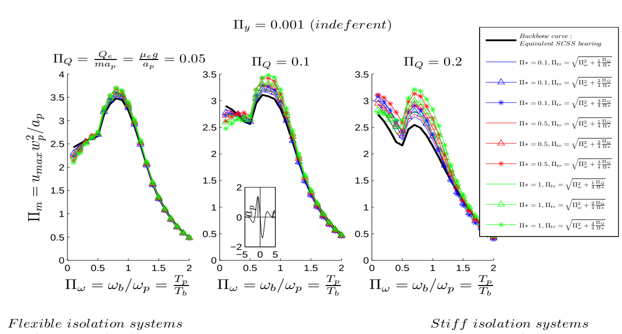

Figure 5. Dimensionless maximum inelastic displacement of a rigid deck supported on DCSS bearings with a wide range of parameters when subjected to an antisymmetric Ricker pulse.

SEGMENTATION OF PIERS AND ABUTMENTS INTO VERTICAL LAYERS WITH EXPANDED POLYSTYRENE INSERTIONS

Sevasti D. Tegou[1], Ioannis A. Tegos[2] and Thomas N. Salonikios[3]

[1,2] Aristotle University of Thessaloniki, Dept. of Civil Engineering, Greece
[3] Institute of Engineering, Seismology and Earthquake Engineering (ITSAK)
e-mail: [1]stegou@civil.auth.gr, [2]itegos@civil.auth.gr, [3]salonikios@itsak.gr

ABSTRACT: In the present study, the accommodation of the serviceability and earthquake resistance requirements of bridge structures is attempted through the segmentation of the piers and abutments into vertical layers. The resultant construction problems are properly accommodated and the proposed alternative design methodology is implemented in a long railway seismic isolated bridge.

KEY WORDS: Abutment; Bridge; Concrete wall; Seismic; Serviceability.

1 INTRODUCTION

Integral Abutment and Jointless Bridges (IAJB) has become an increasingly popular alternative to conventional bridge design in recent years. A recent survey indicates that there are over 13 000 integral abutment bridges in service in the United States [1]. On the other hand, although European experience with Integral Abutments is significantly less [2], the trend is towards making this type of bridges a larger percentage of all newly constructed bridges.

In conventional construction bridge deck typically consists of simply supported spans separated by expansion joints and is supported on the abutments and piers by bearings. The main disadvantage of these bridge systems concerns the installation and maintenance of the expansion joints and bearings [3]. Failed expansion joints by fatigue, leaked expansion joints and corroded bearings are representative phenomena. These problems increase the initial and long-term cost of the structure while a more extensively effort is required for the maintenance of the bridge.

In integral construction the superstructure and the vertical supports, piers and abutments, form a continuous, monolithic structure [4]. The increased popularity of the integral bridges is due to their advantages concerning the cost-effectiveness and durability of these structures [5]. Furthermore, integral bridges are the preferred structures in more seismically regions, due to their increased capacity during seismic events. However, despite the fact that integral abutment and jointless bridges have aesthetics and earthquake resistance advantages over conventional bridges with bearings and expansion joints, the implementation of these systems is restrained due to the serviceability requirements [6], which distress piers, abutments and approach embankments.

The last years, more and more studies are carried out on the known problem of embankment-bridge interaction, which can contribute to the enhancement of the seismic resistance of bridges. Recent studies, [7-10], which have investigated this effect, came up to the conclusion that, generally, the abutment and the backfill can be utilized in order to reduce the movement of the deck and by extension, the structural cost of the bridge [11].

In the first part of the present study a seismic isolated bridge is redesigned according to the current Codes provisions to comprise an integral bridge system. A new type of earthquake resistant abutment, a simpler version of which was presented in a previous work [10], is properly modified to be exploited in this system. In the second part, the experimental investigation on the seismic efficiency of the integral abutment is presented.

2 DESCRIPTION OF THE INTEGRAL ABUTMENT

The proposed integral abutment is illustrated in Figure 1. The abutment consists of the extension of the deck slab of the bridge onto transversely directed R/C walls. These walls are arranged in pairs and are rigidly connected to the so-called continuity slab. The abutment's web consists of five transversely directed walls which are rigidly connected to the deck. The distance between the walls is achieved by the interjection of an expanded polystyrene (EPS) layer, with a small thickness, i.e. 20mm. The walls are constructed in a concrete box-shaped substructure, which replaces the conventional wing walls and retains the backfill material. The longitudinal walls of the box improve aesthetics, as they visually overlap the multi-wall restraining system. The earth pressures affect only the stability of the concrete box-shaped substructure and the abutment's foundation, but not the earthquake resistance of the restraining walls. The foundation of the abutment is designed to have adequate capacity to withstand the in-service and the seismic loading of the abutment. The design of the walls also provides a hierarchy of the resistances of its structural components, which ensures that flexural failure precedes its shear failure. The development of plastic hinges at the top and bottom of the walls is ensured by applying capacity design according to current code provisions [12].

3 OVERVIEW OF THE “REFERENCE” BRIDGE

A seismic isolated railway bridge in Greece was used as the reference case of the study, Figure 2(a). This bridge is straight, has four-spans and a total length equal to 168.0m. The prestressed deck, Figure 2(c), has a hollow T-beam-like section, and is supported on three hollow rectangular piers, Figure 2(d). The

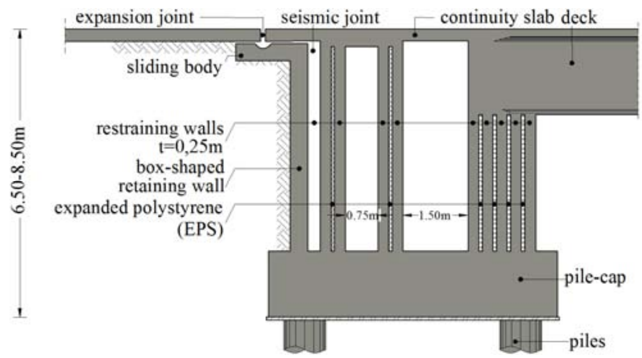

Figure 1. Longitudinal section of the integral abutment.

deck is connected to the abutments and piers through LRB bearings and is separated from the backwall through an expansion joint, Figure 2(b). Each abutment is equipped with two fluid dampers. The bridge was designed for normal loads according to the German Norms [13] while the seismic design was carried out according to the Greek Seismic Code [14] and the relevant Greek standards [15] for the seismic design of bridges. The bridge is founded on a ground type B according to the Greek Seismic Code [14]. The bridge site is located in the Seismic Zone II which is equivalent to a peak ground acceleration of 0.24g. The behaviour factors of the system adopted for design were $q_x=q_y=q_z=1.0$ for the response in the three principal directions, respectively.

4 OVERVIEW OF THE INTEGRAL BRIDGE SYSTEM

4.1 General

The seismic isolated bridge presented in the previous section was redesigned as an integral bridge system which exploits the proposed integral abutment. The modified bridge system has the same length, number of spans, heights of piers and deck cross-section as the reference case, Figure 2(a). The prestressed deck is rigidly connected to the three piers whose cross-section, Figure 2(e), is properly modified to conform to the serviceability requirements of the bridge (see section 4.2). The rigid connection of the deck with the piers and abutments allows the development of their hysteretic behaviour. By extension, the design spectra of the longitudinal design earthquake is divided by a factor of $q_x=3.5$. The relatively lower value of the transverse shear ratio $\alpha_{s,y}$ of the piers leads to the use of a q-factor equal to $q_y=2.25$ [16].

4.2 The piers of the integral bridge system

The rigid connection of the piers with the deck restrains the expansion and contraction of the deck due to the serviceability requirements of the bridge, which require a system as flexible as possible and that makes necessary the modification of the piers' cross-section. A reasonable solution is the selection of

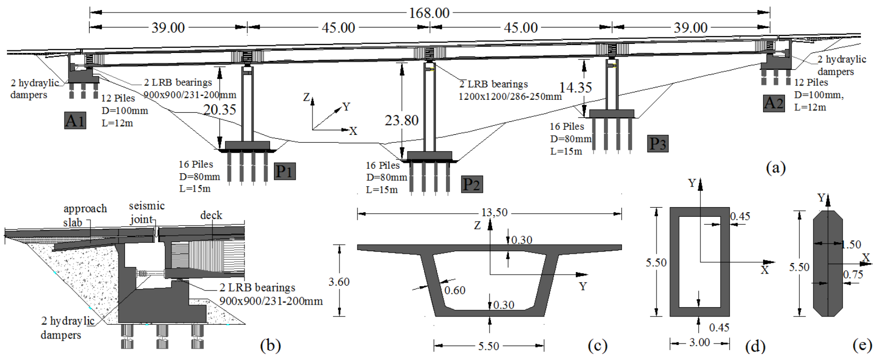

Figure 2. (a) Longitudinal section of the seismic isolated railway bridge, (b) Longitudinal section of the abutment, (c) The cross-section of the deck at the mid-span,(d) The cross-section of the pier in the case of the “reference” bridge and (e) The new cross-section of the pier.

wall-like columns whose weak axis is longitudinally oriented and their depth is equal to the depth of the initial cross-section. Considering that the piers’ height is fixed, the selection of their width is based on the demand limitation of their in-service loading under the inevitable constraint-type movements of the deck. The in-service constraint movements are maximized at the bridge’s ends and minimized at the middle of the deck. As a result, piers P_1 and P_3 are the ones which suffer more distress due to the in-service loading of the bridge. A parametric investigation was performed in order to optimize the piers’ thickness. Figure 3 shows the maximum allowable thickness of the piers by serviceability loading as a function of their height. It can be deduced that the maximum required thickness for the most critical pier (P_3) is 0.78m. In order to increase the longitudinal stiffness of the bridge, each pier of the initial bridge system is replaced by two wall-like columns whose thickness is equal to 0.75m. Consequently, the piers of the new integral bridge system have a total thickness equal to 1.50m, Figure 2(e).

4.3 The abutment of the integral bridge system

The integral abutment described in Section 2 replaces the conventional abutment of the “reference” bridge. The critical point, as far as the serviceability requirements of the bridge is concerned, is the selection of the height of the abutment’s web. The height of the walls behind the web is equal to the sum of the height of the abutment’s web and the deck’s cross-section height. Consequently, the more flexible walls will respond in an elastic manner under the total in-service maximum constraint-type movement of the deck, considering that they have the same cross-section and reinforcement with the stiffer walls.

A parametric investigation was performed in order to select the optimum geometry and reinforcement of the walls. An example concerning this investigation is given in Ref. [10]. The investigation showed that, in general, the reduction in the longitudinal reinforcement ratio yields to an increase in the minimum required height of the walls. Considering that the height of a conventional abutment's web is about 4.0m-5.0m, it is obvious that this height must be kept constant in order to keep the construction cost in a low level. On the other hand, the use of high walls would lead to a lower seismic efficiency of the restraining system. The increase of the walls' thickness also increases the minimum required height and consequently the construction cost. As a result, the thickness of the walls, fixed in both wall types, was selected to be the minimum required by the Codes (e.g. 25 mm) [17]. For this thickness, a abutment's height equal to 4.5m is required in order for the serviceability requirements of the bridge to be fulfilled. The serviceability check also showed that D16@50mm longitudinal reinforcement (ρ=3.2%) is required in the case of the stiffer walls. Considering that the height of the abutment's web is 4.5m, the walls arrayed behind it have a height equal to 7.7m. The serviceability check showed that D16@100mm (ρ=1.6%) longitudinal reinforcement is adequate for these walls.

5 DISCUSSION ON THE STRUCTURAL COST

The integral bridge described in the previous section was designed according to the current Code's provisions. It is noted that the deck was not redesigned because its design is mainly based on serviceability loading of the bridge, which is almost constant in the bridge alternative studied in the present study. Figure 4 represents the percentage increases or decreases in the cost of each re-designed structural member. It can be deduced that the total structural cost of the integral bridge system is about 5% lower comparatively with the cost of the seismic isolated bridge. The increase by up to 28% and 35% which is noticed in the construction cost of the abutments and their foundations respectively is due to the part of the induced seismic energy which is dissipated by the earthquake resistant walls.

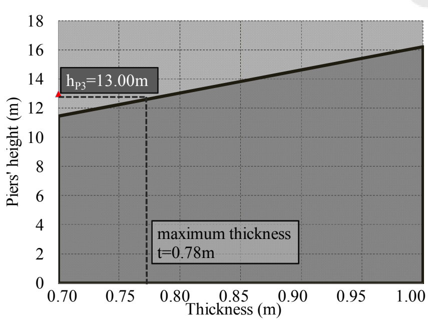

Figure 3. Maximum thickness of the piers due to the serviceability requirements of the bridge.

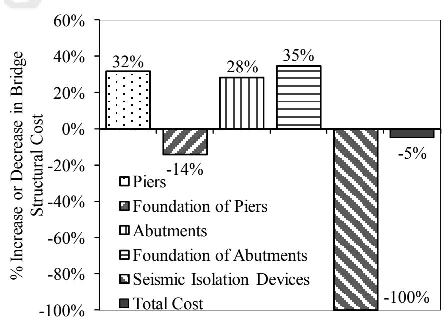

Figure 4. The percentage (%) alteration in the cost of each re-designed structural member and the total bridge structural cost alteration.

6 EXPERIMENTAL INVESTIGATION

6.1 Description of specimens and overview of experimental setup

The experimental program presented in this work involves 2 specimens (denoted as SPEC1 and SPEC2). Each specimen, Figure 5, represents an 1:2 scale pair of walls of the integral abutment presented in Section 2. SPEC1 has a longitudinal reinforcement ratio equal to 1.6% while the longitudinal reinforcement ratio of SPEC2 is 2.9%, Figure 5(b). Figure 5(a) illustrates the experimental setup, consisted of the two steel beams HEB 320, which substitute the bridge deck and pile-cap respectively. The double-acting hydraulic actuator is connected to the one steel beam, which has the ability to slip through two steel bars fixed at the laboratory's floor. It is noted that the connection between this steel beam and the specimen allows the partial rotation of the specimen's head. In cases that the serviceability requirements impose the construction of abutments' web with height greater than 4.5m (this height corresponds to the 1:2 scale of the experiment), but it is not possible, due to other parameters' limitations (i.e. construction cost etc.), these rotations accommodate part of the in-service induced movements. The second steel beam is fixed at the laboratory's floor. The aforementioned specimens were subjected to a number of cycles of quasi-static cyclic loading, Figure 5(c).

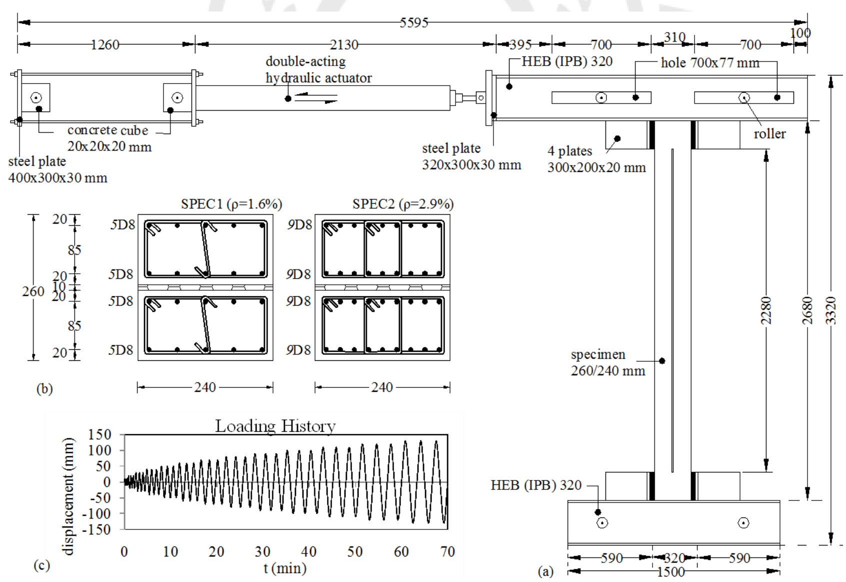

Figure 5. (a) Experimental setup (b) cross-section of the specimens and (d) loading history.

6.2 Discussion of Results

Hysteresis loops for the two specimens are shown in Figure 6. Regardless of the large relevant displacements between the specimen's head and foot, the failure of the specimens was not reached. The noticed plastic branch has short length in both cases and consequently, a conclusion about the ductility of the specimens it is not possible to be extracted. However, the observation of the last loop indicates that, both specimens have available ductility, as the three last loops corresponding to the maximum displacement are coincided. The intended non-full impaction of the specimens' head caused rotations, which affect the results.

Any relevant movement between the specimen's head and base causes (a) linear variant bending moments along the height of the walls, (b) tension and compression axial forces corresponding to the direction of the head's movement (the presence of the tensile axial loading is confirmed by the appearance of flexural cracks in the middle of the tensile wall of the specimen during the loading) and (c) second-order effects. The described above parameters affect the loops' shape and cause the loops' pinching. In any case, the area enclosed by the envelope, which is quite large, indicates that the energy dissipation is significant in both specimens.

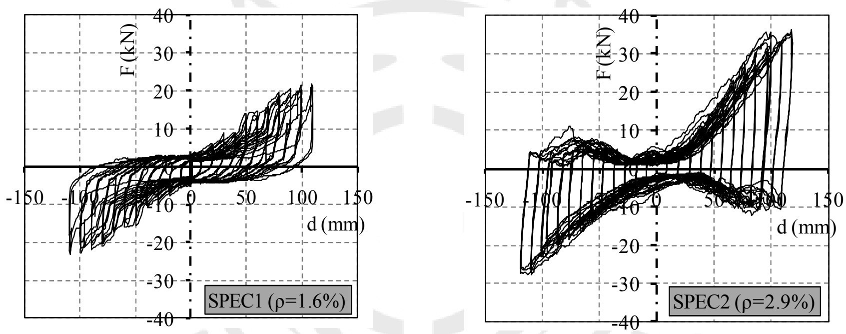

Figure 6. Hysteresis loops for the two specimens.

7 CONCLUSIONS

In the first part of the present study, the applicability and cost-effectiveness of the new integral bridge system was assessed, while in the second part, the experimental investigation on the seismic efficiency of the integral abutment was presented. The study resulted in the following conclusions:

- The new integral bridge system has explicit advantages concerning durability and driving convenience.
- The critical loading for the design of the new integral bridge is the one caused by the in-service movements of the deck, which are accommodated for by the flexibility of the walls and piers.
- The total structural cost of the new integral bridge system is reduced by up to 5%. This percentage is increased in long bridges as the higher total cost absorbs the increases observed in the cost of each structural member. Considering that the maintenance cost of the redesigned system is quite low, the long-term cost-effectiveness is greater than this one presented in this study.

- The experimental investigation showed that the energy dissipation capability of the integral abutment is significant. The hysteresis loops' shape proves that many parameters affect the response of the system.

ACKNOWLEDGEMENTS

This research is co-funded by the European Union (European Social Fund-ESF) and National Resources, in the framework of the program "HRAKLEITOS II" of the "Operational Program for Education and Initial Vocational Training".

Acknowledgements are due to METE SYSM S.A. for kindly providing the original study of the bridge for the purposes of the present study. The Authors wish also to express their gratitude and sincere appreciation to MASOUTIS S.A. for kindly offering the experimental setup.

REFERENCES

[1] Maruri R.F. and Petro S.H., "Integral abutments and jointless bridges (IAJB), 2004 survey summary", *in FHWA Integral Abutment and Jointless Bridges Conference*, pp. 12 – 29, 2005.

[2] White H. et al. "Integral Abutment Bridges: The European Way." Practice Periodical on Structural Design and Construction, 15: 201, 2010.

[3] Mistry V.C., "Integral abutment bridges", *Conference of High Performance Steel Bridge Others*, Nov 30-Dec 1, Baltimore Maryland, 2000.

[4] Burke M. P., *Integral and semi-integral bridges*, Wiley- Blackwell Pub., 2009.

[5] Hassiotis, S. and Roman E. K. "A survey of current issues on the use of integral abutment bridges", Bridge Structures 1(2): 81 – 101, 2005.

[6] Arockiasamy M. et al., "State-of-the-Art of Integral Abutment Bridges: Design and Practice", Journal of Bridge Engineering, Vol. 9, No. 5, September 1, 2004.

[7] Mitoulis S.A., Tegos I.A. "An unconventional restraining system for seismically isolated bridges", Engineering Structures, Vol. 32, Issue 4, pp. 1100-1112, 2010.

[8] Kotsoglou A., Pantazopoulou S., "Bridge-embankment interaction under transverse ground excitation", Earth. Eng. & Struct.Dyn., Volume 36, Issue 12, p. 1719-1740, 2007.

[9] Mikami T. et al., "The effect of abutments as displacement limiting measure on seismic performance of bridges", www.pwri.go.jp, Accessed 15 Oct 2010.

[10] Tegou S.D., Mitoulis S.A., Tegos I.A., "An unconventional earthquake resistant abutment with transversely directed R/C walls", Eng. Struct., Vol. 32, Issue 11, pp. 3801-3816, 2010.

[11] Nutt R.V. and Mayes R.L., *Comparison of Typical Bridge Columns Seismically Designed With and Without Abutment Participation Using AASHTO Division I-A and Proposed AASHTO LRFD Provisions*, Task F3-1(a),2000.

[12] CEN, *Eurocode 8: Design of structures for earthquake resistance, Part 1: General rules, seismic actions and rules for buildings*, 2003.

[13] DIN 1075: *Betonbrucken; Bemessung und Ausfuhrung. Ausgabe*, April 1981.

[14] Ministry of Environment, Physical Planning and Public Works, *Greek Seismic Code—EAK 2000*, Athens, 2000 (amended 2003, in Greek).

[15] Ministry of Environment, Physical Planning and Public Works, *Circular 39/99: Guidelines for the Seismic Design of Bridges*, Athens, 1999 (in Greek).

[16] CEN, *Eurocode 8: Design of structures for earthquake resistance, Part 2: Bridges*, 2003.

[17] CEN, *Eurocode 2: Design of concrete structures-Part 1: General rules and rules for buildings*, 2004.

SEISMIC DESIGN OF CIRCULAR SECTION PIERS UNDER AXIAL LOAD AND BIAXIAL BENDING BELONGING TO LOW DUCTILITY BRIDGES

Analytical and Experimental Investigation of Bending Resistance

Ioannis A. Tegos[1], Nikolaos C. Giannakas[2]
and Theodoros A. Chrysanidis[3]

[1,2,3] Aristotle University of Thessaloniki, Dept. of Civil Engineering, Greece
e-mail: itegos@civil.auth.gr, giannakasnikos@gmail.com, thchrysa@civil.auth.gr

ABSTRACT: The case of seismic design of bridges with bearings which are designed for a value of behaviour factor equal to 1 constitutes a special case and their design should not be allowed to take place by using the familiar diagrams in the bibliography, which refer exclusively to ductile structures (q>1). This happens because these diagrams have resulted based on the section resistances, which exceed in terms of value the yield value of reinforcement bars. In other words, yield stress is demonstrably less than the failure stress. In the framework of the current work, diagrams regarding circular sections were developed. Based on these diagrams, the problem of calculating the necessary longitudinal reinforcement is dealt rationally, when q=1 exists in the problem as a fact. Experimental investigation of the mechanical behaviour of circular compact section piers is included.

KEY WORDS: BRIDGES; CIRCULAR SECTION; LOW DUCTILITY; SEISMIC DESIGN.

1 INTRODUCTION

A simple look at the effective area of an M-N interaction diagram, Fig. 1, proves the following statements to be right. E.g. column with a normal axial force ν=-0.18 appears to be in the balanced state, where the tensile failure strain of steel takes place simultaneously with the compressive failure strain of concrete. This fact means that the yield state preceded for a smaller moment compared to the failure moment. In other words, it means that a design based on the yield moment would have as a result more reinforcement bars at the column. Stated otherwise, a design which assumes the yield strain as a failure strain underestimates the need for reinforcement and this fact results to a clear decrease of the safety factor.

In the case of circular section columns, noticing the relative interaction diagram, it seems that the difference between the states of yield and failure reduces but there is still a difference. Similarly, there is a difference in the case of circular hollow sections, too. This difference is bigger compared to the corresponding circular compact sections. Especially, as far as the circular hollow sections are concerned, it is meaningful to mention that it is advisable these sections to be used only in bridges which are designed with q=1 and the safety of structures should not be risked because of the well-known sensitivity of those sections under seismic actions.

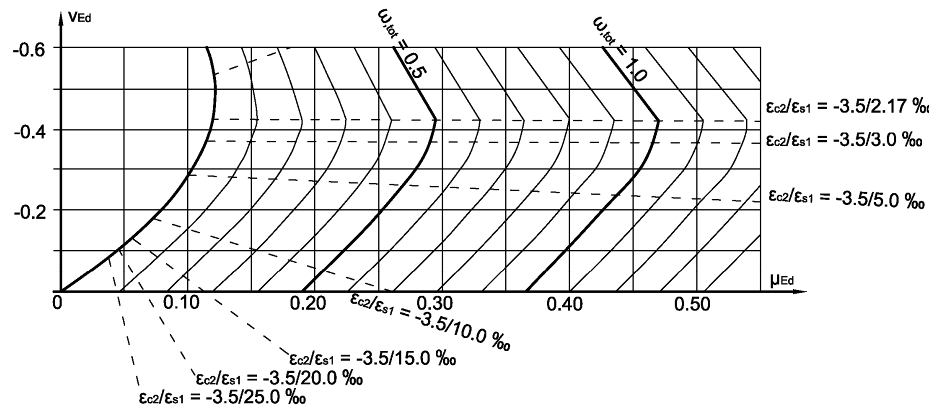

Figure 1. Effective area of seismic design of columns.

2 BASIC DESIGN ASSUMPTIONS

At this point, it should be clarified what yield moment means, since there is the well-known confusion regarding its definition. In some cases, yield moment is related to the yield of the extreme tensile fiber and in other cases (which is more logical), it is related to the yield of the ideal reinforcement which exists at the center of gravity of the tensile zone. The two cases of yield moment are shown in Fig. 2, meaning the yield of the extreme fiber and the yield of the center of gravity of the tensile zone. It is obvious that for the resistance against the same moment from the same, geometrically, section, according to the first case, the definition of yield would be baptized as failure moment and the resultant reinforcement bars would be less. Therefore, it is interesting, if not completely necessary, interaction diagrams of normal forces to be constructed. Based on those diagrams, the mechanical ratio of the necessary longitudinal reinforcement of circular section columns will be defined more rational.

Finally, it must be noted that due to the seismic origin of the forces, there is no meaning for the presence of reduction factor α=0.85 for permanent loads in the calculation against normal forces. Of course, at this point, it must be recognized that the use of the factor of permanent loads brings about a small lifting of the unsafety which was underlined above, but this constitutes an accidental (random) result and in any case non-controlled.

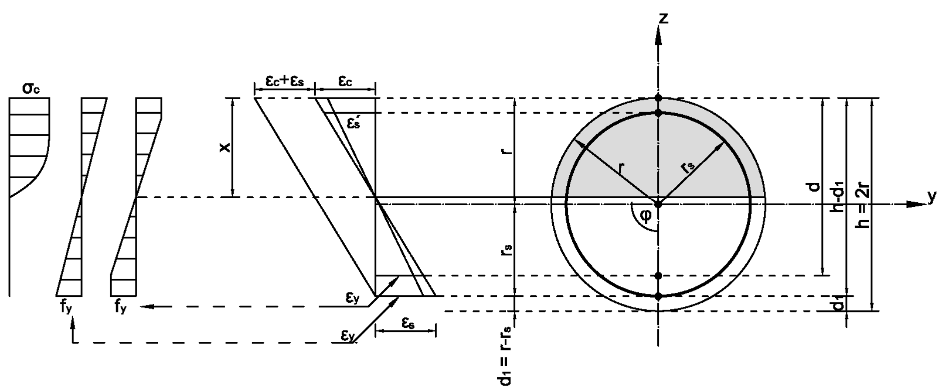

Figure 2. Section stresses at failure state of a circular section column with elastic behaviour.

As far as the influence of the confinement to the construction of the proposed interaction diagrams is concerned, it is obvious that it would be wrong to seek its influence, since it is well-known that the results of the confinement are revealed only during the inelastic states of the sections.

3 METHODOLOGY OF CONSTRUCTING DESIGN DIAGRAMS

For the construction of interaction diagrams of circular section piers, which are calculated having in mind a value for the behaviour factor q equal to one, appropriate software of technical programming (MATLAB 7.0.1) was used. Equilibrium equations of section were applied in this program and the design parameters were defined. The procedure of calculating the diagrams was carried out as follows:

- A section of unit diameter was chosen, its characteristics were defined, like the position of the longitudinal reinforcement d_1 and the quality of the concrete, which did not include the permanent load factor α [3], and the equations of the stress-deformation curves of materials were applied.
- The internal forces of concrete and steel of the section were calculated for every case of shortening of the extreme compressive fiber ε_c and for a specific volumetric ratio of longitudinal reinforcement.
- From the solution of Eq. 1 and Eq. 2, the normal forces, which correspond to every case of mechanical reinforcement ratio and concrete shortening from 0 to 3.5‰, were resulted.

$$N_E = F_{c,c} + F_{s,c} + F_{s,t} = \int\int \sigma_c dA + \sum_i (\sigma_{si,c} - \sigma_{ci,c}) \cdot A_{si,c} + \sum_i \sigma_{si,t} \cdot A_{si,t} \quad (1)$$

$$M_E = M_{c,c} + M_{s,c} + M_{s,t} = \iint \sigma_c z dA + \sum_i (\sigma_{si,c} - \sigma_{ci,c}) \cdot A_{si,c} + \sum_i \sigma_{si,t} \cdot A_{si,t} \quad (2)$$

- The results were imprinted on a diagram having results μ on abscissa axis and results ν on ordinate axis, Fig. 3. Such diagrams have been constructed for ratios $d_1/D = 0.05$, $d_1/D = 0.10$ and $d_1/D = 0.15$. The present work shows only the diagram corresponding to the ratio $d_1/D = 0.05$, Fig.3. Moreover, the basic «radiuses», which correspond to the relative shortening of concrete ε_c and to the elongation at the position of the resultant of tensile stresses ε_s=2.175‰, were calculated and designed with a discontinuous line.

4 EXAMPLE

In order to evaluate the results of the analytical investigation and of the interaction diagrams, which were resulted above, examples of bibliography were utilised and the case of bending design with a behaviour factor q=1 was examined.

$$\nu_{Ed} = \frac{N_{Ed}}{A_c f_{cd}} = \frac{2.668 \cdot 1.5}{1.824 \cdot 27.6 \cdot 0.85} = 0.0935 \quad (3)$$

$$\omega = 0.02 \cdot \frac{455}{27.6 \cdot 0.85} \cdot \frac{1.5}{1.15} = 0.506 \rightarrow \mu = 0.195 \quad (4)$$

$$M_{Ed} = \mu_{Ed} \cdot A_c \cdot D \cdot f_{cd} = 0.195 \cdot 1.824 \cdot 1.524 \cdot 27.6 \cdot 0.85/1.5 = 8.478\text{kNm} \quad (5)$$

Taking into account as actions the values of the forces which were resulted from the conventional method, the normalized forces for q=1 turn up:

$$\nu_{Ed} = \frac{N_{Ed}}{A_c f_{cd}} = \frac{2.668 \cdot 1.5}{1.824 \cdot 27.6} = 0.08 \quad (6)$$

$$\mu_{Ed} = \frac{M_{Ed}}{A_c D f_{cd}} = \frac{8.478 \cdot 1.5}{1.824 \cdot 1.524 \cdot 27.6} = 0.1658 \quad (7)$$

From the application of the diagrams and the necessary linear interpolation for $d_1/D = 0.033$ (D=h), it turns up that $\omega_{tot} = 0.567$ and required reinforcement ratio is:

$$\rho_t = 0.567 \cdot \frac{27.6 \cdot 1.15}{455 \cdot 1.5} = 2.64\% \quad (8)$$

Consequently, an increase by 32.0% arises in the required longitudinal bending reinforcement.

Similarly, in two examples, which were taken from german bibliography [1] and [2], a design was realized, on one hand with the use of valid until today diagrams, and on the other hand under seismic actions with a behaviour factor q=1 based on the new interaction diagrams. The results of the corresponding calculations are displayed synoptically at Table 1:

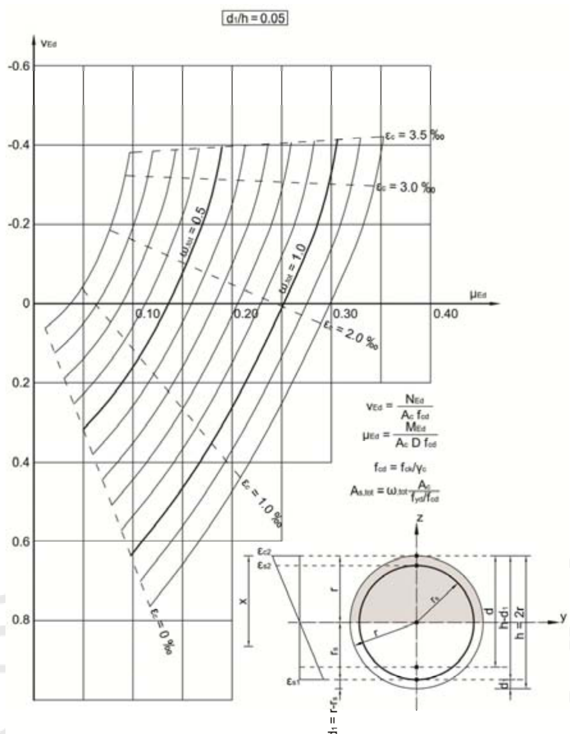

Figure 3. Interaction diagrams for $d_1/D=0.05$ and for behaviour factor q=1.

Table 1. Comparison of results of proposed method versus conventional method

	q [-]	d_1/h [-]	μ_{ed} [-]	ν_{ed} [-]	ω_{tot} [-]	A_s [cm^2]	Variation [%]
Schindler, Bender, Mark	>1.0	0.10	0.272	-0.197	0.80	131	19
	1.0		0.231	-0.168	0.81	156	
Obst	>1.0	0.075	0.146	-0.366	0.20	73.7	45
	1.0		0.124	-0.311	0.248	107	

4.1 Evaluation of results

The following remarks have resulted from a close look of diagrams and from the comparison of results of the aforementioned design examples:

- The seismic design of bridge piers based on the proposed diagrams of the current work for a behaviour factor q=1 has as a result (as it was expected) the increment of the requirement of longitudinal reinforcement.
- The design diagrams, although they constitute an approximate solution (since the code stress-strain diagrams of materials and mainly of concrete

were taken into account and not the real diagrams), are more realistic than the diagrams in effect of bibliography and they produce more credible solutions. It should be noted that the proposed diagrams were roughly cross-checked through the proposed design diagrams of compact circular sections under serviceability actions by assuming as a steel stress in those diagrams the steel yield limit ($\sigma_s = 435$ MPa).

- More investigation is required about the elastic seismic behaviour of centre piers, so solutions even closer to reality can arise in the future.
- Experimental research is needed in order to investigate the real mechanical behavior and mainly the resistance of piers having a circular compact section.

5 EXPERIMENTAL RESEARCH

5.1 Scope

The scope of the experimental research is the comparison of the calculated values of the bending resistances based on diagrams of bibliography [4] and the proposed diagrams to the experimental bending resistances.

5.2 Test specimens

Experimental research consisted of 3 test specimens in total. Longitudinal reinforcement ratio was different for each specimen in order to investigate the differentiation in the mechanical behavior. All specimens were constructed under a scale 1:3. Geometrical and loading characteristics of all test specimens are given at Table 2.

Table 2. Geometrical and loading characteristics of test specimens

Test specimen	D [m]	L [m]	A_s	f_c [MPa]	f_y [MPa]	α	α_{eff}
KQb1	0.20	1.50	16Ø10	32	550	0.50	3.75
KQb2	0.30	1.50	2x16Ø10	21	550	0.525	2.50
KQb3	0.30	1.70	2x24Ø10	25	550	0.75	2.80

5.3 Test setup

Test specimens were subjected to loading coming from two symmetrically placed single loads, Fig. 4. Test setup is shown in Photo 1.

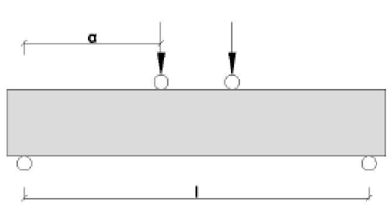

Figure 4. Experimental loading.

Photo 1. Test setup.

5.4 Results

All test specimens failed due to bending. The variation of the deflection in the middle of the specimens with the increment of the load is displayed in Fig. 5 for all specimens. Failure of specimen KQb3 is shown in Photo 2.

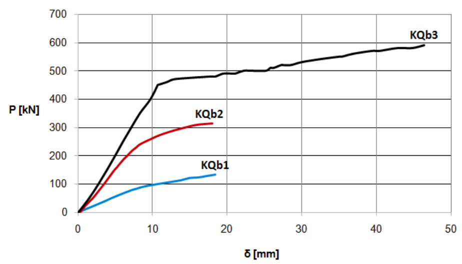

Figure 5. P-δ diagram (All specimens).

Photo 2. Failure (Specimen KQb3).

5.5 Evaluation of results

In order to evaluate the experimental results, the analytical values of the bending resistances are calculated based on the diagrams of the bibliography [4] and the proposed diagrams and then all the analytical results are compared to the experimental results of the bending resistance. Table 3 shows the analytical and experimental results of the bending resistances.

Table 3. Analytical and experimental results of the bending resistances

Test specimen	P_{max} [kN]	Experimental bending resistance M_{exp} [kNm]	Calculated bending resistance (Diagrams of bibliography) $M_{cal,B}$ [kNm]	Calculated bending resistance (Proposed diagrams) $M_{cal,P}$ [kNm]	$M_{cal,B}/M_{cal,P}$
KQb1	135	67.50	45.24	36.17	1.29
KQb2	310	162.75	130.81	106.88	1.22
KQb3	590	309.75	249.04	156.31	1.59

Diagram of Fig. 6, which shows experimental results of work conducted by Priestley [5], displays for the same section the various loading capacities according to three different out of the four different criteria which have been mentioned in the present work. The criterion which is not mentioned is the second criterion which corresponds to the yield of the centre of gravity of the tensile zone. If this criterion was displayed in Fig. 6, it would have been somewhere between "First yield" and "Computed resistance".

6 CONCLUSIONS

The following conclusions have derived from the aforementioned research:

- In the current article, a series of diagrams is proposed for the seismic design of bridges, which are calculated with behavior factor q=1 because of the catholic presence of elastometallic bearings at points of support. A design under seismic normal forces could be possible to take place with the help of those diagrams, in such a way so that the longitudinal reinforcements during the extreme seismic action reach simply the yield point. In this case, it must be noted that the resultant longitudinal reinforcement based on those diagrams is increased, compared to the corresponding reinforcement which results based on the conventional diagrams of bibliography, by a ratio of 20% till 60%.

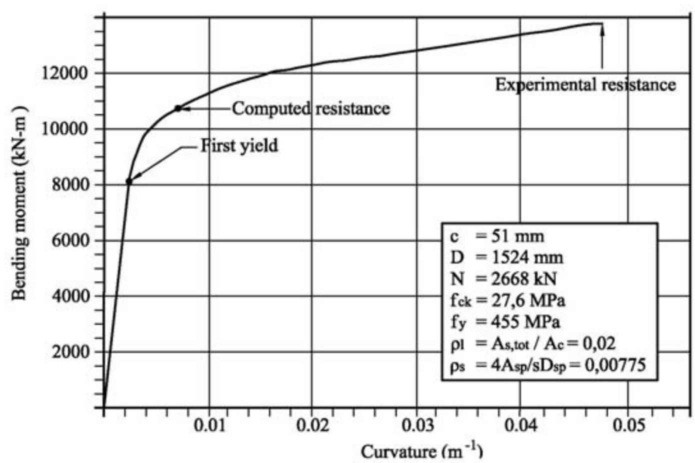

Figure 6. Moment – curvature diagram of an experiment of bibliography [5].

- The comparison of the experimental bending resistances to the corresponding bending resistances calculated either with the diagrams of bibliography either with the proposed diagrams shows, as it was expected, that the experimental results are bigger than the corresponding calculated results based on both types of diagrams.

REFERENCES

[1] Schindler, S, Bender, M, and Mark, P, “Erweiterung der klassischen M-N Interaktionsdiagramme”, Beton- und Stahlbetonbau, Heft 8, pp. 539-547, 2007.

[2] Obst, A, “Bemmesung von Kreisquerschnitten auf Schub. Beton - und Stahlbetonbau”, Heft 12, pp. 297-301, 1981.

[3] Giannakas, N, Tegos, I, “The reinforcement of circular section columns under axial load and biaxial bending of earthquake resistance structures”, Proc. 3rd Greek Conference on Earthquake Engineering and Engineering Seismology, Athens, 2008.

[4] Schneider, K-J, Goris, A, “Bautabellen für Ingenieure”, Werner Verlag, 17 Auflage, 2007.

[5] Priestley, MJN, Seible, F, Calvi, GM, “Seismic design and retrofit of bridges”, John Wiley & Sons, Inc., 1996.

A PROPOSAL FOR COST-EFFECTIVE DESIGN OF PRECAST I-BEAM BRIDGES

Sevasti D. Tegou[1] and Ioannis A. Tegos[2]

[1,2] Aristotle University of Thessaloniki, Dept. of Civil Engineering, Greece
e-mail: stegou@civil.auth.gr, itegos@civil.auth.gr

ABSTRACT: The Codes include provisions about the use of seismic stoppers in the longitudinal direction of bridges. These stoppers are provided with adequate margins in order for the serviceability requirements to be accommodated and are activated only during earthquake. The seismic efficiency and cost-effectiveness of this methodology, which offers the opportunity to design precast I –beam bridges as ductile structures, is investigated in the present study.

KEY WORDS: Bridge; Cost-effectiveness; Longitudinal; Seismic stoppers.

1 INTRODUCTION

Bridge design is mainly concerned with the ability of the deck to withstand traffic loads. The selection of the most properly structural system is affected by parameters such as the topography, traffic requirements and construction method which will be implemented. However in many cases, the seismic performance of the structure proves to be determinative for the whole structural system, as well as critical for the earthquake resistant members of the bridge.

As it is known, the design of the bridge structures must meet specific requirements concerning their structural and serviceability performance. The bridge engineer seeks to design new bridges which will incorporate desirable features such as design and construction economy in both time and money, good appearance, ride quality and safety, ease of access for inspection and maintenance, ease of repair, possible strengthening and possible modification or replacement during road widening [1]. In earthquake resistant bridges, the parameter of economy is concerned with the selection of the most properly structural system. The cost-effectiveness concerning the design of the earthquake resistant members, e.g. piers, constitutes an interesting issue which has not been systematically investigated until now.

The criteria concerning the safety and serviceability performance of the structure are prescribed by Codes [2]. The role of the structural engineer is to strike a socially acceptable balance between the risk of failure and the cost of the structure by applying the Codes' rules and standards. In this regard, the previous experience of the Civil Engineer on similar projects is quite important.

The construction cost of a bridge is mainly affected by the selected structural system. However, the basic design idea includes not only the selection of the structural system but also the configuration of the structural members as well as the structural details. The basic idea, concerning the design of a structure, constitutes the most important, interesting and creative part of Civil Engineers' work. An apposite initial idea minimizes the difficulties concerning the design and the construction of the structure. Considering that, the modern computational methods give the opportunity to design complicated structural systems, many designers assume that, in this way, the design completeness is achieved.

Apart from the main idea, however, there are also the several issues arising during design. In many cases, the comparison between these issues with the whole project makes them seem unimportant. However, as Michelangelo said "trifles make perfection and perfection is not a trifle". This means that when the Engineer faces all the problems arising during the design with accountability, a perfect structure is probable to be designed. An important issue of this category is the one referring to the optimum and cost-effective design of the bridge members.

Precast I – beam bridges are of the most widely constructed bridge types due to their compatibility with the design parameters referring above. More specifically, the simplicity of the structural system and the construction rapidity are of their most important advantages [3]. For bridges with relatively tall piers whose height exceed ten meters, precast beams are the appropriate method for deck construction, which has proven to be both fast and cost effective. The investigation on the improvement of the earthquake resistance and cost effectiveness of these bridge systems constitutes a quite interesting subject. In the present study the efficiency of a proposed seismic design methodology, which not only corresponds to the Code provisions [2], but also accomplish the aforementioned intention, is evaluated.

2 DESCRIPTION OF THE PROPOSED METHODOLOGY

The present study investigates the possible seismic design of precast I- beam bridges considering a value of the behaviour factor in the longitudinal direction greater to one. Seismic stoppers are used to transmit the longitudinal design seismic action to two contiguous central piers, preferably the tallest ones, provided that serviceability requirements are preserved. The simplified proposed methodology assumes that the seismic stoppers are continuously activated and restrain the movements of the deck. The aforementioned seismic stoppers are combined with elastomeric bearings which allow the free rotation of the supported nodes. The transverse movement of the deck is also restrained through seismic stoppers.

The proposed methodology is based on the provisions of Eurocode 8-Part 2 [2] about the use of seismic stoppers in the longitudinal direction of the bridge. This Code in paragraph 6.6.3.1 assigns that elastomeric bearings may be used in combination with seismic stoppers which are designed to carry the design seismic actions. These stoppers shall be provided with adequate margins, so as to remain inactive under any non- seismic actions and to be activated only under seismic actions. Namely, the Code assigns that the longitudinal seismic stoppers must allow the free deformation of the bearings due to the in - service loading. On the other hand, during earthquake, seismic stoppers must not allow the movement, but simultaneously, they must not prevent the rotation of the supported nodes around the horizontal axes. In transverse direction, in which the serviceability requirements are not critical, the movement of the deck shall be restrained through stoppers. Figure 1 illustrates two cases with active and inactive respectively longitudinal seismic stoppers. It is noted that, the Greek Code for Seismic Resistant Bridges [4] included similar provisions about the use of longitudinal seismic stoppers. However, the insufficient reliability of the aforementioned provision, made engineers suspicious to the proposed methodology in the past. The insecurity is due to the difficulty in the compromise of the proposed methodology with the serviceability requirements of the bridge. The existence of the margins causes the non-simultaneous activation of the stoppers during earthquake, which leads either to a possible failure of the inadequate designed stoppers or, in the case that a capacity design procedure is used in order for the hierarchy of strengths of the various structural components to be ensured, to disproportional stopper dimensions.

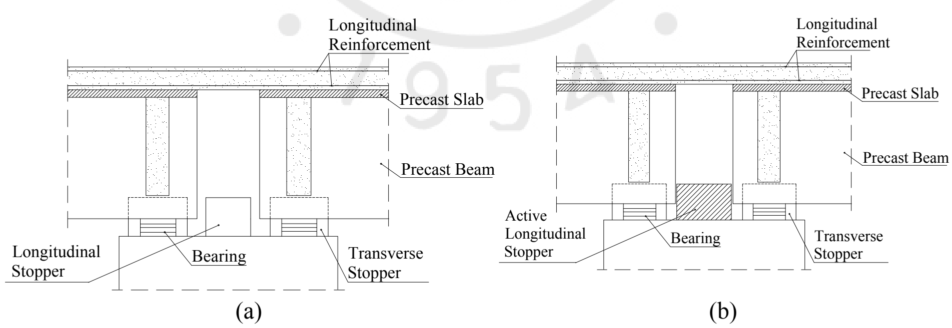

Figure 1. Longitudinal section of a pier with (a) inactive and (b) active longitudinal seismic stoppers.

The possible seismic design of precast I – beam bridges for a value of the behaviour factor greater to one, as well as the consequent reduction in the design seismic actions leads to a more rational design which requires smaller pier cross-sections. On the other hand the usual seismic design of these bridge systems for a value of the behaviour factor equal to one requires huge pier cross-sections. In these cases, it is desirable the use of hollow circular or hollow rectangular cross-sections. During the investigation on the efficiency of the proposed methodology, were checked the consequences of the reduction of the pier cross-section, which were found to be positive as far as the constructability is concerned, and negative as far as the occurrence of second order effects is concerned. It is known that if the diameter of a circular cross-section is greater than 2.5m, it is desirable the use of a hollow than a solid cross-section [5]. Solid pier cross-sections with a diameter greater than 2.5m must be avoided, because the heat diffusion has negative influence on the concrete strength.

3 ANALYTICAL INVESTIGATION

3.1 The "reference" bridges

The efficiency of the proposed design methodology was assessed by utilizing two precast I-beam bridges, a long bridge with tall piers (L=136.0m) and a shorter one (L=75.20m).

The first "reference" bridge R1 is located in Northern Greece and crosses the Aliakmonas river. The bridge was constructed downriver from a narrow and old bridge which had been constructed during the'50s. Although the crossing width as well as the height of the bridge allowed the construction of a cast in-situ bridge, the Engineers selected to construct the new bridge using the prefabrication method which as referred in the introduction, is a method which is characterized for the rapidity of the construction. This bridge, Figure 2(a), has three spans and a total length equal to 75.2m. The transverse dimension of the bridge deck is equal to 10.50m, Figure 2(b), and consists of five simply supported precast and prestressed I-beams, precast deck slabs and a cast in-situ part of the slab. The deck is supported on both abutments and on the piers through low damping rubber bearings. The piers, Figure 2(c), are circular sections with a diameter equal to 1.8m. The bridge is founded on a ground type A according to the Greek seismic design code [6]. The design ground acceleration was equal to 0.16g. The importance factor adopted was equal to γ_I=1.0, while the behaviour factors were equal to 1.0 for both horizontal directions and also 1.0 for the vertical seismic action.

The second "reference" bridge R2 is located at Asprovalta territory of Egnatia Odos Motorway and is given in Figure 3(a). This bridge has four spans and a total length equal to 136.0m. The deck, Figure 3(b), is consisted of five simply supported precast and prestressed I-beams, precast deck slabs and a cast in-situ part of the slab. The deck is supported on both abutments and on the piers through low damping rubber bearings. The piers, Figure 3(c), are hollow rectangular sections with external dimensions 3.1x5.1m and a web thickness equal to 0.45m. The bridge is founded on a ground type B according to the

Greek seismic design code [6]. The design ground acceleration was equal to 0.16g. The importance factor adopted was equal to γ_I=1.3, while the behaviour factors were equal to 1.0 for the three directions.

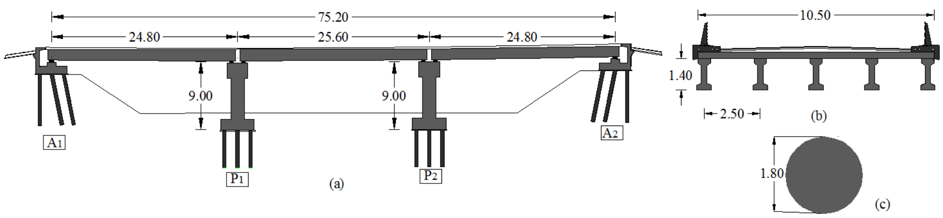

Figure 2. The first "reference" bridge R1 (a) Longitudinal section, (b) Cross –section of the deck and (c) Cross – section of the piers.

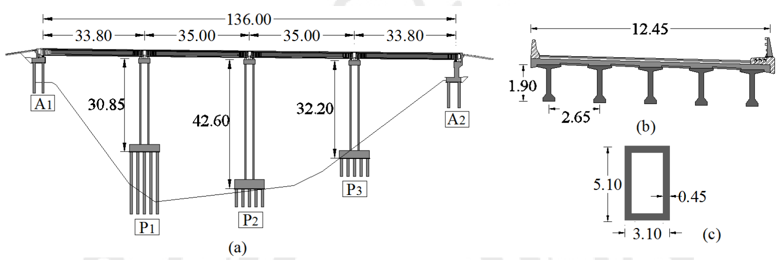

Figure 3. The second "reference" bridge R2 (a) Longitudinal section, (b) Cross –section of the deck and (c) Cross – section of the piers.

3.2 Modelling

The as-built bridge systems given in Figure 2 and 3 and the modified, according to the proposed methodology, bridges were modeled and analyzed for the purposes of the present study. The typical stick model of the first "reference" bridge systems is given in Figure 4. The bearings were modeled by link elements, Detail (a) in Figure 4, which model the corresponding translational and rotational stiffnesses of each bearing. These values were calculated according to Naeim and Kelly model [7]. Stiff zones were used in order to take into account the distance of the center of gravity of the deck's cross-section from the head of the bearings and also the width of the pier's head. The flexibility of their foundations was also taken into account by assigning six spring elements -three translational and three rotational. The modeling of the longitudinal active stoppers was made by considering that the precast beams are connected to the pier head through moment hinge connections, Detail (b) in Figure 4. All bridge systems were analyzed using the FE commercial code SAP 2000 ver. 11 [8]. Linear modal response spectrum analysis was implemented according to Codes [2] [9].Table 1 presents the bridge alternatives studied in the present study. It is noted that, the complete calculation progress of the integral bridge alternative M1-2 can be found in [10].

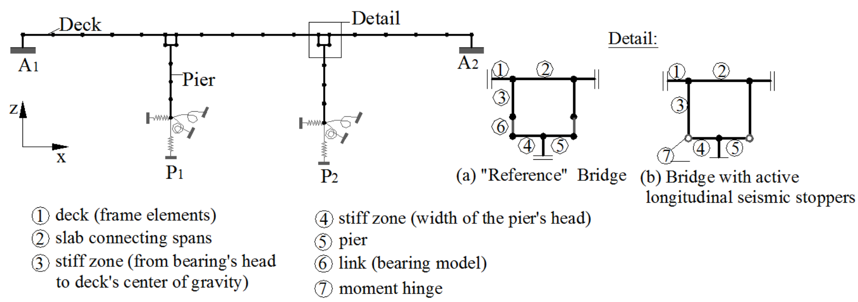

Figure 4. Typical modeling of the analyzed bridge systems.

Table 1. Analyzed Bridge systems (R1and R2 are the initial bridge systems, Figure 2 and 3, and Mi-j is the j system which results from the i initial bridge).

Bridge system	Piers	Bearings	Piers' Foundation
R1 Initial Bridge	Solid Circular d=1.8m	NBC 4 450x181(77)	4.5x4.5x1.5m pile-cap 3x3 piles/ d_p=0.45m/ L_p=5.0m
M1-1 Active stoppers at the piers	Solid Circular d=1.5m	NBC 4 450x181(77)A_1,A_2 NBC 4 450x121(33) P_1,P_2,P_3	3.5x3.5x2.0m pile-cap 4 piles/ d_p=0.45m/ L_p=5.0m/
M1-2 Integral Bridge	Solid Circular d=1.5m	NBC 4 450x181(77) A_1,A_2	3.5x3.5x2.0m pile-cap 4 piles /d_p=0.45m /L_p=5.0m/
R2 Initial Bridge	Hollow Rectangular	NBC 4 500x271(143)	10.0x10.0x2.5m pile-cap 25 piles /d_p=0.80m/ L_p=20.5(6.0)m
M2-1 Active stoppers at piers P_2, P_3	Hollow Circular d=3.0m	NBC 4 900x328 (198) A_1,A_2,P_1 NBC 4 500x121(33) P_2,P_3	11.0x11.0x2.5m pile-cap 9 piles /d_p=1.20m /L_p=20.5 (6.0)m
M2-2 Active stoppers at piers P_2, P_3	Solid Circular d=2.0m	PNu 6000/160-700 A_1,A_2, P_1 NBC 4 500x121(33) P_2, P_3	11.0x11.0x2.5m pile-cap 9 piles /d_p=1.20m /L_p=20.5m (6.0m)
M2-3 Active stoppers at piers P_2, P_3	Solid Circular d=2.5m	PNu 6000/160-700 A_1,A_2, P_1 NBC 4 500x121(33) P_2, P_3	11.0x11.0x2.5m pile-cap 9 piles /d_p=1.20m /L_p=20.5m (6.0m)

3.3 Results

The bridge alternatives, presented in Table 1 were re-designed according to current code provisions [2],[9],[11]. The members that were re-designed in all cases, apart from the case M1-2, which is referred to an integral alteration of the first "reference" bridge, were: (a) piers, (b) bearings and (c) foundations. It is noted that, the deck was re-designed only in the case M1-2, because its design is mainly based on serviceability loading of the bridge, which is almost constant in the other bridge alternatives studied in the present study. Figure 5 shows the cost of the re-designed bridge members in the case of the two bridges used as "reference" cases in this study. The figure shows that, in the case of the short bridge R1, the members that were re-designed represent a percentage equal to

32% of the total structural cost of the bridge, while in the case of the longer bridge the aforementioned percentage is about double and is equal to 65%.
Figure 6 shows the percentages reductions in the costs of the materials (concrete, steel), bearings, as well as the total structural cost for the bridge alternatives presented in this study. It can be deduced that the proposed methodology is more cost-effective in the case of the long bridge R2, as the total structural cost is reduced by up to 31%. This is due to the greater participation of the cost of the redesigned members in the case of the long bridges in comparison with the corresponding one in the case of the short bridges (see Figure 5). Furthermore, the use of elastomeric bearings for the support of the deck either decreases or increases the initial cost. On the other hand the use of sliding bearings for the support of the deck at the third pier and the abutments decreases the initial cost up to 31%. Finally, it seems that an integral solution (case M1-2) is preferable in the case of short bridges, which leads to a decrease of the total structural cost equal to 13%.

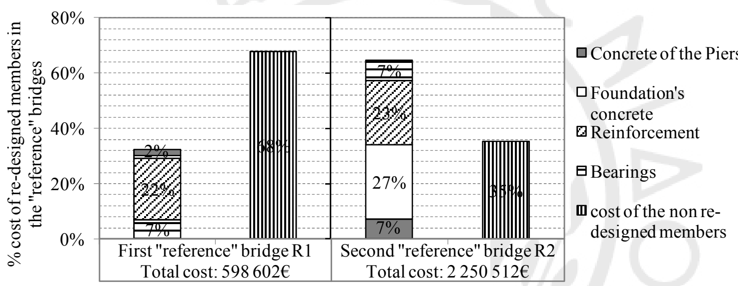

Figure 5. The total percentage cost of the re-designed members in the “reference” bridges.

4 CONCLUSIONS

The efficiency of a proposed methodology which aims on the improvement of the cost-effectiveness and safety of precast I – beam bridges was investigated in the present study. The investigation reached the following conclusions:

- According to the results of the analytical investigation, precast I – beam bridges with stoppers which restrain the longitudinal deck movements, can be designed as ductile structures. As a result, a behaviour factor less or equal to 3.5 may be used.
- The proposed methodology is characterized as technically integrated and approaches the design methodology which is implemented in monolithic bridges. The use of active seismic stoppers to two or three contiguous piers does not restrain the in-service constraint movements of the deck.
- The implementation of the proposed technique leads to smaller pier cross-sections, which are advantageous as far as concerns their earthquake resistance and aesthetics. Also the dimensions of their foundations are effectively reduced.

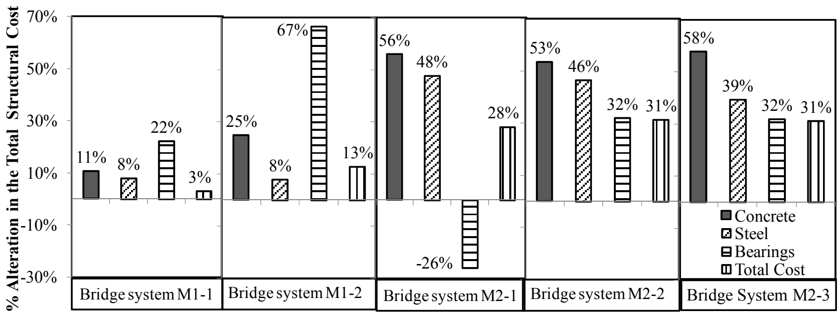

Figure 6. The percentage alteration in the total structural cost of the bridge alternatives presented in the study (according to Table 1).

- The reduction in the dimensions of the pier cross-sections and their foundations leads to significant reductions in the concrete volume and steel weight. The dimensions of the bearings are also reduced. As a result, the structural cost of the re-designed bridge system is effectively decreased.

ACKNOWLEDGMENTS

This research is co-funded by the European Union (European Social Fund-ESF) and National Resources, in the framework of the program “HRAKLEITOS II” of the “Operational Program for Education and Initial Vocational Training”.

The authors would like to thank METE SYSM S.A., Egnatia Odos S.A. and the Civil Engineer Mr. I. Mavrakis, for their kind decision to provide the studies of the two bridges for the purposes of the present study.

REFERENCES

[1] Pritchard, B. *Bridge design for economy and durability: concepts for new, strengthened and replacement bridges*, Thomas Telford, 1992.
[2] CEN, *Eurocode 8: Design of structures for earthquake resistance, Part 2: Bridges*, 2003.
[3] CEB-FIB, *Precast concrete bridges State-of-the-art report*, bulletin 29, Switzerland, 2004.
[4] Ministry of public works of Greece, *Guidelines for Seismic Design of Bridges in Combination with DIN-FB 102 103, 104*, Athens, 2007.
[5] Priestley M, Seible F. and Calvi G., *Seismic Design and Retrofit of Bridges*, John Wiley and Sons, Inc., New York, 1996.
[6] Ministry of public works of Greece, *Greek seismic code-EAK2000*, Athens, 2000.
[7] Naeim F, Kelly J.M., *Design of seismic isolated structures, From theory to practice*, John Wiley and Sons, Inc., New York, 1999.
[8] Computers and Structures Inc., *SAP 2000 Nonlinear Version 11.0.3, User’s Reference Manual*, Berkeley, California, 2007.
[9] CEN, *Eurocode 8: Design of structures for earthquake resistance, Part 1: General rules, seismic actions and rules for buildings*, 2003.
[10] Mougaidis M., Pantazidis P., Design *alternatives of a precast I-beam bridge of Egnatia Odos Motorway, Diploma Thesis*, Aristotle University of Thessaloniki, Civil Eng. Dep., 2010.
[11] CEN, *Eurocode 2: Design of concrete structures-Part 2: Bridges*, 2004.

EFFECTS OF THE SOIL-STRUCTURE-INTERACTION ON THE REGULAR SEISMIC BEHAVIOUR OF BRIDGES

Mira Petronijević[1], Djordje Ladjinović[2] and Andrija Rašeta[3]

[1] University of Belgrade, Faculty of Civil Engineering, Serbia
[2,3] University of Novi Sad, Technical Faculty, Serbia
e-mail: pmira@grf.bg.ac.rs, ladjin@uns.ac.rs, araseta@uns.rs

ABSTRACT: The effects of soil-structure-interaction (SSI) on the regular seismic behaviour of bridges were investigated. The simplified dynamic analysis, proposed in EC8-2, of 18 idealized bridges in transverse direction was carried out using the substructure method, considering three different types of soil. Different criteria for regular behaviour of bridges were applied and discussed.

KEY WORDS: Bridge; Regular behaviour; Soil-structure-interaction; EC8/2.

1 INTRODUCTION

In a recent years earthquake caused unexpected collapse of the affected bridges. In many cases the reasons were influence of soil conditions on dynamic response of structures. Numerical investigations have shown that the additional base flexibility introduced by the soil-foundation system could play an important role in altering the overall response of the bridge system. Whether the SSI will have beneficial or detrimental effect on the bridge behaviour depends on the characteristics of the structure and earthquake ground motion [4], [5].

In this paper presented is the influence of SSI on regularity of 18 cases of idealized four span bridges. The regularity of these bridges was first analyzed by Isakovic, Fischinger and Kante [3]. Their paper investigated the influence of the relevant parameters on the dynamic translatory response of viaducts with fixed-base. The responses of SDOF and MDOF models for elastic and inelastic analysis were compared and in many models significantly different results were obtained. Based on the differences in the responses the regularity index, as a new quantitative measurement of bridge regularity, was proposed.

In this paper the influence of the soil was taken into account using impedance functions and substructure method. The regularity was checked, according to EC8/2, concerning the eccentricity, mass participation factor of the first mode of vibration, relative displacement of the centre of mass for fixed and flexible base and parameter ρ, defined in EC8/2 [2] for ductile bridges.

2 BRIDGE MODELS AND SEISMIC LOAD

2.1 Bridge models

The parametric study of the response in transverse direction was carried out for 18 different types of bridges. The typical bridge has 180 m long deck and three single column piers. The abutments are pinned in the transverse direction. In the longitudinal direction fixed support at the left abutment and roller support at the right abutment are assumed. The heights of the columns vary from 7 m, to 2·7=14 m and 3·7=21 m resulting in 27 different combinations. Each particular combination is defined by *Vijk*, where *i*, *j* and *k* denote the multipliers of the unit height of 7 m, for the first, second and third piers, respectively, *Fig.1*.

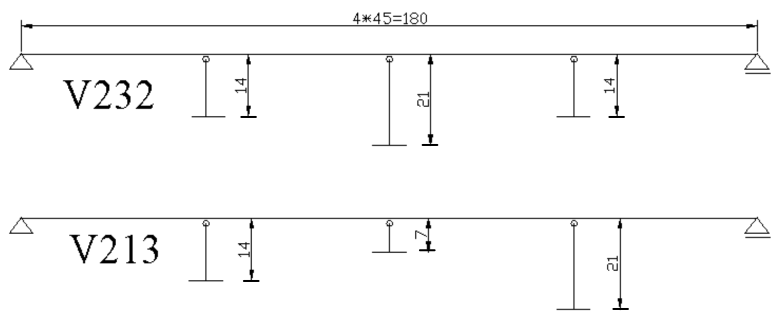

Figure 1. Layout of bridges V213 and V232

The deck is continuous, prestressed concrete box girder, *Fig. 2*. Steel B500 and concrete C25/30 are used.

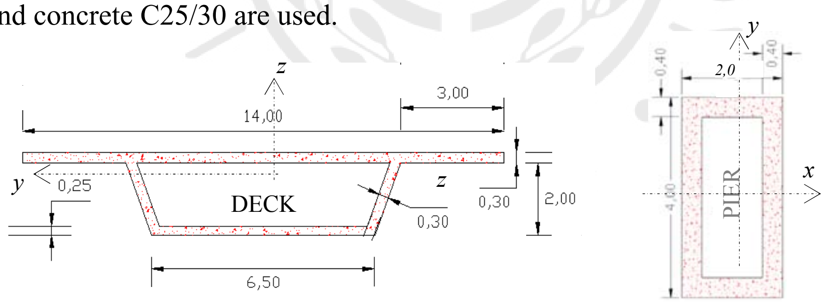

Figure 2. Cross-sections of deck and piers

The characteristics of the cross-sections of a deck and piers are given in Table 1.

Table 1. Cross-section properties

	A	A_s	I_x	I_y	I_z
deck	6.97 m^2	4.025 m^2	-	5.37 m^4	88.45 m^4
piers	4.16 m^2	-	7.3899 m^4	2.2059 m^4	-

2.2 Seismic load

The design response spectrum type I, according to EC8-2, and design ground acceleration of $a_g = 0.35 \cdot g$ are considered.

3 SOIL AND FOUNDATION

3.1 Soil

The subsoil is assumed to be half space. In order to analyze the influence of the soil properties on the regularity of bridges, three different types of soil B, C and D according to EC8, were analyzed. The soil characteristics are given in Table 2. Shear modulus G and shear wave velocity v_s are reduced, according to ATC (1978), to the values G_0=0.385G and v_{s0}=0.625v_s, that correspond to the effective soil acceleration $a_g=0.35g$.

Table 2. Soil characteristics

Soil type	v_s (m/sec)	ν	γ (kN/m^3)	ρ (t/m^3)	G (kPa)	G_0 (kPa)	v_{s0} (m/sec)
B	600	0.33	20.0	2.04	734400	282744	375.0
C	300	0.33	19.0	1.94	174600	67221	187.5
D	160	0.33	18.0	1.84	47104	18135	100.0

3.2 Dynamic stiffness of foundation

The influence of the soil and foundations on the dynamic response of bridges was taken into account using superstructure supported on springs and dashpots.

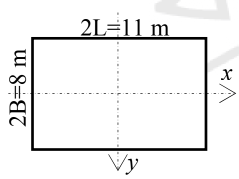

Figure 3. Foundation

The dynamic stiffnesses of prismatic foundations (*l_x=l_y=l_z=8*x*11*x*2m) Fig. 3,* resting on a half-space were calculated taking the solutions for arbitrary shaped foundation given by Dobry and Gazetas [1]. The dynamic stiffness K_i in $i=x,y,z,\varphi$ direction is presented in the following form:

$$K_i = K_{i,stat}\left(k_i + i a_o c_i\right) = \mathrm{K}_i + i\mathrm{C}_i \quad , \; i=x,y,z,\varphi \tag{1}$$

where: $K_{i,stat}$ is static stiffness,

a_o is dimensionless frequency ($a_o = \omega B/c_s$) ,

$k_{i.}\ c_i$ are dimensionless stiffness and damping coefficients [1].

Dynamic stiffness of the foundation is a complex number. The real part presents spring stiffness K_i while imaginary part presents dashpot damping C_i. Although the dynamic stifnesses of the foundation are in general frequency-dependent quantities, their low frequency values do not fluctuate appreciably with frequency and can be replaced with frequency independent springs and dashpots. The stiffness of spring K_i and damping of dashpot C_i for soils type B, C, and D were calculated for driving frequency equal to the first frequency of the structure, and given in Table 3. The damping in the soil is assumed to be 5%.

Table 3. Spring and dashpots characteristics

	Stiffness [MN/m], [MNm/rad]			Damping [MNs/m]		
	B	C	D	B	C	D
K_z	9.033	2.148	0.579	0.115	0.055	0.0276
K_x	7.436	1.768	0.477	0.093	0.044	0.022
K_y	7.224	1.718	0.463	0.106	0.050	0.025
$K_{\varphi x}$	284.938	67.743	18.276	0	0	0

4 NUMERICAL ANALYSIS

Finite element analyses (FE) were carried out using the commercial FE package SAP2000 [6]. In all models, the damping of the bridge superstructure was approximated with the Rayleigh damping, by assuming a 5% modal damping ratio in the first and the second modes. The masses of the piers were concentrated at the top and bottom of each pier. The stiffness of the piers was reduced to 50% of uncracked section.

4.1 Fix-base structures

The analysis of regularity of 18 bridges with fix-base was carried, using fundamental mode method (FMM) and response spectrum method (RSM). The regularity of bridges was considered according to the following parameters:

- eccentricity e between the centre of mass and the centre of stiffness, relative to the bridge length l

$$e=\left(x_m-x_s\right)/l \quad , \tag{2}$$

- relative difference Δ between the areas bounded by the deck displacement diagrams obtained by RMS and FMM methods:

$$\Delta=\frac{\left|(d_{i,RSM}-d_{i,FMM})\Delta x_i\right|}{d_{i,RSM}\Delta x_i}\cdot 100 \tag{3}$$

where: $d_{i,RSM}$ is displacement in point i obtained by RSM method,
$d_{i,.FMM}$ is displacement in point i obtained by FMM
Δx_i is the length between two points of girder

- modal mass participation factor.

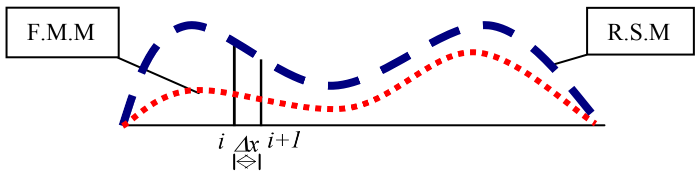

Figure 4. Displacement diagrams

According to EC8-5, a bridge is regular if eccentricity *e* is less than 5%. In that case, the simplified fundamental mode method can be used. For all non-symmetric bridges *e* is higher than 5%, except for the bridge type V213 where *e* is equal to 1.9%, see Table 4. It means that all non-symmetric bridges, except V213, behave as irregular.

Table 4. Eccentricity *e* [%]

Model	V112	V122	V132	V113	V123	V133	V213	V223	V233
e [%]	103	175	188	118	207	224	19	77	11

The normalized diagrams of displacement along the deck due to FMM and RSM were determined and the relative differences Δ between the areas bounded by the normalized displacement diagrams were calculated. In order to evaluate the behaviour of bridges the relative mass participation factors and eccentricity were compared. Analyzing the results following conclusions were made:

- Eccentricity is not relevant factor for regularity of bridges. The structure V213 whose eccentricity *e* is just 1.9% has very high difference of 55.7%, between areas of displacements Δ obtained by FMM and RSM, due to the influence of the second mode. The application FMM is not adequate;
- The symmetric bridges with stiff end columns, V121 and V131, have Δ=11.8% and Δ=6.7%, respectively, which means that they behave as irregular ones, due to the influence of higher modes;
- All structures which have modal mass participation factor in the first mode greater than 90% have Δ<3.5%, which ranks them to the regular bridges. This group includes all symmetric bridges except V121 and V131, and two non-symmetric bridges V223 and V233 (e>5%).

4.2 Flexible base structures

The springs and dashpots were used for modelling the supports of a finite-element model using the commercial FE package SAP2000. The link elements were connected with superstructure by short rigid elements having lengths 1 m. The foundations' mass was taken into account. The effects of wave propagation were neglected, only the influence of soil stiffness and damping on the regular behaviour of bridges was analyzed for three different types of soil B, C and D according to EC8. The case of fixed foundation was treated as the fourth limiting case, G=∞. The impedance functions of the foundations are given in Section 3.2. Among 18 types of the structure presented are the results obtained for three regular bridges: V111, V232P and V333 and three irregular ones: V131, V123 and V213.

The SSI prolongs the period of vibrations. The fundamental periods of vibration T_1 and the relative differences between the fundamental periods T_1 of structures with fixed and flexible base are presented in Table 5. The biggest change of the period of vibration of the first mode happened in the case of symmetric bridge with the shortest columns V111.

Table 5. Periods of vibrations

	T [s]	T [s]	T [s]	T [s]	ΔT (%)	ΔT (%)	ΔT (%)
type	fixed	B	C	D	B	C	D
V111	0.242	0.265	0.329	0.489	9.5	36.0	102.1
V232	0.774	0.793	0.846	0.836	2.5	9.3	8.0
V333	1.031	1.045	1.071	1.198	1.4	3.9	16.2
V131	0.413	0.434	0.497	0.666	5.1	20.3	61.3
V123	0.609	0.622	0.697	0.817	2.1	14.4	34.2
V213	0.423	0.434	0.481	0.64	2.6	13.7	51.3

The EC8/2 [2] indicates that SSI should be used when the relative displacement

$$\Delta_\mathrm{d} = \frac{\left| d_{flex} - d_{fix} \right|}{d_{flex}} \cdot 100\% \qquad (4)$$

due to the soil flexibility in the centre of mass of the desk is greater than 30%. The flexibility of the soil caused larger displacements of the deck. The relative displacements were calculated for all cases and are presented in Table 6. For soil type B, Δ_d is less than 30%. SSI is not important. For soil type C, Δ_d is higher than 20% for the bridges V111 and V213. For the soil type D displacements due to the soil flexibility Δ_d is higher than 30% for all bridges, except for the symmetric bridges V232 and V333. In all these cases SSI should be taken into account.

Table 6. Δ_d

	Δ_d [%]		
type	B	C	D
V111	9.3	20	41.3
V232	2.3	7.6	11.3
V333	1.2	3.6	14.3
V131	4.7	15.9	31
V123	2.4	14.2	38.9
V213	11.4	25.8	37.5

In *Fig.5* only two diagrams of displacements for fixed and flexible structures, V111 and V213, soil type D, are presented. Part of flexible structures displacement is due to the rigid body rotation of piers caused by soil deformation at the base. The displacements are larger as soil is softer. In the case of irregular bridges, V213, with irregular arrangement of the columns, the soil flexibility has beneficial effect on the deck displacements, smoothing the diagram of displacements.

4.3 Flexible base, ductile bridges

In the case of ductile structures the regular behaviour of bridges was checked using clause 4.8.1, EC8/2. The behaviour factor q is assumed to be 3.5. The effective moment of inertia was taken as 26.2% of uncracked pier section, according to EC8/2, Annex C.

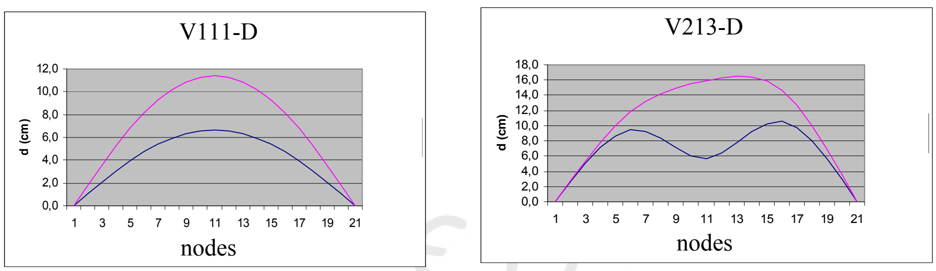

Figure 5. Diagrams of displacement for soil type D: — fixed and — flexible base

The regular behaviour was checked comparing the maximum and minimum local force reduction factor r obtained for individual pier. If the ratio of r_{max} and r_{min} differs for a factor larger than 2, the bridge is considered to have irregular behaviour.

All piers have the same cross section and percentage of steel is 1% of section area. As the flexural resistance is the same for all piers, the ratio between maximum and minimum reduction factor can be expressed as:

$$\rho = \frac{\max M_{Ed,i}}{\min M_{Ed,i}} \tag{5}$$

where: $M_{Ed,i}$ is maximum value of the design moment at the plastic hinge,
$M_{Ed,i}$ is minimum value of the design moment at the plastic hinge, of member i.

The parameters ρ for bridges with fixed base and flexible base were calculated and are given in Table 7.

Table 7. Parameters ρ

	ρ					
	B		C		D	
type	fix	flexible	fix	flexible	fix	flexible
V111	1.4	1.4	1.4	1.4	1.4	1.4
V232	1.4	1.5	1.4	1.4	1.4	1.3
V333	1.4	1.4	1.4	1.4	1.4	1.4
V131	2.9	2.9	2.8	2.7	2.8	2.1
V123	1.9	1.9	1.8	1.9	1.8	2.0
V213	4.4	4.3	4.4	4.2	4.4	3.8

In the case of all symmetric bridges ρ is less than 2, except for the bridge with stiff ends columns - V131, which means that all symmetric bridges except bridge V131 have regular behaviour. The most irregular bridge appears to be V213 – the structure with stiff central column and small eccentricity (e=1.9%). The soil flexibility tends to diminish irregular behaviour of this structure increasing the flexibility of the central part, but the ρ remains still high, far from the proposed values. According to EC8/2 such bridge can be designed using either a reduced q-value or a non-linear time/history analysis.

5 CONCLUSIONS

A parametric study demonstrates that eccentricity-based criterion given in EC8/2 is not always adequate, especially in the case of the structure with stiff end (or central) column and relatively small eccentricity. Neglecting of higher mode leads to unsatisfactory results, thus FMM is not adequate for analysis. In such case RSM or time history analysis should be applied.

SSI should be taken into account in the case of very soft soil. SSI does not affect the regularity of regular bridge structures. The SSI effect is more pronounced in the case of irregular bridges, where its influence is more beneficial than detrimental. In comparison with fixed base structure, flexible base caused larger deck displacements, equalizing displacements and smoothing the curvature of the displacement diagram. The base flexibility causes the diminishing of ρ, but not so significantly to change the irregular behaviour of such bridges.

ACKNOWLEDGMENTS

The results presented in this paper are part of the Project TR 36043 supported by the Ministry of Science and Technology, Republic of Serbia.

REFERENCES

[1] Dobry R, Gazetas G, "Dynamic Response of Arbitrary Shaped Foundations", JGED, ASCE, Vol. 112, No. 2, pp 109-135, 1986
[2] prEN 1998-2, Eurocode 8: Design of structures for earthquake resistance, Part 2: Bridges, DRAFT No 5, European Committee for Standardization, June 2004
[3] Isaković T, M. Fischinger, P. Kante, Bridges: "When is single mode seismic analysis adequate?", Structures & Buildings, Vol 156, Issue 2, pp. 165-173, May 2003
[4] Mylonakis G, Gazetas G, "Seismic soil–structure interaction: beneficial or detrimental?" Journal of Earthquake Engineering, Vol 4, No 3, pp 277–301, 2000
[5] Sextos A, Kappos A, Pitilakis K, "Inelastic dynamic analysis of RC bridges accounting for spatial variability of ground motion, site effects and soil-structure phenomena. Part 2: Parametric study", Earthquake Engng. and Struct. Dyn, Vol 32, pp. 629-652, 2003
[6] SAP2000 Analysis Reference Manual, Computers and Structures, Inc., Berkeley, California, July, 2002

USE OF BRIDGE APPROACH EMBANKMENTS AS SEISMIC RESTRAINERS

Ioannis Tegos[1], Sevasti Tegou[2], Afroditi Spanou[3] and Thomas Salonikios[4]

[1,2,3] Aristotle University of Thessaloniki, Dept. of Civil Engineering, Greece
[4] Institute of Engineering, Seismology and Earthquake Engineering (ITSAK)
e-mail: [1]stegou@civil.auth.gr, [2]itegos@civil.auth.gr, [3]aspanou1@hotmail.com,
[4]salonikios@itsak.gr[4]

ABSTRACT: In the present study an unconventional fusing mechanism is proposed for earthquake resistant bridges. The unconventional system consists of a concrete slab, which is rigidly connected to the bottom flange of the deck's section. This slab is embedded in the approach fill and resists to the seismic movements of the deck through the friction, which is developed, while the deck moves.

KEY WORDS: Abutment; Bridge; Embankment; Friction.

1 INTRODUCTION

As it is known, bridge design has to compromise both serviceability and earthquake resistance requirements. Serviceability requirements, which mainly affect the longitudinal direction of the bridge, require the free expansion and contraction of the deck due to thermal effects, creep and shrinkage. In current Bridge Engineering, the accommodation of these requirements is achieved through the support of the deck by the abutments through bearings and its separation of the approach embankment by expansion joints. The desirable use of the embankments as seismic restrainers is possible, provided that the serviceability requirements of the bridge are properly accommodated. On the other hand, in cases that the deck is rigidly connected to the abutment, the wedging of soil behind the abutment namely the "ratcheting effect" which results in the long-term build-up of soil pressures, is a significant problem. This phenomenon was successfully faced by Horvath who proposed structural techniques to minimize the in-service distress of the abutments and their approach fills [1-2]. The response of the aforementioned systems, which consists of the reinforced backfill and the compressible inclusion (EPS), was experimentally tested by Potzl and Naumann in Germany [3]. Figure 1 and 2 show cases where Horvath's structural techniques are implemented in US and German bridges.

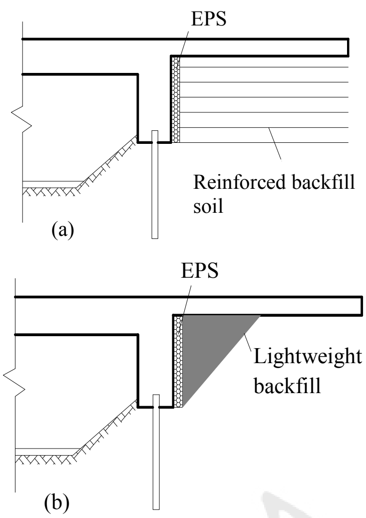

Figure 1. Horvath's proposed structural techniques for the minimization of the ratcheting effect: (a) reinforced backfill and (b) lightweight backfill.

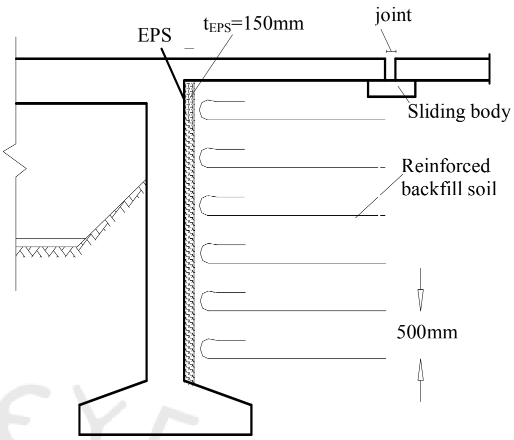

Figure 2. The reinforced backfill and the interjection of the compressible inclusion (EPS), between the abutment and the earth, in the case of a German bridge with full height abutments.

In recent years, more and more researchers turn their attention to the embankment- bridge interaction, which can contribute to the enhancement of the earthquake resistance of bridges [4-5]. Recent studies came up to conclusion, that in general, the seismic participation of the abutment and approach embankment reduces the bridge movements [6-8]. An extensive research is conducted concerning the effective reduction of bridge seismic actions through the participation of the abutments and approach embankments, in the laboratory of Reinforced Concrete and Masonry Structures of Aristotle University of Thessaloniki. Methods of reducing the bridge pounding through the exploitation of the abutments and approach embankments as seismic restrainers, are investigated in such a way so as, the expected effect to be maximized.

In the present study, the approach embankments are properly used so as to dissipate part of the induced seismic energy. The proposed fusing mechanism, without causing problems to the serviceability performance of the bridge, effectively reduces the longitudinal seismic movements of the deck. It is, also, mentioned that this system can achieve during the longitudinal earthquake, even the immobilization of a bridge, whose length is approximately 200m, without effects on the serviceability performance of the bridge. The proposed methodology is economical and reliable and is proposed as an alternative choice to the equivalent and continuously expanding in recent years, seismic isolation practice.

2 DESCRIPTION OF THE PROPOSED FUSING MECHANISM

2.1 General

The aim of the proposed, in the present study, mechanism is the prevention of the seismic vibration of the bridge as well as the dissipation of the induced seismic energy. The system, Figure 3, consists of a thin plate, which is embedded in the backfill and is rigidly connected to the bottom flange of the deck's cross-section. The width of the plate is equal to distance between the wing-walls, while its length is proportional to the bridge's length. The friction forces that are developed during the movement of the plate due to the constant weight of the overlying soil, are easily overcome in the case of the in-service constrained movements of the deck due to creep, shrinkage and thermal effects.

On the other hand, these forces resist to the longitudinal movement of the deck during earthquake. The friction forces are constant and are related to the aforementioned depth and area of the plate. The proposed mechanism can achieve a desirable control of the seismic movements of the deck and therefore reduces the seismic actions of the piers and their foundations. Furthermore, this system can be applied in both integral and simply supported bridges. The effect of the loading speed on the efficiency of the proposed mechanism is experimentally investigated in this paper.

2.2 Exit plate

The so-called "exit plate" of the bridge deck, is either cast in-situ or prefabricated and is embedded at a depth of about 2.0 m below the road surface. Its thickness is t_s=0.25m while its width is equal to the distance between the abutment's wing-walls, which are rigidly connected to the abutment's web. Its length is related to the length of the bridge and varies from 4.0 m to 8.0 m.

2.3 Embankments

The approach embankment, in which the exit plate is moved into during the serviceability and earthquake loading of the bridge, includes two layers of crushed material above and below the plate, as shown in Figure 3. It is noted that the embankment is composed of a common backfill material without special requirements, which would lead to an increase of the construction cost of the proposed system.

3 IN-SERVICE AND SEISMIC PERFORMANCE OF THE PROPOSED SYSTEM

The seismic contribution of the proposed unconventional fusing mechanism, which brings to mind the story of the "Egg of Columbus", is based on use of the resultant constant friction force, which resists to the movement of the bridge deck. The friction forces F_f, developed during earthquake both ends of the

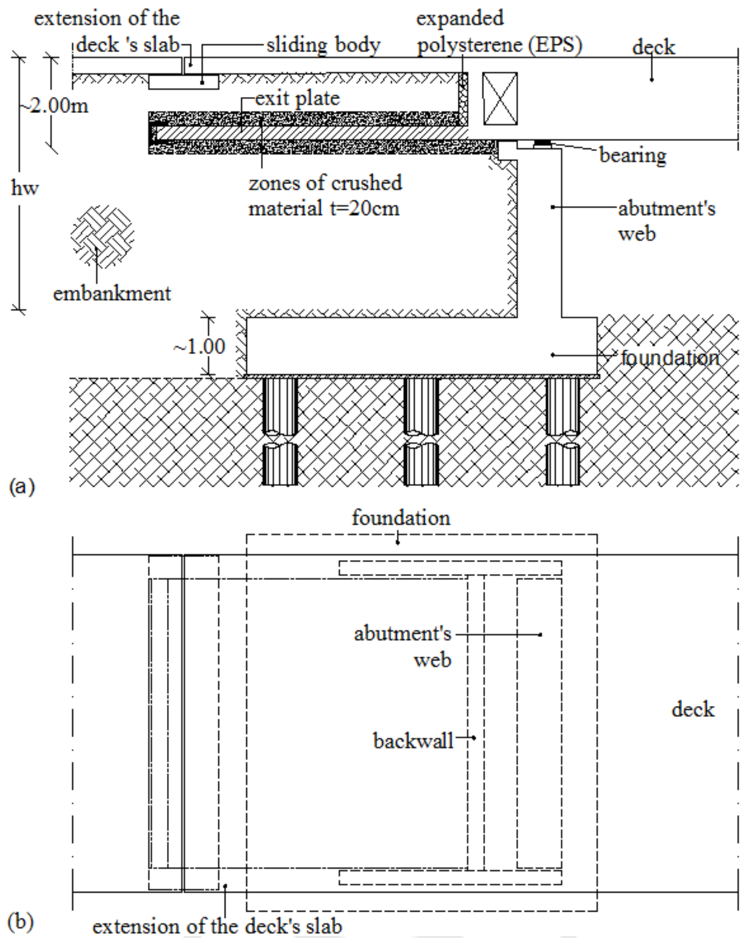

Figure 3. The proposed system: (a) longitudinal section and, (b) plan view.

bridge, have the same direction and when they occur, their value is constant. Of course, for ground acceleration's values lower than F_f/m_{ol}, where m_{ol} is the bridge's mass, the system is not oscillated, but is moved parallel to the ground's motion. When the ground acceleration exceeds the above value, then the oscillation of the system is activated. The friction force F_f resists to the system's oscillation.

Figure 4 presents two typical hysteresis loops, of which the one refers to an initial bridge system, while the other refers to the bridge which develops the proposed fusing mechanism. This figure shows that the percentage of the seismic energy absorbed by the proposed system is equal to $100 \cdot F_f/[m_{ol} \cdot S_a(T)]$. The above quantification of the absorbed energy shows that ductile bridge structures, in which the behaviour factor q is greater than 1.5, respond effectively to the proposed upgrade because the value of $S_a(T)$ is much lower than in the cases of the low ductility systems (i.e. precast bridge systems with q<1.5). However, these systems have the advantage of the increased period due to the support of the deck to the piers and abutments by rubber bearings and therefore, in many cases, the possibility of covering the difference that is referred above cannot be excluded.

The aforementioned friction force is subtracted from the inertial force of the bridge. This means that the dynamic response spectrum analysis of the system can be implemented, using a modified response spectrum whose ordinates are reduced by F_f/m_{ol}, where F_f is the frictional force of the exit plate and m_{ol} is the total mass of the system. Eq. 1 quantifies the calculation of the ordinates of the design response spectrum used for the dynamic analysis of bridge structures which exploit the proposed fusing mechanism.

$$DF_{inertial} = m_{ol} \cdot S_a(T)\text{-}F_f \tag{1}$$

where: $S_a(T)$ is the spectral acceleration and
$DF_{inertial}$ is the reduction of the inertial force due to earthquake.

4 EXPERIMENTAL INVESTIGATION

4.1 Description of the experimental setup

The experimental setup includes a suitable, without parasitic frictions, system as well as a double acting hydraulic actuator, Figure 5 and Photo 1. The system is consisted of a rectangular concrete slab 1.00x0.60m, whose thickness is 0.18m. The double acting hydraulic actuator is properly connecting to the slab's end. This slab slides under the quasi-static cyclic loading within two thin layers of gravel, which are surrounded by two steel frames, Figure 5. The maximum diameter of the gravels is between 8 to 16 mm. The dead load imposed on the concrete slab is 5kN. The experiment was repeated for two loading speeds, namely, the slow speed which represent the movement of the plate during the serviceability loading and the fast speed which represents the seismic loading of the slab.

4.2 Test results

Figure 6 gives, for the two different loading speeds, the hysteresis loops derived from the response of the system to the loading imposed by the double acting hydraulic actuator.

In the first case, Figure 6(a), which refers to the slow loading of the system (158 mm/min) the the frictional resistance was almost 13,5kN, while in the second one, Figure 6(b), which refers to the fast loading (1800 mm/min), the frictional resistance was almost 15 kN. The area enclosed by the envelope of the hysteresis loop, which is quite large, indicates that the energy dissipation is significant in both cases.

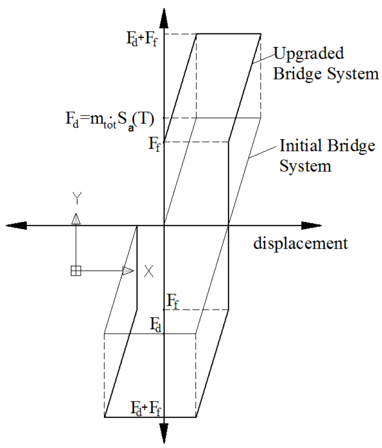

Figure 4. Typical hysteretic loops of the initial and the upgraded bridge system.

Photo 1. Experimental setup.

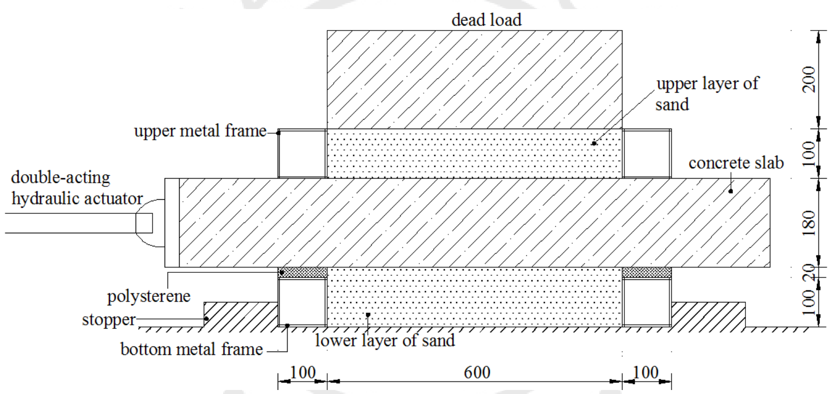

Figure 5. Experimental setup.

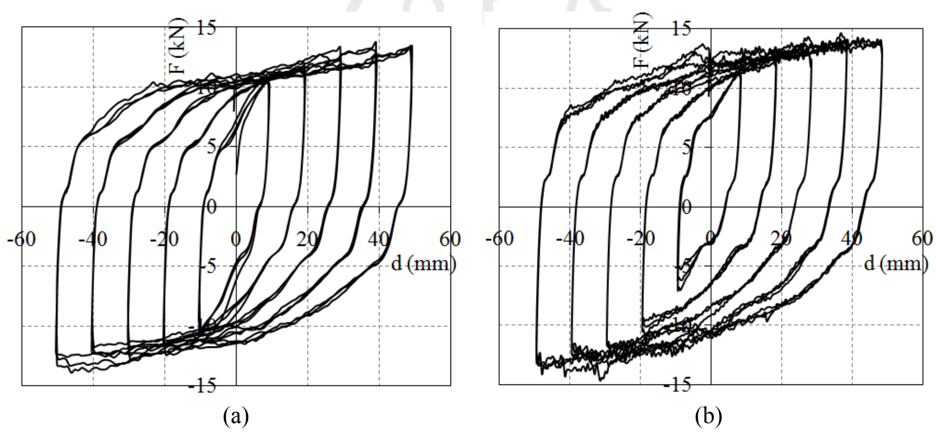

Figure 6. Hysteresis loops (a) slow loading (158 mm/min),(b) fast loading (1800 mm/min).

5 CONCLUSIONS

In the present study was experimentally investigated the seismic efficiency of a fusing mechanism, which is consisted of a thin slab, rigidly connected to the bottom flange of the deck's cross-section. This slab is embedded in the approach fill and resists to the seismic movements of the deck through the friction, which is developed while the deck moves. The investigation reached the following conclusions:

- The resultant hysteresis loops are impressive and can be contrasted with the seismic efficiency of the most efficient seismic dampers. The energy dissipation of the system is significant.
- The influence of the loading's speed on the frictional resistance is obvious. This influence is expected to be much higher for realistic speed values of the seismic loading, in cases, of course, that they can be simulated in the laboratory. In the experiment presented in this study, the friction resistance is increased about 10% due to the increase of the loading's speed. The friction coefficient is increased by the same percentage.
- The friction resistance of the plate's surface is about three times the imposed dead load. As a result, the measured value of the coefficient of friction between the concrete surface and the gravels' layer is about 1.5. This value was obtained without any improvement of the adjacent surfaces.

REFERENCES

[1] Horvath J.S., "The compressible-inclusion function of EPS Geofoam: Analysis and design methodologies", Manhattan College Research Report No. CE/GE-98-2, New York, USA, 1998.

[2] Horvath J.S., "The compressible-inclusion function of EPS Geofoam: An overview of concepts, Applications and Products", Manhattan College Research Report No.CE/GE-98-1, New York, USA, 1998.

[3] Pötzl M. and Naumann F., "Fungenlose betonbrucken mit flexiblen widerlagern", Beton-und Stahlbetonbau, Heft 8, 2005.

[4] Zhang, J., and Makris, N., "Kinematic response functions and dynamic stiffnesses of bridge embankments", Earthquake Eng. Struct. Dyn., 31, pp. 1933–1966, 2002.

[5] Mylonakis, G, Simeonov, V.K., Reinhorn, A.M., and Buckle, I.G., "Implications of Spatial Variation of Ground Motion on the Seismic Response of Bridges: Case Study," ACI International - Special Publication SP-187 (K. Krishnan Editor), pp. 299-327, 1999.

[6] Mikami T. et al., "The effect of abutments as displacement limiting measure on seismic performance of bridges", www.pwri.go.jp/eng/ujnr/tc/g/pdf/19/4-1mikami.pdf, Accessed 15 Oct 2008, 2003.

[7] Mitoulis S.A., Tegos I.A. "An unconventional restraining system for seismically isolated bridges", Engineering Structures, Vol. 32, Issue 4, pp. 1100-1112, 2010.

[8] Tegou S.D., Mitoulis S.A., Tegos I.A., "An unconventional earthquake resistant abutment with transversely directed R/C walls", Engineering Structures, Vol. 32, Issue 11, pp. 3801-3816, 2010.

EXCITATION OF HIGHER MODES OF LONG BRIDGES DUE TO SPATIAL VARIABILITY OF EARTHQUAKE GROUND MOTION

Savvas P. Papadopoulos[1], Anastasios G. Sextos[2]

[1] Aristotle University of Thessaloniki, Department of Civil Engineering, Thessaloniki, Greece, Civil engineer, MSc, Ph.D. Candidate

[2] Aristotle University of Thessaloniki, Department of Civil Engineering, Thessaloniki, Greece, Assistant Professor

e-mail: savvaspp@civil.auth.gr, asextos@civil.auth.gr,

ABSTRACT: In the present study, the excitation of higher modes due to spatially variable earthquake ground motions is examined for the case of an existing, seismically isolated R/C bridge; the Lissos river bridge. The results reveal a systematic trend to excite the higher modes of the bridge when this is subjected to non-uniform earthquake motion and a subsequent increase in seismic demand.

KEY WORDS: higher modes; asynchronous motion; spatial variability; bridges.

1 INTRODUCTION

During the last decades, a great progress has been made in earthquake engineering and the use of advanced numerical analysis methods has been incorporated in most modern seismic codes worldwide, some of them proving rules and guidelines for obtaining a reliable estimate of the seismic structural response in the time domain. Notwithstanding these advancements in predicting the linear and/or nonlinear seismic response of a structure, the outcome still heavily relies on the appropriate selection of an input motion scenario representative to the seismic hazard at the site of interest. The latter however, is deemed to be associated with the highest level of uncertainty within the entire design or assessment process. This problem of defining the earthquake scenario becomes even more complex and multi-parametric in the cases of structures of significant length, such as bridges, where, for a number of reasons [1] related to wave propagation, soil conditions and topography, the structure is excited by motions that differ considerably among its support points both in terms of phase and amplitude; a phenomenon called spatial variability of earthquake ground motion (SVEGM).

Since the early '60s, many empirical, semi-empirical and analytical methodologies have been proposed to estimate the effect of asynchronous excitation on long structures. However, modern seismic codes still dealt with this problem through either simplified code-based calculations or indirect measures involving larger seating deck lengths (AASHTO 1996, ATC-32 (ATC 1996), JRA 2002). It is only in EC8-Part 2 [2] that proposes both a simplified (pseudo-static) and a more detailed procedure (in the frequency domain) for considering SVEGM effects; again though recent studies [3] have revealed large discrepancies compared to more comprehensive methodologies [4], primarily attributed to their inability to capture the dynamic component of structural response.

The scope of this paper therefore, is to focus on the modification of the dynamic response of an existing bridge when it is subjected to non-uniform ground motion. This is achieved by quantifying the excitation of higher modes of vibration as a means to investigate a simple measure for predicting in advance the beneficial or detrimental effect of asynchronous excitation on the seismic response of long bridges. The description of the case studied, as well as the analysis results and the subsequent discussion are presented in the following.

2 METHODOLOGY

2.1 Overview of the bridge studied

The Lissos' bridge [5] is used for the particular case study. It is an 11-span, base-isolated R/C structure of an overall length of 433m that is constructed along the Egnatia Highway in northern Greece (Figure 1 and Table 1). The deck rests through elastomeric bearings on 10 piers and through roller bearings at the two abutments. Expansion joints of 330mm have also been prescribed while transverse displacements of the deck larger than 10cm are prevented by stoppers of 1.20m height. The sections of the piers and the deck are illustrated in Figure 2. This bridge was adopted as a case study for two primary reasons. First, the bridge is long enough to be, in principle, sensitive to asynchronous earthquake excitation (based on both research findings and EC8 criteria) and secondly, because the large number of piers generates the required sample for detailed statistical processing of the response quantities.

2.2 Parametric analysis scheme

An extensive parametric analysis was performed in order to investigate whether higher modes are excited under non-uniform earthquake excitation scenarios. The parameters modified were the soil class (A, B, C, D according to the EC8 as seen in Table 2) and PGA (taken equal to 0.16g, 0.24g, 0.36g). To account for different target frequency content of the earthquake motion three real records were used for each combination of the above parameters. These records were selected from the PEER strong motion database complying with the corresponding pair of soil category and PGA. The motions were applied in each support as displacement time histories after appropriate baseline correction. It is noted that, due to paper length limitations, it is only the results of the wave passage effect that are presented and discussed herein.

Figure 1. Overview of the Lissos' bridge along Egnatia Highway in northern Greece.

Table 1. Pier height [m] and span length [m].

A1	P1	P2	P3	P4	P5	P6	P7	P8	P9	P10	A2
	5.50	5.83	6.12	6.40	10.24	10.58	7.92	8.26	8.60	4.40	
29.56	37.05	37.05	37.05	44.35	44.35	44.35	44.35	44.35	44.35	26.50	

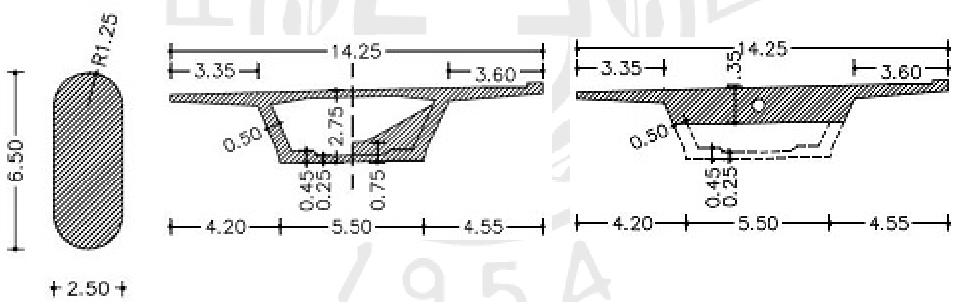

Figure 2. Pier section (left), typical deck section (middle) and deck section at the last span (right).

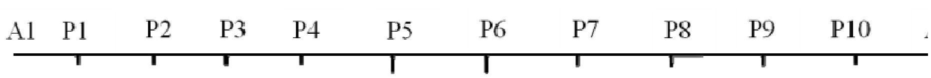

Figure 3. Layout of the Lissos river bridge.

In order for the dynamic soil-structure interaction (SSI) to be taken into account, the foundations of the bridge were individually designed for each combination of the above pairs of soils class and PGA according to Eurocodes 8 [2] and 7 [6], while impedance of the surface and pile foundation was derived according to Mylonakis et. al. [7-8]. Due to the fact that the deck rests on the piers through elastomeric bearings, piers were not redesigned for different values of earthquake intensity. It is noted that in the particular study, it was only the transverse response of the bridge that was studied.

Table 2. Soil properties used in the parametric study.

Category	V_s[m/sec]	N_{spt}	φ[^{o}]	c [kPa]	γ [kN/m^3]	v	β [%]	G [MPa]
A	Piers are assumed fixed							
B	500	60	43	0	22	0.4	3.0	550
C	250	30	36	15	19	0.4	3.5	120
D	100	10	30	8	16	0.4	4.0	16

2.3 Numerical analysis aspects

All the analyses were performed using the computer program SAP2000v.10 [9]. Beam elements were used to model the piers, the deck and the stoppers, while bearings, gaps, foundation dashpots and locations of potential plastic hinge development at the base of the stoppers were modeled using nonlinear link elements. Apart from the pier-dependent 6-DOF foundation impedance, abutment stiffness was introduced in the form of linear springs characterized by horizontal (transverse and longitudinal) stiffness equal to 10^6 kN/m. As the scope of this study is the investigation of the potential excitation of higher modes, geometric nonlinearities were deliberately neglected at a first stage, in order to ensure that the predicted dynamic characteristics of the bridge would not change in time. However, a second set of analyses that was in parallel performed considering the above geometric nonlinearity, revealed that, at least for the particular levels of earthquake intensity (PGA up to 0.36g) examined, the stoppers were activated 12 times as a minimum. These results are also discussed in terms of assessing the effect of asynchronous excitation on the overall dynamic response of the bridge but inevitably no comparison is made on the basis of the (time-dependent) dynamic characteristics of the bridge.

2.4 Criteria set quantifying higher modes excitation

In order to investigate the excitation of higher modes and most importantly, to attempt to correlate it with the increase in the response quantities of the bridge studied, the Fourier spectra of the accelerations derived at specific points along the deck were computed and were then compared with the modal frequencies of the structure. As explained previously, for linear elastic response, the peak frequencies observed in the Fourier spectra coincide well with the dynamic characteristics of the bridge. However, *excitation* of a specific mode *due to asynchronous motion* is less apparent, and as such, specific quantitative criteria need to be defined. The criteria adopted herein for spotting an excited mode Φ_{Ti} are the following:

- the Fourier amplitude at a specific modal period T_i under asynchronous motion ($FA_{asyn}(T_i)$) is at least 20% of the maximum Fourier amplitude ($maxFA_{syn}$) observed at the entire frequency range under synchronous excitation, *and*

- the Fourier amplitude at a specific modal period T_i under asynchronous motion ($FA_{asyn}(T_i)$) is higher than the respective one under synchronous excitation ($FA_{syn}(T_i)$) *and*
- the mode i (Φ_{Ti}) corresponding to modal T_i activates at least 5% of the modal mass in the transverse direction or around the vertical axis. In other words:

$$\varphi_{Ti} : \begin{cases} FA_{asyn}(T_i) > 0.2 \cdot maxFA_{syn} \\ FA_{asyn}(T_i) > FA_{syn}(T_i) \\ \frac{\varphi_{Ti}^T \cdot \boldsymbol{M} \cdot \varphi_{Ti}}{\Sigma(\varphi_i^T \cdot \boldsymbol{M} \cdot \varphi_i)} > 5\% \end{cases} \tag{1}$$

3 ANALYSIS RESULTS

3.1 Linear elastic response

The amplitude of the deck's displacements in the transverse direction at the locations of the pier top and the corresponding bending moments at the base of all piers have been examined for both synchronous and asynchronous input motion. The effect of the SVEGM is revealed through the ratio ρ of maximum displacements or bending moments in time for asynchronous excitation over the respective values due to synchronous excitation. These results are presented in Figure 4 and the statistics of this response are summarized in Tables 3 and 4. It is shown that both the deck displacements and the pier base bending moments have been considerably increased in a number of cases examined (i.e, displacements by up to 100% and bending moments by up to 50%), despite the fact that on average the asynchronous over synchronous ratios ρ were found less than 1 in the case of 6 out of 10 piers. It is also observed in Figure 4 that displacements are far more sensitive to non-uniform ground motion compared to uniform excitation (i.e., the associated discrepancy is higher).

Cases where higher modes have been excitated under asynchronous excitation are also illustrated in Figure 4 as filled squares. It is evident from Tables 3 and 4 that higher modes are systematically excited at the edge piers (i.e., in 44% to 69% of the cases studied for P1 to P4 and in 75% to 94% of the cases for P7 to P10) in contrast to the middle piers P5 and P6. Another interesting observation is that in the vast majority (i.e., more than 70%) of the cases where higher modes were indeed excited, this has resulted into an increase (ρ>1) of both the deck displacements and the pier base bending moments. Again this does not apply to piers P5 and P6 which were not significantly affected by SVEGM.

An explanation for the above observation is given in Table 5 where it is made clear that the primary mode excited is the principal antisymmetric one which strongly affects the transverse response of piers P1-P4 and P7-P10 but leaves relatively unaffected piers P5 and P6.

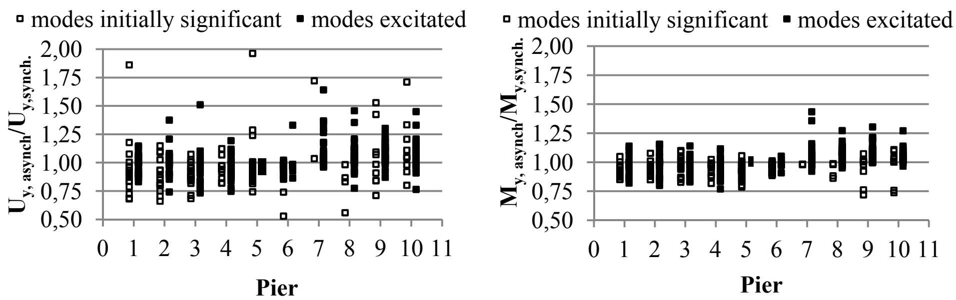

Figure 4. Comparison of the maximum displacements of the deck (left) and of the maximum bending moments at the base of each pier (right) in the case of asynchronous and synchronous excitation (36 cases). Filled squares represent the cases in which higher modes were excited.

Table 3. Comparison of the deck displacements resulted due to asynchronous and synchronous ground motion and correlation with higher modes excitation (36 cases).

Piers:	P1	P2	P3	P4	P5	P6	P7	P8	P9	P10
% where $U_{asyn.}>U_{syn.}$	38.9	38.9	25.0	33.3	13.9	8.3	80.6	72.2	77.8	75.0
average ratio of $U_{asyn.}/U_{syn.}$	0.98	0.95	0.93	0.96	0.98	0.94	1.11	1.04	1.08	1.09
standard dev. σ of $U_{asyn.}/U_{syn.}$	0.19	0.15	0.14	0.10	0.19	0.11	0.17	0.15	0.15	0.17
% where higher modes were excited	55.6	52.8	44.4	69.4	5.6	25.0	94.4	88.9	75.0	75.0
% where $U_{asyn.}>U_{syn}$ and higher modes were excited	71.4	71.4	55.6	83.3	20.0	33.3	93.1	100	85.7	77.8

Table 4. Comparison of the pier bending moments resulted due to asynchronous and synchronous ground motion and correlation with higher modes excitation (36 cases).

Piers:	P1	P2	P3	P4	P5	P6	P7	P8	P9	P10
% where $M_{asyn.}>M_{syn.}$	33.3	27.8	33.3	25.0	11.1	11.1	66.7	75.0	77.8	86.1
average ratio of $M_{asyn.}/M_{syn.}$	0.95	0.96	0.96	0.95	0.93	0.96	1.04	1.05	1.05	1.04
standard dev. σ of $M_{asyn.}/M_{syn.}$	0.08	0.09	0.08	0.08	0.06	0.04	0.10	0.08	0.11	0.09
% where higher modes were excited	55.6	52.8	44.4	69.4	5.6	25.0	94.4	88.9	75.0	75.0
% where $M_{asyn.}>M_{syn.}$ and higher modes were excited	66.7	60.0	33.3	77.8	25.0	25.0	100.0	96.3	78.6	67.7

Table 5. Distribution of the mode shapes excited at each pier.

Mode's shape	P1	P2	P3	P4	P5	P6	P7	P8	P9	P10
	4.1	0.0	0.0	0.0	0.0	11.1	18.8	41.2	45.4	51.4
1st antisymmetric	79.2	95.0	88.9	33.3	50.0	88.9	46.4	54.9	50.0	17.1
	0.0	0.0	0.0	63.3	0.0	0.0	34.8	2.0	2.3	25.7
other mode shapes	17.7	5.0	11.1	3.3	50.0	0.0	0.0	2.0	2.3	257

Table 6. Comparison of the deck displacements and the pier bending moments resulted due to asynchronous and synchronous ground motion (12 non-linear cases).

	P1	P2	P3	P4	P5	P6	P7	P8	P9	P10
Deck displacements										
% where $U_{asynch.}>U_{synch.}$	33.3	25.0	33.3	25.0	8.3	16.7	83.3	75.0	50.0	75.0
average ratio of $U_{asynch.}/U_{synch.}$	0.91	0.95	0.98	1.00	0.92	0.96	1.05	1.04	0.99	1.03
σ of $U_{asynch.}/U_{synch.}$	0.12	0.13	0.15	0.14	0.06	0.04	0.06	0.11	0.15	0.12
Pier base bending moments										
% where $M_{asynch.}>M_{synch.}$	25.0	33.3	33.3	25.0	8.3	0.0	83.3	83.3	66.7	75.0
average ratio of $M_{asynch.}/M_{synch.}$	0.92	0.94	1.03	0.91	0.88	0.94	1.03	1.13	1.12	1.03
σ of $M_{asynch.}/M_{synch.}$	0.07	0.13	0.22	0.13	0.09	0.04	0.05	0.17	0.26	0.20

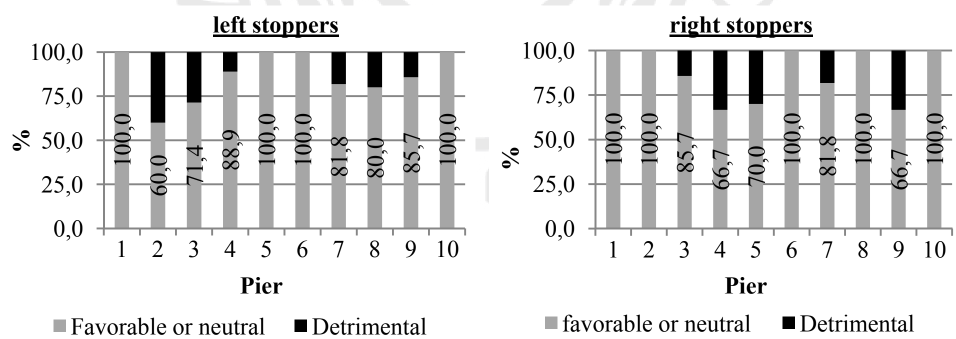

Figure 5. The effect of the asynchronous motion on the closure of the gaps at each pier.

3.2 Non-linear response

As already explained, in the twelve analyses where geometrical nonlinearities were taken into consideration, it was only the impact of SVEGM that was investigated and not the excitation of higher modes. As previously, depending on the pier examined, the average response of the ratio ρ was varied by ±10% for both response quantities, i.e., displacements and bending moments.

Moreover, as seen in Figure 5, it was found that during asynchronous excitation the stoppers were activated more frequently than in the case of uniform excitation at piers P2, P3, P4, P7, P8, P9 (for the left stopper) and P3, P4, P5, P7 and P9 (for the right stoppers) in a non-negligible number of cases which varies from 10-25%. Again piers P5 and P6 were rather unaffected. Despite the fact that modal frequencies cannot be defined in non-linear systems, it is hinted that spatial variability of earthquake ground motion leads to increased structural damage at the location of the stoppers, especially those associated with the excited 1^{st} antisymmetric mode.

4 CONCLUSIONS

The scope of this study was to investigate the correlation between the potential excitation of higher modes and the increase in the seismic demand. For this purpose a set of parametric analyses was conducted for the case of an existing R/C bridge of a total length of 433m. The results indicate that independently of the soil class, the reference earthquake records used and the ground motion intensity, the 1st antisymmetric mode is systematically excited and this in turn leads to non-negligible increase of the bridge response quantities at all piers associated with the particular mode shape.

REFERENCES

[1] A. Der Kiureghian, P. Keshishian, and A. Hakobian, Multiple Support Response Spectrum Analysis of Bridges Including the Site-Response Effect & the MSRS Code, Technical Report, UCB/EERC-97/02, 1997.

[2] CEN [Comité Européen de Normalisation] (2005) Eurocode 8: Design provisions of structures for earthquake resistance—Part 2: Bridges (EN1998-2). CEN, Brussels

[3] A.G. Sextos and A.J. Kappos, "Evaluation of seismic response of bridges under asynchronous excitation and comparisons with Eurocode 8-2 provisions," *Bulletin of Earthquake Engineering*, vol. 7, pp. 519-545, 2009.

[4] A.G. Sextos, A.J. Kappos, and K.D. Pitilakis, "Inelastic dynamic analysis of RC bridges accounting for spatial variability of ground motion, site effects and soil-structure interaction phenomena. Part 2: Parametric study," *Earthquake Engineering & Structural Dynamics*, vol. 32, pp. 629-652, 2003.

[5] I.F. Moschonas, A.J. Kappos, P. Panetsos, V. Papadopoulos, T. Makarios, and P. Thanopoulos, "Seismic fragility curves for Greek bridges: methodology and case studies," Bulletin of Earthquake Engineering, vol. 7, pp. 439-468, 2008.

[6] CEN [Comité Européen de Normalisation] (2004) Eurocode 7: Geotechnical Design - Part 1: General rules (EN1997-1). CEN, Brussels

[7] G. Mylonakis, S. Nikolaou, and G. Gazetas, "Footings under seismic loading: Analysis and design issues with emphasis on bridge foundations," *Soil Dynamics and Earthquake Engineering*, vol. 26, pp. 824-853, 2006.

[8] S. Nikolaou, G. Mylonakis, G. Gazetas, and T. Tazoh, "Kinematic pile bending during earthquakes: analysis and field measurements," *Géotechnique*, vol. 51, pp. 425-440, 2001.

[9] CSI, *SAP 2000* Nonlinear Ver. 10.01, *User's Reference Manual, Berkeley*, California, U.S.

THE INFLUENCE OF CURVATURE TO THE RESPONSE OF CURVED BRIDGES SUBJECTED TO EARTHQUAKE LOADING

Vassilis Sentzas [1], Nikolaos Pnevmatikos [2]

[1] Hellenic Open University, Earthquake Enginnering and Seimic-Resistan Structure, Greece
[2] Department of Civil Infrastructure Works, Faculty of Technological Application, Technological Educational Institution of Athens, Greece
e-mail: bsentzas@gmail.com, nikos_pnevmatikos@hotmail.com

ABSTRACT: This paper focuses on the seismic response of the curved and post-tensioned concrete box girder bridges. More specifically, it investigates how the curvature influences the response of a bridge subjected to earthquake action. Parametric analysis of different radius of curvature is performed and the internal forces, torsion moment, axial and shear as well as the displacements and rotations at specific points along the bridge are calculated. Two types of connection are investigated, the monolithic connection and the connection with rubber bearing, between the deck, the bents and the abutments. The response spectrum seismic analysis was performed. The models were designed, according to the provisions of EC8-part 2, EC2 and the Greek regulations E39/99. Diagrams relating the curvature with the torsion moment have been obtained from the results of parametric analysis. These diagrams could be used by engineers for preliminary design of such kind of bridges.

KEY WORDS: Box girder bridge; Curved bridges; isolated bridge; Torsion;

1 INTRODUCTION

Over the past few decades, in the modern road networks, traffic congestion, increasing demands on highways and multilevel interchanges, adaptation in the formulation of major highways that have to reduce the distances between cities.and aesthetic and economic factors have rendered horizontal curved bridges popular, both in urban and non urban areas on major highways

The curved bridge body can constitute of steel beams or inline pre-stressed concrete beams used as strings in the formation of the curve, steel girders with U profile with shear links beetween the beam and the deck plate and prestressed concrete beams with box cross section. The latter are inherently strong in torsion which is important because curved bridges subject great torsional strain due to the curvature. Provisions and directions in the design of curved bridges can be found in EC2 [1]& [2] , EC8 [3], AASHTO [5], Leonhardt F. [6].

In this study the influence of curvature on torsional moment of bridge subjected to self weight and seismic loadings is investigated.

2 PARAMETRIC ANALYSIS OF CURVED BRIDGE

2.1 Description and modelling of the bridge

For the purpose of the parametric analysis were examined four models of bridges that have common geometrical section characteristics for deck and bents. The only parameter that changes is the radius of curvature of the models. Two types of connections between the piers and the deck were taken into consideration.

The first type is a monolithic connection between deck and piers while the edge abutment is connecting through bearings. In the second type the monolithic connection is limited only to the central pier and the rest piers are connected with the deck through sliding bearings.

In the first type of connection the pier section was taken as compact circular with a diameter of 3 m, while the second type of connection the middle pier is box section with exterior dimensions 4,00 x 2,00 m and 0,50 m thick while the other piers remain unmodified. The section profile of both piers types does not vary with the height, which was taken equal to 12m. The total length of the model is 212 m, with four openings. The two edge openings are 51m long and the two centers are 55m long.

The cross section of the model consists of a single – cell box, 0,50 m thick. The height of the section varies from 2.5 m at abutments and exposures to 4.00 meters at intermediate supports. Section diaphragms exist at the edge of each span. Prestressing force 25 MN was applied at the web of the box section in all models.

The cross section of the model and a 3d view is shown in figure 1.

Apart from the straight model four other curved models were studied with 550m, 350m, 150m and 70m respective radii of curvature.

All models are subjected to self weight, prestressing force and seismic action according to Eurocode 8. The method of analysis used, was the response spectrum analysis. Forty (40) modes were considered to participate in the total response of the bridge. The equivalent static linear analysis wasn’t used because with this method the influence of higher important modes is neglected.

Shell elements were used to simulate the deck of the bridge, and concrete properties were assigned to them. The piers were modeled as a series of frame (beam) elements. The nodes at the ends of the beam elements representing the base of the piers, were fully fixed against translation and rotation in all directions. The connection between abutment and deck were via non linear link elements with properties of rubber bearings. All the simulations were performed using the non linear software SAAP2000 v14.

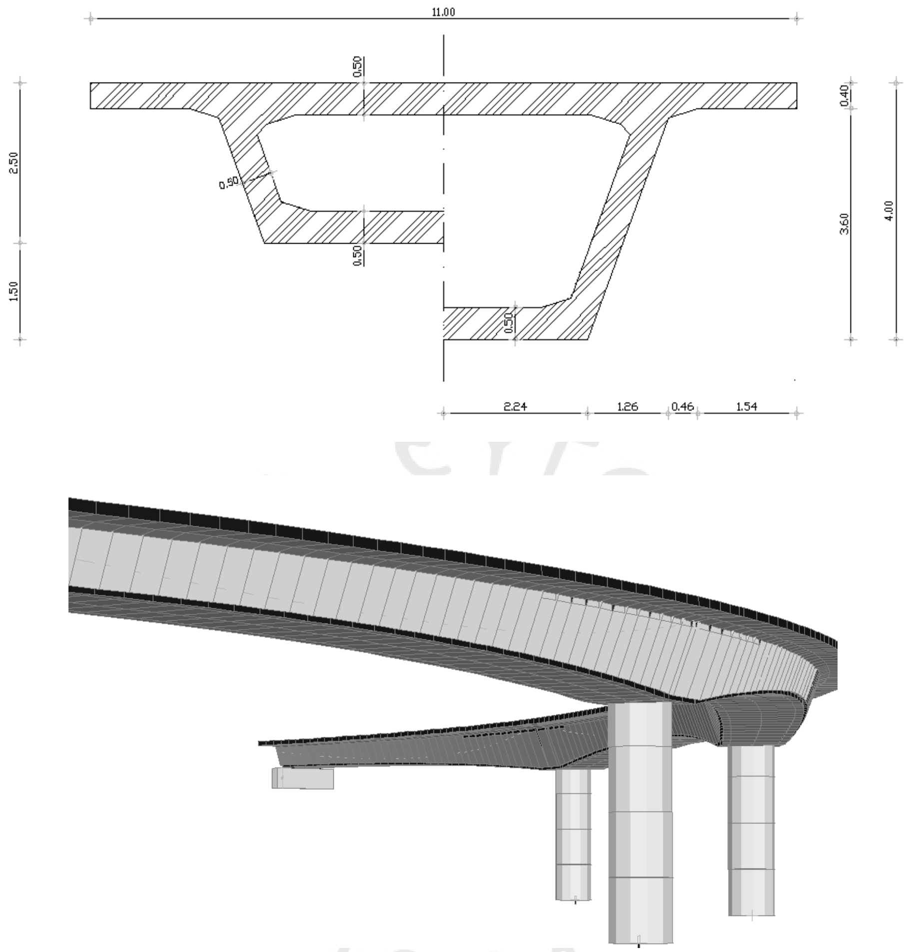

Figure 1. Cross section at the support and at the span of the bridge and 3d view of a curved model with monolithic connection.

3 RESUTS AND DISCUSSIONS

The numerical results were obtained by applying the gravity the prestressing force and the seismic actions to all models. The ratio of maximum forces (maximum bending moments at the spans and supports, maximum shear and maximum torsion moment) corresponding to models with different value of curvature to the maximum force of the model with the greater curvature , with monolithic connection, under dead load appears in Figure 2. It is shown that the moments and shear have zero variation while the torsion moment varies when the curvature increases. The same behavior is observed for the isolated bridge.
In the following figures 3 to 5 the torsion moment ratio with respect to the

curvature for both types of connection subjected to seismic actions are shown
In monolithic bridges the direction of seismic force does not cause such a great variation in the torsion moment of the deck. It should be pointed out that the torsion moment is affected by the flexural stiffness of the bents. Thus the usage of isolators relieves the torsion moment on the deck.

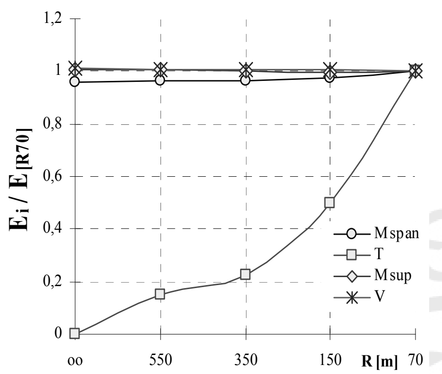

Figure 2. Distribution of moment shear and torsion under dead load.

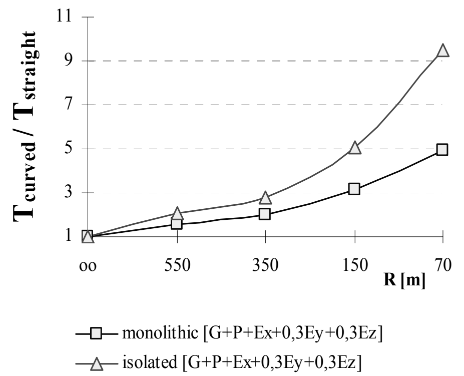

Figure 3. Moment ratio along with the curvature for main earthquake component Ex.

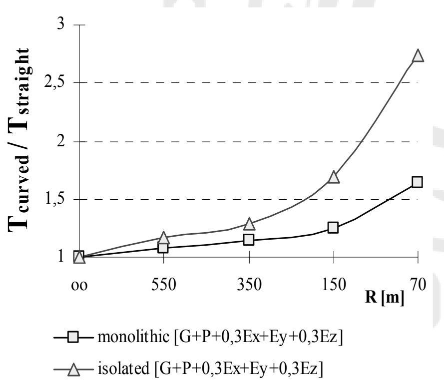

Figure 4. Moment ratio along with the curvature for main earthquake component Ey.

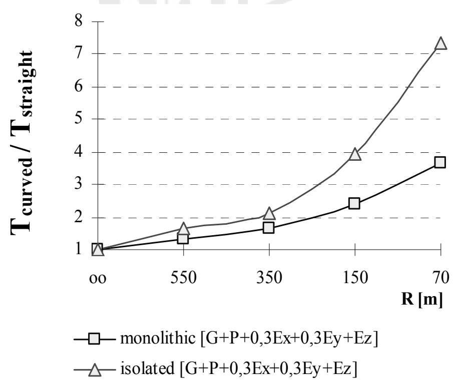

Figure 5. Moment ratio along with the curvature for main earthquake component Ez.

Figure 6 presents the torsion moment ratio (moment of curved bridge over the moment of straight, isolated bridge) along with the curvature for both types of connection subjected to seismic actions. It is observed that the increase of the curvature decreases the influence of the way of the connection between the piers and deck. Two combination of seismic actions were taken into consideration. In this figure it is shown that when the curvature increases, the torsion increases as expected. The combination G+P+0.3Ex+Ey+0.3Ez is more critical since the force (Ey), which is applied vertically to the chord of curved bridge, results in higher torsion than the force (Ex), which is applied along the chord of the bridge. Another observation is that the isolated bridge has been subjected to less torsion than the monolithic one.

Figure 7 presents the torsion moment ratio along with the curvature for both types of connection subjected to prestressing force. From this figure is concluded than the way of connection between deck and piers does not influence the torsion moment caused by the prestressing force.

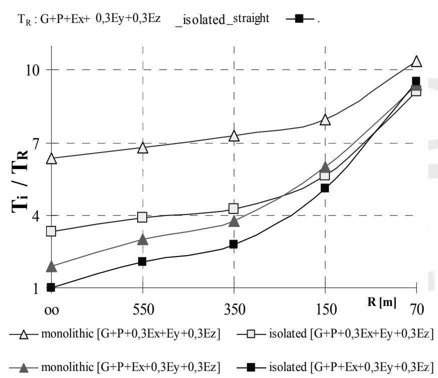

Figure 6. Normalized torsion moment diagram with the value T_R .

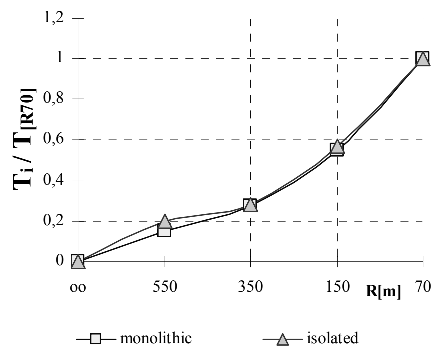

Figure 7. Moment ratio along with the curvature for prestressing force.

Fitting the above results for a monolithic connection and for the G+P+0.3Ex+Ey+0.3Ez combination which is the most critical, the equation (1) is appears. This equation helps the engineers to estimate the additional torsion moment due curvature.

$$y = 3{,}50x^{-0{,}20} \tag{1}$$

The same procedure was followed for the isolated models with the same combination and resulted in equation (2)

$$y = 15x^{-0{,}40} \tag{2}$$

The resulting value multiplied with the corresponding torsion moment of the straight model provides the torsion moment in the different curve radii.

The change in the period of the rotational mode of models due to the change of curvature appears in figure 8, while its percentage of contribution is laid out in figure 9. It is observed that the rotational period increases from straight bridge to 550 m curvature bridge and then remains constant when increasing the curvature. On the top of the diagram in figure 9 is presented the sequence of modes in which appears the rotational modal. The numbers in the brackets show the number of the modes in which the rotational modal appears for the isolated model. It is observed that for the straight isolated model, 25 modes in the analysis should be taken into consideration, in order for the percentage of contribution to remain at about 60 percent. Based on this figure it is concluded that when a response spectrum analysis is used an adequate number of modes should be considered in contribution to the total response of structure. In this example at least 25th modes should be included for SRSS combination method. Particularly in all parametric analysis the first 40 modes were considered to participate to the response of the models.

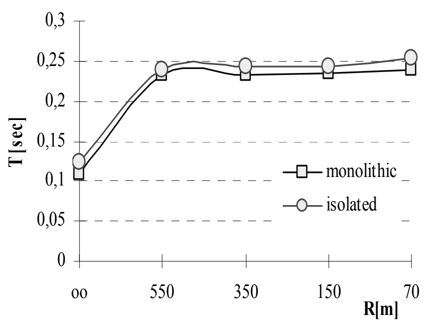

Figure 8. The period of the rotational mode.

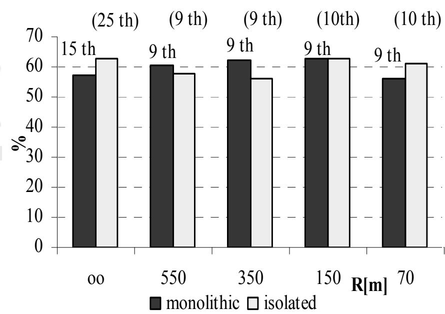

Figure 9. The percentage of contribution.

4 CONCLUSIONS

The present work is an attempt to investigate the influence of the curvature to the torsion moment of horizontally curved concrete box – girder bridge subjected to seismic action.

From the results it is shown that the Ex and Ey components of earthquake plays important role to the torsion moment and cause the magnitude to increase as the curvature increases. Thus the angle of earthquake attack is a significant factor to the torsion moment of the deck.

The way the deck and the piers are connected can also affect the torsion moment of bridge. Isolated bridges experience less torsion moment than the monolithic ones, when the curvature is low. As the curvature increases the connection does not play important roll since both types have the same magnitude of torsion moment.

The AASHTO provisions, [5] suggest that for radii of curvature higher than 200 m the torsion moment due to curvature can be neglected, while Leonhardt F., [6] collocates this limit to 105m. In the present study, it is seems that for radii of curvature about 350m is the limit from with the moment should be neglected or not.

Finally the proposed close form relations can be used to estimate the additional torsion moment due to curvature for preliminary design from practice engineers.

REFERENCES

[1] EN 1992-1-1 Eurocode 2: design of concrete structure; Part 1-1: general rules and rules for buildings 2004; European Committee for Standardization, Brussels
[2] EN 1992-2:2005 Eurocode 2: Design of concrete structures — Concrete bridges — Designand detailing rules 2005; European Committee for Standardization, Brussels
[3] EN 1998-2:2005 Eurocode 8: Design of structures for earthquake resistance — Part 2 : bridges 2005; European Committee for Standardization, Brussels
[4] NCHRP (2008) Development of Design Specifications and Commentary for Horizontally Curved Concrete Box-Girder Bridges Washington, D.C.
[5] AASHTO (2005), AASHTO LRFD Bridge Design Specifications, 3nd Edition with Interims, American Association of State Highway and Transportation Officials, Washington, D.C.
[6] Leonhardt F**.,** Ολόσωμες Γέφυρες**,** Εκδόσεις Γκιούρδας, Αθήνα, 2000.
[7] Computers and Structures, Inc. (1998) "SAP2000 – Integrated Finite Element Analysis and Design of Structures," CSI, Berkeley, California.
[8] Υπουργείο Περιβάλλοντος , Χωροταξίας και Δημοσίων Έργων (Υ.ΠΕ.ΧΩ.Δ.Ε.) (1999) «Εγκύκλιος Ε39/99, Οδηγίες για την Αντισεισμική Μελέτη Γεφυρών», Απόφαση ΔΜΕΟγ/Ο/884/24.12.99.

A SEISMIC RESTRAINING SYSTEM FOR BRIDGES
Analytical study of a strut-ties mechanism

Ioannis Tegos[1], Olga Markogiannaki [2]

[1] Professor, Aristotle University of Thessaloniki, Dept. of Civil Engineering, Greece
[2] Aristotle University of Thessaloniki, Dept. of Civil Engineering, Greece
e-mail: itegos@metesysm.gr, omarkogiannaki@civil.auth.gr

ABSTRACT: In this paper a system that restrains the longitudinal seismic displacements of bridges is presented. It includes four symmetrical bundles of struts-ties bars, in the deck and anchored at their ends, that bound the deck with the abutments' wing walls; while their length between the anchorages is unbonded. The proposed method was applied in a long span bridge and proved a significant reduction in the seismic displacements and loads of the bridge.

KEY WORDS: Bridge; Earthquake; Restrain; Steel bars; Struts-Ties

1 INTRODUCTION

In earthquake prone areas bridge design focuses on limiting the seismic stress developed in bridge's structural system. During earthquakes bridges experience high stress levels that can cause from minor service problems to major failures of the structural members of bridges.

There is a wide range of strategies in recent literature for upgrading the seismic performance of bridges. An extensive number of papers deal with isolating the bridge structural system, deck-piers, from the abutments either with bearings[1] or dampers[2], which can be described as an attempt to reduce the seismic forces on the superstructure by letting the system to oscillate and limit the inelastic deformations [3].The aforementioned methods have quite satisfactory results on the seismic response of bridges, but there is an issue risen regarding their maintenance cost. The isolating devices that are used appear to have much shorter lifetime than the bridge itself and to require periodical maintenance operations. Thus, the cost of the maintenances added to the construction cost, can raise that total budget of such bridges and turn these methods uneconomic. Therefore, in the last years the development of alternative methods focusing on reducing the bridges' cost without, always, endangering the safety and reliability of bridge structural systems becomes more and more intriguing. A wide range of these alternative strategies introduce the restrain of the bridge oscillation. There are methods proposed in studies that utilize bridge members which formerly, were not considered in evaluating the seismic performance of bridges, for instance abutments [4],[5] and the backfill soil [6].These methods limit the maintenance expends by avoiding the use of devices that have short lifetime and shall be replaced periodically. Additionally, other methods include the combined use of external stoppers[7] and even the activation of sidewalks [8].

In this paper, towards the aforementioned direction of alternative strategies, a suggestion of applying bundles of steel bars in bridges in order to improve their seismic resistance is presented. This strategy limits the seismic displacements of bridges by preventing their oscillation. Moreover, the overall goal is to reduce the total cost, construction and maintenance, of bridges by developing a reliable and effective antiseismic design method.

2 DESCRIPTION OF THE SUGGESTED RESTRAINING SYSTEM

The proposed method is characterized by simplicity and is described with the following:

Four bundles of steel bars are anchored in their ends; the one in the bridge superstructure (the horizontal part of the bridge where the vehicles move) and the other in the 4 wing walls of the 2 abutments of the bridge. The direction of these bar bundles is parallel to the longitudinal direction of the bridge. Moreover, appropriate measures are taken so that the incorporation of the steel bars in the bridge concrete will be avoided during concreting. Their incorporation through anchorage is achieved only in their ends. Their body incorporation is possible to be avoided through the same way that is used in superstructures that are prestressed before concreting (un-bonded prestressing), by utilizing plastic ducts for the steel bars in desirable lengths. Furthermore, a medium steel bar diameter, Φ14 or Φ16, is chosen as the appropriate steel bar diameter. This selection is due to the pursue of limiting the length of the bars up to 14m, which is the common production length of steel mills supplied in the market. The mechanism is presented in Figure 1.

Additionally, it should be underlined that it is desirable that the bars of each bundle, for reasons of safety anchoring, will not have the same length but will be anchored in teams of four in the same position.

The steel bars are not utilized only in tension as ties but also as compressive members since their placement in the superstructure protects them from buckling. A critical part against buckling is at the outer expansion joint between the abutment and the superstructure. However, it is possible to take appropriate measures at that position in order to avoid buckling. Regarding the width of the outer joints of the bridge, although there are multiple ways, only one will be presented due to the limited length of the paper. This is the harmonization with Eurocode 8 Part II, which includes in the definition of the joint width only the 40% of the seismic displacement. I t should be noted that the presence of strut and ties reduces it drastically and results in economic outer joints for the bridge.

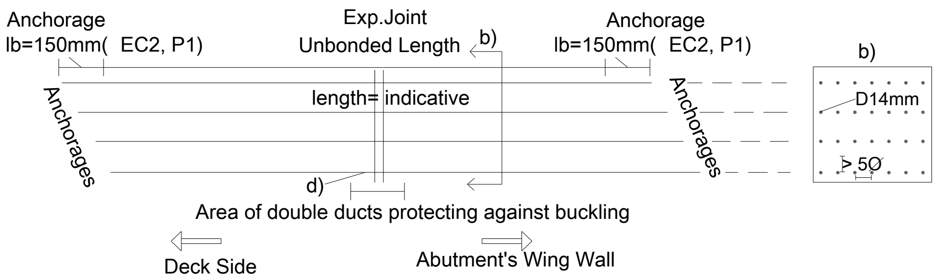

a) Steel bundle of 28 steel bars – layout (indicative)

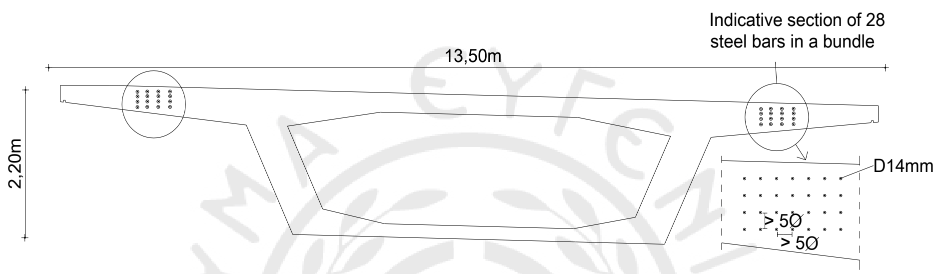

c) Cross section of the deck

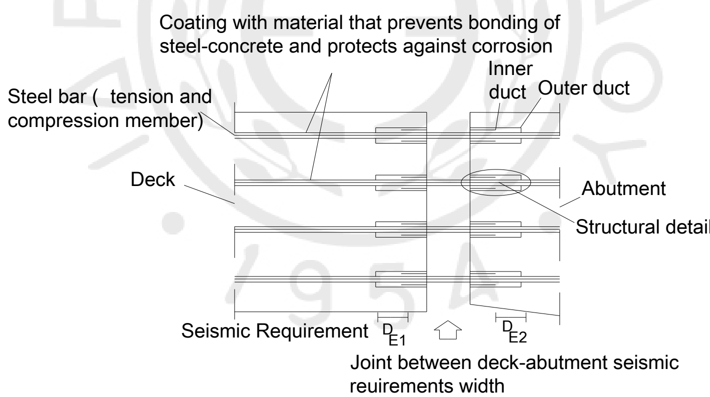

d) Construction detail at the outer joint

Figure 1. (a) Steel bundle of 28 steel bars – layout (indicative), (b) 28 steel bars in a bundle (indicative), (c) Cross section of the deck , (d) Construction detail at the outer joint

Regarding the transverse earthquake, the ducts in the joint that are utilized for avoiding the buckling of the bars can protect them against an awry earthquake. This can be understood since there will be appropriate stoppers in each abutment through which the displacement of the system edges is eliminated and the angle of the elastic line that the transverse earthquake creates is minor. The steel bars are activated not only during the earthquake but also during the service limit state, for instance during winter, when the superstructure is shrinked they are in tension and during summer when the superstructure is lengthened they are compressed. Consequently, this results in the creation of additional stress that although it is of small scale, it shall be taken into account for designing the abutments and the superstructure. The steel bars' activation during earthquakes certainly fulfills their application's aim, since they act as reins through which the restrain of the seismic displacement is achieved. These "reins" have a direct effect on relieving the involved in the earthquake members, for instance the piers, the bearings and the joints.

One critical issue of the aforementioned simplified method is the steel fatigue factor. Although the steel bars are secured against buckling are subjected to the danger of failure from fatigue due to the large number of cycles of alternative sign of high stress level. This danger is not possible to be ignored despite the doubtless improvement of steel ductility. Consequently, a revision of the required lengths of the ties becomes necessary taking into account the Code requirements for fatigue [9]. This means that around the double of the scalable lengths of the steel bars will be required for reducing the service state stress. Furthermore, it is noted that the requirement of larger lengths from 14m, which, as it is already mentioned, is the largest supplied length by the steel industry, is not an obstacle; since, lately, there are coils of steel bars of unlimited length, of diameter up to 16mm that are supplied in the market.

The presence of struts- ties in the structural system during the serviceability limit state and the seismic, too, obviously, introduces forces at the anchorages of each bar in the superstructure and in the wing walls that shall be considered in the design of the system. The introduced forces develop moments due to the eccentricity of the anchorage points which, however, affect only the longitudinal direction and not the transverse due to the symmetrical application of the bars. Moreover, axial forces with alternative sign are introduced in the structural system.

The aforementioned introduced forces, on the one hand, affect the capacity of the wing walls, in which are introduced directly, on the other hand the stability of the close abutments.

3 AN APPLICATION OF THE PROPOSED METHOD

3.1 Description of the bridge system

In the present study the valuation of the proposed method was attempted by utilizing a monolithic prestressed bridge of Egnatia Motorway, located in Veroia territory in north Greece (Figure 2). The bridge is skewed in plan by 51.84 degrees, has three spans and total length of 135.80m. The end spans are 45.10m and the middle span is 45.60m long. The deck of the bridge has concrete box cross section and is 13.5m wide and 2.20 m high. The deck is connected to the piers monolithically. The piers are circular with 2m diameter and are founded on 3x3 pile groups, which are connected to 7.5mx7.5m pile-caps. The piles have circular cross section of 1m diameter. Moreover, the deck is seated on the abutments, which are of conventional type, through bearings and the movements in transverse direction are controlled with stoppers, placed on the abutments. The bridge earthquake response was analyzed according to the Eurocode 8 requirements [10]. It is founded on ground of soil class B and the basic ground acceleration is taken 0.16g for seismic zone I. The importance factor is taken 1.30. The behavior coefficient in the longitudinal direction was considered 3.00 and in the transverse direction 3.50.

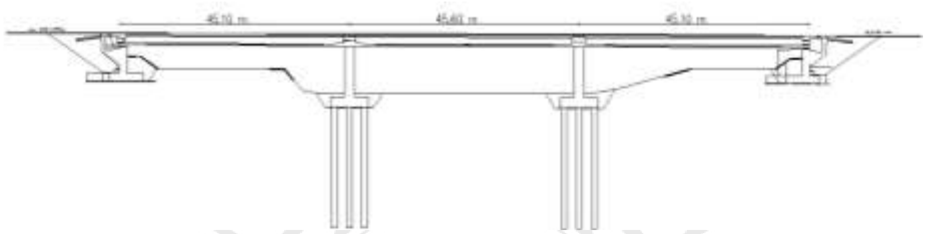

Figure 2. Longitudinal section of the bridge

3.2 Description of the application of the proposed method in the bridge

The performance of the proposed introduced4 bundles of steel bars in the bridge system was studied with gradual increase of their size. The minimum length of the steel bars was determined 6.20 m based on the maximum steel allowed deformation (2.5%) and the maximum seismic displacement of the bridge. The initial length was taken larger in order to accommodate the serviceability requirements, too. In the first case, 4 steel bars, 6.5m long were applied at each wing wall and anchored in the deck. Next, 4 steel bars, with an 1 meter increase to their length were added to each of the 4 bundles. Gradually with a step of 4 steel bars which had 1m added to their length each time, the steel bundle at each wing wall arrived to 28 bars. Each step was analyzed and evaluated regarding the effects on the seismic performance of the bridge.

3.3 Analytical results

The analysis was performed in SAP2000 and the results of the analysis for each application are presented in the following figures. In Figure 3 the total performance of the bridge system against the longitudinal design earthquake is presented. In the x axis is the total displacement of the system and the y axis is the total seismic force produced at each application of the steel bars. The angle created with the x axis represents the stiffness of the system which appears to get larger as the number of bars is increased

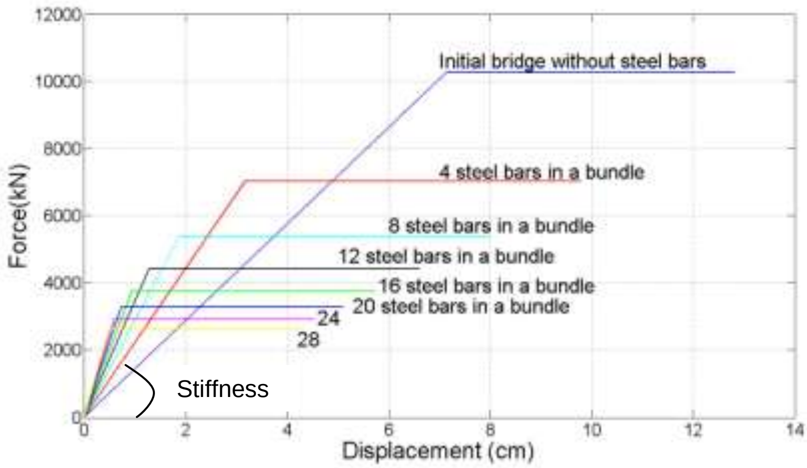

Figure 3. Perfomance of the system with gradual increase of steel bars

In Figure 4 the longitudinal seismic displacement and the corresponding displacement reduction depending on the size of the bundles are presented.

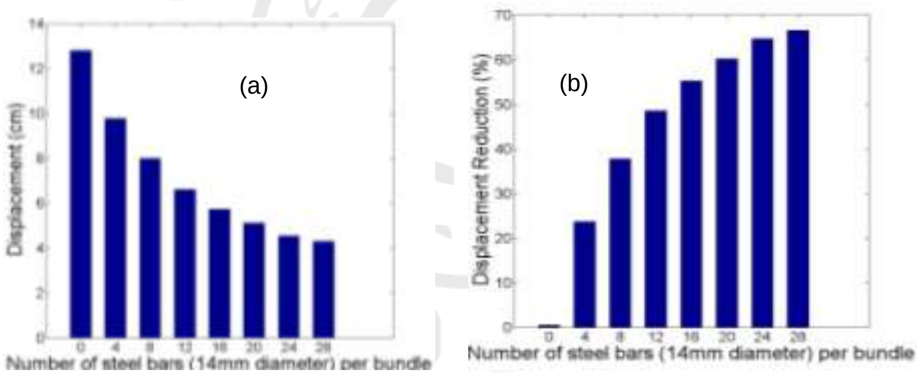

Figure 4. (a) Seismic Displacement depending on the size of bundles, (b) Seismic Displacement Reduction depending on the size of bundles

In Figure 5 the base seismic shear and the force transferred to each abutment that are developed depending on the size of the bundle are presented.

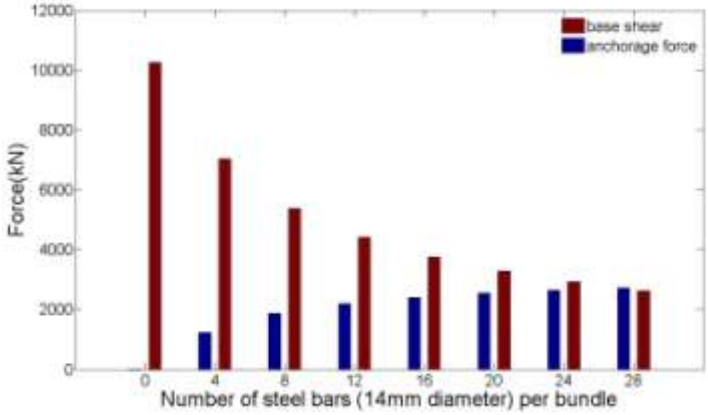

Figure 5. Seismic Force and Anchorage Force transferred to the abutment depending on the number of steel bars per bundle

In Figure 6 the reduction of the base moment of the piers depending on the steel bars applied are presented.

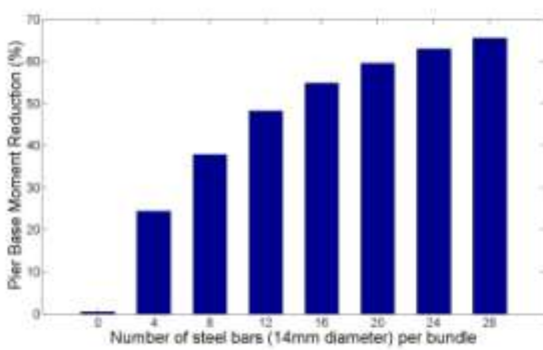

Figure 6. Pier Base Moment Reduction

4 CONCLUSIONS

A mechanism of undertaking the longitudinal earthquake is proposed in the extents of this paper, which was studied for a gradual increase of the cross sections used. It is desirable to outline the following, as the main results of the delivered parametric study.

a. Major reduction of the seismic actions is achieved. It is possible to have a reduction to 1/3 of the seismic actions without using very dense bundles of struts-ties

b. The forces transferred to the two abutments through the anchorages are of such a magnitude that the required adjustments in the abutments are minor. This is due to the passive resistance of the one of the abutments each time that is activated by the longitudinal earthquake, which undertakes the largest part of the seismic action. Consequently, the other abutment, which does not have an ally to its stability the at rest earth pressure of its wall, is relieved drastically.

c. From the economic point of view, the suggested restraining system has minor cost compared to other solutions, regarding the results for the longitudinal earthquake which is generally more difficult to be treated than the transverse.
d. Concluding from the above the proposed method could probably belong to those called as Columbus' Egg solutions.

ACKNOWLEDGMENTS

Acknowledgements to METESYSM Company for providing all the necessary information and drawings for the studied bridge.

REFERENCES

[1] Makris N., Zhang J, "Seismic Response Analysis of a Highway Overcrossing Equipped with Elastomeric Bearings and Fluid Dampers", Journal of Structural Engineering, Vol 130, Issue 6, pp 830-845, 2004

[2] Ruangrassamee A., Kawashima K., "Control of nonlinear bridge response with pounding effect by variable dampers",Engineering Structures 25 (2003) 593–606

[3] Jangid R. S., "Seismic Response of Isolated Bridges", Journal of Construction Steel Research, Vol. 9, Issue 2, pp. 156-166, 2004.

[4] Nutt R.V. and Mayes R.L., "Comparison of Typical Bridge ColumnsSeismically Designed With and Without Abutment Participation Using AASHTODivision I-A and Proposed AASHTO LRFD Provisions", Task F3-1(a), 2000

[5] Tegos I.A., Mitoulis S.A., Tegou S.D., "A proposition for a complexearthquake resistantabutment for continuous deck slab long bridges", FifthEuropean Workshop on the Seismic Behaviour of Irregular and ComplexStructures, Faculty of Engineering Structures, Catania, 2008

[6] Tegos I.A., Mitoulis S.A., "Seismic response analysis of highwaybridges,including backfill deck interaction, through improved participation of backfills",ECCOMAS Thematic Conference on Computational Methods in StructuralDynamics and Earthquake Engineering, Rethymno, 2007

[7] Mitoulis S.A, Tegos I.A, "Restrain of a seismically isolated bridge by externalstoppers", Bulletin of Earthquake Engineering,Vol. 8, No. 4, pp.973-993, 2010

[8] Tegos I.A., Tsitotas M.A., Tegou S.D., Mitoulis S.A**, "**Reduction in seismic actions of bridges by utilizing thesidewalks as restrainers", 16th Hellenic Concrete Conference, Pafos, 2009

[9] EN 1993-1-9:2005 Eurocode 3: Design of steel structures – Part 1-9: General – Fatiguestrength

[10] CEN [Comité Européen de Normalisation], "Eurocode 8: Design of structures for earthquake resistance, Part 1: General rules, seismic actions and rules for buildings", 2003

INPUT-BASED LATERAL FORCE PATTERN STUDY
For Pushover Analysis of Elevated Pile Foundation System of Bridges

Sasa Cao[1], Wancheng Yuan[2]

[1,2]State Key Laboratory of Disaster Reduction in Civil Engineering, Tongji University, China
e-mail:lifeng_4315052@163.com, yuan@tongji.edu.cn

ABSTRACT: A new lateral force distribution pattern is proposed to conduct the pushover analysis for elevated pile foundation system of bridges. Based on a specific ground motion record, the proposed lateral force pattern is confirmed by the dynamic characteristics which have been derived from a linear time-history analysis of the system.

KEY WORDS: Elevated pile foundation system; Input-based lateral force pattern; Pushover analysis

1 INTRODUCTION

Currently, elevated pile foundation system is widely used in the bridge structure. Generally, an elevated pile foundation system has only two levels. One is the pile level and the other is the pier level. The mass is concentrated on the cap and on the top of the pier where the mass of the superstructure acts at.

Seven common lateral force patterns are presented in the FEMA-440: concentrated load, first mode, inverted triangular, uniform (rectangular), code force distribution, adaptive first mode, SRSS[1]. The FEMA-440 recommended three lateral force patterns: first mode, code distribution and the triangular, which are refered as common patterns in this paper. However, these lateral force patterns are not fit for high-rise buildings in which the contributions of the higher modes are significant. Chopra and Geol have proposed a modal pushover analysis procedure (MPA) to include the influence of higher modes[2]. In such a procedure, multiple pushover analysis with a lateral load corresponding to the considered elastic mode shapes are conducted separately, and then the total seismic response is estimated by combining the responses due to each modal load. A modified version of the MPA (MMPA), Wherein the response contributions of higher vibration modes are computed by assuming the structure to be linearly elastic, has been proposed by Chopra et al[3]. Both the MPA procedure and the MMPA procedure use SRSS combination rule and assume that there is no interaction between the modes[1].

However, when the structure goes into the post-yield range, its dynamic properties are changing with time. To describe the changing properties, some researchers have proposed the adaptive lateral force patterns[4-6]. In each step of the PHA, the lateral force pattern is updated according to the mechanism and the stiffness state of the structure. An interesting displacement adaptive force pattern has been proposed by Antonious and Pinho[7]. In this method, a set of updated lateral displacements, rather than force, are imposed on the structure. These adaptive lateral force patterns can provide more accurate dynamic response of the structure, but they also need more computation effort. Furthermore, the procedure to form them is complicate.

Based on the MPA, Kalkan and Kunnath have proposed an adaptive modal combination procedure (AMC) method[8]. The AMC is same as the MPA except that the modes are updated at each step of the pushover procedure. It is demonstrated that the AMC can reasonably estimate critical demand parameters such as roof displacement and inter-story drift for both far-fault and near-fault records. However, there is no rigorous theoretical foundation for the SRSS combination rule. Additionally, the superposition method of the vibration mode effects is no longer valid in the inelastic range.

Based on the work done by Wancheng Yuan and Jun Yang[9], this paper aims to proposed an invariant input-based lateral force pattern and simplify the procedure. This new pattern will provide a simple and practical procedure for the pushover analysis of the elevated pile foundation system.

2 DEVELOPMENT OF THE NEW PROCEDURE

The main differences between common procedures used in pushover analysis (such as the first mode, code distribution and the triangular) and the proposed procedure are:

a) The new lateral force pattern is based on a specific earthquake ground motion;

b) The new lateral force pattern contains only two lateral forces;

c) The proposed lateral force pattern is confirmed by the dynamic characteristics which have been derived from a linear time-history analysis of the system.

2.1 Develop the new force pattern

Given an elevated pile foundation model, we can obtain two lateral flexural factors: δ_{11}, δ_{12}. Where, δ_{11}、 δ_{12} is the lateral top displacement of the model when the model is subject to a unit force acting at the pier top or at the cap respectively. Obviously, $\delta_{11} > \delta_{12}$. Conduct a linear time-history analysis of the model and record the two controlling parameters V_b、 U_n. We assume two single forces f_1 acting at the top and f_2 acting at the cap causing the same values of the two controlling parameters. The values of the two single forces can be computed by Eq. (1) and (2).

$$f_1 + f_2 = V_b \tag{1}$$

$$f_1 * \delta_{11} + f_2 * \delta_{12} = U_n \tag{2}$$

Regularizing the lateral force vector $\begin{Bmatrix} f_1 \\ f_2 \end{Bmatrix}$, we can get the regularized proposed lateral force pattern $\begin{Bmatrix} 1 \\ \eta \end{Bmatrix}$. In which,

$$\eta = \frac{f_2}{f_1} \tag{3}$$

Where: η is the lateral force acting at the cap in the proposed force pattern.

For integrity, it is necessary to verify the uniqueness of the new force pattern. Define ξ as

$$\xi = \frac{U_n}{V_b} \tag{4}$$

Substituting the Eq. (1)、(2) and (3) into Eq. (4), we find

$$\xi = \frac{U_n}{V_b} = \frac{f_1 * \delta_{11} + f_2 * \delta_{12}}{f_1 + f_2} = \frac{\delta_{11} + \eta * \delta_{12}}{1+\eta} = \delta_{12} + \frac{\delta_{11} - \delta_{12}}{1+\eta} \tag{5}$$

Since $\delta_{11} > \delta_{12}$, Eq. (5) indicates that ξ is a monotonic decreasing function about η. For each value of ξ, only one value of η will be confirmed. In other words, for each linear dynamic analysis only one lateral force pattern can be confirmed.

2.2 Basic steps of the new procedure

The main steps of the proposed procedure are as follows:

a) Create a reasonable mathematical model of the elevated pile foundation system. The SAP2000 program is employed in this paper for computation.

b) Conduct two linear static analyses of the model assuming that it is subjected to a unit force acting at the pier top or at the cap individually to get δ_{11}, δ_{12}.

c) Choose a specific ground motion record and scale it down to ensure a linear time-history analysis of the model.

d) Conduct a linear time-history analysis of the model with the scaled acceleration record. The two controlling parameters, V_b、U_n, are obtained.

e) Confirm f_1、f_2 using Eq. (1) and (2).

f) Regularize the lateral force vector $\begin{Bmatrix} f_1 \\ f_2 \end{Bmatrix}$ to form the proposed lateral force pattern $\begin{Bmatrix} 1 \\ \eta \end{Bmatrix}$.

g) Conduct the pushover analysis of the system with the new force pattern.

3 VALIDATION OF THE PROPOSED METHODOLOGY

An elevated pile foundation system is chosen to evaluate the effectiveness and correctness of the proposed procedure. Pushover analyses of the system with common lateral force patterns (the proposed three patterns in FEMA 440: first mode, code distribution and the triangular) and the proposed pattern are conducted respectively. The IDA of the system is also conducted to provide the benchmark. Three earthquake records (El-centro, Loma Prieta and Northridge) are chosen for the IDA and for obtaining the new lateral force patterns.

3.1 Model of an elevated pile foundation system

Based on the work done by Wancheng Yuan and Jun Yang, the systems of the model 6 in [9] is chosen for case study. The parameters of the model are shown in Table 1.

Table 1. Model information

System	Equivalent mass of the superstructure/t	Mass of the cap*(t)*	Numble of piles	Pier/tower length*(m)*	Equivalent pile length*(m)*	$T_1(s)$
Model 6	3000	6000	6	20	8	1.5445

The fundamental period, T_1, is listed in Table 1 too. The interaction between the piles and the soil is neglected. The piles are assumed to be fixed into the earth in a predetermined depth. The length from the fixed point to the top of the pile is regarded as the equivalent pile length, which is 8m in this model. The properties of the sections of model 6 are shown in Table 2. The three dimensional model is constructed and shown in Figure 1. Focused plastic hinge model is introduced into the model to represent the plastic behavior of the structure. The effect of p-delta is included.

Table 2. Sectional material characteristics

Member	Material type	Dimension	Ratio of longitudinal bars	Ratio of stirrup
Pier	C30	2.6×5.5m	2.20%	0.80%
Pile	C30	Diameter1.8m	1.80%	1.00%

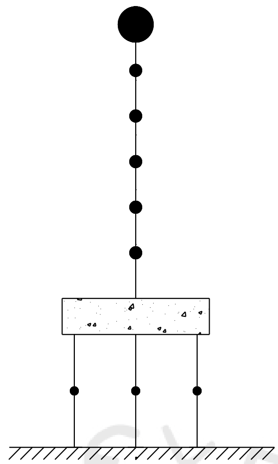

Figure 1. Elevated pile foundation model (Model 6)

3.2 lateral force pattern

The procedure of how to extract the proposed input-based lateral force pattern is shown as bellow.

a) The lateral flexural factors δ_{11}, δ_{12} of the model are 2.01e-8m/N 、7.301e-10m/N.We can see $\delta_{11} > \delta_{12}$. This verified our assumption in section 2.1.

b) When the model of the elevated pile foundation system is subjected to the three acceleration records, the controlling parameters and the corresponding lateral force patterns are displayed in the following table:

Table 3. Model information

System	Earthquake ground motion	U_n (*m*)	V_b (*kN*)	f_1 (*kN*)	f_2 (*kN*)	η	ξ (*m/kN*)
Model 6	El-centro	0.038933	11424	1579.375	9844.625	6.2332	3.408e-6
	Loma Prieta	0.115276	21992.619	5122.339	16870.28	3.2935	5.242e-6
	Northridge	0.019611	13855.935	490.1823	13365.775	27.267	1.415e-6

ξ is also listed in Table 3.

c) According Table 3, we can get the proposed lateral force vector for the systems.

3.3 Comparison of the results

As in [9], the criterion of maximum displacement versus maximum bash shear is adopted to match the controlling parameters in this paper.

The capacity curves of the model 6 derived by the six lateral force patterns are illustrated in Figure 2. Several points of relationship between biggest top displacement, U_n, and the biggest base shear, V_b, derived by the IDA of the system are also illustrated to give the benchamark.

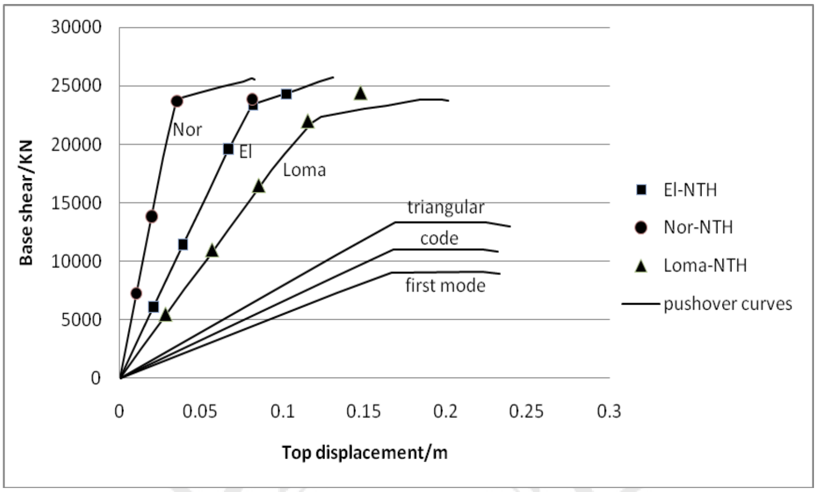

Figure 2. Comparison of the results for model 6

From Figure 2, we can see that:
a) When an elevated pile foundation system is subjected to different earthquake ground motions, the dynamic characteristics of it are different. The input-based lateral force pattern can depict this phenomenon well;
b) Pushover analyses with common lateral force patterns severely undervalued the base shear of the system;
c) Compared with the common lateral force patterns, the proposed lateral force pattern can give more accurate predictions of the dynamic characteristics of the system;
d) The proposed procedure can exactly capture the response of the system subjected to a specific ground motion before the system yielding. In the post-yield range, the new procedure can't exactly capture the response of the system. However, the erroneous is not too big to accept for practical use.

4 CONCLUSIONS

An input-based lateral force pattern has been proposed for the pushover analysis of the elevated pile foundation system of bridges. The principle and specific steps of the new pattern are illustrated. A case study of an elevated pile foundation system is conducted to evaluate the effectiveness and correctness of the new pattern. The predictions of the foundation system obtained from the new pattern are compared with results derived by rigorous NL-THA as well as PHA with common patterns. The main conclusions of this study are summarized as bellow:

a). The capacities of a structure should be different when it is subjected to different ground motion inputs. When an elevated pile foundation system is subjected to different earthquake ground motions, its dynamic responses are different. The input-based lateral force distribution pattern can reflect this discrepancy, while the common lateral force patterns can not.

b). The mass of the cap is very large in the elevated pile foundation system. When the structure is subjected to earthquake ground motion, the inertial force of the cap is so large that common lateral force patterns will severely undervalue the base shear of the system. The proposed lateral force pattern can give more accurate predictions of the system.

c). When an elevated pile foundation system is subjected to a specific ground motion, the proposed procedure can exactly capture the response of the system before yielding. In the post-yield range, the new procedure can't exactly capture the response of the system. However, the erroneous is not too big to accept. In a word, the new procedure provides a simple and practical way for the seismic evaluation of the elevated pile foundation system.

ACKNOWLEDGMENTS

This research is supported by Ministry of Science and Technology of China under Grant No. SLDRCE 09-B-08, and the National Science Foundation of China under Grant No.50978194 and No.90915011.

REFERENCES

[1] FEMA, *Improvement of Nonlinear Static Seismic Analysis Procedures[R]*, FEMA 440, Washington (DC): Federal Emergency Management Agency, 2005.

[2] Anil K. Chopra, Rakesh K. Geol, *A Modal Pushover Analysis Procedure to Estimate Seismic Demands for Buildings:Theory and Preliminary Evaluation*[R], Report No: PEER 2001/03, Pacific Earthquake Engineering Research Center, University of California, Berkeley, 2001.

[3] Chopra AK, Goel RK, Chintanapakdee C, Evaluation of a modified MPA procedure assuming higher modes as elastic to estimate seismic demands, Earthquake Spectra[J], Vol. 20, No. 3, pp. 757–78, 2004.

[4] Gupta B, Kunnath SK, Adaptive spectra-based pushover procedure for seismic evaluation of structures, Earthquake Spectra[J], Vol.16, No.2, pp.367–91, 2000.

[5] Elnashai, A. S. Advanced inelastic static (pushover) analysis for earthquake applications, Structural Engineering and Mechanics[J], Vol.12, No.1, pp.51-69, 2001.

[6] Antoniou S, Pinho R, Advantages and limitations of force-based adaptive and non-adaptive pushover procedures[J], Earthq Eng, Vol.8, No.4, pp.497-522, 2004.

[7] Antoniou S, Pinho R, Development and verification of a displacement-based adaptive pushover procedure[J], Earthq Eng[J],Vol.8, No. 5, pp.643-61, 2004.

[8] Kalkan E, Kunnath SK, Adaptive modal combination procedure for nonlinear static analysis of building structures, ASCE Journal of Structural Engineering, 2006 [in press].

[9] YUAN Wancheng, YANG Jun, Lateral load pattern study of pushover analysis for elevated pile foundation of bridge[J]. Journal of Tongji University: nature science, Vol.36, No.11, pp.1467~1472, 2008.

INFLUENCE OF SEISMIC INCIDENT DIRECTION ON THE LINEAR RESPONSE OF A BRIDGE

Milto Skordeli[1], Asimina Athanatopoulou[2] and Ioannis Tegos[3]

[1,2,3] Aristotle University of Thessaloniki, Dept. of Civil Engineering, Greece
e-mail: miltws@gmail.com, minak@civil.auth.gr, itegos@civil.auth.gr

ABSTRACT: The present paper investigates the influence of the seismic incident angle on the response of a bridge by analyzing a two-span bridge for several earthquake records and comparing the maximum response over all incident angles with the conventional one. The results show that the influence of the seismic incident angle on the bridge response is significant.

KEY WORDS: Incident angle; Linear time history; Maximum response; Seismic response.

1 INTRODUCTION

In general seismic analysis is performed for the three translational components of ground motion. These components are recorded by accelerographs, the orientation of which is arbitrary. In time history analysis the recorded horizontal components are applied along the longitudinal and transverse axis of a bridge simultaneously. Alternatively the principal components of ground motion are applied along the horizontal axes of the bridge. The vertical accelerogram is applied along the vertical z-axis.

The orientation of a future earthquake is unknown. Therefore, it is prudent to design a structure for the most adverse orientation (the orientation that produces maximum response). Seismic input axes are not clearly defined in seismic codes [1, 2]. Therefore, the recorded or uncorrelated accelerograms are applied along the longitudinal and the transverse axes of a bridge.

Several researchers have investigated the influence of seismic incident angle on structural response [3, 4, 5, 6]. They concluded that the common practice to apply the accelerograms along the structural axes can lead to very unconservative results. Moreover analytical formulas were developed for the determination of maximum response over all incident angles under three seismic components [3].

The objective of the present paper is to compare the maximum response over all incident angles with the response produced by accelerograms applied along the longitudinal and the transverse axis of a bridge. For this purpose a straight two-span bridge is analyzed by time history analysis due to seven ground motions represented by both the three recording correlated accelerograms and the corresponding uncorrelated ones. The results indicate that accelerograms applied along the bridge axes can underestimate maximum response.

2 MAXIMUM RESPONCE

The structure is subjected to bidirectional horizontal seismic motion consisting of the accelerograms $\ddot{u}_{ag}(t)$ and $\ddot{u}_{bg}(t)$. Since the direction of the seismic motion is unknown, they can form any angle θ with the X and Y structural axes *Fig.1(a)*. We consider the following orientations for the seismic excitation:

- Excitation ‘αθ’: The accelerogram $\ddot{u}_{ag}(t)$ is applied along the direction of p axis and the accelerogram $\ddot{u}_{bg}(t)$ is applied along the direction of w axis, i.e. the angle of seismic incidence is θ *Fig.1(a)*. A typical response quantity R is donated as $R_{,\alpha\theta}$.
- Excitation ‘α0’: The accelerogram $\ddot{u}_{ag}(t)$ is applied along the direction of the X axis while the accelerogram $\ddot{u}_{bg}(t)$ is applied along the direction of the Y axis, i.e. the angle of seismic incidence is θ=0° *Fig.1(b)*. A typical response quantity R is donated as $R_{,\alpha 0}$.
- Excitation ‘α90’: In this case the roles of $\ddot{u}_{ag}(t)$ and $\ddot{u}_{bg}(t)$ are interchanged: the accelerogram $\ddot{u}_{ag}(t)$ is applied along the direction of the Y axis, while the accelerogram $\ddot{u}_{bg}(t)$ is applied along the direction of X axis, i.e. the angle of seismic incidence is θ=90° *Fig.1(c)*. A typical response quantity R is donated as $R_{,\alpha 90}$.

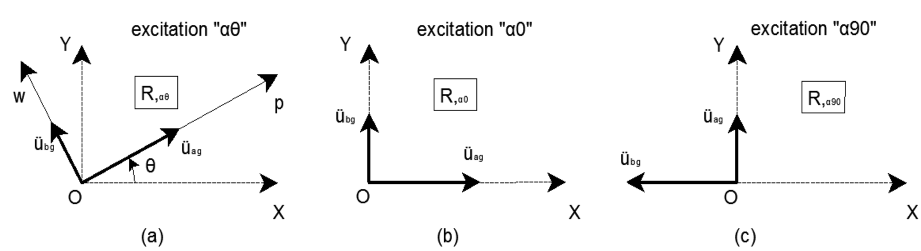

Figure 1. Excitations ‘αθ’ (a), ‘α0’ (b) and ‘α90’ (c).

It has been proven [3] that the maximum/minimum value of a response parameter for any angle θ of seismic incidence is given, as a function of time, by the relation:

$$R_1(t) = +\sqrt{R_{,a0}^2(t) + R_{,a90}^2(t)} + R_{,z}(t) \tag{2.1a}$$

$$R_2(t) = -\sqrt{R_{,a0}^2(t) + R_{,a90}^2(t)} + R_{,z}(t) \tag{2.1b}$$

The plot of the functions $R_1(t)$ and $R_2(t)$ provides the maximum and the minimum value of the required response parameter as well as the time instants t_{cr1} and t_{cr2} at which these maximum/minimum occur.

$$\max R = R_1(t_{cr1}) \quad \text{and} \quad \min R = R_2(t_{cr2}) \tag{2.2}$$

The corresponding critical angles θ_{cr1} (maximum value) and θ_{cr2} (minimum value) are given by the equations [3]:

$$\theta_{cr1} = \tan^{-1}\left(\frac{R,_{a90}(t_{cr1})}{R,_{a0}(t_{cr1})}\right) \text{ and } \theta_{cr2} = \tan^{-1}\left(\frac{R,_{a90}(t_{cr2})}{R,_{a0}(t_{cr2})}\right) - \pi \tag{2.3}$$

3 PRINCIPAL COMPONENTS OF GROUND MOTION

In most of the ground motion databases the horizontal components $\alpha_i(t)$ and $\alpha_j(t)$ are given for the direction in which they were recorded. This direction does not coincide with any of the bridge axes. However the accelerograms can be transformed to any set of axes forming with the initial axes an angle θ. The accelerograms $\alpha_{x(\theta)}(t)$ and $\alpha_{y(\theta)}(t)$ along the new axes are given by the relation [7]:

$$\begin{pmatrix} a_{x(\theta)}(t) \\ a_{y(\theta)}(t) \end{pmatrix} = \begin{pmatrix} \cos\theta & \sin\theta \\ -\sin\theta & \cos\theta \end{pmatrix} \cdot \begin{pmatrix} a_i(t) \\ a_j(t) \end{pmatrix} \tag{3.1}$$

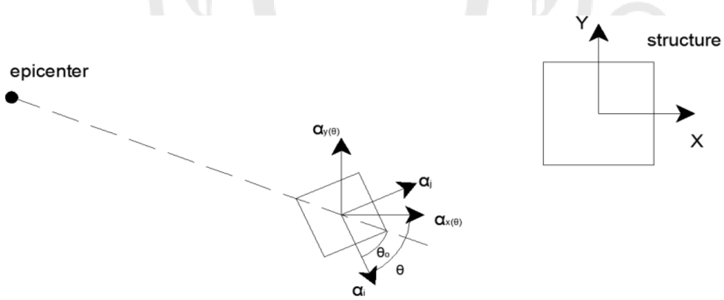

Figure 2. Recorded and transformed components of ground motion

Moreover, there exists a specific single axis system for which the correlation between the components of the earthquake excitation vanishes. This axis system defines the principal directions of ground motion. The one principal direction is approximately vertical, as demonstrated by the [7]. The two others directions are defined by the angle θ_0 given by the equation:

$$\tan 2\theta_0 = \frac{2\sigma_{xy}}{\sigma_{xx} - \sigma_{yy}} \quad , \quad \sigma_{ij} = \frac{1}{s}\int_0^s a_i(t) \cdot a_j(t)\,dt \tag{3.2}$$

where $\alpha_{ij}(t)$ are the ordinates of accelerograms and s is the total duration.

4 APPLICATIONS

4.1 Analysis model

The present study utilizes a straight two-span bridge with a total length equals to 55.0 m. The length of each span is 26.8 m *Fig.3.* The deck of the bridge is continuous and monolithically connected to the piers, while it is supported on the abutments through two low damping rubber bearings, which are symmetrically installed. The cross section of the deck is a T-shaped wide flange, while the pier has a circular cross section with a diameter 1.2 m.

The finite element model of the bridge is shown in *Fig.4*. The SAP2000 program is used for the analysis [8].

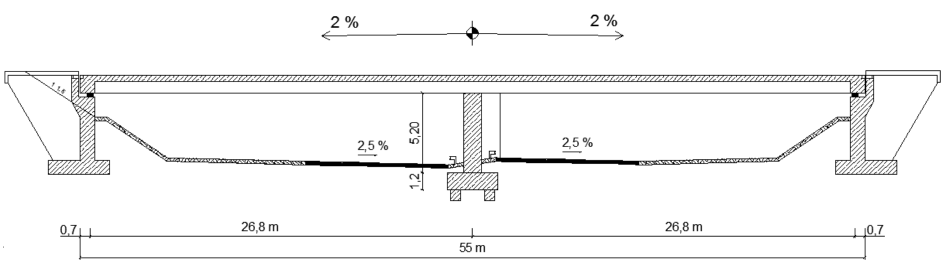

Figure 3. Longitudinal section of bridge

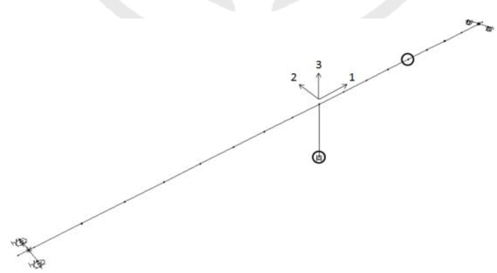

Figure 4. Finite element model

4.2 Earthquake ground motions

In this study, a suite of three-components ground motion records shown in Table 1 are used as input motion in time history analyses [9].

Table 1. Earthquake records

Earthquake	Station	Magnitude	PGA (g)
Landers Amboy	21081	7.28	0.1298
Landers Sillent Vall	12206	7.28	0.0463
Loma Prieta Point Bonita	58043	6.93	0.0712
Loma Prieta Rincon Hill	58151	6.93	0.0855
Northridge Antelope Buttes	24310	6.69	0.0559
Northridge L.A. Wonderland	90017	6.69	0.1343
Northridge San Gabriel	90019	6.69	0.2087

4.3 Time History Analyses (THA)

Firstly, the analyses are performed for the correlated components of ground motions. The maximum response is computed by the following two procedures: i) the three accelerograms are applied simultaneously along the structural axes of the bridge (the two horizontal accelerograms along the longitudinal axis and the transverse one and the third one vertically along the vertical axis); ii) the maximum response over all seismic incident angles is computed using the procedure presented in section 2. According to the last procedure three analysis cases are required: (1) due to two horizontal components applied along the horizontal axes of the bridge (excitation ‘α0’, *Fig.1b*), (2) due to two horizontal components rotated by an angle of 90-degrees counter-clockwise with regard to the analysis (1) (excitation ‘α90’, *Fig.1c*) and (3) due to the vertical accelerogram, along the vertical axis. The results of these three analyses provide all necessary data for the computation of the maximum response values (moments, displacements, stresses) over all seismic incident angles.

In addition, all the above mentioned analyses cases are carried out for the uncorrelated components of ground motions. The uncorrelated components are calculated using the equations (3.1) and (3.2), presented in section 3.

4.4 Response Spectrum Analysis (RSA)

Furthermore the response is computed by the response spectrum method on the basis of the acceleration response spectra corresponding to the seven ground motions used for Time History Analysis. These spectra are obtained by the following procedure.

Firstly the response spectra corresponding to the uncorrelated components of each ground motion for 5% damping ratio are determined. Then, the geomean spectrum corresponding to the two horizontal components of each ground motion is calculated. After that, the average spectrum corresponding to the seven geomean spectra is calculated. This spectrum is used for both horizontal components. The vertical component is represented by the mean spectrum corresponding to the seven vertical response spectra of the ground motions.

4.5 Analyses Results

In *Figure 5* the maximum normal stress at the centre of the pier base due to all ground motions produced by both procedures presented in section 4.3, are given. It is obvious that accelerograms (correlated or uncorrelated) applied along the bridge axes produce smaller response values than the maximum ones over all incident angles. Also, we see that both the recorded correlated accelerograms and the uncorrelated ones produce the same maximum values over all incident angles. However they produce different response values when they are applied along the bridge axes. Moreover, we observe that for some ground motions the uncorrelated components applied along the structural axes produce larger response values than the correlated components (No. 2, No. 3 and No. 7) while, for other ground motions the opposite is true (No. 4 and No. 6).

In order to judge the difference between the maximum response over all incident angles and the response values obtained by accelerograms applied along the longitudinal and the transverse axis of the bridge the following ratio r_i (where i the ground motion used for the analysis) is defined:

$$r_i = \frac{\max\left|R,_{\theta}\right|}{\max\left|R,_{code}\right|} \tag{4.5.1}$$

where: $\max\left|R,_{\theta}\right|$ is the maximum absolute value of the response parameter over all incident angle determined by equations (2.1) and (2.2),

$\max\left|R,_{code}\right|$ is the maximum absolute value of the response parameter produced by acceleration loads applied along the bridges axes.

Fig.6 shows the values of the ratio r_i for the bending moment M in the middle of the span (*Fig. 4*) due to all ground motions for both correlated and uncorrelated seismic components. Additionally *Fig. 7* presents the values of the ratio r_i corresponding to the vertical displacement in the middle of the span (*Fig. 4)*. It is observed that the values of the ratio r_i are larger than one. This means that the maximum value over all incident angles is larger than the value produced by accelerograms applied along the bridge axes. The ratio is extremely large under specific ground motions (e.g. No. 5 under correlate accelerograms and No. 6 under uncorrelated accelerograms for bending moment, *Fig. 6*). Similarly, the results illustrated in *Fig.7* show that the maximum value of vertical displacement can be up to 2.12 times for correlated and 1.90 times for uncorrelated accelerograms larger than the value produced when the accelerograms are applied along the bridges axes.

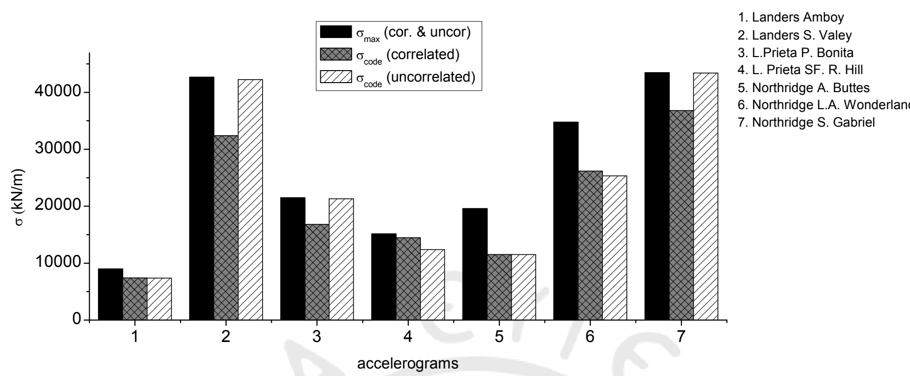

Figure 5. Maximum normal stress at the centre of the pier base.

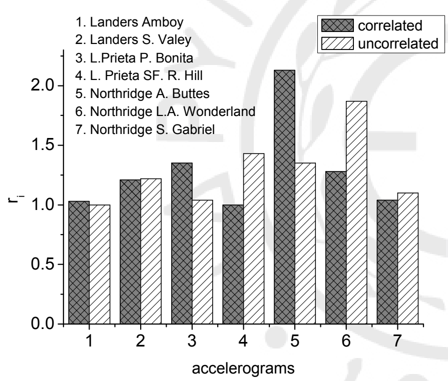

Figure 6. Ratio r_i for bending moments in the middle of the span.

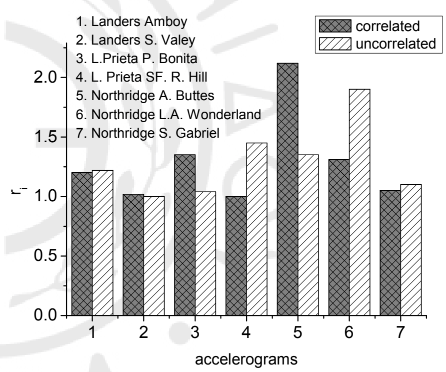

Figure 7. Ratio r_i for vertical displacement in the middle of the span.

In Table 2 the average response values produced by all ground motions in the middle of the span, obtained by both Time History analysis and Response Spectrum method are given. The maximum values for Time History analysis correspond to the mean value of the 7 maximum values over all incident angles. In Response Spectrum method, the maximum response value does not depend on the earthquake input angle, since the two horizontal components are represented by the same spectrum [10]. It is noted that CQC rule was used for modal combination and SRSS rule for directional combination. We observe that the maximum response values over all incident angles produced by Time History analysis are larger than the respective response values obtained by Response Spectrum Method. The increase ranges between 1.28 and 1.45.

Table 2. Maximum response values produced by RSA and THA

RESPONSE	THA (average for $maxR_{,\theta}$)	RSA	THA/RSA
M_{22}	3713.12	2891.77	1.28
M_{33}	2304.80	1578.66	1.45
u_1	0.00458	0.00354	1.29
u_2	0.00442	0.00345	1.28
u_3	0.00933	0.00658	1.41

5 CONCLUSIONS

The results of the present study indicate that the bridge response depends strongly on the seismic input angle under a single ground motion. Moreover, the response produced by accelerograms applied along the bridge axes depends on the application of recorded correlated or uncorrelated accelerograms. The commonly chosen input axes such as longitudinal and transverse axis of bridge may lead to very unconservative results. The existing analytical formulas for maximum response computation over all incident angles produce response values which do not depend on the application of the recorded correlated or uncorrelated accelerograms. These formulas can be easily incorporated into existing software and require very little additional computational effort.

REFERENCES

[1] American Association of State Highway and Transportation Officials (AASHTO), *AASHTO LRFD bridge design specifications*, Second Edition, AASHTO, Washington, DC, 1998.

[2] CEN Eurocode 8, *Design of structures for earthquake resistance, Part2: Bridges*, European Committee for Standardization, Brussels, 2005.

[3] Athanatopoulou, AM, "Critical Orientation of Three Correlated Seismic Components", Engineering Structures, Vol. 27, No. 2, pp. 301-312, 2005.

[4] MacRae, GA, Mattheis, J, "Thee dimensional steel building response to near-fault motions", ASCE Journal of Structural Engineering, Vol. 126, No. 1, pp. 117-26, 2000.

[5] Maleki, S, Bisadi, V, "Orthogonal Effects in Seismic Analysis of Skewed Bridges", J, Bridge Engrg, Vol. 11, No. 1, pp. 122-130, 2006.

[6] Rigato, AB, Medina, RA, "Influence of angle of incidence on seismic demands for single-storey structures subjected to bi-directional ground motions", Engineering Structures, Vol. 29, No. 10, pp. 2593-2601, 2007.

[7] Penzien, J, Watabe, M, "Characteristics of 3-D earthquake ground motions", Earthquake Engineering and Structural Dynamics, Vol. 4 , No. 3, pp. 365-373, 1975.

[8] SAP2000, *Integrated Finite Element Analysis and Design of Structures*, Computers andStructures, Inc, Berkeley, California, USA, 2000.

[9] Pacific Earthquake Engineering Research Center (PEER), Strong Motion Database, http://peer.berkeley.edu/smcat/, 2005.

[10] Anastassiadis, K, Avramidis, IE, and Panetsos, PK, "Concurrent design forces in structures under three-component orthotropic seismic excitation", Earthquake Spectra, Vol. 18, No. 1, pp. 1–18, 2002.

EFFECT OF ISOLATION BEARING MODELING ON THE SEISMIC FRAGILITY OF BRIDGES

Anastasios Sextos[1], Ioannis Kilanitis[2], Ioannis Moschonas[3]

[1,2,3] Aristotle University of Thessaloniki, Dept. of Civil Engineering, Greece
e-mail: asextos@civil.auth.gr, giakila@yahoo.gr, imoschon@civil.auth.gr

ABSTRACT: In the present paper, the epistemic uncertainty related to the finite element modeling of low damping rubber bearings (LDRB) is investigated for the case of an existing 11-span bridge. Several time-history analyses are performed for increasing levels of earthquake intensity and the effect of bearing-related modeling uncertainty is quantitatively assessed.

KEY WORDS: base isolation, bearing modeling, bridges, fragility analysis

1 INTRODUCTION

The common practice in the design of isolated bridges involves the execution of response spectrum analyses and the assumption of linear elastic behaviour for the base isolation devices. This approach often involves a number of iterations until a reliable estimate of the earthquake intensity-dependent bearing stiffness is achieved. However, when non linear time-history analyses have to be carried out, primarily for assessment purposes, the equivalent linear approach is not valid anymore since there the bearing damping and stiffness varies at each earthquake loading cycle. Due to the inherent complexity of the bearing cyclic response though, the above problem has to be tackled on the basis of various simplifying assumptions and alternative implicit modeling approaches. As the seismic response of an isolated bridge greatly depends on the mechanical properties of the bearings though, the issue of the reliable modeling of the bearings cyclic response becomes of paramount importance. Despite this fact, the effect of the bearing-related modeling decisions has not yet been quantified. Along these lines, the objective of this paper is to investigate alternative analytical models that are commonly used in the framework of the seismic assessment of isolated bridges and to quantify the corresponding modeling uncertainty introduced, in terms of the predicted vulnerability. For this purpose an existing R/C bridge is parametrically assessed and the uncertainty associated with bearing finite element modeling is estimated. The theoretical and numerical backgrounds as well as the analysis results are presented in the following.

2 BACKGROUND

2.1 Cyclic behaviour of low damping rubber bearings

There are numerous experimental studies related to the mechanical properties of different types of bearings but only a few of them [1], [2] have investigated the behavior of low damping rubber bearings. However, the principles of LDRB cyclic response have been identified and it is quite common to be accounted for in numerical modeling. As regard to the horizontal stiffness of the bearings, it has been observed that their stress-strain relationship is typically of mild non-linearity, presenting a softening up to 100% stain and then a hardening for larger strain levels. This hardening can be primarily attributed to material nonlinearity in the natural rubber due to crystallization effects at high strains.

The hysteresis loops observed in all the experiments were thin and stable providing an equivalent viscous damping ratio that ranged from 3% to 6% depending on the applied strain rate (Fig. 1). It should be also noted that loading frequency has only a minor influence on the equivalent stiffness and damping ratio values that are used in design. As regard to the vertical stiffness of the bearings it has been observed to increase with increasing load and to decrease with increasing horizontal deflection.

2.2 Common approaches for modeling the LDRB

Due to the highly non linear behavior that have that have been described in the previous section, finite element modeling of low damping rubber bearings is inevitably made on the basis of simplifying assumptions. Most seismic codes propose that LDRBs are modeled by linear elastic elements with an equivalent viscous damping ratio (commonly taken approximately 6%) and an effective linear stiffness K_{eff} that is calculated based on elastic theory as:

$$K_{eff} = \frac{GA}{t_r} \tag{1}$$

where G is the shear modulus of the elastomer (rubber), A is the overall cross-sectional area, and t_r is the total thickness of the rubber. Similar equations have also been proposed for the estimation of vertical and bending stiffness [3].

However, the thin hysteresis loops that low damping bearings form under cyclic loading, can be also approximated by a bilinear model which is most commonly used for the modeling of other types of bearings (such as, lead-rubber bearings and friction pendulum system). The parameters needed in this case for the bilinear modeling of the LDRB isolation device are the elastic stiffness K_1, the post-elastic stiffness K_2, and the characteristic strength Q (Fig. 2).

In a more sophisticated modeling approach, a multi-linear law that takes into account the hardening effect could be used.

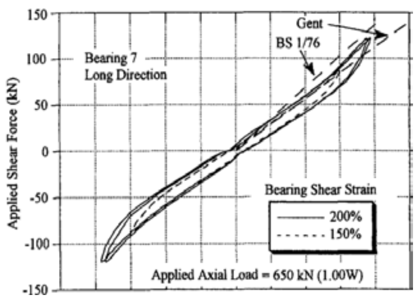

Figure 1. Typical hysteretic behaviour of low damping rubber bearings [1]

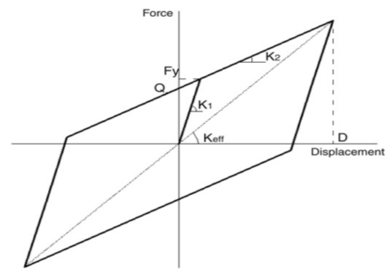

Figure 2. Bi-linear model of the cyclic response of LDR bearings [3]

3 OVERVIEW OF THE CASE STUDY

3.1 Description and modeling of the Lissor river bridge

The bridge studied is crossing the Lissos River along the Komotini-Mesti part of the 680km long Egnatia Motorway in Northern Greece. It is a 60/30 class bridge consisted of two similar branches, for serving the traffic in each traffic direction. The superstructure consists of a continuous, single-cell pre-stressed concrete box girder. It is straight with a total length of 433.31m and rests on 10 piers (hereafter denoted as M1÷M10) and 2 abutments (A1 and A11) through twenty, 1000x1000x175mm, low damping rubber bearings. The height of the deck is 2.75m except from the last span where the height is reduced to 1.35m and the section becomes solid. In order to prevent excessive movements in the transverse direction in case of a strong earthquake, seismic links (stoppers) of 1.2m height have been placed on the top of each pier permitting a clearance of ±10cm. Piers are wall-type having a section of 2.5x6.5m and rounded edges, while pile foundations comprising of 100mm diameter piles have been used to support the bridge. Lissos bridge has been designed according to the 1995 Greek Seismic Code provisions for soil conditions of Class C considering a design PGA value equal to 0.16g and a behaviour factor equal to 1.0 for both principal directions (longitudinal and transverse).

For the numerical analysis of the system, the computer program SAP2000 v.14 was used. The piers, the deck and the seismic links were modeled by frame elements, while various properties of the link elements have been used to model the cyclic behavior of the bearings in compliance to the different modeling approaches each time adopted. In order to filter-out any possible systematic bias attributed to the dynamic interaction between the superstructure, the foundation and the soil, fully fixed support conditions were assumed for all analyses conducted. Based on the actual boundary conditions of the system the deck-abutment connection was assumed free at the longitudinal direction and fixed at the transverse one.

3.2 Description and numerical modelling of the bearings

Four different analytical approaches where used herein to model the cyclic behavior of the bearings (Table 1) in the framework of the nonlinear dynamic analysis required for the assessment of the bridge vulnerability, in particular:

- *a linear model :* the common linear model which is proposed in most seismic codes [4] was used with 5% equivalent viscous damping ratio and an equivalent horizontal stiffness that was calculated by Eq.(1) as equal to K_{eff}=4457KN/m.
- *two alternative bilinear models*: in the first bilinear model (b1), the post-elastic stiffness K_2 was determined according to Eq.(1), while the initial stiffness K_1 was taken as a function of K_2 ($K_1=5K_2$). The required strength Q was obtained by assuming a yielding displacement ($u_y=0.1t_r$) [5]. The second model (b2) was also bilinear; however, it was made the assumption that the equivalent viscous damping ratio 5% occurs at a strain of 200% according to [6]. It should be noted that the estimation of the above parameters is rather arbitral. That is because, as opposed to other types of bearings, low damping rubber bearings do not have a specific yielding point and the bi-linearization of their actual force-displacement relationship essentially depends on the assumptions made as regard to their actual yielding point and the sharpness of the stress-strain curve close to yield.
- *a tri-linear model:* the tri-linear model was derived by introducing a third branch to the (b2) stress-strain curve with stiffness identical to the initial one (i.e., $K_3=K_1$) in order to take into account the hardening that occurs when the strain exceeds 100%. As the multi-linear link element provided by the computer program used was found to produce unstable hysteresis loops, the foreseen tri-linear stress-strain relationship was achieved by combining a Wen and a gap element in a series system (Fig. 3).

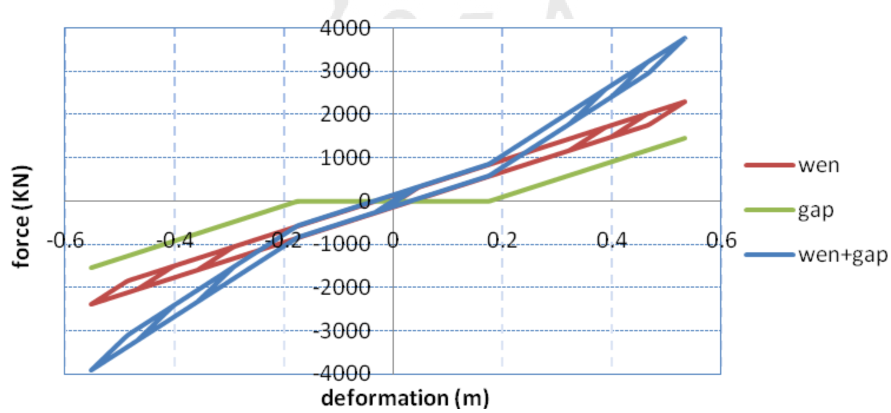

Figure 3. The tri-linear force-displacement model

Table 1. Alternative bearing models used in the framework of the fragility analysis

mode	material law	modeling approach	assumptions made
a	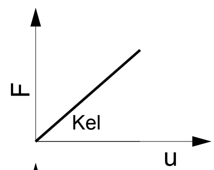	linear elastic theory	• nominal G
b1	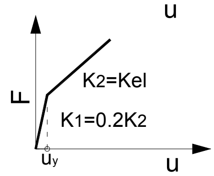	wen model	• nominal G • factor a = 0.2 • yielding diplacment uy = 0.10 tr • $K_2=K_{el}$
b2	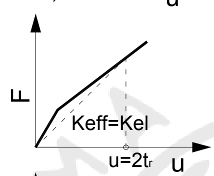	wen model	• nominal G • factor a = 0.5 • $K_{eff}=K_{el}$ for u = $2t_r$ • β_{eff} = 5% for u = $2t_r$
c	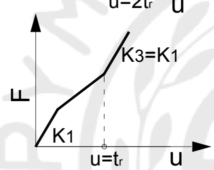	multi-linear model	• for u < t_r same as b2 law • for u >= tr $K_3=K_1=K_{el}$

3.3 Nonlinear time history analysis

Twenty ground motion records were selected from the PEER-NGA strong motion database [7]. Each ground motion was scaled to 20 increasing levels of spectral acceleration at the fundamental period of the bridge (T_1=2.44 sec) which was considered as the most appropriate intensity measure (IM) [8]. The response of the bridge was computed by inducing the selected acceleration time-histories as support excitation along the longitudinal direction. For the case of the linear elastic bearings, a constant modal damping of 5% was assumed for the entire structure, while for the remaining models the bearing damping was taken into account explicitly through their individual hysteresis loops, in addition to a 5% modal damping prescribed for the concrete parts.

3.4 Fragility analysis

The impact of the aforementioned modeling assumptions has been studied on the basis of the predicted bridge vulnerability. Four damage states, namely, slight, moderate, major, and collapse were defined to express the damage, corresponding at 0.5, 1.5, 2.0 and 5.0 bearing shear strain (the last three values are adopted from [9]). A log-normal distribution of the intensity measure over each DS was assumed, hence, the fragility functions (i.e. the probability of reaching or exceeding a certain damage state) can be written as:

$$P_f = \Phi\left[\frac{1}{\beta}\ln\left(\frac{S_a}{S_{am}}\right)\right] \quad (2)$$

where Φ is the standard normal cumulative distribution function, S_{am} is the median threshold value of spectral acceleration for a certain damage state and β is the lognormal standard deviation of the natural logarithm of S_a.

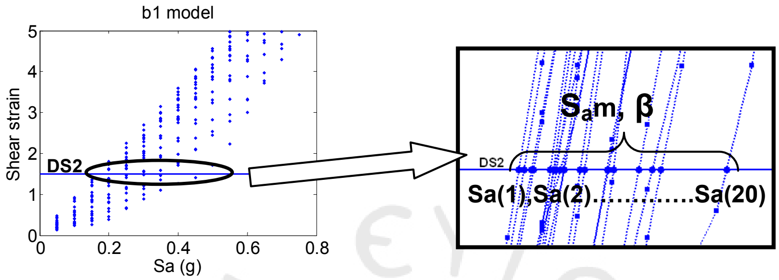

Figure 4. Derivation of the median value and the standard deviation of the natural logarithm of Sa values at which the bearing reaches the threshold of damage state 2.

These S_a values for each DS are specified by linearly interpolating the values of two consecutive S_a levels (Figure 4). Figure 5 compares the fragility curves derived for the four alternative bearing models and for each individual damage state. It can be noted that at the DS1 and DS2, the linear model leads to higher conditional probabilities of failure for the entire range of earthquake intensity, as expressed by S_a. This implies that the linear model is a rather conservative approach for design purposes that commonly correspond to such levels of bearing deformation (i.e., $\gamma<1.5$). However, when it comes to examine the probability of collapse (DS4), the bilinear2 model tends to predict the highest vulnerability, therefore it can be claimed that the assumption of linear behavior for the bridge bearings underestimates the probability of collapse. Another interesting issue is related to the high slope observed for the fragility curve that corresponds to the linear model. This can be attributed to the fact that for the particular structural system, the mass that is activated in the first mode is high, hence the variability in the response of a linear elastic system under earthquake records that have been scaled to the spectral acceleration at the fundamental period, is naturally, very low.

Table 2 summarizes the two parameters of the lognormal distribution S_{am}, β for the four alternative bearing modeling approaches. A comparison of the four models can be made on the basis of their median value (S_{am}) that corresponds to the value of S_a that has 50% probability of exceedance. It can be seen that $S_a m$ varies from 0.059g to 0.107g for DS1, 0.178g to 0.249g for DS2, 0.237g to 0.31g for DS3 and 0.518g to 0.619g for DS4.This difference of 81,4%, 39,9%, 30,8% and 19,5% (for DS1-DS4) between the highest and the lowest S_{am} value clearly reflects the fact that as the seismic demand increases the response dispersion among the four bearing models decreases, hence, for more critical damage states, the decisions related to bearing modeling are less significant, although still non-negligible. It is notable that the linear and bilinear2 model have similar median values at DS3, a fact which was anticipated since both models have the same equivalent viscous damping ratios and stiffness at 200% shear strain. Finally, it is seen that the linear model is associated to the lowest standard deviation (β) which is approximately equal to 0.005 while bilinear1 (DS1, DS2, DS3) and tri-linear (DS4) lead to significantly higher values of β.

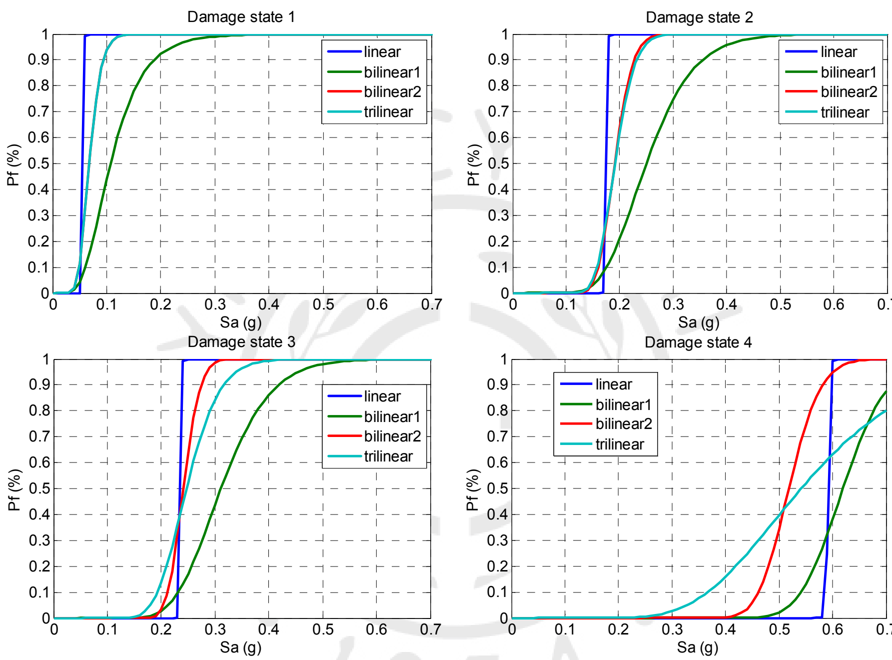

Figure 5. Fragility curves for the four different modeling approaches adopted for the bearings and the four damage states examined

Table 2. Lognormal distribution parameters for the four alternative bearing modeling approaches

		linear	blinear1	bilinear2	trilinear
DS1	S_am (g)	0.059	0.107	0.067	0.067
	β	0.005	0.440	0.253	0.253
DS2	S_am (g)	0.178	0.249	0.191	0.191
	β	0.005	0.274	0.136	0.150
DS3	S_am (g)	0.237	0.310	0.241	0.246
	β	0.005	0.231	0.101	0.193
DS4	S_am (g)	0.592	0.619	0.518	0.539
	β	0.005	0.105	0.090	0.304

4 CONCLUSIONS

This paper attempts to quantify the uncertainty introduced in the fragility analysis of an existing R/C bridge due to different assumptions made regarding the finite element modeling of specific bearings used in design. As all other vulnerability analyses remained deliberately identical, the particular study revealed dispersions in the predicted probability of failure that can be solely attributed to the interplay between the force-displacement relationships adopted for the bearings, the dynamic characteristics of the bridge and the frequency content of the earthquake motions used. Through the fragility analysis that has been carried out, it was shown that different assumptions related to the modeling of bridge bearings may significantly alter the median values of the intensity measure associated to a particular damage state. It was also shown that the assumption of linear elastic bearings leads to a conservative estimate of the probability of exceedance of the lower (i.e., less critical damage states), a situation that is reversed for the case of major damage and collapse. Finally, it was shown that the more critical the damage stage, the less significant the decisions on the bearing modeling become; however, the associated dispersion is certainly non-negligible and hence, further research towards the quantification of the epistemic uncertainty are certainly needed.

REFERENCES

[1] Mori, A., Moss, P. J., Cooke, N., & Carr, A. J."*The behavior of bearings used for seismic isolation under rotation and axial load*",Earthquake Spectra*, Vol. 15,No.* 2,pp. 225-244, 1999
[2] Abe, M., Yoshida, J., & Fujino, Y. " *Multiaxial behaviors of laminated rubber bearings and their modeling. I: Experimental study*" *Journal of Str Eng, Vol. 130*, No. 8,pp. 1119-1132
[3] Naeim, F., Kelly, J. "Design of seismic isolated structures", 1st edition, Wiley, 1996
[4] CEN "*Eurocode 8: Design of structures for earthquake resistance, Part 2: Bridges, European standard, EN 1998-2*", Brussels, 2005
[5] Zhang, J., Huo, Y. "Evaluating *effectiveness and optimum design of isolation devices for highway bridges using the fragility function method*", *Eng Struct ,Vol. 31,*No.8,pp 1648-1660
[6] Moschonas, IF, *Seismic Fragility Analysis of Concrete Bridges*, PhD Thesis (in Greek), Civil Engineering Department, Aristotle University of Thessaloniki , 2010
[7] Katsanos, EI, Sextos, AG, Notopoulos, T, "ISSARS: An Integrated System for Structural Analysis and Earthquake Record Selection", *CD-ROM Proc. ECCOMAS Thematic Conference on Computational Methods in Structural Dynamics and Earthquake Engineering - COMPDYN 2011*, Paper No. 224, Corfu, 2011.
[8] Mackie KR, Stojadinović B. "*Performance-based seismic bridge design for damage and loss limits States*", Earthquake Eng Struct Dyn, Vol. 36, pp. 1953–1971, 2007
[9] Moschonas, IF, Kappos, AJ, Panetsos, P, Papadopoulos, V, Makarios, T, Thanopoulos, P, "Seismic fragility curves for greek bridges: methodology and case studies", Bulletin of Earthquake Engineering, Vol. 7, No. 2, pp. 439-468, 2009.

DESIGN AND CONSTRUCTION OF BRIDGE G7
Egnatia Motorway, NW Greece

Ioannis Lefas[1], Tilemachos Tsiknias[2] and Vassiliki Georgiannou[3]

[1] AKTOR SA, Greece
[2] T Tsiknias & Associates (TTA), Greece
[3] National Technical University of Athens, Dept. of Civil Engineering, Greece
e-mail: ilefas@etae.com, ttsiknias@tta.gr, vngeor@civil.ntua.gr

ABSTRACT: The paper describes the design and construction process followed for a valley bridge in an area of high seismicity and adverse ground conditions. Attention is paid to the system used to provide seismic isolation and the treatment of difficult site conditions during the construction of pier foundations.

KEY WORDS: Bridge; High Seismicity; Adverse ground; Seismic Isolation.

1 INTRODUCTION

Egnatia Motorway in Greece is one of the largest civil engineering projects in Europe with over 600 bridges on its main axis alone. The motorway traverses a wide range of seismically active terrains lending to the design and construction of a variety of bridge forms and earthquake protection systems [1], [2].

Bridge G7 carries Egnatia Motorway, a new 650km dual motorway crossing North Greece from West to East, through a valley close to the area of Paramithia town some 35km east of the major port link of Greece with Italy and Western Europe.

From contract award in late 1997, the Contractor had determined that a valley bridge (with two independent branches) constructed with precast prestressed beams would be economical and would lend to rapid construction. With those directives specialist bridge designer TTA began evaluating various ways of designing the bridge in an area of severe seismic input and difficult ground conditions with the additional constraints of the avoidance of excavating new access roads and the use of the data of the existing site investigation.

2 STRUCTURAL FORM

The structure is curved in plan with a radius R=1445.1 m for the south branch and 1754.9 m for the north branch and the deck section is laterally inclined (in the transverse direction) by 3.5% and 4% respectively. In elevation, the south branch has a slope of 5.35%, while the north branch has a slope of 2.85%, after the first 48 m which are horizontal.

Each branch consists of two lanes plus emergency lane and pavement in the external side. The overall width of each branch is 12.7 m. The north and south branches have an overall length between the expansion joints of the abutments of 166.9 m and 133.4 m respectively. The north branch consists of 4 spans: 32.15+2*33.5+32.15 m, while the south branch consists of 5 spans: 32.15+3*33.5+32.15 m (see *Photo 1*).

Photo 1. North and South branches of bridge G7

During the planning phase there was particular concern about the vulnerability of the bridge to seismic events and the overall economics of the solution to be adopted. A system of elastomeric or PTFE bearings was selected to connect the piers/abutments with the beams/deck superstructure. Hydraulic dampers, a pair in the longitudinal direction and a pair in the transverse direction connect each abutment with the superstructure.

3 DESIGN

3.1 Geology and geotechnical conditions

The geology along the route of Egnatia Motorway is diverse since it crosses some ten different main zones, most of which have been overthrusted on one another from east to west [3]. The diversity results from the intense folding, thrusting, faulting and uplifting of strata that took place during the Alpine period at the boundary between oceanic and continental plates. Heavily sheared zones have drastically degraded the rock quality.

The geological conditions of the foundation of the abutments/piers of bridge G7 are as follows (see Figure 1):

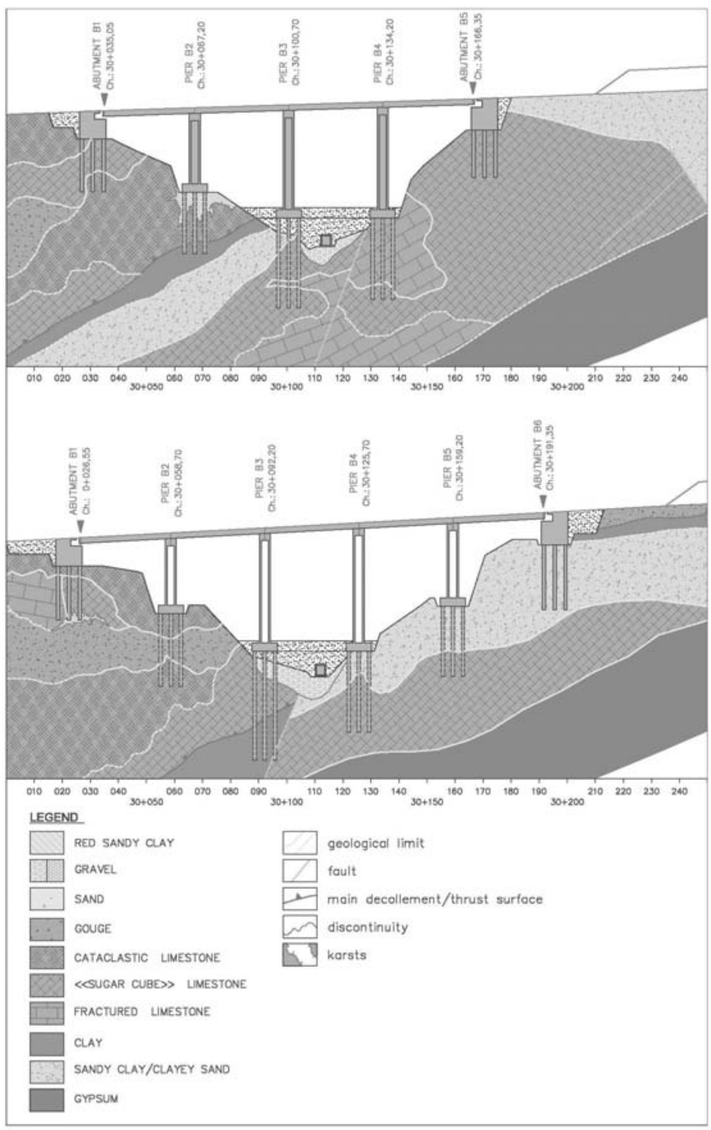

Figure 1. Schematic geological conditions along bridge G7

Limestone dominates in the area of the bridge. The limestone [4] is subdivided into fractured limestone, sugar cube limestone, cataclastic limestone and cataclasite or gouge, depending on the structure and the block size of the rock mass. Karstic voids within the limestone are present in the area and are found filled with red clay or clayey gravels. A 30m thick intercalation of a sedimentary sequence (blue clay and sandy, clayey gravel) is found within the limestone which is exposed at the area of B4, B5 and B6 piers of the south branch of the bridge. Blue Clay is firm to very stiff, thin bedded and exhibit slickensided anastomosing surfaces. Sandy, clayey gravel is not bedded, medium dense to very dense.

The basement of the above mentioned geological units is weak to moderately weak, grey, thin bedded, crystalline gypsum. This gypsum layer which lay some tens of meters underneath the foundation piles of the B6, B5 and B4 piers of both branches. Along the axis of the stream, 5 to 10m thick, recent river bed deposits are found consisting mainly of sandy gravel with boulders. All geological formations are cut by a fault, trending parallel to the axis of the stream, running almost at the stream bed. Small scale structural failures took place in the sedimentary sequence during excavation and formation of the slope for the construction of B5 pier (south branch)).

3.2 Foundations

The presence of relatively small bridge spans combined with high seismic actions resulted in the development of high bending moments combined with relatively low axial forces at founding levels. Part of this detrimental effect was reduced in the mid high piers by the construction of an embankment from selected material.

Bored piles, 1.2m in diameter, were used in various combinations for the foundations of abutments and piers. The piles were designed to DIN 4014 [5]. Most of the piles in both branches were bored in limestone, either throughout their entire length (piers B1, B4, B5 of the north branch and B1, B2 of the south branch) or at their end (pier B3 of the north branch and B4, B5 of the south branch), thus acting as end bearing piles. In the cases were the piles ended within the sedimentary sequence (pier B2 of the north branch and B3, B6 of the south branch) their length was enlarged in order to counterbalance the reduction of the base resistance of the piles with the increase of their shaft resistance. The settlement of the ground due to the loading from the embankment has been ignored to be on the safe side. A total length of 1242m of piles was used for the north branch with the equivalent number of the south branch being 1410m.

3.3 Abutments and piers

The piers are of rectangular hollow section with overall external dimensions of 4m by 7m. Wall thickness is 0.45m. The abutments are of multi-cell wall construction with transverse stiffening walls. The superstructure deck is continuous over the piers. Expansion joints are placed only over the abutments and permit horizontal movement at the tangential and radial directions of the bridge axes.

3.4 Superstructure

The superstructure was constructed with precast prestressed beams. With the use of a purpose-built launching truss five beams (31.8m long by 2.0m deep each) per span have been put in place. The beams were prestressed in a purpose-built precast bed using linear tendons. The beams are supported on elastomeric bearings some of which also work as sliding bearings. The gaps between the flanges of the beams have been filled with conventionally reinforced precast slabs with a minimum thickness of 0.20m. The overall structural dimensions of the superstructure are 2.23m in height and 12.20m in width.

3.5 Dynamic behaviour and the use of seismic isolation

In accordance with current Greek legislation, bridges are designed in accordance with the Greek Seismic Code (very similar to Eurocode 8, [6]). The peak ground acceleration (PGA) at the bridge site is 0.24g. This value represents a seismic event with a 475-year return period. Due to the fact that Egnatia Valley bridges are considered to be seismically important viaducts and should be designed for a higher reliability, the PGA was multiplied by an importance factor 1.30 thus yielding a Design Ground Acceleration (DGA) of 0.312g. This value corresponds to a major earthquake event with a return period 1000 years approximately.

Due to the magnitude of the seismic action, the main design challenge is the reduction of the forces transferred from the deck to the substructure. An effective way to reduce seismic actions is to install a seismic isolation system between the deck and the substructure [7]. The main properties of a seismic isolation system are:

a) the ability to provide the so called ‘period-shift’ (moving the fundamental vibration period of the structure to the lower spectral accelerations),

b) the ability to provide additional damping in order to reduce the displacements resulting from the ‘period-shift, and

c) the ability to provide re-centering of the deck at the end of the dynamic response so that there will be no remaining displacement of the deck .

The seismic isolation system selected for bridge G7 is comprised of a combination of normal rubber bearings (with and without PTFE sliding sheets) and Viscous Hydraulic Dampers [8], [9]. The bearings provided the ‘period shift’; the hydraulic dampers provide the additional damping. The re-centering of the deck is provided by the normal elastomeric bearing (without PTFE sliding sheets).

The dampers were installed at the abutments, in order to achieve easy access for inspection and maintenance. Two dampers were installed in the longitudinal and two in the transversal direction at each abutment.

For the north branch bridge the longitudinal dampers were specified for a damping force of 500KN and a piston total stroke of 520mm whereas the transversal dampers were specified for damping force of 400 KN and a piston total stroke of 460. For the south branch bridge the corresponding values were 600KN/550mm for the longitudinal dampers and 440KN/470mm for the transversal.

Due to the nonlinear behaviour of the dampers, a nonlinear dynamic analysis of the whole structure was performed by using a series of synthetic acceleration time histories generated to closely fit the design acceleration spectrum of the code [10]. The effect of seismic isolation in quantitative terms was the reduction of seismic actions on the substructure elements (piers and foundations) by more than 60% comparing to the non-isolated case.

4 TREATMENT OF SPECIAL CASES DURING CONSTRUCTION

The construction of bridge G7 has necessitated the use of innovative solutions for mitigating effects on the natural and man-made environment.

4.1 Presence of gypsum

Early site investigation works on specimens from the boreholes in the deep trough of the valley close to the founding position of the middle piers has indicated the presence of sulphate salts in the chemical analysis of groundwater. Concentrations as high as 500mg/litre of sulphate anions SO_4 were recorded and confirmed from further tests just before the commencement of foundation works. To counteract the detrimental effect of such aggressive environment for the concrete, sulphate resistant concrete with max w/c ratio of 0.50 and minimum cement content of 400kg/m^3 were used for the construction of almost 25% of the piles and pile caps particularly of the south branch.

4.2 Embankment from selected material at foundation of middle piers

The construction of a small embankment from selected material (together with the associated hydraulic works) at foundation level of middle piers resulted in the drastic reduction of unwanted overturning moments combined with low axial forces during the earthquake.

4.3 Geotechnical conditions at pier positions – Slope stability issues

Small scale structural failures took place in these materials, while excavating and forming the slope for the construction of eastern pier (right branch).To achieve the trouble free construction of foundations and piers in these highly unpredictable ground conditions met during slope excavation, the following techniques were used as required:

Steep slopes and loose rock masses were present at or above the area of abutments and piers founding areas of the right branch of the bridge. For safety reasons, initially the excavated temporary slopes were protected with wire mesh, shotcrete and rock bolts. Drain pipes were also installed to discharge any water blocked within the various interfaces of permeable and impermeable layers. Photo 2 below depicts the end product in the steep cliff edges leading to the Paramithia valley.

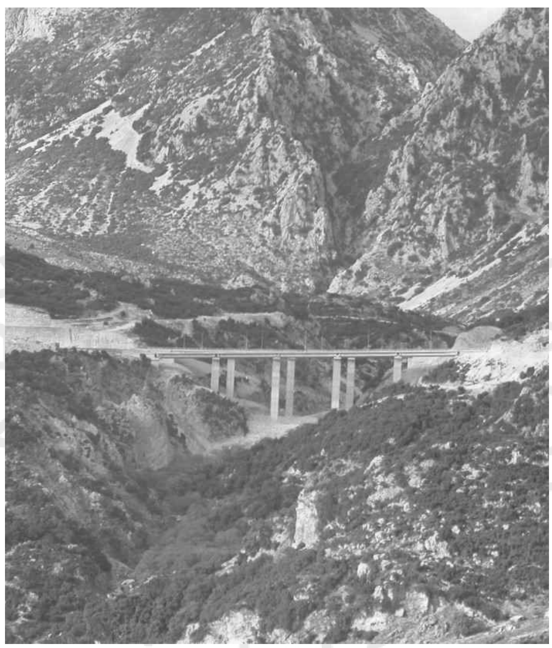

Photo 2. Valley Bridge G7 in operation close to the town of Paramithia

5 COMPARATIVE COST STUDY

During checking the client asked for a comparative study of the cost benefits by the use of the seismic isolation technique for bridge G7 versus the conventional technique for resisting lateral forces and moments stemming from an earthquake during the lifetime of the bridge.

The non use of hydraulic dampers increases the seismic actions to the piers by 310%. The end result of this is the need of an area of pier flexural reinforcement at the base of 3.9% of the overall sectional area compared with 1.54% for the seismically isolated case. Similarly the shear reinforcement requirement in the pier's web reduces by 50%. Adding these two beneficial effects, the overall reduction in reinforcement requirement of the piers reaches 55%.

In addition, the base moments at foundation level are three times larger in the conventional approach. This would have meant a significant increase in the required pile head cross sectional area and volume per pier, number and length of piles per pier together with an increase in the area of steel ratios within each pile.

The non use of hydraulic dampers would have also resulted in an increase of displacements during the design earthquake from 14 cm to 27cm. This increase affects significantly the sizing of both elastomeric bearings and expansion joints. The influence of the above beneficial effects from the use of the seismic isolation system proposed, as compared to the overall cost of the bridge constructed using the conventional method was in the range of 25%.

6 CONCLUSIONS

Valley Bridge G7 was built in an area of high seismicity and adverse ground conditions. The final solution adopted was the result of close liaison between the designer, the construction team and the engineers carrying out the design and detailing of the works. The provision of seismic isolation combined with proper treatment of difficult site conditions during the construction of pier foundations resulted in a solution that managed to deliver successfully all the objectives of the design process.

ACKNOWLEDGMENTS

The authors would like to thank EGNATIA ODOS S.A. for fruitful discussions during the finalization of design and execution of the works.

REFERENCES

[1] Ahmadi-Kashani K. “Seismic Design of Egnatia Motorway Bridges, Greece”, Journal of Bridge Engineering, Vol. 2, pp. 83-91, 2004.
[2] Hindley G., Gibbons P., Agius M., Carr B., Game R., and Kashani K. “Linking Past and Future”, ASCE, Civil Engineering Magazine, , Vol. 74, No. 5, 2004.
[3] IFP-IGRS, *Etude Geologigue de l'Epire*, Ed. Technip, 1966.
[4] Georgiannou V.N., Lefas I.D. and Boroncay C.A. “Monitoring of tunnel behaviour through cataclastic rocks”, ICE, Journal of Geotechnical Engineering, Vol. 159, pp. 113-123, 2006.
[5] DIN 4014 : “Bored Piles”
[6] Eurocode 8 – “Design provisions for earthquake resistance of structures – Part 2 : Bridges”
[7] AASHTO, “Guide Specifications for Seismic Isolation Design”, 1999
[8] Kelly J.M., *Earthquake Resistant Design with Rubber*, Springer, 3rd Edition, 1997, 243pp.
[9] Fazrad Naeim and James M. Kelly, *Design of Seismic Isolated Structures : From Theory to Practice*, 1999
[10] Chopra A.K., *Dynamics of Structures – Theory and Applications to Earthquake Engineering*, Prentice-Hall Inc., International Series in Civil Engineering and Engineering Mechanics, Englewood Cliffs, New Jersey, 3rd Edition, 2006, 912pp.

BRIDGE WITH UN-BONDED POST-TENSIONED PIERS
Dynamics Simulation under Base Excitation

Dimitrios Sophianopoulos, Panagiotis Tsopelas

University of Thessaly, Dept. of Civil Engineering, Volos,Greece
e-mail: dimsof@civ.uth.gr, tsopelas@civ.uth.gr

ABSTRACT: The dynamics of bridges with un-bonded post-tensioned piers under ground motion is considered. The actual bridge structure is modeled as a 3-DOF with 2-masses excited at the base by a simulated seismic motion. The effect of the parameters controlling the system dynamics is captured and important conclusions for structural design purposes are drawn.

KEY WORDS: Bridges, un-bonded post-tensioned piers, base excitation.

1 INTRODUCTION

Following the large number of strong seismic events striking large urban centers around the world the last 30 years, modern societies have been pushing towards the establishment of modern seismic design approaches which favor/require construction techniques (e.g. pre-casting), and innovative technologies (e.g. seismic isolation) aiming to limit damage, and limit cost of repairing and downtime after a seismic event. Traditional design approaches based on the development of ductile mechanisms within the structure cannot adequately satisfy those requirements. For infrastructure systems and especially for bridges the interruption of functionality as well as the repair costs resulting from earthquake damages are of great concern, and have lead engineers to propose modern design approaches for these structures. One such modern design approach is the utilization of un-bonded post–tensioned piers to support the deck [1-7]. This approach limits the strength of the structure in an attempt to limit the accelerations in the deck and accordingly minimize the base or pier shear forces. Although such reduction of acceleration response is beneficial, it comes with the increase of deformations which could become unacceptable causing structural instability.

To the authors' knowledge, this quite novel and intuitively correct approach lacks theoretical validation, as far as its dynamic instability and bifurcations are concerned, in the context of a strictly non-autonomous vector-field formulation, dictated by the theory of dynamical systems. The main control parameters of the aforementioned problem, the influence of the variation of which will be studied, are the masses and the characteristics of the springs. The strongly coupled dynamic equations of motion are tackled within the framework of non-autonomous vector fields.

2 PROPOSED MODEL: FEATURES - MOTION EQUATIONS

2.1 Model description and properties

The considered 3-degrees-of-freedom, two-mass system is depicted in Figure 1, and proposed herein for simulating the dynamics of bridges with un-bonded post-tensioned piers.

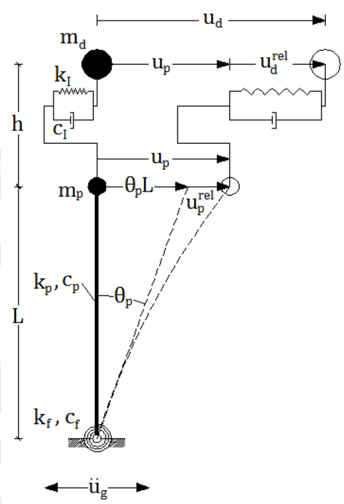

Figure 1. Proposed 3-DOF model

This simplified (stick) model consists of a concentrated mass representing the deck, supported by a linear viscoelastic spring representing the bridge bearings (expansion or seismic isolation with mild nonlinearities). This pier mass is connected to the foundation, via a massless flexible column (modeling the pier), which is pin connected to the ground with an additional linear rotational spring, simulating the connection of the pier to the foundation and characterized by a mild energy dissipation, coming from a linear viscous rotational dashpot. In the aforementioned illustration the subscripts “d”, “p”, “I” and “f” refer to the deck, the pier, the isolation system and the foundation respectively, while “m”, “k” and “c” represent the related masses, spring stiffnesses and damping coefficients of each of the above components, where applicable.

2.2 Equations of motion and local trivial instability

Two translational and one rotational generalized coordinates describe the dynamic response of the above model, which under simulated earthquake base excitation is governed by the system of strongly coupled linear non-autonomous equations of motion that follow ($\dot{} = d/dt$)

$$m_d\left(\ddot{\theta}_P L + \ddot{u}_P^{rel} + \ddot{u}_d^{rel}\right) + k_I u_d^{rel} + c_I \dot{u}_d^{rel} = m_d \ddot{u}_g(t) = F_1(t) \tag{1a}$$

$$m_P\left(\ddot{\theta}_P L + \ddot{u}_P^{rel}\right) - k_I u_d^{rel} - c_I \dot{u}_d^{rel} + k_p u_P^{rel} + c_P \dot{u}_P^{rel} = m_P \ddot{u}_g(t) = F_2(t) \tag{1b}$$

$$m_d\left(\ddot{\theta}_P L + \ddot{u}_P^{rel} + \ddot{u}_d^{rel}\right)(L+h) + m_P\left(\ddot{\theta}_P L + \ddot{u}_P^{rel}\right)L + k_f\theta_P + c_f\dot{\theta}_P = (L+h)F_1(t) + LF_2(t) \tag{1c}$$

In the right hand sides of these equations the ground motion is simulated, for the cases of remote and near earthquakes, via an acceleration function envelope $\ddot{f}(t)$ with its characteristics shown in Figure 2.

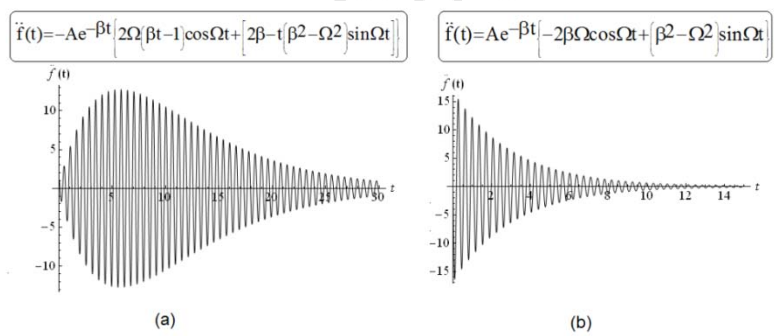

Figure 2. Typical plots of simulated ground motion for (a) remote and (b) near earthquakes

Evidently, for these simulations, the range of the parameters involved is:

$$\begin{aligned} &\text{Case (a)}: 0.01 \le A \le 0.10 \;,\; 0.05 \le \beta \le 0.30 \;,\; 5 \le \Omega \le 20 \\ &\text{Case (b)}: 0.01 \le A \le 0.10 \;,\; 0.15 \le \beta \le 0.50 \;,\; 1 \le \Omega \le 12 \end{aligned} \tag{2}$$

Introducing the following dimensionless parameters

$$\left.\begin{aligned} &\tau = t\sqrt{\frac{k_p}{m_p}} \;,\; u_1 = \frac{u_p^{rel}}{L} \;,\; u_2 = \frac{u_d^{rel}}{L} \;,\; \sigma = \frac{h}{L} \;,\; m = \frac{m_d}{m_p} \;,\; \theta_p(t) = \phi(\tau) \\ &\alpha = m(1+\sigma)+1 \\ &k_1 = \frac{k_I}{k_p} \;,\; k_2 = \frac{k_f}{k_p L^2} \;,\; c_1 = \frac{c_I}{\sqrt{k_p m_p}} \;,\; c_2 = \frac{c_p}{\sqrt{k_p m_p}} \;,\; c_3 = \frac{c_f}{L^2\sqrt{k_p m_p}} \end{aligned}\right\} \tag{3}$$

the system of motion equations 1(a-c) is written in dimensionless form as:

$$m\varphi''(\tau) + u_1''(\tau) + u_2''(\tau) + k_1 u_2(\tau) + c_1 u_2'(\tau) = m\gamma(\tau) \tag{4a}$$

$$\varphi''(\tau)+u_1''(\tau)+c_2u_1'(\tau)-c_1u_2'(\tau)+u_1(\tau)-k_1u_2(\tau)=\gamma(\tau) \tag{4b}$$

$$\varphi''(\tau)+u_1''(\tau)+(\alpha-1)u_2''(\tau)+\frac{c_3}{\alpha}\varphi'(\tau)+\frac{k_2}{\alpha}\varphi(\tau)=\gamma(\tau) \tag{4c}$$

where prime indicates differentiation with respect to τ, while the excitation function $\gamma(\tau)$ is the dimensionless base acceleration according to Figure 2.

The system is considered perfect and at rest before the initiation of the ground motion. Since no external loading exists, the trivial state represents the only valid equilibrium configuration. It would thereafter be of major importance to seek out the local stability of this state, by exploring the nature of the roots of the corresponding 6^{th}-order characteristic polynomial (which in fact are the eigenvalues of the trivial equilibrium), via the possible violation of one or more of the Liénard-Chipart conditions [8]. Employing advanced symbolic manipulations in *Mathematica* [9], the above polynomial, equal to:

$$G(\rho)=\rho^6+\alpha_1\rho^5+\alpha_2\rho^4+\alpha_3\rho^3+\alpha_4\rho^2+\alpha_5\rho+\alpha_6 \tag{5}$$

possesses coefficients α_i (i=1,…,6) given by:

$$\alpha_6=\frac{k_1^2k_2}{(m-1)m(1+\sigma)(1+m+m\sigma)}\ ,\ \alpha_5=\frac{k_1\left(c_3k_1+(c_1-c_2)k_2\right)}{(m-1)m(1+\sigma)(1+m+m\sigma)} \tag{6a,b}$$

$$\alpha_4=\frac{-c_1c_2k_2+k_1^2(1+m+m\sigma)+k_1(1+c_1c_3-c_2c_3+m+m\sigma)}{(m-1)m(1+\sigma)(1+m+m\sigma)} \tag{6c}$$

$$\alpha_3=\frac{\begin{pmatrix}c_1\left(1-c_2c_3+k_1-2k_2+m+k_1m+(1+k_1)m\sigma\right)\\ -c_2\left(k_2+k_1(1+m+m\sigma)\right)\end{pmatrix}}{(m-1)m(1+\sigma)(1+m+m\sigma)} \tag{6d}$$

$$\alpha_2=\frac{-1+c_1c_2+m(1+\sigma)+k_1\left(m^2(1+\sigma)\right)+\dfrac{2c_1c_3+c_2c_3+k_2}{1+m(1+\sigma)}}{(m-1)m(1+\sigma)} \tag{6e}$$

$$\alpha_1=\frac{(m-1)(c_1+c_2+c_2m)+c_2m^2\sigma-\dfrac{c_3}{1+m(1+\sigma)}}{(m-1)m(1+\sigma)} \tag{6f}$$

Rational values of the involved parameters will be used in obtaining numerical results. For moderate dimensions of deck and piers and commonly used values of damping and stiffness, the following range shall be utilized, in seeking possible unstable trivial situations as well as forced dynamic responses:

$$0.1 \le k_1 \le 1 \ , \ 0.002 \le k_2 \le 0.005 \ , \ \sigma \le 0.10 \ , \ 2 \le m \le 10$$
$$0.02 \le c_1 \le 4 \ , \ 0.04 \le c_2 \le 0.1 \ , \ 0.005 \le c_3 \le 0.08 \tag{7}$$

Utilizing the powerful *FindMinimum* and *Reduce* commands embedded in *Mathemetica*, it was found that only coefficient α_3 may be less or equal to zero within the range given in (7). This fact however leads to at least one eigenvalue of the trivial state with positive real part, implying local instability, i.e. the possibility, for an infinitesimal disturbance, of the system to exhibit at least a divergent motion, and, under ground motion, the occurrence of complicated dynamic phenomena. Two typical situations of such a possibility are given in the contents of Table 1.These two cases represent actual bridge structures; e.g. a typical 2-span seismic isolated highway overpass.

Table 1. Two characteristic cases of local trivial instability

Case No	m	σ	k_1	k_2	c_1	c_2	c_3	eigenvalue(s) with positive real part(s)
1	3	0.05	0.5	0.0035	0.05	0.05	0.04	0.004±0.37i
2	1.5	0.03	0.1	0.004	1	0.07	0.08	0.18±1.14i

Solving numerically the system of equations 4(a-c) for $\gamma(\tau)=0$ and $\varphi'(\tau)=0.0001$, for both cases shown in the above Table, an unbounded motion response was found, validating the unexpected theoretical prediction described earlier. This response is depicted in the phase-plain portraits $[u_1(\tau), u'_1(\tau)]$ of Figure 3.

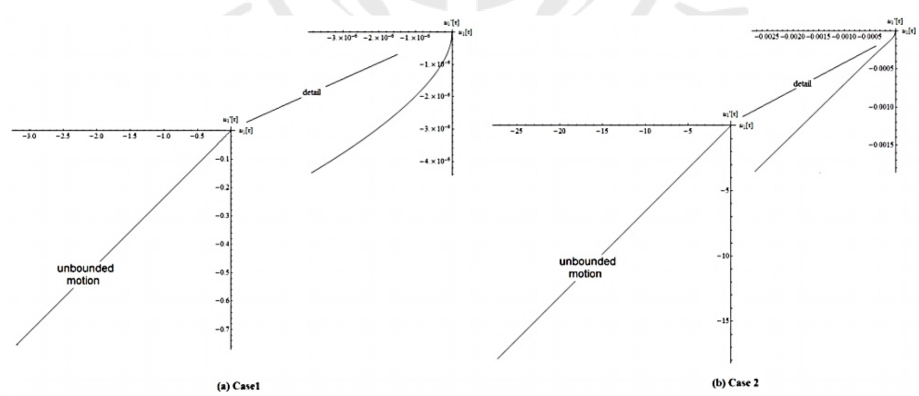

Figure 3. Unbounded motion exhibited by the system at its trivial state (for both Cases shown in Table 1), for an infinitesimal initial disturbance in the absence of base excitation

2.3 Some aspects of non-autonomous formulation

The forced oscillations of the model governed by eqs.(4) can also be treated as a linear non-autonomous 6^{th}-order vector field, within the context of the theory of dynamical systems [10]. For such a type of systems, a variety of responses have been reported, and as far dynamic stability is concerned, these may vary from unbounded motions and simple periodic orbit bifurcations to complicated resonance phenomena, without excluding strange or chaotic behaviour [11]. Evidently, to perform a rigorous non-autonomous formulation regarding the multi-parameter foregoing system would be very intriguing, but for reasons of space limitation such an approach is not included herein, but proposed for future research. Instead, a straightforward dynamic analysis will be hereafter adopted, which as it will be demonstrated may produce very important qualitative results.

3 NUMERICAL RESULTS AND DISCUSSION

For typical remote and near earthquake simulations, it would be of great interest to compare between the dynamic responses of the system corresponding to cases related to stable and unstable trivial configurations. In what follows, Cases 1 and 2, as in Table 1, will be considered for the unstable situation, while two more combinations of parameters (for which the trivial state is stable) will be used, namely Cases 3 and 4, with details given in Table 2.The parameters for these cases are also representative of actual bridge structures.

Table 2. Two characteristic cases of local trivial stability

Case No	m	σ	k_1	k_2	c_1	c_2	c_3
3	10	0.05	0.1	0.004	0.2	0.07	0.05
4	6	0.02	0.3	0.004	0.8	0.02	0.05

In obtaining numerical results, the following simulated ground motion parameters were used for assessing the excitation function $\gamma(\tau)$:

- Remote earthquake simulation : $A=0.05$, $\beta=0.20$, $\Omega=5$
- Near earthquake simulation : $A=0.05$, $\beta=0.15$, $\Omega=2$

The straightfarward dynamic analysis lead to two totally different responses, which are illustrated throughout Figures 3 and 4, corresponding to iniatially unstable and stable trivial states respectively, in terms of phase – plain plots $[u_1(\tau), u_1'(\tau)]$. More specifically, the system under both remote and near eartquake simulated excitation was found to exhibit small amplitude vibrations, which decay to zero after the end of the forcing function, i.e. to finally rest at its trivial stable equilibrium; the free vibration was not depicted in Figure 3 for clarity.

On the other hand, the dynamics of the intially unstable system configurations were related to an unbounded motion, leading to very large chatastrophic displacements. Same qualitative results were also obtained for other combinations of parameters regarding the ground motion (within the afore mentioned ranges) not shown herein for brevity. It is postulated that the above findings are directly dependent on the nature of the stability of the trivial state, a fact implying that during design this should be taken inti account, in order to avoid potential unfavorable and rather unexpected dynamic behavior.

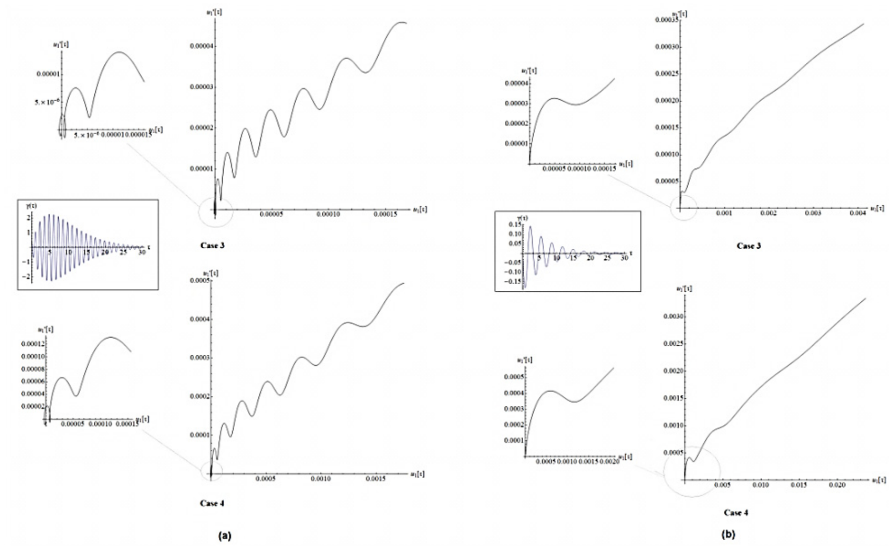

Figure 4. Dynamic response of the initially stable system under (a) remote and (b) earthquake simulations

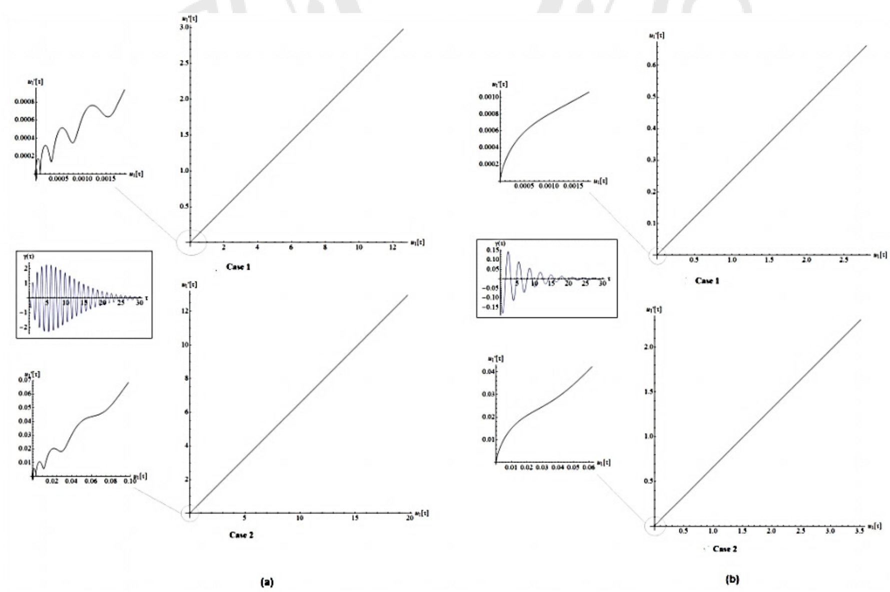

Figure 5. Dynamic response of the initially unstable system under (a) remote and (b) earthquake simulations

4 CONCLUSIONS

The non-dimensional formulation of the equations of motion of a bridge structure supported by un-bonded post-tensioned piers is presented. The behavior of the springs of the model is assumed linear. This assumption is considered valid as long as the potential nonlinearities of the springs representing bridge bearings and pier to foundation connection are small. It was shown that there are cases which could represent real bridge structures where the dynamic behavior can become unstable. These phenomena are not common but they might become catastrophic and as such the bridge designers should be aware and take appropriate actions even at the preliminary design phases. Considering the assumptions and limitations of this study, additional work is required, focusing on the following issues, in order to reach a much more integrated prediction of the real structural response:(a) Adopt a more detailed non-linear model to capture bearing and pier-foundation springs behavior, (b) Seek the dynamics of thebridge model under real (recorded) seismic excitations, and (c) Employ perturbation techniques and capture possible resonance phenomena associated with both the linear model utilized in this study and the non-linear model for the future study.

REFERENCES

[1] Kwan, W-P, Billington SL, "Unbonded Posttensioned Concrete Bridge Piers. I: Monotonic and Cyclic Analyses", Journal of Bridge Engineering, Vol. 8, No. 2, pp. 92-101, 2003.

[2] Kwan, W-P, Billington SL, "Unbonded Posttensioned Concrete Bridge Piers. II: Seismic Analyses", Journal of Bridge Engineering, Vol. 8, No. 2, pp. 102-111, 2003.

[3] Palermo, A, Pampanin, S, Calvi, GM, "Concept and development of hybrid solutions for seismic resistant bridge systems", Journal of Earthquake Engineering, Vol. 9, No. 6, pp. 899-921, 2005.

[4] Palermo, A, Pampanin, S, Marriott, D, "Design, Modeling, and Experimental Response of Seismic Resistant Bridge Piers with Posttensioned Dissipating Connections", Journal of Structural Engineering, Vol. 133, No. 11, pp. 1648-1661, 2007.

[5] Marriott, D, Pampanin, S, Palermo, A, "Quasi-static and pseudo-dynamic testing of unbounded post-tensioned rocking bridge piers with external replaceable dissipaters", Earthquake Engineering and Structural Dynamics, Vol. 38, No. 3, pp. 331-354, 2009.

[6] Ou, Y-C, Wang, P-H, Tsai, M-S, Chang, K-C and Lee, GC, "Large Scale Experimental Study of Precast Segmental Unbonded Posttensioned Concrete Bridge Columns for Seismic Regions", Journal of Structural Engineering, Vol. 136, No. 3, 2010.

[7] Roh, H, Reinhorn, AM, "Nonlinear Static Analysis of Structures with Rocking Columns", Journal of Structural Engineering, Vol. 136, No. 5, pp. 532-542, 2010.

[8] Sophianopoulos, DS, Michaltsos, GT, Kounadis, AN, "The Effect of Infinitesimal Damping on the Dynamic Instability Mechanism of Conservative Systems", Mathematical Problems in Engineering, Vol. 2008, Article ID 471080, 25 pages, 2008.

[9] Dubin, D, *Numerical and Analytical Methods for Scientists and Engineers using Mathematica*, John Wiley & Sons, Hoboken, New Jersey, 2003.

[10] Lynch, S, *Dynamical Systems with Applications using Mathematica*, Birkhäuser, Boston, 2007.

[11] Guckenheimer, J, Holmes, P, *Nonlinear Oscillations, Dynamical Systems, and Bifurcations of Vector Fields*, Second Edition, Springer, 1983.

SEISMIC DESIGN PRINCIPLES OF CABLE-STAYED BRIDGES OF WHOLE FLOATING SYSTEM WITH ELASTIC CABLE CONNECTION

Zhenghua Wei[1], Jian Zhong[2], Wei Hu[3], Wancheng Yuan[4]

[1] State Key Laboratory of Disaster Reduction in Civil Engineering, Tongji University, Shanghai 200092, China
e-mail: wzhyicheng@gmail.com, china01zhong@126.com, daisay@126.com, yuan@tongji.edu.cn

ABSTRACT: Cable-stayed bridges of whole floating system can survive excessive displacements of girder and excessive bending moment in the tower. So elastic cable device is introduced and its seismic isolation mechanism is analyzed through finite element analysis. It reveals that through reasonable parameter design, the seismic response of the bridge can be controlled well.

KEY WORDS: cable-stayed bridge of whole floating system; elastic cables; mechanic characteristics; seismic isolation mechanism.

1 INTRODUCTION

Cable-stayed bridges which are famous for their reasonable load-transferring path, relatively low cost, and beautiful appearance usually constitute an integral part of many national highway systems[1]. The worldwide application of cable-stayed bridges began in the 1970s, but rapid progress had been made since the 1990s in the design and construction technologies of cable-stayed bridges. A new era of long-span cable-stayed bridges was opened with the completion of Normandy Bridge in France and the Tatara Bridge in Japan[2]. The construction of Sutong Bridge in China shows that the maximum span of cable-stayed bridges can reach the level of 1,000 meters, which used to be only occupied by suspension bridges in the past[3]. In the recent years, design theories and construction methods are gradually improved and high-strength lightweight materials are widely applied in this field, which makes the cable-stayed bridges play a more and more important role in the bridge constructions [2].

Usually cable-stayed bridges experience either excessive displacement of the girder or excessive bending moments of the tower. So some seismic reduction devices are adopted to reduce seismic response of cable-stayed bridges. There had also been a large number of studies aimed at characterizing and studying the dynamic behavior of cable-stayed bridges adopting these devices under severe earthquakes, but more concerned are the development and application of these seismic reduction devices, although some studies tried to discuss the seismic isolation mechanism of these devices, there were still a lot of work need to undertake. So in this paper, the mechanism of seismic reduction for cable-stayed bridges using elastic cables devices between the tower and girder is illustrated in details, based on the dynamic analysis of a finite element model of a 440m length cable-stayed bridge.

2 THE MECHANISM OF ELASTIC CABLES

2.1 The seismic isolation principle of cable-stayed bridges

For super-long-span cable-stayed bridges, with the increase of girder length, the weight of the girder and the seismic inner force of the tower increase largely, which all will induce the risk of bridge structures' serious damage inevitably. The floating system is considered to be an effective solution to the problem. In this situation, energy concentration can be avoided through extending the natural period of cable-stayed bridges, consequently, the seismic force can be decreased significantly[2][4]. At the mean time, it is inevitable to generate the excessive girder displacement, which may exceed the displacement capacity of the expansion joints, causing the possibilities of immense damages such as the collision between the main girder and approach girders.

2.2 The elastic cable devices

In order to constrain the seismic displacement of girder to an acceptable value and minimize the bending moment at the bottom of tower effectively, some elastic connection devices are usually adopted to provide additional longitudinal stiffness[5-7]. There are many types of elastic connection devices used in the construction of former bridges, such as large rubber bearing, steel strand cables. In this paper, elastic cables will be adopted to analyze the seismic reduction effect of the elastic connection devices on the cable-stayed bridges.

3 BRIDGE DESCRIPTION

A three-dimensional cable-stayed bridge of single tower is adopted in this study. The bridge have a span arrangement of 55m+2×165m+55m＝440m and a height of 81m from the top of the concrete tower to the deck. The cross section of the main girder and the side girder is π shape and box shape respectively with a height of 3.955 m at the supporting locations, and 2.468 m at the middle span. Cables are arranged symmetrically to the tower which are parallel to each other and have a distance of 8m on the girder and 4.434m on the tower. The structural scheme of the cable-stayed bridge is shown in Figure 1.

The whole floating system is adopted in the case with no bearing located between the tower and the main girder while longitudinal sliding bearings set on the other piers.

In order to effectively constrain the displacement of the girder as well as reduce the bending moment at the bottom of the tower, elastic cables are adopted in the paper to set between the main girder and the tower.

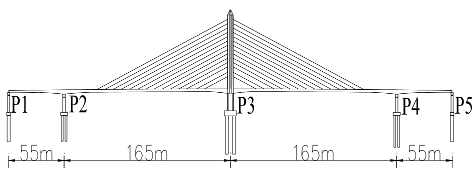

Figure 1. Structural schematic of bridge

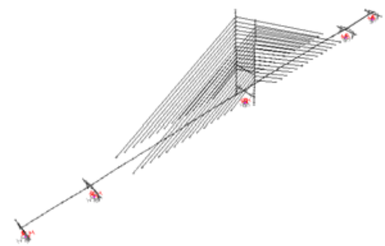

Figure 2. Finite element model of bridge

4 SEISMIC REDUCTION OF ELASTIC CABLES ANALYSIS

4.1 Analytical model of reference bridge

The 3-D finite element model of the reference bridge that is used as the basis for the comparison in this study is depicted in Fig.2, and the model is developed and analyzed using SAP2000 finite element program.

In the finite element model, the bridge girder, towers pier and cables are all developed using beam elements, and the geometric stiffness reduction due to the sag effect of cables caused by the weight is considered in the simulation of cables [8]. The elastic cables are developed using elastic bearing connection elements, and six-spring-element system is adopted to consider the effect of soil-structure interaction (SSI)[9].

The sensitivity of elastic cable stiffness is analyzed by response spectrum method, considering different site condition I and III specified in Chinese Guidelines for Seismic Design of Highway Bridges(2008)(Fig.3). The input response spectrum in horizontal and vertical directions are adopted, and the damping ratio is 5%[4].

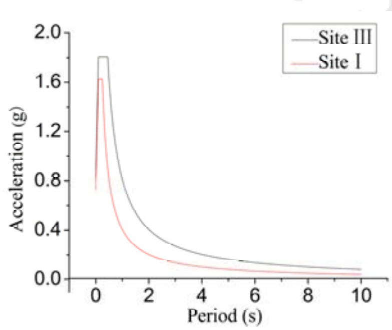

Figure 3. Response spectrums in different site conditions

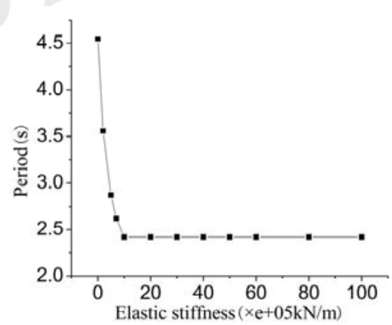

Figure 4. Elastic stiffness vs first period

4.2 The changes in the dynamic characteristics

Fig.4 shows the impact of elastic cable stiffness on the first natural period of the cable-stayed bridge, which can be divided into two different stages: rapid reduction stage and gentle changing stage. In the rapid reduction stage, with elastic cable stiffness ranging from 0 to 1.0×10^{6}kN/m, the first natural period decreases rapidly. However, in gentle changing stage, the first period grows gently. It means that after reasonable elastic stiffness design, natural period can be decreased, which can effectively reduce seismic responses of the structure.

The influence the elastic cables have on the mode participation coefficients of the cable-stayed bridge is showed in Table 1. It is can be seen that the two modes of whose participation coefficients are the two biggest with elastic cables (the stiffness is 3.0×10^{6}) lag significantly behind those without elastic cables. That is to say elastic cables can achieve the purpose of reducing the seismic response of structure.

Table 1. Dynamic characteristics varied with the change of elastic stiffness

Stiffness of Elastic Cable (kN/m)					
0			3.0×10^{6}		
mode	period	Participation coefficient	mode	period	Participation coefficient
1	4.55	0.55	2	2.26	0.06
3	2.33	0.18	4	1.61	0.72

4.3 Force transferring path analysis

The force transferring path can be changed by setting elastic cable at tower-girder connections. The impacts of elastic cable stiffness on the bending moment and shear force at tower-girder connection are shown in Fig.5 and Fig.6 respectively. For different site I and III, the trends are basically the same.

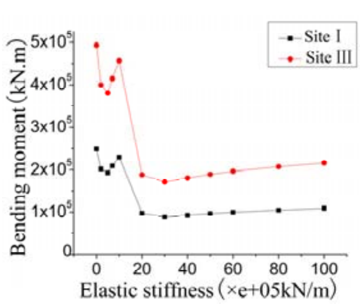

Figure 5. Elastic stiffness vs bending moments at the tower-girder connection

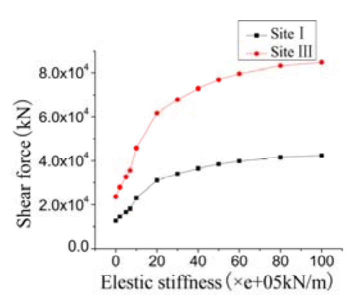

Figure 6. Elastic stiffness vs shear forces at the tower-girder connection

As shown in Fig.5, the bending moment at tower-girder connection does not vary monotonically, but inclined to fluctuate. For a cable-stayed bridge, the seismic force is mostly transmitted to the tower through the stay cables. While setting elastic cables, seismic force is partly transmitted through elastic cables, which decreases the moment arm considerably, and bending moment decreases correspondingly. Therefore, with the increase of elastic cable stiffness, the proportion of the seismic force transmitted through the elastic cables is gradually increasing, while that transmitted from stay cables to tower is gradually decreasing. So the bending moment at tower-girder connection is significantly decreased. But with the further increase of the elastic cable stiffness, the seismic force transferred through the elastic cables keeps on increasing, however, the limitation to the girder displacement by the elastic cables increases at the same time. Therefore, the bending moment at the tower-girder connection will increase. Different from bending moment, the shear force at tower-girder connection increases monotonically. It shows that only the bending moment at tower-girder connection can be properly decreased though setting the elastic cable devices.

4.4 Structure displacement analysis

One of the prominent problems of the long span cable-stayed bridges is that the displacement of the structure will exceed the deformation capacity of expansion joints. The impacts of elastic cable stiffness on the girder displacement and tower-girder relative displacement are shown in Fig.7 and Fig.8 respectively, and there is a similar trend for site I and III. It is clear from both Fig.7 and Fig.8 that with the increase of the elastic cable stiffness, the displacement decreases correspondingly. When the stiffness is less than 3.0×10^{6}kN/m, the displacement is sensitive to the elastic cables stiffness. After that, the displacement changes relatively gently.

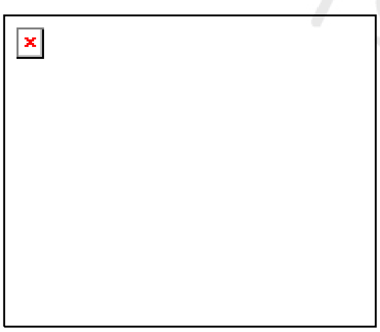

Figure 7. Elastic stiffness vs relative displacement

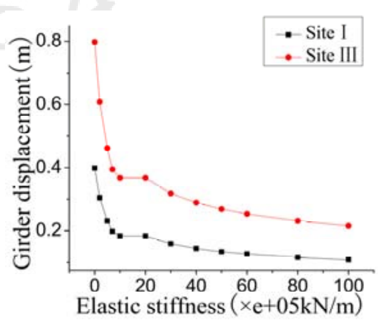

Figure 8. Elastic stiffness vs girder displacement

4.5 Analysis of seismic force at the bottom of tower

The impacts of elastic cable stiffness on the bending moment and shear force at the tower bottom are shown in Fig.9 and Fig.10 respectively, and there is a similar trend for site I and III. As shown in Fig.9, the bending moment at the tower bottom does not increase monotonically, even less than the case without setting elastic cables when the stiffness within the range of 2.0×10^5 kN/m～7.0×10^5kN/m. In Fig.10, the shear force at the tower bottom is monotonically increasing, and it changes very gently in the above stiffness range.

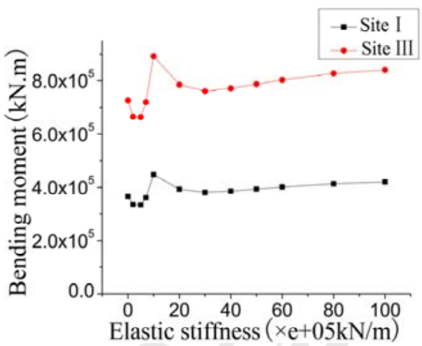

Figure 9. Elastic cable stiffness vs bending moments at the bottom of tower

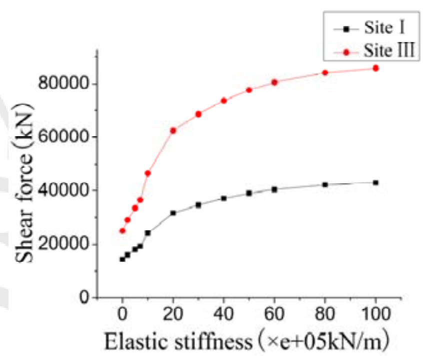

Figure 10. Elastic cable stiffness vs shear force at the bottom of tower

4.6 Seismic reduction analysis

It shows above that s with elastic cable stiffness ranging from 2.0×10^5kN/m to 7.0×10^5kN/m, the girder displacement and tower-girder relative displacement can be significantly decreased, while bending moment and shear force at the tower bottom increase gently, so in this paper, the elastic cable stiffness is set to 5.0×10^5kN/m the seismic reduction effects for site III of elastic cables are compared. The results are shown in Table 2.

Table 2. Comparison of seismic reduction effects of elastic cables devices

	Without elastic cables	With elastic cables
Tower-girder displacement(m)	0.747	0.407
Girder displacement(m)	0.798	0.462
Bending moment at tower bottom(kN/m)	726396.9	663956.2

As shown in Table 2, the displacement can be controlled well and the reduction of girder displacement is up to 42.1%. Meanwhile, the reduction of bending moment at the tower bottom is also up to 8.6%. The results show that by setting the optimum elastic cables stiffness, both structural displacement and bending moment can be controlled well.

5 CONCLUSION

Cable-stayed bridge of whole floating will develop great girder displacement and bending moment at the bottom of the tower in an earthquake. To solve this significant problem, elastic cables set at the location between the tower and girder is introduced in this paper, the mechanism of elastic cables for seismic reduction of cable-stayed bridges is illustrated in details. The results shows that by adopting reasonable parameters, the dynamic characters of structure including the first previous natural vibration periods, vibration mode participating ratio and so on can be changed, the seismic force-transferring-path can be also changed, thus the displacement of the structure as well as seismic force of the tower can be decreased significantly.

ACKNOWLEDGMENTS

This research is supported by Ministry of Science and Technology of China, Grant No. SLDRCE 09-B-08, and the National Science Foundation of China, Grants No.50778131, No.50978194 and No.90915011.

REFERENCES

[1] Chenglong Jia, Yumei Shen, "Seismic Analysis of Single-tower Double-sided Cable-stayed Bridge", Transport Standardization, Vol. 218, No. 1, pp. 166-169, 2010.

[2] Dong Yan, Wancheng Yuan, "Conceptual Seismic Design for Long-span Cable-stayed Bridges", Journal of Tongji University, Vol. 32, No. 10, pp. 1344-1348, 2004.

[3] Aijun Ye, Shide Hu, Lichu Fan, "Seismic Displacement Control For Super-long-span Cable-stayed Bridge", China Civil Engineering Journal, Vol. 37, No. 12, pp. 38-43, 2004.

[4] "Chinese Guidelines for Seismic Design of Highway Bridges", JTG/T B02-01-2008, pp. 16-18, 2008

[5] Reginald DesRoches, Gregory L.Fenves, "Design of Seismic Cable Hinge Restrainers for Bridges", Journal of Structural Engineering, Vol. 126, No. 4, pp. 500-509, 2004

[6] M.Saiidi, M.Randall, E.Maragakis, "Seismic Restrainer Design Methods for Simply Supported Bridges", Journal of Bridge Engineering. Vol. 6, No. 5, pp. 307-315, 2001

[7] Panos Trochalakis, Marc O.Eberhard, John F.Stanton "Design of Seismic Restrainers for Iin-span Hinges", Journal of Structural Engineering, Vol. 123, No. 4, pp. 469-478, 1997

[8] Dong Yan, Chunxiang Qi, Qinghai Feng, *SAP2000 structural engineering analysis and examples explanation*. China Architecture & Building Press, Beijing, China, 2009.

[9] Experimental and Theoretical Studies on Seismic Performance of Elevated Pile Cap Bridge, Ph. D. thesis, Department of Bridge Engineering, Tongji University, Shanghai, China, 2008

ISOLATION CAPACITY OF CONTINUOUS GRIDER BRIDGES USING CSFAB UNDER NEAR FAULT GROUND MOTIONS

Xinzhi Dang[1] ,W. Yuan[2]

[1,2] State Key Laboratory of Disaster Reduction in Civil Engineering, Tongji University, Shanghai, China
e-mail: leodangxz@163.com, yuan@tongji.edu.cn

ABSTRACT: In this paper, a new seismic bearing, CSFAB, was introduced. A model of continuous girder bridge with CSFAB was established and the seismic response of the bridges subjected to near fault ground motions were analyzed. The results showed that the effectiveness of the CSFAB in controlling the girder displacement and reducing the base shear are obvious.

KEY WORDS: Cable-sliding friction aseismic bearing; Isolation capacity; Continuous girder bridge; Near fault ground motions.

1 INTRODUCTION

The concept of seismic isolation has been considered an attractive strategy over the past decades to mitigate the damaging effects of earthquakes on civil structures such as buildings, bridges and nuclear power plants. One of the goals of the seismic isolation is to shift the fundamental frequency of a structure away from the dominant frequencies of earthquake ground motion and fundamental frequency of the fixed base superstructure. The other purpose of an isolation system is to provide an additional means of energy dissipation, thereby reducing the transmitted acceleration into the superstructure. In general, a seismic isolation system should have (i) high lateral flexibility in order to lengthen the period of the structure to reduce lateral earthquake forces, (ii) adequate energy dissipation capacity and a good re-centering mechanism to avoid excessive bearing deformations and instability, (iii) a means of providing rigidity under service load levels and (iv) high vertical load carrying capacity [1]. A variety of isolation devices including elastomeric bearings (with and without lead core), frictional/sliding bearings and roller bearings have been developed and used practically for aseismic design of buildings during last 20 years in many new buildings in countries like USA, Japan, UK, Italy, New Zealand etc [2]. Frictional/sliding isolation systems are one of the most popular and effective techniques for seismic isolation . The sliding systems perform very well under a variety of severe earthquake loading and are very effective in reducing the large levels of the superstructure's acceleration. These isolators are characterised by insensitivity to the frequency content of earthquake excitation. This is due to tendency of sliding system to reduce and spread the earthquake energy over a wide range of frequencies. The simplest sliding isolation system is the pure friction (P-F) system [3]. The P-F type base isolator is essentially based on the mechanism of sliding friction. The horizontal frictional force offers resistance to motion and dissipates energy. However, P-F systems lack re-centering ability result in the large sliding and residual displacement. Friction pendulum system (FPS) [4] overcomes this disadvantage by combine the concept of sliding systems with the action of the pendulum to provide restoring force. There are some other isolation systems such as EDF base isolator [5], S-RF base isolator [6], SMA isolation systems [7] etc.

Although seismic isolation has become one of the most popular solutions for seismic protection of bridge structures, the performance of the isolated bridges against near-field earthquakes has been questioned by several researchers in recent years [8-9]. As the name implies, near fault fault ground motion is derived from the distance to the rupturing fault line. Caltrans [10] defines that a structure of interest should be within 10 miles (approximately 15 km) of a fault in order to be classified as near fault. Ground motions outside this range are classified as far-field motions. According to Somerville, near fault ground motions differ from far-field ground motions in that they often contain a long period high velocity pulse in the fault-normal direction and permanent ground displacement [11]. These pulses are obviously going to have large impact on the isolation system with a period in this range and can lead to a large isolator displacement. In particular, the isolation devices experience very large displacements which may cause critical problems such as instability in the isolator, pounding as well as unseating of the grider. In order to reduce large displacements in a sliding isolation system, researchers have proposed the supplemental device. In such a study, Yuan and Cao [12] proposed a new seismic bearing named as cable-sliding friction aseismic bearing (CSFAB). The Teflon plate was used as a sliding friction device and the cable was used for limiting the displacement as well as providing a restoration force. Wei etal. [13] evaluated the effectiveness of the CSFAB in controlling the girder displacement and limiting the shear force and bending moment demands on the bridge piers.

The focus of this study is to investigate the dynamic behavior of continuous girder bridges isolated by an optimal CSFAB system to the non-isolated ones subjected to near-fault ground motion excitations. In order to assess the benefits of the CSFAB system, the performance of a bridge isolated by the LRB isolation system are also considered.

2 SYNOPSIS OF CSFAB

CSFAB is the combination of ordinary sliding bearing and restrainer cables, and the types of cable materials can be high strength steel tendon or carbon fiber. The configuration of a fixed bearing is shown in *Fig.1* .

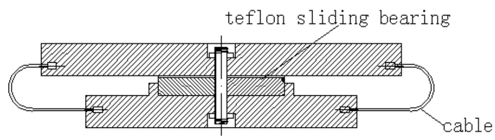

Figure 1. Configuration of fixed CSFAB

While setting on the fixed pier of a continuous bridge, CSFAB ensures the bearing keep fixed by the effect of shear bolt in normal conditions of ambient vibrations and small magnitude earthquakes. For large earthquake, the shear bolt is sheared off as the horizontal loads exceed a certain value. As a result, the bearing is changed into a sliding one, which alters the characteristics of load transfer mechanism of the system and distributes the horizontal loads to all piers.

Fig.2 shows the typical force-deformation curves of the sub-components of the CSFAB system, i.e. supplemental cable device and steel-Teflon sliding bearing and the combined hysteresis. The steel-Teflon sliding bearing offers resistance to motion and dissipates energy and the cables provide a large longitudinal stiffness to limit the excessive relative displacement between the superstructure and the substructure. Here, the cable device has a simple design, which avoids extra fabrication costs. It simply consists of two high strength restrainer cables on each side.

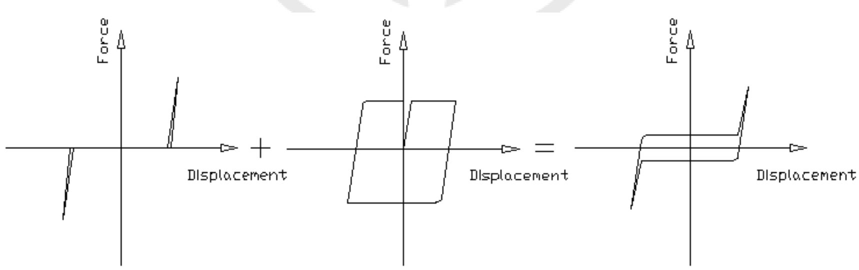

Figure 2. Force–deformation curves of the CSFAB and its sub-components

Although to some degree considered as an improved version of sliding isolation devices, this new aseismic bearing system is characterized by its insensitivity to the frequency content of earthquake excitations. It can be used in various types of bridge systems. Compared to other isolation bearings, this bearing system has the advantages of simplicity in principle, wide application, stable performance and low cost.

3 STRUCTURAL MODEL AND SEISMIC EXCITATIONS

3.1 Numerical model of continuous girder bridge

Fig.3 shows the reference structure of the present study. It is a perfectly symmetric bridge with single-column piers having the same height and cross section and sustaining a horizontal continuous girder. The bridge has a total length of 165m, and each pier is 20m tall. The total dead load W which includes the superstructure is 78.9 MN. The natural period for the non-isolated bridge in the longitudinal direction is 0.78s.

To demonstrate the effect of isolation bearings, two types of bridge system have been adopted here for analysis. One of them is the isolated bridge and the other is the non-isolated bridge. The bearing system of the non-isolated bridge in longitudinal direction that there are a fixed bearing on top of the left-of-center pier and sliding bearings at the other piers. For the isolated bridge, the bearing system in longitudinal direction is cable-sliding friction aseismic bearings on top of the fixed piers.

The bridges are assumed to stand on rigid foundation, the dynamic soil-structure interaction is neglected and only the longitudinal motion is considered, the transverse and vertical components are ignored. The concrete box girder and the concrete piers is assumed to behave linear-elastically and non-linear occur only in cable-sliding friction aseismic bearing.

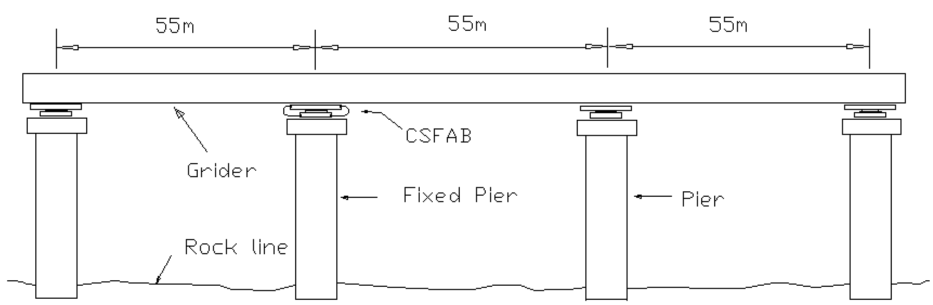

Figure 3. Model of an isolated bridge with CSFAB

3.2 Seismic ground motions used in this study

In this study, a total of six historical earthquakes presenting near fault characteristics are selected as as input ground motions. The characteristics of the ground motions such as recording station, magnitude, PGA, PGV, PGD, and the closest distance to the fault plane are depicted in Table 1. These near fault seismic records all possess significantly long-period acceleration or velocity pulse(*Fig.4*), and it is quite distinct from other without long-period pulse ground motions. The ground motion records are obtained from the PEER Strong Motion Database.

Table 1. Description of the near fault ground motions used in the analyses

Serial number	Earthquake	Recording station	Magnitude (Mw)	PGA (g)	PGV (cm/s)	PGD (cm)	Distance to the fault(km)
1	1999 Duzce,Turkey	Duzce	7.1	0.348	60.0	42.09	8.2
2	1994 Northrige	Newhall Fire	6.7	0.590	97.2	38.05	7.1
3	1994 Northrige	Rinaldi	6.7	0.472	73.0	19.76	7.1
4	1992 Cape mendocino	Petrolia	7.1	0.662	89.7	29.55	9.5
5	1989 Loma Prieta	LGPC	6.9	0.563	51.0	11.5	6.1
6	1979 Imperial Valley	EC Array #7	6.5	0.463	109.3	44.74	0.6

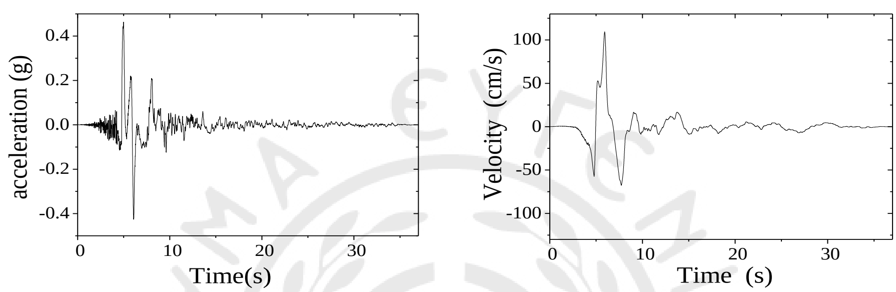

Figure 4. Near fault ground motion recorded at station EC Array #7 in Imperial Valley earthquake (a) Acceleration time histories, and (b) velocity time histories

4 NUMERICAL STUDIES

4.1 Earthquake response of the CSFAB isolated bridge subjected to near-fault ground motions

In order to assess the effectiveness of the CSFAB system, the response of the bridge isolated by the CSFAB system is compared with the response of the non-isolated bridge. The response of the bridge is analyzed in the longitudinal direction independently; the dynamic responses in the transverse and vertical directions are ignored. The peak ground acceleration of these near-fault records are scaled to the design level (PGA=0.4g), and a damping ratio of 5% are adopted. The values of the CSFAB parameters considered are cable stiffness k_c=1.0×10^{6}kN/m, Critical displacement u_0= 20cm and sliding friction coefficient μ=0.02.

The time histories of the base shear of the fixed pier and grider displacements under the 1999 Turkey Duzce earthquake motion is shown in *Fig.5*. It can be seen that there is a significant reduction in the pier base shear, implying that the CSFAB is effective for the aseismic design of bridges. The peak grider displacement in the longitudinal direction is 0.23m for isolated bridge and o.12m for non-isolated bridge. It can be conclued that the isolated bridge increase the peak grider dispalcement in a acceptable range.

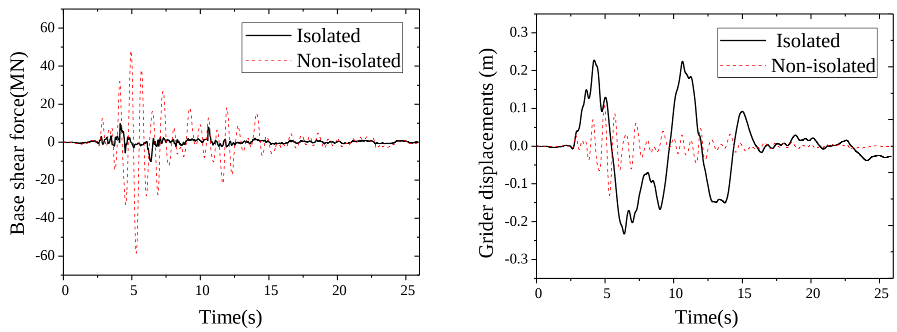

Figure 5. Time histories of the pier base shear and grider displacements in the longitudinal direction subjected to 1999 Turkey Duzce earthquake motion

Table 2. Peak Response Quantities for Isolated and Non-isolated Conditions

Earthquake number	Non-isolated bridge				Isolated bridge				effect
	①*F*(kN)	*M*(kN.m)	*x*(m)	*d*(m)	②*F*(kN)	*M*(kN.m)	*x*(m)	*d*(m)	(①-②)/①
1	58482	708841	0.120	0.120	10170	124382	0.231	0.021	0.826
2	64898	784172	0.132	0.132	12776	139218	0.235	0.023	0.803
3	43899	518378	0.085	0.085	10516	125349	0.231	0.021	0.760
4	44776	547174	0.093	0.093	9381	107192	0.225	0.017	0.790
5	66820	804679	0.134	0.134	21948	259375	0.261	0.042	0.672
6	58662	709197	0.119	0.119	22829	274145	0.267	0.046	0.611

In addition, the peak values of various response quantities under different earthquake motions for both non-isolated and isolated conditions are presented in Table 2. The response quantities of interest for the bridge system under consideration are the base shear in the fixed piers (*F*), the bending moment in the fixed piers (*M*), the displacement at the center of the bridge grider (*x*), and the displacement at the tom of the fixed grider (*d*). From this table, it is observed that there is a significant reduction in the peak base shear and base bending moment for all these near-fault ground motions, confirming the effectiveness of the CSFAB for near-fault ground montions. Further, it also shows the longitudinal isolation effect (the ratio of decreasing base shear at the bottom of isolated piers to that of non-isolated ones), the maximum reduction of base shear at the bottom of the fixed pier is 82.6%, and the minimum reduction of shear force at the bottom of fixed pier is 61.1%. It also can be observed that the maximum longitudinal displacements of the bridge grider is limited about 25cm induced by each near fault ground motions. This is an important feature of CSFAB which can control the displacement of girder to an controllable value.

4.2 A compared study with a LRB isolated bridge

In order to assess the benefits of the CSFAB system, the performance of the bridge isolated by a CSFAB system is compared with the response of the same bridge isolated by the lead-rubber bearing (LRB) isolation system which was most commonly used base isolation system. LRB bearings were settled on each pier. For the LRB isolated bridge, the designed yield force for the LRB bearings on each pier is about 2.5% of the weight of the girder, the post-yielding stiffness adopted herein is 15.4% of the initial stiffness. The specifications of LRB are shown in Table 3. The force-deformation behavior of the LRB is considered as bilinear.

Table 3. Specifications of LRB used in the isolated continuous bridge

specification	bearing capacity	yield force	yield stiffness	post yield stiffness ratio	equivalent stiffness	permit deformation
J4Q1520×1520	21000kN	1234kN	45500kN/m	0.154	11700kN/m	15cm

Table 4. Maximum horizontal displacement of LRB

Earthquake number	1	2	3	4	5	6
displacement	19.6cm	19.5cm	21.5cm	19.3cm	23cm	34.1cm

Table 4 shows the maximum horizontal displacement of the LRB are all exceed 15cm induced by these near fault ground motions. It can be concluded that the pulse effect of near fault seismic motion on the displacement of the bridge isolated by LRB was so extraordinary prominent, excessive displacement will directly result in the failure of LRB which the maximum allowable shear deformation is 15.0cm, causing possible failure of superstructure. It is obvious that the LRB is not suitable for the isolated bridge subjected to these near fault ground motions.

5 CONCLUSIONS

This study explores the non-linear dynamic response characteristics of bridges isolated by CSFAB subjected to near fault ground motions. Six historical earthquakes presenting near fault characteristics are utilized as input to analyze the dynamic behavior of the bridges. In order to serve as a benchmark for evaluating effectiveness of the CSFAB system, the responses of the non-isolated bridge are also provided. It is found that the CSFAB system can effectively mitigate the response of continuous girder bridge against near fault earthquakes. Also, it is observed that the bridge isolated by the CSFAB system can control the displacement of girder to an controllable value. Additionally, the earthquake response of the bridge isolated by the CSFAB is compared with that by the lead-rubber bearing (LRB). It is found that the LRB system was not available no longer since it excessive shear deformation has overrun its utmost. Noting that the high cost of the LRB is mostly cited as one of the main barriers that precludes the use of LRB in a full-scale seismic application, and considering the earthquake response of the CSFAB system, it can be concluded that the CSFAB system which combines restrainer cables with sliding bearings has more favorable properties than the LRB isolation system against some near fault earthquakes.

ACKNOWLEDGMENTS

This research is supported by the Ministry of Science and Technology of China under Grant No. SLDRCE09-B-08, and by the National Natural Science Foundation of China under Grants No.50978194 and No.90915011. Their supports are gratefully acknowledged.

REFERENCES

[1] Osman E. Ozbulut, Stefan Hurlebaus, "Optimal design of superelastic-friction base isolators for seismic protection of highway bridges against near-field earthquakes", Earthquake Engineering and Structural Dynamics, Vol. 40, No. 3, pp. 273-291, 2011.

[2] M.C. Kunde, R.S. Jangid, "Seismic behavior of isolated bridges: A-state-of-the-art review", Electronic Journal of Structural Engineering, No. 3, pp. 140-170, 2003.

[3] Westermo, B, Udwadia, F, "Periodic response of a sliding oscillator system to harmonic excitation", Earthquake Engineering and Structural Dynamics, Vol. 11, No. 1, pp. 135-146, 1983.

[4] Zayas, V.A., Low, S.S. and Mahin, S.A., "A simple pendulum technique for achieving seismic isolation", Earthquake Spectra, Vol. 6, No. 2, pp. 317-334, 1990.

[5] Gueraud, R., N.-Leroux, J.P., Livolant, M. and Michalopoulos, A.P., "Seismic isolation using sliding-elastomer bearing pads", Nuclear Engineering and Design, Vol. 84, No. 3, pp. 363-377, 1985.

[6] Su, L., Ahmadi, G. and Tadjbakhsh, I.G., "Performance of sliding resilient friction base isolation system", Journal of Structural Engineering, Vol. 117, No. 1, pp. 165-181, 1991.

[7] Cardone D, Dolce M, Ponzo FC., "The behaviour of SMA isolation systems based on a full-scale release test",. Journal of Earthquake Engineering, Vol. 10, No. 6, pp. 815–842, 2006.

[8] Shen J, Tsai M H, Chang K C and Lee G C, "Performance of a seismically isolated bridge under near-fault earthquake ground motions", Journal of Structural Engineering, Vol. 130, No. 6, pp. 861-868, 2004.

[9] Liao W I, Loh C H and Lee B H, "Comparison of dynamic response of isolated and non-isolated continuous girder bridges subjected to near-fault ground motions", Engineering Structural, Vol. 26, No. 14, pp. 2173-2183, 2004.

[10] California Department of Transportation (CALTRANS), "Seismic Design Criteria," Sacramento, California, 2004.

[11] Somerville, P.G., "Characterizing Near Fault Ground Motion for the Design and Evaluation of Bridges", Third National Seismic Conference and Workshop on Bridges and Highways. Portland, Oregon. April 28 - May 1, 2002.

[12] Wancheng Yuan, Xinjian Cao, Zhaojun Rong, "Development and experimental study on cable-sliding friction aseismic bearing", Journal of Harbin Engineering University, Vol. 31, No. 12, pp. 1593-1600, 2010.

[13] Zhenghua Wei, Wancheng Yuan, Pak-chiu Cheung, Xinjian Cao, Zhaojun Rong. "Seismic Performance of Continuous Girder Bridges Using Cable-Sliding Friction Aseismic Bearing", The Twelfth East Asia-Pacific Conference on Structural Engineering and Construction (EASEC-12), China, Hong Kong SAR, 26-28 January, 2011

COST BENEFITS OF SEISMIC ISOLATION ON CONSTRUCTED BRIDGES

Dimitrios K. Kolios[1], George K. Pantazopoulos[2],
Panos O. Theodoropoulos[3] and Tilemachos G. Tsiknias[4]

[1,2,3,4] TTA S.A. Structural Engineers, Athens Greece
e-mail: dkolios@tta.gr, gpantazopoulos@tta.gr, ptheodoropoulos@tta.gr, ttsiknias@tta.gr

ABSTRACT: The paper focuses on overall cost comparisons between constructed bridges with Normal Elastomeric Bearings (NEB) and bridges with Lead Rubber Bearings (LRB). Based on real case studies, it is demonstrated that LRBs (that also provide additional damping to the structure), although more expensive than NEBs, contribute to significant savings in the overall construction cost.

KEY WORDS: Bridge; Cost; Isolation; LRB; Real case studies.

1 INTRODUCTION

It is common practice among designers in Greece (and also internationally) to use Normal Rubber Bearings (NEBs) for seismic design. This is due to the following main reasons: a) the design properties and criteria of NEB are well established and provided by the applicable code hence the specific design is straightforward and no testing is required for verification c) normal elastomeric bearings are cheaper than Lead Rubber Bearings (LRBs) of similar volume.

Bridge decks supported on either NEB's or LRB's are seismically isolated since both type of isolators contribute to the so called 'period shift' of the structure. The difference between them is that while NEBs do not offer any additional damping to the inherent damping of the structural system (5% for concrete bridges) , the LRBs due to their elastoplastic behavior increase the equivalent viscous damping to as much as 25%-30% of the critical.

The purpose of this paper is to show that in areas of high seismicity the use of LRBs even though more expensive than NEBs leads to significant reduction on the overall construction cost of the bridge.

The conclusions drawn in this paper are based on real case studies of two Motorway Bridges in the New Section of the Motorway Concession Project Korinthos-Patra-Pyrgos-Tsakona; namely the bridge of crossing Ladopotamos River (B269) and the Bridge crossing Alfeios Bridge (B900). The resulting overall construction costs of two alternative designs are presented and compared for each bridge. The 1st alternative is based on NEBs and the 2nd on

LRBs. Since the concrete bridge deck is practically not affected, the two alternative designs are compared in terms of cost of:
a) The normal elastomeric bearings versus the Lead Rubber Bearings.
b) The construction of the piers
c) The construction of the abutments
d) The foundation (pile caps and piles)

Additional costs that are related to the excavations, temporary (or permanent) retaining structures, construction phasing, etc. are not quantified, but are taken into account in each case to derive the benefits of one isolator type over the other.

2 CASE STUDIES

2.1 B269 r. Ladopotamos Bridge

B269 Bridge is a two-branch bridge with a total length of 130m. The superstructure consists of two simply supported box girders of a theoretical span of 63.5m (*Figure 1*).

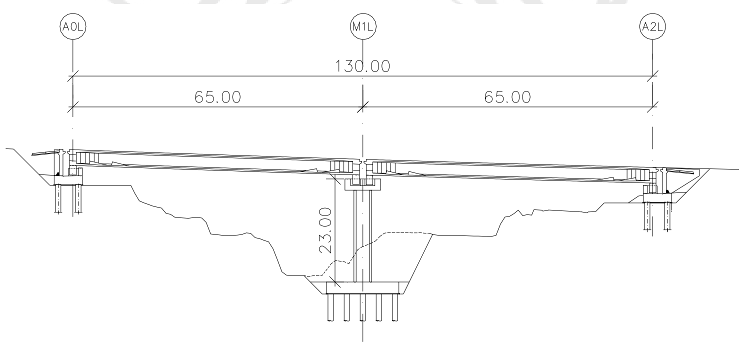

Figure 1. Longitudinal Section of Bridge B269

The cross section is 14.75m wide and its height is 3.5m, constant along the length of the bridge. The width of the flanges and the web, however, is (linearly) increased towards the supports. Diaphragms are designed at the support axes. The pier has a rectangular box cross section of outer dimensions of 4x7m. Its height is 20.5m and a 2.5m high pier table is constructed on top of it. The bridge designed for a peak ground acceleration a_g of 0.36g (0.24x1.5) due to the proximity to active faults.

2.1.1 Bridge Design with Lead Rubber Bearings

In the original design, the superstructure is supported on Lead Rubber Bearings (two at each support). The characteristics of the LRBs are:

- Diameter of Bearing: 1100mm

- Lead Core Diameter: 200mm
- Total Thickness of Rubber: 264mm (24 layers of 11mm each)
- Rubber Shear Modulus: 0.7MPa

The pier is supported on a grid of 4x5 piles of Ø120 diameter through a 2.5m thick pile cap (rectangular plan view 12.6x16.2m). The length of the piles is 20.0m. All piles have minimum axial distance of 3D=3.60m. The abutments are supported on two rows of five piles of Ø120 diameter and 28.0m length.

The properties of the bridge relating to the seismic response are summarized in *Table 1*. The joints that were used allowed for simultaneous displacements in both horizontal directions (dx=±260mm, dy=±65mm and dx=±115mm, dy=±215).

Table 1. Bridge Properties with LRBs

	T_{eff} (s)	ξ_{eff} (%)	η_{eff}	Sa (m/s^2)	Sd (mm)
LDPV	2.51	22	0.60	1.29	207
UDPV	2.24	26	0.56	1.36	173

2.1.2 Bridge Design with Normal Elastomeric Bearings

In the new design, normal rectangular elastomeric bearings of dimensions 1100x1100mm and height 132mm (12 layers of 11mm each) are used. The properties of the Bridge relating to the Seismic response are summarized in *Table 2*.

Table 2. Bridge Properties with NEBs

	T (s)	ξ (%)	η	Sa (m/s^2)	Sd (mm)
LDPV	2.14	5	1.00	2.55	295
UDPV	1.77	5	1.00	3.10	245

The seismic forces at the base of the pier were almost doubled compared to the original design as presented in *Table 3* below.

Table 3. Forces Comparison between two designs

	Longitudinal Direction		Transversal Direction	
	M (kNm)	V (kN)	M (kNm)	V (kN)
Elas. Bear.	$2.05*10^5$	8292	$2.52*10^5$	9492
LRBs	$1.14*10^5$	5530	$1.30*10^5$	6200

Consequently, the reinforcement demands at the base of the pier increased by 60%. The existing foundation is no longer adequate to bear the new loads. The bearing capacity of the existing piles is exceeded, so the new foundation consists of 20 piles of Ø150 diameter and 24m length. The pile cap plan view dimensions are 15.6x20.10m and its thickness is 3m. The foundation of the abutments increased in plan view from 6.3x15.45m to 6.6x20.1m and the pile diameter to Ø150.

2.1.3 Comparison

In this paragraph the conclusions that are drawn from both designs and presented in §2.1.1 and §2.1.2 are summarized and tabulated in *Table 4* and *Table 5*. The cost savings for this bridge is approximately 15% of the overall construction cost. In the case of Ladopotamos Bridge the design with LRBs had additional benefits:

a) Due to the steep terrain the smaller foundation resulted in much smaller excavations and even bigger temporary retaining works were avoided.

Table 4. B269 Ladopotamos river Bridge with LRBs

	Quantity	Total Length (m)	Dimensions (BxL, D)	Concrete (m^3)	Steel Rein/nt (Kg)	Cost (€)
Pier Piles	20x2=40	20x40=800	Ø 120	905	112140	320000
Pier Pile Cap	2	-	12.60x14.20	1020	91860	357000
Pier	2	20.50	7x4-6x3	410	118900	160000
Abutment Piles	2x2x210=40	1120	Ø 120	1270	291410	448000
Ab/nt Pile Cap	2x2=4	-	15.45x6.30	390	35100	136500
Bearings	2x8=16	-	Ø 1100x264	-	-	176000
					TOTAL:	1597500

Table 5. B269 Ladopotamos river Bridge with NEBs

	Quantity	Total Length (m)	Dimensions (BxL, D)	Concrete (m^3)	Steel Rein/nt (Kg)	Cost (€)
Pier Piles	20x2=40	24x40=960	Ø 150	1700	210250	576000
Pier Pile Cap	2	-	15.60x20.10	1885	169320	658500
Pier	2	20.50	7x4-6x3	410	131200	168000
Abutment Piles	2x2x10=40	1120	Ø 150	1980	554400	672000
Ab/nt Pile Cap	2x2=4	-	6.60x20.10	530	47760	185500
Bearings	2x8=16	-	1100x1100	-	-	144000
					TOTAL:	2404000

b) The enlarged pile cap of the abutment that resulted from the new design would not be feasible to be constructed due to the proximity to the abutment foundation of the other branch.

2.2 B900 r. Alfeios Bridge

River Alfeios Bridge is the longest bridge of the Korinthos – Patra – Tsakwna Motorway with a total length of 402.10m. The first and last span of the bridge are 38.75m long and the other eight spans are typical with a length of 40m.

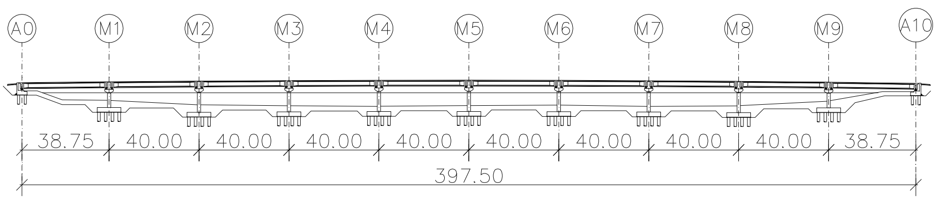

Figure 2. Longitudinal Section of Alfeios river Bridge

The deck at every span is formed by eight prestressed – precast concrete beams and a concrete deck slab cast in situ over the precast beams top flanges. The deck is 20m wide and carries both motorway branches. The structure is supported on the piers through lead rubber bearings. The deck slab has structural joints only above the abutments and piers M3 and M7. The piers have solid rectangular cross section with curved ends of total external dimensions of 16.00m x 1.50m and height 6.50m for pier M1 and M9 and 9.00m for the rest.

Each pier is supported on a grid of 4x6 piles of Ø100 diameter through a 2.00m thick pile cap (rectangular plan view 10.60x19.10m). The length of the piles varies from 30 to 40m. All piles have minimum axial distance of 3D=3.00m. The abutments are supported on two rows of six piles of Ø100 diameter and 30.00m length.

The bridge is constructed right next to the existing Alfeios bridge on weak soil, with very small bearing capacity. The soil is classified as category 'C' as per Greek Seismic Code. Due to the hydraulic and environmental studies the bridge layout had to be the same with that of the existing bridge. The designed performed for peak ground acceleration of 0.31g (0.24*1.3).

2.2.1 Bridge Design with Lead Rubber Bearings

In the original bridge design, the superstructure is supported on Lead Rubber Bearings (eight at each support). The characteristics of the LRBs are:

- Diameter of Bearing: 550mm
- Lead Core Diameter: 120mm
- Total Thickness of Rubber: 165mm (15 layers of 11mm each)
- Rubber Shear Modulus: 0.7MPa

The properties of the bridge relating to the seismic response are summarized in

Table 6. The joints that were used allowed for simultaneous displacements in

both horizontal directions (dx=±190mm, dy=±50mm and dx=±90mm, dy=±150).

Table 6. Bridge Properties with LRBs

	T_{eff} (s)	ξ_{eff} (%)	η_{eff}	Sa (m/s^2)	Sd (mm)
LDPV	1.68	27	0.56	2.06	147.85
UDPV	1.53	29	0.54	2.18	129.65

2.2.2 Bridge Design with Normal Elastomeric Bearings

In the alternative design, normal rectangular elastomeric bearings of dimensions 650x650mm and height 187mm (17 layers of 11mm each) are used. The properties of the bridge relating to the Seismic response are summarized in *Table 7*.

Table 7. Bridge Properties with NEBs

	T (s)	ξ (%)	η	Sa (m/s^2)	Sd (mm)
LDPV	0.79	5	1.00	4.96	199.65
UDPV	0.95	5	1.00	5.97	164.36

The seismic forces at the base of the pier were doubled compared to the original design as presented in *Table 8* below.

Table 8. Forces Comparison between two designs

	Longitudinal Direction		Transversal Direction	
	M (kNm)	V (kN)	M (kNm)	V (kN)
Elas. Bear.	$1.22*10^5$	11100	$1.50*10^5$	10900
LRBs	$0.64*10^5$	5200	$0.67*10^5$	4460

Consequently, the reinforcement demand at the base of the pier became 1.60 times bigger. The existing foundation is no longer adequate to bear the new loads.

The bearing capacity of the existing piles is exceeded, so the new foundation consists of longer piles of Φ120 diameter. The dimensions of the pile cap plan view are 12.6x19.80 and its thickness is 2m.

2.2.3 Comparison

In this paragraph the conclusions that are drawn from both designs and presented in §2.2.1 and §2.2.2 are summarized and tabulated in tables

Table 9 and *Table 10*. The cost savings for this bridge is approximately 16.5%

of the overall construction cost.

Table 9. B900 Alfeios river Bridge with LRBs

	Quantity	Total Length (m)	Dimensions (BxL, D)	Concrete (m^3)	Steel Rein/nt (Kg)	Cost (€)
Pier Piles	24x9=216	7440	Ø 100	5845	752000	2752800
Pier Pile Cap	9	-	19.1x10.6x2	3645	363850	1275500
Pier	9	76	16x1.5	1790	319250	626500
Abutment Piles	12x2=24	720	Ø 100	815	72780	266500
Ab/nt Pile Cap	2	-	19.4x4.6x1.5	500	53170	171300
Bearings	160	-	Ø 550	-	-	416000
					TOTAL:	5508600

Table 10. B900 Alfeios river Bridge with NEBs

	Quantity	Total Length (m)	Dimensions (BxL, D)	Concrete (m^3)	Steel Rein/nt (Kg)	Cost (€)
Pier Piles	24x9=216	7704	Ø 120	8715	1021800	4083100
Pier Pile Cap	9	-	19.8x12.6x2	4490	545700	1571700
Pier	9	76	16x1.5	1790	354700	626500
Abutment Piles	24	840	Ø 120	950	111600	445200
Ab/nt Pile Cap	2	-	19.8x5.2x1.5	545	66470	189300
Bearings	160	-	650x650	-	-	336000
					TOTAL:	7251800

3 CONCLUSIONS

Bridge Decks on Lead Rubber Bearings LRBs as compared to Bride decks on Normal Elastomeric Bearings (NEBs) leads in cost savings in the overall bridge construction even though LRBs per se are more expensive than NEBs. The cost savings for areas with high seismic accelerations (PGA =0.31g) is in the order of 16% of the overall bridge cost.

The effectiveness of LRBs in reducing overall costs increases in the following cases:

a) High Seismicity. Ground accelerations of 0.24g or even of 0.316g (0.24x1.3) when it comes to bridges are frequent in Greece.
b) Soft soils where spectra present a wider range in which the acceleration is

constant at its maximum value. It should be noted however that on stiff soils with better characteristics (e.g. type A as per EAK), the cost savings is not that significant as in soft soils.

c) Valley bridges with piers on steep slopes, whereas the foundation footprint should be minimized as much as possible in order to reduce excessive and expensive excavations and retaining works.

ACKNOWLEDGMENTS

We would like to express our sincere thanks to Independent Engineer's Structures Manager Mr. Thanassis Kontizas for his constructive comments and advice throughout the structural design process of both bridges.

DISCLAIMER

All prices presented hereinafter are TTA's educated estimations based on market prices.

REFERENCES

[1] APION KLEOS C.J.V / ELEFSINA - KORINTHOS - PATRAS - PYRGOS - TSAKONA MOTORWAY / FINAL DESIGN OF BRIDGE B269 (r.LADOPOTAMOS) (G.U. 27, CH:71+115.00KM) / FIL-KP1-CON-B269-1TT-F-99269-A-.

[2] APION KLEOS C.J.V / ELEFSINA - KORINTHOS - PATRAS - PYRGOS - TSAKONA MOTORWAY / FINAL DESIGN OF BRIDGE B900 (r. ALFEIOY) (G.U. 43, CH:00+460.900KM) / FIL-KP3-CON-B900-3TT-F-99900-A-.

TOPIC 2

Old Bridges and Maintenance

Stone Bridges

SEISMIC RETROFIT OF 74M PRESTRESSED CONCRETE OVERPASS BRIDGE WITH V-TYPE ABUTMENTS

Nestoras Loukatos[1], Neonellis Tzanetos[1]and Ilias Kritikos[1]

[1] N.Loukatos & Associates SA, Greece
e-mail: info@stand.gr

ABSTRACT: The article presents the design of the seismic retrofit of a prestressed concrete bridge overpass with abutments of V shape. It is one of the almost 10 old similar bridges passing over the highway Corinthos-Patra that must be upgraded to meet the modern seismic design criteria.

KEY WORDS: BRIDGE SEISMIC ISOLATION; BRIDGE SEISMIC RETROFIT; BRIDGE STRENGTHENING.

1 INTRODUCTION

The aim of this project was to understand the behavior of the specific type of bridge, examine the existent capacities and find a solution for upgrading the bridges with low cost and negligible traffic disturbance instead of replacing them with new constructions. It had been used realistic assumptions by examining Aigio's overpass which was accompanied by the prototype as built drawings. Moreover, in situ tests, site inspection including excavations and laboratory testing have been made for the confirmation of the drawings information.

Photo 1. General view

2 AS BUILT PRESENTATION

The inclined columns of the abutments of the specific bridge are made of B300 (C20/25) with dimensions 1.20~2.00x0.80m (variable) for the internal columns and 1.20x0.80m (constant) for the external columns, creating 3 spans of 20, 34 and 20m. The bridge was designed at 1969 having a class of 30T according to DIN. The deck is a voided slab of 1,10m height with 6 cyclic gaps of 0.85m made of B450 (C30/37). The width of the bottom flange is 7.30m. The slab becomes solid at the area close to the inclined columns for the reinforcement's anchorage. A cross beam at the middle helps the better function of the deck. 24 prestressed tendons ($\sigma_{S/B}$ = 160/180kg/mm2) comprising 12 cables of ½' each (1130mm2) with an initial prestress force of 123T per tendon, crossing all the length and are anchored at the two deck edges.

The 4 columns of every abutment end up at a uniform spread footing 9.00x5.00m made of B300 (C20/25) with an inclination such that the self weight causes no horizontal reactions.

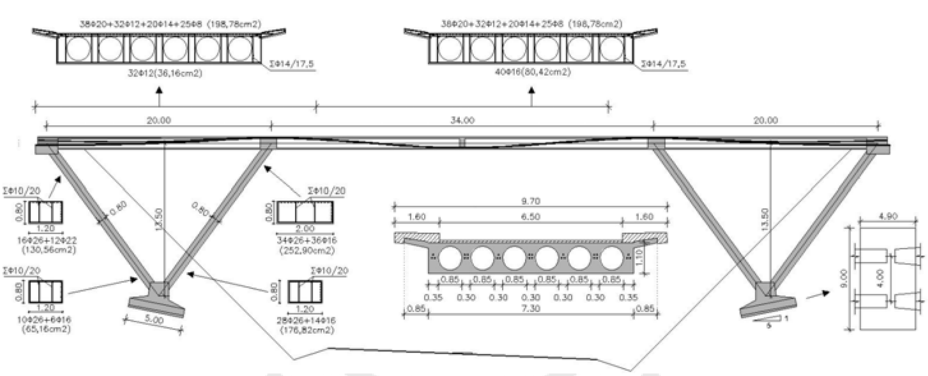

Figure 1. Basic geometric information

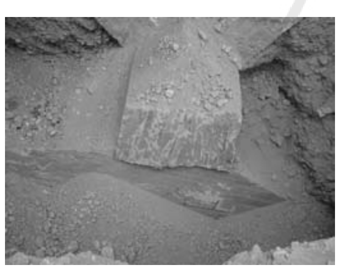

Photo 2. Spread footing

Photo 3. Joint of inclined columns

3 STATIC AND SEISMIC BEHAVIOUR

The total vertical load of the bridge is 17363kN caused by the dead load 13924 kN (80.1%), the rest dead load 2691kN (15.5%) and the quasi-permanent live load 20%*3738=748kN (4.3%). A modal and a response spectrum analysis with β_0=2,5, γ_I=1, θ=1, q=1, A(g)=0.36, T_1= 0.15s, T_2=0.60s and n=1 [1], showed the following:

- At the longitudinal direction, the deformation against horizonal loads depends on the bending of the middle span of the deck between the abutments. The system of the inclined columns with the end span rotates as a rigid body.
- The columns are mainly axially loaded and impose tension to the edge spans and compression to the middle span.
- The two footings is necessary not to be movable. Even a very small support's horizontal displacement creates huge bending moments to the middle part of the deck. The rotational stiffness of the supports doesn't play a significant role to the static model.
- At the vertical direction, the system that withstands the seismic forces is the frames composed of the columns and the deck. The columns act as restrained at their ends.

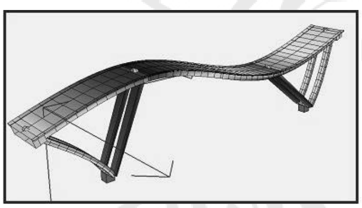

Figure 2. 1st mode (X), T = 1.04s

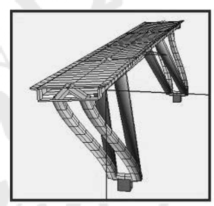

Figure 3. 2nd mode (Y), T = 0.98s

Table 1. Response Spectrum Analysis

Earthquake	Displacement	Shear Force
X	13.5cm	7444kN
Y	15.5cm	9974kN

The analysis of the structure has shown the available peak ground accelerations for which the critical sections fail. These accelerations are from 0.075g to 0.100g, about 21%~28% of the required PGA 0.36g.

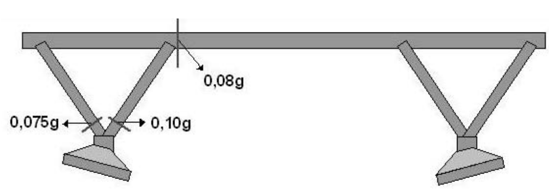

Figure 4. Available peak ground accelerations

4 SEISMIC RETROFIT

4.1 General

The seismic retrofit of the bridge could be achieved with strengthening, increase of ductility and seismic isolation [3].

The seismic isolation of the structure is not applicable on this type of structures without extended changes of the frame for certain reasons :

- No traditional cut of the columns for the embodiment of seismic devices can be done without restoring the static equilibrium of the system columns-deck and the strengthening of the foundation which is inappropriate for any other state except the current static state.
- The percentage of the required decrease of the seismic force due to energy dissipation cannot be achieved by keeping the same static system because of the low level of the available PGA.

Moreover the ductility of the deck which is the weak point of the longitudinal deformation cannot be improved. That means that the deck's contribution to the system that withstands the seismic forces must be limited or even stopped. On the contrary, the other direction can be improved by conventional strengthening, enlarging the inclined columns or placing additional shear walls including the existent columns.

In addition to the aforementioned facts, for the solution to be chosen we must take into account the following parameters :

- An acceptable static system must be formed.
- The available height between the subjacent road and the deck's bottom flange is enough to accommodate new structural elements under the bridge so that the traffic is not interrupted.
- It would be better to limit the works at the two edges for minimizing the traffic disturbance.
- A nice aesthetics result would be preferable.
- The connection between the old and new frame is a matter of high importance.
- The minimization of the cost and time is the criterion for deciding the most appropriate solution.

After the testing of many solutions we have concluded in two solutions that are presented bellow.

4.2 Solution with a new frame

The first solution comprises of a new steel arch formed as a triangular space truss beneath the deck. The two upper and the one lower chord are of CHS813*16 and CHS813*20 respectively. The maximum distance between the chords is 4.6m horizontally and 3m vertically. The bracings are of CHS273*10 and the struts are of CHS159*4.5. The existent columns are enlarged with new reinforced concrete jackets of 12cm thickness. For the anchorage of the new reinforcement, the top and bottom area between the inclined columns is fulfilled with reinforced concrete. Moreover, the footings are enlarged to new bigger spread footings 14x10.25m with variable height 1.5~4.5m or alternately they are changed to pilecups with new piles at their perimeter. The connection between the old and the new frame is accomplished with special shear keys surrounding the middle cross beam.

The total vertical load of the bridge is 20062kN caused by the concrete's dead load 15951 kN (79.5%) and the steel's dead load 673.4kN (3.4%), the rest dead load 2691kN (13.4%) and the quasi-permanent live load 20%*3738=748kN (3.7%).

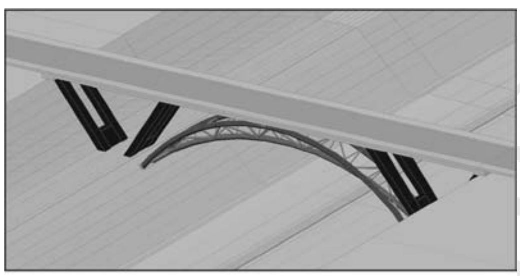

Figure 5. Photorealistic illustration of 1st solution

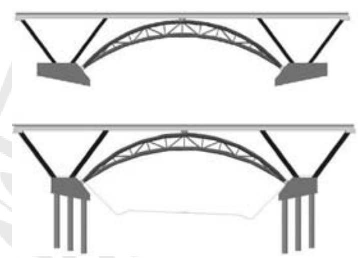

Figure 6. Views of 1st solution

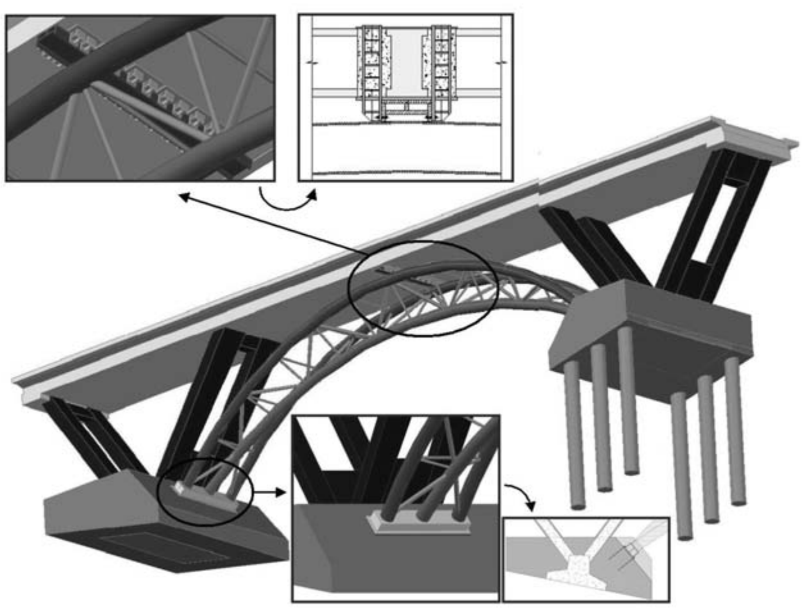

Figure 7. Available peak ground accelerations

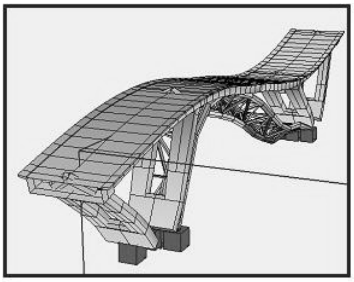

Figure 8. 2^{nd} mode (X), T = 0.33s

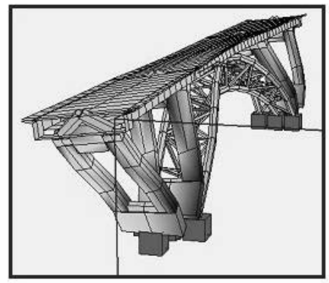

Figure 9. 1^{st} mode (Y), T = 0.43s

The response spectrum analysis was made according to the greek seismic code for β_0=2,5, γ_I=1, θ=1, q=1, A(g)=0.36, T_1= 0.15s, T_2=0.60s and n=1 [1]. The new structure is more stiff which implies bigger seismic forces. However in the longitudinal direction the new arch took almost the total seismic force. In the transverse direction the strengthened concrete frame could withstand satisfactory to the implied seismic loads. The checks included ULS checks, stresses check and crack design.

Table 2. Analysis results for the first solution

Earthquake X	Current state	1^{st} solution
Seismic force X	7444kN	12904kN
Seismic force X- old frame	7444kN	1589kN
Seismic force X- new arch	-	11315kN
Seismic force Y	9974kN	14793kN
Seismic force Y- old frame	9974kN	13640kN
Seismic force Y- new arch	-	1150kN
Check Results	a) Deck: FAIL b) Columns: FAIL c) Ground bearing resistance: FAIL d) Sliding resistance: FAIL e) Overall stability: FAIL	a) Deck: OK b) Columns with new concrete jackets 12cm with new reinforcement ρ =2.5% : OK c) Ground bearing resistance: OK d) Sliding resistance: OK e) Overall stability: OK

The construction of the arch has to be done parallel to the final position, temporary supported to the new footing on a surface with specific inclination so that the arch produces only a perpendicular reaction and does not open. Afterwards, the completed arch have to slide at its final position. Finally the base of the arch would be covered with concrete of second phase.

4.3 Solution with seismic isolation

For the seismic isolation of the bridge, the deck must be cut from the columns. For that reason firstly the static equilibrium of the system columns-deck must be restored with the construction of new horizontal prestressed beams with new tendons. Simultaneously new shear walls will be constructed at both directions that will embody the existent inclined columns. For the anchorage of the new concrete's reinforcement and for the safe transition of the bridge's actions to the ground, the foundation will be enlarged with new reinforced concrete. Moreover the footing will be lengthened for the foundation of the new shear walls having a thickness of 1m.

After the strengthening of the abutment, appropriate hydraulic jacks and chocks will be placed between the deck and the top of the strengthened abutments. The procedure continues with the cut of the joints of the inclined columns with the deck. New appropriate bearings will be installed after the preparation of the final upper and bottom surfaces.

In this solution, the deck does not bend during the seismic deformation and the previous deck's bending moments are not developing any more. Moreover the seismic isolation with the increase of the fundamental period of the structure means smaller required abutments [2].

Finally, the deck's is upgraded from class 30T to 60/30T with new external prestress tendons.

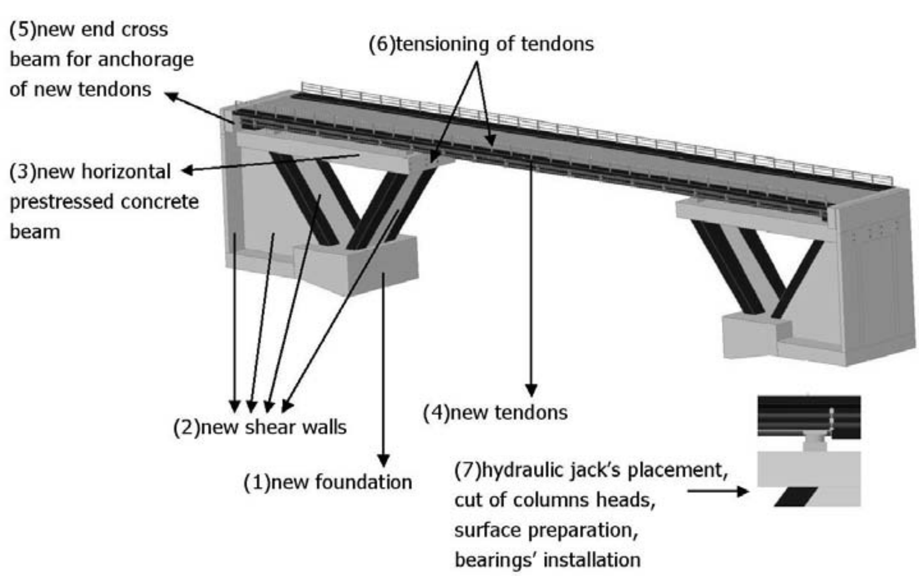

Figure 10. Seismic retrofit with seismic isolation

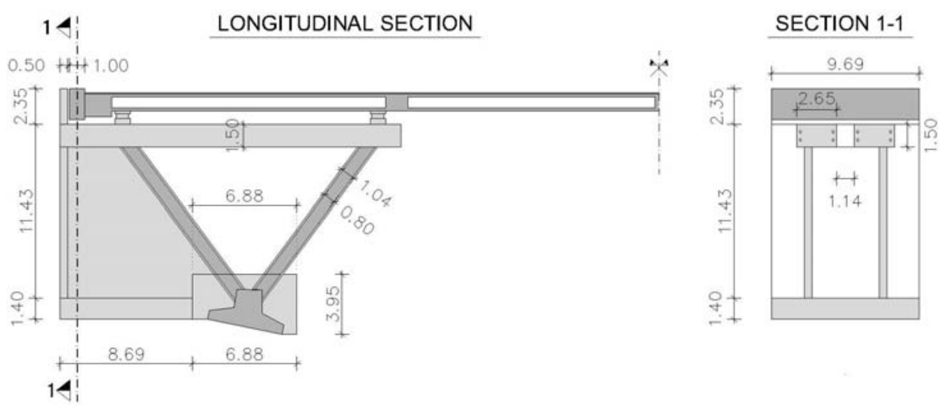

Figure 11. Seismic retrofit with seismic isolation

5 CONCLUSIONS

Seismic retrofit has been widely developed during the last years. However the behavior and the particularities of each individual structure cannot always make clear what is the appropriate solution to be chosen. In this project the strengthening of the structure with the addition of a steel arch and the enlargement of the existent concrete elements seems to be a simple and efficient seismic retrofit solution. Alternately the seismic isolation of the deck which is also an efficient solution requires a more complicated procedure due to the specific type of the bridge.

REFERENCES

[1] Greek code for the Seismic Resistant Structures EAK2003.

[2] Greek guidelines for the design of bridges with seismic isolation, Hellenic Ministry of Environment, Country Planning and Public Works , June 2007.

[3] M.J.N. Priestley, F. Seible, G.M. Calvi, *Seismic Design and Retrofit of Bridges*, First Edition, John Wiley & Sons, Inc., New York, 1996.

SEISMIC RETROFIT OF 144M ROAD PRESTRESSED CONCRETE BRIDGE

Nestoras Loukatos[1], Neonellis Tzanetos[1], Panagiotis Mergos[1] and Ilias Kritikos[1]

[1] N. Loukatos & Associates SA, Greece
e-mail: info@stand.gr

ABSTRACT: This paper presents a potential retrofit solution of a two branches road prestressed concrete bridge. According to this solution, the existing concrete deck is replaced by a new composite steel-concrete one. The solution is completed with the application of friction pendulum bearings, which reduce significantly seismic forces transferred to the bridge piers and abutments.

KEY WORDS: Bridge; Retrofit; Composite deck; Friction pendulum bearings

1 INTRODUCTION

In Greece as well as in other countries, a significant number of existing bridges has been constructed prior to modern bridge and seismic design provisions. Total replacement of these bridges is not always feasible due to insufficient funds and the problems imposing to the traffic volume served by these structures.

For these cases, retrofit of the existing bridges is required in order to enhance structural performance, especially in the case of a major seismic event.

Herein, the case of an existing 144m road prestressed concrete bridge is examined. Initially, the structure is assessed for vertical and seismic loading in its current condition. The assessment procedure reveals the necessity for structural upgrading in order for the bridge to meet modern design provisions.

On the other hand, structural upgrading of this bridge is subjected to several constraints. The bridge is fully operational and the length of detour resulting from bridge closure is considerably long. Hence, the time required for the retrofit solution should be minimal. Furthermore, the bridge crosses a significant river and the piers and abutments are almost completely covered by its debris. Consequently, strengthening of the understructure is not feasible.

In the following, a potential retrofit solution is proposed for the bridge under examination, which takes into consideration all of the aforementioned constraints and updates sufficiently structural performance to meet current design criteria.

2 ASSESSMENT OF EXISTING STRUCTURE

2.1 Existing bridge description

The bridge examined herein (Fig. 1, Photo 2) is named B289 and it is located at Selinountas river (G.U. 29, CH 85+674) of the Korinthos-Patra motorway in Greece. It was originally designed in 1969. It is composed by two independent branches. Each branch consists of three equal length spans of 48m. The class of the bridge is 60T. Bridge details were determined by both the original study and in situ and experimental measurements conducted by N. Loukatos and Associates, as assigned by AKTOR S.A..

The deck of each branch of the bridge is composed by five prestressed concrete T-beams with 2.50m height. On top of these beams, the width of the cast in place concrete slab is 0.18m and the width of the asphalt layer is 0.17m. In the transversal direction of the bridge and along each span, the prestressed concrete beams are connected by cast in place reinforced concrete crossbeams (Photo 3).

The piers of the bridge (Fig. 4) are of a wall section type, constructed by reinforced concrete and they are supported on spread footings with dimensions in plan 10.8mX7.0m. The height of the pier cross section is 8.9m. The width is 1.4m at the base of the piers and reduces to 1.0m in distance 2m above. Concrete quality is classified as B225 by both the original study and the experimental measurements. Longitudinal reinforcement consisted of 2Φ22/20 and 2Φ24/20 at the critical cross-sections A-A and B-B respectively. According to the original study, shear reinforcement is Φ10/30 in the transversal and 4Φ10/m^2 in the longitudinal direction of the bridge. Nevertheless, reinforcement exposures revealed that the actual horizontal reinforcement in the transversal direction is Φ10/70, which is importantly lesser than the prescribed one.

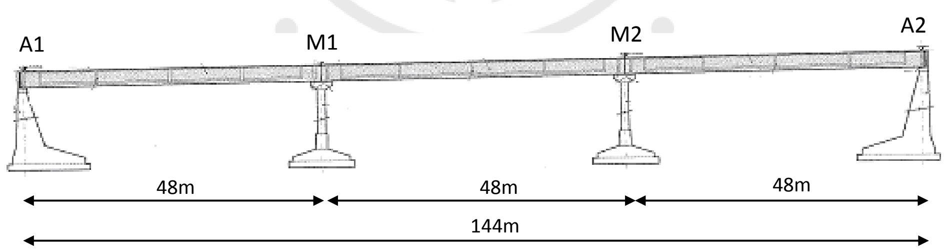

Figure 1. Longitudinal section of the existing bridge

The abutments (Fig. 5) are again of a wall section type, constructed by reinforced concrete and they rest on spread footings. The stem width increases linearly from 1.10m at the top to 3.50m at the bottom. Concrete quality in the original study is classified as B225. However, the experimental measurements revealed significant discrepancies between the material characteristics of the four different abutments. Abutment concrete class ranges from B160 to B300.

Vertical reinforcement at the critical cross section A-A is Φ24/20 and Φ12/30 on the soil and bridge side respectively. Horizontal reinforcement is Φ12/30.

Regarding reinforcement steel strength, a sample was subjected to the tensile strength test in the laboratory. The yield and ultimate steel strengths were measured 356MPa and 545MPa respectively.

Photo 1. Existing bridge view

Photo 2. Existing bridge deck

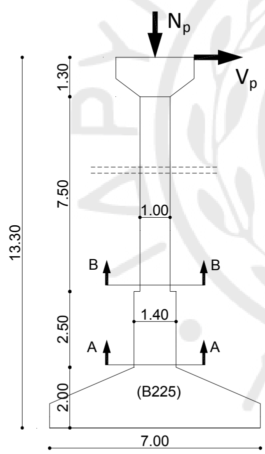

Figure 2. Bridge pier section

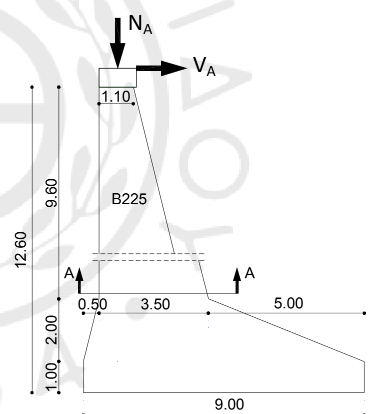

Figure 3. Bridge abutment section

2.2 Assessment of the existing bridge

As mentioned previously, the class of the existing bridge is 60T. Hence, upgrading of the existing deck is unavoidable in order to be compatible with the modern 60/30 bridge class.

The existing deck is assumed to work as three independent simply supported beams resting on the abutments and piers. Hence the reactions of the superstructure can be easily calculated. In addition, due to the symmetry of the structure, both bridge piers may be assumed to undertake the same vertical load N_P. The same is valid for the abutments carrying deck reactions N_A.

Based on the above, deck reactions for the ‘quasi permanent’ combination are calculated N_P=12133.0kN and N_A=6066.5kN for the piers and abutments respectively.

In the following, the adequacy of the existing understructure to sustain the design seismic action (10% probability of exceedance in 50 years) is examined. The design seismic action is determined according to [1] for design ground acceleration 0.36g, soil type C (T_B=0.20sec, T_C=0.60sec and T_D=2.50sec) and behavior factor q=1.0. The latter is chosen due to the non-ductile configuration of the existing piers and abutments.

Table 1 summarizes the demand/capacity ratios obtained by the safety checks for the design seismic action at the bridge piers. It is evident that the existing pier is not able to undertake this level of earthquake action.

Similarly, Table 2 presents the demand/capacity ratios obtained by the safety checks for the design seismic action at the bridge abutments. Again, the inadequacy of the existing abutments is clearly concluded.

Table 1. Demand/capacity ratios for the existing piers without retrofitting

Location/Check	Bending		Shear	
	Longitudinal direction	Transversal direction	Longitudinal direction	Transversal direction
Section A-A	8.46>1.00	1.57>1.00	1.96>1.00	2.14>1.00
Section B-B	8.80>1.00	1.14>1.00	2.43>1.00	2.57>1.00

Table 2. Demand/capacity ratios for the existing abutments without retrofitting

Location/Check	Bending	Shear
Section A-A	1.72>1.00	0.94<1.00

Taking all of the above into consideration, the following conclusion is drawn. Retrofit actions are necessary to enhance structural performance of both the superstructure and the understructure in order to meet current design criteria. To serve this goal, a potential retrofit solution is described in the following paragraphs.

3 RETROFIT OF EXISTING BRIDGE

3.1 Introduction

The main characteristic of the bridge under examination is the fact that retrofitting of the understructure is not feasible due to the existence of Selinountas river (Photo 2). Since capacity of the existing understructure cannot be upgraded, the only solution remaining is to reduce seismic forces transmitted by the deck to the understructure. Application of seismic isolation between bridge superstructure and its supporting substructure is the best strategy to achieve this target.

Retrofitting of the existing concrete superstructure to undertake the additional vertical loads is attainable due, for example, the use of external prestressed tendons. Nevertheless, additional concrete degradation caused by the environmental factors could raise some important issues regarding the integrity of the existing deck in the future years.

To avoid these problems, the replacement of the existing concrete deck with a new composite steel-concrete box girder one is proposed herein. The new deck, apart from the being able to carry the additional vehicle loads, holds a very important advantage. Its mass is significantly lesser than the existing deck reducing considerably the potential seismic forces transmitted to the supporting piers and abutments.

3.2 New composite steel-concrete box girder deck

The configuration of the new continuous composite steel-concrete box girder deck is shown in Figs. (6). The static height of the deck is set 3.2m as restrained by the height of the existing red line. The width of the concrete slab is 0.20m.

The deck is composed by four longitudinal steel HEB450 sections connected in the transversal direction by HEA360 steel sections placed every 3m. At the bottom, two longitudinal welded box girder steel sections with 500mm height are applied in the longitudinal direction.

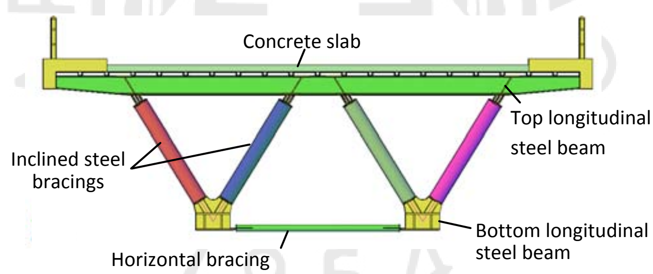

Figure 4. Composite steel-concrete box girder deck

To form diaphragms at the bottom and top level of the composite deck, horizontal bracings of steel CHS139.7X5.6 section are placed. In this way, instability of the steel girders in their weak direction is restrained. The webs of the composite box girder are formed by four inclined steel bracings of CHS323.9X6.3 section in the span and CHS323.9X11.0 close to the supports.

It is important to mention that due to the continuous function of the new deck, the locations close to the supports are highly stressed. To avoid over sizing of the entire deck which drives to serious increase of the dead load, it is more efficient that the static height of the deck is increased locally in the support regions. To achieve this, shearing of the existing piers for 3.3m underneath the composite steel deck is required. This also has the benefit of reducing the moments acting at the base of the piers in the case of a seismic event.

The continuous, composite deck was analyzed by applying the finite element model presented in Fig. (7), formed in the general finite element analysis and structural design program SOFISTIK [4] (Version 21.0). Dead and permanent loading as well as vehicle loading combinations described in [5] were taken into consideration. Design according to EC3 for the Ultimate Limit State (ULS) verifies the adequacy of the steel-concrete sections under the prescribed vertical loading combinations.

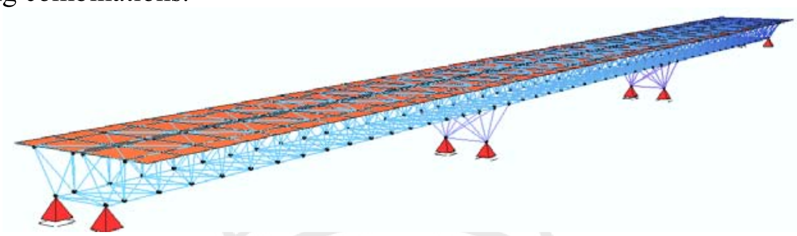

Figure 5. Finite element model of the new composite steel-concrete deck

A very significant advantage of the new composite deck is its reduced dead load which decreases importantly the seismic forces transmitted to the understructure. In particular, the reaction forces transmitted by the new deck to the piers for the ‘quasi permanent’ combination is N_P=6714kN (45% reduction) and to the abutments is N_A=2521kN (58% reduction). It is worth noting, that the reduction of the reaction forces acting on the piers is smaller than the respective one of the abutments. This is due to the continuous static function of the new deck.

3.3 Seismic isolation

Reduction of deck reactions leads to an analogous decrease of the seismic forces transmitted to the understructure. However, this is not enough for the bridge examined herein. This is evident by the demand over capacity ratios of Tables 1 and 2, where it can be seen that these ratios don’t become smaller than unity for the respective reduction of seismic forces. This is especially the case for the moment capacity of the existing piers in the longitudinal direction of the bridge. To overcome this problem, the application of seismic isolation is proposed herein between the superstructure and the substructure.

Seismic isolation is implemented via two spherical friction pendulum bearings with friction coefficient μ and radius R at each pier and abutment of the bridge (Fig. 8). The aim of this isolation system is to further decrease seismic forces resisted by the substructure through energy dissipation and lengthening of the fundamental period.

To analyze the behaviour of the seismic isolation proposal, an equivalent SDOF system is applied [4]. The main properties of this SDOF system are the effective period T_{eff}, the equivalent viscous damping ξ_{eff} and the spectral acceleration $S_e(g)$, which determines the level of shear forces passing to the substructure.

In order to design the seismic isolation solution, several constraints are taken into consideration. First, the seismic shear forces transmitted to the piers and abutments should be sufficiently small to preclude failures in shear and bending in these locations. For this reason, it is calculated that $S_e(g)$ should be lesser than 0.15. Furthermore, mostly for safety and reliability reasons, it is chosen that for all cases the following limitations should hold: $T_{eff} \leq 2.50s$ and $\xi_{eff} \leq 0.40$.

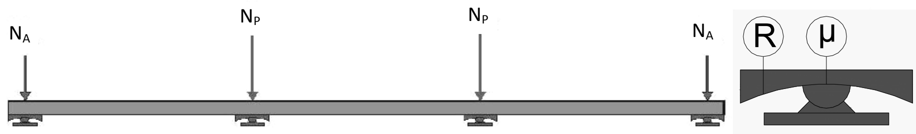

Figure 6. Seismic isolation with friction pendulum bearings

For all the potential combinations of μ and R of the friction pendulum bearings, iterative calculations are conducted and the properties of the equivalent SDOF system are evaluated. The results of these properties are summarized in Table 3.

Table 3. Properties of the equivalent SDOF system (T_{eff} [s] / ξ_{eff} / $S_e(g)$) for the potential combinations of μ and R of the friction pendulum bearings.

μ / R	0.991m	1.549m	2.235m	3.048m	3.962m	6.198m
3%	1.88/0.07/0.26	2.29/0.10/0.19	2.66/0.14/0.14	2.94/0.19/0.10	3.15/0.24/0.08	3.46/0.33/0.06
4%	1.82/0.11/0.24	2.20/0.14/0.18	2.53/0.18/0.14	2.75/0.24/0.10	2.91/0.30/0.09	3.13/0.39/0.07
5%	1.76/0.14/0.22	2.09/0.19/0.17	2.38/0.24/0.13	2.58/0.29/0.11	2.71/0.34/0.09	2.88/0.43/0.08
6%	1.69/0.18/0.21	1.98/0.24/0.16	2.22/0.29/0.13	2.41/0.33/0.11	2.54/0.38/0.10	2.67/0.45/0.08
7%	1.62/0.22/0.20	1.87/0.28/0.16	2.07/0.33/0.13	2.22/0.38/0.12	2.34/0.42/0.11	2.51/0.48/0.09
8%	1.55/0.25/0.20	1.76/0.32/0.16	1.93/0.37/0.14	2.05/0.42/0.12	2.14/0.45/0.11	2.27/0.50/0.10
9%	1.48/0.29/0.20	1.66/0.35/0.16	1.80/0.41/0.14	1.90/0.45/0.13	1.97/0.48/0.12	2.07/0.53/0.11
10%	1.41/0.32/0.20	1.57/0.39/0.17	1.68/0.44/0.15	1.76/0.48/0.13	1.82/0.50/0.13	1.90/0.54/0.12
11%	1.34/0.35/0.20	1.48/0.41/0.17	1.57/0.46/0.15	1.64/0.50/0.14	1.69/0.52/0.13	1.75/0.56/0.13
12%	1.28/0.37/0.20	1.40/0.44/0.18	1.48/0.48/0.16	1.53/0.51/0.15	1.57/0.54/0.14	1.62/0.57/0.13

When applying friction pendulum bearings, the variation of the friction coefficient μ should be taken into account. According to [?], the friction coefficient ranges between 0.80μ and 1.68μ.

In order to fulfill the aforementioned constrains of the seismic isolation solution for the whole range of μ coefficient, it is shown in Table 3 that a basic value of μ=5% in combination with a radius R=2.235m should be chosen. This is the case because for R=2.235m and μ ranging between 0.8·5%=4% and 1.68·5%=8.4% the following limitations are simultaneously fulfilled:

$S_e(g)<0.15$, $T_{eff} \leq 2.50s$, $\xi_{eff} \leq 0.40$.

Taking all of the above into consideration, the maximum shear forces (envelope values for the different values of μ) transmitted to the piers and abutments are now reduced to V_P=926.6kN and V_A=345.9kN respectively.

3.4 Seismic assessment of the retrofitted bridge

In this section, the adequacy of the existing substructure to undertake the seismic forces of the retrofitted bridge is examined.

Table 4 summarizes the demand/capacity ratios obtained by the safety checks for the design seismic action at the bridge piers. It is evident that the existing piers are able now to undertake the reduced level of earthquake action.

Table 5 presents the demand/capacity ratios obtained by the safety checks for the reduced seismic action at the bridge abutments. Similarly, the adequacy of the existing abutments is established.

Table 4. Demand/capacity ratios for the existing piers after retrofitting

Location/Check	Bending		Shear	
	Longitudinal direction	Transversal direction	Longitudinal direction	Transversal direction
Section A-A	0.72<1.00	0.13<1.00	0.17<1.00	0.18<1.00
Section B-B	0.75<1.00	0.10<1.00	0.21<1.00	0.22<1.00

Table 5. Demand/capacity ratios for the existing abutments after retrofitting

Location/Check	Bending	Shear
Section A-A	0.75<1.00	0.42<1.00

4 CONCLUSIONS

In this paper, the potential retrofit scheme of a 144m road prestressed concrete bridge is presented. To enhance the class of the existing bridge, replacement of the existing concrete deck with a steel-concrete composite one is proposed. The additional advantage of this solution is the reduction of the deck dead load, which leads to significant decrease of the seismic forces transmitted to the substructure. The retrofit solution is completed with the application of the friction pendulum isolation bearings between the superstructure and the substructure. It is verified that by applying this retrofit scheme, additional strengthening of the existing piers and abutments is not required.

REFERENCES

[1] Deutches Institut für Normung, *DIN 1072: Road and Foot Bridges- Design Loads*, 1985.
[2] Hellenic Society of Civil Engineers, *EAK 2000*: *Hellenic Seismic Code*, 2000.
[3] Hellenic Ministry of Public Works, *Guidelines for Bridges with Seismic Isolation*, June 2007.
[4] Priestley, MJN, Seible, F, Calvi, GM, *Seismic Design and Retrofit of Bridges,* Wiley and Sons, New York, 1996.

CAISSON FOUNDATION ASSESSMENT FOR SEISMIC VULNERABILITY ANALYSIS OF EXISTING BRIDGES

Giovanni Lanzano[1], Mariella Mancini[1], Filippo Santucci de Magistris[1], Giovanni Fabbrocino[1]

[1] Structural and Geotechnical Dynamics Lab. StreGa, Department SAVA, University of Molise, Italy
e-mail: giovanni.lanzano@unimol.it, mariella.mancini@unimol.it, filippo.santucci@unimol.it, giovanni.fabbrocino@unimol.it

ABSTRACT: Large diameter caissons were frequently used in the past years as massive foundations for bridges and deep off-shore structures. Concerning the bridges, the caissons were generally used as deep foundation in order to reach layers with larger strength. Moreover, the massive shape of these foundations was used in order to limit the soil movements due to landslides along the slopes where the structures were established.

Examples of this foundation type can often be found in existing bridges, so that an insight on structural and geotechnical response to seismic actions is of some interest in view of vulnerability analyses. The seismic design of caisson foundation was based on pseudo-static formulation with simplifying assumptions for the evaluation of lateral ultimate response. Starting from the geotechnical and structural characterization of these structures, the caisson foundation was analyzed using a FEM model in order to compare available simplified methods with the numerical analyses. The analyses were performed in order to evaluate the lateral resistance of the caisson, on the analogy with a pier foundation. Moreover, a set of pseudo-static analyses were carried out to perform a parametric study on the shape ratio and to check the limits of the simplified seismic design method.

KEY WORDS: caisson foundation, existing bridges, seismic performances, soil-structure interaction

1 INTRODUCTION

The caisson foundations were generally used as massive foundations for bridge piers and abutments, offshore structures and tower structure, when a strong lateral action was expected on the superstructure. These structures are generally considered as intermediate foundation and transfer the superstructure loads to the deeper soil layers, which are stiffer and resistant. For the on ground bridges, this type of foundation was frequently used when the bridge passes through unstable slopes and in seismic areas; for offshore bridges, it was adopted when strong actions of wind and water waves on the structure was expected. The caissons were generally made by masonry or concrete, with circular, elliptic or rectangular sections; the in-plane dimensions of the caisson are generally larger in the transverse direction of the bridge alignment, in order to increase the stiffness in that direction.

The seismic design of caisson foundation is traditionally based on pseudo-static formulation with simplifying assumptions for the evaluation of lateral ultimate response. Starting from the geotechnical and structural characterization of these structures, the caisson foundation was analyzed using a FEM model in order to compare available simplified methods with the numerical analyses. The analyses were performed to evaluate the lateral resistance of the caisson, on the analogy with a pier foundation. Moreover, a set of pseudo-static analyses were carried out to perform a parametric study on the shape ratio and to check the limits of the simplified seismic design method.

2 DESIGN METHODS

The Eurocode [1] and the Italian codes [2] relative to the design and control of geotechnical structures, does not contain explicit indications for caisson foundation, but only for shallow and pile foundation.

The lateral and seismic response of bridge foundations was obtained with a number of methods of varying degrees of accuracy [3]. However, few of them concerned the caissons. The methods of solution developed for (rigid) surface embedded foundation and for (flexible) piles have been frequently adapted to deal with the caisson problem. Gazetas (1991) [4] obtained semi−analytical expressions and charts for stiffness and damping of horizontally and rotationally loaded arbitrarily−shaped rigid foundations embedded in homogeneous soil. Gerolymos et al. (2006) [5,6,7] focused on caissons, developing a Winkler model accounting the ultimate horizontal resistance of a cohesive soil.

The evaluation of the horizontal bearing capacity of caisson foundation was usually based on an old formulation, centered on simplified hypotheses about geometry and soil/structure interaction. In the following section the closed form solution for ultimate horizontal load obtained by Frohlich (1936) [8] was described.

2.1 Limit equilibrium method

The ultimate horizontal capacity of the caisson was based on the limit equilibrium of the caisson inside the soil [8]. The behavior of the caisson was supposed as rigid; the soil/structure interaction was accounted using equilibrium equations only. The loading scheme (Fig.1) considers a horizontal force applied on top of the pier. Frohlich (1936) [8] considered a parabolic distribution of the pressures along the walls of the caisson, assuming that the rotation point is inside the caisson. The distribution of the normal stresses along the structure was also showed in Fig. 1. The horizontal pressure at a generic depth x is:

$$\sigma_x = \pm\left(\sigma_p \frac{x}{t} - \left(\sigma_p - \sigma_2\right)\frac{x^2}{t^2}\right) \tag{1}$$

where:

$$k_2\gamma = \frac{1}{2}\left(k_p\gamma - \frac{6\left(H + fV\right)}{at^2}\right) \tag{2}$$

In the previous expressions (1) and (2), the variables are: H, V horizontal and vertical (weight of caisson and pier and overloads) force acting on the caisson; h arms of the force H from the top of the caisson; t height of the caisson; a width of the base caisson; k_p passive resistance ratio; f = tanδ tangent of interface friction.

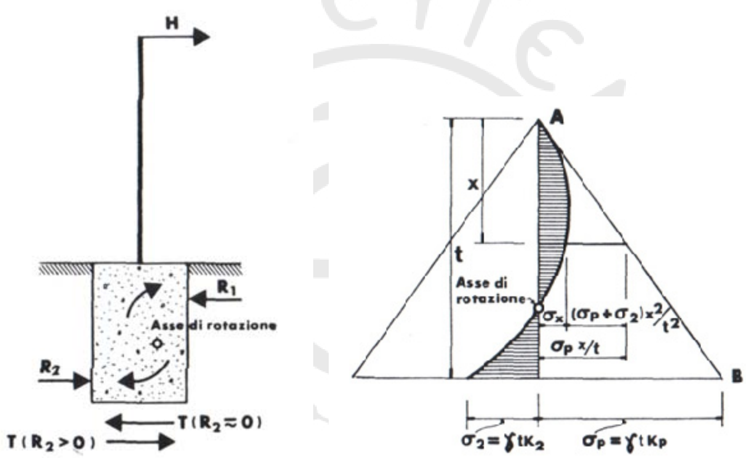

Figure 1. Loading scheme and distribution of the net horizontal pressure along the caisson (Asse di rotazione = Rotation axis) [9]

3 PSEUDO-STATIC ANALYSES

The basic and most common seismic analysis of geotechnical systems consists in pseudo-static calculations, in which the soil/structure seismic interaction is studied modeling the dynamic action as an equivalent static force.

In the following part, numerical analyses were described, in which the ultimate horizontal capacity of the caisson was evaluated in order to obtain the maximum horizontal force which could be applied to the caisson as pseudo-static action.

The numerical analyses were performed considering the geometry of an existing caisson, used as a pier foundation for an existing bridge located in the Molise Region, Italy, approximately 250km S-E of Rome. The area is characterized by a very complex and heterogeneous geology and morphology.

Many bridges of the most important highways of the Region were built in sites with a high hydro-geological hazard. Moreover the seismic hazard of the Region is spanning from moderate to high [10].

The caisson has cylindrical shape with a base diameter of D_e=14 m and a trunk diameter of D_i=12,4m. The height of the foundation structure is H=16m. In Fig. 2 a view of the original design documents with the geometry of the caisson was showed. In order to carry out the numerical analyses the caisson were considered perfectly cylindrical, without the enlargement at the base, setting the diameter as D=D_i. The caisson was made by concrete. The superstructure was constituted by a 30 m high pier.

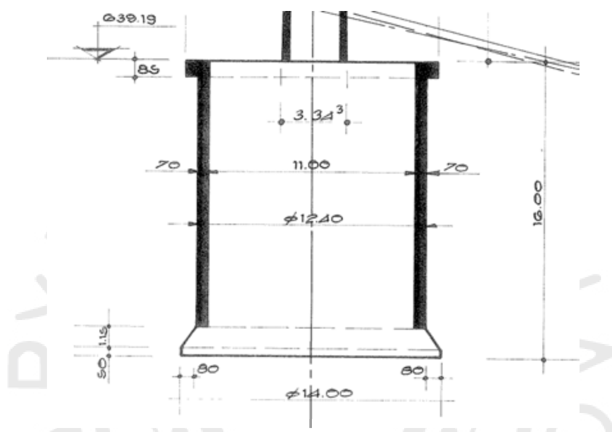

Figure 2. View of the original design drawings of the bridge.

3.1 2D FEM analyses

The caisson model was created using Plaxis 8.0 [11], a FEM code optimized for geotechnical problems. The model was built in plane strain conditions, differently from the 3D behavior of the caisson foundation. The geometry of the numerical model is showed in Fig. 3. The domain was not symmetric around the structure because of the non-symmetry of the load and the failure volume.

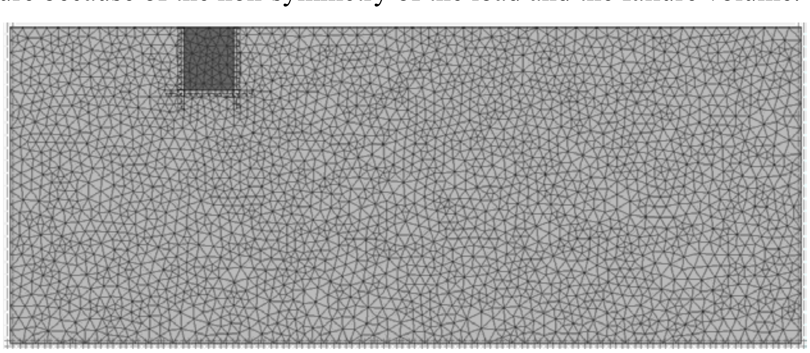

Figure 3. View of the FEM model

Table 1. Material properties for the numerical analyses

Parameter		**Soil**	**Foundation material**
γ	(kN/m^3)	19	14,78
E	(kN/m^2)	14600	30000000
ν	(-)	0,3	0,3
ϕ	(°)	31,5	-

The soil materials properties used for the analyses were showed in Table 1. The soil was considered as a purely frictional material (loose sand). A Mohr-Coulomb model was adopted to control the soil failure due to the horizontal force. No water table was considered in the analyses; therefore the analyses were carried out in total/effective stresses. In the Table 1, γ is the unit weight, E is the Young modulus, ν is the Poisson ratio and φ is the friction angle of the soil. At first, in the numerical analyses the ratio between the friction at soil/caisson interface δ and the friction of the soil ϕ was set as δ/ϕ = 0,1. From this assumption a strong reduction of the interface friction angle δ was adopted, which was 10% of the soil friction angle.

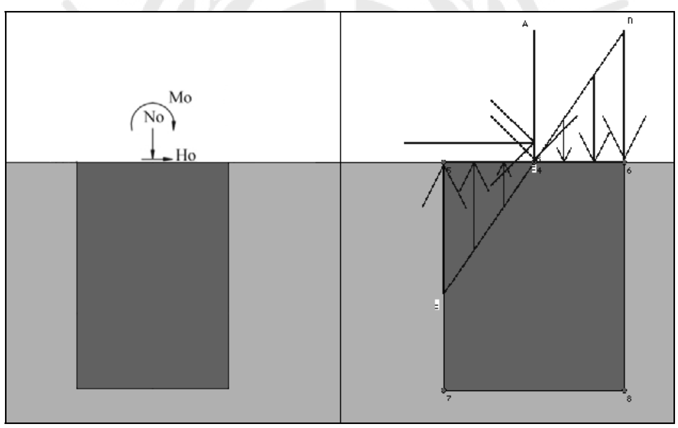

Figure 4. System of load applied to the caisson.

In the Table 1, the mechanical properties of the caisson itself were showed: the parameters were chosen considering the caisson made by concrete. The material model for the structure was linear elastic. Concerning the value of unit weight of the foundation γ_f, the original value for the concrete was modified in order to account for the differences between the 2D model and the 3D real foundation. Starting from the true weight of the caisson, which was W = 3,7x10^4 kN, the caisson was modeled as a square base parallelepiped, with side B=12,5 m and height H=16 m. In order to obtain the same caisson weight, the difference between the volume of the cylinder and the volume of the parallelepiped determined a reduction of the unit weight to γ_f=14,8 kN/m^3.

The caisson model were submitted on the top to a set of loads (Fig.4): a vertical force N_0, which was derived by the superstructure loads (pier weight, beam load and overload); a horizontal load $H_0=H_u$, which represented the horizontal bearing capacity of the caisson; a bending moment M_0, which was given by the product of the horizontal force H_0 and the arm h between the point of application of H_0 and the top of the caisson (height of the pier). The horizontal and vertical forces were applied as point loads, instead the bending moment was applied as a linear distribution of loads (Fig. 4).The results of the analyses were showed in terms of normal stresses on the lateral walls of the caisson (Fig. 5). The horizontal stresses were compared with the theoretical values obtained from the Rankine's theory (in the hypothesis of no soil/structure friction).

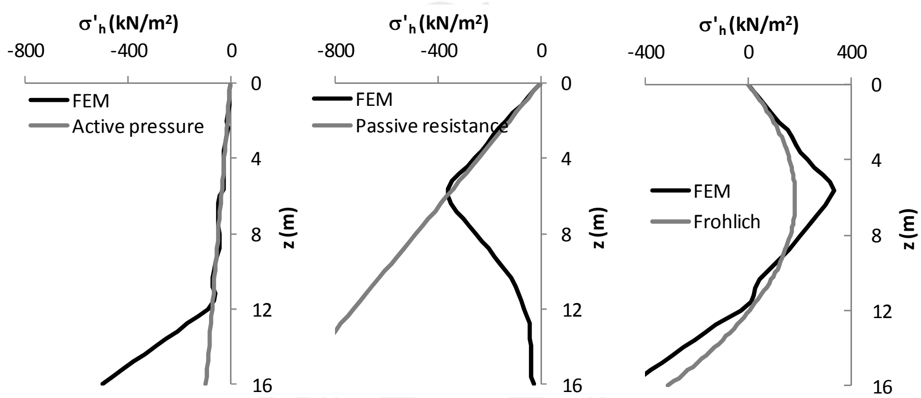

Figure 5. Distribution of horizontal pressure along the caisson: left, right and net diagram.

The horizontal stresses followed the closed-form Rankine's distribution in the top part of the caisson. The change occurred because the rotation centre is inside the caisson: the counter-rotation caused in the bottom part of the caisson (from the rotation centre to the bottom side) an increment of horizontal stresses on the left side, and a reduction in the right side. Net graphs of the normal horizontal stresses, difference between left and right components, were also plotted in Fig. 5 together with the analytical distribution [5].

The numerical and analytical results gave a good agreement: the graph inversion point was similar between the two distributions, which determined a very similar kinematics (same height of the rotation point).

4 PARAMETRIC ANALYSES

A set of parametric analyses were performed, starting from the initial one, varying the geometry of the caisson and the interface properties.

Seven different geometries were prepared, considering a constant value of the base of the caisson and changing its height, in order to obtain different slenderness ratios (λ=H/D=0,5; 0,75; 1; 1,25; 1,5; 2; 3). This ratio values were organized to cover possible construction ranges of these structures, from the squat caisson (low λ) to the slender caisson (high λ). Therefore this type of structures in an ideal hyphen between the shallow foundations (squat caisson) to single large diameter pile (slender caisson).

For each geometry three different interface friction ratios were considered (δ/ϕ=0,1; 0,5; 1). Totally 21 models were analyzed. In each analysis the vertical force value N was obtained as the summation of the initial N_0, which was kept constant in all the analyses, and the weight of the caisson W, which was variable depending on the caisson geometry. Also the bending moment M_0 was evaluated considering a constant value for the force arm.

In Fig.6 the dimensionless ratio H_u/N, between the ultimate horizontal load e the total vertical force were displayed against the slenderness ratio λ=H/D. Three curves were plotted for the three values of the interface friction ratio δ/ϕ.

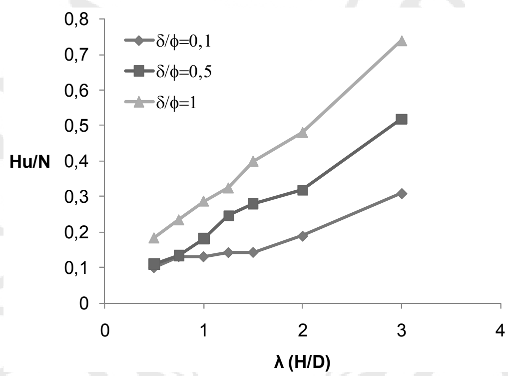

Figure 6. Dimensionless ratio H_u/N against slenderness ratio λ=H/D

The trend of the H_u/N curves was clearly linear with the value of λ. Same increments were observed together with the increment of friction ratio δ/ϕ.

In order to plot the net diagrams of the normal horizontal stresses σ'_h for all the models, these pressure were reported against a dimensionless height of the caisson z/H in Fig.7 for two values of friction ratio δ/ϕ (0,1 and 0,5).

The maximum values of the net horizontal stresses were increased with the value of the slenderness ratio, because of the increments of the horizontal ultimate load capacity. The rotation centre varied with λ, observing a downward shift with the increment of the slenderness ratio. For the δ/ϕ=0,1, the rotation centre were located in a range between 70÷80% of the total height; for the δ/ϕ=0,5, the range was between 86÷93% of H.

5 CONCLUSIONS

The paper described a parametric study based on the results of numerical pseudo-static analyses of caisson foundation. The horizontal bearing capacity was evaluated for seven different slenderness ratio λ=H/D and three interface soil/structure ratio δ/ϕ. The analyses showed a good agreement with the analytical formulation despite of the model simplification (2D instead of 3D). The following research step will be the execution of 3D pseudo-static analyses, and dynamic analyses in order to account the effect of kinematic soil/structure interaction on the response of the caisson.

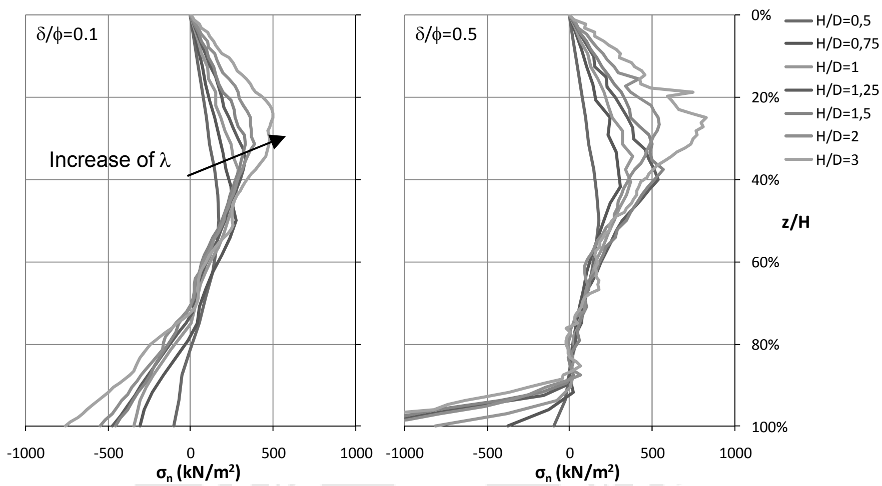

Figure 7. Horizontal net pressure against z/H

REFERENCES

[1] EUROCODE 7 , PART 1 , BS EN 1997-1 “Geotechnical Design”, CEN European Committee for Standardization, Bruxelles, Belgium.

[2] DM 14/1/2008, “Norme tecniche per le costruzioni. Testo unico”, G.U. (in Italian).

[3] Mylonakis G, Nikolau S, Gazetas G, “Footings under seismic loading: Analysis and design issues with emphasis on bridge foundations”, Soil Dynamics and Earthquake Engineering 26, 2006, 824–853.

[4] Gazetas, G, “Formulas and charts for impedances of surface and embedded foundations”, J Geotech Eng ASCE 1991;117(9):1363–81.

[5] Gerolymos, N, Gazetas, G, “Winkler model for lateral response of rigid caisson foundation in linear soil”, Soil Dynamics and Earthquake Engineering, 347-361, 2006.

[6] Gerolymos N, Gazetas G. “Development of Winkler model for static and dynamic response of caisson foundations with soil and interface nonlinearities”. Soil Dyn Earthq Eng, 2006.

[7] Gerolymos N, Gazetas G. “Static and dynamic response of massive caisson foundations with soil and interface nonlinearities—validation and results”. Soil Dyn Earthq Eng, 2006.

[8] Frohlich, X, “Beitrag fur Berechnung von Mastfundamenten”, Ernest, Berlin, 1936 (in German).

[9] Cestelli Guidi, C, “Geotecnica e Tecnica delle Fondazioni”, Hoepli, Milan, 1991 (in Italian).

[10] M. Caccavale, V. Convertito, M. Mancini, G. Fabbrocino, “Seismic hazard disaggregation in the Molise region, Italy: the case study of Campobasso”, 14 ECEE 30 Agosto- 3 Settembre 2010, Ohrid, Macedonia

[12] Brinkgreve, R.B.J, “Plaxis 2D version8”, A.A. Balkema Publisher, Lisse, 2002.

CONDITION ASSESSMENT AND RETROFIT OF A HIGHWAY STEEL BRIDGE

Ioannis G. Raftoyiannis[1], George I. Ioannidis[2] and Anastasios G. Veis[3]

[1,2,3] National Technical University of Athens, Dept. of Civil Engineering, Greece
e-mail: rafto@central.ntua.gr

ABSTRACT: This paper presents an analytical study to access the condition of an existing highway steel bridge and to propose strengthening measures. A validated analytical model is employed to evaluate the capacity of the bridge to carry traffic, seismic and wind loads specified by the current design codes. An estimation of the remaining fatigue life of the bridge in its present condition and after the suggested strengthening is also made.

KEY WORDS: Steel bridges; highway bridges; field measurements; retrofit.

1 INTRODUCTION

At the early 1980s, the Greek Government developed a series of steel highway bridges in the Athens suburbs on locations where traffic problems started rising rapidly. All of those steel bridges but the one under study have been gradually replaced by concrete ones. The present work concerns the strengthening study of an existing steel bridge located on the junction of Athens Avenue (Kavalas) with the Kifissos Avenue that was manufactured in 1980. Part of the study concerns the structural performance of the bridge under the loads from the current regulations (traffic loads, wind loads, seismic loads etc). The study provides the necessary technical details for the required stiffening and improvement measures of the bridge.

The bridge structure is constituted by thirteen steel decks simply resting on steel pylons with variable height. The five extreme parts at both ends of the bridge have span lengths 20.90m and height of main beams 1.20m. More specifically, the fifth span (from each side) has variable height from 1.20m to 1.40m. The central part has span length 22.10m and height 1.40m, while the 2 neighboring parts of 38.50m have height 1.40m as well. These parts have been manufactured by a central part similar to the 22.10m part on both sides of which there are bolted two parts with length 8.25m. Each part has been formed by main beams, transverse cross-girders and orthotropic deck. The orthotropic deck constitutes by a metal-sheet 12mm thick for the 20.90m spans and 25mm for the 22.10m and 38.50m spans. The metal-sheets of the deck are stiffened by typical closed form stiffeners (U-type) 8mm thick and dimensions 180mm at the bottom and 300mm at the top (on the deck) and total height 220mm. The stiffeners are perpendicular to the cross beams on which they are based via welded connections and thus determining the main direction (stiff) of the orthotropic plate. A detailed arrangement of the stiffeners, the main beams, the cross girders and the orthotropic plate is shown in *Fig. 1*. A perspective view of the bridge structure and the arrangement of main beams and pylons are shown in *Fig. 2*.

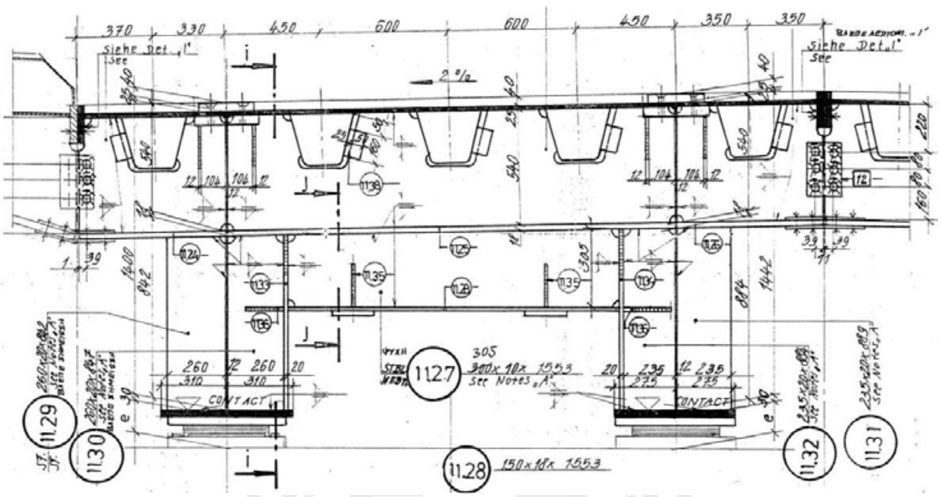

Figure 1. Half-section of the bridge deck, cross-girder and bearings

Figure 2. Perspective and underneath view of the entire bridge

The steel quality is St 37-2 corresponding to the current category S235. Each part has four main beams simply supported on twin pylons (per direction). The pylons (4 per axis of support) are manufactured from rectangular hollow cross-section with dimensions 700x730mm shaped by welding steel plates with thickness 15mm as shown in *Fig. 3*. The drawings of the existing structure (*Figs 1* and *3*) constitute among others the basis for the structural checks and the relative calculations, for which sampling confirmation has been performed.

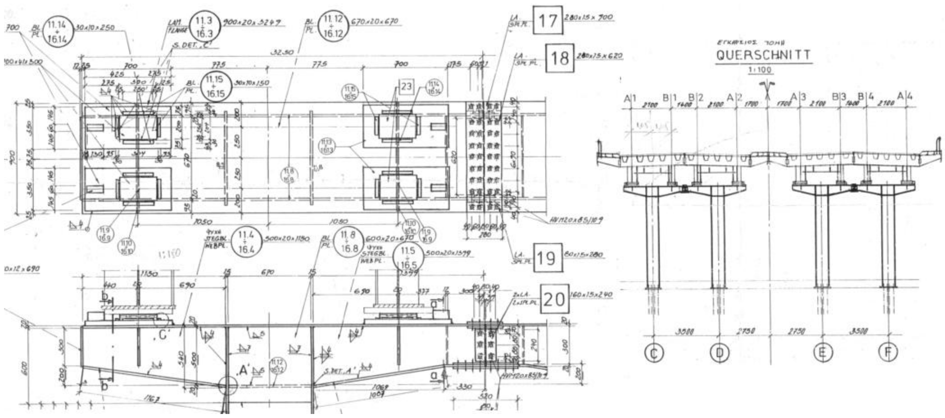

Figure 3. Bearing details and arrangement of pylons

2 DEVELOPMENT OF VALIDATED ANALYTICAL MODELS

Extensive field measurements as well as analytical work have been performed to assess the condition of the steel superstructure and propose a proper strengthening scheme.

Separate analyses were performed for each of the three different spans by considering the simply supported parts resting on elastometallic bearings (see *Fig. 4*), respectively, for the parts with lengths 20.90m, 22.10m, 38.50m and one for the entire bridge including the pylons (see *Fig. 5*). In order to construct the corresponding detailed finite element models, the Sofistik engineering software has been employed. Based on these analyses, the level of developing stresses and deformations (due to bending) under the operation loads were determined together with the need of stiffening measures for the deck parts.

Next, a spectral seismic analysis of the full bridge structure (all openings, pedestals and pylons) is performed based on which the determination of the finally required dimensions for elastometallic bearings (that will replace the existing ones) as well as the metal joints between successive parts and at the bridge ends is done. From the analysis of the full bridge model result also the stresses in pylons and at the foundation.

In order to check for fatigue, the fatigue model 3 that corresponds to an individual vehicle described in EN 1991 Part 2, has been employed for the checking of critical connections against fatigue. However, due to the particularly high traffic loads of the examined bridge, but also its significant importance for the transportation network of Athens City, the fatigue load model 1 has also been examined for comparison purposes. Note that the above bridge is overloaded with traffic loads classified into the category of very heavy traffic (according to the Technical Notes of the Ministry of Public Works for bridges with traffic over 8,000 vehicles per day) and, moreover, due to the fact that the actual number of passages exceeds by far the previous limit (over

25,000 vehicles per day). Consequently, it is appropriate to consider also a more conservative model for fatigue calculations (such as the fatigue load model 1).

In order to apply the traffic loads and to check the strength of the structure, the provisions of Eurocode 1-Part 3 "Traffic loads on bridges" and of Eurocode 3 - Part 2 "Steel bridges" have been applied for the loads and the strengths, respectively, since these provisions were similar to the ones of the DIN Fachberichten and since the application of Eurocodes in the area of bridges was imminent at the time of this study.

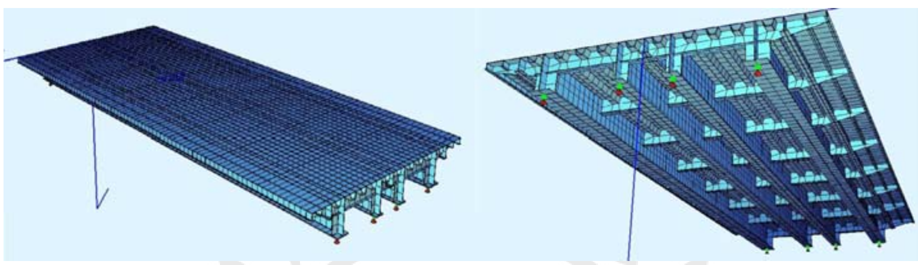

Figure 4. Detailed FE model of the 20.90m simply supported bridge deck

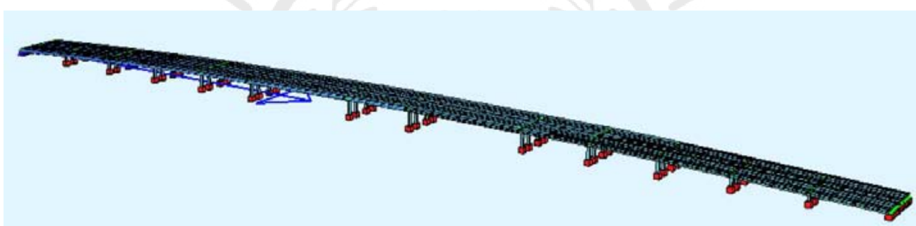

Figure 5. FE model of the entire bridge including the pylons

Regarding the bending deformations (deflections) due to traffic loads, the relative provisions of AASHTO "Standard Specifications for Highway Bridges" have been adopted which consider a maximum acceptable deflection smaller than 1/500 of the span length for traffic loads. Moreover, the provisions of Greek Aseismic Regulation (EAK 2000) and of Directive E39/93 "Directives on the aseismic studies of bridges" have been taken into account, based on which the design of bearings is performed.

The self-weight of the metal structure (load case LC-1) has been taken directly into account by the program, where it is considered γ_S=78.5 kN/m^3. For the concrete pavements a plate thickness t=20 cm is considered with γ_b=25.0 kN/m^3, while for the asphalt layer a thickness t=8 cm is considered with γ_a=22.5 kN/m^3.

For the main traffic lane a uniform load 9.0 kN/m^2 is considered over the entire length of the bridge, while for the secondary lane it is taken 2.5 kN/m^2. A live load of 2.5 kN/m^2 was also considered for the pavements. These uniform loads constitute load case LC-2.

Concentrated loads due to heavy vehicles were applied according to EC-1 as follows: the vehicle in the main lane has 4 wheels with total load 300 kN per axis while the vehicle in the secondary lane has also 4 wheels with total load 200 kN per axis. The load of each wheel is distributed over a surface 0.40x0.40m according to EC-1. The vehicles are placed at 6 different positions (load cases LC-3 to LC-8), which are expected to give the most unfavorable results for the various elements of the bridge.

Regarding the acceleration and deceleration loads due to traffic (load case LC-9), a uniformly distributed horizontal load s taken into account, which is acting over the main traffic lane (width 3.0 m) on the entire length of the bridge and is:

$Q_{fk} = 0.6\ (2Q_{1k}) + 0.10\ f_{1k}\ w_1 \cdot L = 0.6 \times (600) + 0.10 \times 9.0 \times 3.0 \times L$

where L the span length of the bridge. The above load takes the following values: 463.95 kN, 419.67 kN and 416.43 kN for span lengths 38.50m, 22.10m and 20.90m, respectively.

Two 4-wheel vehicles in line with 120kN per axis, which abstain between them 6.00 m as required by the fatigue model 3 of EC-1, are considered in load case LC-10 for fatigue. The forces of each wheel were uniformly distributed over an area with dimensions 0.40x0.40m based on the provisions of EC-1.

A wind pressure $w=1.51\ kN/m^2$ is considered (load case LC-11) that is acting transversely to the bridge with area of influence the height of the main beam plus the height of lorries (that is taken 2.0 m), which is totally 3.40 m. The wind pressure was calculated analytically as follows:

$w=q_{ref} \cdot c_e(z) \cdot c_d \cdot \psi_\lambda \cdot c_{fx,0}$, $q_{ref}= 0.81\ kN/m^2$, $c_e(z) = 2.8$ (zone II), $c_d = 0.95$, $\psi_\lambda=0.70$, $c_{fx,0} = 1.0$, and hence, $w = 0.81 \cdot 2.8 \cdot 0.95 \cdot 0.7 \cdot 1.0 =1.51\ kN/m^2$.

A uniform temperature change $\Delta T=35°C$ (load case LC-12) and a linear temperature variation $\delta T= + 18°C / -13°C$ (load case LC-13) that corresponds to deck category 1, were also considered. The factor of surface k_{sur} was taken 1.0.

Seismic forces acting along X, Y and Z directions (load cases LC-17, LC-18 and LC-19, respectively) were also considered. Since the examined individual parts are simply supported on bearings, an equivalent static analysis for seismic loads has been adopted with seismic factor ε that is

$$\varepsilon = \gamma \frac{\eta\theta\beta_o}{q}\alpha = 1.0\frac{1.08x1.0x2.5}{1.0}0.16 = 0.432 \tag{1}$$

where for seismic zone I, it is $\alpha=0.16$, the significance factor is $\gamma=1.0$, the damping factor is $\eta=1.08$, the magnification factor is $\beta_o=2.5$ and the factor of seismic behavior is $q=1$. It must be pointed out that besides the analysis per each individual span with the assumptions reported above, an aseismic analysis of the entire bridge has also been performed.

For the design of bearings, their resistance in vertical loads and their acceptable shear deformation in combination with the requirements of Eurocode 3 and Directive E39/93 were taken into account. The types ALGABLOC NB4

400x300x123 (48) for the small spans (20.90m and 22.10m) and ALGABLOC NB4 600x300x123 (48) for the spans of 38.50m have been selected. The bearings are enclosed within a top and a bottom metal plate suitable to allow connection of the bridge to the piers in a stable manner.

From the analysis of the entire bridge model results the fundamental period of bridge oscillation T_1 = 0.733s that corresponds to translational motion in the transverse direction (perpendicular to the traffic) and the second T_2 = 0.692s that corresponds to translational motion along the length of the bridge.

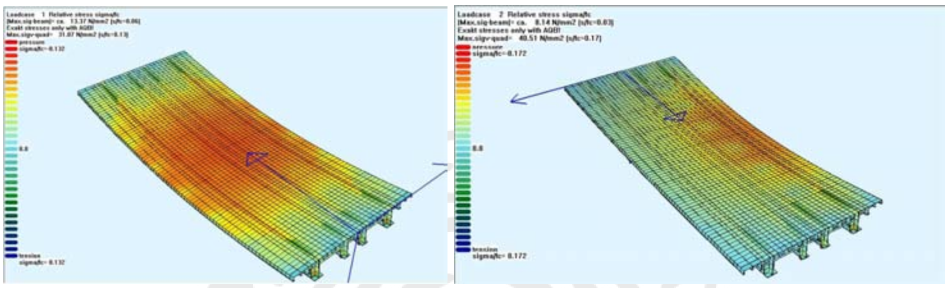

Figure 6. Stress and deformed states for permanent and traffic loads

Regarding the 20.90m spans, the highest developing stress in the most unfavorable position under the most unfavorable loading combination was determined equal to 212.6MPa. The highest acceptable stress for marginal failure is equal to 235/1.10=213.6MPa. The biggest deformations (due to bending) are computed equal to 9.6mm for the permanent loads and 39.3 for traffic loads. As biggest acceptable deformation under the traffic loads only it is taken 1/500 of the span length, that is 20900/500=41.8 mm>39.1 mm. The bridge deck (12mm steel plate) is fully effective due to the existing stiffeners. In *Fig. 6* one can see the stress and deformed states for permanent and traffic loads of the 20.90m span model. Fatigue calculations were done for web - bottom flange connections. The typical stress deviation that expresses the strength for $2x10^6$ cycles is taken from EC-3 Part 1.9. The increase of stress deviation by a factor λ is done according to EC-3 Part 2, in order to relate the actual number of cycles to the typical for $2x10^6$ cycles. Based on fatigue model 3, the stresses of the bottom flange were adequate against the limit value by 13%. Based on fatigue model 1, it was observed a significant divergence of fatigue and resistance values. More specifically, the design value was 95MPa compared to the fatigue one 152MPa (divergence 60%).

Similar results were obtained for the 22.10m spans. The biggest developing stress was determined equal to 194.7MPa<213.6MPa. The biggest deformations (due to bending) are computed equal to 8.9mm for the permanent loads and 32.6 for traffic loads. Based on fatigue model 3, the stresses of the bottom flange were adequate against the limit value by 23%, while for fatigue model 1 a significant unfavorable divergence of fatigue and resistance values by 43% was observed.

Regarding the 38.40m spans, the highest developing stress was determined equal to 273.6MPa that is higher than 213.6MPa by almost 30%. The biggest deformations (due to bending) are computed equal to 51.5mm for the permanent loads and 117.3 for traffic loads which is significantly higher than the limit value of 38500/500=77.0 mm. In these spans strengthening is essential. A 30mm thick steel plate is welded on the bottom flange of the main beams over the entire length (up to a distance of 1.50m from the theoretical axis of support). The additional plate has dimensions 660x30 for the extreme beams and 440x30 for the intermediate ones as shown in *Fig. 7*. After strengthening, the biggest developing stress is 220.5MPa and the maximum deflection due to traffic loads becomes 95.7mm, which can be marginally accepted. Fatigue calculations were also done for web - bottom flange connections. Similar observations as in the previous cases are valid for fatigue.

Figure 7. Strengthening of the 38.40m main beams

Figure 8. Replacement of bearings

There are four pylons per axis of support which have the same rectangular hollow cross-section with external dimensions 700x730mm and wall thickness 15mm. Each pylon group has different height (maximum 5720mm). From the analysis of the entire bridge model it is concluded that the existing pylons have adequate strength despite the big increase of the seismic loads according to seismic regulations (EAK 2000) due to the favorable shift on the design spectrum. The pylons are considered fixed at their base. No anchoring failure at the foundation was predicted by the above analysis.

3 CONCLUDING RESULTS AND STRENGTHENING

Based on the analysis of the bridge and the evaluation of the preceding results one can point out the following:

- The pylons of bridge were adequate and no strengthening was required.
- All existing bearings were replaced by new elastometallic bearings according to the results of the above analysis.
- During retrofit a detail inspection of all welded and bolted connections was performed and in places of failure the connection was re-established.
- In the spans of 20.90m and 22.10m, where a welded connection of joists was realized, stiffening plates were placed at the bottom flange on the main beams since at these places a severe possibility of fatigue type failure exists.
- In the spans of 38.50m, stiffening plates were placed at the bottom flange on the main beams in order to increase the bending strength and decrease the vertical deflection. The web of the main beams was also strengthened in the mid-span zone against fatigue.

Figure 9. Replacement of joints

REFERENCES

[1] DIN 18800, Teil 1–4, Stahlbauten. Berlin: Beuth Verlag GMBH, November, 1990.
[2] ENV 1993-2, Eurocode 3: Design of steel structures. Part 2: Steel Bridges, CEN, European Committee for Standardization, 1997.
[3] ENV 1991-3, Eurocode 1: Basis of design and actions on structures. Part 3: Traffic loads on Bridges, CEN, European Committee for Standardization, 1995.
[4] Ermopoulos J. Steel and composite bridges in Greek, Kleidarithmos Publ., Athens, 2000.
[5] Greek Aseismic Code (EAK 2000), Athens 2000.
[6] Miner MA. Cumulative damage in fatigue. ASME, J Appl Mech 1945;12(3):159–164.
[7] Directive E39/93. "Directives on the aseismic studies of bridges", Athens 1993.
[8] AASHTO. Standard Specifications for Highway Bridges, USA 1989.

THE MEDIEVAL BRIDGE OF KREMASTI IN LESVOS:
Documentation, Assessment & Proposed Interventions

Elizabeth Vintzileou[1], Alkimos Papathanassiou[2], Angelos Zagkotsis[3] and Aikaterini-Anna Manoledaki[4]

[1,4] National Technical University of Athens, Dept. of Civil Engineering,
Laboratory of Reinforced Concrete, Greece
[2,3] Civil Engineer, Athens, Greece
e-mail: [1] elvintz@central.ntua.gr, [2] apapatha@tee.gr, [3] angeloszag@hotmail.com,

ABSTRACT: The bridge of Kremasti is a stone masonry arch bridge. In-situ and in-laboratory investigations were carried out to document the materials, the bearing system and the pathology of the monument. FE analyses contributed to the assessment of the structure and the interpretation of damages. Intervention measures are proposed for the preservation of the monument.

KEY WORDS: FE analysis; Interventions; Masonry; Arch bridge.

1 INTRODUCTION

The bridge (*Photo 1* and *Fig. 2*) is located in the island of Lesvos, Greece, 3km NE from the village of Aghia Paraskevi; it was built during the domination of the island by the Genovese family of Gattilussi (1355-1462 AD). It is a single span stone masonry arch bridge, 8.5 m high and 40 m long. The arch, made of cut stones, is of semi-circular shape (radius equal to 5.8 m approximately) with span length of 11.5 m. The spandrel walls (s.w.) of the bridge, made of rubble stone masonry, are of different inclination, to follow the geomorphology of the terrain. The orientation of the longitudinal axis of the bridge is ESE-WNW.
The aim of the work presented in this paper was to assess the current state of the bridge and to propose adequate intervention measures for its conservation.

Photo 1. General view of the bridge (from south)

2 DESCRIPTION OF THE STRUCTURE

The construction of the arch is of remarkable accuracy; its width is equal to 3.0 m, whereas its thickness is equal to 0.6m. Sphenoid stones are used to form the circular shape of the arch. The arch is founded on stone masonry abutments made of the same materials as the arch. Both abutments are resting on solid rock; they are of different width, however, as shown in *Fig. 2*.

The s.w. are made of rubble stone masonry, although one can discern some large-size cut stones close to the abutments, mainly at the western part of the bridge (*Photo 1*). The width of the eastern s.w. is constant (approx. equal to 3.0m), whereas the width of the western s.w. varies between 2.85m and 3.40m (*Fig. 2*). Both s.w. are founded on solid rock over their entire length.

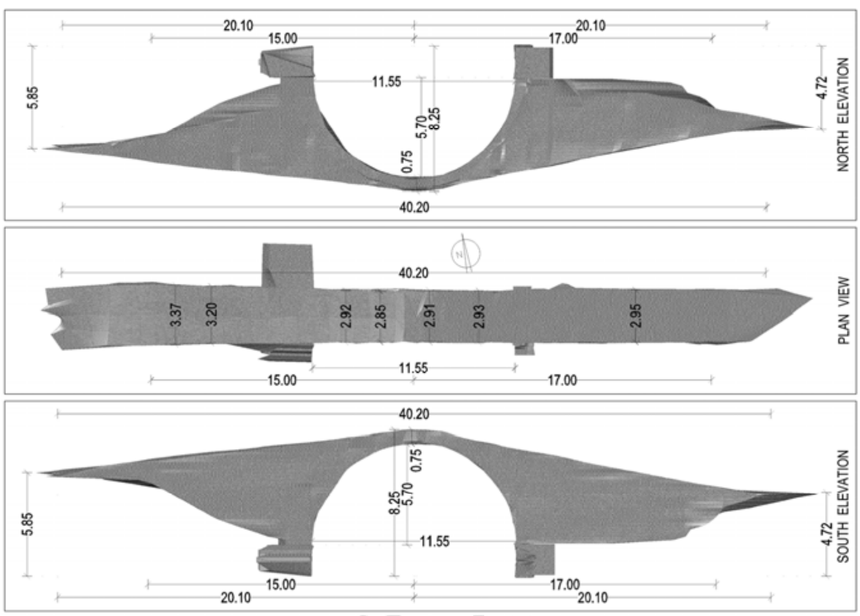

Figure 2. The geometry of the bridge.

In order to identify the construction type of masonry within its thickness, the stone pavement was locally removed in selected places, and boroscopy was applied through existing holes. This investigation revealed that the western s.w. is made of three-leaf masonry, consisting of two external leaves (0.8 m in thickness, each) and an internal leaf made of stones laid without mortar. On the contrary, the eastern s.w. is made of solid rubble stone masonry throughout its thickness (equal to 3.0m). These differences (a) in the construction type of the two s.w. and (b) in their width, may insinuate that the bridge was damaged in the past and partly reconstructed. However, as no information about the history of the monument is available, this interpretation cannot be confirmed.

Photo 3. Central region of the arch. Cracked stones and out-of-plane displacement of stones.

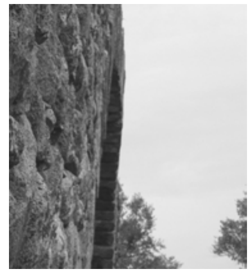

Photo 4. Out-of-plane displacement of the arch.

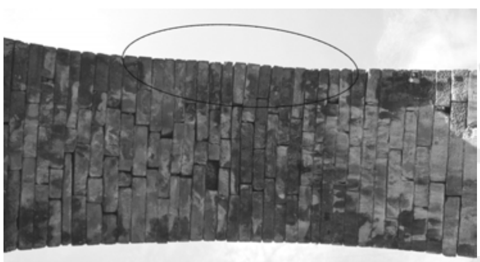

Photo 5. Out-of-plane displacement of the central region of the arch.

Photo 6. Eastern abutment. Wide horizontal joints are shown.

3 PATHOLOGY

The general condition of the bridge is good, given its age, as well as the high seismicity of the area [7], [8].

Damages are concentrated in the arch, especially in its central region, where several stones are cracked and displacement of stones out of the plane of the arch are observed (*Photo 3*). This damage results to significant out-of-plane displacement of the arch (*Photos 4, 5*). The maximum value of the relative displacement between the arch and the north face of the s.w. reaches 0,15m. At the intrados of the arch, decay of materials is observed due to rain water penetrating the pavement. As expected, decay of stones and disintegration of the mortar joints is more pronounced in the central region of the arch, where the thickness of the pavement is very small.

At the abutments, wide horizontal joints are observed (*Photo 6*), filled with wedges. Few vertical cracks in stones are also detected, mainly at the south edge of the western abutment. These damages, however, do not affect the horizontality of the upper face of the abutments. Although there is no sign of damages that could be attributed to foundation problems, this aspect should be further studied.

The s.w. are slightly inclined out of their plane (1.5% maximum). Extensive decay of materials is observed throughout the s.w. Disintegration of mortar (it is washed out at a depth that reaches 100mm) led to local disintegration of masonry. Moreover, debonding between the arch and the s.w. is observed.

4 MECHANICAL PROPERTIES OF MATERIALS

Samples of mortars and stones were taken and tested in the Laboratory of Reinforced Concrete NTUA, with the purpose to evaluate their mechanical properties. Twenty four samples of mortar (from various regions of the bridge) and five samples of stones were taken. The fragments method [2] was applied to measure the tensile strength of the mortars. Depending on the region of sampling, the tensile strength of mortar varies between 0.04 MPa and 0.40 MPa. The compressive strength of stones, measured on prismatic specimens, is approximately equal to 45 MPa.

The mechanical properties of masonry are estimated, taking into account the measured strength values, as well as the construction type of masonry per region of the bridge. In order to estimate the compressive strength of the arch (along its axis), a conservative value was assumed for the compressive strength of the stones, equal to 40 MPa, since sampling of (better quality) stones from the arch was obviously not possible. Thus, a design value of the compressive strength of the arch equal to 4.0 MPa was estimated; the estimated value for its long term modulus of elasticity is equal to 4,500 MPa.

Although the two s.w. are different in construction type within their thickness, due to the very poor quality of the mortar in the interior of the eastern s.w., the lower of the calculated design values of compressive strength (equal to 1.0 MPa) is adopted for both s.w. Similarly, the same value (equal to 2000 MPa) was adopted for the E-modulus. It should be noted that when calculating the mechanical properties of masonry, it was assumed that the mortar joints are full, although extensive disintegration of mortar is observed. This is because re-jointing of the entire surface of the monument is one of the interventions which are proposed for its preservation. Moreover, it is assumed that re-jointing does not contribute to the enhancement of the mechanical properties of masonry.

5 NUMERICAL ANALYSES

5.1 FE Model

The numerical analysis was performed using the computer program Sofistik [9]. Area elements were used to model the structure. The bridge is assumed to be fixed on the ground. Moreover, the end zones of the s.w. lower than 1.5m, were not included in the model (*Fig. 7*).

Three different materials were used in the model to simulate the arch, the s.w. and the pavement. The properties attributed to those materials are derived from the data of Section 4. Although the pavement is not a bearing element, it was included in the model (assuming that its mechanical properties are very poor), in order to take into account accurately the self weight of the bridge.

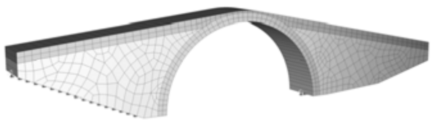

Figure 7. View of FE model of the bridge

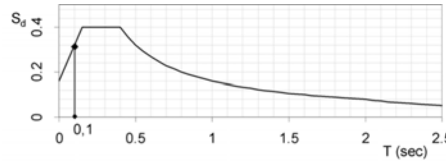

Figure 8. Design spectrum EC8 (Type 1, soil class A, q=1.5).

5.2 Vertical loads and Seismic Action

The vertical loads on the bridge include its self weight (G), as well as a live load (Q) equal to 5kN/m^2. Due to the limited use of the bridge, the seismic loading was applied (in two independent orthogonal directions) combined with dead load only. X and Y directions coincide with the longitudinal and the transverse axis of the bridge respectively. In order to calculate action-effects to be used for the verification of the critical regions of the bridge, the equivalent seismic load method was selected (with uniform distribution of actions along the height of the structure). Two values of spectral acceleration (S_d) were considered, namely: Case 1: S_d = 0.30(g), Case 2: S_d = 0.40(g).

As shown by preliminary analyses, Case (1) corresponds to the seismic action that the structure can withstand with no major damages to be expected. Case (2) is the maximum design spectral acceleration according to the Greek Aseismic Code [4], assuming a behaviour factor q equal to 1.50 and taking into account that the peak ground acceleration for Lesvos is equal to 0.24(g). Modal analysis was also carried out.

5.3 Results

It was proven that the bridge can safely withstand the design vertical loads. Actually, the maximum compressive stresses developed in the arch (=0.65 MPa), as well as in the s.w. (=0.21 MPa) are significantly smaller than the compressive strength in the respective regions.

For the seismic action X along the longitudinal axis of the bridge, the arch is subjected to bending (*Fig. 9)*. Tensile stresses develop in the intrados, in the central region of the arch (*Fig. 12*). The depth of the tensioned zone of the arch was calculated for both values of the imposed seismic action (Cases 1 and 2). Assuming linear distribution of stresses within the height of the arch (equal to 0.6m), it was found that the depth of the tensioned zone is equal to 20mm in Case (1) and 120mm in Case (2). The maximum stress in the compressed zone of the arch under Case (2) is small (= 0.35 MPa) and, therefore, no failure of the arch is expected. However, cracks are expected to develop in the central region of the arch.

Considering the spandrel walls, as shown in *Fig. 11*, there is no region in which the combination of vertical (compressive) stress and the respective shear stress is critical.

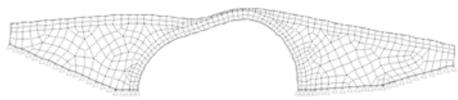

Figure 9. Deformed shape of the bridge under seismic action in +X direction.

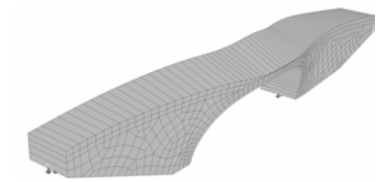

Figure 10. Deformed shape of the bridge under seismic action in +Y direction.

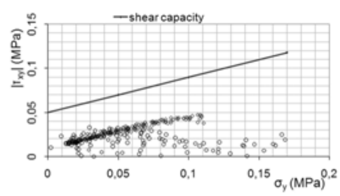

Figure 11. Case (2). Shear stress vs. compressive stress in spandrel walls. Seismic action in + X direction.

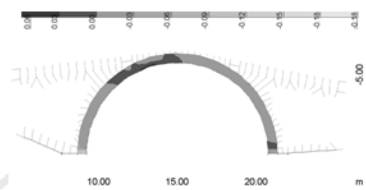

Figure 12. Case (2). Maximum principal stress distribution. Seismic action in +X direction (dark areas: tensile stresses).

When the bridge is subjected to a seismic action in the Y direction, the arch is subjected to out-of-plane bending (*Fig. 10*). Assuming linear distribution of stresses along the width of the arch (equal to 3.0m), one finds that in Case (1) the length of the tensioned zone of the arch is equal to 0.5m, whereas in Case (2), the tensioned zone is as long as 1.2m. It is to be noted that these results are in accordance with the observed damages in the central region of the arch (*Photos 3, 5).* Again, the maximum compressive stress developed in the arch (~0.50 MPa) is significantly smaller than the design value of the compressive strength of the arch (=4.0 MPa).

The same checks at the base of the arch give a length of the tensioned zone equal to 1.1m and 1.8m for Cases (1) and (2) respectively, whereas compressive stresses as high as 2.0 MPa develop in the compressed zone. Taking into account that the real out-of-plane deformations of the bridge will be definitely larger than those calculated on the basis of an elastic analysis, both the out-of-plane displacement of the arch (*Photo 4*) and the vertical cracks in the abutments may be interpreted.

Modal analysis provided further data that allow to interprete the response of the bridge to past earthquakes, in a qualitative way, though. For modal analysis, the spectrum included in Eurocode 8 [6] for soil class A (rock) was used. The assumed values for the behaviour factor q, the damping and the peak ground acceleration are equal to 1.5, 5% and 0.24g respectively (*Fig. 8)*. The results of the modal analysis show that the bridge is of remarkably high stiffness, whereas the vibration modes that contribute most to the response of the bridge are of a period smaller than 0.1 sec (*Fig. 13*). This observation is of key importance both for the interpretation of the actual state of the bridge and for the selection of the scheme of interventions to the monument (see Section 6). For these values of period, the actually demanded spectral acceleration is well below the maximum values of the spectrum (*Fig. 8*). The base shear was calculated by CQC method for the 20 first modes, and found 640 kN and 775 kN in X and Y direction respectively, against 2800 kN in each direction for the equivalent seismic load method in Case (2), where $S_d(T)$ is equal to 0.24(g). Although the activated mass in modal analysis does not exceed 80% of total mass, the results indicate that the equivalent seismic load method clearly overestimates the effect of seismic actions on the bridge.

The mode shapes (*Fig. 13*) show that the central region of the arch is critical, both for in plane and out of plane response. This is in accordance with the observed pathology (*Photos 3, 4,* and *5*).

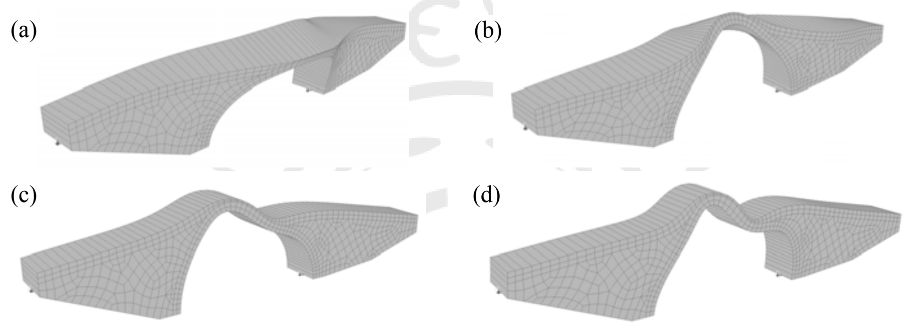

Figure 13. Vibration modes that contribute the most in modal analysis. (a) Mode 1, T1=0.103sec; (b) Mode 4, T4=0.044sec; (c) Mode 3, T3=0.056sec; (d) Mode 8, T8=0.031sec

6 PROPOSED INTERVENTIONS

In general, the observed pathology of the structure was successfully interpreted by numerical analyses. At a first glance, there is an inconsistency between the rather limited intensity of the damages in the arch and the historical seismicity of the island of Lesvos [10, 11]. It seems, however, that due to the high stiffness of the bridge, even along its out-of-plane direction, the actual spectral demand is significantly smaller than that the equivalent seismic load method would predict. This fact gave the authors of this paper the reasoning to avoid heavy interventions in the arch (e.g. steel jacket) that would alter the appearance of a monument - landmark of the island. Thus, the proposed remedial measures comprise (a) the re-jointing of the entire bridge, including arch and abutments, (b) repair of damages, (c) grouting of the s.w. and (d) protection against environmental actions.

More specifically, deep re-jointing of the spandrel walls (using a hydraulic lime based mortar, physico-chemically compatible with the in situ materials) is required to restore the integrity of masonry, to ensure its impermeability to rain water and to ensure adequate mechanical properties.

Grouting of the spandrel walls, using a hydraulic lime-based grout, contributes to the homogenization of the s.w. It also contributes to the improvement of the bond between the spandrel walls limiting, therefore, their vulnerability to out-of-plane actions and, eventually, to the enhancement of their mechanical properties. Grouting will also contribute to the re-instatement of the bond between the arch and the s.w. which is quite poor, as the pathology of the bridge indicates. An intervention of major significance for the in-time behaviour of the bridge is the protection of the monument from water impregnation through the pavement. Thus, the pavement should be completely removed and the stones should be laid on a new layer of lime-pozzolan mortar which may ensure adequate waterproof properties.

7 CONCLUSIONS

The stone arch bridge of Kremasti was systematically documented, using both in-situ and in-laboratory techniques. Its pathology was surveyed and qualitatively interpreted. The structure was modeled and analysed. The analytical work allowed for the pathology of the bridge to be quantitatively interpreted, as well as for the necessary interventions to be specified. The proposed interventions are efficient, being at the same time fully compatible with the architectural and historical value of the monument.

ACKNOWLEDGMENTS

The project was funded by the Municipality of Aghia Paraskevi, Lesvos.

REFERENCES

[1] E. Vintzileou: "Mechanics of Masonry" (in Greek) NTUA, Athens, 2005
[2] T.P. Tassios, C. Vachliotis, C. Spanos: "In-Situ strength measurements of masonry mortars", Structural Conservation of Stone Masonry, International Technical Conference, ICCROM, Athens, September 1989.
[3] T. Tassios, M. Chronopoulos: "Aseismic Dimensioning of Interventions on Low Strength Masonry Buildings", Conference on Low Strength Masonry, Ankara, 1986.
[4] Ministry of Environment, Planning and Public Works, Greek Aseismic Code (EAK 2000, In Greek), Athens, 2000
[5] Eurocode 6: EN1996-1-1, "Design of Masonry Structures, Part 1-1: Common rules for reinforced and unreinforced masonry structures".
[6] Eurocode 8: EN1998-1-1, "Design of Structures for Earthquake Resistance, Part 1-1: General rules, seismic actions and rules for buildings".
[7] B.C.Papazachos, Ch.A.Papaioannou: "Long-term Prediction in the Aegean Area Based on a Time and Magnitude Predictable Model", PAGEOPH, Vol. 140, No4 pp. 593-612, 1993.
[8] N.N. Ambraseys and C.F.Finkel: "Long-term Seismicity of Istanbul and of the Marmara Sea", Terra Nova, 3, pp. 527-539, 1991.
[9] SOFISTIK, Structural Analysis Software, Ver. 23, Sofistik AG, Oberschleissheim, Germany.
[10] Seismological catalogues, Greek Institute of Geodynamics (www.gein.noa.gr)
[11] Seismological catalogues, University of Athens, Faculty of Geology, Dept. of Geophysics & Geothermics (www.geophysics.geol.uoa.gr).

EASTERN MEDITERRANEAN STONE BRIDGES
Structural and Aesthetic Aspects

Gerasimos Thomas[1]

[1] Dr Civil Engineer National Technical Univesrity of Athens, Greece,
Athens School of Fine Arts Gratuate
e-mail: tomjerry78@hotmail.com

ABSTRACT: The monumental stone bridges that still survive in the eastern Mediterranean, from the Mycenaean era till the 19th century, show us the ways of historical construction (architectural forms, structural types and materials). An aesthetic approach to the stone bridges focuses on optical components of beauty: geometry, forms, harmony, scale, architectural orders, material, age etc.

KEY WORDS: Aesthetic, IBSBI 2011; Mediterranean; Stone Bridges.

1 INTRODUCTION

Man has always had to face several problems, which had to be solved by the junction of two sides, metaphorically or literally. In the second case belong the projects, which are described by the Greek word "zeuxis" and include the monumental stone bridges from the antiquity till the present.

2 STRUCTURAL FEATURES

2.1 Historical overview -The three main structural systems

We are able to understand the ways of historical construction through the stone bridges that still survive in the eastern Mediterranean. The dominant material of monumental bridges for four millennia had been the stone; only one hundred and fifty years ago do new materials appear such us reinforced concrete and several types of metals. This follows from the peculiarity of this corner of the world: first because of the high availability of stone, then because of the long tradition of stone working, originating from ancient times. As we study the history of bridges, we distinguish three main structural systems [1]:

a) Horizontal coverage or the so-called system of "beam on poles",
b) The system of arch with horizontal layers or "epexoche" or "ekphora",
c) The radial stone-axis arch, which is the most recent and the most common.

The first stone bridges date from the 2nd B.C. millennium in the Minoan Crete and the Mycenaean Peloponnese. They were made according to the structural system of "ekphora", with the upper stones approaching each other, in a pointed vault. The prehistoric bridges of Argolis (e.g. Kazarma -Photo 1) and Thriassion field are constructed with massive stones in the cyclopean or polygonal [2]. Essentially they have a function similar to gravity structures, which resemble small water dams. The bridges of Classical and Hellenistic era are very impressive, thanks to their special stonemasonry. We should mention the double-arched Selinountas Bridge in Sicily, which is constructed with well carved pentagonal elongated blocks (Figure 1) and the surviving bridge from the 4th century B.C. in Eleutherna in Crete. During the era of the Roman Empire enormous bridges-aqueducts were constructed on several series of arches. In these years new structural methods were used, based on the setting up of wood-formed vaults of smaller stones connected with strong mortar. Worthy of mention are the bridges of the Roman era in several places in Greece (Macedonia, Laconia, Patras, Rhodes, Ilissos of Eleusis), Asia Minor and Italy. During the years of the Byzantine Empire and later, from the Ottoman invasion till the end of the 19th century, there is no comparable revolution in structural ways, but only in architectural forms. Important structures worthy of mention include: The Early Byzantine three-arched bridge on the river Afrin in Syria [3], the one in Sakarya River in Bithynia -Asia Minor dating from the Justinian's rule, the single-arch "Black Cave" Bridge or "Karamagara" in Cappadokia with the pointed arch (Photo 2), the three-arched Byzantine bridge in Moscholourion in Karditsa-Greece (Photo 3), the nine-arched bridge in Larissa-Greece (which was partially destroyed by the British in 1941 and completely destroyed by the Germans in 1944 - Photo 4), the twelve-arched bridge of 15th century in Skopje (Photo 5) etc.

The most well preserved bridges belong to the last two or three centuries. The length of their arch diameter is often remarkably big, reaching 45 meters, which surpasses the monumental vaults of the Pantheon and St. Peter in Rome, Hagia Sophia in Istanbul, Santa Maria dei Fiori in Florence. Some bridges have only one large arc (e.g. in Greece: the bridge in Argithea-Thessaly - Figure 2a, in Albania: the Ali pasha's bridge in Argyrokastron) but in other cases they have more arcs (Figure 2b-d). In the second case belong plenty examples, like these:

<u>Greece:</u> the bridges of Aggista and Aziz Aga in Macedonia [4], the bridges of Papastathis, of Arta and Kalogeriko (Figure 2c) in Epirus [5], the Kompsatos in Thrace (Figure 2d), the Kopanos in Peloponnesus, the Kremasti in Lesvos.

<u>Albania:</u> The Golik Bridge in Pogradets, the seven-arched Goritsa in Berati.

<u>Serbia-Montenegro:</u> the bridge in Visegrad (Photo 6a).

<u>Bosnia-Herzegovina:</u> the Neretva Bridge in Mostar.

<u>Turkey:</u> the bridges in Konya Meram, Adrianople and Side.

2.2 The construction

The stone bridges have four main difficult points of construction: i) the organization of the whole project, ii) the foundation in a plain [6], iii) the design and setting up of the arch, iv) the selection of the period of building.

It should be noted that in any case of construction of a bridge, the final result is just a part of total work. Besides the actual construction work there is the design, the manning and supplying of the site, work in quarries, transport by means characteristic of each era, the stone work of craftsmen, the careful layout of the scaffolding and the rest wooden frames, removal of these and, of course, with these steps accompanied by the risk of accident and the continuing stress on a large group trying to secure success.

The foundation of a bridge had to be done on a rock surface; otherwise it was necessary to enlarge the base and use a frame of wooden stakes. Traditional artisans of the past century talk about the method of creating a system of long vertical stakes and headband-grate of oak or chestnut in soils lacking strength (a similar method of foundation exists in buildings in Venice). The upper parts of the stakes must be carbonized or covered by tar. The base had to be durable and fusiform (like a boat), because this could help the bridge to be more stable and to resist the water impetuosity. There is a "cutter" of water in front of the base and a "lock" behind it, which is a kind of buttress. The lower parts being fully or even partially wetted must be resistant to corrosion. This explains the use of hydraulic and generally strong mortar in foundations [7]. There is use of mortars with crushed tile ("kourasani") or other specific components that increase the coherence, flexibility and endurance: eggs, vegetable fiber (bran), animals' fiber (sheep-wool or the so-called "giagli"), milk, sand etc.

The arch is the main skeleton of a stone bridge, the thin zone that conducts the static loads to the earth. It includes one or more adjacent zones of radially placed and tightly connected cuneiform stones. It was necessary to use a tall wood frame to form the arc and to support the material until the mortar coagulates. The main force is compression and follows the axis of the arc. When large tensile forces develop, there is the risk of unlocking or collapse. In order to counteract the tension force in an earthquake, there were also metal tendons between the two faces of a bridge. Usually, the construction of an arch proceeds from both ends of the bridge towards the center, which requires two teams alternating in the project to avoid construction unevenness. The average stonemason was able to prepare three or four blocks per day, using hammers and needles. At the end is the "keystone", of the arch (corresponding to the "harmonia-stone" of the vaults of the Mycenaean tombs [8]). In the lowlands, given the need to bridge not only the river, but also the whole area that is expected to be flooded, the length of bridges is increased.

The danger of water pressure is really great. There are few modern structures, which failed because of the power of water flow. In recent memory is the destruction of the modern Malpasset arched dam (1959), which claimed thousand of lives. The reduction of the projected surface of a stone bridge in very high water levels is absolutely necessary for its stability; because the water needed to be able to overflow, the architects were forced to design some extra smaller arches between the main ones (Figure 2d).

In the final phase the bridge deck and parapets were constructed. The deck is made by embankments; it is sloping and usually has steps. In any case the deck must be able to serve pedestrians and sometimes (in a plain) to also serve wheeled vehicles. The barriers consist of either small solid walls or standing stones and are designed to offer practical and psychological safety to people.

The selection of the season during which to build was a very important consideration, as the collapse of a bridge and the death of many workers was a serious and not rare event. The suitable time was when the river's level was low enough to avoid flood damages. Tradition talks about human fear against the spirit of the flooding rivers and the sacrifice of people. In Macedonia, Epirus, Thrace and other places of Greece, the period from July to September was often chosen, so they had a short deadline to finish the project.

The strength of stone bridges is admirable, given that the Eastern Mediterranean is a region plagued by numerous earthquakes every year. Of course, there are plenty of cases apart from earthquakes that act on a structure like a bridge: the self-weight of the material and the dead-weight of super structure, snow, the stress applied by water and wind etc. We should not undervalue the old craftsmen of bridges, considering that they had no idea about these risks because they did not use software programs. Accidents of the past served as lessons for later craftsmen, in a trial and error process. So, what are the features that give durability and longevity to these bridges? Among other things we could mention the adequacy of sections and foundation, the correct choice of forms and materials, the correct shape of bases, the regularity of the building, without major asymmetries or eccentricities, the correct distribution of mass in all levels, the systematic interlocking of stones thereby avoiding large vertical joints, the use of cuneiform stones in arcs, the occasional construction of two concentric arcs (hyperstatic skeleton), the elasticity of mortar and the occasional use of additional means of support (tendons, anchorage, buttresses).

3 AESTHETIC ASPECTS

3.1 Values of monumental stone bridges

The values that all these monuments reflect are scientific, historical, archeological, architectural, structural, technological, symbolic, landmark, authenticity, aesthetic and artistic ("venustas" [9]). Let us clarify that our engagement today with the aesthetics of the stone bridges may exceed the intentions of the manufacturers of the past, who had to complete primarily a technical work and only secondarily a masterpiece. However the aesthetic qualities of these bridges are so obvious, that it would be remiss not to highlight them. Irrefutable evidence of their aesthetic value is given by the numerous pictures (plans, paintings, stamps, posters) of scientists, travellers, artists, photographers etc. Especially, stone bridges with large and thin arches have been characterized as “stone poems” or “orbits awe”.

3.2 Aesthetic aspects and theories

Talking about the aesthetics of stone bridges includes various aspects of the morphological features and specifically: forms, types, material, scale, rhythm, modulus, harmony, colours etc.

The concept of measure in the three versions according to P. Michelis [10], the external measure (by human scale), the interior (based on ratio of construction) and the absolute one (e.g. depending on the material) are elements that determine a particular design. In their books Wölfflin [11] and Papanoutsos [12] talk about the aesthetic categories of Beauty: the sublime, the cute and the tragic. On the basis of their theories would not be inappropriate to claim that if the bridges are small and subtle may belong to the aesthetic category of cute; if they are huge, imposing and awe-inspiring they can relate to the aesthetic category of sublime. If one adds knowledge of history, we may have emotions that are specific to the aesthetic category of tragic (e.g. bridges that have been marked by human drowning or have witnessed the execution of innocent people in world wars).

One could also consider the mathematical aspect, especially the geometric interpretation of the curves formed by the arches (e.g. parabolic or circular). The charm of these dynamic patterns fascinates many lovers of analytical geometry. The simulation of those curves with second or higher degree functions, their quantification and their comparative study inspire today many architects, designers, artists or town planners to incorporate relevant features in their work. It is very important to notice the rhythmic visual repetition of structural elements in facades: horizontal or vertical joints, colored stones in the manner of a Byzantine mosaic, the linear line-shadow impression created by the arches in a multi-arched bridge (Photo 6a-b). As in music, here also there is a harmony -not audio but visual- and a well-calculated balance between quantities of volumes, shapes, material, blocks, lines. The dominant element of composition is the stone, a strong and beautiful material that comes from the earth. Stone has its own special type, weight, hardness, transparency, color, tone, density, durability. If we combine all these characteristics with the numerous traces of tools on the stones, we set a specific visual impression.

Apart from the deliberate artistic creation, there is another factor that contributes to the aesthetic quality of the stone bridges: The charm of their antiquity. The ravage of time, wars and thunderstorms, overflowing rivers, strong winds, earthquakes and the timeworn red-brown surfaces are the features that constitute the rhythm of a long disarticulation. The aesthetic impression is also mediated by some factors external to the bridge itself, such us the weather conditions, the transparency of the atmosphere, the surrounding landscape (barren, rough, flat, mountainous, wooded), the special position of the bridge (e.g. in a gorge), the peculiar scattering of the sun or moonlight on the stone surfaces, the reflection of the bridge in the water and so on.

4 FIGURES

Photo 1. Mycenean bridge in Kazarma *Peloponnesus* (Greece).

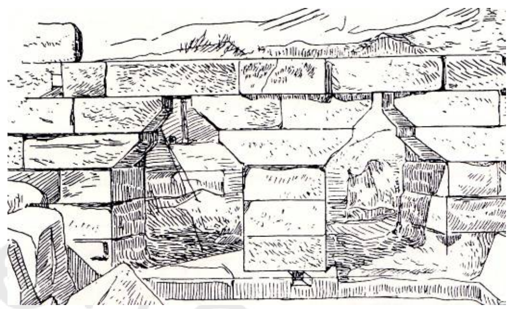

Figure 1. Roman bridge in Selinuntas Sicily (Italy), [by Durm].

Photo 2. Karamagara Bridge in Asia Minor (Turkey).

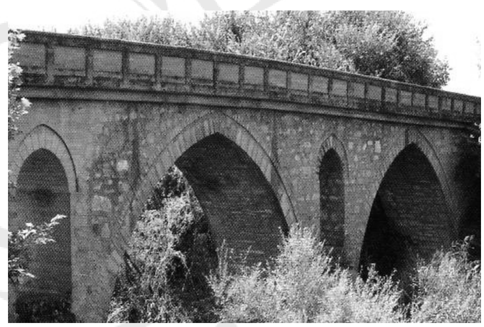

Photo 3. Byzantine Bridge in Moscholourion in Karditsa - Thessaly (Greece).

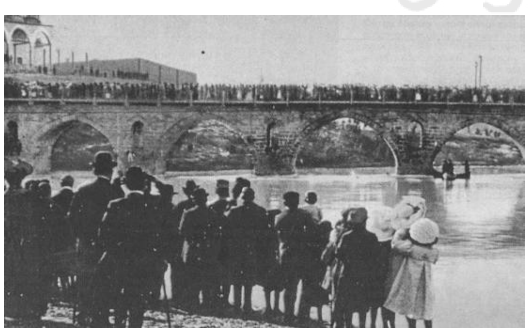

Photo 4. The destroyed large bridge in Larissa - Thessaly (Greece), [Cart postal of G. Velonis].

Photo 5. 15th century bridge in FYROM (Skopje).

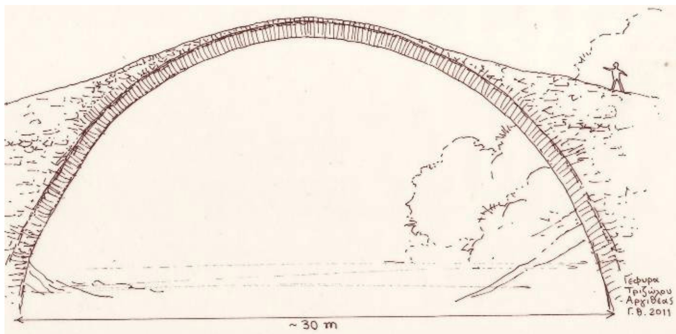

a

b

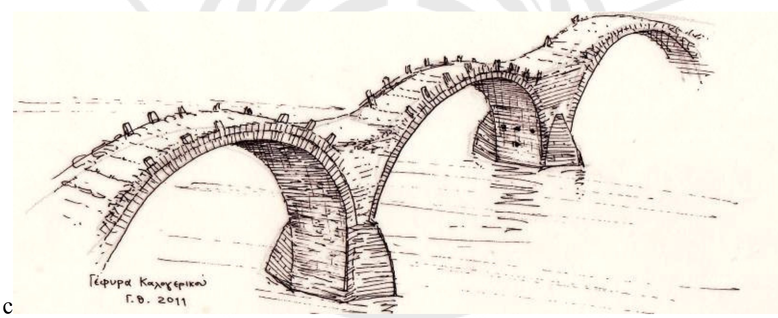

c

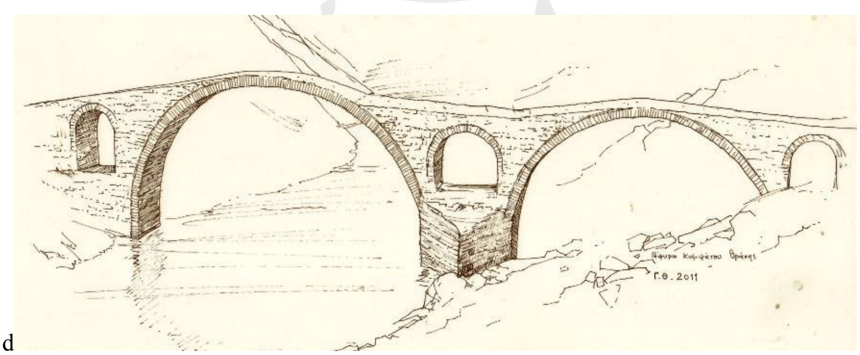

d

Figure 2. Historical bridges of Greece: a. Argithea -Thessaly, b. Karditsomagoula - Thessaly, c. Kalogeriko - Epirus, d. Kompsatos - Thrace. [by Ger. Thomas].

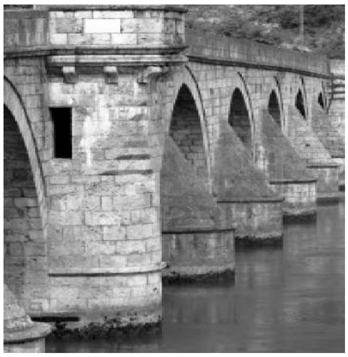
a

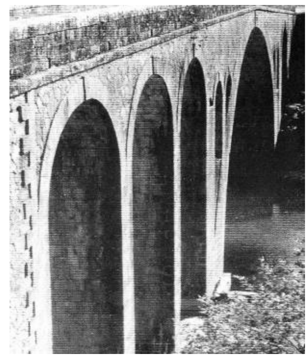
b

Photo 6. Means of rhythm: The linear line-shadow impression created by the arches in multi-arched bridges: *a.* Visegrad - Serbia-Montenegro, b. Karditsa - Greece.

5 CONCLUSIONS

Today, in the beginning of the 21st century, the human interest in monuments of universal cultural heritage is increasing; so knowledge about stone bridges of the past is essential for their conservation and restoration. Humans are the only creatures on earth, who not only managed to bridge the watery chasms of our planet, but also the chaotic gap between earth and space.

The great challenge of the future for humanity is not only the titanic effort to build bridges with the unknown universe, but first and foremost to build durable and beautiful bridges of affection between human souls.

REFERENCES

[1] Petronotis A., "How the stone bridges were constructed", Traditional Architecture, Journal Seven Days, Kathimerini, Vol. 24, pp. 64-73, Athens, 1995.
[2] Bougia P., FM, "Ancient Bridges in Greece and Coastal Asia Minor", Ph.D. Thesis, University of Pennsylvania, 1996.
[3] Albani J., "Byzantine bridges", Traditional Architecture, Journal Seven Days, Kathimerini, Vol. 24, pp. 80-83, Athens, 1995.
[4] Tsotsos G., "Bridges in Macedonia", Thessalonica, 1997.
[5] Mantas S., "Bridges in Epirus", Athens, 1984.
[6] Galerides A., "Stone bridges in the Thessalian plain", Traditional Architecture, Journal Seven Days, Kathimerini, Vol. 24, pp. 105-109, Athens, 1995.
[7] Thomas G., Paulides E., "Restoration of Trichinon Bridge in Livadeia - Boiotia", Technical Study, Athens, 2008.
[8] Orlandos A., "The building material of the ancient Greeks and their means of use", Library of Archaeological Society in Athens, No 37, Second Edition, Athens, 1994.
[9] Vitruvius "De Architectura", Plethron Editions, Second Edition, Athens, 1994.
[10] Michelis P., "Architecture as Art", Foundation of P. & E. Michelis, Athens, 2002.
[11] Wöllflin H., Hart J., "Encyclopaedia of Aesthetics", Oxford Univ. Press, Vol. 4, 1998.
[12] Papanoutsos ., "Aesthetics", Fourth Edition, Athens, 1969.

SEISMIC PERFORMANCE AND REHABILITATION OF OLD STONE BRIDGES IN EARTHQUAKE-PRONE AREAS: THE CASE OF DEBOSSET BRIDGE IN GREECE

Emmanouil Rovithis[1] and Kyriazis Pitilakis[2]

[1] Institute of Engineering Seismology and Earthquake Engineering (ITSAK), Greece
[2] Aristotle University of Thessaloniki, Dept. of Civil Engineering, Greece
e-mail: rovithis@itsak.gr, kpitilak@civil.auth.gr

ABSTRACT: The seismic performance of a monumental stone bridge in an earthquake-prone area of Greece is investigated. The study refers to the DeBosset bridge in Cephalonia comprising of successive arches and stiff block-type abutments founded on deformable soil. The strong 1953 M_s=7.2 earthquake induced severe damages to the bridge that were partially or totally restored with reinforced concrete. The observed damage pattern is adopted to assess transverse load effects based on actual strength properties that were obtained from laboratory tests as part of a recent multidisciplinary project. Extensive geotechnical surveys were also performed providing natural and dynamic characteristics of the foundation soil. The latter are employed in soil response analyses to study soil amplification effects at the bridge site by utilizing a well-documented set of real earthquake recordings. The seismic motion computed at the foundation is then implemented in a stress-based evaluation of the bridge seismic response focusing on foundation soil bearing capacity by means of a 3D finite-element model which encompasses soil-bridge interaction. A set of rehabilitation measures is proposed combining foundation soil improvement and bridge strengthening. Comparison of pre- and post-rehabilitation seismic response of the bridge indicates the favorable effect of the interventions.

KEY WORDS: stone bridges; soil-structure interaction; finite element analysis; foundation soil intervention.

1 INTRODUCTION

Seismic analysis of stone arch bridges exposed to high seismic risk and/or unfavorable environmental conditions poses strong engineering challenges originated from complex geometry, variation in construction materials, strength deterioration and unknown vulnerability of the structure [1-2]. The problem becomes more complex in the case of deformable foundation soil requiring consideration of soil-structure interaction. The latter has been investigated

Photo 1. The DeBosset bridge under study

Photo 2. Out-of-plane collapse of the bridge induced by 1953 earthquake

mainly in the basis of arch wall-to-filling material interaction [3]. However, for stiff massive foundations such as those of stone bridges, soil compliance may possess an equally important role in controlling the dynamic characteristics of the structure and the effective seismic motion imposed at the foundation.

In this study, the seismic response of the historical bridge DeBosset (*Photo 1)* in the earthquake-prone area of Cephalonia (Greece) is analyzed. The investigation is based on in-situ inspections, geotechnical field surveys and laboratory tests performed within a recent multidisciplinary project [4] providing knowledge of mechanical and dynamic properties of the soil-bridge system. The latter were adopted in a stress-based evaluation of the bridge seismic performance focusing on transverse strength and foundation soil bearing capacity by implementing both simplified methods based on fracture line patterns and three-dimensional (3D) finite-element (FE) models. A set of real earthquake recordings is utilized to define seismic motion imposed at the foundation as affected by non-linear soil response. Soil-structure interaction is examined by comparing fixed- and flexible-based bridge response in the realm of elastodynamic considerations. Based on the identified critical zones of structural instability a set of intervention measures is proposed leading to seismic performance upgrade by combining foundation soil improvement and bridge strengthening.

2 DEBOSSET BRIDGE: A BRIEF OVERVIEW

The DeBosset bridge was constructed in 1830 comprising of successive stone arches founded on stiff block-type abutments. The bridge has a total length of 750m and its height varies in the range of 2-4m. The strong 1953 earthquake (M_s=7.2 [5]) induced severe damages to the bridge (*Photo 2)* related to out-of-plane collapse of the arch walls and the filling material [6]. Extensive rehabilitation works were undertaken with reinforced concrete to reconstruct the collapsed parts of the bridge. It is noted that the authentic dry stone material was preserved only in the first two of the fifteen arches in total.

In-situ inspections performed as part of a recent multidisciplinary project [4] revealed significant longitudinal and transverse cracks in the tensile zones, especially under the arches. Furthermore, laboratory tests on construction materials indicated deep corrosion, loss of mass and poor condition of joint mortars for the stone parts and significant loss of strength, delamination and detachment of covering for the concrete parts of the bridge due to detrimental environmental conditions [7].

3 GEOTECHNICAL SURVEY AND LOCAL SITE EFFECTS

Geotechnical and geophysical field surveys were also performed in properly selected sites along the bridge axis (*Fig.1*) including sampling boreholes, SPT tests, Cross-Hole and microtremor array measurements complemented by laboratory tests on soil specimens to provide natural, mechanical and dynamic properties of the foundation soil at the bridge site. Further details can be found in Pitilakis [4]. Synthesis of the above data resulted in the detailed foundation soil profile shown in *Fig.2* in terms of shear wave propagation velocity variation with depth. Of particular interest is the presence of a soft surface silty-clay layer (V_s=140-170m/sec) that has probably contributed to the observed deformation of the bridge. At the level of 35m the stiff sandstone layer (V_s=1000m/sec) was considered as seismic bedrock.

3.1 Soil response analysis

A set of twenty five earthquake events ($3.7<M_s<5.2$, 0.02g<PHGA<0.2g) recorded by an accelerometric station at a close distance from the bridge were utilized to investigate soil amplification effects. The station is operated by ITSAK (www.itsak.gr) as part of the Greek National Network. The selected motions were deconvoluted to define outcrop motion normalized to 0.36g corresponding to the peak bedrock acceleration for the particular seismic zone according to the Greek Aseismic Code [8]. The computed motions were then specified at the base of the bridge foundation soil to perform equivalent-linear soil response analyses utilizing the experimentally derived G-γ-D curves. Three shear wave velocity profiles (i.e. A1-A4, A5-A9 and A10-A15) were analyzed to account for variation in foundation soil properties along the longitudinal axis of the bridge (*Fig.3*). Surface-to-bedrock peak acceleration ratios computed for each seismic motion specified at bedrock are plotted in *Fig.4*. These ratios correspond to a mean horizontal acceleration of 0.6g at ground surface indicating strong amplification effects, especially for deeper soil deposits (i.e. A5-A9, A10-A15). *Fig.5* shows acceleration elastic response spectra obtained at the ground surface of A1-A4 profile. The high-frequency content of the selected recordings is reflected in the mean response spectrum (thick black line) compared with the elastic design spectrum corresponding to soil category D and C according to EAK2000 [8] and EC8 [9] code respectively.

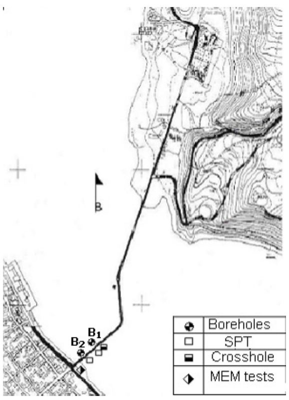

Figure 1. Geotechnical and geophysical field tests.

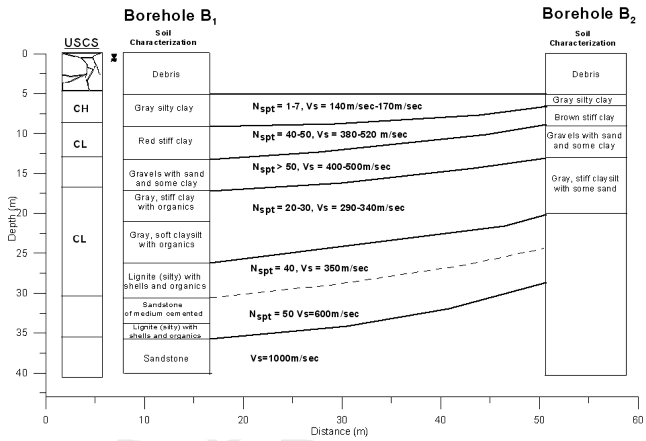

Figure 2. 2D cross-section of the soil profile at the bridge site

4 TRANSVERSE STRUCTURAL STRENGTH

Transverse load effects were investigated by implementing the fracture line method proposed by Erdogmus and Boothby [10]. The method requires the selection of fracture line patterns according to the boundary conditions, geometry and material properties of the bridge. The spandrel wall is considered as a retaining wall of the material fill volume above the arch inducing active-state pressures that may be computed from classical earth pressures theories. Maximum allowable lateral pressure is computed from virtual work principle:

$$\sum W_i = \sum M_f L\theta = \sum (f_r S) L\theta = \sum W_e = \sum Q\theta d \tag{1}$$

where W_i is the internal work by the resisting wall, M_f $(= f_r S)$ is the bending moment producing fracture, f_r being the tensile strength of masonry and S is the section modulus, L is the length of the fracture line and θ stands for the rotation along the fracture line. The external work (W_e) is the product of the resultant force Q and the distance d from the point of application of Q to the facture line.

In the case of DeBosset bridge, the fracture pattern of *Fig. 6* was considered appropriate based on the 1953 earthquake-induced damages. The Mononobe-Okabe approach was adopted to estimate seismic lateral earth pressures utilizing the mean peak ground horizontal acceleration (0.6g) computed from soil response analyses. The tensile strength (f_r) was set at 0.08Mpa due to the poor mortar connection as suggested by the OPCM 3274 [11] norm and verified by the laboratory tests. *Table 1* summarizes the above calculations leading to a safety factor against transverse structural strength at 0.7. The latter denotes detrimental transverse load effects contributing to the generation of longitudinal cracks in the stone arch barrels in agreement with in-situ observations.

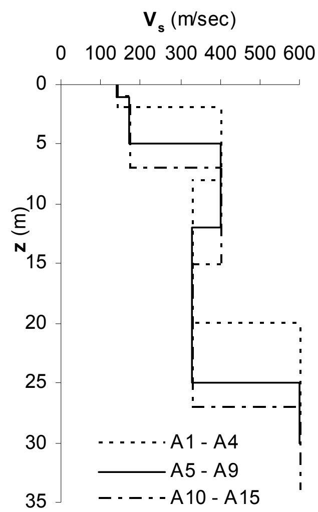

Figure 3. V_s models considered for soil amplification study

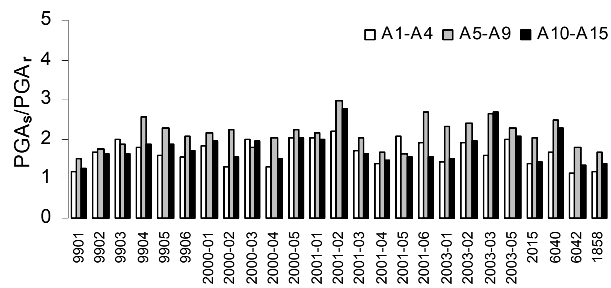

Figure 4. Surface-to-bedrock PGA ratios computed from soil response analysis of the Debosset site (The abscissa shows the code-names of the 25 seismic recordings)

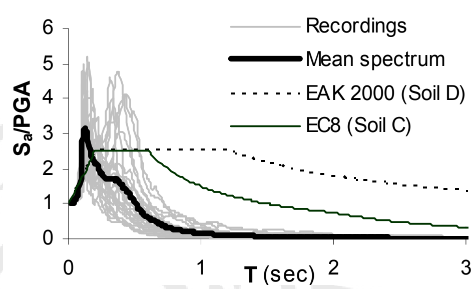

Figure 5. Normalized response spectra computed from soil response analysis of A1-A4 model

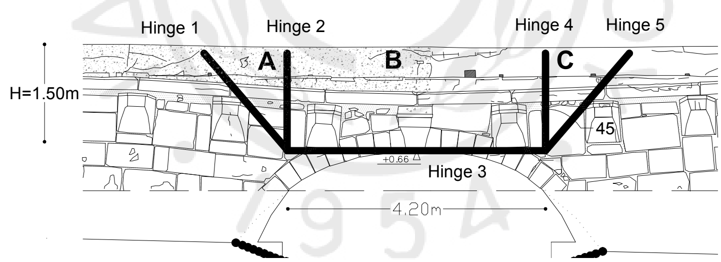

Figure 6. Fracture line pattern considered for transverse load effects

5 BEARING CAPACITY OF THE FOUNDATION SOIL

The structural stability of the bridge was further examined in terms of foundation soil bearing capacity by means of a 3D finite element model. To minimize computational cost a representative part of the bridge was modelled having proper boundary conditions to obtain equivalent modal characteristics with the actual bridge [12]. Cubic elements were employed to reproduce the actual geometry of the bridge assuming perfect bonding. However, mean elastic material properties (i.e E=15GPa, $\rho=2t/m^3$) were adopted based on laboratory test results [7] as a modelling approximation of cracked sections and material

Table 1. Assessment of transverse load effects based on the fracture line method

Panel	Hinge	L (m)	θ	M_f (KNm/m)		$W_i=M_fL\theta$ (KNm)
A	1	2.12	$\theta\sqrt{2}$	4.32		13.81θ
	2	1.5	θ	4.32		$6.91\ \theta$
B	3	4.2	θ	4.32		$18.14\ \theta$
C	4	1.5	θ	4.32		$6.91\ \theta$
	5	2.12	$\theta\sqrt{2}$	4.32		$13.81\ \theta$
					Total ΣW_i	$\mathbf{57.01\theta}$
Panel	L (m)	H (m)	θ	Q (KN)	d (m)	$W_e=Qd\ \theta$ (KNm)
A	1.5	1.5	$\theta\sqrt{2}$	$0.375q_{max}$	0.75	$0.397\ q_{max}\ \theta$
B	4.2	1.5	θ	$3.15q_{max}$	0.5	$1.58\ q_{max}\ \theta$
C	1.5	1.5	$\theta\sqrt{2}$	$0.375q_{max}$	0.75	$0.397\ q_{max}\ \theta$
					Total ΣW_e	$2.37\ q_{max}\ \theta$
				Maximum allowable pressure $\boldsymbol{q_{max}}$ (KPa) = $\Sigma W_i/\Sigma W_e$		24.05
Mononobe-Okabe method						
H (m)	k_h/g k_v/g	Fill internal friction φ(°)	ψ (°)	Seismic coeff. K_{AE}	Total active thrust P_{AE} (KN/m)	Normalized active thrust $\mathbf{q_{AE}}$ (KPa)
1.5	0.6 0.25	37	38.7	1.738	25.2	**33.6**
		Safety factor against tranverse failure $\mathbf{SFs=q_{max}/q_{AE}}$				**0.71**

inhomogeneity [11]. Modal analysis of the fixed-base bridge model revealed a first mode natural period at 0.03sec with a dominant translational component in the transverse direction. Flexible-base models were then analyzed to evaluate SSI effects by introducing spring supports at the abutments base computed from pertinent analytical formulas of surface footings [13]. As expected, soil compliance modified substantially the bridge modal response leading to a remarkably increased effective natural period of the system at 1.68Hz. Having identified the vibrational characteristics of the bridge, a series of response spectrum analyses were performed to estimate the stress field under the abutments. Mean acceleration response spectra obtained from soil response analysis (i.e A1-A4, A5-A9 and A10-A14) and code-defined elastic spectra (EAK, EC8) were consecutively specified at the base of the bridge model as a conservative loading in the transverse direction [6]. The numerical results were reviewed in terms of a mean vertical stress developed under the abutment area.

On the other hand, bearing capacity of the foundation soil under seismic loading was computed from the available geotechnical data according to EAK2000 [8]. Safety factors in the form of bearing capacity to mean stress ratios are plotted in *Fig.7a* and *7b* for fixed- and flexible-base (SSI) conditions respectively. Each bar refers to a different spectrum loading as mentioned above. It is observed that safety factors related to bearing capacity of the foundation are below unity indicating a critical section of the bridge.

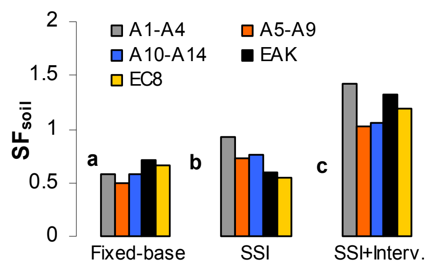

Figure 7. Safety factor against bearing capacity of the foundation soil

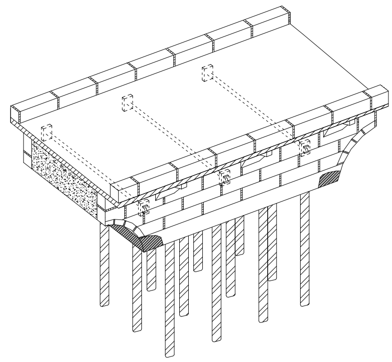

Figure 8. Proposed rehabilitation measures

6 REHABILITATION MEASURES

Based on the identified zones of inadequate strength, a set of rehabilitation measures was designed combining foundation soil improvement and bridge strengthening (*Fig.8*). The basic concepts of the proposed interventions are:

- Maintenance of the monumental nature of the bridge by partial or total restoration of the detached stones and the concrete facades of the bridge with stone elements compatible to the authentic material.
- Increase of the transverse strength with highly-resistant mortar connecting the new stone elements and closely spaced lateral tendons contributing to the monolithic behavior of the structure under lateral seismic loading.
- Improvement of the foundation soil by a group of slender piles (micropiles) designated to increase the corresponding safety factor above unity.

Particular emphasis was placed on the design of micropiles as an additional bearing mechanism of the superstructure loads transmitted to the foundation. The above design concept resulted in a 4x5 pilegroup (D=0.25m, L=15m) embedded at the foundation soil of each bridge abutment. A new series of response spectrum analyses was performed taking into account the group of micropiles as a set of point springs computed from single-pile analytical solutions [14] since pile-to-pile interaction was considered negligible due to the large normalized pile spacing (S/D=8). Safety factors related to bearing capacity of the soil-micropiles system are plotted in *Fig.7c* in the same spirit as in the initial SSI system mentioned above. The favorable effect of the interventions reflected in the increase of the safety factors above unity is evident.

7 CONCLUSIONS

An integrated approach for evaluating the seismic performance of a historical stone bridge in an earthquake-prone area of Greece was presented. The results indicate that:

- Apart from structural inspection and testing of old stone bridges, knowledge of foundation soil conditions may be equally important allowing study of soil amplification effects on the seismic motion imposed at the structure.
- Soil-structure interaction is expected to modify substantially the vibrational characteristics of a massive stone bridge founded on deformable soil that should be accounted for in analysis or design of rehabilitation measures.
- Inadequate transverse strength of old stone bridges was identified as a critical parameter related to out-of-plane failure mechanisms due to excessive lateral pressures on the spandrel walls.
- For a strongly deteriorated system rehabilitation measures as the ones proposed in this study aiming at foundation soil improvement and bridge strengthening may be an efficient solution for seismic performance upgrade of old stone bridges.

REFERENCES

[1] Page, J, "Repair and strengthening of masonry arches" , *Proc. IABSE Symposium on Structural Preservation of the Architectural Heritage*, Rome, 1993.

[2] Proske, D, and Van Gelder, P, *Safety of Historical Stone Arch Bridges*, Springer Publications, 2009.

[3] Cavicchi, A,. and Gambarotta, L, "Collapse analysis of masonry bridges taking into account arch -fill interaction", Engineering Structures, Vol. 27, pp. 605-615, 2005.

[4] Pitilakis, K, "Restoration and Consolidation of the DeBosset bridge in Argostoli, Cephalonia', Final Report, Laboratory of soil mechanics and Earthquake Geotechnical Engineering, A.U.T.H., 2006.

[5] Papazachos, B, *Earthquakes of Greece*, Ziti publications, Thessaloniki, 1997.

[6] Rota, M, Pecker, A, Bolognini, D, and Pinho, R, "A methodology for seismic vulnerability of masonry arch bridge walls", Journal of Earthquake Engineering, Vol. 9, Special Issue 2, pp. 331-353, 2005.

[7] Papayianni, I, Pachta, V, and Alexiou, A, "Study of the constructing materials, techniques and pathology symptoms of the stone bridge DeBosset in Kefalonia", *Proc. 5th International Conference on Arch Bridges,* pp. 147-154, Madeira, 2007.

[8] EAK2000, Greek Seismic Code, OASP, Athens, 1999

[9] CEN, European Committee for Standardization (2002) "prEN 1998-5: Eurocode 8: Design of Structures for Earthquake Resistance, Part 5: Foundations, Retaining structures and Geotechnical Aspects, Brussels.

[10] Erdogmus, E, and Boothby, T, "Strength of spandrel walls in masonry arch bridges", Journal of Transportation Research Board, Vol. 1892, pp. 47-55, 2004.

[11] OPCM 3274. Ordinanza del Presidente del Consiglio dei Ministri n. 3274 del 20 Marzo 2003: Primi elementi in materia di criteri generali per la classificazione sismica del territorio nazionale e di normative tecniche per le costruzioni in zona sismica, 2005 (ANNEX 11.D).

[12] Rovithis, E, Pitilakis, K, and Apostolidis, P, "Rehabilitation of the historic bridge De-Bosset in Argostoli", Proc. 1st Hellenic Conference on restoration of monuments, 2006

[13] Gazetas, G, "Formulas and charts for impedance functions of surface and embedded foundation", Journal of Geotechnical Engineerning, ASCE, Vol. 177, pp. 1363-1381, 1991.

[14] Pender, M, J, "Aseismic Pile Foundation Design Analysis", Bulletin of the New Zealand National Society on Earthquake Engineering, Vol. 26, pp. 49-161, 1993.

TOPIC 3

Design Methods

MOVING LOADS ON MULTI-SPAN BRIDGES

Theodore G. Konstantakopoulos[1], Ioannis G. Raftoyiannis[2]
and George T. Michaltsos[3]

[1,2,3] National Technical University of Athens, Dept. of Civil Engineering, Greece
e-mail: theokons@central.ntua.gr, rafto@central.ntua.gr, michalts@central.ntua.gr

ABSTRACT: The present paper concludes via an analytical method to conversion formulae for determining the eigenfrequencies and eigenmodes of multi-span continuous beams with spans of different lengths and bending rigidities. The rigorous determination of eigenfrequencies and eigenmodes allows us to focus on the derivation of the time function for the forced vibrating beam subjected to the action of moving loads.

KEY WORDS: conversion formulae, continuous beams, moving loads

1 INTRODUCTION

Despite the extensive bibliography on the vibrations of single-span beams, the dynamic behavior of continuous (multi-span) beams has not been thoroughly studied since the solution of the problem becomes evidently more cumbersome as the number of beam spans increases. There are two commonly used approaches for computing the eigenfrequencies of continuous beams. The F.E.Method and the analytical one. The precision of the FEM requires a very large number of dynamic elements, while the analytical one concludes to extremely great matrixes for the solution of the eigenvalue problem. The corresponding bibliography on this topic is rather poor. One must refer Dmitrief [1], who presented a method for determining the dynamic deflections of multi-span beams with equal spans, while other authors used the classical Ritz method [2], or the method of the eigenfunctions expansion [3], or an extension of the complex mode superposition [4], or the Green's functions [5]. The present work concludes through an analytical method to conversion formulae for determining the eigenfrequencies and eigenfunctions of multi-span continuous beams with spans of different lengths and rigidities. The dynamic response of a continuous beam subjected to a load moving with constant velocity is thoroughly studied. The analysis is carried out by the modal superposition method.

2 MATHEMATICAL FORMULATION

Let us consider the multi-span beam of Fig. 1.The continuous beam consists from ν spans with lengths ℓ_i , cross-section areas A_i, moments of inertia I_i and masses per unit length m_i, with i=1, 2, …,ν.

2.1 The free vibrating beam

Neglecting the influence of longitudinal motion and damping, the equations of motion of the freely vibrating beam are:

$$EI_i w_i''''(x_i,t) + c\,\dot{w}(x_i,t) + m_i \ddot{w}_i(x_i,t) = 0 \;,\quad (i=1,2,\cdots\nu) \tag{1}$$

where c is the damping coefficient.

Searching for a solution of separate variables: $w_i(x_i,t) = X_i(x_i)\cdot T(t)$

we conclude to the following equations:

$$EI_i X_i''''(x_i) - m_i\omega_i^2 X_i(x_i) = 0$$

$$\ddot{T}_i(t) + 2\beta_i \dot{T}_i(t) + \omega_i^2 T_i(t) = 0\,,\quad \text{where}:\ \beta_i = \frac{c}{2m_i}\,,\ \text{and}\ i=1,2,\cdots,\nu \tag{2a,b,c}$$

The solution of equation (2a) is given by the following relation:

$$X_i(x_i) = A_i \sin k_i x_i + B_i \cos k_i x_i + C_i \sinh k_i x_i + D_i \cosh k_i x_i \quad,\quad i=1,2,\cdots,\nu \tag{3}$$

By setting:

$$k_i^4 = \frac{m_i\omega^2}{EI_i},\quad c_i^4 = \frac{m_i I_1}{I_i m_1},\quad k_i = c_i k,\quad k = k_1,\quad d_i = \frac{I_i}{I_1}\quad i=1,2,\cdots,\nu \tag{4}$$

eq(3) becomes:

$$X_i(x_i) = A_i \sin c_i k\, x_i + B_i \cos c_i k\, x_i + C_i \sinh c_i k\, x_i + D_i \cosh c_i k\, x_i \quad,\quad i=1,2,\cdots,\nu \tag{5}$$

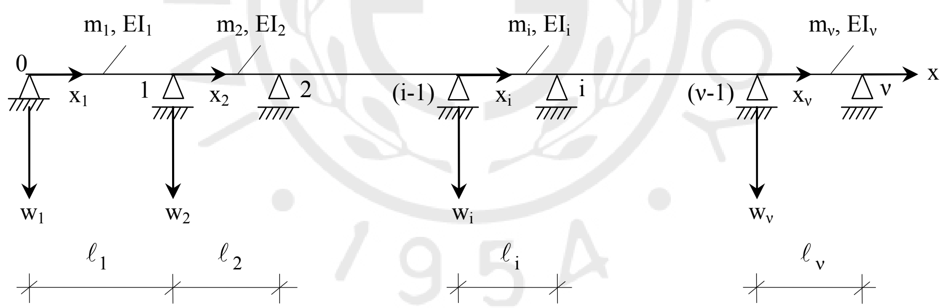

Figure 1. Geometry and sign convention of a ν-span continuous beam

The corresponding boundary conditions for each span are:

$$1^{st}:\quad X_1(0)=0,\quad X_1(\ell_1)=0,\quad X_1''(0)=0,\quad X_1''(\ell_1)=d_2X_2''(0),\quad X_1'(\ell_1)=X_2'(0)$$

$$i^{th}:\quad d_{i-1}X_{i-1}''(\ell_{i-1})=d_iX_i''(0),\quad X_{i-1}'(\ell_{i-1})=X_i'(0),\quad X_i(0)=0,\quad X_i(\ell_i)=0,\quad d_iX_i''(\ell_i)=d_{i+1}X_{i+1}(0),\quad X_i'(\ell_i)=X_{i+1}'(0) \tag{6}$$

$$\nu^{th}:\quad d_{\nu-1}X_{\nu-1}''(\ell_{\nu-1})=d_\nu X_\nu''(0),\quad X_{\nu-1}'(\ell_{\nu-1})=X_\nu'(0),\quad X_\nu(0)=0,\quad X_\nu(\ell_\nu)=0,\quad X_\nu''(\ell_\nu)=0$$

The above conditions provide the following linear homogeneous system without second member:

$$\begin{vmatrix} |\theta_1| & 0 & 0 & \cdots & 0 & 0 & 0 & \cdots & 0 & 0 \\ |\delta_1| & |\theta_2| & 0 & \cdots & 0 & 0 & 0 & \cdots & 0 & 0 \\ 0 & |\delta_2| & |\theta_3| & \cdots & 0 & 0 & 0 & \cdots & 0 & 0 \\ \cdots & \cdots & \cdots & \cdots & \cdots & \cdots & \cdots & \cdots & \cdots & \cdots \\ 0 & 0 & 0 & \cdots & |\delta_{i-1}| & |\theta_i| & 0 & \cdots & 0 & 0 \\ 0 & 0 & 0 & \cdots & |\delta_i| & |\theta_{i+1}| & 0 & \cdots & 0 & 0 \\ \cdots & \cdots & \cdots & \cdots & \cdots & \cdots & \cdots & \cdots & \cdots & \cdots \\ 0 & 0 & 0 & \cdots & 0 & 0 & 0 & \cdots & |\delta_\nu| & |\theta_\nu| \\ 0 & 0 & 0 & \cdots & 0 & 0 & 0 & \cdots & 0 & |\delta_\nu| \end{vmatrix} \begin{vmatrix} A_1 \\ B_1 \\ C_1 \\ D_1 \\ \cdots \\ A_i \\ B_i \\ C_i \\ D_i \\ \cdots \\ A_\nu \\ B_\nu \\ C_\nu \\ D_\nu \end{vmatrix} = 0 \tag{7}$$

2.2 Conversion formulae for eigenfrequencies

In order for the system to have non-trivial solutions, the determinant of the coefficients of the unknowns of the above system (7) must be equal to zero:

$$|\Delta_\nu| = 0 \tag{8}$$

with:

$$|\theta_1| = |\,0 \; -1 \;\; 0 \;\; 1\,|\,, \quad |\delta_1| = \begin{vmatrix} 0 & 1 & 0 & 1 \\ \sin k\ell_1 & \cos k\ell_1 & \sinh k\ell_1 & \cosh k\ell_1 \\ -\sin k\ell_1 & -\cos k\ell_1 & \sinh k\ell_1 & \cosh k\ell_1 \\ \cos k\ell_1 & -\sin k\ell_1 & \cosh k\ell_1 & \sinh k\ell_1 \end{vmatrix}, \quad |\theta_2| = \begin{vmatrix} 0 & 0 & 0 & 0 \\ 0 & 0 & 0 & 0 \\ 0 & d_2c_2^2 & 0 & -d_2c_2^2 \\ -c_2 & 0 & -c_2 & 0 \end{vmatrix} \tag{9a,b,c}$$

$$|\delta_i| = \begin{vmatrix} 0 & 1 & 0 & 1 \\ \sin c_i k\ell_i & \cos c_i k\ell_i & \sinh c_i k\ell_i & \cosh c_i k\ell_i \\ -d_i c_i^2 \sin c_i k\ell_i & -d_i c_i^2 \cos c_i k\ell_i & d_i c_i^2 \sinh c_i k\ell_i & d_i c_i^2 \cosh c_i k\ell_i \\ c_i \cos c_i k\ell_i & -c_i \sin c_i k\ell_i & c_i \cosh c_i k\ell_i & c_i \sinh c_i k\ell_i \end{vmatrix} \tag{9d}$$

$$|\theta_i| = \begin{vmatrix} 0 & 0 & 0 & 0 \\ 0 & 0 & 0 & 0 \\ 0 & d_i c_i^2 & 0 & -d_i c_i^2 \\ -c_i & 0 & -c_i & 0 \end{vmatrix} \tag{9e}$$

$$|\delta_{\nu-1}| = \begin{vmatrix} 0 & 1 & 0 & 1 \\ \sin c_{\nu-1} k\ell_{\nu-1} & \cos c_{\nu-1} k\ell_{\nu-1} & \sinh c_{\nu-1} k\ell_{\nu-1} & \cosh c_{\nu-1} k\ell_{\nu-1} \\ -d_{\nu-1} c_{\nu-1}^2 \sin c_{\nu-1} k\ell_{\nu-1} & -d_{\nu-1} c_{\nu-1}^2 \cos c_{\nu-1} k\ell_{\nu-1} & d_{\nu-1} c_{\nu-1}^2 \sinh c_{\nu-1} k\ell_{\nu-1} & d_{\nu-1} c_{\nu-1}^2 \cosh c_{\nu-1} k\ell_{\nu-1} \\ c_{\nu-1} \cos c_{\nu-1} k\ell_{\nu-1} & -c_{\nu-1} \sin c_{\nu-1} k\ell_{\nu-1} & c_{\nu-1} \cosh c_{\nu-1} k\ell_{\nu-1} & c_{\nu-1} \sinh c_{\nu-1} k\ell_{\nu-1} \end{vmatrix} \tag{9f}$$

$$|\theta_\nu| = \begin{vmatrix} 0 & 0 & 0 & 0 \\ 0 & 0 & 0 & 0 \\ 0 & d_\nu c_\nu^2 & 0 & -d_\nu c_\nu^2 \\ -c_\nu & 0 & -c_\nu & 0 \end{vmatrix}, \quad |\delta_\nu| = \begin{vmatrix} 0 & 1 & 0 & 1 \\ \sin c_\nu k\ell_\nu & \cos c_\nu k\ell_\nu & \sinh c_\nu k\ell_\nu & \cosh c_\nu k\ell_\nu \\ -\sin c_\nu k\ell_\nu & -\cos c_\nu k\ell_\nu & \sinh c_\nu k\ell_\nu & \cosh c_\nu k\ell_\nu \end{vmatrix} \quad \text{(9g,h)}$$

Expanding the matrix of eq(8), we determine the following conversion formulae:

$$|\Delta_\nu| = U_\nu \cdot |\widetilde{\Delta}_{\nu-1}| + V_\nu \cdot |\Delta_{\nu-1}|, \quad |\widetilde{\Delta}_\nu| = V_\nu \cdot |\widetilde{\Delta}_{\nu-1}| + W_\nu \cdot |\Delta_{\nu-1}| \quad \text{(10a,b)}$$

with:

$$\begin{aligned} U_\nu &= 4\, d_\nu c_{\nu-1} c_\nu^2 \cdot \sin c_\nu k\ell_\nu \cdot \sinh c_\nu k\ell_\nu \\ V_\nu &= 2\, d_{\nu-1} c_{\nu-1}^2 \; c_\nu (\sin c_\nu k\ell_\nu \cdot \cosh c_\nu k\ell_\nu - \cos c_\nu k\ell_\nu \cdot \sinh c_\nu k\ell_\nu) \\ W_\nu &= 2\, c_{\nu-1} c_\nu (1 - d_{\nu-1} c_{\nu-1} \cos c_\nu k\ell_\nu \cdot \cosh c_\nu k\ell_\nu) \end{aligned} \quad \text{(10c)}$$

where:

$$|\Delta_\nu| = \begin{vmatrix} |\theta_1| & 0 & 0 & \cdots & 0 & 0 & 0 & \cdots & 0 & 0 \\ |\delta_1| & |\theta_2| & 0 & \cdots & 0 & 0 & 0 & \cdots & 0 & 0 \\ 0 & |\delta_2| & |\theta_3| & \cdots & 0 & 0 & 0 & \cdots & 0 & 0 \\ \cdots & & & & & & & & & \\ 0 & 0 & 0 & \cdots & |\delta_{i-1}| & |\theta_i| & 0 & \cdots & 0 & 0 \\ 0 & 0 & 0 & \cdots & |\delta_i| & |\theta_{i+1}| & 0 & \cdots & 0 & 0 \\ \cdots & & & & & & & & & \\ 0 & 0 & 0 & \cdots & 0 & 0 & 0 & \cdots & |\delta_\nu| & |\theta_\nu| \\ 0 & 0 & 0 & \cdots & 0 & 0 & 0 & \cdots & 0 & |\widetilde{\delta}_\nu| \end{vmatrix} \quad \text{(11a)}$$

$$|\widetilde{\delta}_\nu| = \begin{vmatrix} 0 & 1 & 0 & 1 \\ \sin c_\nu k\ell_\nu & \cos c_\nu k\ell_\nu & \sinh c_\nu k\ell_\nu & \cosh c_\nu k\ell_\nu \\ \cos c_\nu k\ell_\nu & -\sin c_\nu k\ell_\nu & \cosh c_\nu k\ell_\nu & \sinh c_\nu k\ell_\nu \end{vmatrix} \quad \text{(11b)}$$

$$|\Delta_1| = 4 \sin k\ell_1 \sinh k\ell_1 \quad |\widetilde{\Delta}_1| = 2 \sin k\ell_1 \cosh k\ell_1 - 2 \cos k\ell_1 \sinh k\ell_1 \quad \text{(11c,d)}$$

2.3 Conversion formulae for shape functions

Let us consider now the equations related to the span "i".

$$\begin{aligned} & c_i A_i + c_i C_i = G_{i-1} \\ & A_i \sin c_i k\ell_i + B_i \cos c_i k\ell_i + C_i \sinh c_i k\ell_i + D_i \cosh c_i k\ell_i = 0 \\ & -d_i c_i^2 A_i \sin c_i k\ell_i - d_i c_i^2 B_i \cos c_i k\ell_i + d_i c_i^2 C_i \sinh c_i k\ell_i + d_i c_i^2 D_i \cosh c_i k\ell_i = d_{i+1} c_{i+1}^2 (D_{i+1} - B_{i+1}) \\ & B_i + D_i = 0 \qquad \text{for } i = 2 \text{ to } (\nu - 1) \end{aligned}$$

(12a,b,c,d)

where we put:

$$G_i = (A_i \cos c_i k\ell_i - B_i \sin c_i k\ell_i + C_i \cosh c_i k\ell_i + D_i \sinh c_i k\ell_i) c_i \quad \text{(13)}$$

Because of (12d), that is valid also for (i-1), the above system can be written:

$$
\begin{aligned}
& c_i A_i + c_i C_i = G_{i-1} \\
& B_i + D_i = 0 \\
& A_i \sin c_i k\ell_i + B_i \cos c_i k\ell_i + C_i \sinh c_i k\ell_i + D_i \cosh c_i k\ell_i = 0 \\
& -d_i c_i^2 A_i \sin c_i k\ell_i - d_i c_i^2 B_i \cos c_i k\ell_i + d_i c_i^2 C_i \sinh c_i k\ell_i + d_i c_i^2 D_i \cosh c_i k\ell_i = -2\, d_{i+1} c_{i+1}^2 B_{i+1}
\end{aligned}
\tag{14a,b,c,d}
$$

Solving the above system we find:

$$
\begin{aligned}
A_i &= a_i G_{i-1} + \tilde{a}_i B_{i+1} \quad , \quad B_i = b_i G_{i-1} + \tilde{b}_i B_{i+1} \\
C_i &= \gamma_i G_{i-1} + \tilde{\gamma}_i B_{i+1} \quad , \quad D_i = \delta_i G_{i-1} + \tilde{\delta}_i B_{i+1}
\end{aligned}
\tag{15a,b,c,d}
$$

where:

$$
\begin{aligned}
& a_i = \frac{\cos c_i k\ell_i \sinh c_i k\ell_i}{c_i \Lambda_i} \quad , \quad \tilde{a}_i = \frac{-d_{i+1} c_{i+1}^2 (\cosh c_i k\ell_i - \cos c_i k\ell_i)}{d_i c_i^2 \Lambda_i} \\
& b_i = \frac{-\sin c_i k\ell_i \sinh c_i k\ell_i}{c_i \Lambda_i} \quad , \quad \tilde{b}_i = \frac{d_{i+1} c_{i+1}^2 (\sinh c_i k\ell_i - \sin c_i k\ell_i)}{d_i c_i^2 \Lambda_i} \\
& \gamma_i = \frac{-\sin c_i k\ell_i \cosh c_i k\ell_i}{c_i \Lambda_i} \quad , \quad \tilde{\gamma}_i = \frac{d_{i+1} c_{i+1}^2 (\cosh c_i k\ell_i - \cos c_i k\ell_i)}{d_i c_i^2 \Lambda_i} \\
& \delta_i = \frac{\sin c_i k\ell_i \sinh c_i k\ell_i}{c_i \Lambda_i} \quad , \quad \tilde{\delta}_i = \frac{-d_{i+1} c_{i+1}^2 (\sinh c_i k\ell_i - \sin c_i k\ell_i)}{d_i c_i^2 \Lambda_i} \\
& \Lambda_i = \cos c_i k\ell_i \sinh c_i k\ell_i - \sin c_i k\ell_i \cosh c_i k\ell_i
\end{aligned}
\tag{16a,b,c,d,e}
$$

We have now to determine the conversion formulae for G_i. From the system:

$$
\begin{aligned}
& B_1 = D_1 = 0 \\
& A_1 \sin k\ell_1 + C_1 \sinh k\ell_1 = 0 \\
& -A_1 \sin k\ell_1 + C_1 \sinh k\ell_1 = -2\, d_2 c_2^2 B
\end{aligned}
$$

we find that:

$$
\begin{aligned}
& A_1 = \frac{d_2 c_2^2}{\sin k\ell_1} B_2 \ , \quad C_1 = -\frac{d_2 c_2^2}{\sinh k\ell_1} B_2 \\
& G_1 = d_2 c_2^2 (\cot k\ell_1 - \coth k\ell_1) B_2 = \varepsilon_1 B_2 \ , \quad \text{where}: \varepsilon_1 = d_2 c_2^2 (\cot k\ell_1 - \coth k\ell_1)
\end{aligned}
\tag{17a,b,c,d}
$$

In general, we set: $G_i = \varepsilon_i B_{i+1}$ (18)

Then, because of (15b) we get:

$B_i = b_i \cdot \varepsilon_{i-1} \cdot B_i + \tilde{b}_i \cdot B_{i+1}$ and thus $B_i = \dfrac{\tilde{b}_i}{1 - b_i \cdot \varepsilon_{i-1}} B_{i+1}$ or finally:

$$
B_i = \zeta_i \cdot B_{i+1} \quad , \quad \text{where}: \ \zeta_i = \frac{\tilde{b}_i}{1 - b_i \cdot \varepsilon_{i-1}}
\tag{19a,b}
$$

Therefore, eqs(15) are written:

$$
\begin{aligned}
A_i &= (a_i \cdot \varepsilon_{i-1} \cdot \zeta_i + \tilde{a}_i)\, B_{i+1} \\
B_i &= (b_i \cdot \varepsilon_{i-1} \cdot \zeta_i + \tilde{b}_i)\, B_{i+1} \\
C_i &= (\gamma_i \cdot \varepsilon_{i-1} \cdot \zeta_i + \tilde{\gamma}_i)\, B_{i+1} \\
D_i &= (\delta_i \cdot \varepsilon_{i-1} \cdot \zeta_i + \tilde{\delta}_i)\, B_{i+1}
\end{aligned}
\tag{20a,b,c,d}
$$

Introducing eq(20) into eq(13), we get:

$$G_i = [c_i(a_i\varepsilon_{i-1}\zeta_i + \tilde{a}_i)\cos c_i k\ell_i - c_i(b_i\varepsilon_{i-1}\zeta_i + \tilde{b}_i)\sin c_i k\ell_i + c_i(\gamma_i\varepsilon_{i-1}\zeta_i + \tilde{\gamma}_i)\cosh c_i k\ell_i + c_i(\delta_i\varepsilon_{i-1}\zeta_i + \tilde{\delta}_i)\sinh c_i k\ell_i]\cdot B_{i+1} \quad (21)$$

and:

$$\varepsilon_i = c_i(a_i\varepsilon_{i-1}\zeta_i + \tilde{a}_i)\cos c_i k\ell_i - c_i(b_i\varepsilon_{i-1}\zeta_i + \tilde{b}_i)\sin c_i k\ell_i + c_i(\gamma_i\varepsilon_{i-1}\zeta_i + \tilde{\gamma}_i)\cosh c_i k\ell_i + c_i(\delta_i\varepsilon_{i-1}\zeta_i + \tilde{\delta}_i)\sinh c_i k\ell_i \quad (22)$$

with $\varepsilon_1 = d_2 c_2^2(\cot k\ell_1 - \coth k\ell_1)$

Finally, from the system

$$B_v + D_v = 0$$
$$A_v \sin c_v k\ell_v + B_v \cos c_v k\ell_v + C_v \sinh c_v k\ell_v + D_v \cosh c_v k\ell_v = 0$$
$$-A_v \sin c_v k\ell_v - B_v \cos c_v k\ell_v + C_v \sinh c_v k\ell_v + D_v \cosh c_v k\ell_v = 0$$

we determine the coefficients A_v and B_v as follows:

$$A_v = -B_v \cdot \cot c_v k\ell_v$$
$$C_v = B_v \cdot \coth c_v k\ell_v \quad (23)$$
$$D_v = -B_v$$

Hence, every coefficient is expressed as a function of B_v. Constant B_v is a random number that can take any value. Usually, we set B_v=1.
Thus, we get the following relations:

Span 1: $$X_1 = d_2 c_2^2\, \zeta_2\zeta_3\cdots\zeta_{v-1}\left(\frac{1}{\sin k\ell_1}\sin kx_1 - \frac{1}{\sinh k\ell_1}\sinh kx_1\right) \quad (24a)$$

Span i=2 to v-1: $$X_i = \zeta_{i+1}\zeta_{i+2}\cdots\zeta_{v-1}[(a_i\varepsilon_{i-1}\zeta_i + \tilde{a}_i)\sin c_i k\ell_i + (b_i\varepsilon_{i-1}\zeta_i + \tilde{b}_i)\cos c_i k\ell_i + (\gamma_i\varepsilon_{i-1}\zeta_i + \tilde{\gamma}_i)\sinh c_i k\ell_i + (\delta_i\varepsilon_{i-1}\zeta_i + \tilde{\delta}_i)\cosh c_i k\ell_i] \quad (24b)$$

Span v: $$X_v = -\cot c_v k\ell_v \sin c_v kx_v + \cos c_v kx_v + \coth c_v k\ell_v \cdot \sinh c_v kx_v - \cos c_v kx_v \quad (24c)$$

2.4 The forced vibrating beam

The equation of motion of a beam under the action of a moving load is: $EIw''''(x,t) + cw(x,t) + m\ddot{w}(x,t) = P\cdot\delta(x - \upsilon t)$. When the load P crosses the i span, in time interval $\sum_1^{i-1}\frac{\ell_i}{\upsilon} \le t \le \sum_1^{i}\frac{\ell_i}{\upsilon}$, the following equations are valid:

$$EI_1 w_1''''(x_1,t_i) + cw_1(x_1,t_i) + m_1\ddot{w}_1(x_1,t_i) = 0$$
$$\cdots\cdots\cdots$$
$$EI_{i-1} w_{i-1}''''(x_{i-1},t_i) + cw_{i-1}(x_{i-1},t_i) + m_{i-1}\ddot{w}_{i-1}(x_{i-1},t_i) = 0$$
$$EI_1 w_i''''(x_i,t_i) + cw_i(x_i,t_i) + m_i\ddot{w}_i(x_i,t_i) = P\cdot\delta(x_i - \upsilon t_i)$$
$$EI_{i+1} w_{i+1}''''(x_{i+1},t_i) + cw_{i+1}(x_{i+1},t_i) + m_{i+1}\ddot{w}_{i+1}(x_{i+1},t_i) = 0 \quad (25)$$
$$\cdots\cdots\cdots$$
$$EI_v w_v''''(x_v,t_i) + cw_v(x_v,t_i) + m_v\ddot{w}_v(x_v,t_i) = 0$$

where: $t_i = t - \sum_1^{i-1}\frac{\ell_i}{\upsilon}$ and δ is the Dirac unit function

We are searching for a solution under the form:

$$w_i(x_i, t) = \sum_n (X_{in} T_n) \quad , \quad (i = 1, 2, \cdots, \nu) \tag{26}$$

Thus, eqs(25) become:

$$\begin{aligned} & EI_j \sum_n X''''_{jn} T_{in} + c \sum_n X_{jn} \dot{T}_{in} + m_j \sum_n X_{jn} \ddot{T}_{in} = 0 \qquad \text{for} \quad j \neq i \\ & EI_j \sum_n X''''_{jn} T_{in} + c \sum_n X_{jn} \dot{T}_{in} + m_j \sum_n X_{jn} \ddot{T}_{in} = P\,\delta(x_j - \upsilon t_i), \text{ for} \quad j = i, \text{ and } j = 1, 2, \cdots, \nu \end{aligned} \tag{27a,b}$$

Taking into account that eq(3a) are valid, eqs(27) become:

$$\begin{aligned} & m_j \sum_n \omega_n^2 X_{jn} T_{in} + c \sum_n X_{jn} \dot{T}_{in} + m_j \sum_n X_{jn} \ddot{T}_{in} = 0 \qquad \text{for} \quad j \neq i \\ & m_j \sum_n \omega_n^2 X_{jn} T_{in} + c \sum_n X_{jn} \dot{T}_{in} + m_j \sum_n X_{jn} \ddot{T}_{in} = P\,\delta(x_j - \upsilon t_i), \text{ for} \quad j = i, \text{ and } j = 1, 2, \cdots, \nu \end{aligned}$$

Multiplying the correspond equation j by X_{jk}, integrating the outcome from 0 to ℓ_j, and adding the resulting expressions we get:

$$\ddot{T}_{in} + 2\beta_i \dot{T}_{in} + \omega_n^2 T_{in} = \frac{P}{\sum_\nu \left(m_i \int_0^{\ell_i} X_{in}^2 dx\right)} \cdot X_{in}(\upsilon t_i) , \quad \text{with } t_i = t - \sum_1^{i-1} \frac{\ell_i}{\upsilon} \tag{28a,b}$$

The solution of eq(28a) is given by the Duhamel's integral:

$$T_{in}(t_i) = \frac{P}{\tilde{\omega}_n \sum_\nu \left(m_i \int_0^{\ell_i} X_{in}^2 dx\right)} \int_0^{t_i} X_{in}(\upsilon\tau) e^{-\beta_i (t-\tau)} \sin \tilde{\omega}_n (t-\tau) d\tau \text{ , with : } \tilde{\omega}_n = \sqrt{\omega_n^2 - \beta_i^2} \tag{29}$$

3 NUMERICAL RESULTS AND DISCUSSION

Let us consider the multi-span beam of Fig. 1 with E=2.1x10^{10} kN/m^2. The beam consists of five spans with lengths $\ell_1 = \ell_5$=24m, and $\ell_2 = \ell_3 = \ell_4$=30m respectively, I_b=0.05m^4, m_b=500 kg/m and damping parameter β=20.

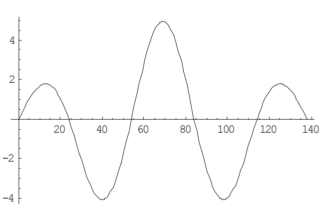

Figure 2. The fundamental eigenshape of the vibrating beam (ω_1=17.5324sec^{-1})

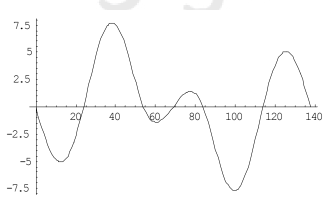

Figure 3. The 2nd eigenshape of the free vibrating beam (ω_2=21.9206sec^{-1})

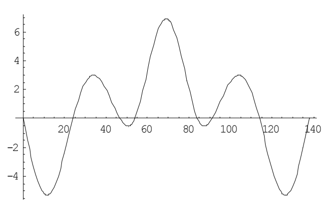

Figure 4. The 3rd eigenshape of the free vibrating beam (ω_3=28.0297sec^{-1})

Then, the corresponding eigenshapes are obtained using the relations (24a,b,c). In Figs 2, 3 and 4 one can see in graphical form the first three eigenshapes.

Let us consider now a load with constant magnitude F=50000kN moving with constant velocity v=20m/s and v=40m/s along the length of the beam. In Figs 5, 6 and 7 one can see the dynamic influence lines referring to the midpoints of the first three spans, i.e. $w_1(\ell_1/2, t)$, $w_2(\ell_2/2, t)$ and $w_3(\ell_3/2, t)$.

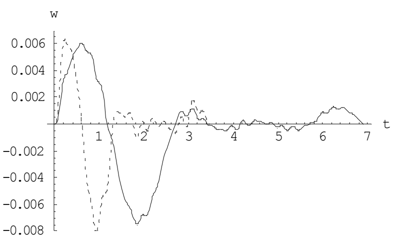

Figure 5. Influence lines at $w_1(\ell_1/2, t)$ for forced vibration of the beam

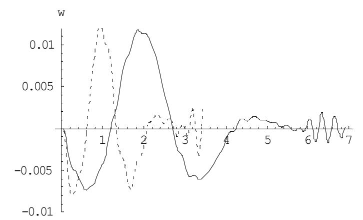

Figure 6. Influence lines at $w_2(\ell_2/2, t)$ for forced vibration of the beam

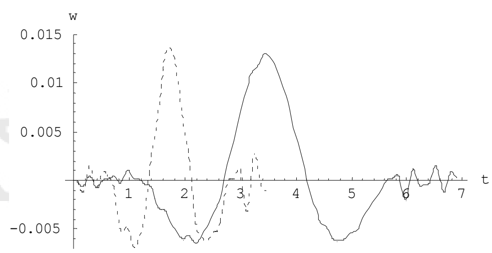

Figure 7. Influence lines at $w_3(\ell_3/2, t)$ for forced vibration of the beam

The continuous influence line refers to velocity v=20m/s, while the dotted influence line refers to velocity v=40m/s.

4 CONCLUSIONS

A simple but very easy and efficient analytical method for obtaining conversion formulae in order to determine the eigenfrequencies and eigenmodes of multi-span continuous beams with spans of different lengths and bending rigidities is presented. The results can be readily employed for studying the dynamic response of multi-span beams subjected to any type of dynamic actions.

REFERENCES

[1] DMITRIEV, A.S.: Dynamic of continuous multi-span beams under a moving force, International Applied Mechanics, **18**(2), 179-186 (1982).

[2] KOMG, J., CHEUNG, Y.K.: Vibration of continuous beams using modified beam vibrating functions, Communications in Numerical Methods in Engineering, **12**, 107-114 (1996).

[3] ICHIKAWA, M., MIYAKAWA, Y.: MATSUDA, A.: Vibration analysis of the continuous beam subjected to a moving mass, J. of Sound and Vibration, **230**(3), 493-506 (2000).

[4] GRECO, A., SANTINI, A.: Dynamic response of a flexural non-classically damped continuous beam under moving loading, Computers and Structures, **80**, 1945-1953 (2002).

[5] MEHRI, B., DAVAR, A., RAHMANI, O.: Dynamic Green function solution of beams under a moving load with different boundary conditions, Sharif Univ. of Technology, Transaction B: Mechanical Engineering, **16**(3), 273-279 (2009).

THE DESIGN OF THE CONTINUITY SLABS OF PRECAST I-BEAM BRIDGES

Ioannis A. Tegos[1] and Sevasti D. Tegou[2]

[1,2] Aristotle University of Thessaloniki, Dept. of Civil Engineering, Greece
e-mail: itegos@civil.auth.gr, stegou@civil.auth.gr

ABSTRACT: In this study, the design of the continuity slabs of the precast I-beam bridges is analytically presented. A precast I-beam bridge of P.A.TH.E. Motorway in Greece is used for the purposes of this study. The investigation is focused on the study of the available ductility of the continuity slabs and on their controllable resistance on the end rotations of the spans.

KEY WORDS: Continuity slab; Precast I-beam bridge; Seismic; Serviceability.

1 INTRODUCTION

The large growth of road traffic and the construction of new motor ways in the fifties and sixties, create a need for fast and economic solutions for bridges with a little as possible disturbance of the ongoing traffic. In many countries, precast bridges are accepted as a good variant solution to cast in-situ bridges as they offer rapidity construction.

There are many partly or completely precast bridge systems which have been developed during the past 40 years [1]. However, span by span simply supported construction of multi-span bridges using form of precast concrete or steel longitudinal beam elements constitute the main solution for precast bridges built from the sixties on. In these cases, the bridge deck is composed of several inverted T – or I- shaped beams positioned at a certain distance. After erection of the beams, a deck slab is cast on site, while expansion joints were provided over all the bridge supports. However inspection of these bridge systems revealed that the salt water penetration through the joints was lead to the damage of the deck ends and their supported elements [2].

During the sixties in USA and seventies in Europe, researches had been focused on the elimination of the expansion joints. The resulting continuous deck slab eliminates the intermediate support joints and consequently the deterioration of the supported elements. In short bridges two joints are only preserved at the abutments, while in long bridges the continuity of the deck slab is separated every five or six spans due to the serviceability requirements of the bridge, which require the free expansion and contraction of the deck. The elimination of the end expansion joints is avoided, as it affects the serviceability performance of the bridge. More specifically, the design process is greatly complicated due to effects such as temperature, shrinkage and creep [3]. Especially in low seismicity countries such as Germany and England, the only advantage of the integral connection of the deck slab to the abutment is the protection to the salt water penetration and the consequential damage to the support elements.

As referred above, multi-span bridges are now mostly designed as continuous structures. The continuous deck provides traffic comfort, reduces the maintenance cost due to the elimination of the expansion joints and ensures the membrane action of the deck slab under horizontal seismic actions. There are two alternatives, either with partial, or with full continuity [4-5]. Partial continuity is a method to provide only continuity of the deck slab, while the beams are designed as simply supported. This means that no distribution of vertical load effects between the intermediate decks can occur. On the other hand fully continuity is realized by the integration of the bridge beams into a reinforced concrete crosshead on the top of the piers. However, the main disadvantage of this method derives from the time dependent effects (mainly creep of concrete) which causes the deflection of the girders in the hogging mode after continuity is established. In this study, the problem of the design of the continuity slabs providing partial continuity of the deck over the piers is analytically presented for the persistent and seismic design situations. A precast I-beam bridge of P.A.TH.E. Motorway in Greece is used for the purposes of this study.

2 DESIGN METHODOLOGY

2.1 General

Bridge deck should in general be designed to avoid damage during earthquake. However, formation of plastic hinges is allowed in the flexible ductile concrete slabs providing continuity between adjacent simply-supported precast concrete girder spans. These members are included in the model of seismic analysis, taking into account their eccentricity relative to the deck axis and a reduced stiffness of their flexural stiffness. However, the design and detailing of these members is usually based on the designer’s experience as their failure is very possible and acceptable during earthquake.

The design of the continuity slabs follows the basic Code’s requirements [6] about the two main limit states namely, (1) the serviceability limit state, which deals with the restriction on the stresses and the crack width under the regular service conditions and (2) the ultimate limit state, which is indented to ensure that the slab has the adequate strength the resist the significant load combinations that a bridge will experience in its life.

The next paragraphs discuss the main subjects concerning the rational design of the continuity slabs.

2.2 Load cases

Table 1 summarizes the main load cases affecting the design of the continuity slabs. The traffic loads should also be included in the combination of the actions according to load Model 1 of Eurocode 1 [7], which cover the most normally foreseeable traffic situation. This model includes concentrated loads due to double-axle vehicles and uniformly distributed loads. The distance between the axles is 1.20m, while the distance between the wheels of the same axle is 2.00m. These loads are applied in each notional lane in which the carriage width is divided. Considering that the analysis and design of the slabs includes a unit strip, only one wheel of each axle will be on this strip.

The wheel concentrated loads should be taken as transversely distributed. The effective width of the concentrated load (transversely to the direction of the main reinforcement) depends on the type of the support at the slab's ends, as well as the distance *x* of the centroid of the load from the support. In this case, the slab is considered as fixed along its edges, due to the high stiffness of the adjacent spans. Eq. 1-3 give the effective width of the concentrated loads for three different situations, namely, when the calculation concerns (1) the maximum bending moment at the mid-span, (2) the maximum bending moment at the support and (3) the maximum shear at the support.

$$b_{m,f} = t_y + x\left(1 - \frac{x}{l}\right),\ \ t_{x,max} = l,\ \ t_{y,max} = 0.4l \tag{1}$$

$$b_{m,s} = t_y + 0.5x\left(2 - \frac{x}{l}\right),\ \ t_{x,max} = l,\ \ t_{y,max} = 0.4l \tag{2}$$

$$b_{m,v} = t_y + 0.3x,\ \ t_{x,max} = 0.2l,\ \ t_{y,max} = 0.4l \tag{3}$$

where: $b_{m,i}$ is the effective width of the concentrated load (the index i indicates the maximum bending moment at the support *s* or at the mid-span *f*, while the index *v* indicates the maximum shear at the support),

t_y, t_x, are the dispersal widths of the concentrated load at the middle surface of the slab in the two directions.

The adjacent spans behave as simply-supported, as the beams are not integrated over the piers. On the other hand the slab's ends are fixed, as the adjacent spans restrain any possible rotation. The loading of the spans due to the additional permanent loads, traffic loads as well as the time-dependant effects e.g. creep, shrinkage and prestressing, causes constraint rotations at the fixed slab's ends, Figure 1(a). These constraint rotations must also be included in the combination of the design actions, as Eurocode [8] assigns for the serviceability limit states. It is noted that the spans' self-weight (beams and deck slab) is excepted from the above load case, as the construction of the continuity slabs is performed after the erection of the beams. As a result, any possible rotation at the ends of the spans due to their self-weight does not affect the slabs. Constraint deformations also imposed at the slab's ends due to the longitudinal earthquake, Figure 1(b).

The effect of the creep on the constraint rotation at the slab's ends consists, on one hand, in the shortening of the compressive zone of the deck's cross-section and, on the other hand, in the increase of the prestressing losses. A simplified consideration of this effect is possible through the multiplication of the constrained rotations caused by dead loads by the creep coefficient φ. In any case, a more accurate solution is possible.

Table 1. Design situations of the continuity slabs

Check		Design Situation	Load Cases	Check position 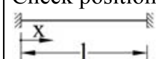
Bending	ULS	Non-Seismic	1. Self-weight *g* 2. Additional permanent loads *g΄* 3. Wheel load *Q*	x=0 x=l/2 x=l
		Seismic	1. Quasi-permanent actions 2. Seismic imposed deformations	x=0 x=l
	SLS	Non-Seismic	1. Self-weight *g* 2. Additional permanent loads *g΄* 3. Wheel load *Q* 4. Vertical linear temperature difference component ΔT 5. Uniform temperature component T 6. Constraint rotations at the slab's ends due to: 6.1 additional permanent 6.2 traffic loads 6.3 creep 6.4 shrinkage	x=0 x=l/2 x=l
Shear	UDL	Non-Seismic	1. Self-weight *g* 2. Additional permanent loads *g΄* 3. Wheel load *Q*	x=d x=2d
		Seismic	1. Quasi-permanent actions 2. Seismic imposed deformations	x=d
Punching	UDL	Non-Seismic	Wheel load *Q*	x=l/2

2.3 Shear Design

The verification of the slab's shear resistance follows the Code's requirements [6]. In cases that there is a concentrated load near the support of the member (in this problem the wheel load may be in any position on the slab), the shear check must be implemented in two positions, as much higher shear strengths can be obtained in these cases. The closer the load is to the support, the greater the proportion of the load which will be transmitted to the support in this way. The Code [6] assigns that when the load is applied on the upper side within a distance $0{,}5d \leq a_v \leq 2d$ from the edge of a support, the contribution of this load to the shear force V_{Ed} may be multiplied by $\beta = a_v/2d$. As a result the shear check is implemented in two critical sections, whose distance from the support is d and 2d respectively.

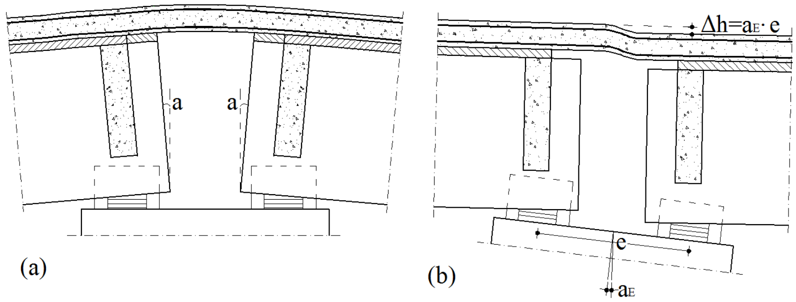

Figure 1. Modes of flexure of the continuity slab due to (a) constraint rotations and (b) constraint movement at the slab's end.

3 APPLICATION

The example presented in this study corresponds to the design of the continuity slabs of a precast I-beam bridge located at Skarfeia-Raches territory of P.A.TH.E. Motorway in Greece. This bridge, see Figure 2(a), is straight and asymmetric and has five span 34.75m+3x36.00m+34.75m and a total length equal to 177.50m. The superstructure consists of six prestressed and precast beams, Figure 2(b), precast deck slabs and a cast in-situ part of the slab. The continuity of the deck over the piers is achieved through slabs whose length is 2.0m while their thickness is 0.25m. The piers are hollow circular sections, Figure 2(c), and are supported on a 3x3 pile group system of 1m diameter. The bridge is founded on Ground Type B and a Peak Ground Acceleration equal to a_g=0.24g is adopted and corresponds to Seismic Zone II. The importance factor adopted is equal to γ_I=1.00, while the behavior factor is equal to q=1 in both directions.

Table 2 summarizes the loads applied to a typical continuity slab of the reference bridge, while Table 3 summarizes the design process of the slab for the ultimate and serviceability limit states. Figure 3 illustrates the reinforcement detailing of the slab's cross-section. The longitudinal reinforcement requirement resulted from the non-seismic design situation is quite smaller than the one required by the seismic design situation. The selected D20@100mm (top and bottom) longitudinal reinforcement corresponds to a ratio equal to 3.2%, which is close to the upper limit assigned by the Code. The increase of the longitudinal reinforcement ratio due to the seismic design requirement increases the stiffness of the slab and consequently the developing bending moment, which lead to a higher reinforcement requirement. As a result, plastic hinges will be formatted at the slabs critical sections due to the design earthquake. Besides the Code [9] accepts the formation of plastic hinges in flexible ductile members such as the continuity slabs provided that the rotational capacity θ_{pu} is less or equal to the allowable plastic rotation θ_{pl}. This rotation is calculated according to Eurocode's 2 provisions and depends on the ratio x_u/d where x_u is the depth of the neutral axis at the ultimate limit state and d is the effective depth of the slab, as well as the classes of the reinforcement and concrete. The allowable plastic rotation for the slab of this example is θ_{pl}=21.0 mrad (x_u/d=0.266, concrete class C30/37, steel class B500C). The R/C section moment-curvature (M-φ) relationship and the corresponding ultimate and yield values, Figure 4, are calculated through the fiber-analysis code RCCOLA-90 [10]. The rotational capacity θ_{pu} is equal to 8.5 mrad and is estimated by multiplying the plastic curvature φ_{pl} by an equivalent plastic hinge length equal to d=20mm. As a result the verification of the plastic rotation in the ultimate limit state is considered to be fulfilled.

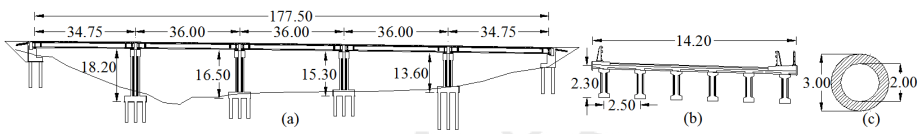

Figure 2. (a) Longitudinal section of the "reference" bridge, (b) Cross-section of the deck at the span, (c) Cross-section of the piers.

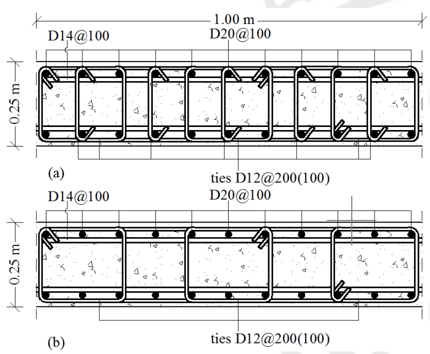

Figure 3. Reinforcement detailing of the slab (a) plastic hinge region and (b) non-critical region.

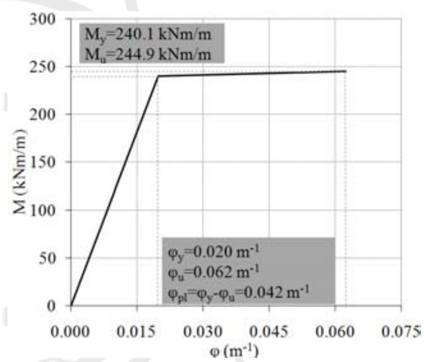

Figure 4. Bilinear moment-curvature relationship for the slab's cross-section.

A significant advantage resulting from the high longitudinal reinforcement ratio of the slab, is the reduction in the seismic bending moment at the pier's base. The shear force of the continuity slab due to the application of the moments of resistance at the two ends of the slab is transferred to the pier through the bearings' reactions. These reactions cause a bending moment which is opposite to the seismic bending moment at the pier's base. In the example presented in this study, the flexural resistance of the slab is about 3410 kNm while the bending moment at the pier's base is 23800 kNm. The increase of the slab's longitudinal reinforcement ratio increases its flexural resistance. The relation of the static parameters of the system always leads to the yield of the top and bottom longitudinal reinforcement of the slab during the longitudinal earthquake. As a result, the bending moment at the pier's base is reduced.

As far as the calculation of the required shear reinforcement is concerned, it is noted that the seismic design situation is critical. The strut inclination, θ, is taken equal to 45° (cotθ=1), in the critical region of the slab, while a cotθ=1.25 is considered in the other cases.

Shear and punching shear are two strongly related effects. However there is a main difference between them: The required shear reinforcement concerns the area of the slab beyond the distance d of the support. On the other hand, the transverse reinforcement required by the punching check is placed in a distance not greater that 1,5d around the concentrated load. As a result, there is an interaction zone between the shear and punching required reinforcement. In this example, the punching shear resistance of the slab without shear reinforcement is higher than the maximum punching shear stress of the slab (see Table 3) and consequently no punching shear reinforcement is required.

Table 2. Loads of the slab (b_m is the effective width of the concentrated load)

Dead Loads	Self Weight g = 6.25 kN/m^2 Additional Permanent loads g' = 4.08 kN/m^2
Live Loads	Wheel Load Q (L.M. 1) =120/b_m^* kN/m Uniformly distributed Load q =9.00 kN/m^2
Vertical Linear Temperature Difference	ΔT =15°C
Uniform temperature Component	T =±25°C
Constraint rotations at the slab's ends	a =8.36·10^{-4} rad
Seismic constraint movement of the support	Δh =15.46·10^{-3}m (a_E=7.73·10^{-3} rad)

Table 3. Design of the continuity slab for bending, shear and punching shear

Bending							
ULS	Design Situation	Position	M_{sd} (kN-m/m)	N (kN/m)	$A_{s.req}$ (cm^2)	$A_{s.prov}$ (cm^2)	Longitudinal Reinforcement
	Non-Seismic	support	-41.75	-	6.5	31.4	D20@100
		mid-span	42.07	-	6.6	31.4	D20@100
	Seismic	support	639.64	553.68	95.0	31.4	D20@100
SLS	Design Situation	Position	M_{sd} (kN-m/m)	N (kN/m)	σ_s (MPa)	Maximum Bar size (mm)	s (mm)
	Non-Seismic	support	-92.31	773.00	175.6	30	280
		mid-span	92.35	773.00	175.7	30	280
Shear							
ULS	Design Situation	Position	V_{sd} (kN/m)	$V_{Rd.c}$ (kN/m)	$V_{Rd.s}$ (kN/m)	$V_{Rd,max}$ (kN/m)	Transverse reinforcement
	Non-Seismic	x=d	125.73	173.35	552.7	927.2	D12@100
		x=2d	212.19	173.35	552.7	927.2	D12@100
	Seismic	x=d	392.46	173.35	442.2	950.4	D12@100
Punching Shear							
ULS	Design Situation	Position	V_{sd} (kN/m)	Critical perimeter u (m)	v_{sd} (kN/m^2)	$v_{Rd.c}$ (kN/m^2)	Check
	Non-Seismic	mid-span	252.00	4.11	291.74	304.31	$v_{Ed} < v_{Rd.c}$

4 CONCLUSIONS

In this study, the design of the continuity slabs of the precast I-beam bridges was analytically presented for the persistent and seismic design situations. The study resulted in the following conclusions:

- The effect of the constraint rotations at the fixed ends of the slab due to the loading of the adjusted spans affect the serviceability performance of the slab. The minimum required effective slab's length due to the serviceability requirements of the bridge is from 1.5m to 2.0m
- As far as the shear design of the slab is concerned, the seismic situation is critical. The required transverse reinforcement is calculated considering a value of $\cot\theta=1$ in the plastic hinge region, while a value of $\cot\theta=1.25$ is considered in the case of the non-critical sections.
- The formation of plastic hinges at the slabs' ends during the longitudinal design earthquake is inevitable. In these regions, the rotational capacity θ_{pu} must be less or equal to the allowable plastic rotation θ_{pl}.
- In plastic hinge regions whose length is about 2d, the Code's requirements about the transverse reinforcement must be fulfilled.

ACKNOWLEDGMENTS

The authors would like to thank METE SYSM S.A for kindly providing the original study of the bridge used for the purposes of the present study.

REFERENCES

[1] CEB-FIB, *fib bulletin 29: Precast concrete bridges State of the art report*, Switzerland, 2004.

[2] Pritchard, B., *Continuous and Integral Bridges: Proceedings of the Henderson Colloquium Towards Joint-Free Bridges,* Organized by the British Group of the International Association for Bridge and Structural Engineering, Pembroke College, Cambridge, UK 20-21 July 1993, Taylor & Francis, 1994.

[3] PCI, *Precast, prestressed concrete bridges, the high performance solution, Comprehensive Bridge Design Manual*, Available via DIALOG. www.pci.org/publications/bridge Accessed: May 5, 2011.

[4] Miller R.A. et al., *Connection of Simple-Span Precast Concrete Girders for Continuity*, NCHRP Report 519 Transportation Research Board, Washington, D.C., 2004.

[5] Saleh A., Einea A. and Tadros M., Creating Continuity in Precast Prestressed Girder Bridges, *Concrete International*, pp 27-32, Aug. 1995.

[6] CEN, *Eurocode 2: Design of concrete structures - Part 1-1: General rules and rules for buildings*, 2003.

[7] CEN, *Eurocode 1: Actions on structures - Part 1-2 Traffic actions on bridges, Final Draft prEN1991-1-2*, 2003.

[8] CEN [Comité Européen de Normalisation], *Eurocode Bases of structural analysis*, 2002.

[9] CEN Eurocode 8: Design of structures for earthquake resistance, Part 2: Bridges, 2003.

[10] Kappos AJ. RCCOLA-90: *A microcomputer program for the analysis of the inelastic response of reinforced concrete sections*, Aristotle University of Thessaloniki, Greece, 2002.

A SPECIAL FORM OF CABLE-STAYED BRIDGES

Ioannis G. Raftoyiannis[1] and George T. Michaltsos[2]

[1,2] National Technical University of Athens, Dept. of Civil Engineering, Greece
e-mail: rafto@central.ntua.gr, michalts@central.ntua.gr

ABSTRACT: A mathematical model suitable for static and dynamic analysis of curved-in-plane cable-stayed bridges is proposed. By expressing the tensile forces of the cables in relation to the deck and pylon deformations, the problem is reduced to the solution of a beam curved-in-plane that is subjected to the usual permanent and external loads and to the tensile forces of the cables.

KEY WORDS: C-Stayed bridges; Curved beams; Dynamic structural analysis;

1 INTRODUCTION

Cable-stayed bridges are a particular type of bridge structures that have been of great interest in recent years (Troitsky [1]). Numerous publications dealing with the dynamic behavior of cable-stayed bridges have presented significant results. We must mention those of,, Chatterjee et al. [2], Bruno and Golotti [3] and Virlogeux [4]. The bibliography on the curved c-s-bridges is rather poor. The most interesting publications are those of J. Brownjohn et al. [5] who studied the dynamic behavior of a 100 m span curved c-s-bridge based on full-scale testing and Sirigoringo and Fujino [6] assessed the dynamic characteristics of the 455 m Katsushika harp-type curved c-s-bridge. In this paper, a mathematical model for the static and dynamic solution of the problem of the cable-stayed bridges curved-in-plane is proposed. Due to the limited length of a conference paper it is impossible to develop such an object. Therefore in this study the equations of the complete problem and the free vibration are presented. The problems of the static behavior and of the forced vibrations are formulated by the Lagrange equation and solved by the Laplace transformation. These topics are presented in detail in a paper, which is in printing in Int. J. of Struc. Stability and Dynamics.

2 PRELIMINARY CONCEPTS

In fig.1 the model of a curved c-s-bridge is shown. The bridge is suspended by μ cables starting from point 1 with angle ρ_1, and ending at point 2 with angle ρ_2, and anchored at the top of the pylon PG. The deck is referred to the three-orthogonal, clockwise, curvilinear coordinates system, while the 1-1 and 2-2 axes are the main ones of the pylon. For this paper, the following relations are useful:

$$L = R \cdot \rho \;, \qquad PG = h/\cos\gamma_1 \;, \qquad PC = h/\cos\gamma_2 \tag{1),(2),(3}$$

$$\cos\beta_1 = (R^2 + \ell_1^2 - \ell_2^2)/(2\,\ell_1 R)\,, \quad \cos\beta_2 = (R^2 + \ell_2^2 - \ell_1^2)/(2\,\ell_2 R)\,, \quad OA = 2R\sin\frac{\vartheta}{2} \tag{4}$$

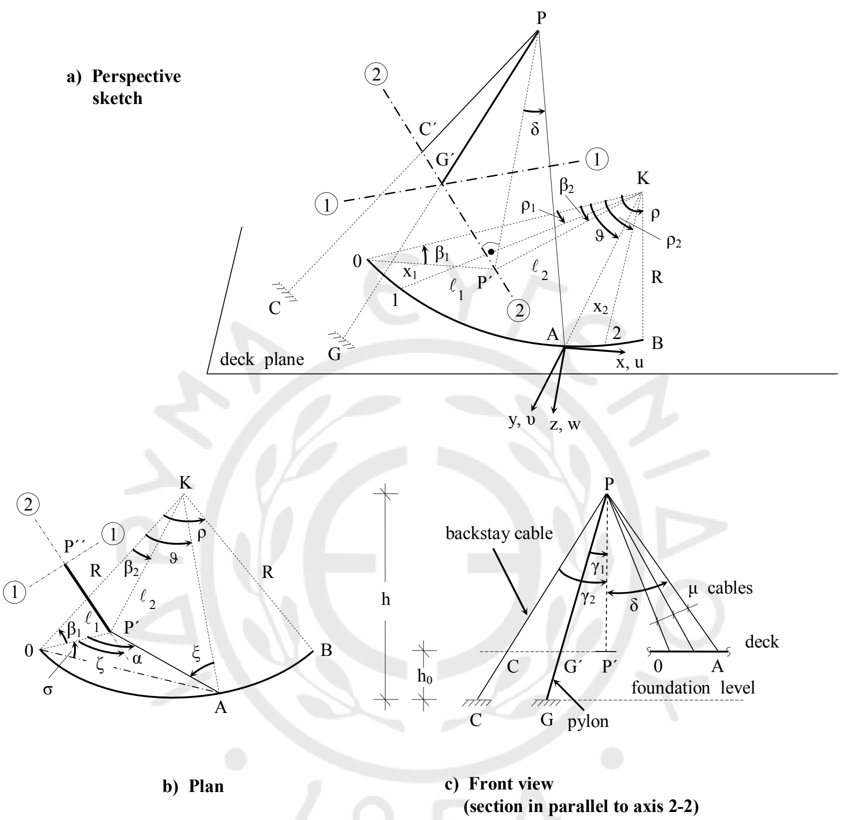

Figure 1. (a) perspective sketch, (b) plan, (c) front view

$$\sigma = \frac{\pi}{2} - \frac{\vartheta}{2} - \beta_1 \quad , \quad P'A = \sqrt{\ell_1^2 + 4R^2\sin^2\frac{\vartheta}{2} - 4\,\ell_1 R\sin\frac{\vartheta}{2}\sin\left(\frac{\vartheta}{2} + \beta_1\right)} \tag{5),(6a}$$

$$\cos\alpha = \frac{\ell_1^2 + (P'A)^2 - (OA)^2}{2\,\ell_1 (P'A)} = \frac{\ell_1 - 2R\sin\frac{\vartheta}{2}\sin\left(\frac{\vartheta}{2} + \beta_1\right)}{\sqrt{\ell_1^2 + 4R^2\sin^2\frac{\vartheta}{2} - 4\,\ell_1 R\sin\frac{\vartheta}{2}\sin\left(\frac{\vartheta}{2} + \beta_1\right)}} \tag{6b}$$

$$\tan\delta = \frac{P'A}{P'P} = \frac{\sqrt{\ell_1^2 + 4R^2\sin^2\frac{\vartheta}{2} - 4\,\ell_1 R\sin\frac{\vartheta}{2}\sin\left(\frac{\vartheta}{2} + \beta_1\right)}}{h - h_o} \tag{7}$$

$$\xi = \alpha - \beta_1 - \vartheta \quad , \quad s_i = \frac{h - h_o}{\cos\delta} \quad , \quad \text{where: } s_i=(PA) \tag{8}$$

3 THE DEFORMED STATE OF THE SYSTEM

Let us consider now the system in its deformed state, as shown in Fig. 2(b). From Fig.3(a) we get:

$$F_{i1} = F_i \cdot \sin\delta \cdot \sin(\alpha_i - \zeta), F_{i2} = F_i \cdot \sin\delta \cdot \cos(\alpha_i - \zeta), F_{iV} = F_i \cos\delta_i \tag{9}$$

From Fig. 3(c) for the vertical plane containing the main axis 2-2, we get:

$$h = \ell \cdot \cos\gamma_1 \ , \ F = F_{i2}\cos\gamma_1 + F_{iV}\sin\gamma_1 \ , \ F_{bo} = F_{bc} \cdot \sin(\gamma_2 - \gamma_1) \ ,$$
$$f_{i2} = f\cos\gamma_1 \quad , \quad f_{bc} = f_{bo} \cdot \cos\gamma_1$$

We can find (with $\tan\eta = f_1 / f_2$):

$$f_1 = \sum_{i=1}^{\mu} \frac{h^3}{3E_p J_2} \cdot \frac{F_i}{\cos^3\gamma_1} \cdot \sin\delta_i \cdot \sin(\alpha_i - \zeta)$$
$$f_2 = \sum_{i=1}^{\mu} \frac{h^3 F_i}{3E_p J_1} \cdot \frac{\sin\delta_i \cdot \cos(\alpha_i - \zeta)}{\cos^2\gamma_1} + \sum_{i=1}^{\mu} \frac{h^3 F_i}{3E_p J_1} \cdot \frac{\sin\gamma_1 \cos\delta_i}{\cos^3\gamma_1} - \frac{h^3 F_{bc}}{3E_p J_1} \cdot \frac{1}{\cos^3\gamma_1} \tag{10a,b}$$

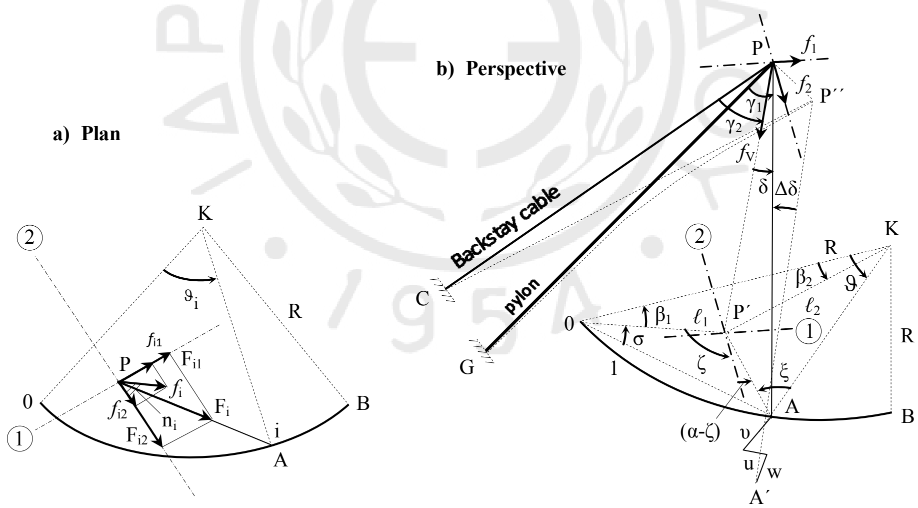

Figure 2. Deformed configuration of a curved-in-plane cable-stayed bridge. (a) Plan view, and (b) perspective view

Taking into account that $f_o^2 = f_1^2 + f_2^2$ and $f_i = f_{io}\sin\delta_i$, for the deformation f_i of the i^{th} cable, we get:

$$f_{io} = f_o \cdot \cos(\alpha_i - \zeta - \eta) = \sqrt{f_i^2 + f_2^2} \cdot [\cos(\alpha_i - \zeta) \cdot \frac{f_2}{\sqrt{f_i^2 + f_2^2}} + \sin(\alpha_i - \zeta) \cdot \frac{f_1}{\sqrt{f_i^2 + f_2^2}}]$$

And finally: $$f_{io} = f_1 \cdot \sin(\alpha_i - \zeta) + f_2 \cdot \cos(\alpha_i - \zeta) \tag{11}$$

For the back-stayed cable, we have: $F_{bc} = \frac{E_c \cdot A_{bc}}{s_{bc}} \cdot \frac{\sin(\gamma_2 - \gamma_1)}{\cos\gamma_1} \cdot f_2$ and Eq. (10b) becomes:

$$f_2 = \frac{h^3}{3 K E_p J_1} \cdot \sum_{i=1}^{\mu} (\frac{\sin\delta_i \cos(\alpha_i - \zeta)}{\cos^2\gamma_1} + \frac{\sin\gamma_1 \cos\delta_i}{\cos^3\gamma_1}) \cdot F_i \tag{12a}$$

where: $$K = 1 + \frac{h^3 E_c A_{bc} \cdot \sin^2(\gamma_2 - \gamma_1)}{3 E_p J_1 \cdot s_{bc} \cdot \cos^4\gamma_1} \tag{12b}$$

From the generic cable i, by projecting its deformed and undeformed states on the $(PP'A)$ plane (Fig. 2(b)), we can obtain the following equation: $\Delta s_i = u_i \sin\xi_i \sin\delta_i + \upsilon_i \cos\xi_i \sin\delta_i + w_i \cos\delta_i - f_i \sin\delta_i$ which with $\Delta s_i = \frac{s_i F_i}{E_c A_i}$ becomes:

$$\begin{aligned} \frac{s_i}{E_c A_i} \cdot F_i &= u_i \sin\xi_i \sin\delta_i + \upsilon_i \cos\xi_i \sin\delta_i + w_i \cos\delta_i \\ &\quad - \sin\delta_i \sin(\alpha_i - \zeta) \cdot \frac{h^3}{3 E_p J_2 \cos^3\gamma_1} \cdot \sum_{j=1}^{\mu} F_j \sin\delta_j \sin(\alpha_j - \zeta) \\ &\quad - \sin\delta_i \cos(\alpha_i - \zeta) \cdot K \cdot \frac{h^3}{3 E_p J_1 \cos^3\gamma_1} \cdot \sum_{j=1}^{\mu} F_j \sin\delta_j \cos(\alpha_j - \zeta) \end{aligned} \tag{13}$$

Equation (13), assuming that the cables are densely distributed on the bridge-deck, after some manipulations is written:

$$\begin{aligned} F(x) &= \frac{E_c A(x)}{s(x)} \cdot [u(x) \sin\xi \sin\delta + \upsilon(x) \cos\xi \sin\delta + w(x) \cos\delta] \\ &\quad - c \cdot \int_{x_1}^{x_2} (\overline{B}_1 d + \overline{B}_2 r) \cdot [u(x) \sin\xi \sin\delta + \upsilon(x) \cos\xi \sin\delta + w(x) \cos\delta] dx \\ &\quad - \varepsilon \cdot \int_{x_1}^{x_2} (\overline{B}_3 d + \overline{B}_4 r) \cdot [u(x) \sin\xi \sin\delta + \upsilon(x) \cos\xi \sin\delta + w(x) \cos\delta] dx \end{aligned} \tag{14}$$

where:

$$\overline{B}_1 = \frac{1}{\overline{B}_5} \cdot \left(1 + \int_{x_1}^{x_2} \varepsilon(x) r(x) dx\right), \quad \overline{B}_2 = -\frac{1}{\overline{B}_5} \cdot \int_{x_1}^{x_2} \varepsilon(x) d(x) dx \tag{15a}$$

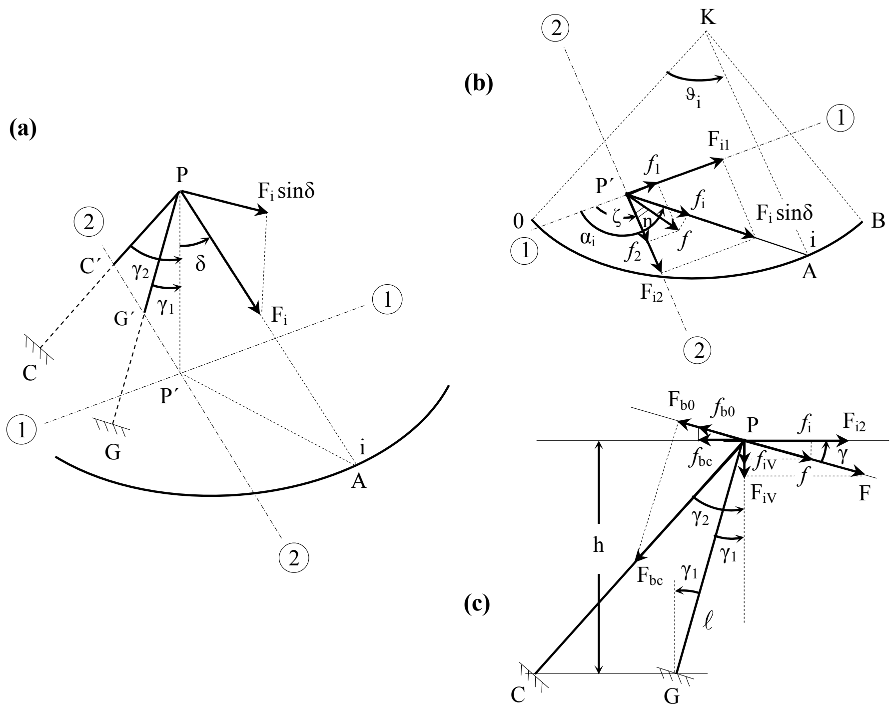

Figure 3. Analysis and equilibrium of cable tensions and deformations. (a) Plan view, (b) Top view, and (c) Front view in plane CGP

$$\overline{B}_3 = -\frac{1}{\overline{B}_5} \cdot \int_{x_1}^{x_2} c(x)\, r(x)\, dx \ , \quad \overline{B}_4 = \frac{1}{\overline{B}_5} \cdot \left(1 + \int_{x_1}^{x_2} c(x)\, d(x)\, dx \right) \tag{15b}$$

$$\overline{B}_5 = \left(1 + \int_{x_1}^{x_2} c(x)\, d(x)\, dx \right) \cdot \left(1 + \int_{x_1}^{x_2} \varepsilon(x)\, r(x)\, dx \right) - \int_{x_1}^{x_2} c(x)\, r(x)\, dx \cdot \int_{x_1}^{x_2} \varepsilon(x)\, d(x)\, dx \tag{15c}$$

$$c(x) = \frac{E_c A(x)}{s(x)} \cdot \frac{h^3}{3 E_p J_2} \cdot \frac{\sin(\alpha - \zeta) \sin\delta}{\cos^3 \gamma_1} \ , \quad d(x) = \sin(\alpha - \zeta) \sin\delta$$

$$\varepsilon(x) = \frac{E_c A(x)}{s(x)} \cdot \frac{h^3 \cdot K}{3 E_p J_1} \cdot \frac{\cos(\alpha - \zeta) \sin\delta}{\cos^3 \gamma_1} \ , \quad r(x) = \cos(\alpha - \zeta) \sin\delta \tag{16}$$

and $\alpha(x)$, $\xi(x)$, $\delta(x)$, $s(x)$ are functions of x already defined in Eqs. (6c), (8), (7) and (9), respectively, (by setting $\delta = x/R$, $\rho_1 = x_1/R$, $\rho_2 = x_2/R$, $L = R\rho$).

When the distance between two successive cables is $\overline{\delta}$, the tension of the cable in position x_i will be: $F_i = F(x) \cdot \overline{\delta}$.

4 THE DECK

According to the theory of curved beams with thin-walled cross-sections, and considering that for a sufficiently large R, the effect of flexural tensions caused by the lateral deformation are negligible (i.e., it does not affect the axial force), we arrive at the following system of equations of motion:

$$EA\left(u'' + \frac{u}{R^2}\right) - m\ddot{u} = -q_x \tag{17a}$$

$$EJ_z\upsilon'''' + \frac{2EJ_z}{R^2}\cdot\upsilon'' + \frac{EJ_z}{R^4}\cdot\upsilon + m\ddot{\upsilon} = q_y \tag{17b}$$

$$\left(EJ_y - \frac{EJ_\omega}{R^2}\right)w'''' + \frac{GJ_d}{R^2}\cdot w'' - \frac{EJ_y - GJ_d}{R}\cdot\varphi'' - \frac{EJ_\omega}{R}\cdot\varphi'''' + m\ddot{w} = q_z \tag{17c}$$

$$EJ_\omega\varphi'''' - GJ_d\varphi'' - \frac{EJ_y}{R^2}\cdot\varphi + \frac{EJ_\omega}{R}\cdot w'''' + \frac{EJ_y - GJ_d}{R}\cdot w'' + J_{px}\ddot{\varphi} = m_x \tag{17d}$$

5 THE FREE VIBRATING BRIDGE

In order for us to apply Eqs. (17) for the case of a freely vibrating bridge, we set

$$\left.\begin{aligned} &q_x = -F(x)\sin\xi\sin\delta\,,\quad q_y = -F(x)\cos\xi\sin\delta\,,\quad q_z = -F(x)\cos\delta \\ &m_x = F_y e_z + F_z e_y = -F(x)\left(e_y\cos\delta + e_z\cos\xi\sin\delta\right) \end{aligned}\right\} \tag{18}$$

We are searching for a solution in the form of separate variables:

$$\left.\begin{aligned} &u(x,t) = U(x)\cdot T(t),\quad \upsilon(x,t) = V(x)\cdot T(t), \\ &w(x,t) = W(x)\cdot T(t),\quad \varphi(x,t) = \Theta(x)\cdot T(t) \end{aligned}\right\} \tag{19}$$

Introducing Eqs.(19) into Eqs.(17), and taking into account Eqs.(14), we arrive at a differential system of equations which can be solved via the Galerkin procedure. Thus, we arrive at the following equations

$$\int_0^L \sum_{i=1}^n \left[EA\, b_i X_i'' + \left(\frac{EA}{R^2} + m\omega^2\right) b_i X_i\right] X_\sigma dx = \int_0^L \overline{F} X_\sigma \sin\xi\sin\delta\, dx \tag{20a}$$

$$\int_0^L \sum_{i=1}^n \left[EJ_y c_i Y_i'''' + \frac{2EJ_y}{R^2} c_i Y_i'' + \left(\frac{EJ_y}{R^4} - m\omega^2\right) c_i Y_i\right] Y_\sigma dx = -\int_0^L \overline{F} Y_\sigma \cos\xi\sin\delta\, dx \tag{20b}$$

$$\int_0^L \sum_{i=1}^n \left[S_1 d_i Z_i'''' + \frac{GJ_d}{R^2} d_i Z_i'' - S_2 f_i \Phi_i'' - \frac{EJ_\omega}{R} f_i \Phi_i'''' - m\omega^2 d_i Z_i\right] Z_\sigma dx = -\int_0^L \overline{F} Z_\sigma \cos\delta\, dx \tag{20c}$$

$$\begin{aligned} &\int_0^L \sum_{i=1}^n \left[EJ_\omega f_i \Phi_i'''' - GJ_d f_i \Phi_i'' - \frac{EJ_y}{R^2} f_i \Phi_i + \frac{EJ_\omega}{R} d_i Z_i'''' + S_2 d_i Z_i'' - J_{px}\omega^2 f_i \Phi_i\right] \Phi_\sigma dx = \\ &= -\int_0^L \overline{F}\Phi_\sigma (e_y\cos\delta + e_z\cos\xi\sin\delta)\, dx \end{aligned} \tag{20d}$$

where:

$$\overline{F}=\sum_{i=1}^{n}(A_1 b_i X_i + A_2 c_i Y_i + A_3 d_i Z_i)+\sum_{i=1}^{n} c\int_{x_1}^{x_2}(\Gamma_1 b_i X_i + \Gamma_2 c_i Y_i + \Gamma_3 d_i Z_i)dx + \\ +\sum_{i=1}^{n}\varepsilon\int_{x_1}^{x_2}(E_1 b_i X_i + E_2 c_i Y_i + E_3 d_i Z_i)dx \quad , \quad \text{for} \quad \sigma=1 \quad \text{to} \quad n \tag{20e}$$

Equations (20) represent a linear system of homogeneous equations without second member. Therefore, the determinant of the coefficients of the unknowns must be zero, from which the eigenfrequencies of the bridge can be determined.

6 NUMERICAL RESULTS AND DISCUSSION

In this section, a number of numerical investigations based on the equations obtained in the preceding section have been developed. In our study, we consider three bridges with lengths L=100m, 200m and 300m, but different radii of curvature: R=100m, 300m, and 500m. We consider in addition the sets of decks' and pylons' showed in table 1. The following data are used: x_1=L/5, x_2=4L/5, $\ell_1 = 100\,\text{m}$, $\beta_1 = \pi/3$, h=150 m, h_o=50 m, $\gamma_1 = \pi/6$ and $\gamma_2 = \pi/4$. For the law of the cables' cross-section change, we modify the one proposed by by Bruno and Golotti [4] as follows: $A(x) = g/(\sigma_g \cdot \cos\delta)$, where g is the uniformly distributed deck's own load, σ_g is the initial tension of the stays' curtain due to the above g, i.e., $\sigma_g = \sigma_\alpha \cdot g/(g+p)$, where σ_a is the allowable stress of the cables (in this example σ_a =12,000 dN/cm^2) and p is the design live load (in this example p=g).

Table 1. Decks' and pylons' properties

	m	J_y	J_z	J_d	J_{px}	J_ω	A_p	J_1	J_2	A_{bc}
S_1	550	1	10	1.2*10^{-5}	6	10	0.20	4	4	0.005
S_2	700	2	15	1.2*10^{-4}	12	30	0.35	8	8	0.015
S_3	900	4	20	1.2*10^{-3}	20	50	0.50	20	20	0.030

By applying the relations given in Section 5, we can obtain Table 2 for the first three eigenfrequencies of the bridge. From these results, we can observe the influence of the pylon's and deck's stiffness on the eigenfrequencies of the bridge (for the same L and R) in comparison with the corresponding values of the straight bridge (R→∞). For ω_1: the deviations are 54.70%, 54.90%, 70.70% for R=500 m, 300 m, 100m, respectively. Correspondingly, for ω_2 we have: 26.50% for R=500 m, 41.50% for R=300 m, 35.80% for R=100m, and for ω_3 we have: 57.50% for R=500 m, 50.00% for R=300 m, 10.70% for

R=100m. One can see that the fundamental eigenfrequency ω_1 is severely affected by both the length of the bridge as well as by the relatively small curvature radii.

The influence of the deck and pylon properties on the eigenfrequencies of the system (for the same L and R) in comparison with the corresponding values of the straight bridge (R→∞) has as follows: For ω_1: 120.0% for S_1, 130.0% for S_2, 290.0% for S_3. For ω_2: 280.0% for S_1, 120.0 % for S_2, 295.0% for S_3. And for ω_3: 45.0% for S_1, 56.0 % for S_2, 105.0% for S_3. On the other hand, we observe that the influence of the eccentric anchorage of cables ranges from 4% to 51% for ω_1, from 15% to 150% for ω_2 and for 5% to 94% for ω_3, with respect to the eigenfrequencies of the corresponding straight bridge.

Table 2. Bridge eigenfrequencies

			R = 100 m			R = 300 m			R = 500 m		
			S_1	S_2	S_3	S_1	S_2	S_3	S_1	S_2	S_3
L =100	e_y=0	ω_1	4.20	3.48	2.46	6.95	8.05	9.76	6.49	5.23	9.76
		ω_2	6.45	7.24	8.76	24.45	16.13	34.67	9.73	8.20	12.32
		ω_3	23.57	29.86	37.30	25.85	30.58	38.80	24.43	22.53	38.41
	e_y=5	ω_1	4.78	4.65	3.76	10.55	8.45	9.57	7.09	5.82	9.88
		ω_2	7.42	7.37	8.79	24.50	12.88	29.52	24.10	8.05	11.58
		ω_3	23.74	29.86	37.10	25.62	30.52	38.11	25.20	22.55	38.40
L =200	e_y=0	ω_1				1.22	1.51	1.85	1.19	1.46	1.75
		ω_2				6.62	5.65	5.07	6.45	5.71	5.11
		ω_3				14.05	8.05	9.77	9.71	7.84	9.76
	e_y=5	ω_1				1,28	1.60	1.95	1.31	1.52	1.97
		ω_2				7.49	6.34	5.64	7.71	6.87	6.07
		ω_3				10.53	8.52	9.85	15.07	8.06	9.87
L =300	e_y=0	ω_1				0.51	0.64	0.79	0.53	0.67	0.82
		ω_2				1.97	2.12	2.21	1.26	4.88	5.06
		ω_3				5.83	5.26	4.76	5.68	8.20	9.83
	e_y=5	ω_1				0.53	0.65	0.81	0.62	0.69	0.81
		ω_2				2.23	2.23	2.96	1.01	2.19	1.91
		ω_3				6.22	5.55	4.95	5.59	5.68	5.05

REFERENCES

1. M.C. Troitsky, *Cable-stayed bridges* (Crosby Lockwood Staples, London, 1977).
2. P.K. Chatterjee, T.K. Datta and C.S. Surana, Vibration of cable-stayed bridges under moving vehicles, *Journal of Structures Engineering International* **2** (1994) 116-121.
3. D. Bruno and V. Golotti, Vibration analysis of cable-stayed bridges, *Journal of Structures Engineering International* **1** (1994) 23-28.
4. M. Virlogeaux, Recent evolution of cable-stayed bridges, *J. of Engineering Structures* **21** (1999) 737-755.
5. J.M.W. Brownjohn, J. Lee and B. Cheong, Dynamic performance of a curved cable-stayed bridge. *Engineering Structures* **21** (1999) 1015-1027.
6. D.M. Siringorino and Y. Fujino, Dynamic characteristics of a curved cable-stayed bridge identified from strong motion records. *Engineering Structures* **29**(8) (2006) 2001-2017.

IBSBI 2011, October 13-15, 2011, Athens, Greece

DYNAMIC BEHAVIOR OF A BRIDGE ON FLOATS

Theodore G. Konstantakopoulos[1], Ioannis G. Raftoyiannis[2] and George T. Michaltsos[3]

[1] University of Thessaly, Dept. of Civil Engineering, Greece
[2,3] National Technical University of Athens, Dept. of Civil Engineering, Greece
e-mail: tkonstadak@civ.uth.gr, rafto@central.ntua.gr, michalts@central.ntua.gr

ABSTRACT: Bridges on floats are usually temporary structural systems carrying moving loads while consisting from at least two or more floating piers (pontoons). In this work, an analytical model suitable for the dynamic analysis of bridges on floats is presented. When a moving load is passing the bridge with constant velocity both the beams as well as the piers become in motion. The theoretical formulation is based on a continuum approach employing the modal superposition technique. Various cases of geometrical and loading parameters are studied and the analytical results obtained in this work are tabulated in the form of dynamic response diagrams.

KEY WORDS: Pontoon bridges; floats; moving loads; bridge dynamics.

1 INTRODUCTION

Floating bridges were used since ancient times to cross wide rivers. In our days floating structures are still in wide use in both military and civil constructions. Many floating bridges have been constructed in several countries across rivers and seas instead of conventional bridges based on piers and abutments. One of the most well known floating bridges in Europe is the double deck steel pontoon bridge in Instanbul spanning over the Bosporos, which was constructed in the beginning of the 20th century. Other floating bridges are the Lacey V. Murrow Bridge, the Hood Canal Bridge in USA, the Bergs Ysundet Floating Bridge in Norway and the Daxie Island Floating Bridge in China.

Some of the advantages of the floating bridges compared to the conventional ones include the reduced environmental impact, the ability of relocation and the significant low costs in deep water structures.

Two different structural forms have been used until now for floating bridges: a continuous-pontoon type bridge which is made of interconnected pontoons and ramps pressed to the shore banks and a discrete pontoon type bridge which has a beam deck and several discrete pontoons functioning as piers. In both cases the support forces for dead and live loads on the bridge are due to the buoyancy of water.

Floating bridges are usually designed by applying the theory of elastic foundation where the hydrodynamic effects are neglected or more realistically by considering hydrodynamic effects using hydrodynamic masses and dampers. Seif & Inoue [1] investigated the dynamic behavior of a discrete pontoon floating bridge under the condition of wave effects with the finite element method. Fleischer & Park [2] used modal analysis to study the hydroelastic vibration of a beam under a uniformly moving one-axis vehicle. The studies of other researchers such as Wang, Liu-Chao Qiu, Chonan, Sneyd etc. are also worth mentioning. The problem can be divided into a hydrodynamic problem for the liquid flow and an elastic problem for the pontoons' oscillations. In the restricted length of this paper, the hydrodynamic influence of the liquid flow is omitted. This is the object of a next, more extensive, paper.

In this study the dynamic response of a bridge on floating piers under a moving load is presented. Using Laplace transformations, the analytical solutions for the dynamic deflections of the joints between pontoons are determined. The water surface is taken to be in calm and its level remains invariable. The floating piers are assumed to be non-deformable and are in dynamic equilibrium by taking into account, the moving load and the buoyancy forces developed.

2 THEORETICAL ANALYSIS

In order to analyze the dynamical behavior of bridges on floats, we consider a n-span bridge with n-1 intermediate floating piers as shown in *Fig. 1*. The first and the last span are simply supported at points 0 and n, respectively, which are immovable and at points 1 and n-1, which are resting on floats 1 and n-1 that are allowed to move only in the vertical direction. Consequently, all intermediate spans slide vertically and rotate as well. All parts of the bridge are connected to each other with hinged connections.

In order to analyze the system, we assume the following:

1. The system equilibrates in a horizontal position at time instant t=0 under its self-weight only. The waves' influence is neglected.
2. When a load P with constant magnitude crosses the bridge with constant speed υ, the system is deformed as shown in *Fig. 1*.
3. The buoyancy forces at the floating supports are:
$$V_i = A_i \cdot s_i \qquad (i = 1,..., n-1) \tag{1}$$
where A_i is the area of the i^{th} pontoon's cross-section and s_i is its corresponding settlement (sinking).
4. Each span ″i″ of the bridge has mass per unit length m_i and bending stiffness EI_i (i=1,…,n).
5. The so-called ″influence functions″ which express the geometrical movement of an undeformed beam for unit settlement of each support (see *Fig. 2*) are the following:

$$g_{(i+1)i} = \frac{x_i}{\ell_i}, \qquad g_{i(i+1)} = \frac{\ell_i - x_i}{\ell_i} \tag{2}$$

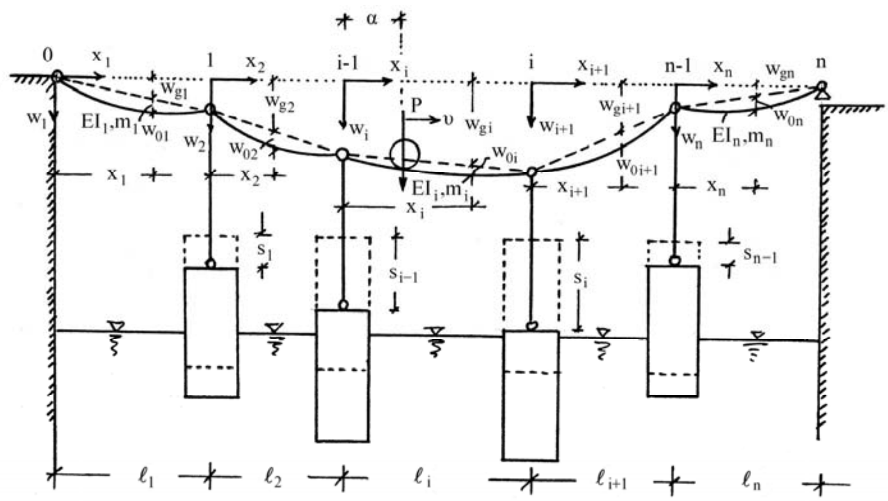

Figure 1. Deformed state of a bridge on floating piers

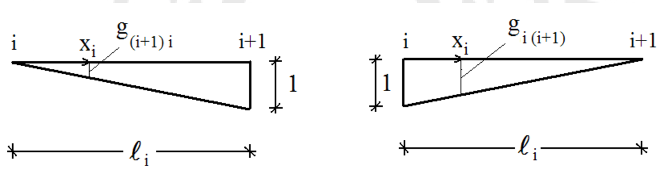

Figure 2. Influence functions for beam support unit settlements

We assume that a load P with constant magnitude moves on the i^{th} span. For the random span ρ according to *Fig. 1* and Eqs(2) we have:

span ρ:
$$w_\rho = \frac{\ell_\rho - x_\rho}{\ell_\rho} s_{\rho-1} + \frac{x_\rho}{\ell_\rho} s_\rho + w_{o\rho} \tag{3}$$

The forces acting on the random joint ρ and on the joints (i-1),i are:

joint ρ:
$$V_\rho = -\frac{m_\rho}{\ell_\rho}\int_0^{\ell_\rho} x_\rho \ddot{w}_\rho \, dx_\rho - \frac{m_{\rho+1}}{\ell_{\rho+1}}\int_0^{\ell_{\rho+1}} (\ell_{\rho+1} - x_{\rho+1})\ddot{w}_{\rho+1}\, dx_{\rho+1}$$

joint i-1:
$$V_{i-1} = \frac{P(\ell_i - \alpha)}{\ell_i} - \frac{m_{i-1}}{\ell_{i-1}}\int_0^{\ell_{i-1}} x_{i-1}\ddot{w}_{i-1}\, dx_{i-1} - \frac{m_i}{\ell_i}\int_0^{\ell_i} (\ell_i - x_i)\ddot{w}_i \, dx_i \tag{4}$$

joint i:
$$V_i = \frac{P\cdot\alpha}{\ell_i} - \frac{m_i}{\ell_i}\int_0^{\ell_i} x_i \ddot{w}_i \, dx_i - \frac{m_{i+1}}{\ell_{i+1}}\int_0^{\ell_{i+1}} (\ell_{i+1} - x_{i+1})\ddot{w}_{i+1}\, dx_{i+1}$$

Because of Eqs(3) and Eq(1) and after some manipulation, Eqs(4) become:

joint ρ:

$$A_\rho s_\rho + \frac{m_\rho \ell_\rho}{6}\ddot{s}_{\rho-1} + \frac{m_\rho \ell_\rho + m_{\rho+1}\ell_{\rho+1}}{3}\ddot{s}_\rho + \frac{m_\rho}{\ell_\rho}\int_0^{\ell_\rho} x_\rho \ddot{w}_{o,\rho}\,dx_\rho + \frac{m_{\rho+1}}{\ell_{\rho+1}}\int_0^{\ell_{\rho+1}}(\ell_{\rho+1} - x_{\rho+1})\,\ddot{w}_{o,\rho+1}\,dx_{\rho+1} = 0 \tag{5a}$$

joint i-1:

$$A_{i-1}s_{i-1} + \frac{m_{i-1}\ell_{i-1}}{6}\ddot{s}_{i-2} + \frac{m_{i-1}\ell_{i-1} + m_i\ell_i}{3}\ddot{s}_{i-1} + \frac{m_i\ell_i}{6}\ddot{s}_i + \frac{m_{i-1}}{\ell_{i-1}}\int_0^{\ell_{i-1}} x_{i-1}\ddot{w}_{o,i-1}\,dx_{i-1} + \frac{m_i}{\ell_i}\int_0^{\ell_i}(\ell_i - x_i)\,\ddot{w}_{o,i}\,dx_i = \frac{P(\ell_i - \alpha)}{\ell_i} \tag{5b}$$

joint i:

$$A_i s_i + \frac{m_i\ell_i}{6}\ddot{s}_{i-1} + \frac{m_i\ell_i + m_{i+1}\ell_{i+1}}{3}\ddot{s}_i + \frac{m_{i+1}\ell_{i+1}}{6}\ddot{s}_{i+1} + \frac{m_i}{\ell_i}\int_0^{\ell_i} x_i\ddot{w}_{o,i}\,dx_i + \frac{m_{i+1}}{\ell_{i+1}}\int_0^{\ell_{i+1}}(\ell_{i+1} - x_{i+1})\,\ddot{w}_{o,i+1}\,dx_{i+1} = \frac{P\cdot\alpha}{\ell_i} \tag{5c}$$

The equations of motion are:

$$\begin{aligned} &EI_\rho w_\rho'''' + m_\rho \ddot{w}_\rho = 0 \qquad (\text{for } \rho \neq i,\ \rho = 1,\ldots,n) \\ &EI_i w_i'''' + m_i \ddot{w}_i = P\cdot\delta(x_i - \alpha) \end{aligned} \tag{6a}$$

The above because of Eqs(3) become:

$$\begin{aligned} &EI_\rho w_{o,\rho}'''' + m_\rho \ddot{w}_{o,\rho} = -m_\rho \frac{\ell_\rho - x_\rho}{\ell_\rho}\ddot{s}_{\rho-1} - m_\rho \frac{x_\rho}{\ell_\rho}\ddot{s}_\rho \\ &EI_i w_{o,i}'''' + m_i \ddot{w}_{o,i} = P\cdot\delta(x_i - \alpha) - m_i \frac{\ell_i - x_i}{\ell_i}\ddot{s}_{i-1} - m_i \frac{x_i}{\ell_i}\ddot{s}_i \end{aligned} \tag{6b}$$

The system of Eqs(5) and Eq(6b) gives the unknowns $w_{o,i}$ and s_i (i=1 to n). We are searching a solution in the form of separate variables in the form:

$$w_{o,i} = \sum_k X_{ik}(x_i)\cdot T_{ik}(t) \tag{7}$$

where X_{ik} are the shape functions of the i^{th} beam, while T_{ik} are the time functions to be determined. Introducing the above expressions (7) into Eqs(6a) and Eqs(5) and taking into account that the shape functions of a simply supported beam are $\sin(k\pi x_i/\ell_i)$ and satisfy the equations for free motion, we obtain:

$$m_\rho\sum_k X_{\rho k}\ddot{T}_{\rho k}+m_\rho\sum_k \omega_{\rho k}^2 X_{\rho k}T_{\rho k}=-m_\rho\frac{\ell_\rho-x_\rho}{\ell_\rho}\ddot{s}_{\rho-1}-m_\rho\frac{x_\rho}{\ell_\rho}\ddot{s}_\rho\quad(\rho=1,\dots,n,\ \rho\neq i)\tag{8a}$$

$$m_i\sum_k X_{ik}\ddot{T}_{ik}+m_i\sum_k \omega_{ik}^2 X_{ik}T_{ik}=P\cdot\delta(x_i-\alpha)-m_i\frac{\ell_i-x_i}{\ell_i}\ddot{s}_{i-1}-m_i\frac{x_i}{\ell_i}\ddot{s}_i\quad(\rho=i)\tag{8b}$$

$$\begin{gathered}\frac{m_\rho}{\ell_\rho}\sum_k(\ddot{T}_{\rho k}\int_0^{\ell_\rho}x_\rho X_{\rho k}dx_\rho)+\frac{m_{\rho+1}}{\ell_{\rho+1}}\sum_k(\ddot{T}_{\rho+1,k}\int_0^{\ell_{\rho+1}}(\ell_{\rho+1}-x_{\rho+1})X_{\rho+1,k}dx_{\rho+1})=\\-A_\rho s_\rho-\frac{m_\rho\ell_\rho}{6}\ddot{s}_{\rho-1}-\frac{m_\rho\ell_\rho+m_{\rho+1}\ell_{\rho+1}}{3}\ddot{s}_\rho-\frac{m_{\rho+1}\ell_{\rho+1}}{6}\ddot{s}_{\rho+1}\end{gathered}\tag{8c}$$

$$\begin{gathered}\frac{m_{i-1}}{\ell_{i-1}}\sum_k(\ddot{T}_{i-1,k}\int_0^{\ell_{i-1}}x_{i-1}X_{i-1,k}dx_{i-1})+\frac{m_i}{\ell_i}\sum_k(\ddot{T}_{i,k}\int_0^{\ell_i}(\ell_i-x_i)X_{i,k}dx_i)=\\\frac{P(\ell_i-\upsilon t)}{\ell_i}-A_{i-1}s_{i-1}-\frac{m_{i-1}\ell_{i-1}}{6}\ddot{s}_{i-2}-\frac{m_{i-1}\ell_{i-1}+m_i\ell_i}{3}\ddot{s}_{i-1}-\frac{m_i\ell_i}{6}\ddot{s}_i\end{gathered}\tag{8d}$$

$$\begin{gathered}\frac{m_i}{\ell_i}\sum_k(\ddot{T}_{i,k}\int_0^{\ell_i}x_iX_{i,k}dx_i)+\frac{m_{i+1}}{\ell_{i+1}}\sum_k(\ddot{T}_{i+1,k}\int_0^{\ell_{i+1}}(\ell_{i+1}-x_{i+1})X_{i+1,k}dx_{i+1})=\\\frac{P\upsilon t}{\ell_i}-A_is_i-\frac{m_i\ell_i}{6}\ddot{s}_{i-1}-\frac{m_i\ell_i+m_{i+1}\ell_{i+1}}{3}\ddot{s}_i-\frac{m_{i+1}\ell_{i+1}}{6}\ddot{s}_{i+1}\end{gathered}\tag{8e}$$

Multiplying Eq(8a) by $X_{\rho1}$, $X_{\rho2},\dots$, $X_{\rho n}$, successfully, integrating the outcome from 0 to ℓ_ρ ($\rho=1,\dots,n$), then Eq(8b) by X_{i1}, $X_{i2},\dots$, X_{in} and integrating the outcome from 0 to ℓ_i etc., we conclude to the following system:

$$\frac{m_\rho\ell_\rho}{2}\ddot{T}_{\rho k}+\frac{m_\rho\ell_\rho\omega_{\rho k}^2}{2}T_{\rho k}=-\frac{m_\rho\ell_\rho}{k\pi}\ddot{s}_{\rho-1}-(-1)^{k+1}\frac{m_\rho\ell_\rho}{k\pi}\ddot{s}_\rho\tag{9a}$$

$$\frac{m_i\ell_i}{2}\ddot{T}_{ik}+\frac{m_i\ell_i\omega_{ik}^2}{2}T_{ik}=P\cdot\sin\Omega_i t-\frac{m_i\ell_i}{k\pi}\ddot{s}_{i-1}-(-1)^{k+1}\frac{m_i\ell_i}{k\pi}\ddot{s}_i\tag{9b}$$

$$\begin{gathered}\sum_k(-1)^{k+1}\frac{m_\rho\ell_\rho}{k\pi}\ddot{T}_{\rho k}+\sum_k\frac{m_{\rho+1}\ell_{\rho+1}}{k\pi}\ddot{T}_{\rho+1,k}=\\-A_\rho s_\rho-\frac{m_\rho\ell_\rho}{6}\ddot{s}_{\rho-1}-\frac{m_\rho\ell_\rho+m_{\rho+1}\ell_{\rho+1}}{3}\ddot{s}_\rho-\frac{m_{\rho+1}\ell_{\rho+1}}{6}\ddot{s}_{\rho+1}\end{gathered}\tag{9c}$$

$$\begin{gathered}\sum_k(-1)^{k+1}\frac{m_{i-1}\ell_{i-1}}{k\pi}\ddot{T}_{i-1,k}+\sum_k\frac{m_i\ell_i}{k\pi}\ddot{T}_{i,k}=\\\frac{P(\ell_i-\upsilon t)}{\ell_i}-A_{i-1}s_{i-1}-\frac{m_{i-1}\ell_{i-1}}{6}\ddot{s}_{i-2}-\frac{m_{i-1}\ell_{i-1}+m_i\ell_i}{3}\ddot{s}_{i-1}-\frac{m_i\ell_i}{6}\ddot{s}_i\end{gathered}\tag{9d}$$

$$\sum_k (-1)^{k+1} \frac{m_i \ell_i}{k\pi} \ddot{T}_{i,k} + \sum_k \frac{m_{i+1} \ell_{i+1}}{k\pi} \ddot{T}_{i+1,k} = \frac{P\upsilon t}{\ell_i} - A_i s_i - \frac{m_i \ell_i}{6} \ddot{s}_{i-1} - \frac{m_i \ell_i + m_{i+1} \ell_{i+1}}{3} \ddot{s}_i - \frac{m_{i+1} \ell_{i+1}}{6} \ddot{s}_{i+1} \tag{9e}$$

Where: $\Omega_i = \dfrac{i\pi\upsilon}{\ell_i}$.

The above system of equations (9) with unknowns the terms $T_{\rho 1}$, $T_{\rho 2}$,…, $T_{\rho k}$ (k=1 to n) and s_1, s_2,…, s_{n-1} and can be solved using the Laplace transformation. Thus, we set:

$$\begin{aligned} L T_{\rho k}(t) &= \overline{T}_{\rho k}(p) \\ L s_i(t) &= \overline{s}_i(p) \end{aligned} \tag{10}$$

From the above Eq(10) we get:

$$\begin{aligned} L\ddot{T}_{\rho k}(t) &= p^2\, \overline{T}_{\rho k}(p) - p\, T_{\rho k}(0) - \dot{T}_{\rho k}(0) \\ L\ddot{s}_i(t) &= p^2\, \overline{s}_i(p) - p\, s_i(0) - \dot{s}_i(0) \end{aligned} \tag{11}$$

where $T_{\rho k}(0), \dot{T}_{\rho k}(0), s_i(0), \dot{s}_i(0)$ are the initial conditions, which are known. Therefore, from Eqs (9), (10) and (11) we conclude to the following system:

$$\begin{aligned} &\left(\frac{m_\rho \ell_\rho}{2} p^2 + \frac{m_\rho \ell_\rho \omega_{\rho k}^2}{2}\right)\overline{T}_{\rho k} + \frac{m_\rho \ell_\rho}{k\pi} p^2\, \overline{s}_{\rho-1} + (-1)^{k+1} \frac{m_\rho \ell_\rho}{k\pi} p^2\, \overline{s}_\rho = \\ &\quad \frac{m_\rho \ell_\rho}{2}[pT_{\rho k}(0) - \dot{T}_{\rho k}(0)] - \frac{m_\rho \ell_\rho}{k\pi}[p s_{\rho-1}(0) + \dot{s}_{\rho-1}(0)] + (-1)^{k+1} \frac{m_\rho \ell_\rho}{k\pi}[p s_{\rho-1}(0) + \dot{s}_{\rho-1}(0)] \end{aligned} \tag{12a}$$

$$\begin{aligned} &\left(\frac{m_i \ell_i}{2} p^2 + \frac{m_i \ell_i \omega_{ik}^2}{2}\right)\overline{T}_{ik} + \frac{m_i \ell_i}{k\pi} p^2\, \overline{s}_{i-1} + (-1)^{k+1} \frac{m_i \ell_i}{k\pi} p^2\, \overline{s}_i = \frac{P\Omega_i}{p^2 + \Omega_i^2} + \\ &\quad + \frac{m_i \ell_i}{2}[pT_{ik}(0) - \dot{T}_{ik}(0)] - \frac{m_i \ell_i}{k\pi}[p s_{i-1}(0) + \dot{s}_{i-1}(0)] + (-1)^{k+1} \frac{m_i \ell_i}{k\pi}[p s_{i-1}(0) + \dot{s}_{i-1}(0)] \end{aligned} \tag{12b}$$

$$\begin{aligned} &\sum_k (-1)^{k+1} \frac{m_\rho \ell_\rho}{k\pi} p^2\, \overline{T}_{\rho k} + \sum_k \frac{m_{\rho+1} \ell_{\rho+1}}{k\pi} p^2\, \overline{T}_{\rho+1,k} + \Big[\frac{m_\rho \ell_\rho}{6} p^2\, \overline{s}_{\rho-1} + \Big(\frac{m_\rho \ell_\rho + m_{\rho+1} \ell_{\rho+1}}{3} p^2 + A_\rho\Big)\overline{s}_\rho + \\ &\quad + \frac{m_{\rho+1} \ell_{\rho+1}}{6} p^2\, \overline{s}_{\rho+1}\Big] = \sum_k (-1)^{k+1} \frac{m_\rho \ell_\rho}{k\pi}[p\, T_{\rho k}(0) + \dot{T}_{\rho k}(0)] + \sum_k \frac{m_{\rho+1} \ell_{\rho+1}}{k\pi}[p\, T_{\rho+1,k}(0) + \dot{T}_{\rho+1,k}(0)] + \\ &\quad + \Big\{\frac{m_\rho \ell_\rho}{6}[p s_{\rho-1}(0) + \dot{s}_{\rho-1}(0)] + \frac{m_\rho \ell_\rho + m_{\rho+1} \ell_{\rho+1}}{3}[p s_\rho(0) + \dot{s}_\rho(0)] + \frac{m_{\rho+1} \ell_{\rho+1}}{6}[p s_{\rho+1}(0) + \dot{s}_{\rho+1}(0)]\Big\} \end{aligned} \tag{12c}$$

$$\begin{aligned} &\sum_k (-1)^{k+1} \frac{m_{i-1} \ell_{i-1}}{k\pi} p^2\, \overline{T}_{i-1,k} + \sum_k \frac{m_i \ell_i}{k\pi} p^2\, \overline{T}_{i,k} + \Big[\frac{m_{i-1} \ell_{i-1}}{6} p^2\, \overline{s}_{i-2} + \Big(\frac{m_{i-1} \ell_{i-1} + m_i \ell_i}{3} p^2 + A_{i-1}\Big)\overline{s}_{i-1} + \\ &\quad + \frac{m_i \ell_i}{6} p^2\, \overline{s}_i\Big] = \sum_k (-1)^{k+1} \frac{m_{i-1} \ell_{i-1}}{k\pi}[p\, T_{i-1,k}(0) + \dot{T}_{i-1,k}(0)] + \sum_k \frac{m_i \ell_i}{k\pi}[p\, T_{i,k}(0) + \dot{T}_{i,k}(0)] + \\ &\quad + \Big\{\frac{m_{i-1} \ell_{i-1}}{6}[p s_{i-2}(0) + \dot{s}_{i-2}(0)] + \frac{m_{i-1} \ell_{i-1} + m_i \ell_i}{3}[p s_{i-1}(0) + \dot{s}_{i-1}(0)] + \frac{m_i \ell_i}{6}[p s_i(0) + \dot{s}_i(0)]\Big\} + \\ &\quad + P\frac{p\,\ell_{i-1} - \upsilon}{p^2\, \ell_{i-1}} \end{aligned} \tag{12d}$$

$$\sum_k(-1)^{k+1}\frac{m_i\ell_i}{k\pi}p^2\,\overline{T}_{i,k}+\sum_k\frac{m_{i+1}\ell_{i+1}}{k\pi}p^2\,\overline{T}_{i+1,k}+[\frac{m_i\ell_i}{6}p^2\,\overline{s}_{i-1}+(\frac{m_i\ell_i+m_{i+1}\ell_{i+1}}{3}p^2+A_i)\overline{s}_i+$$
$$+\frac{m_{i+1}\ell_{i+1}}{6}p^2\,\overline{s}_{i+1}]=\sum_k(-1)^{k+1}\frac{m_i\ell_i}{k\pi}[p\,T_{i,k}(0)+\dot{T}_{i,k}(0)]+\sum_k\frac{m_{i+1}\ell_{i+1}}{k\pi}[p\,T_{i+1,k}(0)+\dot{T}_{i+1,k}(0)]+ \tag{12e}$$
$$+\{\frac{m_i\ell_i}{6}[p\,s_{i-1}(0)+\dot{s}_{i-1}(0)]+\frac{m_i\ell_i+m_{i+1}\ell_{i+1}}{3}[p\,s_i(0)+\dot{s}_i(0)]+\frac{m_{i+1}\ell_{i+1}}{6}[p\,s_{i+1}(0)+\dot{s}_{i+1}(0)]\}+$$
$$+P\frac{\upsilon}{p^2\,\ell_i}$$

The above system of Eqs(12) is a linear system with respect to the unknowns $\overline{T}_{\rho k}$, $\overline{s}_{\rho k}$ (ρ=1,…,n). Solution of the above system gives the unknowns in the form:

$$\overline{U}(p)=\frac{N(p)}{M(p)}$$

where N(p) and M(p) are polynomials with respect to p, with M(p) of equal or higher order than N(p). Hence, Heaviside's rule can be applied, which leads finally to the following expression for the unknowns U(t):

$$U(t)=L^{-1}\overline{U}(p)=L^{-1}\,\frac{N(p)}{M(p)}=\sum_{j=1}^{r}\frac{N(\theta_i)\,e^{\theta_i t}}{M'(\theta_i)} \tag{13}$$

where θ_i are the r roots (j=1 to r) of the polynomial M(p).

3 NUMERICAL RESULTS

We consider a three-span bridge with lengths $L_1=L_3=10m$ and $L_2=15m$ which rests on two pontoons with area $A=40m^2$. The beams are made from steel with modulus of elasticity $E=2.1X10^6$ dN/cm^2, moment of inertia $I=0.00045m^4$ and mass per unit length m=100kg. At time t=0sec, a load P=20000 dN enters the bridge moving with speed υ.

Applying the equations of the preceding paragraphs for different values of the speed υ (55, 90, 160km/h), we obtain the diagrams in *Fig. 3* and *Fig. 4*, which show the oscillations of the middle of the three spans w_{o1}, w_{o2}, w_{o3}, and the sinking s_1 and s_2 of the two pontoons, respectively.

4 CONCLUSIONS

A very simple approach to determine deflections of a bridge on floats based on closed form solutions is presented. From the above results, one can draw the following conclusions: The influence of the moving load velocity to the dynamic response of the bridge is significant, especially for the intermediate span. As the load velocity increases, the maximum deflection also increases and becomes maximum after the load pass. The oscillation of the intermediate span is strongly affected by the ones of the neighboring spans due to the pier sinking.

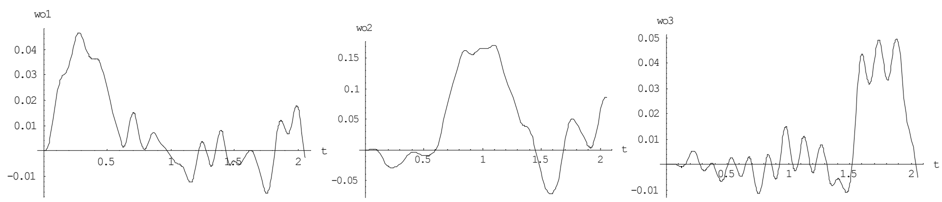

(a) 55km/h – 15m/s

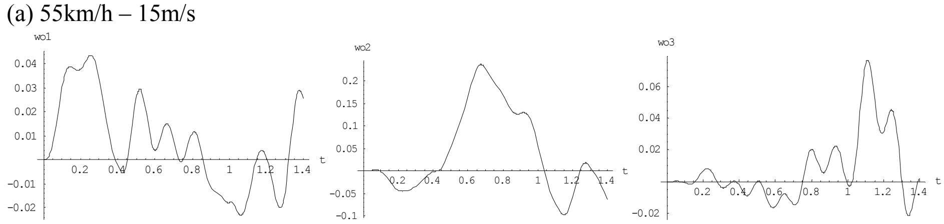

b) 90km/h – 25m/s

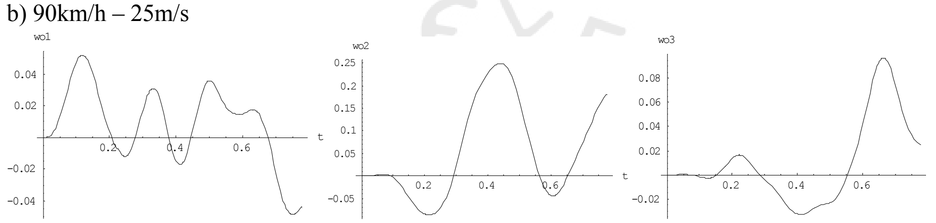

c) 160km/h – 45m/s

Figure 3. Mid-span oscillations w_{o1}, w_{o2}, w_{o3} for various speeds υ of the moving load P

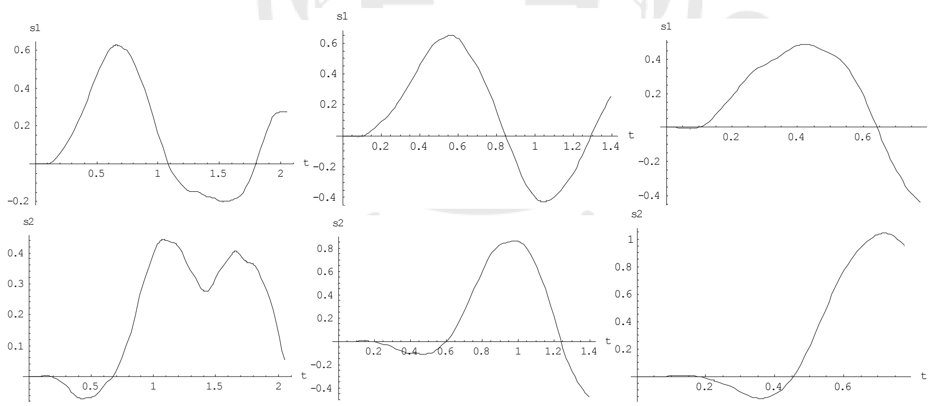

Figure 4. Pontoon sinking s_1 (first raw) and s_2 (second raw) for speeds υ (55, 90 and 160km/h) of the moving load P

REFERENCES

[1] Seif M.S., Inoue Y., "Dynamic analysis of floating bridges", Journal of Marine Structures, Vol.11(1),pp. 29-46, 1998.

[2] Fleischer D., Park S.-K., "Plane hydroelastic beam vibrations due to uniformly moving one axle vehicle", Journal of Sound and Vibration, Vol. 273, pp. 585-606, 2004.

CONCEPTUAL DESIGN OF THE YONGDING RIVER BRIDGE IN BEIJING

Ru-cheng Xiao[1], Dong-li Zhuang[2], Li-jun Jia[3], Jin Cheng[4], Bin Sun[5], Wan Zhang[6] and Jia Gao[7]

[1-7] Department of Bridge Engineering, Tongji University, Shanghai, 200092, P.R.China
e-mail: Xiaorc@mail.tongji.edu.cn, donlea_zhuang@163.com, jialj@mail.tongji.edu.cn, chengjin@mail. Tongji edu.cn, sunbin@mail.tongji.edu.cn, zwxc815@126.com

ABSTRACT: This paper examines the process of conceptual design of the YongDing River Bridge in Beijing, China. The bridge is located at ChangAn Avenue in Beijing, which is lined by prestigious buildings such as Wangfujing shopping area, Tiananmen Square and the Peoples' Congress Hall. This conceptual design considers issues of structural form, mathematical analysis, construction methods, and the relationship of the structure to the site. Specifically, the paper will show how the designer developed a design by starting with an initial aesthetically driven but structurally reasonable decision about form. Several innovative concepts in the design are also described.

KEY WORDS: Bridge; Conceptual design; Innovative concepts.

1 INTRODUCTION

Beijing Chang'an avenue Xiyan is well known as "the first street in china", which has an important political significance. The length of Changan avenue is about 6.4km from the Gucheng road in east to Sanshi road, this road is designed as major thoroughfare, of which design speed is 60km/h. The Yongding River Bridge is an important node of this extension road, whose length is about 650m from Shougang factory in east, and over Fengsha railway, DongBin river road, Yongding river and Hedi road. The Width of Urban Street is about 80m. Just as shown in Figure 1.

Figure 1. Schematic diagram of bridge position

Because of its important geographical location in Beijing, Yongding River Bridge is not only significant traffic hinge, but also an important landmark building which can combine economy, politics, history and culture together.

Yongding river bridge crosses the Rongding river in beijing, closes to industrial transformation zone of Shougang Company. It is about 1300m from Shijing mountain which is located in the north of Beijing (Figure 2). Changan avenue is center axis of Yongding River Bridge. Shijing mountain, Yongding River and Capital Steel Company are three indispensable surrounding environmental elements of this bridge.

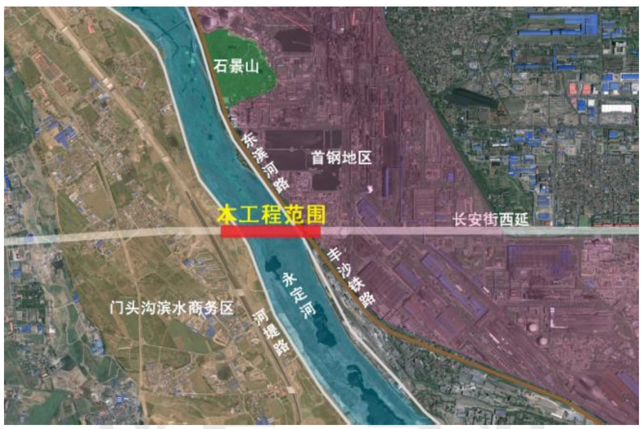

Figure 2. Surrounding environment

2 CONCEPT CREATION AND CHOICE

2.1 Design concept

In the whole design process, some factors are considered as follows: geographic and geomorphic conditions, weather, hydrology, geology, navigation, history, culture, lay-out and landscape et al. It is for satisfying nature condition and functional requirement as much as possible and making scheme be easily designed and constructed. This ideation is shown in Figure 3.

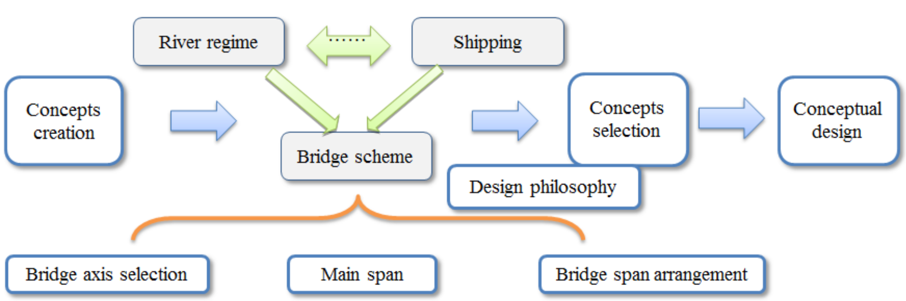

Figure 3. Ideation of bridge design

- Bridge style. Because its location condition is special, the peculiar style is not selected. But it is not appropriate that too conservative and traditional.
- Structure size. The surrounding environment coherence should be consider, example for Shijing mountain and Shougang condensing tower. In addition, the structure height should be lower in order not to block “Visual Corridors” from south to east along Dongbin river road.

In the design, the bridge sustainable development and green low carbon concept is long advocated. And it follows the 21st century international bridges six principles that are safety, appropriateness, economy, beauty, durability and environment.

2.2 Bridge span

The factors that influence span are shown as follows: 1) the route obliquely crosses riverway, and the skew angle is about 53 degrees; 2) the route in east over double-line electric railway; 3) the route in east over Dongbin river road, and the road width is 40m; 4) the route in west over Hedi road, and the road width is 30m. These are given in Figure 2.

Based on lay-out data and environment conditions, the piers in the location of dike is not permitted, or else it can do damage to dike. For this reason, the bridge only over Fengsha railway, Dongbin river road and dike in east with one span and over Hedi road and dike in west. And the Minimum span is about 120m. The navigation doesn’t affect span, however, the flood discharge capability of riverway must be considered. From statistical data of built Bridges up and downstream, the most bridge span in riverway is about 40m.

For all the above reasons, the span in east and in west is set about 120m, and the span in riverway is set about 40m.

2.3 Cross section

The width of red line is 80m. The width of road surface is 60m, of which layout is 5m (pavement) +7m (side road) +3m (lane separator) +30m (carriageway) +3m (lane separator) + 7m (side road) + 5m (pavement). Just as shown in Figure 4.

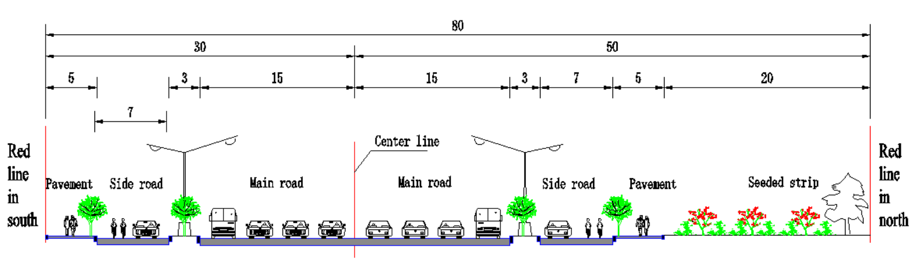

Figure 4. Road sectional drawing

Chang'an Street West Spur is urban trunk road which combines with Xiliuhuan expressway to form interchange and combines with Fengsha railway to form separate overpass highway. Therefore, Chang'an Street West Spur is also planned the separate overpass highway with Dongbin river road and Hedi road. That is shown in Figure 5.

Figure 5. Traffic planning of bridge surrounding

The single-layer bridge deck width is set more than 54m, if double width bridge is selected, the style selection will be limited, if the arch bridge with 120m span is adopted, the view of bridge in transverse will be affected by four arch ribs and the traffic will also be slow because of separate belt which is installed in location of two arch ribs, however, these problem can be solved with double-deck section which has the advantages as follows:

- Segregation of bicycle lane, pavement and carriageway. It offers advantageous condition to carry out interchange with Xiliuhuan: the traffic is more fluent, because pedestrian flow, motor vehicles flow and non-motor vehicles flow don’t cross that is impossible in the case of single-layer bridge deck; non-motor vehicles and pedestrian are safer.
- The bicycle lane and pavement can intersect the Guihuayi road on the same plane; the carriageway can over Guihuayi road.
- More styles can be chosen due to the small width of double-deck section.

So, the double-deck section is a right section in this bridge. Just as shown in Figure 6.

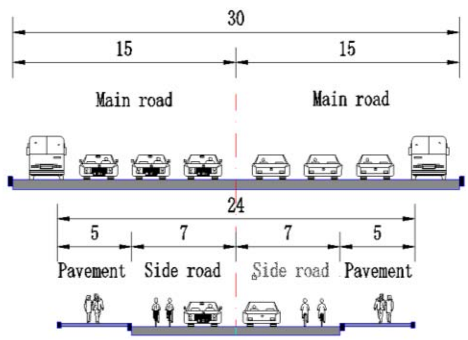

Figure 6. Cross section of double-deck

2.4 Bridge type

Four types of bridge are suitably constructed here, which include beam bridge, arch bridge, cable-stayed bridge and suspension bridge. The layout drawings of schemes are shown in figures as follows.

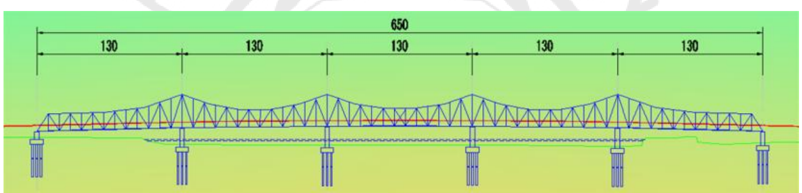

Figure 7. Five-span continuous truss beam bridge

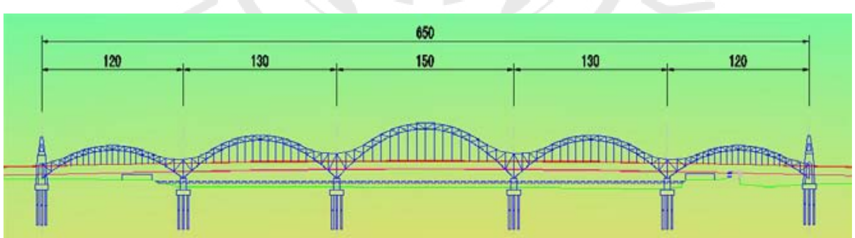

Figure 8. Five-span continuous truss arch bridge

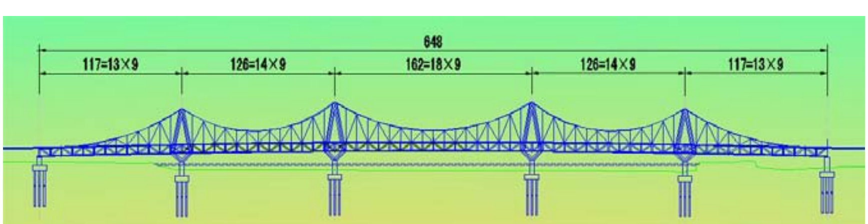

Figure 9. Five-span suspension bridge

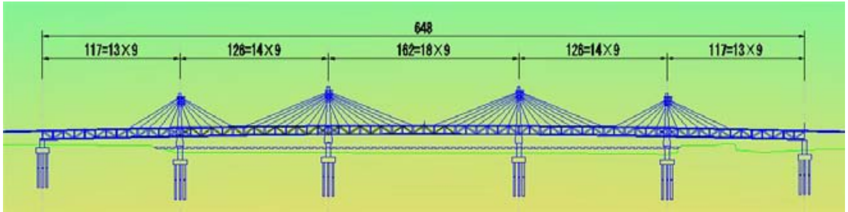

Figure 10. Five-span cable-stayed bridge

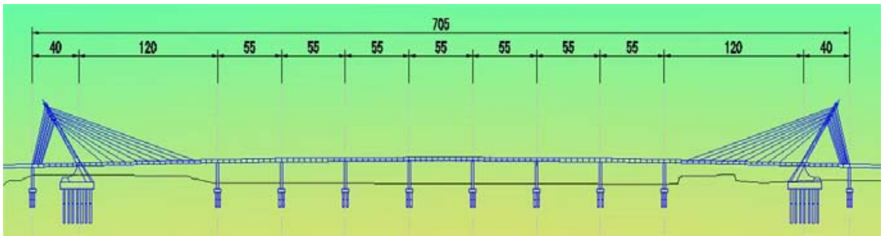

Figure 11. The bridge consists of cable-stayed bridge and beam bridge

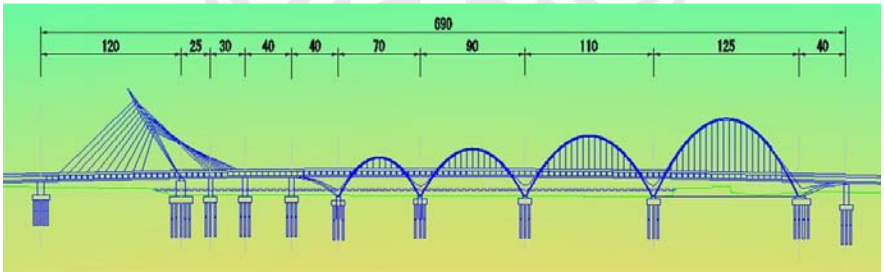

Figure 12. The bridge consists of cable-stayed bridge and arch bridge

These schemes have their own characteristics and advantages. After analysis and comparison, the bridge consisting of cable-stayed bridge and arch bridge is considered to be the best scheme. Just as shown in Figure 13.

Figure 13. Effect drawing of bridge consisting of cable-stayed bridge and arch bridge

3 THE SCHEME OF "DRAGON AND PHOENIX BRINGING AUSPICIOUSNESS"

This scheme consists of single pylon cable-stayed bridge and half-through multi-span arch bridge. The span is laid out as follows: (120m + 25m + 30m) + (40m + 40m + 70m + 90m + 110m + 125m + 40m) = 690m.

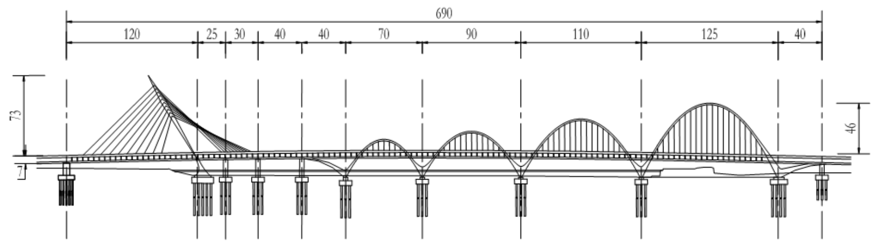

Figure 14. Elevation drawing of bridge

The pylon of cable-stayed is oblique with a skew angle of 30°. The pylon height is 88m, and the height of what above deck is 70m. The pylon cross section is circular. And the section size tends to decrease in direction of tower top and bottom, of which maximum diameter is 5m. The anchor point interval is 3.6m in pylon and 8m in main span girder. The distribution of anchor point in side span girder is curved that makes cable form spacial cable planes.

The arch rib of multi-span arch bridge is oblique inward with a skew angle of 11°. The arch rib height above deck tends to increase from 9.5m to 45.5m according to the golden ratio towards bank. The shape of arch rib is quadric curved lines. The segment above deck is rectangular steel box girder of which width is 2.5m, height is 1.5m, and thickness is 40mm, however, the segment below deck is concrete structure. The high-strength steel wires what PE layers protect are used for making suspender of which interval is 5m.

The girder consists of double decks, either of which is flat steel box girder. The upper deck, of what height is 2m, and of what width is 32m in arch bridge and 34m in cable-stayed bridge, is used for motor vehicles. The lower deck, of what width is 27m and height is 1.5m, is used for non-motor vehicles and pedestrian.

For arch bridge, the span continuous changed and the arch rib uneven shape makes bridge like a dragon in appearance which produces a strong sense of rhythm through repeating, gradient and similar form. By this, arch bridge, the old type, is given a new life powerful and vitalized. For cable-stayed bridge, the middle tower of the cable bridge leans to one side which results in "Tendentious Tension" and produces dynamic effect of volatilization outwards; the ends of the tower are tightened up which highlight the strong impression of structure. On the other side, two groups of the cable twist each other in space compose a space cable plane what likes a phoenix dancing in the sky with the fanning wings. These two types of the bridge, the masculinity and the femininity, the new and the old, are in sharp contrast, however, perfect match with each other. It is not only meets the internal balance of the structure and the force in mechanics, but also reflects the strength on an even profounder level. The design idea comes from the limiting factor. The main span of the cable bridge and the maximum span of the arch bridge are designed to cross the embankment and the railroad; meanwhile, the short ones are designed to cross riverway which needn't meet the navigation expectation. Through this way, the demand both of function and cost can be satisfied. The unique style and design theory of the bridges reflect the spirit of innovation and the future development, highlighting its status of landmark site.

Figure 15. Effect drawing of "Dragon and Phoenix Bringing Auspiciousness" in night

4 CONCLUSIONS

The conceptual design of Beijing Chang'an avenue Xiyan Yongding river bridge meets traffic function in region of west Chang'an avenue. In the design process, the factors, what include environment condition, human landscape, historical and cultural background, what emphasize urban landscape organization and reasonable coherence with surrounding landscape, and what consider harmony with the adjacent structure, geography and environment, is analyzed that cause the scheme of "Dragon and Phoenix Bringing Auspiciousness". This scheme creatively combines two bridge types that make the bridge beautiful, novel, practical and economy. And the solution of double-deck achieves the separation of people and vehicles what provide good conditions for reasonable traffic organization surrounding.

REFERENCES

[1] XIANG Hai-fan, XIAO Ru-cheng. *Conceptual Design of Bridge*. Beijing: China Communications Press, 2011, 03.
[2] Architectural Design＆Research Institute of Tongji University. Design of Chang'an Venue Xiyan Yongding River Bridge.

FLOATING BRIDGES UNDER MOVING LOADS

Tassos Avraam[1], Ioannis G. Raftoyiannis[2] and George T. Michaltsos[3]

[1,2,3] National Technical University of Athens, Dept. of Civil Engineering, Greece
e-mail: avraamt@central.ntua.gr, rafto@central.ntua.gr, michalts@central.ntua.gr

ABSTRACT: The dynamic response of a floating bridge consisted of simply connected non-deformable pontoons under a moving load with constant velocity is presented. Taking into account the moving load and the buoyancy forces, the dynamic equilibrium ends to dynamical equations of motion for the joints between pontoons. Using Laplace transformations, analytical solutions are determined for the dynamical deflections of the joints, which are shown in related diagrams for several velocities of the moving load.

KEY WORDS: Floating Bridge; Moving Loads; Pontoons; Dynamic Behavior

1 INTRODUCTION

Pontoon bridges were used since ancient times to cross wide rivers. In our days floating structures are still in wide use in both military and civil constructions. Many floating bridges have been constructed across rivers and seas instead of conventional bridges based on piers and abutments in several countries. One of the most well known pontoon bridges in Europe is the double deck steel pontoon bridge in Instanbul spanning over the Bosporos, which was constructed in the beginning of the 20th century. Other floating bridges are the Lacey V. Murrow Bridge, the Hood Canal Bridge in USA, the Bergs Ysundet Floating Bridge in Norway and the Daxie Island Floating Bridge in China.

Some of their advantages compared to conventional structures include the reduced environmental impact, the ability of relocation and the significant low costs in deep water structures.

Two different structural forms have been used until now for floating bridges: a continuous-pontoon type bridge which is made of closely connected pontoons and ramps pressed to the shore banks and a discrete pontoon type bridge which has a beam deck and several discrete-pontoons functioning as piers. In both cases the supports for the dead and the live loads on the bridge due to the buoyancy of water.

Floating bridges usually are designed by applying the theory of elastic foundation (neglecting hydrodynamic effects) or more realistically by considering hydrodynamic effects using hydrodynamic masses and dampers [1]. Fleischer and Park [2] used modal analysis to study the hydroelastic vibration of a beam under an uniformly moving one axle vehicle. Seif and Inoue [3] investigated the dynamic behavior of a discrete-pontoon floating bridge under the condition of wave effects with the finite element method.

We must mention the studies of Wang et al [4], Liu-chao Qiu [5], Chonan [6] and Sneyd et al [7-9].

The problem can be divided into a hydrodynamic problem for the liquid flow and an elastic problem for the pontoons' oscillations. In the restricted length of this paper, the hydrodynamic influence of the liquid flow is omitted. This is the object of a next, more extensive, paper.

In this study the dynamic response of a continuous floating bridge with closely connected pontoons under a moving load is presented. Using Laplace transformations analytical solutions for the dynamic deflections of the joints between pontoons are determined. The water surface is taken to be in calm and its level remains invariable. The pontoons supposed to be non-deformable and situated in dynamic equilibrium by taking into account, the moving load, the buoyancy forces and the vertical forces, which are developed between pontoons (the horizontal ones are neglected).

2 MATHEMATICAL MODEL

2.1 Acceptances

2.1.1 We consider a floating bridge with individual elements (pontoons) of equal length "ℓ", width b and height h, while the thickness of walls are t.

2.1.2 The pontoons are practically non-deformable, while m is the mass of each pontoon.

2.1.3 Each element of the bridge is of homogeneous beam with rectangular cross-section while its supports are fixed, allowing the element's free rotation. This is a suitable model for continuous floating bridges with closely connected pontoons.

2.1.4 During the bridge's oscillations, we omit the horizontal forces acting between individual elements.

2.1.5 The level of the water remains invariable.

2.1.6 A load P moves on the central axis of the bridge with constant speed υ. At t=0 the load enters the bridge.

2.1.7 On the random pontoon "i" the following forces act:
The moving load P, the reactions of the neighbouring pontoons (i-1) and (i+1), the buoyancy forces, the inertia forces $m\ddot{w}$ and the inertia mass-moments $J_p \cdot \ddot{\varphi}$.

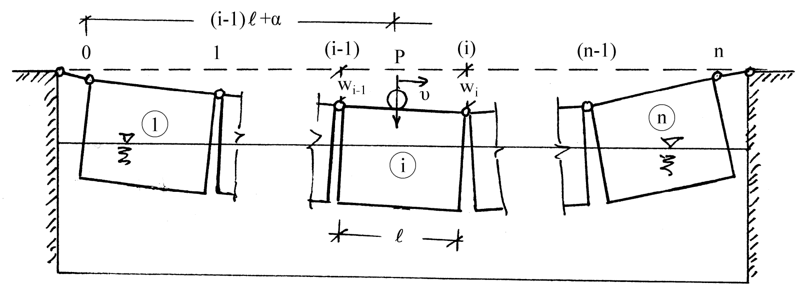

Figure 1. Floating bridge model

2.1.8 In order for us to determine the mass-moment of inertia J_p, we have (Fig.3):

Sides 1.

$$I_x = 2\rho \cdot t \cdot \ell \cdot b \cdot \left(\frac{h}{2}\right)^2 , \quad I_z = 2\rho \cdot t \cdot b \cdot \frac{\ell^3}{12}$$

Sides 2.

$$I_x = 2\rho \cdot t \cdot b \cdot \frac{h^3}{12} \quad , I_z = 2\rho \cdot t \cdot h \cdot b \cdot \left(\frac{\ell}{2}\right)^2$$

Sides 3.

$$I_x = 2\rho \cdot t \cdot \ell \cdot \frac{h^3}{12} \quad , \quad I_z = 2\rho \cdot t \cdot h \cdot \frac{\ell^3}{12}$$

For the entire pontoon:

$$I_x = \frac{\rho \cdot t}{6} \cdot \left(3\ell \cdot b \cdot h^2 + b \cdot h^3 + \ell \cdot h^3\right)$$

$$I_z = \frac{\rho \cdot t}{6} \cdot \left(3b \cdot h \cdot \ell^2 + b \cdot \ell^3 + h \cdot \ell^3\right) \tag{1}$$

$$I_p = \frac{\rho \cdot t}{6} \cdot \left(3b \cdot h \cdot \ell \cdot (\ell + h) + \cdot h^3 (\ell + b) + \ell \cdot^3 (b + h)\right)$$

where ρ is the specific mass of the pontoon's material.

2.1.9 Given that the random pontoon "i" is deformed as it is shown in Fig. 2,we have :

$$\varphi = \frac{w_i - w_{i-1}}{\ell} \quad \text{and thus :} \quad \ddot{\varphi} = \frac{\ddot{w}_i - \ddot{w}_{i-1}}{\ell}$$

Therefore the developed forces V_{Jp} are:

$$V_{J_p} = J_p \cdot \frac{\ddot{\varphi}}{\ell} = J_p \cdot \frac{\ddot{w}_i - \ddot{w}_{i-1}}{\ell^2} \tag{2}$$

with directions as they are shown in Fig. 2.

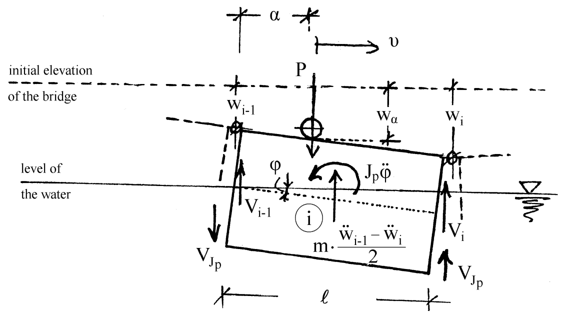

Figure 2. Equilibrium of a pontoon

3 ANALYSIS

Equilibrium of random elements (i-1) , I ,and (i+1) gives:

Pontoon (i-1):

$$V_{i-2} = -(\frac{m\ell^4}{4} + \frac{J_p}{\ell^2})\ddot{w}_{i-2} - (\frac{m\ell^4}{4} - \frac{J_p}{\ell^2})\ddot{w}_{i-1} - \frac{b\ell^2}{3} w_{i-2} - \frac{b\ell^2}{6} w_{i-1} \quad (3a)$$

$$V_{i-1} = -(\frac{m\ell^4}{4} - \frac{J_p}{\ell^2})\ddot{w}_{i-2} - (\frac{m\ell^4}{4} + \frac{J_p}{\ell^2})\ddot{w}_{i-1} - \frac{b\ell^2}{6} w_{i-2} - \frac{b\ell^2}{3} w_{i-1} \quad (3b)$$

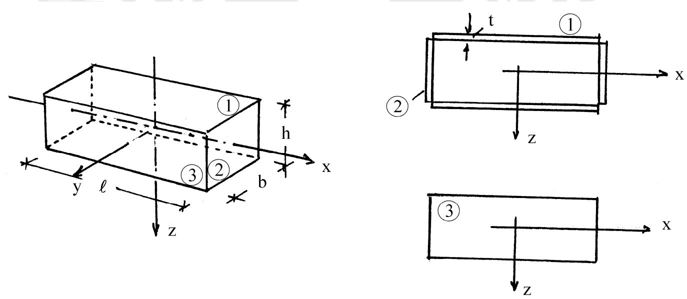

Figure 3. Pontoon geometry

Pontoon i:

$$V_{i-1} = -(\frac{m\ell^4}{4} + \frac{J_p}{\ell^2})\ddot{w}_{i-1} - (\frac{m\ell^4}{4} - \frac{J_p}{\ell^2})\ddot{w}_{i} - \frac{b\ell^2}{3} w_{i-1} - \frac{b\ell^2}{6} w_{i} + P(\ell - \alpha) \quad (3c)$$

$$V_{i} = -(\frac{m\ell^4}{4} - \frac{J_p}{\ell^2})\ddot{w}_{i-1} - (\frac{m\ell^4}{4} + \frac{J_p}{\ell^2})\ddot{w}_{i} - \frac{b\ell^2}{6} w_{i-1} - \frac{b\ell^2}{3} w_{i} + P \cdot \alpha \quad (3d)$$

Pontoon (i+1):

$$V_{i} = -(\frac{m\ell^4}{4} + \frac{J_p}{\ell^2})\ddot{w}_{i} - (\frac{m\ell^4}{4} - \frac{J_p}{\ell^2})\ddot{w}_{i+1} - \frac{b\ell^2}{3} w_{i} - \frac{b\ell^2}{6} w_{i+1} \quad (3e)$$

$$V_{i+1} = -(\frac{m\ell^4}{4} - \frac{J_p}{\ell^2})\ddot{w}_i - (\frac{m\ell^4}{4} - \frac{J_p}{\ell^2})\ddot{w}_{i+1} - \frac{b\ell^2}{6} w_i - \frac{b\ell^2}{3} w_{i+1} \qquad (3f)$$

For the random joint j, the following condition must be fulfilled:

$$V_{j_{right}} = V_{j_{left}}$$

Joint (j)

$$(\frac{m\ell^4}{4} - \frac{J_p}{\ell^2})\ddot{w}_{j-1} + 2(\frac{m\ell^4}{4} + \frac{J_p}{\ell^2})\ddot{w}_j + (\frac{m\ell^4}{4} - \frac{J_p}{\ell^2})\ddot{w}_{j+1} + \frac{b\ell^2}{6} w_{j-1} + \frac{2b\ell^2}{3} w_j + \frac{b\ell^2}{6} w_{j+1} = 0 \qquad (4a)$$

Joint (i-1)

$$(\frac{m\ell^4}{4} - \frac{J_p}{\ell^2})\ddot{w}_{i-2} + 2(\frac{m\ell^4}{4} + \frac{J_p}{\ell^2})\ddot{w}_{i-1} + (\frac{m\ell^4}{4} - \frac{J_p}{\ell^2})\ddot{w}_i + \frac{b\ell^2}{6} w_{i-2} + \frac{2b\ell^2}{3} w_{i-1} + \frac{b\ell^2}{6} w_i = P(\ell - \upsilon t) \qquad (4b)$$

Joint (i)

$$(\frac{m\ell^4}{4} - \frac{J_p}{\ell^2})\ddot{w}_{i-1} + 2(\frac{m\ell^4}{4} + \frac{J_p}{\ell^2})\ddot{w}_i + (\frac{m\ell^4}{4} - \frac{J_p}{\ell^2})\ddot{w}_{i+1} + \frac{b\ell^2}{6} w_{i-1} + \frac{2b\ell^2}{3} w_i + \frac{b\ell^2}{6} w_{i+1} = P \cdot \upsilon t \qquad (4c)$$

The solution of eqs(4) , gives the unknown w_i (i=1 to n-1) given that w_0=w_n=0

3.1 The free vibrating bridge

For the random element j will be:

$$\alpha\ddot{w}_{j-1} + \beta\ddot{w}_j + \alpha\ddot{w}_{j+1} + 1 + \frac{b\ell^2}{6} w_{j-1} + \frac{2b\ell^2}{3} w_j + \frac{b\ell^2}{6} w_{j+1} = 0 \qquad (5a)$$

with j=1 to n and $\alpha = \frac{m\ell^2}{4} - \frac{J_p}{\ell^2}$, $\beta = 2 \cdot (\frac{m\ell^2}{4} + \frac{J_p}{\ell^2})$ (5b)

Considering that $w_j = \overline{w}_j \cdot e^{i\omega t}$ (6)

eqn(5) changes to

$$(\frac{b\ell^2}{6} - \alpha\omega^2) \cdot \overline{w}_{j-1} + (\frac{2b\ell^2}{3} - \beta\omega^2) \cdot \overline{w}_j + (\frac{b\ell^2}{6} - \alpha\omega^2)\overline{w}_{j+1} = 0 \text{ with j=1 to n} \qquad (7)$$

In order for the above system to have nontrivial solutions, the determinant of the unknowns' coefficients must be equal to zero:

$$\|\Delta\| = 0 \qquad (8)$$

The above gives the eigenfrequency of the system. Neglecting the first of equation 7 (j=1), one can determine the $\overline{w}_j$ (j=2 to n) in relation to $\overline{w}_1$.

Therefore the free vibration of the j joint is given by the following equation:

$$w_j(t) = \overline{w}_j(w_1) \cdot (A_j \cdot \sin\omega t + B_j \cdot \cos\omega t) \qquad (9)$$

3.2 The forced vibrating bridge

Equations (4) , describe the bridge's motion caused by a load P, which enters the element (I) at t=0 with speed υ . For t<0, the bridge oscillates because of the motion of P on (i-1) element.

We set: $$Lw_j(t) = W_j(p) \tag{10}$$

And with initial conditions because of the motion of P on the (i-1) element will be: $$L\ddot{w}_j(t) = p^2 W_j(p) - pw_j(0) - \dot{w}_j(0) \tag{11}$$

Therefore, equations (4) with the symbolisms of eqs (5) become:

Joint j: $$(\alpha p^2 + \frac{b\ell^2}{6})W_{j-1} + (\beta p^2 + \frac{2b\ell^2}{3})W_j + (\alpha p^2 + \frac{b\ell^2}{6})W_{j+1} =$$
$$= \left[\alpha w_{j-1}(0) + \beta w_j(0) + \alpha w_{j+1}(0)\right]\cdot p + \left[\alpha\dot{w}_{j-1}(0) + \beta\dot{w}_j(0) + \alpha\dot{w}_{j+1}(0)\right] \tag{12a}$$

Joint (i-1): $$(\alpha p^2 + \frac{b\ell^2}{6})W_{i-2} + (\beta p^2 + \frac{2b\ell^2}{3})W_{i-1} + (\alpha p^2 + \frac{b\ell^2}{6})W_i =$$
$$= \left[\alpha w_{i-2}(0) + \beta w_{i-1}(0) + \alpha w_i(0)\right]\cdot p + \left[\alpha\dot{w}_{i-2}(0) + \beta\dot{w}_{i-1}(0) + \alpha\dot{w}_i(0)\right] + P(\frac{L}{p} - \frac{\upsilon}{p^2}) \tag{12b}$$

Joint i: $$(\alpha p^2 + \frac{b\ell^2}{6})W_{i-1} + (\beta p^2 + \frac{2b\ell^2}{3})W_i + (\alpha p^2 + \frac{b\ell^2}{6})W_{i+1} =$$
$$= \left[\alpha w_{i-1}(0) + \beta w_i(0) + \alpha w_{i+1}(0)\right]\cdot p + \left[\alpha\dot{w}_{i-1}(0) + \beta\dot{w}_i(0) + \alpha\dot{w}_{i+1}(0)\right] + \frac{P\upsilon}{p^2} \tag{12c}$$

The solution of the above system gives the unknowns $W_j(p)$.

Therefore, it will be: $w_j(t)=L^{-1}\, W_j(p)$

4 NUMERICAL EXAMPLE

Let us consider now a bridge composed by 5 pontoons with dimensions ℓ=15m, b=6m and h=5m, or $A=15\cdot 6=90m^2$ B=60000 dN. A load-mass $P = M\cdot g = 30000$ dN enters the bridge with speed υ.

Applying the equations of the previous paragraphs and studying the bridge's motion during the time of the moving load passage, plus for time $3\ell/\upsilon$ after the load exit, we gather the following diagrams of Figures 4 and 5.

5 CONCLUSIONS

1. A very simple approach to determine deflections of a floating bridge is presented. The results have been obtained by closed form from analytical solutions.
2. The influence of the moving load velocity to the dynamic response of the bridge is significant, especially for usual velocities 10-20 m/sec.
3. The restricted length of a conference presentation does not allow an extensive study of the influence of the rotational-mass moment of inertia to the bridge deformation.
4. The latter as well as the hydrodynamic influence of the liquid flow is the object of a new study, which will be published soon.

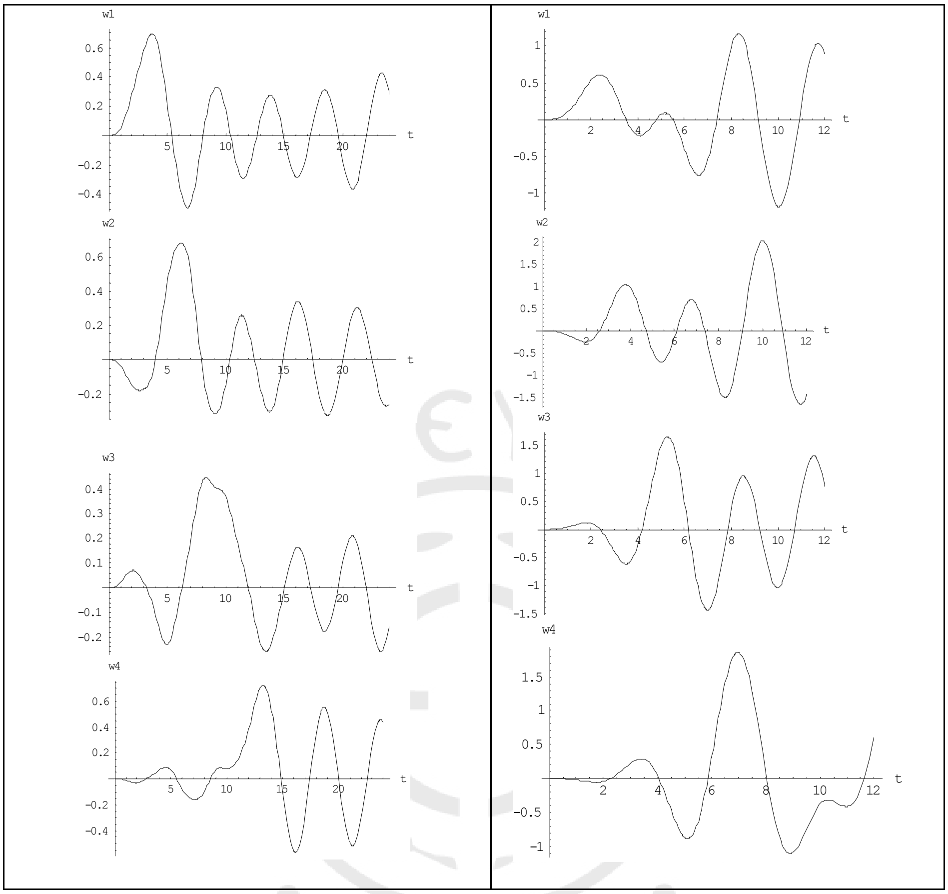

v=5m/sec (18km/h) v=10m/sec (36km/h)

Figure 4. Bridge motion for moving load velocities v=5m/s and v=10m/s

REFERENCES

[1] Vugts J. H., "The hydrodynamic coefficients for swaying, heaving and rolling cylinders in a free surface", International Shipbuilding Progress, Vol. 15, pp. 251-276, 1968

[2] Fleischer D., Park S.-K., "Plane hydroelastic beam vibrations due to uniformly moving one axle vehicle", Journal of Sound and Vibration, Vol. 273, pp. 585-606, 2004

[3] Seif M.S.,Inoue Y., "Dynamic analysis of floating bridges", Journal of Marine Structures, Vol.11(1),pp. 29-46, 1998

[4] Wang C., Fu S.-X., Li N. Et al, "Dynamic anlysis of a pontoon-separated floating bridge subjected to a moving load", Journal of China Ocean Engineering, Vol. 20(3), pp. 419-430, 2006

[5] Qiu L. C., "Modeling and simulation of transient response of aflexible beam floating in finite depth water under moving loads", Journal of Applied Mathematical Modeling", Vol. 33, pp. 1620-1632, 2009

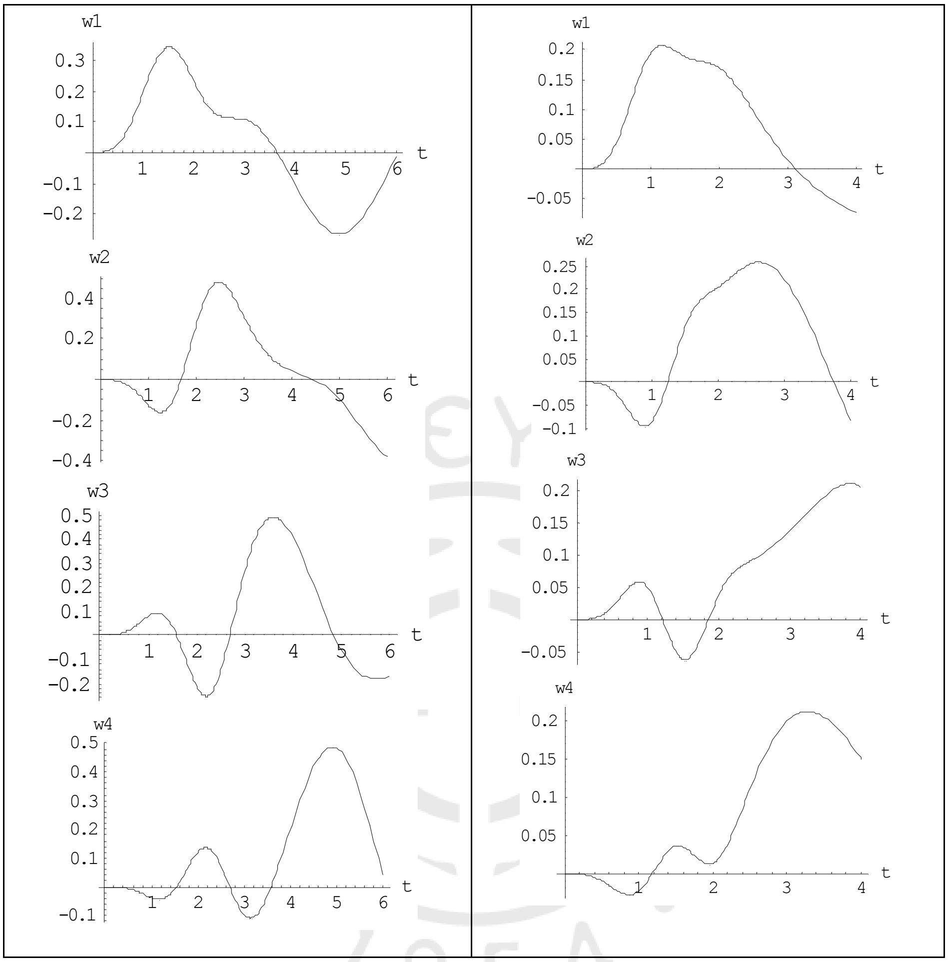

v=20m/sec (72km/h) v=30 m/sec (108km/h)

Figure 5. Bridge motion for moving load velocities v=20m/s and v=30m/s

[6] Chonan S., “Moving load on a pre-stressed plate resting on a half space”, Ingenieur Archiv, Vol. 45, pp. 171-178, 1976

[7] Davys J., Hosking R., Sneyd A., “Waves due to a Steadily moving source on a floating ice plate”, Journal of Fluid Mechanics, Vol. 158, pp. 269-287, 1985

[8] Schulkes R., Hosking R.,Sneyd A., “Waves due to a steadily moving source on a floating ice plate,part 2”, Journal of Fluid Mechanics, Vol. 180, pp. 297-318, 1987

[9] Schulkes R., Sneyd A., “Time-dependant response of floating ice to a steadily moving load”, Journal of Fluid Mechanics, Vol. 186, pp. 25-46, 1988

LATERAL BUCKLING OF UPPER-CORD SECTION IN STEEL TRUSS BRIDGES

Ioannis G. Raftoyiannis[1] and Tassos P. Avraam[2]

[1,2] National Technical University of Athens, Dept. of Civil Engineering, Greece
e-mail: rafto@central.ntua.gr, avraamt@central.ntua.gr

ABSTRACT: In this work, the elastic buckling load of the upper-cord section in steel truss bridges is thoroughly investigated. The elastic critical loads for lateral buckling of the upper cord section are determined and the results are compared with the ones obtained using Eurocode 3 provisions. The findings can be employed for the design of steel truss bridges against lateral buckling.

KEY WORDS: Steel Bridges; Truss Bridges; Upper Cord; Lateral Buckling

1 INTRODUCTION

The problem of determining the critical load of the upper cord section in steel truss bridges was studied in general by numerous researchers (Timoshenko [1], B1eich [2]) by applying a linear stability theory and various approximate methods of calculation have been formulated. The corresponding stability check has been proven necessary for bottom-pass steel truss bridges due to the absence of lateral bracing systems on the upper cord. In this type of bridges, where the distressed upper cords do not allocate any lateral bracing, lateral buckling is prevented via the elastic stiffness of cross frames, each one of which consists from a cross girder and the vertical members of the left and the right main truss beams. These frames are placed at equal distances along the length of the bridge (at the locations of the cross girders) and provide lateral flexible supports to the upper cord sections, thus preventing lateral instability failure. For simplicity reasons and because of the symmetry, we may consider only half of the frame. In order to prevent lateral buckling of the upper cord section (global instability) the stiffness of the half-frame should be bigger than a specific limiting value. In engineering practice, all internal cross frames have the same stiffness properties while the two end frames are designed to be stiffer than the internal ones. When the cross frames are relatively flexible, the upper cord section, being in compression, buckles laterally with one half-wave of length L since the cross frames do not provide sufficient lateral support. Contrarily, when the cross frames are very stiff, the upper cord section is fully supported at the joints and buckles with a number of half-waves (local instability) equal to the number of openings of the main girder. The aforementioned modes of buckling are the two limiting cases of upper cord instability, while numerous intermediate cases exist where lateral buckling of the upper cord occurs with intermediate half-wave lengths and corresponding intermediate critical load values. The above are valid only in cases where both the area of the upper cord section and the internal compression are constant along the length of the bridge while the two end cross-frames are considered fully inflexible. In reality though, the internal compression has a stepped distribution depending on the number of openings while the area of the upper cord section is not constant. Moreover, the two end cross-frames are stiffer than the internal ones but it is advisable to consider their actual flexibility. In *Fig. 1* one can see a bottom pass steel truss bridge with unbraced upper cord main girders and one of the corresponding half cross-frames that provide elastic supports laterally to the upper cord section.

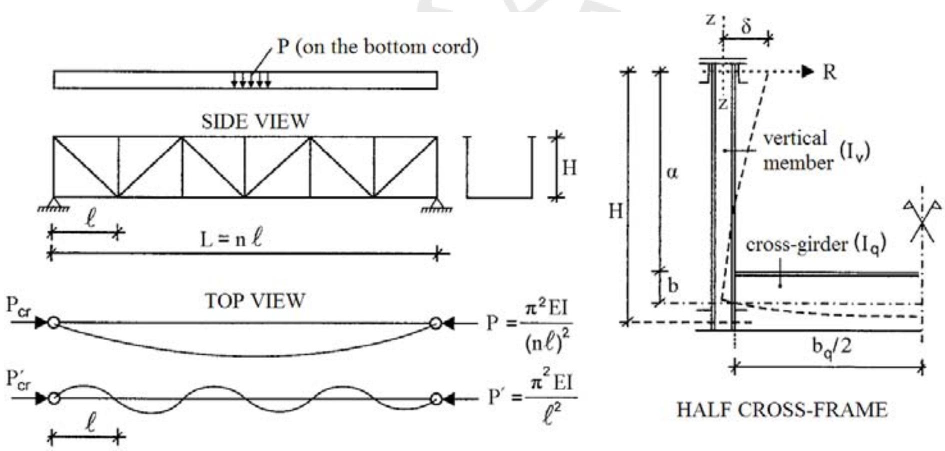

Figure 1. Steel truss bridge (bottom-pass) and half cross-frame

2 ANALYTICAL MODELS

A theoretical solution for this problem has been first developed by Timoshenko and the relative provisions in Eurocode 3 – Part 2 are based on this approach. In this approach, the upper-cord section of the main girder is considered as a simply supported beam resting on elastic foundation where the developed axial compression force follows a parabolic distribution. Let us consider the simply supported beam AB with constant cross section shown in *Fig. 2*, which is loaded by a compressive axial load q_x. The axial load q_x produces an internal compression N_x with parabolic type distribution. This distribution approaches the actual stepped distribution very well only when the number of openings is considerably large. The beam is supposed to be resting on elastic foundation with stiffness constant $c = C_d/\ell$, where C_d is the spring constant of each half cross frame and ℓ are the distances between each other. The degree of accuracy of this assumption depends also on the number of openings. Timoshenko presented a stability approach [1] for this problem and determined the critical load based employing energy methods. The critical load for lateral buckling of this beam is given by:

$$\frac{(q_0 L)_{cr}}{4} = \frac{\pi^2 EI_z}{L^2} \frac{\pi^2 (1 + \frac{cL^4}{\pi^4 EI_z})}{2(\frac{1}{3}\pi^2 - 1)} = \frac{\pi^2 EI_z}{(\beta L)^2} \tag{1}$$

where $q_0L/4$ is the internal compression at the half-length of the beam, β is a factor relating the equivalent buckling length to the actual length of the beam and c is the lateral distributed stiffness constant.

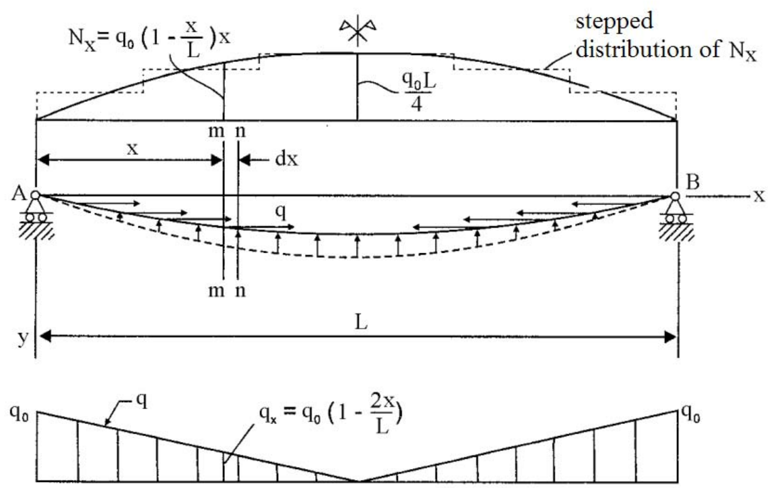

Figure 2. Simply supported compression beam resting on elastic foundation

The equivalent buckling length factor β can be taken from Table 1 as a function of the non-dimensional quantity $\Psi=cL^4/16EI_z$. It can be shown that a beam with constant cross-section along the length and constant axial compression resting on n-1 intermediate elastic lateral supports with spring constant C_d at equal distances between each other, starts behaving as a continuous beam based on immovable supports when the spring constant C_d takes values higher than:

$$C_d = \frac{n^3 \pi^2 EI_z}{\gamma L^3} \tag{2}$$

where n is the number of openings, EI_z is the lateral bending stiffness of the upper cord section, γ is a factor that depends on the number of openings n and L/n is the length of each opening.

Table 1. Values of factor β for the loading in *Fig. 2* with constant cross-section

Ψ	0	5	10	15	22.8	56.5	100	162.8	200	300	500	1000
β	0.696	0.524	0.443	0.396	0.363	0.324	0.290	0.259	0.246	0.225	0.204	0.174

Table 2. Values of factor γ for constant axial force with constant cross-section

n	2	3	4	5	6	7	9	11	∞
γ	0.500	0.333	0.293	0.276	0.268	0.263	0.258	0.255	0.250

The spring constant C_d of each half cross-frame can be computed from the following relation:

$$\frac{1}{C_d} = \frac{\alpha^3}{3EI_v} + \frac{(\alpha + b)^2 b_q}{2EI_q} \tag{3}$$

where I_v and I_b are the moments of inertia of the vertical member and the cross-girder, respectively, while the distances α, b and b_q are defined in *Fig. 1*. The critical load N_{cr} for buckling with n half-waves is

$$N_{cr} = mN_E \tag{4}$$

where N_E is the Euler load of the upper cord corresponding to buckling with a single half-wave and m is a coefficient [3] given by

$$m = \frac{2}{\pi^2}\sqrt{\gamma} \tag{5}$$

It should be pointed out at this stage that the buckling behavior of a compression beam resting on a Winkler type elastic foundation depends strongly on the lateral spring value c as well as on the boundary conditions and presents no similarities to the corresponding behavior of a simply supported beam. According to Bazant & Cedolin [4], the critical length (equivalent buckling length) is not related to the total length of the beam but to the bending stiffness EI and the lateral spring value c. Hence, overall buckling of the upper cord (one half-wave) is not likely to occur since it corresponds to a value higher than the critical load [5]. Thus, an analytical investigation of the upper cord lateral buckling is necessary in parametric sense.

Let us next consider the beam shown in *Fig. 3* with n equal length openings, which is axially compressed by a stepped internal force N(x) and it is resting on lateral springs with constants c_0 and c. Solution of the governing equation gives the expression for w(x) for opening i, which is:

$$w_i(x_i) = A_i \sin k_i x_i + B_i \cos k_i x_i + C_i x_i + D_i \quad (i=1,2,...n) \tag{6}$$

with

$$k_i^2 = \frac{N_i}{EI_i} \tag{7}$$

where N_i is the internal axial compression and EI_i is the bending stiffness for beam part i, respectively.

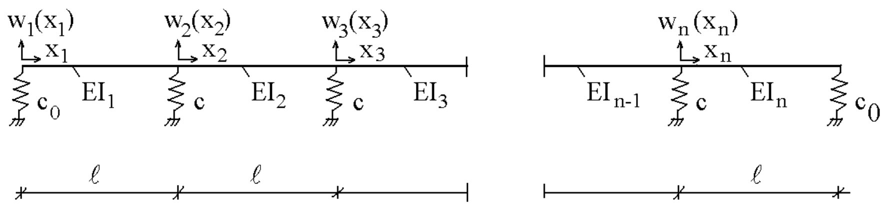

Figure 3. Model of the upper cord section with lateral supports

The coefficients A_i, B_i, C_i and D_i (i=1,2,...n) are determined by employing the boundary conditions for the first and the last part, which are

$$\begin{aligned} &M_1(0) = 0 \\ &V_1(0) - c_0 \cdot w_1(0) = 0 \\ &M_n(\ell) = 0 \\ &V_n(\ell) + c_0 \cdot w_n(\ell) = 0 \end{aligned} \tag{8}$$

while the continuity conditions for each intermediate part i (i=2,..,n-1) are

$$\begin{aligned} &w_{i-1}(\ell) = w_i(0) \\ &w'_{i-1}(\ell) = w'_i(0) \\ &M_{i-1}(\ell) + M_i(0) = 0 \\ &V_{i-1}(\ell) - V_i(0) + c \cdot w_i(0) = 0 \end{aligned} \tag{9}$$

The expressions for moment and shear are given by

$$\begin{aligned} &M_i(x_i) = -EI_i \cdot w''_i(x_i) \\ &V_i(x_i) = -EI_i \cdot w'''_i(x_i) - N_i w'_i(x_i) \end{aligned} \tag{10}$$

Substituting the expressions for w(x) from Eq.(6) and the expressions for moments and shear forces from Eq.(10) into Eq.(8) and Eq.(9) we obtain a linear homogeneous system of equations with respect to the unknowns A_i, B_i, C_i and D_i. In order that this system acquires a non-trivial solution, the determinant of the coefficients of the unknowns must be zero (buckling equation), thus corresponding to an eigenvalue problem. The first zero value of the determinant corresponds to the smaller buckling load, which is the critical load. At this point, we define the following non-dimensional quantities

$$\overline{A}_i = A_i / \ell, \;\; \overline{B}_i = B_i / \ell, \;\; \overline{C}_i = C_i, \;\; \overline{D}_i = D_i / \ell \tag{11}$$

$$\overline{k}_i^2 = N_i \ell^2 / EI_i = k_i^2 \ell^2 \qquad \text{(i=1,..,n)} \tag{12}$$

$$\overline{c}_0 = c_0 \ell^3 / EI_1, \;\; \overline{c} = c\ell^3 / EI_1 \tag{13}$$

as well as the stiffness ratios $r_i = EI_i/EI_1$ and the load ratios $\lambda_i = N_i/N_1$, for i=2,...,n. In the case where the stiffness EI and the axial compression N are constant (i.e. $r_i = 1$ and $\lambda_i = 1$ for all i), the buckling equation simplifies to:

$$\begin{vmatrix} [D_0] & [0] & [0] \\ [0] & [D_{i-1,i}] & [0] \\ [0] & [0] & [D_n] \end{vmatrix} = 0 \tag{14}$$

where the sub-matrices D_0, $D_{i-1,i}$ and D_n are

$$D_0 = \begin{bmatrix} 0 & -\bar{k}^2 & 0 & 0 \\ 0 & -\bar{c}_0 & -\bar{k}^2 & -\bar{c}_0 \end{bmatrix} \tag{15a}$$

$$D_{i-1,i} = \begin{bmatrix} \sin\bar{k} & \cos\bar{k} & 1 & 1 & 0 & -1 & 0 & -1 \\ \bar{k}\cos\bar{k} & -\bar{k}\sin\bar{k} & 1 & 0 & -\bar{k}^2 & 0 & -1 & 0 \\ \bar{k}^2\sin\bar{k} & \bar{k}^2\cos\bar{k} & 0 & 0 & 0 & -\bar{k}^2 & 0 & 0 \\ 0 & 0 & -\bar{k}^2 & 0 & 0 & \bar{c} & -\bar{k}^2 & \bar{c} \end{bmatrix} \tag{15b}$$

$$D_0 = \begin{bmatrix} -\bar{k}^2\sin\bar{k} & -\bar{k}^2\cos\bar{k} & 0 & 0 \\ \bar{c}_0\sin\bar{k} & \bar{c}_0\cos\bar{k} & \bar{c}_0 - \bar{k}^2 & \bar{c}_0 \end{bmatrix} \tag{15c}$$

and i is the intermediate spring number and $\bar{k}^2 = N/EI$.

3 NUMERICAL EXAMPLES

Let us consider the bottom-pass pedestrian steel truss bridge, which is 10.0m wide and is build as shown in *Fig. 4*. The design load on each main girder is q_{sd}=55.5kN/m. The critical load for lateral buckling of the upper cord will be determined according to the provisions of EC3 - Part 2, Timoshenko's theoretical approach and the analytical method developed herein. The two end cross-frames are considered fully stiff, while the cross sectional area of the upper cord is considered constant along the length of the bridge.

First, the distribution of the axial compression force in the upper cord is determined as follows N_1=555kN, N_2=888kN and N_3=999kN. Next, the equivalent spring stiffness C_d of each cross-frame is determined from Eq. (3)

$$C_d = \left(\frac{\alpha^3}{3EI_v} + \frac{(\alpha+b)^2 b_q}{2EI_q} \right)^{-1} = \left(\frac{356^3}{3 \cdot 21000 \cdot 11260} + \frac{386^2 \cdot 976}{2 \cdot 21000 \cdot 171000} \right)^{-1} = 11.93\,\text{kN/cm}$$

while the distributed stiffness is $c = C_d/\ell = 11.93/400 = 0.03\,\text{kN/cm}^2$. The factor $\gamma = cL^4/EI_z = 0.03\text{x}2400^4/21000\text{x}50990 = 929.5$ is determined according to EC3 from which we compute $m = 2\sqrt{\gamma}/\pi^2 = 6.18$ and finally $N_E = \pi^2 EI_z/L^2 = 1835$kN and $N_{cr} = mN_E = 6.18\text{x}1835 = 11340$kN.

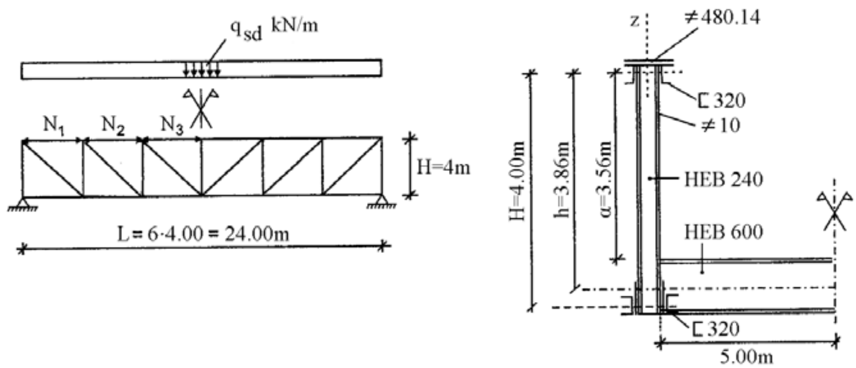

Figure 4. Steel truss bridge with 6 openings

According to Timoshenko's approach, we determine the non-dimensional quantity $\Psi=cL^4/16EI_z=0.03x2400^4/16x21000x50990=58.09$ and from Table 1 we obtain $\beta=0.323$. Thus, the critical load is $N_{cr}=\pi^2EI_z/(\beta L)^2=17586$kN.

Based on the analytical method developed herein, and assuming constant axial compression along the length of the bridge N=999kN we determine $\beta=2.38$ and hence, the critical load is $N_{cr}=\pi^2EI_z/(\beta\ell)^2=11660$kN. In the case of a stepped axial compression with $N_1=555$kN, $N_2=888$kN and $N_3=999$kN we get $\beta=2.20$ and hence, the critical load is $N_{cr}=\pi^2EI_z/(\beta\ell)^2=13650$kN. A FEM analysis using NASTRAN gives $N_{cr}=13980$kN (see *Fig. 5a*).

Finally, if we assume that the two end cross-frames are twice as stiff as the intermediate ones ($c_0=2c$) we obtain $\beta=2.51$ and hence, it is $N_{cr}=\pi^2EI_z/(\beta\ell)^2=10480$kN. The critical load is in this case smaller than the corresponding previous one since the two end cross-frames are contributing to the total deformation, thus increasing the buckling length of the upper cord.

As a second example, we consider the same pedestrian bridge with the same cross-sections, which has now 4 openings ($\ell=6.00$m) as shown in *Fig. 5b*. The distribution of the internal axial compression in the upper cord is $N_1=416.25$kN and $N_2=999$kN. The distributed stiffness is $c=C_d/\ell=11.93/600=0.02$kN/cm^2 and the factor γ is $\gamma=cL^4/EI_z=0.02x2400^4/21000x50990=619.5$ from which we determine the coefficient $m=2\sqrt{\gamma}/\pi^2=5.04$ and finally, the corresponding critical load $N_{cr}=mN_E=5.04x1835=9250$kN. According to Timoshenko, we determine first the non-dimensional quantity $\Psi==38.72$ and $\beta=0.3445$. Thus, the critical load is $N_{cr}=15460$kN.

Based on the analytical method developed herein, and assuming constant axial compression along the length of the bridge N=999kN we determine $\beta=2.37$ and hence, the critical load is computed $N_{cr}=5225$kN. In the case where we consider stepped distribution of the axial compression with $N_1=416.25$kN and $N_2=999$kN we obtain $\beta=1.774$ and thus, the critical load is $N_{cr}=\pi^2EI_z/(\beta\ell)^2=9330$kN.

A FEM analysis using NASTRAN (see *Fig. 5b*) gives N_{cr}=9470kN

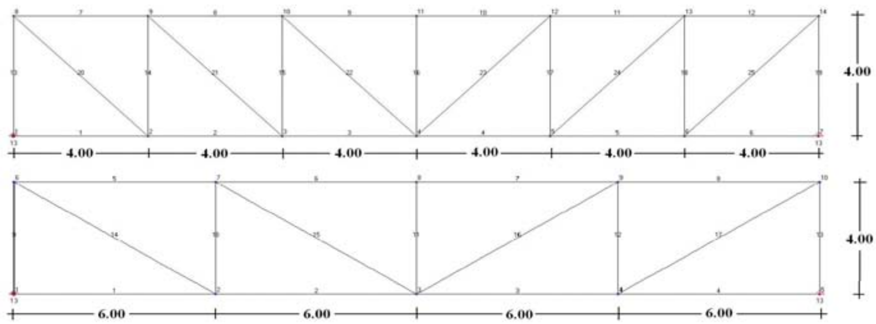

Figure 5. Steel truss bridge FE models with 6 and 4 openings

Finally, if we assume that the two end cross-frames are twice as stiff as the intermediate ones ($c_0=2c$), we obtain β=2.765 and $N_{cr}=\pi^2 EI_z/(\beta\,\ell)^2$ =3840kN. The computed critical load is in this case considerably smaller than the one in all previous cases.

4 SUMMARY & CONCLUSIONS

Based on the results presented herein, the following conclusions can be drawn:

– The effect of distributed stiffness is inaccurate for a relatively small number of openings in truss bridges. This effect diminishes as the number of openings increases.
– The assumption of constant axial compression in the upper cord is very conservative leading to non-economical solutions when designing the bridge against lateral buckling of the upper cord.
– The assumption of inflexible end cross-frames must always be validated since in combination with a small number openings may lead to overestimated values for the critical load and hence, against structural safety.
– The analytical method for determining the critical load of the upper cord in steel truss bridges presented herein must be necessarily followed in cases of main truss girders with small number of openings and relatively flexible end cross-frames. This is also confirmed by finite element analyses employed in this study.

REFERENCES

[1] Timoshenko, SP, Gere, J, *Theory of Elastic Stability*, McGraw-Hill, New York, NY, 1961.
[2] Bleich, F,. *Buckling Strength of Metal Structures*, McGraw-Hill, New York, 1952.
[3] Eurocode 3, *Design of Steel Structures*, *Part 2 - Steel Bridges*, European Committee for Standardization, Brussels, 2004.
[4] Bazant, ZP, Cedolin, L, *Stability of Structures*, Oxford University Press, New York, NY, 1991.
[5] Ermopoulos, J, Steel and Composite Bridges, (in greek) Kleidarithmos Publ, Athens, 2000.

SUSTAINABLE BRIDGE DESIGN IN EGNATIA ODOS MOTORWAY

Theodoros Tzaveas[1], Evgenia Gavaise[2]

[1,2] Egnatia Odos AE, Works Division, Thessaloniki, Greece
e-mail: thtzav@egnatia.gr, egava@egnatia.gr

ABSTRACT: In the paper, the principles adopted during the development of the highway project and bridge design and construction in particular, are described in order to consider the rights of future generations to raw materials and ecological support systems, and also case studies with lessons learnt in order to improve future planning of projects.

KEY WORDS: Sustainability, construction methods, bridge design.

1 INTRODUCTION

During the early stages of the project, EGNATIA ODOS AE designated environmental stewardship and streamlining as one of its three “vital few goals,” along with safety and improved highway infrastructure. Sustainability considerations led to the design and construction of major structures, many of which are considered to be state-of-the-art constructions even worldwide. Their construction was made possible with the use of large self-propelled equipment and advanced construction methods (e.g. cantilevering) taking full advantage of all national and European experience and know-how available today.

Bridge design and construction represent more than simply providing a transportation link between two points. Communities want bridges that are visually pleasing, reflective of their place, and sensitive to the environment. Aesthetics, economy, environmental sensitivity, and sustainability are being combined with function and constructability to provide new bridges that satisfy these expectations.

The commonly accepted definition of sustainability[1], as used by the United Nation’s World Commission on Environment and Development in their 1987 report titled Our Common Future, states “Sustainable development is development that meets the needs of the present without compromising the ability of future generations to meet their own needs.” To the concrete bridge community, this definition means designing, constructing, and maintaining context-sensitive bridges with long-term durability, low life-cycle impacts, sensitivity in the selection of materials and methods, and a minimal impact on the environment throughout the bridge’s life.

2 CONCEPTUAL DESIGN

The conceptual design phase of a bridge project provides the necessary groundwork for the best aesthetic opportunity. The overall alignment and geometry are established at this time, in addition to determining span lengths and the structural depth and dimensioning of superstructure and substructure elements. The conceptual design must call on engineering judgment and an understanding of how to best optimize construction to properly balance economy, functionality, and lasting visual quality. The main design criteria are as follows:

- Functionality, simple and natural forms are followed, aesthetically pleasant and blend with surrounding landscape and minimization of environmental impacts.
- Balancing costs to reach an effective solution both technically and economically.
- Maintain deck continuity and redundant systems to minimize the use of bearings and expansion joints; regular structural systems where possible.
- Assessment of Health and Safety hazards.
- Adequate provisions for inspection to facilitate maintenance.
- Careful detailing of structural elements and selection of materials to improve the durability of the bridge (design life requirement is for 120 years).

Experience has shown that superior bridge aesthetics can be achieved at reasonable construction costs, and, in fact, efficient designs can result in costs savings. An example of this is the Arachthos Bridge (*Photo 1*), where the functional requirement of spanning the valley resulted in a long-span balanced cantilever bridge with a 140m span and an overall length of 1036m.

Photo 1. Arachthos Bridge

2.1 Integrated life cycle design and assessment

Integrated life cycle design [2] is a complex approach implementing all relevant and significant requirements into one single design process. This approach integrates material, component, and structure design and considers selected relevant criterions from a wide range of criterions sorted in three basic groups: environmental, economical and social expressed by corresponding technical quality criteria. Traditionally, design of concrete structures has concentrated on the construction phase, optimizing the construction costs and short-term performance. Sustainable developments raise a strong need for integrated life-cycle design where all phases during the entire service life of the structure have to be considered, see *Fig. 1*.

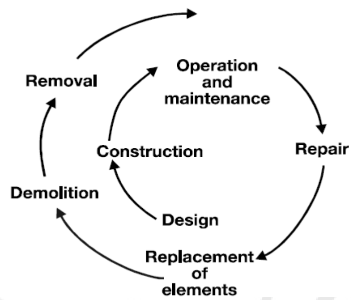

Figure 1. Phases in the life cycle of concrete structures

It is a fact that concrete structures exposed to aggressive environment (i.e. de-icing salt) involves major maintenance and repair activities. The environmental loads associated with maintenance and repairs are very often the dominant sources occurring during the entire service life of the structures. Based on an evaluation covering all relevant durability strategies two or three strategies are selected where the life cycle costs are priced. The life cycle costs in the different phases of the life cycle are priced, being construction, operation, maintenance and repairs.

2.2 Span Length

The individual span lengths of a bridge are based on the alignment, existing site constraints, and potential construction methods. Span lengths are determined after the overall length and alignment have been established and existing site constraints identified. The Venetikos Bridge (*Photo 2*) in the area of Grevena crossing Venetikos Bridge is a 680m long bridge of one continuous unit that consists of six spans with a maximum span length of 120m in order to cross a very steep ravine.

Photo 2. Venetikos bridge during construction

The various combinations of construction methods, span lengths, and unit configurations are evaluated to determine the most feasible alternative. The balanced and repetitive span lengths also provide continuity in appearance, resulting in visually appealing structures.

2.3 Span to Depth Ratio

Determining an ideal span-to-depth ratio is an essential factor in the overall aesthetic appearance of the structure. It influences the visual impact of the structure within the surrounding landscape. Many options exist that can optimize the structural efficiency of the superstructure box girder cross-section while creating an elegant structure. Creating the most aesthetically pleasing combination of span length and superstructure depth is often an iterative process. As the span increases, the magnitude of the forces near the piers normally requires variation in structural height. An example of such an approach is the Votonosi Bridge near Metsovo (*Photo 3*). This bridge has a 230m span with a 13,5m deep section at the pier and a 5,5m deep section at midspan.

Photo 3. Votonosi Bridge during cantilevering

3 CONSTRUCTIONS METHODS

Concrete bridges for long spans are typically erected using the balanced cantilever construction methods *(Photo 4a*). For medium span lengths advancing shoring or incremental launching is implemented (*Photo 4b, 4c*). For shorter spans precast beams is the most favourable method used. Determining the method of construction and bridge type requires taking into consideration the required span length and the existing site constraints. The schedule constraints may also dictate one method over the other, while the contractor's equipment or the size of project may also be determining factors. The advantages and disadvantages of various approaches must be analysed early in the conceptual design phase to determine the best one. Both the span-by-span and balanced cantilever construction methods have been used successfully in the industry and are customary; however, advances in technology and equipment continue to be made. For all projects, a contractor may opt to use unique means and methods that may differ from the assumptions made during the design phase. In these circumstances, further construction analysis is required to verify the design under the revised construction loadings.

Photo 4. (a) balanced cantilever, (b) advancing shoring, (c) incremental launching

The logistics of construction sequences can be an important issue during construction of bridges. Solutions developed in close corporation with the Contractor in order to utilize available equipment and to simplify construction methodology. Considering construction methods in the design is usually a key to minimize risks and to facilitate construction methods fitting to Contractors equipment and knowledge. Value engineering, defined as a structured approach in identifying unnecessary costs in design and construction and in soliciting or proposing alternative design or construction technology to reduce costs without sacrificing quality or performance requirements, has been implemented. An example is precast beams bridges *(Photo 5a*) where pretentioning (*Photo 5b*) combined with steam curing, as opposed to post tensioning, was implemented to achieve faster construction times.

Photo 5. (a) precast beam construction, (b) pretentioning casting bed

4 DESIGN DETAILS – MATERIALS

4.1 Concrete

It is also possible to reduce the environmental impact of concrete by reducing the environmental impact of cement and concrete production. Cement manufacturers undertake many activities concerned with the reduction of environmental impact. Preparing a concrete mix design to incorporate the use of superplisticisers results to concrete with low water to cement ratio as low as 0.4, hence reducing the consumption of water. Also results in a durable, early gain high strength concrete leading to faster construction times hence reducing direct and indirect costs. The use of air entrained concrete is implemented in areas exposed to de-icing slats leading to durable surfaces subjected to freeze-thaw cycles.

4.2 Drainage

The bridge deck drainage is captured and not allowed to freefall onto the ground below, thus implementing a closed drainage system (*Photo 6a*). The water is collected at deck level and piped to an appropriate discharge location, such as a pollution control units (PCU's), see *Photo 6b*. PCU's incorporate a system for the pretreatment of the stormwater by oil/water separators in the inlets and outfall into a natural filtration system. It is given great consideration not only to meet local and state requirements but also to develop a project that is environmentally sensitive.

Photo 6. (a) Closed drainage system, (b) PCU implementation

5 DEALING WITH THE SEISMIC HAZARDS

The earthquake activity and the complex geological conditions are playing an important role in the design. The country is sub-divided into three seismic zones (I, II, III) with peak ground accelerations of 0.16g, 0.24g, 0.36g respectively. The motorway traverses through the zones I & II. A behaviour factor (q), depending on the ductility of the system, from 1,0 to 1,5 for essentially elastic systems up to 3,5 for a ductile design. Current state-of-the art[3] for special bridges is that of limiting, whenever possible, the amount of energy transmitted to the structure through seismic isolation (shift of the fundamental period of the structure in an area of the spectrum poor in energy content). In regions of moderate to high seismicity, the common approach to seismic design both for economic and safety reasons is to design a bridge for ductile behaviour, i.e. to provide it with reliable means to dissipate a significant amount of the input energy via a formation of an intended configuration of flexural plastic hinges that result in a dependable plastic mechanism. In such systems high uplift forces had to be resisted with special pot bearings (*Photo 7a*), and also Shock Transmission Units (*Photo 7b*) have been implemented to distribute the seismic forces in a greater number of piers. Thus, it is tacitly assumed that a certain type and extent of damage on the structural system is acceptable and repair works might be needed following a seismic event equivalent to the design earthquake.

Photo 7. (a) Special pot bearings, Votonosi bridge, (b) STU, Greveniotikos bridge

Seismic isolation is an effective alternative in reducing seismic response without having to make any compromises at all on the level of structural damage, i.e. the response of the seismically isolated structure is mainly elastic (“no damage”). The seismic isolation system installed at the deck-piers interface increases the fundamental period of the structure (period shift) resulting in a reduction of the inertia forces (see *Fig. 2a*). However the negative by-effect of the period shift is the increase of the seismic displacements. Thus seismic isolation systems usually include devices that increase the equivalent damping of the structure (see *Fig. 2b*).

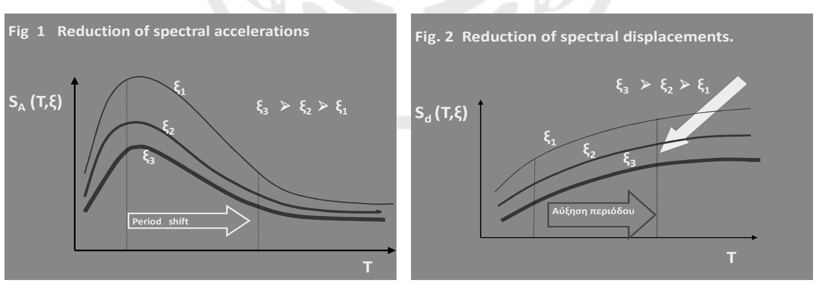

Figure 2. Reduction of spectral accelerations, (b) Reduction of spectral displacements

In valley bridges with very high and flexible piers connected to the deck either monolithically or through horizontally fixed bearings the fundamental period of the bridge may be already within the region of low spectral accelerations. In these cases the beneficial effect of the “period shift’’ is provided by the geometry of the structure itself and thus no further “isolation’’ is needed. However in such cases a further reduction of seismic response is attained by using appropriate devices (*Photo 8*) that increase the damping of the structure (“added-damping’’). The theoretical principle of the concept of seismic isolation is different and should not be confused with the concept of "added damping''. Their similarity may lie only on the effect they have on reducing the seismic response of the structure.

Photo 8. Viscous dampers at the abutments of Arachthos bridge

6 CONCLUSIONS

Bridges are both structure and symbol. Their functionality serves the public good by connecting people and places to enhance the quality of life. As important infrastructures on the landscape, they should merge sustainable design and aesthetic beauty. The bridge engineering community has been practicing many sustainable concepts for decades. Rapid construction, contractor alternate designs, value engineering and extending service life through reliable and durable systems all contribute to sustainable practices. Extending the service life of a structure, through better materials and adaptable designs translates to less time and energy spent on maintenance and future reconstruction. A structure that meets both the needs of today and those of the future will not require premature replacement.

The examples presented in the paper illustrate what is being done to make sustainable bridges an integral part of our national highways network. The future of sufficient funding is uncertain due to the current economic situation despite the increasing importance of additional investments in our nation's infrastructure. We have a wealth of talent, experience and techniques to forge a new generation of sustainable bridges that promise greater strength, safety, service, sensitivity, savings, and stability for all who use them. We need to better promote the exemplary work already being done with high-performance sustainable bridges and their many benefits.

REFERENCES

[1] Azapagic, A,Perdan, S, Clift, R, *Sustainable Development in Practice*, John Wiley & Sons, New York, 2004.

[2] Lounis, Z, Daigle, L, "Environmental benefits of life cycle design of concrete bridges", *Proc. 3rd Intl. Conference on Life Cycle Management*, Paper no.293, pp.1-6, Zurich, 2007.

[3] Naeim, F, Kelly, J.M, *Design of Seismic Isolated Structures*, John Wiley & Sons, New York, 1999.

STABILITY OF PRESTRESSED STEEL BEAMS OF BRIDGES

Theodore G. Konstantakopoulos[1], Charalampos Charitidis[2]

[1] University of Thessaly, Dept. of Civil Engineering, Greece
[2] National Technical University of Athens, Dept. of Civil Engineering, Greece
e-mail: tkonstadak@civ.uth.gr, charitidis@gmail.com

ABSTRACT: The phenomenon of twisting appears in bending beams as a special case of the lateral-torsional buckling of a beam. In this paper, we will study the influence of the prestressing by parabolic tendon on the stability (twisting stability) of a simply supported beam.

KEY WORDS: Stability; Twisting; Bridge's main beams

1 INTRODUCTION

The origin of the prestressed steel members dates beck many years ago. This technique is attributed to Paxton, who in 1851 used prestressed steel beams for the building of Crystal Palace. In 1907, Koenen was the first which proposed prestressed steel bars, many years before the application of prestressing in concrete [1]. The prestressing of members is easily applicable both on new and also for the strengthening of existing bridges [2].As it is generally known, while an installation of prestressing tendons doubles the load-carrying capacity of a structure, it actually increases also the load carrying capacity if buckling of the structure is considered [3,4].The research on this last field of instability, is rather poor, and the existing publications examine this problem mainly through experimental way [5,6]. The instability of a beam, may be appeared not only as the classical buckling of a column, but also as the twisting phenomenon (a special case of the lateral-torsional buckling). This phenomenon, appears in bending beams with or without joins (or obligations) along the beam-span. As an example of the second case we would mention the main-beams of a bridge with deck of under-passage. In this paper we will study the increasing of the stability (twisting-stability) of the main-beam of a steel bridge of under passage, prestressed by rectilinear tendons, that is the usual way of prestressing in steel beams.

2 INTRODUCTORY CONSEPTS

1. The considered beams, have the moment of inertia I_y much bigger than the I_z one. Therefore, appears the phenomenon of twisting.

2. We consider the beam of Fig. 1, which is prestressed by cables of random form, given by the equation:

$$z_o = e_z + z(x) \tag{1}$$

Where we suppose, that the points P of anchorage of the cables at the edges of the beam are located at a distance e_z from the gravity center S of the beam's cross-section.(see Fig. 3).

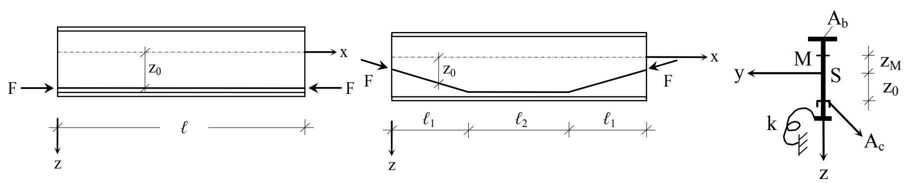

Figure 1. Types of prestressing and beam's model

3. We assume that $w << \upsilon$ and thus the terms due to w can be neglected.
4. Finally the beam may be restrained against torsion, as a member, for example, of a bridge, by a spring of constant k (see fig.1).
5. The external loads produce the moment $M_y(x)$, which after the deformation of the beam is analyzed to (see Fig. 2):

$$\left.\begin{aligned} M_{\bar{y}} &= M_y \cos\varphi \cong M_y \\ M_{\bar{z}} &= -M_y \sin\varphi \cong -M_y \cdot \varphi \end{aligned}\right\} \tag{2}$$

3 ANALYSIS

We will proceed using the method of the developed potential energy. The produced work is due to the external forces and to the internal ones.

3.1 The work of the internal forces

Taking into account the cross-section's warping, the work of the internal forces is:

$$E_i = \frac{1}{2}\int_0^{\ell} (E\, I_z \upsilon''^2 + E\, I_\omega \varphi''^2 + G\, I_d \varphi'^2)dx \tag{3}$$

3.2 The work of the external forces

3.2.1 The work of the force F

Because of F (the force of prestressing), the developed tension at a random point $B(y_B, z_B)$ is equal to $\sigma_B = -F_x(1/A_b + z_B e_z / I_y)$, while the length of the corresponding fibre is equal to $\frac{1}{2}\int_0^{\ell}(\upsilon_B'^2 + w_B'^2)dx$. Therefore the produced work will be:

$$E_F = -\frac{F_x}{2}\int_0^{\ell}\oint_{A_b}\left(\frac{1}{A_b} + \frac{z_B}{I_y}e_z\right)(\upsilon_B'^2 + w_B'^2)dA_b dx \tag{4}$$

The displacement υ_B of the point b, because of the rotation φ, is related to the displacement υ of the gravity center by the following relation:

$$\upsilon_B = \upsilon - \overset{*}{z}_B \varphi \tag{a}$$

On the other hand it is valid: $z_B = z_M + \overset{*}{z}_B$ (b)

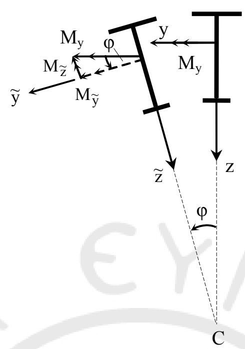

Figure 2. The cross-section in the deformed state

where $\overset{*}{z}$ is shown in figure 3. From the above (a) and (b) we get finally:

$$\left.\upsilon_B = \upsilon - (z_B - z_M)\varphi \quad , \quad w_B = y_B\varphi \quad \right\} \tag{c}$$

From the first of the above we get:

$$\upsilon_B'^{\,2} = \upsilon'^2 + (z_B^2 + z_M^2 - 2z_M z_B)\varphi'^2 - 2\upsilon'\varphi'(z_B - z_M) \tag{d}$$

Given that:

$$\left.\int_{A_b} y_B \, dA_b = \int_{A_b} z_B \, dA_b = \int_{A_b} y_B z_B \, dA_b = 0 \quad , \quad \int_{A_b} y_B^2 \, dA_b = I_z \quad , \quad \int_{A_b} z_B^2 \, dA_b = I_y \right\} \tag{e}$$

Equation (4), because of the above gives:

$$\left.\begin{aligned} &E_F = -\frac{F_x}{2}\int_0^\ell (\upsilon'^2 + i_M^2\varphi'^2 + 2z_M\upsilon'\varphi')dx - \frac{F_x}{2A_b}\int_0^\ell \left[(V_y - 2z_M I_y)\varphi'^2 - 2I_y\upsilon'\varphi'\right]\frac{e_z}{I_y}dx \\ &\text{where: } \quad V_y = \int_{A_b} z_B(y_B^2 + z_B^2)dA_b \quad , \quad i_M^2 = i_p^2 + z_M^2 \quad , \quad i_p^2 = \frac{I_p}{A_b} = \frac{I_y + I_z}{A_b} \end{aligned}\right\} \tag{5}$$

3.2.2 The work of $M_{\tilde z}$

If ψ is the angle between the axis x and the bended axis of the beam, will be $\psi = \upsilon'$ and thus $d\psi = \upsilon'' dx$ or $dE_M = -M_{\tilde z}\upsilon'' dx$ and finally, because of equ (2):

$$E_M = -\int_0^\ell M_{\tilde z}\upsilon'' \, dx = \int_0^\ell M_y \upsilon''\varphi \, dx \tag{6}$$

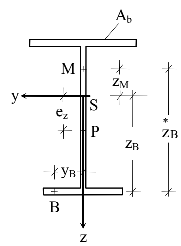

Figure 3. Data of the cross-section

3.3 The produced work by the cables

In figure 4, it is shown the deformed state of a cable of random form. We point out, that in the deformed position of the beam, the cable in addition to the pressure q_z acts also the pressure q_y, which reacts to the beam's displacement. Remembering that w_c is very small compared to υ_c (where w_c, υ_c are the displacements of the cable), we have that υ_c is connected to the displacement of S by the relation:

$$\upsilon_c = \upsilon - z_o \varphi \tag{7}$$

Projecting the cable on the plane (oxz) we have:

$$F_x = \text{constant}\,,\; F_z = F_x z_o'\,,\; dF_z = -q_z\,dx \quad \Big\} \tag{8a}$$

And finally:

$$q_y = -F_x\, z_o'' \tag{8b}$$

Similarly, projecting the cable on the plane (oyz) we have (see fig.4):

$$q_y = -F_x\, \upsilon_c'' \tag{8c}$$

3.3.1 Work produced by the forces q_y, q_z

The produced work by q_y and q_z, taking into account that $w_c \ll \upsilon_c$ and equs (8), will be: $E_{F1} = \int_0^{\ell} (q_y \upsilon_c + q_z w_c)\,dx \cong -F_x \int_0^{\ell} \upsilon_c\, \upsilon_c''\,dx$, or because of equation (7) we get:

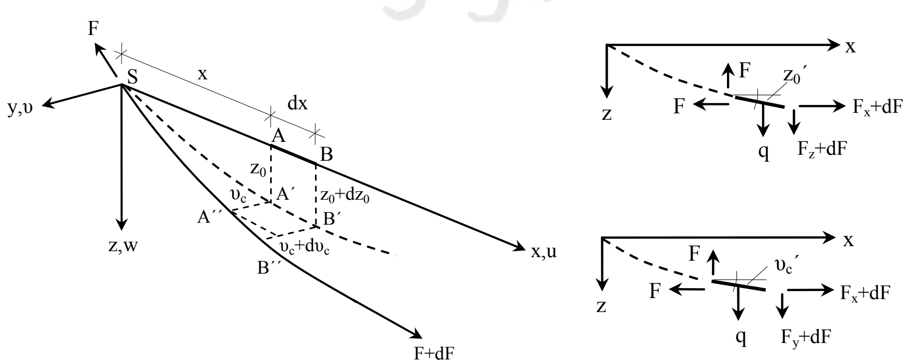

Figure 4. The deformed state of the cable

$$E_{F1} = -F_x \int_0^{\ell} [\upsilon\upsilon'' - z_o\varphi\upsilon'' - \upsilon(z_o\varphi)'' + z_o\varphi(z_o\varphi)'']dx \tag{9}$$

3.3.2 Work produced by the cable it-self

From figure 4 we have: Coordinates of A'': $(x,\ \upsilon_c,\ z_o)$

Coordinates of B'': $(x+dx,\ \upsilon_c + d\upsilon_c,\ z_o+dz_o)$

Therefore the length $A''B''$ will be:

$$A''B'' = \sqrt{dx^2 + d\upsilon_c{}^2 + dz_o{}^2} = dx\sqrt{1+\upsilon_c'^2 + z_o'^2} = dx\left(1+\upsilon_c^2/2 + z_o'^2/2\right),\ \text{or}$$

$ds = \left(1+\upsilon_c^2/2 + z_o'^2/2\right)dx$ and the total length of the cable will be:

$$s = \int_0^{\ell}\left(1+\frac{z_o'^2}{2}+\frac{\upsilon_c'^2}{2}\right)dx \tag{e}$$

On the other hand, we know that the total elongation of a cable of length s and of area of cross-section A_c is:

$$\Delta s = \frac{F}{A_c E}\cdot s \tag{f}$$

Therefore the produced work will be:

$$E_{F2} = F\cdot\Delta s = \frac{F^2}{A_c E}\int_0^{\ell}\left(1+\frac{z_o'^2}{2}+\frac{\upsilon_c'^2}{2}\right)dx \tag{g}$$

Or because of equ. (7), the above equ (g) becomes:

$$E_{F2} = \frac{F^2}{E A_c}\int_0^{\ell}\left(1+\frac{z_o'^2}{2}+\frac{(\upsilon - z_o\varphi)'^2}{2}\right)dx \tag{10}$$

3.4 The work of the spring

We accept that $M=k\varphi$, and therefore: $d E_s = \frac{1}{2}\varphi M\, dx = \frac{1}{2} k\, \varphi^2\, dx$ or finally:

$$E_s = \frac{1}{2}\int_0^{\ell} k\,\varphi^2\, dx \tag{11}$$

3.5 The total work

According to the previous analysis the total produced work is:

$$E = E_i + E_F + E_M + E_{F1} + E_{F2} + E_s \tag{12}$$

The following condition must be fulfilled:

$$\delta E = 0 \tag{13}$$

After partial integration and some manipulation of equ (13), we get integrated terms and integrals. The first are the boundary conditions while the last give the following differential equations of the problem:

$$\left.\begin{aligned}
&E\,I_z\upsilon'''' - \left(F C_o - \frac{F^2}{EA_c}\right)\upsilon'' + FC_o\left(z_M - \frac{e_z}{A_b}\right)\varphi'' + \left(2FC_o + \frac{F^2}{EA_c}\right)(z_o\varphi)'' + (M_y\varphi)'' = 0 \\
&E\,I_\omega\varphi'''' - \left(G\,I_d - i_M^2 FC_o\right)\varphi'' + \left(z_M FC_o + 2z_o FC_o - \frac{e_z FC_o}{A_b} + \frac{z_o F^2}{EA_c}\right)\upsilon'' \\
&+ \frac{e_z FC_o}{A_b I_y}(V_y - 2z_M I_y)\varphi'' + \frac{e_z FC_o}{A_b I_y}(V_y - 2z_M I_y)\varphi'' - \left(2FC_o + \frac{F^2}{EA_c}\right)z_o(z_o\varphi)'' \\
&\qquad\qquad\qquad + k\,\varphi + M_y\upsilon'' = 0 \\
&\text{where : } \quad C_o = \frac{\sqrt{\ell^2 - 16f^2}}{\ell} \quad \text{and thus} \quad F_x = F\cos\varphi = F C_o
\end{aligned}\right\} \tag{14}$$

We note that it is usually: $C_o \cong 1$.

4 NUMERICAL RESULTS

It is obvious, that equs (14) constitute a non linear system and thus it cannot be solved through elementary methods. We will try to solve the above system through an approaching method for an usual case of a beam, with cross-section of double symmetry, prestressed by a rectilinear cable, loaded by a pair of moments M_y=constant, acting at its ends (see fig.5) and is the main beam of a bridge of under passage with k=2.

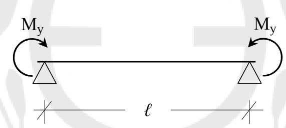

Figure 5. Loading of the beam

For this purpose we will use a beam of different lengths having a cross-section shown in figure 6. Easily, one can find that the above beam has the following data:

$I_y = 0.02082\ m^4$, $I_z = 0.00032\ m^4$, $I_\omega = 0.0002048\ m^6$, $I_d = 9.38\cdot 10^{-6}\ m^4$ $A_b = 0.0496\ m^2$

For the prestressed cables we have: $\sigma_c = 12\cdot 10^6\ kN/m^2$, $z_o = e_z$ and $A_c = 0.001\ m^2$.Beam and cables have the same modulus of elasticity: $E = 2.1\cdot 10^8\ kN/m^2$.

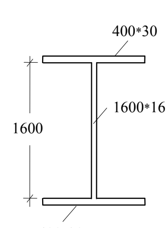

Figure 6. Data of the cross-section

Given that $z_M = 0$, $z_o = e_z = \text{constant}$, $V_y = 0$, $k = 0$, and that the cable is rectilinear, equations (14) get the following form:

$$\left.\begin{aligned} &E\,I_z\upsilon'''' - (F - \frac{F^2}{EA_c})\upsilon'' + (F + \frac{F^2}{EA_c})e_z\varphi'' + M_y\varphi'' = 0 \\ &E\,I_\omega\varphi'''' - (G\,I_d - i_M^2 F)\varphi'' + e_z\,(F + \frac{F^2}{EA_c})\upsilon'' - (2F + \frac{F^2}{EA_c})e_z^2\varphi'' + M_y\upsilon'' = 0 \end{aligned}\right\} \quad (15)$$

We consider solutions of the form:

$$\left.\upsilon = V \cdot \operatorname{Sin}\frac{\pi x}{\ell} \quad , \quad \varphi = \Phi \cdot \operatorname{Sin}\frac{\pi x}{\ell}\right\} \quad (16a,b)$$

Introducing (16) into (15), we get:

$$\left.\begin{aligned} &E\,I_z\left(\frac{\pi}{\ell}\right)^4 V + (F - \frac{F^2}{EA_c})\left(\frac{\pi}{\ell}\right)^2 V - (F + \frac{F^2}{EA_c})e_z\left(\frac{\pi}{\ell}\right)^2 \Phi - M_y\left(\frac{\pi}{\ell}\right)^2 \Phi = 0 \\ &E\,I_\omega\left(\frac{\pi}{\ell}\right)^4 \Phi + (G\,I_d - i_M^2 F)\left(\frac{\pi}{\ell}\right)^2 \Phi - e_z\,(F + \frac{F^2}{EA_c})\left(\frac{\pi}{\ell}\right)^2 V + (2F + \frac{F^2}{EA_c})e_z^2\left(\frac{\pi}{\ell}\right)^2 \Phi \\ &\qquad - M_y\left(\frac{\pi}{\ell}\right)^2 V = 0 \end{aligned}\right\} \quad (17)$$

Remembering that:

$$\left. E\,I_z\left(\frac{\pi}{\ell}\right)^2 = P_e \quad , \quad \frac{1}{i_M^2}\left[E\,I_\omega\left(\frac{\pi}{\ell}\right)^2 + G\,I_d\right] = P_T \right\} \quad (18)$$

are the critical loads of pure buckling and of lateral-torsional buckling respectively, equations (17) conclude to the following ones:

$$\left.\begin{aligned} &A \cdot V + (B - M_y)\cdot\Phi = 0 \\ &(\Gamma - M_y)\cdot V + \Delta\cdot\Phi = 0 \end{aligned}\right\} \quad (19a)$$

Where:

$$\left. A = P_e + F - \frac{F^2}{E\,A_c}, \quad B = -e_z(F + \frac{F^2}{E\,A_c}), \quad \Gamma = B, \quad \Delta = i_M^2(P_T - F) + e_z^2(2F + \frac{F^2}{E\,A_c}) \right\} \quad (19b)$$

In order for the system of equs (19a) to have not only trivial solutions, the determinant of the coefficients of the unknown must be equal to zero. This condition gives the moment M_y as follows:

$$M_y = \frac{1}{2}\left((B + \Gamma) + \sqrt{(B - \Gamma)^2 + 4A\Delta}\right) \quad (20)$$

In the above relations taking F=0 we get the critical load when M_y acts alone, while taking z_o =0, we get the critical M_y for simultaneously action of load F (with out prestress):

$$\left. M_y = i_M\sqrt{P_e \cdot P_T} \quad , \quad M_y = i_M\sqrt{(P_e - F)\cdot(P_T - F)} \right\} \quad (21)$$

Applying the above data, for beams with length 20 and 10 m and different e_z, we get the plots of figure 7.

From these plots we point out the following diagrams:

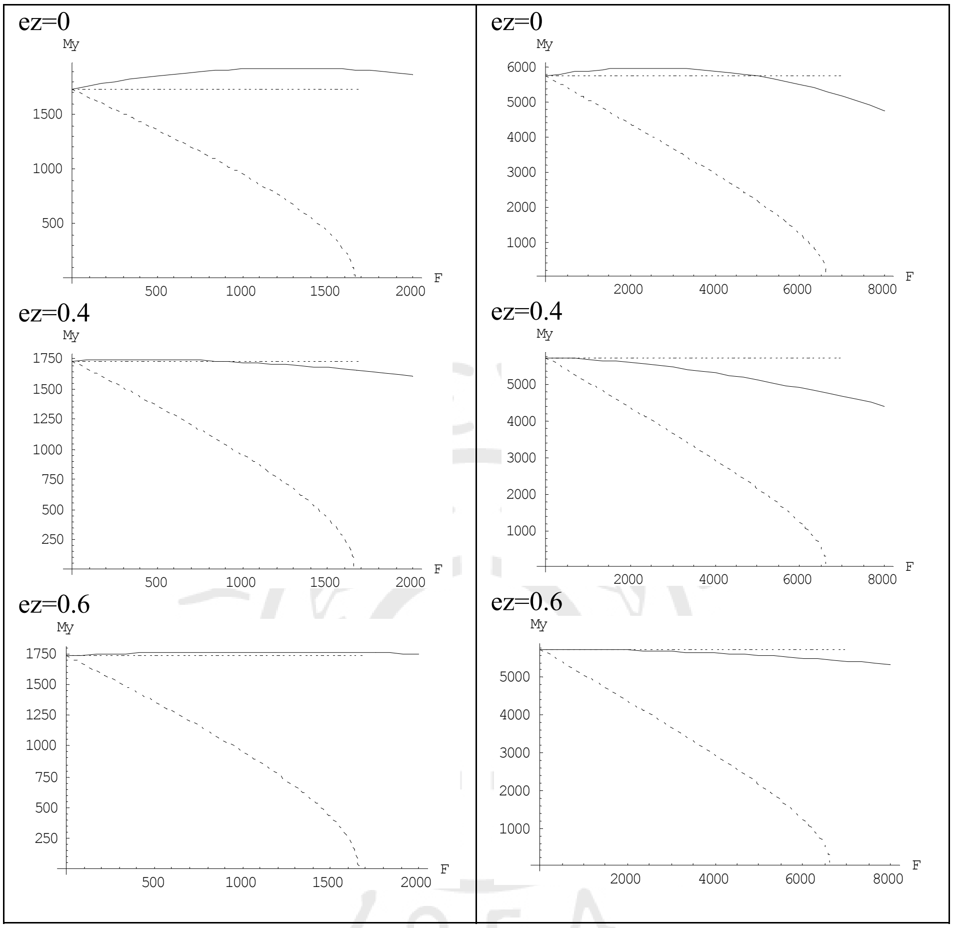

L=20m L=10m

Figure 7. Critical laods – F versus M_y for different e_z

REFERENCES

[1] Nunziata Vinc., “Strutture in acciaio precompresso”, 1999, Palermo, Editore Dario Floccavio.
[2] Troitsky M.S. “Prestressed steel bridges”, 1990, Van Nostrad Co, N. York.
[3] Saadatmanesh H. “Experimental study: Prestressed composite beams”, J. Str. Eng. ASCE, 1989, 115(9), 2348-2363.
[4] Ayyub B.M, Sohn Y.G, Saadatmanesh H., “Prestressed composite girders under positive moments”, J. Str. Eng. ASCE, 1990, 116(11), 2931-2951.
[5] Hambly E.C, “Bridge deck behaviour’ 2nd ed. E&Fnspon, 1986.
[6] Sunkyn Park, Kim T., Kim K., Hang S-H., “Flexural behaviour of steel I-beam prestressed with externally unbonded tendons” J. of Constr. Steel Research, 2010, 66, 125-132

AN ALTERNATIVE PROPOSAL FOR THE DESIGN OF BALANCED CANTILEVER BRIDGES WITH SMALL SPAN LENGTHS

Ioannis A. Tegos[1] and Stergios A. Mitoulis[2]

[1,2] Aristotle University of Thessaloniki, Dept. of Civil Engineering, Greece
e-mail: itegos@civil.auth.gr, mitoulis@civil.auth.gr

ABSTRACT: In balanced cantilever structural method the prestressing is utilised as means to control the strains and to reinforce the top flange of the deck's cross section at the supports. Ordinary strength reinforcements are typically applied within the bottom flange of the deck, after accounting for the unfavorable participation of the prestress. The last check is a critical one at the balanced cantilever-method. Thus the use of ordinary reinforcements at the bottom flange of balanced cantilevers, namely the avoidance of prestressing tendons, seems to be an interesting design alternative which ensures a better construction result. An analytical study on this design alternative had been carried out for cantilever bridges of relatively small span lengths actually built along the Egnatia Highway in Thrace.

KEY WORDS: Bridge; Balanced Cantilever; Small Span; Design; Ordinary Strength Steel (OSS).

1 INTRODUCTION

Safety, serviceability, cost-effectiveness, aesthetics and particular technical issues are typically the controlling factors in the selection of the proper bridge type [1] [2] and construction method. In many cases, a prestressed bridge is a cost-effective choice. Typically, segmental concrete bridge construction is utilized, which is the most common method of bridge construction.

Segmental construction method typically introduces: (a) the conventional cast-in-situ bridge construction, (b) the precast prestressed I-beam deck construction with continuous cast-in-situ slab decks, (c) the balanced cantilever bridge construction, which either utilises scaffolding or precast deck segments and (d) the progressive and span by span incrementally launched bridge construction. Segmental cast-in-situ bridge construction is preferable in case of straight and curved in plan bridges with relatively small bent heights and when prestressing is applied in the longitudinal direction of the superstructure, as shown in Figure 1. The formworks are typically supported directly to the ground or to a well compacted temporary embankment. In most cases, the first span and a 15 to 20% of the length of the second span are casted together. The construction of the next bridge segment follows after the application of the prestressing force, while keeping the immediate prestress losses within normal levels. The final loading of the bridge due to the self-weight of the superstructure is varying with time due to the influence of the creep effect [3] [4].

A new bridge construction method is investigated in this paper. The method has similarities with the balanced cantilever method. The connection of the cantilevers is achieved by the use of tendon couplers. The tendons are straight and the scaffolding, which is used for the deck casting, is removed after the application of the prestressing force. The applicability of the proposed construction method has been attempted to a cast-in-situ benchmark bridge actually built along a major motorway that runs across Northern Greece.

2 THE PROPOSED CONSTRUCTION METHOD

2.1 Structural assumptions

The proposed structural method, which can be utilised for the construction of cast-in-situ bridges, is based on the following structural assumptions: (a) The deck cross section has a variable height along the longitudinal direction of the bridge with a symmetrical bottom flange, which is modulated by a polygonal shape inscribed in a parabolic arch, as shown in Figure 1. The cross section of the deck can be either a box girder or a voided slab. (b) The prestressing tendons are straight and continuous in all the deck spans and they are installed in the top flange of the deck. The appropriate concrete cover [5] [6] is provided to protect the tendons against corrosion. Within the bottom flange of the deck only ordinary strength steel is utilised. (c) The construction of the end spans can follow two different design alternatives: (c_1) The first alternative introduces the construction of the end spans by maintaining the geometry of the intermediate spans for reasons of aesthetics. In that case, the deck is chosen to be seated on a wall-like abutment web, as shown in Figure 1 and 2. (c_2) The second design alternative introduces the construction of the end spans with lengths smaller than the ones of the intermediate ones. Half of the length of the end span has a deck cross section with variable height. This corresponds to the part of the deck which extends from the end pier towards the abutment. The other part of the span is seated through bearings to the abutment, as shown on the right abutment of Figure 1. It extends from the abutment towards the pier and has a constant cross section height. The need for the smaller length of the end spans was found to be dictated by the relatively small height of the deck cross section that is 0,80 m and by the use of ordinary reinforcements in the bottom fibre of the deck.

It is noted that the use of prestressing within the bottom flange of the deck was not deemed to be a rational design selection, as the tendons would induce a large vertical load downwards, due to the variation of the height of the deck cross section. This constraint loading, namely the one induced by possible negative prestressing, would not be compatible with the rational use of tendons, which are typically utilised in order to compensate for the vertical loading.

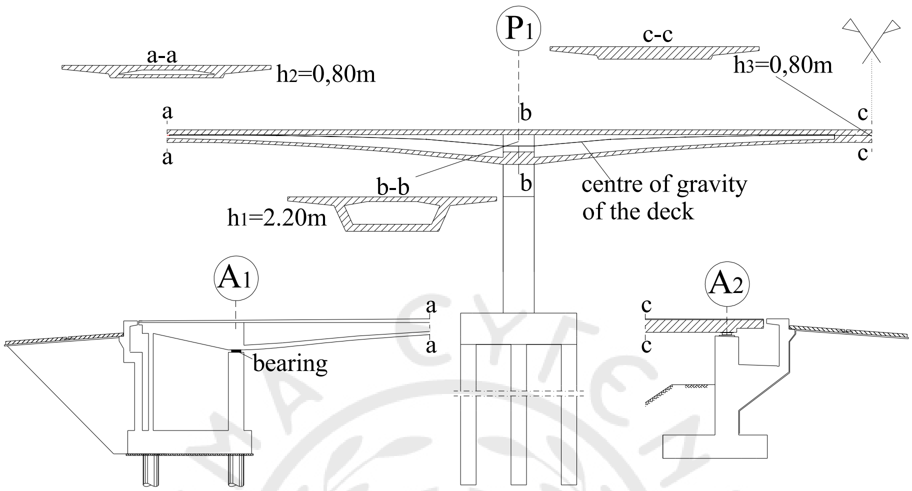

Figure 1. The first stage of the proposed construction method with alternative abutment configurations.

2.2 Particular design issues

The rigid connection of the deck with the abutments was achieved by the construction of a counterbalance that is a cantilever which extends from the abutment towards the backfill soil, as shown in Figure 1 and 2. The length of this cantilever is 5,0 m and its cross section height reduces from the abutment to the backfill. The end cross section of the cantilever is utilised for the anchorage of the tendons. The tendons are slightly lowered at their anchorages in order to provide the appropriate cover for their anchoring devices, namely the bearing plates. A structural tie, namely a reinforced concrete wall with a thickness of 0,30 m, is utilized in order to receive the bending moments of the counterbalance-cantilever, which are developed due to the vertical loading of the deck. In fact this wall, namely the structural tie, is under tension, while the abutment web, which receives the vertical loading through the bearings, is under compression. The structural tie has a transverse dimension equal to the distance between the wing walls, with which it is in contact but not connected. The reinforcement bars of the structural tie are anchored in the pile cap of the abutment's foundation. This pile cap has a relatively small thickness, as the wing walls and the wall that retains the backfill soil formulate a stiff concrete "box", which increases the stiffness of the pile cap. In case the web is integral with the deck, its in-service constrained movements can be accommodated by subdividing it in walls.

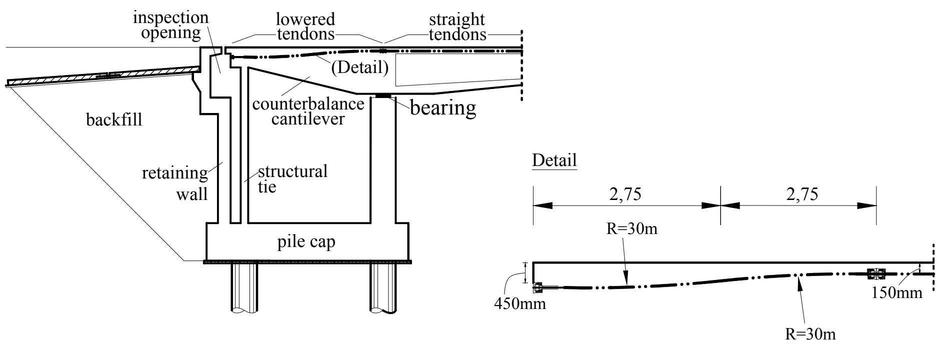

Figure 2. The abutment of the proposed construction method.

The minimum height of the deck cross section is proposed to be not smaller than 0,80 m. After the curing of the casted cantilevers, the tendons are stressed. The design of the prestressing force is based on the objective of the method that is to provide a slight pre-cambering of the cantilevers that is a slight bending deflection upwards. Therefore, at this stage the cantilevers of the deck are set higher than the final design height of the bridge. After the application of prestressing, the steel formwork is removed and the construction procedure is repeated for the adjacent spans. The tendons of the subsequent spans are coupled with the ones of the casted cantilever and the adjacent cantilever is constructed. A detailed description of the prestressing application and the rebar of the deck is given in section 3 of the paper.

After the completion of the deck construction and the application of the prestressing force, positive bending moments, which are caused due to the eccentricity of the straight tendons from the deck's centre of gravity, are induced along the deck. These positive bending moments overbalance the negative ones that are imposed by the self-weight of the deck. Hence, the aforementioned pre-cambering of the cantilevers is achieved. The pre-cambering was deemed necessary in order to compensate for the pre-determined long-term prestress losses due to the creep and shrinkage of the deck and due to the relaxation of prestressing steel. The rest of the vertical loads of the deck that are the additional permanent and the variable loading [7] are imposed after the completion of the total bridge system. Thus, the frame action of the total bridge structure, in which the meeting cantilevers are connected, receives the additional vertical loading. The final bridge system is then checked against the resulting bending moments, the shear actions and the torsion effects after considering the re-distribution of actions. In particular, the design of the deck against shear actions is facilitated due to the beneficial inclination to the horizontal of the compression zone of the deck in the critical section for shear, namely where the maximum shear stress is acting. Possible deficiency of the deck at the supports against the bending moments caused by either the ultimate or the serviceability limit states [6] [8] shall be covered by additional reinforcement bars of ordinary strength steel. The additional reinforcements cover the safety criteria set by codes [6] [8] and the serviceability requirements by limiting the crack width according to the code provisions [5] [6].

3 APPLICATION OF THE CONSTRUCTION METHOD TO A CAST-IN-SITU BRIDGE

3.1 Description of the benchmark bridge

The bridge of Kleidi-Kouloura belongs to Egnatia Motorway that runs across Northern Greece. It is a cast-in-situ structure with a total of three spans and a total length equal to 135.8 m. More details on the bridge are given in an another paper of IBSBI 2011 conference.

3.2 Results

The benchmark bridge was re-analysed and re-designed according to current code provisions concerning serviceability [6] [8] and earthquake resistance [9]. The re-design took into account the construction phases of the proposed method and the following predominant design parameters were revealed:
(1) The required number of straight tendons was less than the one needed in case a classification category A or B was chosen, (table 4.118 in [6] [8]). However, the total number of tendons ensures that the bridge is classified in category C, when this requirement refers to the performance of the top fibre of the deck, while the use of ordinary strength reinforcements in the bottom fibre of the deck leads to the classification category D. It is noted that, the design of the prestressing force and the resulting number of tendons aims at providing the required pre-cambering of the cantilevers against the self weight of the bridge deck, whose length was half of the total span length that is 45,60/2 = 22,80 m. (2) The re-design of the prestressing showed that 15x19T15 (15 tendons of 19 wires with diameter 15mm each) of high strength steel St 1500/1770 are adequate to receive the bending moment of the deck above its support. Additionally, ordinary steel rebar 76Ø16 (76 bars with diameter 16mm each) above the support were utilized, which gradually reduced to 28Ø16 at the bridge mid-span. The tendons and the reinforcements needed in the top flange of the deck are illustrated in Figure 3. The ordinary strength steel bars, which are also required by the code [6], are the ones which allow the safe transition from the uncracked to the cracked deck section and the avoidance of non-ductile failure modes. The lengths of the steel bars were chosen to be sub-multiples, namely half, of the conventionally produced ones by the steel manufactures in order to avoid material waste. Figures 4 and 5 show in detail the reinforcement layout at the support and at the mid-span. Figure 6 shows the steel rebar of the bottom part of the deck. The bars are installed in couples that are 2x71Ø25 (71 couples of bars with diameters 25mm each) at the mid-span, while 2x41Ø25 were found

to be required at the bottom flange of the deck at the supports. The reinforcement splices were required to extend 2,15 m. The lengths of the bars were selected to be 7,0 m and they were set parallel to the sides of the polygonal shape of the bottom flange, as shown in Figure 6. (4) The thickness and the reinforcement of the structural tie, that is the wall that restrains the vertical movements of the counterbalance-cantilever at the abutment shown in Figure 1 and 2, were found to be 0,30m and 3xØ16/100 (3 lines of bars with diameter 16mm at a spacing 100 mm) correspondingly.

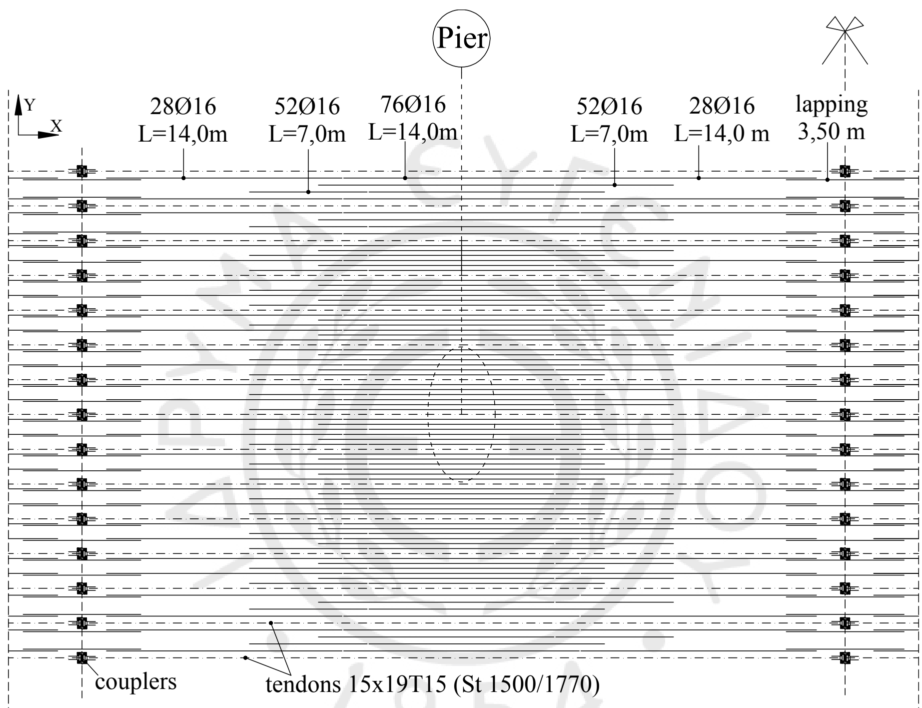

Figure 3. The layout of the straight tendons and the ordinary strength steel bars of the deck's top flange at the support, (the scale is distorted: 1 unit at X equals 2 units at Y axis).

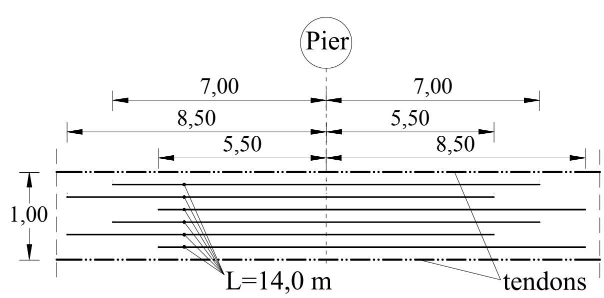

Figure 4. Detail of the straight tendons and the ordinary strength steel bars of the deck's top flange at the support.

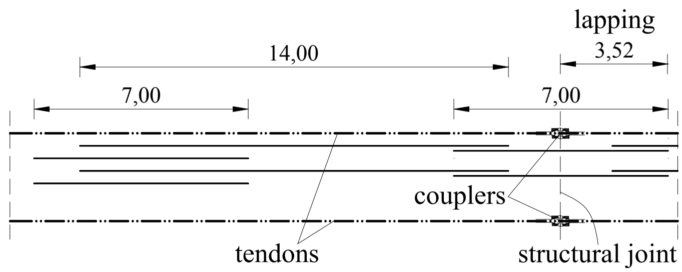

Figure 5. Detail of the ordinary strength steel bars of the deck's top flange at the mid-span and coupling of the tendons.

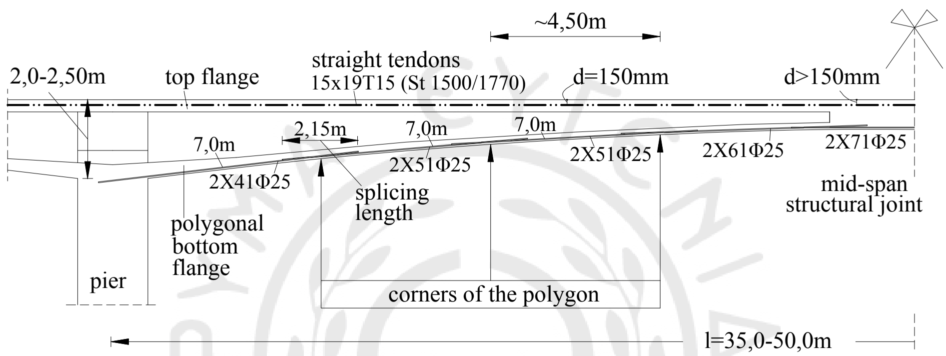

Figure 6. Detail of the ordinary strength steel bars at the bottom flange of the deck.

4 CONCLUSIONS

This paper proposes a new bridge construction method, which can be used as a design alternative to the conventional construction practices. The method has many similarities with the balanced cantilever method. The prestressing tendons are straight and installed within the top flange of the deck cross section, while ordinary strength steel is utilized for the reinforcement within the bottom flange. The deck has a variable cross section height along its longitudinal direction. A benchmark bridge, actually built along the Egnatia Motorway by the conventional segmental cast-in-situ method, was utilized to identify the applicability of the proposed method. The bridge was checked according to the current code provisions and the study came up with the following findings:

- The application of the proposed construction method revealed significant structural benefits. The use of straight tendons for the prestressing of the deck facilitates and accelerates the construction of the bridge. The tendons are installed within the upper slab of the deck's cross section, which is more preferable than using tendons which are installed in the webs of the box girder. It is noted that the use of tendons in the webs of the box-girder decks is not allowed according to current code design, at least for bridges constructed by the balanced cantilever method. Furthermore, the prestressing losses due to friction are significantly reduced when the proposed construction method is employed. The dead load of the bridge deck, which typically constitutes the largest portion of the bridge's vertical loading, is decreased due to the reduction in the height of the deck cross section. However, the variation of the deck cross section along the bridge deck obstructs the falsework as the scaffolding is more demanding in terms of geometry, compared to the conventional segmental bridge construction.

- The bridge aesthetics are significantly improved compared to the conventional segmental bridge construction. This is due to the refined arch-type view of the bridge constructed by the proposed method and the reduced deck cross section height.
- As far as it concerns the cracking of the deck, the proposed construction method can be utilized for the construction of bridges with short to medium spans up to 35 m. The check against cracking due to the short term vertical loading of the deck, namely against the infrequent loading, showed that the deck does not exhibit cracking. In case of bridges with longer spans up to 50m the use of partial prestress shall be used.
- The deflections of the deck were significantly reduced due to the objective set during the design of the prestressing force, which ensured that the cantilevers had a pre-cambering upwards, at least when the scaffolding was removed.
- Possible differential settlements of the piers can be received by the resulting bridge system without developing high bending loading to the deck, due to flexibility of the arch-type superstructure.

REFERENCES

[1] CALTRANS, "Bridge Design Aids Manual", California Department of Transportation, Sacramento, 1994.
[2] Chen WF and Duan L, *Bridge Engineering Handbook*, CRC Press Boca Raton London, New York Washington, D. C., 1999, Chapter 1.
[3] Trost H., *Lastverteilung bei Plattenbalkenbrucken*, Werner Verlag, Dusseldorf, West Germany, 1961.
[4] Kwak H-G and Son J-K, "Determination of design moments in bridges constructed with a movable scaffolding system (MSS)", Computers and Structures, Vol. 84, Issue 31-32, pp. 2141-2150, 2006.
[5] EN 1992-1-1:2004 Eurocode 2: Design of concrete structures, Part 1-1: General rules and rules for buildings, 2004.
[6] DIN-Fachbericht 102, Betonbrücken, DIN Deutsches Institut fuer Normung e.V, 2003.
[7] EN 1991-2:2003 Eurocode 1: Actions on structures - Part 2: Traffic loads on bridges, 2003.
[8] EN 1992-2:2004 Eurocode 2: Design of concrete structures-Part 2: Bridges, 2004.
[9] EN 1998-2:2005 Eurocode 8: Design of structures for earthquake resistance, Part 2: Bridges, 2005.

TOPIC 4

Experimental Research

Bridge Monitoring

REPAIR AND STRENGTHENING OF REINFORCED CONCRETE STRUCTURES THROUGH ULTRA HIGH PERFORMANCE FIBER REINFORCED CEMENTITIOUS COMPOSITES

Alberto Meda[1], Dario Rosignoli[2] and Stefano Maringoni[3]

[1] University of Rome "Tor Vergata", Dept. of Civil Engineering, Rome, Italy
[2,3] Tecnochem Italiana SpA, Barzana, Bergamo, Italy
e-mail: alberto.meda@uniroma2.it, dario.rosignoli@tecnochem.it, stefano.maringoni@tecnochem.it

ABSTRACT: The first application of a new technique based on the use of a specially formulated Ultra High Performance Fiber Reinforced Cementitious Composite jackets for low thickness antiseismic structural strengthening R/C columns and beams is presented herein. In order to verify the effectiveness of the solution, a test on a full scale element has been performed. The applications could be also extended to casting new structures like Bridges or other buildings where low thickness casting or material with high performances are needed.

KEY WORDS: reinforcement, seismic retrofitting, UHPFRCC jackets, low thickness casting

1 INTRODUCTION

In the seismic retrofitting of R.C. elements different techniques are usually proposed (Fib Bulletin 24, 2003; Fib Bulletin 32, 2006; Fib Bulletin 35, 2006; Fib Report 1991). Regarding the strengthening of existing columns, the possibility of using R.C. jacket is usually considered, especially when the element is made of low strength concrete. Traditional jacketing presents some inconvenience, as the jacket thickness is governed by the steel cover (both external and internal). This often leads to a jacket thickness higher than 70-100 mm (Fib Bulletin 24, 2003), with a consequent increase of the section geometry, leading to an increase of both mass and stiffness, which can give some problems with respect to the seismic behaviour. This aspect is particularly important when small columns are considered (e.g. 250-300 mm of side). The traditional reinforcement in the jacket can be avoided allowing the use of a thin HPFRCC layer (30-40 mm). This technique has been demonstrated effective for the strengthening of existing columns if compared with other techniques, such as traditional jacketing or FRP wrapping (Meda et al., 2008), particularly when a low strength concrete is present in the existing structure.

Recent investigations on existing structures built in Italy around the ’60s and ’70s demonstrated that an average concrete compressive strength lower than 15MPa was usually adopted (Ferrini et al., 2008). These buildings not only have problems to carry the design vertical loads but, when a seismic retrofitting is required, they have to be significantly strengthened.

In this situation, the proposed strengthening technique can be easily adopted with the possibility of a remarkable increase of the structure performances.

Herein a real case study concerning the application of the proposed technique is presented: a school building, located in a seismic area near Rome, in which on-site tests showed that a concrete with an average compressive strength of 11 MPa had been used. Accordingly, a complete retrofit of the building in agreement to the new Italian Seismic Code had to be undertaken.

The columns have been strengthened with a 40 mm jacket in high performance fiber reinforced concrete. Before the application of the jackets, a full scale test simulating the behaviour of the existing columns was requested from the Italian Council for Public Works (whom has to be consulted when a non codified structural typology is intended to be used).

Photo 1. Overall view of the outside Zagarolo school after working

Photo 2. Overall view of the outside Zagarolo school before working

The test was performed up to failure by applying cyclic loads of increasing amplitude. Once the results demonstrated the effectiveness of the applied technique, the application in the school building was authorized and eventually executed.

2 SPECIMEN PREPARATION AND TEST SET-UP

A column with a 400x400 mm square section has been tested. The element, 3m high, has been cast on a 500 mm thick foundation (Figure 1). The reinforcement and the concrete strength was typical of this kind of elements in the ’60s: 8Ø16mm diameter longitudinal rebars and 8mm stirrups spaced at 300mm, with a concrete strength of approximately 20MPa.

After casting and a curing period of 14 days, the column surface was sandblasted in order to achieve a roughness of 1-2 mm, that was demonstrated able to ensure a good adhesion between new and old concrete (Martinola et al. 2007).

The specimen has been placed on the testing frame and an axial load equal to 170 kN has been applied by means of two hydraulic jacks (Figure 2). This axial load aims to reproduce the effect of the dead loads acting on the column at the time of the jacket application.

The strengthening jacket, having a thickness of 40 mm was eventually cast (Photo 3) adopting a self-compacting high performance fiber reinforced concrete having a compressive strength of 130 MPa and a tensile strength of 6 MPa.

In order to connect the jacket to the column base, a pocket 50 mm deep was realized in the foundation and a high strength steel mesh (Ø 2 mm/20 mm) was inserted in the jacket for the first 150 mm of the column. This solution has been demonstrated effective in other researches (Marini and Meda, 2009). The same mesh was applied at mid-height of the column, where a cast interruption was forecast. After curing of the jacket, the column was tested.

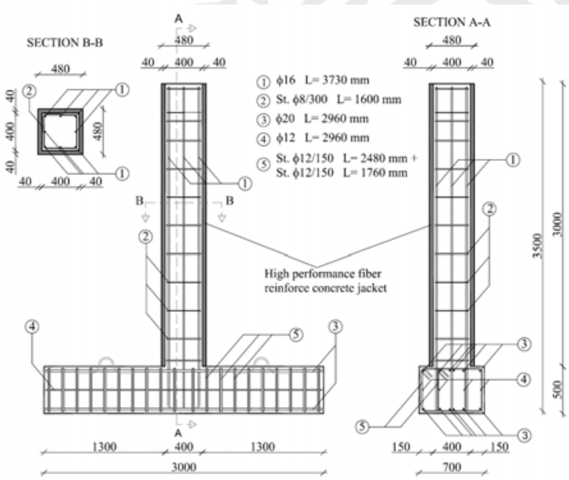

Figure 1. Column geometry and details of the specimen construction

Photo 3. Preparation of formworks of the sample

The column foundation was anchored to the laboratory basement with four pretensioned high strength rebars. The initial axial load was increased up to 645 kN in accordance to the critical design load combination for the column in the building. Eventually, an horizontal cyclic load was applied by means of an electro-mechanical jack fixed to the reaction wall of the laboratory. The jack was linked to the column by means of a hinged bar system in which a load cell was placed. The horizontal force was applied at a height of 2 m from the column foundation connection in order to have the same moment – shear ratio at the critical section (column base section) obtained in the building design.

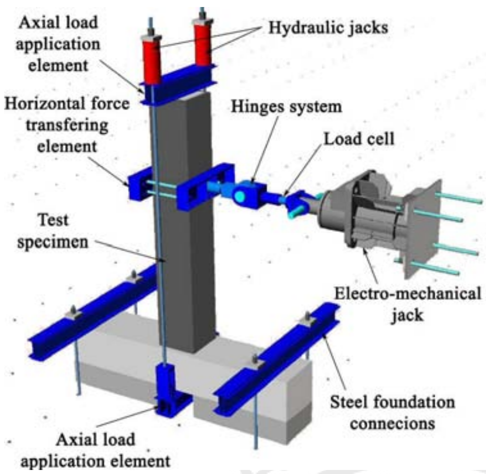

Figure 2. Column geometry and details of the specimen construction

Photo 4. High performance jacket casting

TEST PROCEDURE

Initially, a cyclic horizontal force and a constant vertical force have been applied, aiming to simulate the maximum design actions (axial force N = 645 kN, bending moment M = 144 kNm and shear force V = 72 kN). In this testing phase, five cycles were performed by applying maximum design bending moment and shear action in both directions with a constant axial force. Under these actions the columns has not evidenced any damage and no cracks were detected on the strengthening jacket. As it can be noticed in Figure 3, where the horizontal force versus displacement curve is presented, the behaviour is almost linear elastic. Only the first cycle evidenced some settlement of the loading system.

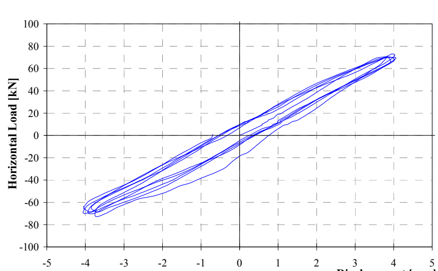

Figure 3. Horizontal load versus displacement for the design load level

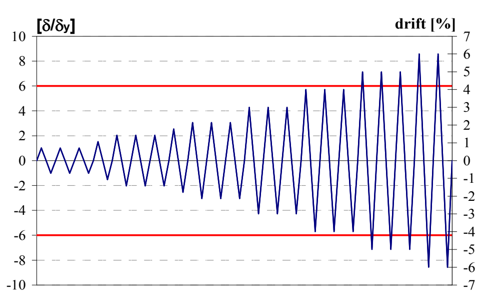

Figure 4. Load history

In order to verify the effectiveness of the strengthening technique, the test was continued by applying the horizontal load with cycles characterized by an incresing amplitude up to failure. Firstly, cycles with a displacement amplitude double respect to the initial one were applied in order to define the structural yielding point. That was found for a horizontal load equal to 115 kN, corresponding to a bending moment equal to 230 kNm, almost 1.6 times the maximum design value.

The structural yielding occurred at a displacement δ_y equal to 1 mm, measured at the load application point level. At this level the yielding drift, defined as the ratio between the displacement δ_y and the lever arm of the horizontal load (2 m) with respect to the column base, was equal to 0.7%. The test has been continued by applying cycles with displacement amplitude proportional to the yielding drift. Initially three cycles at a drift of ±0.7%, one cycle at ±1%, three cycles at ±1.5%, one cycle at ±1.75%, and three cycles at ±2% were applied. Eventually three cycles for increments of drift equal to 1% were applied up to collapse. The adopted load history is summarised in Figure 4, where a ductility limit close to 6 δy is indicated: this value is associated to the behaviour factor for high ductility frame systems given by the Euroccode 8 (EN 1998-1, 2004).

RESULTS

The results in terms of horizontal load versus displacement at the level of the load application point are shown in Figure 5. The column reached the collapse during the third cycle at a drift level equal to 6% (120 mm; δ/δy=8.6). The collapse was due to the rupture of one of the longitudinal rebars.

After the onset of the flexural cracking at a drift equal to 1%, the behaviour was stable up to failure with a limited damage. The main crack was located in correspondence to the end of the high strength steel mesh adopted for linking the high performance concrete jacket to the base foundation. Other cracks developed with a spacing of about 300mm, equal to the stirrups spacing.

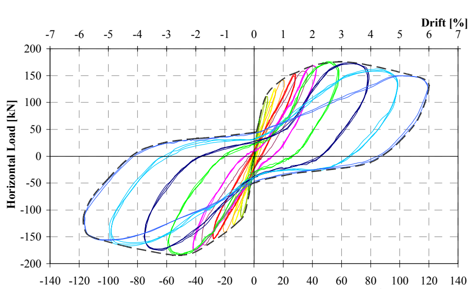

Figure 5. Horizontal load versus displacement at the load application point

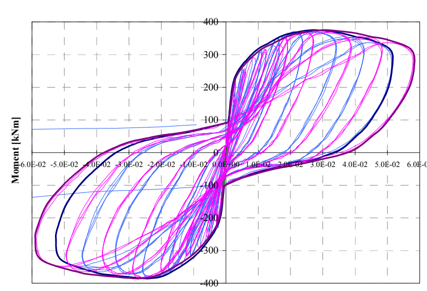

Figure 6. Moment versus curvature curves with and without slip contribution

Photo 5 shows the column deformation at 6% drift. Looking at the envelope curve (dotted line) in Figure 5, it is evident a strength degradation for drift levels higher than 3.5%. The maximum bearing capacity is equal to 175 kN while the horizontal load at failure is equal to 145 kN, 83% of the maximum load. The load decrease can be justified with a progressive slip of the jacket at the foundation base, as highlighted in Photo 6.

Photo 5. Column deformation at failure

Photo 6. Slip between jacket and foundation base

This is confirmed in Figure 6, where the moment versus curvature curves at the column base are drawn: in one curve the curvature has been determined by considering the displacement transducers placed on the column while the other curve is determined by considering the transducers measuring the relative displacement between column and foundation. As a consequence the first curve does not take into account the jacket slip, as the second curve does. The two curves tends to diverge, with the slip mechanism activation, after the maximum moment (horizontal force) is reached. This aspect justifies the load decrease at 3.5% of drift.

JOBSITE

The presented paper illustrates the first application of a new strengthening technique based on the use of high performance fiber reinforced concrete.

Photo 7. Pillars after reinforcement

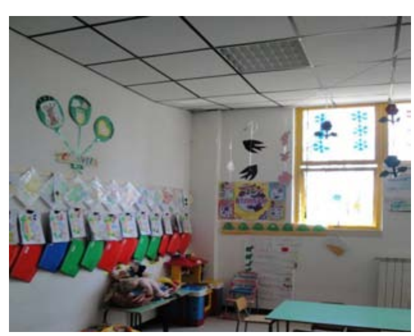

Photo 8. School after seismic retrofitting

Given the good results obtained by experimental evidence, was conducted the casting on the pillars on the jobsite in Zagarolo.

As it can be seen below, this technology has been extended to casting a new bridge. In photos 9 and 10 are shown formworks and UHPFRCC casting about this technology to realize a new bridge in Italy.

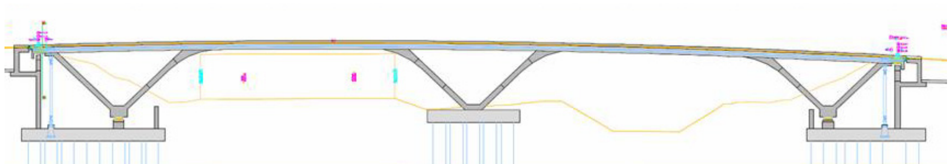

Figure 7. Structural sections of the bridge

Photo 9. Formworks of the pillars

Photo 10. Pillars after casting

CONCLUSIONS

The performed full scale test demonstrated the effectiveness of the jacket application, showing a remarkable increase in terms of bearing capacity and ductility.

The adoption of this technique has advantages with respect to traditional strengthening techniques. In particular, it is possible to limit the increase in the column geometry and, as a consequence in the self weight and stiffness of the structure. The high fluidity of the material allowed to have smooth surfaces. In the application in the school building, it was not necessary to add a plaster layer (20 mm thick) previously present. Hence, the change in geometry was only 20 mm due to the fact that the jacket thickness was 40 mm.

The adopted technique appears particularly useful for static and seismic retroffiting and new constructions with low thickness of structural sections and high static and dynamic loads.

REFERENCES

[1] G. MARTINOLA, A. MEDA, G.A. PLIZZARI, Z. RINALDI, "An application of high

performance fiber reinforced cementitious composites for R/C beams strengthening", FRAMCOS 6. Catania (Italy). 18-21 June 2007.

[2] L. MAISTO, A. MEDA, G.A. PLIZZARI, Z. RINALDI, "R/C beams strengthening and repair with high performance fiber reinforced concrete jacket", 4th International Conference on The Conceptual Approach to Structural Design. Venezia (Italy). 27-29 June 2007.

[3] A. MEDA, G.A. PLIZZARI, Z. RINALDI, G. MARTINOLA, "Strengthening of R/C existing columns with high performance fiber reinforced concrete jacket", 2nd International Conference on Concrete Repair, Rehabilitation, and Retrofitting. Cape Town (South Africa). 21-23 novembre 2005.

EXPERIMENTAL STUDY OF FRP-DFRCC COMPOSITE DECKS

Sung Tae Kim[1], Keunhee Cho[2], Sung Yong Park[3], Jeong-Rae Cho[4] and Byung-Suk Kim[5]

[1,2,3,4,5] Korea Institute of Construction Technology, Structural Engineering & Bridges Research Division, Korea
e-mail: esper009@kict.re.kr, kcho@ kict.re.kr, sypark@ kict.re.kr, chojr@ kict.re.kr, bskim@ kict.re.kr

ABSTRACT: The FRP-DFRCC composite deck (FDCD) is a deck combining Ductile Fiber Reinforced Cementitious Composites (DFRCC) and FRP. Owing to this concept, beam and deck specimens are manufactured and their applicability and stability for use in real bridges are evaluated experimentally.

KEY WORDS: DFRCC; FRP; Composite; Deck; Bridge.

1 INTRODUCTION

Fiber Reinforced Plastic (FRP) is a lightweight material offering high tensile strength and remarkable durability. Such features boosted research to exploit this material for bridges' structural members since early 2000s. Besides, active research is also carried out on high performance concrete. Especially, those focusing on concrete exhibiting smeared-crack effect together with high strength and high toughness superior to those of normal concrete have recognized significant progress. Accordingly, the Korea Institute of Construction Technology started to develop a FRP-concrete composite deck (FCCD) since 2002 [1] and undertook recently the development of the FRP-DFRCC composite deck (FDCD) combining FRP and Ductile Fiber Reinforced Cementitious Composites (DFRCC). This deck concretizes the research results on FCCD and DFRCC and, applies DFRCC at the top of the deck to exploit its outstanding toughness and compressive performance at this zone mainly governed by compression as shown in *Fig. 1*. Moreover, FRP panel is disposed as permanent form at the bottom of the deck mainly subjected to tension in order to replace steel reinforcement owing to its lightweight and non-corrosiveness. Such structure enables to maximize the advantages of both FRP and DFRCC so as to improve the durability and safety of the structural system.

The perfect composition of these two very different materials is realized by the simultaneous application of coarse sand coating and concrete wedge. Coarse sand coating improves the shear bond strength by bonding the coarse sand aggregates on the FRP panel using epoxy prior to placing concrete whereas the concrete wedges enhance the vertical bond strength [2].

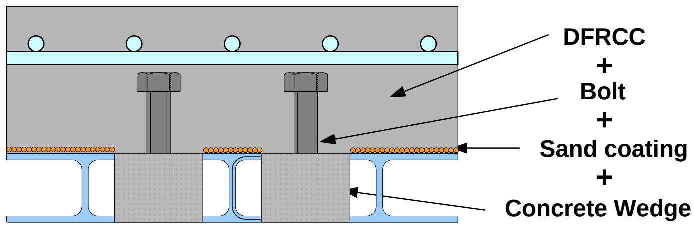

Figure 1. Conceptual drawing of the FRP-DFRCC deck section

Since the so-developed deck uses high performance fiber reinforced cementitious composite, reduction of the construction cost of the bridge can be achieved through significant reduction of the weight by 30~40% compared to conventional RC deck, which is superior than FCCD. However, the lack of knowledge about the actual characteristics of DFRCC and the absence of relevant design specifications impede accurate evaluation of the extent by which the quantity of DFRCC can be reduced. Therefore, FDCD beam specimens were manufactured with various depths of FCCD and DFRCC so as to select experimentally the depth of DFRCC enabling to achieve performances equivalent or superior to specimens using normal concrete and satisfying serviceability and stability. In addition, full scale FCCD and FCCD prototypes were fabricated to fit with the dimensions of real bridges. These two prototypes were subjected to performance tests and their applicability for real bridges and structural stability were evaluated.

2 DESIGN, FABRICATION AND STRUCTURAL PERFORMANCE TEST OF SPECIMENS

2.1 Design of specimens

Due to the absence of accurate design specifications for DFRCC, the design and fabrication of FCCD specimen were conducted prior to the design of FDCD with identical dimensions. The adopted depth of upper concrete was 150 mm so that, added with the depth of the bottom FRP panel, a total depth of 220 mm similar to conventional RC deck was obtained. Besides, this deck uses FRP reinforcement instead of steel reinforcement and was designed in compliance with ACI440 [3] and CHBDC (2006) [4]. Moreover, FCCD was designed as one-way beam with unit width (1 m) for which the flexural behavior can be predicted with very good accuracy using the research results of Cho et al. (2008) [5].

2.2 Beam specimens

2.2.1 Fabrication of specimens

The beam specimens are classified with reference to the use of normal concrete or DFRCC. Three types of DFRCC specimens were manufactured according to the thickness of DFRCC through the process illustrated in *Photo 1*. *Table 1* indicates the characteristics of the specimens where the strength corresponds to the actual compressive strength obtained experimentally. Besides, the specimens being partial models at the beam level, concrete blocks simulating the concrete girder were fabricated and the beams were tied using hydraulic nuts as shown in *Fig. 2*. to consider the effect of the girder's restraint on the deck. This disposition was also adopted to observe the behavior of the deck at the negative moment zone above the girder. FRP reinforcing bars with diameter of 16 mm were installed at intervals of 100 mm in the transverse direction to satisfy the specifications of ACI 440.1R-06 (2006) relative to concrete at the negative moment zone above the girder. *Table 2* lists the test results of the FRP panel and FRP reinforcement used in each of the specimens.

(a) Pultrusion of FRP panel *(b)* Assembling of FRP rebar *(c)* Placing of DFRCC

Photo 1. Fabrication process of FDCD

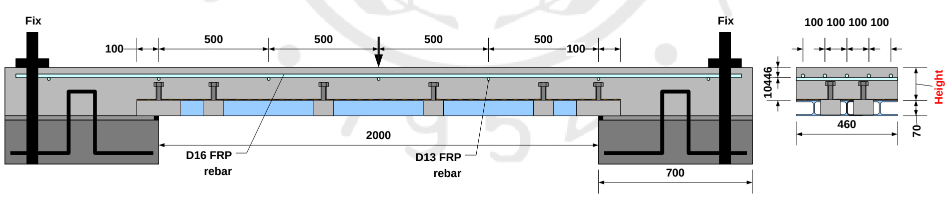

Figure 2. Drawing of specimen at beam level

Table 1. Dimensions and reinforcement of the specimens

Specimen		ea	Concrete			Reinforcement	
			Type	Depth (mm)	Strength (Mpa)	Longitudinal	Transverse
FCCD		2	NC	150	34.8	FRP D13@500	FRP D16@100
FDCD	80	2	DFRCC	80	98.6	FRP D13@500	FRP D16@100
	115	2	DFRCC	115	98.6	FRP D13@500	FRP D16@100
	150	2	DFRCC	150	98.6	FRP D13@500	FRP D16@100

Table 2. Mechanical properties of FRP panel

Properties	Unit	Bottom flange	Web	Top flange	FRP rebar
Tensile strength	MPa	403	425	407	1,000
Tensile modulus	GPa	24.4	24.6	25.1	45.0
Compressive strength	MPa	298	283	226	–
Compressive modulus	GPa	10.3	9.4	8.16	–

2.2.2 Test results and discussion

Load was applied at the center of the specimens as a pressure load with dimensions of wheel load (230 mm × 580 mm). The FCCD specimens placed with normal concrete started to develop flexural cracks in concrete at mid-span with increasing loading and experienced additional flexural cracks at regular spacing with larger loads. Then, final failure occurred through debonding of the FRP-concrete interface following the propagation of diagonal cracks.

The FDCD specimens verified the smeared-crack effect of DFRCC through a cracking pattern different to that of the FCCD specimens as shown in *Photo 2* and *Photo 3*. Cracks initiated in concrete at both negative moment zones of the specimens. In addition, flexural cracking did not occur at mid-span until failure at the FRP-concrete interface when large flexural cracking occurred simultaneously at once. Thereafter, these flexural cracks propagated gradually toward the top and final failure occurred with the damage of the bottom FRP panel. *Table 3* and *Table 4* arrange the test results by type of FDCD specimens.

Table 3. Test results of FDCD beam specimens

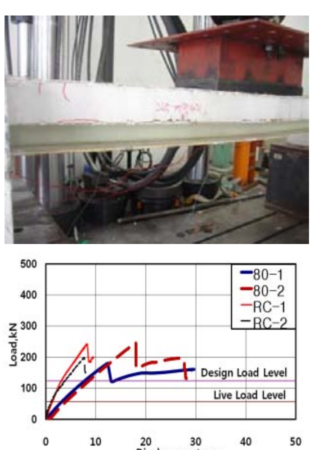	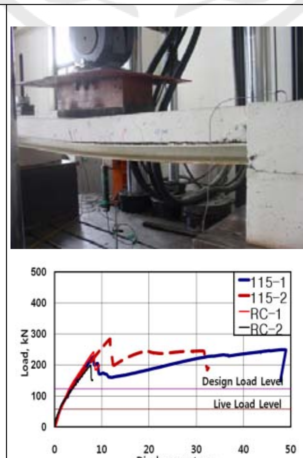	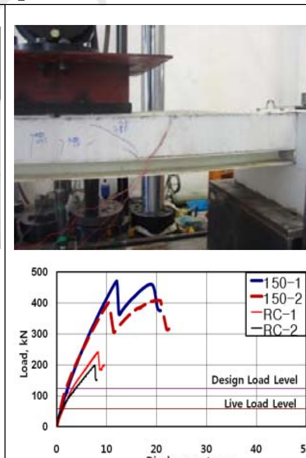
80mm specimens	115mm specimens	150mm specimens

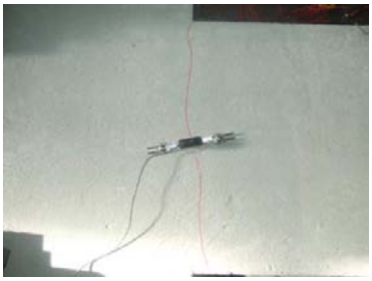

Photo 2. Cracking pattern of FCCD

Photo 3. Cracking pattern of FDCD

Table 4. Measured deflection and crack width of the beam specimens

Type	Allow. deflection (mm)	Deflection (test, mm)	Remark	Allow. crack width (mm)	Crack width (test, mm)	Remark
RC-1	2.5mm	1.46	O.K.	0.3mm	0.14	O.K.
RC-2		1.25	O.K.		0.14	O.K.
80-1		3.40	N.G.		0.012	O.K.
80-2		4.18	N.G.		0.048	O.K.
115-1		1.17	O.K.		No crack	O.K.
115-2		1.21	O.K.		No crack	O.K.
150-1		0.73	O.K.		No crack	O.K.
150-2		0.90	O.K.		No crack	O.K.

From the test results, the failure strength of the specimen with DFRCC depth of 80 mm reached a value of 200 kN similar to that of FCCD but failed to satisfy the allowable deflection (L/800 = 2.5 mm) specified by AASHTO (2004) [6] with a measured deflection ranging between 3.40 mm to 4.18 mm under service load state. This implies that this specimen cannot be applied in real bridges. However, the specimens with DFRCC depths of 115 mm and 150 mm presented failure strengths larger than that of the FCCD specimen by 116% and 199%, respectively. In addition, the deflection measured under service load state ranged respectively within 1.17-1.21 mm and 0.73-0.90 mm, which satisfy sufficiently the design criterion. Moreover, cracking did not occur at the negative moment zones under service load state and the FDCD specimens exhibited improved ductile behavior even after failure. Since the specimens with DFRCC depths of 115 mm and 150 mm achieved performances equivalent or superior to those of the specimens using normal concrete, it could be assessed that no problem would happen in their application in real bridges.

2.3 Deck prototypes

2.3.1 Fabrication of prototypes and tests

The deck prototypes were fabricated with sections identical to the beam specimens and width enlarged to 3 m. The difference was in the decision to adopt a depth of 120 mm for DFRCC so as to secure larger stability. The materials and process adopted for the manufacture of the prototypes were identical to those of the beam specimens. Loading was also applied as a pressure load to simulate wheel loading. *Photo 4* and *Photo 5* illustrate the test setup of the prototypes.

Photo 4. Test of FCCD prototype

Photo 5. Test of FDCD prototype

2.3.2 Test results and discussion

Early longitudinal cracks developed in the FCCD prototype around the supports due to negative moments produced by loading. Then, circular cracks centered at the loading point occurred with larger loads followed by final failure through punching of concrete at load of 694.7 kN.

The FDCD prototype exhibited cracking pattern similar to the FCCD prototype. Final failure occurred at load of 1,502.8 kN with the punching of DFRCC simultaneously with the bonding failure of the bottom FRP panel. *Fig. 3* plots the load-displacement curves measured in both prototypes.

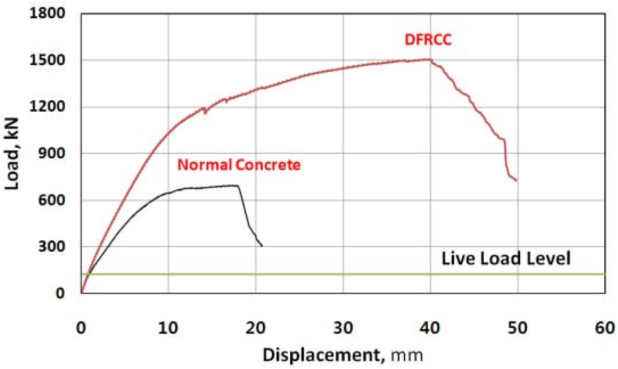

Figure 3. Comparison of load-displacement curves

The deflection of the FCCD prototype under service load state reached 0.8 mm and that of the FDCD prototype reached 0.63 mm. Both prototypes satisfied sufficiently the allowable deflection of 2.5 mm. Moreover, both prototypes did not experience cracking at the negative moment zone under service load state.

In view of the test results of these deck prototypes, the FCCD prototype and the FDCD prototype satisfy with large margin the deflection and crack criteria. Accordingly, it appears that these prototypes provide sufficient applicability and stability for their application to real bridges.

Besides, the failure strength of the FDCD prototype in which the depth of DFRCC was reduced to 120 mm corresponding to 80% of the depth of normal concrete was seen to secure outstanding performance reaching approximately 216% of the failure strength of FCCD. Consequently, it can be predicted that sufficient performance could be secured even with larger reduction of the depth of DFRCC when applied to real bridge. In addition, a reduction of the weight per 1 m^2 of concrete by at least 20% can be realized by reducing the depth of the upper concrete compared to FCCD using normal concrete.

3 CONCLUSIONS

Beam specimens and deck prototypes of FCCD and FDCD were fabricated and subjected to static loading test. The corresponding results made it possible to derive the following conclusions.

1. For the beam specimens with DFRCC depth of 80 mm, the deflection under service load state ranged between 3.40 mm and 4.18 mm, which failed to satisfy the deflection limit of 2.5 mm. This type of specimen appeared thus to be inappropriate for application in real bridges.
2. For the beam specimens with DFRCC depths of 115 mm and 150 mm, the deflection and crack performances were equivalent or superior to those of the specimens using normal concrete. These performances satisfying sufficiently the design criteria enabled to assess that no problem would happen in their application to real bridges.
3. The static loading test results for the FCCD prototype and FDCD prototype with DFRCC depth of 120 mm revealed that both prototypes satisfied the deflection and crack criteria with large margins. Therefore, it appeared that these prototypes provide sufficient serviceability and stability for their application to real bridge.
4. The failure strength of the FDCD prototype reached approximately 216% of that of the FCCD prototype, and its deflection under service load state was 78% smaller. In addition, the absence of cracking showed its outstanding performance. Accordingly, a DFRCC depth smaller than 120 mm can be adopted in real bridges. Moreover, since the specific weight of DFRCC is similar to that of normal concrete, it appears that the weight per 1 m^2 of concrete can be reduced by more than 50% compared RC deck and more than 20% compared to FCCD.

ACKNOWLEDGMENTS

This work is supported by the Construction Core Technology R&D (05 Construction Core D09-HiperCONMAT) of the Ministry of Construction and Transportation and by the “Development of Hybrid Cable-Stayed Bridge Deck”, an in-house project of the Korea Institute of Construction Technology. The authors express their gratitude for the support.

REFERENCES

[1] Korea Institute of Construction Technology, “Development of High Performance Construction Material- Development of Hybrid Bridge System Appling FRP and FRC”, Ministry of Construction and Transportation, 2010.

[2] Cho, K, Park, SY, Kim, ST, Cho, JR, Kim, BS, “Coarse Sand Coating and Concrete Wedge Composite Method for FRP-Concrete Composite Deck , ⅠⅠ”, *Proc. Conference of Korean Society of Civil Engineers*, pp. 1331-1334 and pp. 1339-1342, 2008.

[3] ACI 440.1R-06, “Guide for the Design and Construction of Concrete Reinforced with FRP Bars”, ACI, 2006.

[4] CHBDC, “Canadian Highway Bridge Design Code”, pp. 702-703, 2006.

[5] Cho, K, Park, SY, Cho, JR, Kim, ST, Kim, BS, “Flexural Behaviors of an Innovative FRP-Concrete Composite Deck”, *EASEC-11*, 2008.

[6] American Association of State Highway and Transportation Officials, “AASHTO LRFD Bridge Design Specifications”, pp. 2-11, 2004.

A SUGGESTION OF A QUICK AND ECONOMIC METHOD OF STRENGTHENING BRIDGE PIERS

Alkisti Parapanisiou[1], Dafni Argyropoulou[2], Evangelia Andreadou[3], Xanthi Demertzi[4], Theodoros Chrysanidis[5] and Ioannis Tegos[6]

[1,2,3,4,5,6] Aristotle University of Thessaloniki, Dept. of Civil Engineering, Greece
e-mail: alkhsti@yahoo.gr, dafni_arg@windowslive.com, lina.andr@hotmail.com, xdemertz@yahoo.gr, itegos@metesysm.gr, thchrysa@civil.auth.gr

ABSTRACT: The main subject of the experimental research is the investigation of a new way of strengthening the axial and transverse loading capacity and the confinement of circular cross section piers. The strengthening of the piers took place by the construction of jackets composed by metal semi-pipe systems combined either with high performance cement or with spiral reinforcement and cement.

KEY WORDS: Circular section; Piers; Semi-pipe; Shear; Strengthening.

1 INTRODUCTION

The kind of innovative jackets which are proposed and discussed in this research project consist of metal semi-pipe iron sheets pasted onto the pier with high quality cement of thickness 5 – 10 mm per sheet. Then, the pasted iron sheets of semi-pipe are wrapped with thick conventional spiral reinforcement. Afterwards, the external surface is covered with the appropriate ready-shrinking cement or by using fiber-reinforced concrete. The implementation of the proposed type of jackets takes less time and is easier compared to the existent applied methods of jacketing. Also, the jackets of this type can increase directly, as the traditional jackets, the axial load capacity, [1] [2] [3] [4] [5].

What needs to be considered for the proposed type of jackets is their performance against the basic stresses of a pier. Namely, one should consider the transverse and axial load capacity and the possibility of adding confinement capacity at the strengthened pier. The project was split into two parts which were examined independently one of the other. The transverse and bending load capacity were examined separately from the axial load capacity, which was examined in conjunction with confinement. In particular, the experimental program consisted of 10 specimens. Six of them examine the performance of the proposed jacket against combined bending-shear loads in circular section piers. The remaining four specimens were designed to improve the axial load capacity and the imposed confinement of circular section piers. The conclusions obtained can be considered very encouraging for the performance of the proposed type of jacket and particularly the improvement of all the seismic mechanical properties. Apart from the effectiveness of the method, the constructability, the low cost and the speed of the implementation are some of the main advantages of the proposed method of jacketing, [1] [2].

2 EXPERIMENTAL RESEARCH

2.1 Scope

The test specimens were constructed with strong longitudinal bending reinforcement and weak spiral transverse reinforcement. The reason is that we wanted the test specimens to fail due to shear loads. Then, the transverse load capacity of the test specimens was strengthened using the aforementioned techniques and the experiments will prove if the applied strengthening technique is successful in strengthening the transverse load capacity or not.

2.2 Description of the specimens

This research includes 10 specimens of circular cross section piers. Their specifications are described in the table below, [1] [2].

Table 1. Characteristics of the test specimens.

Specimens	Diameter D (mm)	Length L (mm) Height h (mm)	Longitudinal reinforcement	Transverse reinforcement	Method of strengthening
Test specimens related to the transverse load carrying capacity.					
1	150	1200	12Ø10	Ø4.2/250	Conc. And spiral reinfor. Ø4.2/150
2	150	1200	12Ø10	Ø4.2/250	2 metal semi-pipe systems welded with 2 iron sheets 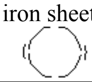
3	150	1200	12Ø10	Ø4.2/250	4 metal semi-pipe systems 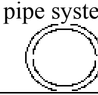
4	150	1200	12Ø10	Ø4.2/250	6 metal semi-pipe systems 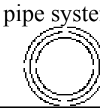
5	150	1200	12Ø10	Ø4.2/250	Metal semi-pipe rings

					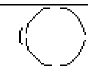
6	200	1200	24Ø8	Ø4.2/250	Conc. And spiral reinfor. Ø4.2/150
Test specimens subjected to axial load (check of the performance of confinement)					
7	200	400	6Ø8	Ø4.2/150	Conc and spiral reinfor. Ø6/200
8	200	400	6Ø8	Ø4.2/150	4 metal semi-pipe systems 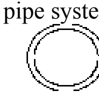
9	200	400	6Ø8	Ø4.2/150	6 metal semi-pipe systems 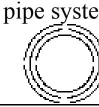
10	200	400	6Ø8	Ø4.2/150	6 metal semi-pipe systems confined from external spiral

*Concrete Quality = C 25/30

2.3 Method of application of strengthening

At first, the spiral reinforcement was constructed. The diameter of the spiral reinforcement was 140 mm for test specimens 1-5 and 190 mm for test specimens 6-10 in order to have a concrete cover of 5 mm at every side of the test specimens. Next step of the construction was the installation of the spiral reinforcement around the strong longitudinal reinforcement. At the end of the specimens 7, 8, 9 and 10, the spiral reinforcement step thickened to 10mm in order to avoid the consequences of the manufacturing defects in these critical areas. These defects may result during the axial load application to premature failure due to phenomena of splitting. For this reason, enlarged "heads" with dimensions 30cm x 30cm and height 20cm were constructed at the ends of test specimens 7–10. In addition, these enlarged "heads" contained a 6mm diameter spiral reinforcement with a step of 2.5 cm, Photo 3. The concrete of the specimens had a maximum aggregate size of 16 mm. After concreting of specimens, their strengthening took place according to the types of strengthening described above. From this point on, the procedure differed for each specimen as the scope of the research was the mechanical response of the different variants of reinforcement. Specimen 1 displayed in Fig. 1 was strengthened using a conventional jacket containing spiral reinforcement of 4.2mm diameter and step of 150mm and high performance cement (EMACO

S88C). Specimens 2-5 displayed in Fig. 2-5 were enhanced by the use of metal semi-pipes that have been pasted to the specimens with the same material EMACO S88C which was used for the jacket of specimen 1. More specifically, specimen 2 shown in Fig. 2 has two metal semi-pipes which are bonded to each other with two iron sheets having a length of 1200 mm, width of 50mm and thickness of 1.5 mm at the points of contact. Specimen 3 displayed in Fig. 3 had two successive layers of metal semi-pipes, namely a total of 4 metal semi-pipes. Specimen 4 displayed in Fig. 4 had three successive layers of metal semi-pipes, namely a total of 6 metal semi-pipes of thickness 1.5 mm. Specimen 5 shown in Fig. 5 was strengthened using metal ring semi-pipes with width 50 mm, thickness 1.5 mm per 50 mm distance between them. These metal ring semi-pipes were pasted on the specimen with using high performance cement EMACO S88C. Specimens 6 and 7 shown in Fig. 6 and 7 were strengthened by using conventional type of jacket containing spiral reinforcement, Ø6/200 mm and Ø4.2/150 mm, respectively. Specimens 8 and 9 presented in Fig. 8 and 9 were strengthened using metal semi-pipes, as in specimens 3 and 4. Specimen 10 shown in Fig. 10 constitutes regarding the strengthening method a hybrid case of strengthening which uses 6 metal semi-pipes surrounded by a common conventional jacket. All specimens were subjected either under a combined bending-shear type of loading (specimens 1-6), or under an axial compressive loading (specimens 7 – 10) while at the same time their shortening was recorded every 50KN. The measurement of elongation took place using an appropriate digital strain gage with wide range of measurement, [1] [2].

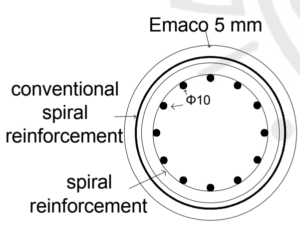

Figure 1. Section of Spec. 1

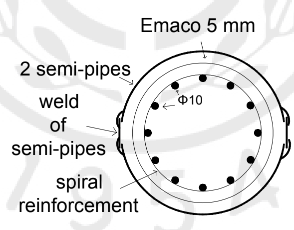

Figure 2. Section of Spec. 2

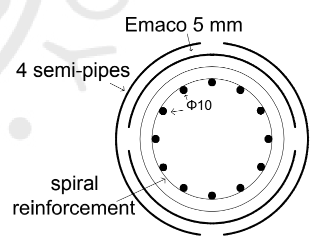

Figure 3. Section of Spec. 3

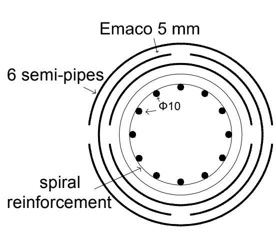

Figure 4. Section of Spec. 4

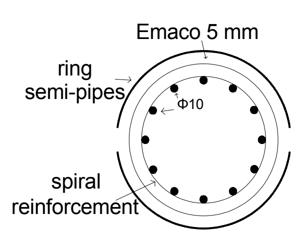

Figure 5. Section of Spec. 5

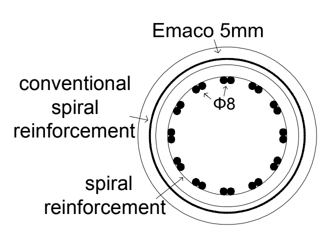

Figure 6. Section of Spec. 6

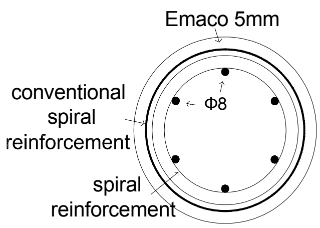

Figure 7. Section of Spec. 7

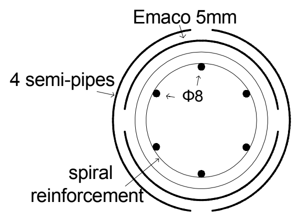

Figure 8. Section of Spec. 8

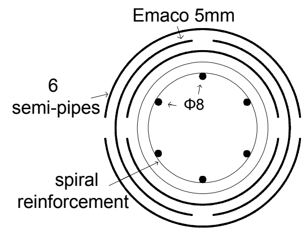

Figure 9. Section of Spec. 9

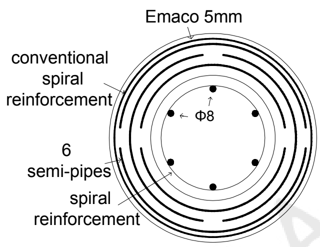

Figure 10. Section of Spec. 10

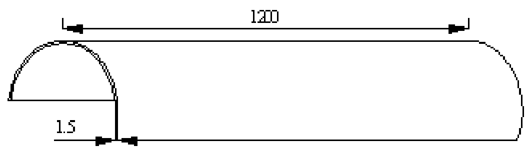

Figure 11. Shape of semi-pipe.

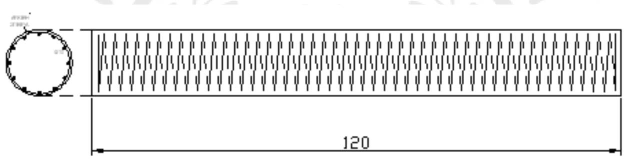

Figure 12. Shape of spiral reinforcement.

3 EXPERIMENTAL RESULTS

Below, the results of this research for all specimens are given in the form of load-displacement diagrams. In these diagrams, the mechanical behaviour of the specimens is displayed. Focus is given on their final resistance and the ductility that they have developed.

3.1 Specimens related to the transverse load carrying capacity

Generally, the specimens failed due to bending. Bending type of cracks formed in the middle of the specimens where formation of plastic hinges took place. Specimens 1 and 6 displayed vertical cracks in their middle part. Specimens 2-5 displayed failure of the semi-pipe systems, mainly in the middle. The relation between the loading and the displacement of specimens can be seen in Fig. 13.

3.2 Specimens related to the axial load capacity and check of the performance of confinement

The relation between the loading and the displacement of specimens can be seen in Fig. 14.

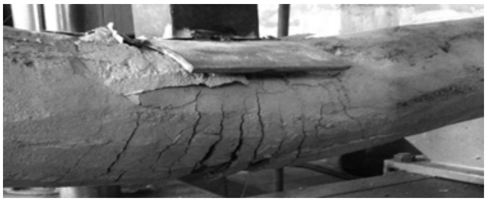

Photo 1. Bending cracks in the middle of specimen 6.

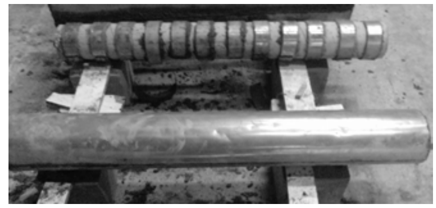

Photo 2. Specimens 4 and 5 after strengthening.

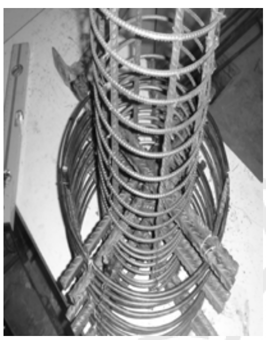

Photo 3. Position of dowels.

Photo 4. Specimen 8 strengthened using 4 semi-pipes.

Photo 5. Specimen 10 after loading.

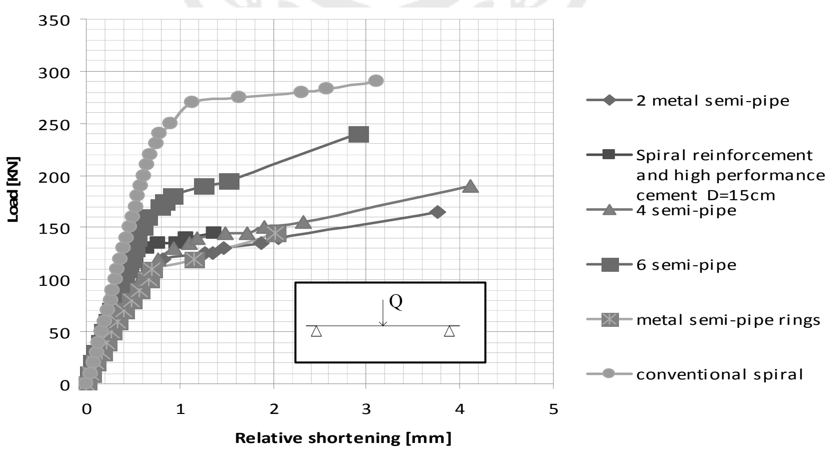

Figure 13. Specimens 1-6 subjected to transverse load.

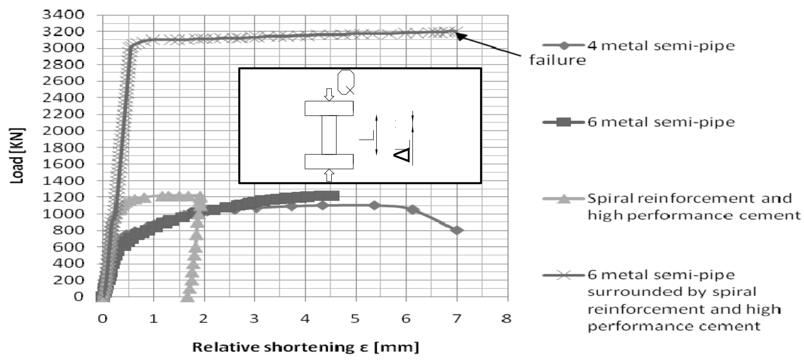

Figure 14. Specimens 7-10 subjected to axial load.

4 CONCLUSIONS

The following main conclusions derive from the conducted experimental research:

4.1 Specimens related to the transverse load carrying capacity

All the specimens failed due to bending, which means that the imposed strengthening, either through conventional jacket or through metal semi-pipe system was effective. It is noted the large plastic branch of the diagrams.

Test specimens 1, 6 which were strengthened using a conventional jacket are considered as a measure for the mechanical behaviour of specimens 2-5 which were strengthened using metal semi-pipe systems. The following specific conclusions are derived:

- Specimen 4 given in Fig. 4 displayed resistance 40% higher and much greater ductility than the corresponding specimen strengthened using a conventional jacket. The appearance of greater bending strength is due to the bending activation of the metal semi-pipe system, [1] [2].
- Specimen 3 given in Fig. 3 displayed a slightly higher bending strength than the corresponding specimen strengthened using a conventional jacket. Obvious superiority compared to the conventional strengthened specimen was displayed in ductility. The deformation was approximately twice the deformation of the conventionally strengthened specimen, [1] [2].
- Specimen 2 shown in Fig. 2 displayed similar load carrying capacity with the conventionally strengthened specimen. However, it should be noted that the weld was incomplete because due to thinness of the iron sheets the electric weld did not work, [1] [2].
- The specimen with the 'rings' semi-pipe system presented in Fig. 5 was defective from the construction, but despite predictions the transverse load carrying capacity was increased so much that the specimen failed due to bending and displayed rich ductile behaviour, [1] [2].

4.2 Specimens related to the axial load capacity and check of the performance of confinement

The mechanical property, which was mostly improved by the new type of strengthening, is the ductility. Unfortunately, premature failure of the enlarged “heads” stopped prematurely the successiveness of the measurements.

As far as the specimens related to the check of the performance of confinement are concerned, specimen 10 can be distinguished, Fig. 10. It overshadows all the other cases and consists the culmination of research, as the increment of the compressive axial load capacity was at least 250% compared to that of the conventional jacket. If the enlarged “heads” at the edges of the specimen did not fail prematurely, the measurements might have given more impressive results for both the resistance and the confinement.

As a final conclusion, it is possible to write that the proposed strengthening methods against transverse loads and confinement, which were tested experimentally in order to verify their effectiveness, displayed high performance. In conclusion, it should be noted that if the semi-pipes were sand-blasted, the conclusions would be obviously more impressive. It is undisputed that the adhesion of cement mortar would be much stronger in semi-pipes system and this fact would lead to better and improved results. Moreover, the intensive transverse buckling phenomena of the semi-pipes would not take place. However, the hybrid type of jacket, which is comprised apart from the external spiral reinforcement and from 3 pairs of semi-pipe systems, does not need the improvements of the sand-blast, since the spiral reinforcement and the semi-pipes support each other and eventually attribute excellent results.

REFERENCES

[1] Andreadou, E, Argyropoulou, D, “Metal jackets: A suggestion of a quick method with the minimum discomfort of strengthening columns, Tests related to the transverse loading capacity, axial loading capacity and confinement on columns with circular cross section”, Thessaloniki, 2010.

[2] Demertzi, X, Parapanisiou, A, “Metal jackets: A suggestion of a quick method with the minimum discomfort of strengthening columns, Tests related to the transverse loading capacity on columns with circular cross section”, Thessaloniki, 2010.

[3] Spirakos Konstantinos, “Strengthening of structures against seismic actions”, Technical Institute of Greece, Athens, 2004.

[4] Penelis, G, Kappos, A, “Earthquake Resistant Concrete Structures”, E and FN Spon, 1997.

[5] Federal Emergency Management Agency, “FEMA 356: Prestandard and Commentary for the Seismic Rehabilitation of Buildings - Chapters 2 and 3”, Washington D.C., November, 2000.

TENSILE TEST OF REINFORCED ULTRA HIGH PERFORMANCE CONCRETE PRISMATIC BARS

Changbin Joh[1], Imjong Kwahk[2], Jungwoo Lee[3] and Byung-Suk Kim[4]

[1,2,3,4] Korea Inst. of Construction Technology, Structural Eng. and Bridge Research Div., Korea
e-mail: cjoh@kict.re.kr, kwakim@kict.re.kr, duckhawk@kict.re.kr, bskim@kict.re.kr

ABSTRACT: This paper investigated the tensile behavior of Ultra High Performance Concrete (UHPC) bars reinforced with rebars. Test results show that the strain localization due to the ductility from the bridging action of steel fibers might reduce the overall ductility of reinforced UHPC bars at the ultimate state.

KEY WORDS: Ultra High Performance Concrete; Tensile Behavior

1 INTRODUCTION

In general, Ultra High Performance Concrete (UHPC) has compressive strength higher than 150 MPa and tensile strength around 10 MPa. These high compressive and tensile strengths of UHPC are essential mechanical properties to design slender and durable structures. However, large difference between compressive and tensile strengths of UHPC makes it necessary to use conventional reinforcement to some degree in the UHPC structures. Therefore, the tensile behavior of reinforced UHPC structures such as cracking, hardening and softening should be understood to design reasonable UHPC structures.

This paper investigated the tensile behavior of reinforced UHPC structures using direct tensile tests of UHPC prismatic bars reinforced with deformed bars. To estimate the effect of steel fibers and reinforcement on the tensile behavior of UHPC structures, crack pattern, ultimate strength and ductility were carefully investigated. Based on the result and discussion, design considerations for the reinforced UHPC structure will be presented as conclusion.

2 TEST SPECIMENS AND SETUP

2.1 UHPC

First, to understand the tensile behavior of UHPC itslef, twenty UHPC tensile specimens with two notches [1] were fabricated using UHPC composition developed by KICT (Table 1) as shown in Fig. 1. Four different volume fraction of steel fibers (0%, 1%, 1.5% and 2%) were used to make UHPC tensile specimens.

Table 1. UHPC composition developed by KICT (by weight except for fibers)

W/B	Cement	Silica fume	Sand	Filling powder	Superplasticizer	Steel Fiber(ρ_f)
0.2	1	0.25	1.1	0.3	0.016	0%, 1%, 1.5%, 2%

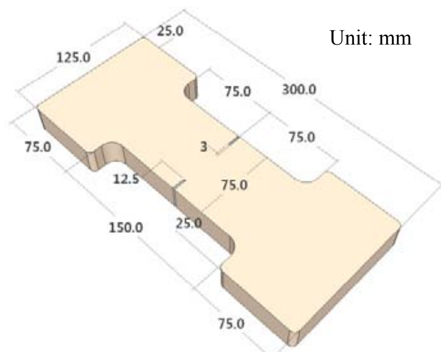

Figure 1. Tensile test specimen with notches

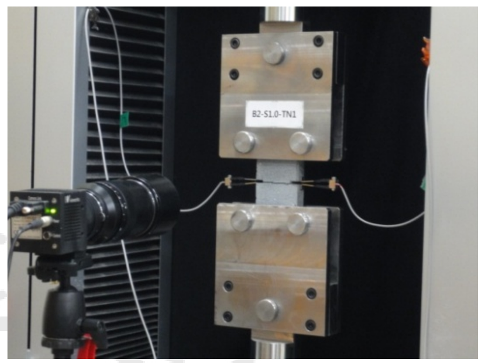

Figure 2. Tensile test setup for UHPC

The UHPC tensile specimens with notches were tested using the UTM with the capacity of 250 kN (Fig. 2). Clip gauges were attached to the notches to measure the crack opening.

2.2 UHPC bar reinforced with rebars

In addition, seven UHPC prismatic bars reinforced with four D13 bars and one without reinforcement were fabricated as shown in Table 2 and Fig. 3.

Table 2. Reinforced UHPC prismatic bars

Specimens	Steel Fiber (ρ_f)	Reinforcement
OD0.0-A	0%	4xD13
OD1.0-A, OD1.0-B, OD1.0-C	1.0%	4xD13
OD1.5-A	1.5%	4xD13
OD2-B, OD2-C	2.0%	4xD13
NR2.0-A	2.0%	None

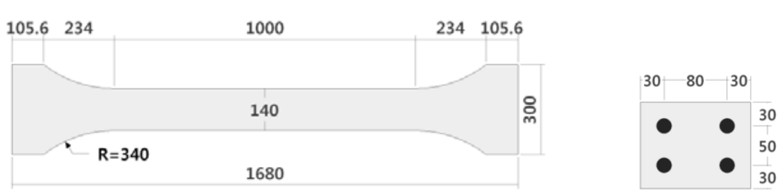

Figure 3. Reinforced UHPC bar and cross section (reinforced with 4 D13 bars, Unit: mm)

Direct tensile tests were performed on reinforced UHPC bars using 2000 kN UTM as shown in Fig. 4. Gauge length was 800 mm and two DTs were used to measure displacement.

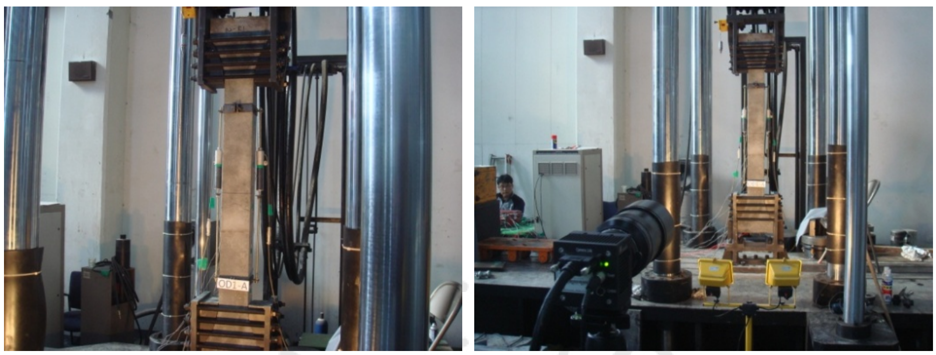

Figure 4. Tensile test setup for reinforced UHPC bars

3 TEST RESULTS AND DISCUSSION

3.1 UHPC

Fig. 5 shows the typical stress-crack width relation of UHPC tensile specimens from the test. The result shows that UHPC becomes more and more ductile with the increase of steel fibers.

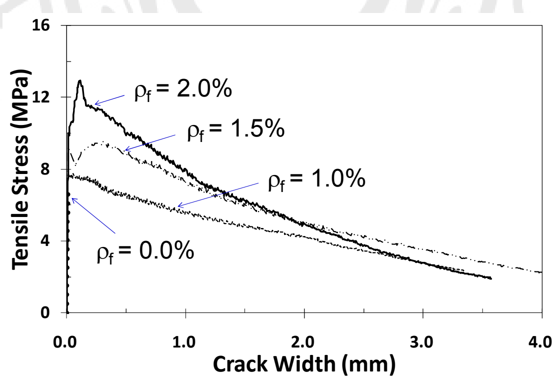

Figure 5. Effect of steel fibers on the tensile behavior of UHPC

The UHPC specimen without steel fibers failed in brittle manner around 8 MPa with the loss of linearity. But the UHPC specimens with steel fibers shows ductile behavior. The bridging action of steel fibers at the cracks make it possible for UHPC to transfer the load through the wide open cracks as shown in Fig. 5. The UHPC specimens with 2% steel fibers even show hardening behavior while others with smaller steel fibers show softening behavior.

The result also shows steel fibers increase the cracking strength of UHPC. The cracking load was determined the load corresponding to the loss of linear elastic behavior. Table 2 summaries cracking loads.

Table 3. Stress and width at initial crack

Steel Fiber (ρ_f)	Crack (MPa)	Load at crack (kN)	Crack width (mm)
OD0.0-A, 0.0%	6.387	7.884	0.009
OD1.0-A, 1.0%	8.659	10.758	0.012
OD1.5-A, 1.5%	8.507	10.59	0.014
OD2.0-B, 2.0%	9.131	11.274	0.01

3.2 UHPC bar reinforced with rebars

Fig. 6 shows contrasting crack patterns of reinforced UHPC bars with and without steel fibers at ultimate limit state. The OD0.0-A specimen with no steel fibers shows typical crack patterns of reinforced concrete bars. Its behavior was relatively ductile with regularly spaced additional cracks developed with the increase of the load after the initial crack. On the other hand, the reinforced UHPC bars with steel fibers (OD1.0-A, OD1.5-A, OD2.0-C), in spite of more ductile UHPC with steel fibers, were failed with cracks localized at the center. Additional cracks were barely observed as shown in Fig. 6. Similar behaviors can be found in the references [2][3].

Figure 6. Effect of steel fibers on the tensile behavior of reinforced UHPC bars at the ULS

The load-displacement relation in Fig. 7 also shows relatively ductile behavior of the reinforced UHPC bar without steel fibers. The displacements at failure were 33 mm for the OD0.0-A specemen and 16 ~22 mm for the OD1.0, OD1.5, OD2.0 specmens respectively. With the increase of steel fibers, the tensile strengths of these specimens were increased, but the descending curves became steeper. It should be noted that the tensile behaviors of the specimens with steel fibers were more or less same regradless of different volums of steel fibers.

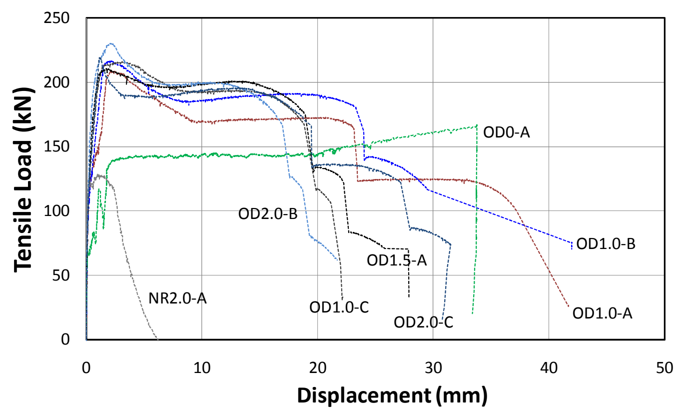

Figure 7. Load-displacement relation of reinforced UHPC bars

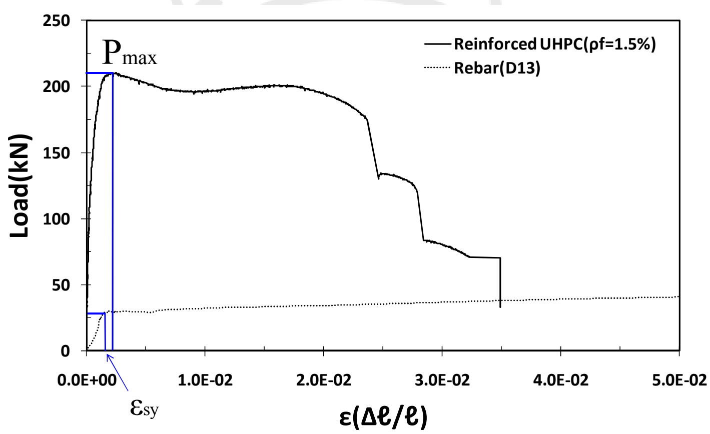

Figure 8. Load strain relation of reinforced UHPC bar and D13 deformed bar

The stress-strain relations of UHPC and deformed bar can explain the strain localization behavior of reinforced UHPC bars. The tensile resistance is the sum of resistance of deformed bars and UHPC. Due to bridging action of steel fibers at crack surfaces, UHPC can still transfer the load although the deformed bars already reach their yield strength. Therefore, as shown in Fig. 8, the tensile strength of reinforced UHPC bars occur at the strain that is greater the yield strain of the deformed bar. Beyond the tensile strength, the load transferred through UHPC begin to decrease as the steel fibers are being pulled out. But since the deformed bars are already yielded, they cannot transfer the load that was transferred through UHPC. If the deformed bars at the initial crack are in the elastic state, additional load can be transferred to other sections and additional cracks can be formed near the outside of transfer length. Otherwise, additional load cannot be transferred and the strain localization is occurred at the first visible crack section that is the weakest section of the bar.

It is obvious that the bridging action of steel fiver is beneficiary to the crack control at the serviceability limite state, but, at the ultimate state, the strain localization due to the ductility from the bridging action of steel fibers might reduce the overall ductility of reinforced UHPC bars.

4 CONCLUSIONS

This paper investigated the tensile behavior of reinforced UHPC bars. Based on the test results and discussion, following conclusions can be made.

- The increase of steel fibers in the UHPC increases the cracking strength and ductility of UHPC.
- At the ultimate state, however, the strain localization due to the ductility from the bridging action of steel fibers might reduce the overall ductility of reinforced UHPC bars.
- Considering the similarity in tensile behavior between the reinforced UHPC bar and the reinforced UHPC girder, this result implies that the ultimate deformation capacity of the reinforced UHPC girder might be smaller than that of the reinforced concrete girder

UHPC can be used to make a bridge lighter. Compared to ordinary reinforced concrete bridges, the reinforced UHPC girder can span longer distance. However, for the design of the bridge with reinforced UHPC girders, it should be noted that its ultimate deformation capacity might be smaller than that can be expected from the reinforced concrete girder due to the strain localization from the ductility in tensile behavior of UHPC.

ACKNOWLEDGMENTS

This work is the result of the research project, the Super Bridge 200 of Korea Institute of Construction Technology. The authors hereby express their appreciation for the support.

REFERENCES

[1] Wille, K, Kim, D. J., Naaman, A. E., "Strain-hardening UHP-FRC with low fiber contents", Materials and Structures, Vol. 44, No. 3, pp. 583-598, 2010

[2] Redaelli, D, Muttoni, A, "Tensile Behaviour of Reinforced Ultra-High Performance Fiber Reinforced Concrete Elements", CEB-FIP Symposium, Dubrovnik, 2007.

[3] Walraven J. C., “High Performance Fiber Reinforced Concrete: Progress in Knowledge and design codes”, Materials and Structures, Vol. 42, No. 9, pp. 1247-1260, 2009

HORIZONTAL SHEAR STRENGTH BETWEEN ULTRA HIGH PERFORMANCE CONCRETE AND NORMAL CONCRETE

Jungwoo Lee [1], Changbin Joh [2], Jongwon Kwark [3], Byung-suk Kim [4]

[1,2,3,4] Korea Inst. of Construction Technology, Structural Eng. and Bridge Research Div., Korea
e-mail: duckhawk@kict.re.kr, cjoh@kict.re.kr, kwakim@kict.re.kr, origilon@kict.re.kr, bskim@kict.re.kr

ABSTRACT: This paper reports the results of fourteen push-off tests to understand shear transfer between UHPC and normal concrete. To recommend a reliable shear transfer formula for the design of composite section of UHPC and normal concrete, the test results are compared to available shear transfer formulas for UHPC and normal concrete.

KEY WORDS: Ultra High Performance Concrete (UHPC); Shear transfer.

1 INTRODUCTION

Ultra High Performance Concrete (UHPC) is an innovative material exhibiting high compressive strength, very high ductility and remarkable durability. The Korea Institute of Construction Technology (KICT) developed UHPC presenting compressive strength larger than 180 MPa and tensile strength exceeding 12 MPa. As part of the research intending to apply this new material for structural purpose, an experimental study was conducted on the composite behavior of UHPC and normal concrete. The developed UHPC provides significantly improved compressive and tensile strengths compared to normal concrete as well as very large bond strength with steel reinforcement. This outstanding material enables to design and construct slender and efficient sections that can be applied to various structures including bridges. However, the lack of relevant studies and other reasons involving the loss of workability and increase of construction costs have impeded its vulgarization to date.

If normal concrete member and UHPC member are combined, the horizontal shear transfer between these two members will constitute a critical factor influencing the composite action. Accordingly, this paper addresses the results of the push-off tests performed to evaluate the horizontal shear transfer at the interface between normal concrete and UHPC using specimens fabricated with varying surface states of the interface, dispositions of the shear connectors and sectional areas.

2 TEST SERIES

A total of 14 push-off test specimens were manufactured to evaluate the horizontal shear transfer at the interface between normal concrete and UHPC. The test members are composed of UHPC at the bottom and normal concrete at the top as shown in *Fig. 1*. The surface state of the interface and the shear connectors were constructed in the shapes depicted in *Photo 1*.

Specimens were manufactured separately for each of the following cases: smooth surface state of the interface, installed shear keys, and chipped surface. The shear keys were fabricated to fit with the shape drawn in *Fig. 1(b)*.

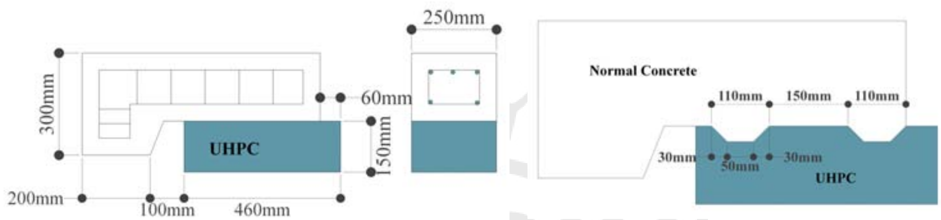

(a) Detailed section of test member (b) Layout of shear key

Figure 1. Details of the test member

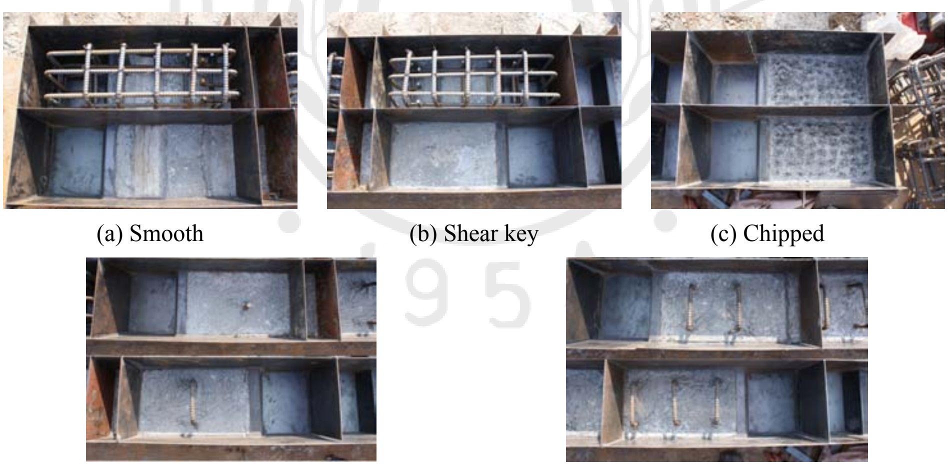

(a) Smooth (b) Shear key (c) Chipped

(d) 1 leg, 2 legs (e) 4 legs, 6 legs

Photo 1. Surface state and arrangement of the shear connectors

Table 1 arranges the main test variables of the 14 members. The arrangement of the shear connectors considered the cases without shear connector, and shear connectors arranged in 1 line, 2 lines and 3 lines. The test members were manufactured accounting only for smooth interface.

Table 1. Specimens and test variables

Specimens	UHPC block size (cm)	Interface area (cm^2)	Legs of D16 shear stirrups	Area of steel (cm^2)	Surface
46D-0L-S-A			0	-	Smooth
46D-0L-S-B			0	-	Smooth
46D-0L-C-A			0	-	Chipped
46D-0L-C-B			0	-	Chipped
46D-0L-K-A			0	-	Keyed
46D-0L-K-B			0	-	Keyed
46D-1L-S-A			1	1.986	Smooth
46D-1L-S-B	15×25×46	1000	1	1.986	Smooth
46D-2L-S-A			2	3.972	Smooth
46D-2L-S-B			2	3.972	Smooth
46D-4L-S-A			4	7.944	Smooth
46D-4L-S-B			4	7.944	Smooth
46D-6L-S-A			6	11.916	Smooth
46D-6L-S-B			6	11.916	Smooth

The mix design strength of normal concrete is 27 MPa and the compressive strength of UHPC is 180 MPa. The horizontal loading in the push-off tests was applied through displacement control with loading speed of 0.01 mm/sec. Loading was applied until decrease of the load after the failure of the specimens. The relative slip between normal concrete and UHPC was measured by means of displacement transducer (DT) throughout the tests. *Photo 2* illustrates the push-off test.

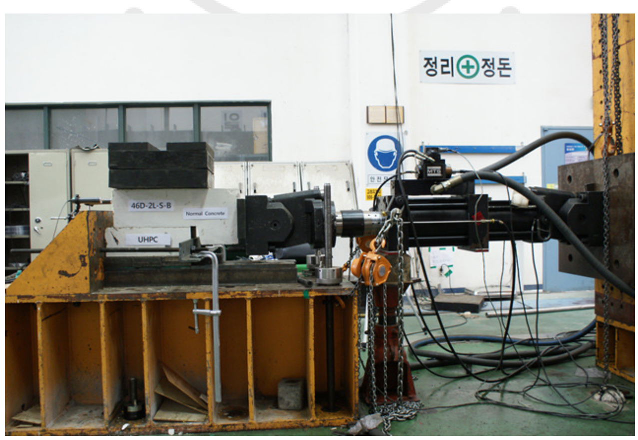

Photo 2. View of the push-off test

3 RESULT OF TEST

3.1 Evaluation of shear strength wrt the interface's surface state

Fig. 2 plots the load-slip curves resulting from the push-off tests according to the surface state of the interface. In order to assess the bond strength characteristics with respect to the composite behaviour, the experimental results are classified according to the interface's surface state as smooth, keyed and chipped. *Fig. 3* plots the bond strength of the interface. *Photo 3* presents the bonding failure pattern according to the interface's surface state.

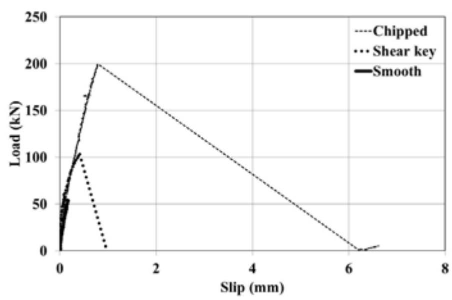

Figure 2. Load-slip curves wrt interface's surface state

Figure 3. Bond strength wrt interface's surface state

(a) Smooth (b) Chipped (c) Shear key

Photo 3. Failure pattern according to interface's surface state

Table 2 compares the test results obtained in the push-off tests of this study with those reported in the study of Banta [1]. Both studies show larger values in the case of chipped surface than when shear keys are installed. Even if it was predicted that larger values would be observed in the case of shear keys than in the case of chipped surface, the actual results showed the contrary. Such disagreement can be attributed to the inaccurate transfer of the horizontal and vertical loads during the push-off test. Additional tests are thus required in the future after improvement of the test method so as to achieve correct transfer of the horizontal and vertical loads. Moreover, it is also recommended to conduct studies clarifying the relationship of the horizontal shear strength with respect to the size of the vertical load.

Table 2. Bond strength results of push-off tests

	Smooth	Chipped	Shear Key
KICT	0.48(1)	2.01(4.19)	1.05(2.19)
Banta , T.E. [1]	0.11(1)	0.45(4.09)	0.35(3.18)

( ) : Ratio of bond strength of interface to that of smooth surface

3.2 Evaluation of shear strength wrt arrangement of shear connectors

Conventional stirrups were adopted as shear connectors in this study. The surface of the specimens was smooth and the vertical load corresponded to the dead load. *Fig. 4* plots the load-slip curves according to the arrangement of the shear connectors and *Fig. 5* presents the bond strength with respect to the arrangement of the shear connectors. The test results of *Fig. 4* do not picture the characteristics of the horizontal shear strength according to the arrangement of the shear connectors but show only the common tendency of the shear strength to increase proportionally to the area of the shear connectors.

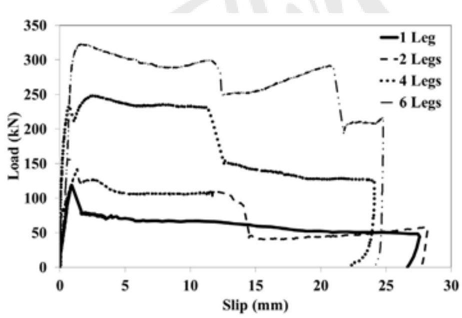

Figure 4. Load-slip curves wrt arrangement of shear connectors

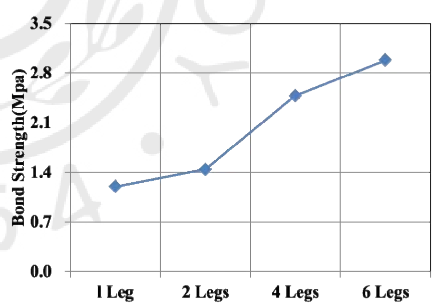

Figure 5. Bond strength wrt arrangement of shear connectors

Among the variables influencing the shear strength of the shear connectors, the size of the vertical load not only increases the frictional resistance but also affects the shear behavior of the connectors[2][3]. Even if the vertical load expressed additionally the dead load in the tests, this effect is relatively insignificant compared to that of the live load in real bridges. This may explain the poor effect of the vertical load on the shear strength. However, since horizontal shear occurs due to the vertical load produced by the live loads in the design of actual bridges and since the size of the vertical load increases the frictional resistance, it appears that the effect of the vertical load must be considered.

Table 3. Push-off test results wrt the arrangement of shear connectors

	1 Leg	2 Legs	4 Legs	6 Legs
Bond Strength (MPa)	1.20	1.44	2.48	2.98

4 CONCLUSIONS

Push-off tests were conducted to evaluate the bond strength at the interface between normal concrete and UHPC. The main variables considered in the tests were the surface state of the interface (smooth, keyed, chipped) and the arrangement of shear connectors and, the effect of each of these variables on the bond strength were evaluated. The bond strength according to the surface state of the interface between normal concrete and UHPC appeared to be the largest in the case of chipped surface. The bond strength when shear keys were installed increased compared to that of the smooth surface but had smaller effect that the chipped surface. However, this result needs to be verified through additional tests adopting the vertical load as variable. In addition, in view of the test results with respect to the arrangement of the shear connectors, it was observed that the horizontal shear strength increased with larger arrangement of shear connectors. Consequently, it was concluded that adopting chipped surface would be effective in the design of a composite member combining normal concrete and UHPC. Future research involving additional tests considering the arrangement type and the amount of shear connectors according to the surface state of the interface are required to propose design formulae for the horizontal shear strength and bond strength characteristics necessary for the composite behavior of normal concrete and UHPC.

ACKNOWLEDGMENTS

This study was supported by “Design Specific Technology for Ultra High Performance Concrete”, a research project of the Korea Institute of Construction Technology.

REFERENCES

[1] Banta, T.E, “Horizontal Shear Transfer between Ultra High Performance Concrete and Lightweight Concrete, 2005.

[2] Korea Road & Transportation Association, *Korea Highway Bridge Design Code*, Gunsuljungbosa: Seoul, Korea, 2005

[3] Hyun, B.H., Chung, C.H., Shim, C.S., Ma, H.W., “Design of Horizontal Shear Strength of the Shear Connectors Between Precast Decks and PSC Girders”, Journal of KSCE, Vol. 25, No. 2A, pp. 327-335, Korea, 2005.

MODELING EXTREME TRAFFIC LOADING ON BRIDGES USING KERNEL DENSITY ESTIMATORS

Cathal Leahy[1], Eugene J. OBrien[1] and Bernard Enright[2]

[1] UCD School of Civil, Structural & Environmental Engineering, Newstead, Dublin 4, Ireland
[2] Dublin Institute of Technology, Bolton Street, Dublin1, Ireland
e-mail: Cathal.Leahy@ucdconnect.ie, eugene.obrien@ucd.ie, bernard.enright@dit.ie

ABSTRACT: Kernel density estimators are a non-parametric method of estimating the probability density function of sample data. In this paper, the method is applied to find characteristic maximum daily truck weights on highway bridges. The results are then compared with the conventional approach.

KEY WORDS: Bridge; Characteristic; Traffic; Kernel Density Estimators; Loading.

1 INTRODUCTION

Bridge safety assessment involves a comparison of load effect (stress, etc.) and the capacity of the bridge to resist that effect. Probabilistic assessment requires the convolution of the probability density functions for load effects and resistances. However, a load and resistance factor approach is commonly applied which requires the calculation or estimation of characteristic levels of load effect and resistance. This paper concentrates on the loading side of this equation and describes a method of estimating characteristic load effects for road bridges using Weigh-in-Motion (WIM) traffic data.

The accurate estimation of characteristic load effect is critically dependent on the extreme upper tail of the load distribution. Relatively few measured values are available for this tail region, and some form of interpolation and extrapolation is required. A popular approach is to plot the measured data on Gumbel probability paper [1] and to fit a type III Generalised Extreme Value (Weibull) distribution to this data [2-4]. Characteristic load effects can be estimated using this fitted distribution. A return period of 1000 years is used in the Eurocode for the design of new bridges, based on a 5% probability of exceedance in 50 years. The U.S. AASHTO design code is based on the distribution of the 75-year maximum loading [5].Lesser periods have been used for assessment, typically in the 5 to 10 year range [6]. One of the disadvantages of this method is that it is assumed that the data comes from a Weibull distribution. Kernel density estimators (KDEs) are a non-parametric method of estimating the probability density function (PDF) of sample data. The PDF is built from the measured data without assuming that it comes from a certain theoretical distribution. As a result, the PDF is 'more true' to the original data as it does not force a theoretical distribution upon it.

1.1 Introduction to kernel density estimators

In the KDE method, each sample data point is replaced by a component density (kernel function), and these densities are then added to form the complete PDF. Rectangular, triangular and Normal kernel functions are common although any distribution can be used. Depending on the parameters of the kernel function used, the resultant PDF will have different characteristics. The KDE method is not then entirely non-parametric but may provide a compromise between a purely non-parametric approach and a parametric approach [7]. *Figs. 1 and 2* illustrate a simple example of how the method works. *Fig. 1* shows the histogram of 30 loads randomly sampled from a Normal distribution. It is clear that the histogram is not an accurate representation of the true distribution. Using the KDE method a normal kernel function of area 1/30 is created for each data point (shown at bottom of *Fig. 2*). These individual kernel functions are then added to create the PDF, which gives a much better approximation of the theoretical normal distribution than the histogram. This simple example uses just 30 data points but the more data points that are available, the more accurate the estimate of the true distribution.

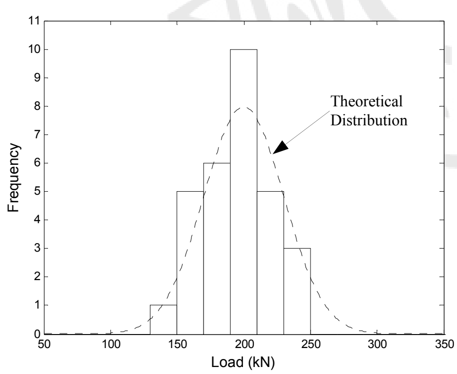

Figure 1. Histogram of 30 sample data points

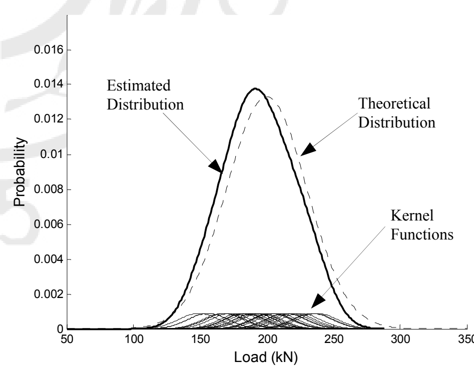

Figure 2. Kernel density estimate of PDF for 30 sample data points

The bandwidth of the kernel functions refers to the width of the individual distributions. In the case of *Fig. 2*, the bandwidth would refer to the standard deviation of the normal kernel functions. This is an important factor in the KDE method and has a significant influence on the smoothness of the estimated PDF. Smaller bandwidths result in fewer data points influencing the estimate at any one point, which gives a 'bumpier' estimate of the PDF [8]. As the bandwidth increases, a smoother PDF is achieved as there is more overlap between the individual kernel functions. A certain degree of smoothness is desirable but as the bandwidth increases, the estimated PDF becomes a poorer fit to the measured data. The optimal bandwidth is therefore a compromise between smoothness and achieving a good fit to the original data. This optimal bandwidth is often chosen by plotting a number of different bandwidths and subjectively picking the one which best fits one's expectations for the density. For many applications this method is sufficient but an objective approach is more appropriate for inexperienced users or if multiple data sets are to be analysed [9, 10].

Towards the peaks of the sample data, where there are many sample data points, small bandwidths are best but towards the tails of the data, where there are very few sample data points, larger bandwidths are required to obtain a smooth PDF and a more appropriate estimate of the density. Scott [11] suggests methods for picking bandwidths and for varying bandwidths based on the distribution of the data.

KDEs are known to work well for interpolation of measured data but less well for extrapolation beyond the measured data [7]. This paper aims to develop a method for improving the accuracy of the method for extrapolation in order to estimate characteristic load events.

2 APPLICATION OF KERNEL DENSITY ESTIMATORS TO LOAD DATA

Measured maximum daily load data is usually assumed to be consistent with the Generalized Extreme Value distribution. Type 1 Generalized Extreme Value (Gumbel) distributions are therefore used here as the kernel functions. In this paper the bandwidth of the kernel function refers to the scale parameter of the Gumbel kernel functions. *Figs. 3* and *4* show the histogram of 1000 truck weights, randomly sampled from a Gumbel distribution. *Fig. 3* uses a fixed bandwidth of 5 kN to estimate the PDF of the data while *Fig. 4* uses a larger fixed bandwidth of 40 kN. The difference in smoothness between the two estimates of the distribution is clear. The smaller bandwidth gives a PDF which follows the data very closely but fails to smooth the local peaks in the histogram (which appear due to the randomness in the limited data set). It is clear in *Fig. 4* that the larger bandwidth has over-smoothed the data set and produced a poor fit to histogram of the data. To achieve a good fit to the original data, while also smoothing the PDF sufficiently, a variable bandwidth can be used. A smaller bandwidth is used where there are high densities of data and the bandwidth increases as the data points become more sparse, i.e., towards the tails of the data.

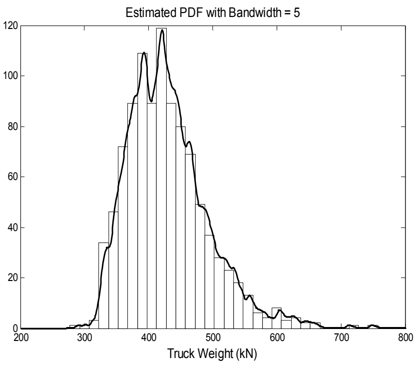

Figure 3. Kernel density estimate of PDF using bandwidth of 5 kN

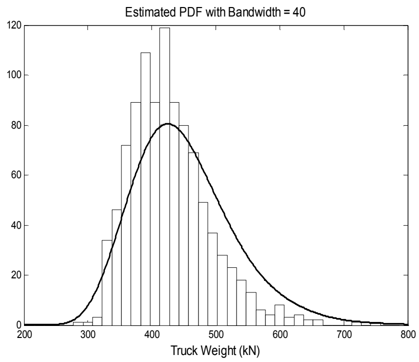

Figure 4. Kernel density estimate of PDF using bandwidth of 40 kN

To find an appropriate starting bandwidth at the mode of the data Eq. (1) is used [11]. This equation is for Normal kernel functions but works well with the Gumbel kernel functions used here.

$$h=1.06\sigma n^{-0.2} \qquad (1)$$

where: h is the bandwidth
σ is the standard deviation of the sample
n is the sample size

Eq. (2) is used to increase the bandwidth with increasing distance from the mode of the data. This approach was developed by Abramson [12] and cited in Scott [11].

$$h_\mathrm{i}=\frac{k}{\sqrt{f(x_i)}} \qquad (2)$$

where: $f(x_i)$ is the density function
k is a constant
h_i is the bandwidth used

Eq. (1) is used to obtain the starting bandwidth at the mode of the data. The constant k is then calculated by substituting this value into Eq. (2). *Fig. 5* shows that using Eq. (2), the bandwidth increases rapidly with increasing distance from the mode of the data. These large bandwidths resulted in overestimation of the value of the PDF in the extrapolation region of the tail. To address this, a bandwidth cap is required to prevent the bandwidth from increasing above a certain level.

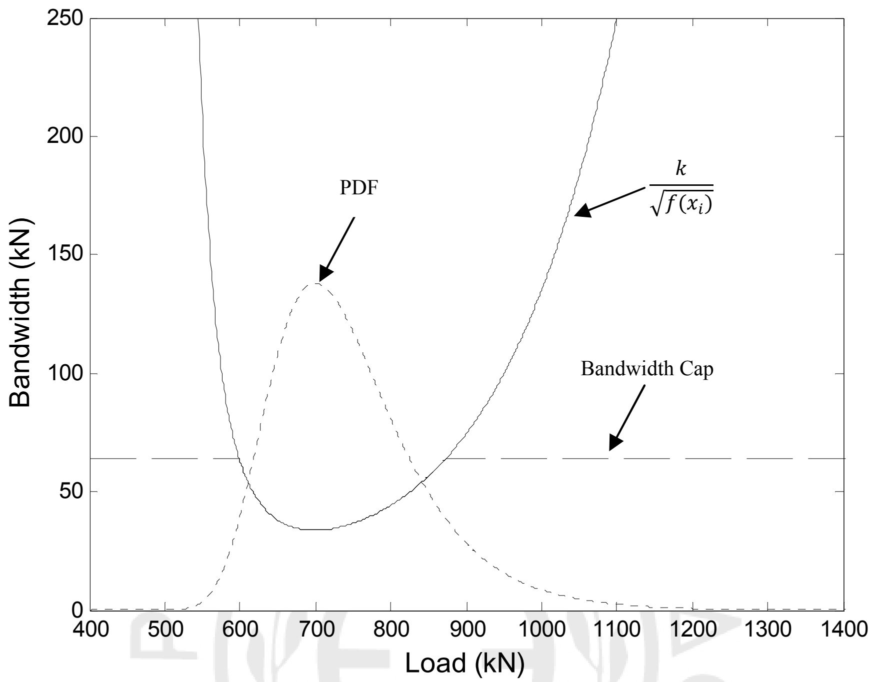

Figure 5. Variation in calculated bandwidth with respect to PDF

Different approaches for calculating the optimal bandwidth cap are investigated. The method which gave the best results is based on the scale parameter of the sample data. The scale parameter of a Gumbel distribution can be estimated using Eq. (3) [13].

$$\sigma = \frac{S\sqrt{6}}{\pi} \tag{3}$$

where: S is the standard deviation of the data and
σ is the scale parameter of the data

To calibrate this method the KDE approach is applied to different data sets using caps of 70, 80 and 90% of the estimated scale parameter for the datasets. These sample data sets are generated from Gumbel distributions using 10 sets of location and scale parameters. Parameters which correspond to typical truck gross vehicle weights and individual, tandem and tridem axle weights are chosen.

Different combinations are selected so as to give different ratios of one parameter to the other. For each set of Gumbel parameters, 10 sets of 100 data points are randomly generated and the KDE method applied to each data set for the three different caps. In all cases the cap of 80% of the estimated scale parameters gives the best estimates of the true distribution.

3 RESULTS

To compare the accuracy of the KDE method to current best practice, 10 datasets, each containing 100 maximum daily truck gross vehicle weights, are randomly generated from a Gumbel distribution with a location parameter of 700 kN and a scale parameter of 80 kN. Maximum daily weigh-in-motion (WIM) data is used as a guide for picking these parameters. Based on a five day week, this would represent 5 months of WIM data. These datasets are first analysed using a conventional approach, i.e., the truck weights are plotted on Gumbel probability paper and a Weibull distribution fitted to the data points. *Fig. 6* shows one of the data sets and the fitted Weibull distribution. The 50 year and 1000 year return period characteristic values are then calculated using the fitted distribution. The estimated return periods for the 10 sets of data are compared with their true theoretical values and a root mean square error (RMSE) calculated.

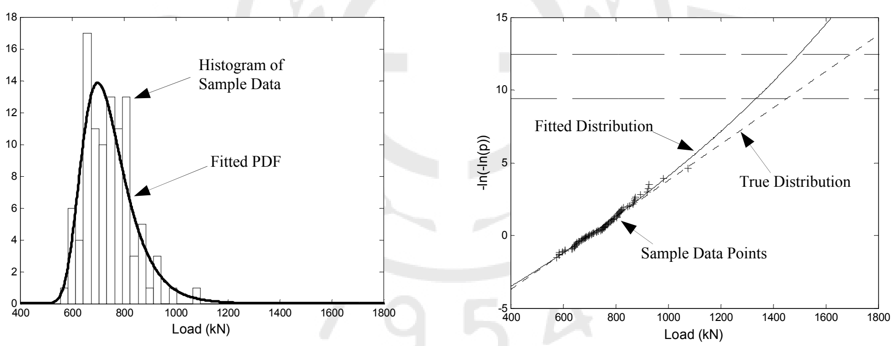

(a) Histogram and fitted PDF

(b) Gumbel probability paper with 50 and 1000 year return period levels shown (- -)

Figure 6. Weibull distribution fitted to data

The KDE method is then applied to the same 10 data sets and the 50 and 1000 year return period values were again estimated and the RMSE calculated. *Fig. 7* shows the KDE estimate of the distribution for the same data set as *Fig. 6*. A comparison of *Figs. 6(a)* and *7(a)* indicates a better fit with the KDE approach but a more realistic theoretical distribution from the conventional approach, as might be expected.

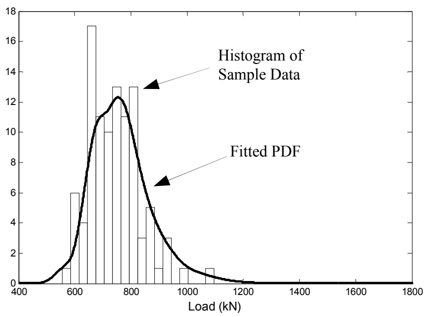

(a) Histogram and fitted PDF

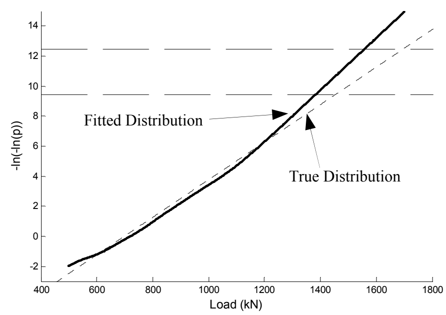

(b) Gumbel probability paper with 50 and 1000 year return period level shown (- -)

Figure 7. Kernel density estimate of distribution of data

Table 1 shows the RMSEs for the two approaches. The KDE method achieves better estimates for both the 50 and 1000 year return period values with an overall reduction in the RMSE of 28%.

Table 1. Root mean squared error of estimated return periods for both methods

	50 yr RMSE	**1000 yr RMSE**
Fitted Weibull	6.12 %	8.51 %
Kernel Density Estimators	3.99 %	6.49 %

4 CONCLUSION

Accurate estimation of characteristic loading is critical for both bridge assessment and design. This estimation process is highly dependent on the extreme upper tail of the distribution of measured data where relatively few data points are available. The kernel density estimator method provides a non-parametric method of interpolating between and extrapolating beyond the data in this region. When applied to the 10 data sets of 100 randomly generated truck gross vehicle weights in this paper, it achieved a substantial reduction in error when estimating the 50 year and 1000 year load events.

ACKNOWLEDGMENTS

The financial support of the Irish National Roads Authority for this research is gratefully acknowledged.

REFERENCES

[1] Castillo, E., *Extreme Value Theory in Engineering*. Academic Press, San Diego, 1988.
[2] Caprani, C.C., OBrien, E.J., McLachlan, G.J., "Characteristic traffic load effects from a mixture of loading events on short to medium span bridges", *Structural Safety*, Vol. 30, No. 5, pp. 394-404, 2008.

[3] Bailey, S.F., Bez, R., "Site specific probability distribution of extreme traffic action effects", *Probabilistic Engineering Mechanics*, Vol. 14, No. 1-2, pp. 19-26, 1999.

[4] Gindy, M., Nassif, H.H., "Comparison Of Traffic Load Models Based On Simulation And Measured Data", *Proc. Joint International Conference on Computing and Decision Making in Civil and Building Engineering*, pp. 2497-2506, Montréal, 2006.

[5] Nowak, A.S., "Live load model for highway bridges". *Structural Safety*, Vol. 13, pp. 53-66, 1993.

[6] Nowak, A.S., Nassif, H.H. and DeFrain, L., "Effect Of Truck Loads On Bridges", *Journal of Transportation Engineering (ASCE)*, Vol. 119, No. 6, pp. 853-67, 1993.

[7] Kim, K.D., Heo, J.H., "Comparative study of flood quantiles estimation by nonparametric models", *Journal of Hydrology*, Vol. 260, No. 1-4, pp. 176-193, 2002.

[8] Moon, Y.I., Lall, U., "Kernel Quantile Function Estimator For Flood Frequency Analysis", *Water Resources Research*, Vol. 30, No. 11, pp. 3095-3103, 1994.

[9] Silverman, B.W., *Density Estimation for Statistics and Data Analysis*, Monographs on statistics and applied probability, Chapman & Hall, London, 1986.

[10] Jones, M.C., Marron, J.S., Sheather, S.J., "A Brief Survey Of Bandwidth Selection For Density Estimation", *Journal Of The American Statistical Association*, Vol. 91, No. 433, pp. 401-407, 1996

[11] Scott, D. W., *Multivariate density estimation : theory, practice, and visualization*, Wiley, New York, 1992.

[12] Abramson, I.S. "On bandwidth variation in kernel estimates - a square root law". *The Annals of Statistics*, Vol. 10, No. 4, pp. 1217-1223, 1982.

[13] Ang, A. H.-S. and Tang, W.H., *Probability concepts in engineering : emphasis on applications in civil & environmental engineering*, Second Edition, Wiley, New York, 2007.

THE STRUCTURAL HEALTH MONITORING SYSTEM OF RION ANTIRION BRIDGE "CHARILAOS TRIKOUPIS"

Panagiotis Papanikolas[1], Aris Stathopoulos-Vlamis[2] and Akis Panagis[3]

[1,2,3] GEFYRA S.A. – Concession Company for the Rion-Antirion Bridge, Greece
e-mail: ppapanikolas@gefyra.gr, gsastructural@gefyralitourgia.gr, panagis.akis@gmail.com

ABSTRACT: Structural monitoring is a relatively newly developed tool particularly useful in structural assessment. "Charilaos Trikoupis" bridge incorporates it as an integral part of inspection, maintenance and management plant. The architecture of system and the operation principles are presented as well as the required maintenance and ongoing enhancements.

KEY WORDS: Rion Antirion Bridge; Structural Monitoring System.

1 INTRODUCTION

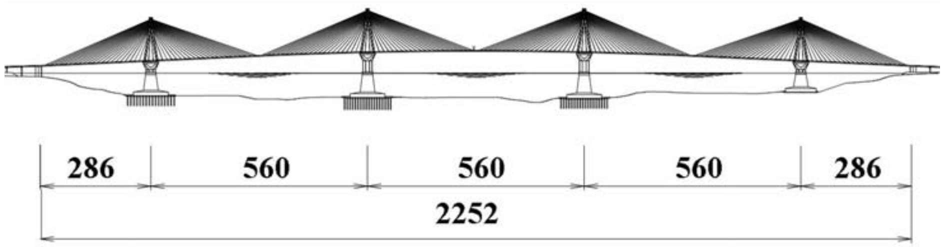

Figure 1. Rion Antirion Bridge elevation

Rion Antirion Bridge "Charilaos Trikoupis" is a 5 span cable-stayed bridge joining Continental Greece with Peloponnesus. The continuous composite deck has total length of 2252 m, with 3 main spans of 560 m and side spans of 286 m, and is suspended by 4 concrete pylons, with total height of 189 up to 227 m, through 368 cables with total length from 79 up to 295 m. At each far end of the deck, a steel rotating frame (RF) supports the structure allowing longitudinal movement that is accommodated by special designed expansion joint. Furthermore, at pylon and RF locations, the deck is transversally restrained through a fusing steel element that releases the deck when the transverse load, on each element, exceeds ±10.500/±3.400 kN (pylon/RF). Their capacity is based on wind ultimate design loads. In case of moderate/strong earthquakes, the deck is released and the induced energy is dissipated through viscous dampers located close to fuse elements.

The size and the importance of the structure, combined with the particularly harsh environmental conditions on site (maximum wind speed up to 266 km/h, design earthquake with p.g.a 0.48 g and tectonic movements up to 2 m between each pylon) required a permanent monitoring system that would provide valuable structural information.

The design, implementation and operation of the system are answering to the selected objectives such as the maximum expected structural response range, measurement accuracy and system robustness.

Through out the operation years (2004-2011) the structural health monitoring system provided invaluable information regarding the actual structure response for very different excitation cases (strong wind/earthquake/accidental events) that were used for both verification of structural integrity and optimization of structural equipment design. Also it should be mentioned the contribution to user safety through real time information regarding weather and road condition (i.e. ice on road/fog).

2 DESCRIPTION OF STRUCTURAL MONITORING SYSTEM

The structural monitoring system of Rion Antirion Bridge was designed according to the structural risk analysis regarding accidental, frequent and permanent load conditions. The selection of the most appropriate sensors and their respective location was done in order to be able to provide all the necessary data, for every possible loading, by minimizing the required number of sensors.

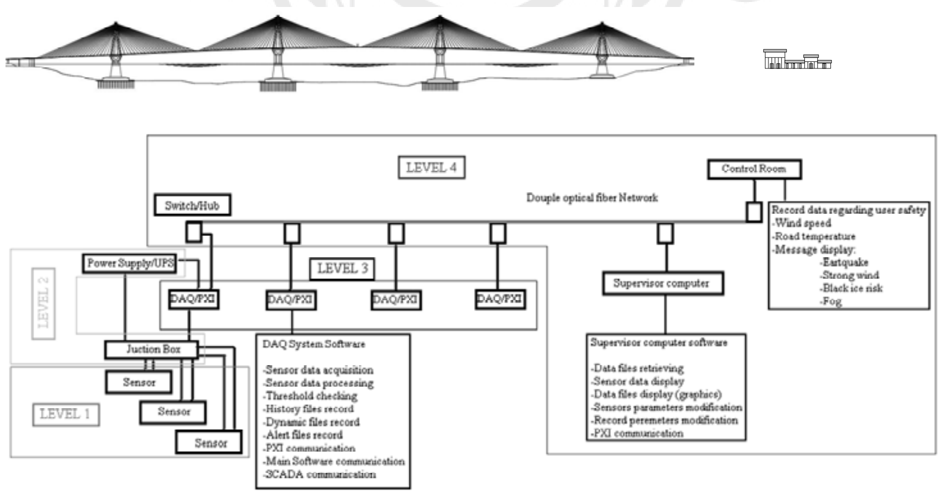

Figure 2. Overview of structural monitoring system

The current architecture of the monitoring system, *Fig.2*, can be divided into 4 different levels:

- Sensors
- Power supply and signal transferring
- Digitalization, acquisition and signal processing
- Communication network and data management.

Each level is equally important for the proper operation of the monitoring system, and the basic features are presented hereunder.

2.1 Sensors

A large variety of sensors are incorporated to the monitoring system in order to record the response of various structural elements under different loading conditions.

Table 1. Sensors description

Sensor	Quantity	Expected range of values	Actual sensor range	Monitored phenomenon
3D anemometers	2	0-50 m/sec	0-60 m/sec	Wind intensity
Temperature and Humidity sensor	2	50º C/0-100%RH	-50ºC, up to 50ºC/ 0-100% RH	Thermal loading
3D Pylon accelerometers	12	±1.9g (top) ±1.0g(base)	±20g(top) ±3g(base)	Pylon vibration (Earthquake/wind)
1D/3D Deck accelerometers	3/12	±2.7g	±3g	Deck vibration (Earthquake/wind)
3D Ground accelerometers	2	±0.48g	±3g	Earthquake
3D Cable accelerometers	13	-	±3g	Cable vibration Wind
Monostrand load of cables	16	0 up to 75% F_{GUTS} (199 kN)	0-320 kN	Cable load variation (Wind/Earthquake/Balance)
Magnetic distance meter	2	+1260/-1150 mm	3 m	Expansion joint opening (Earthquake/Balance/Thermal)
Strain gauges (full bridge)	4	±10500 kN	±1500$\mu\varepsilon$ ±17000 kN	Wind induced lateral load
Road temperature sensors	4	-	-50ºC, up to 50ºC	User safety (black ice risk)
Deck temperature sensors	5	-	-10ºC, up to 80ºC	Thermal loading

The total number of channels exceeds 300. A significant portion is dedicated to the monitoring of the system itself (power supply voltage, surge protection status) in order to be used for proper troubleshooting and maintenance.

In *Fig.3* the position of the sensors that are related with Wind and

Earthquake loads is presented.

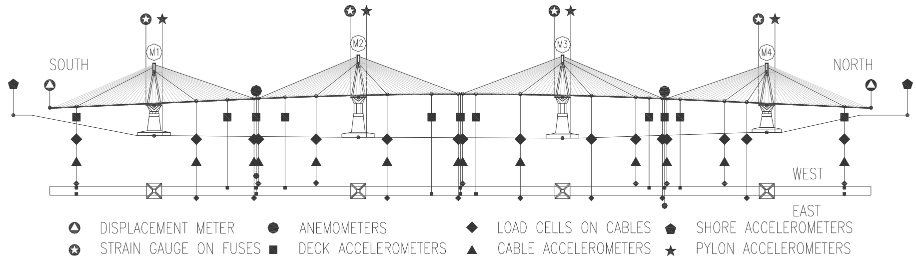

Figure 3. Overview of structural monitoring system

2.2 Power supply and signal transferring

The power supply of the sensors that are up to 400 meters away from acquisition unit, is achieved through the installation of junction boxes (JBs) that contain AC/DC (~230 to 24 VDC) convertors close to the location of sensors. Inside JBs the signal returned from each sensor is amplified (not for all sensors) and transmitted through shielded wires to data acquisition unit. An important design parameter is the surge protection system that should prevent overloads (i.e. lightning) from spreading inside the wiring network and causing damage to sensors. Additionally, it should be noted that even when major power outage occurs, the system remains active, powered by UPS devices and local power generator.

2.3 Digitalization, acquisition and signal processing

Due to the size of the monitored structure (more than 2500 m between extreme sensors), 4 different digitalization and acquisition units (DAQs) are installed, each on one pylon. The DAQs are located in controlled temperature shelters and are specially designed to be operable in harsh environments. The following operations are performed in each DAQ:

- Low pass hardware filtering at 10 kHz
- Digitalization at 500 Hz
- Conversion of signal to engineering units
- Continuous threshold checking
- Data file creation and real time transmission of selected values

A significant aspect, necessary for any further analysis of the recorded signals, is synchronization. In current architecture all the DAQs are synchronized with a server through SNTP protocol.

2.4 Communication network and data management

The communication of each DAQ with the supervisor computer (SE) and with the Control Room of the Bridge is performed through an optic fiber network that is installed along the deck. Thus, the collected data are retrieved, evaluated and permanently stored to dedicated media inside the operation building. Additionally through the SE, the end user can overview all the measurements (real time) and access/modify all record parameters (thresholds, scaling, acquisition parameters etc) that can be adjusted to each monitored event.

3 DATA RECORDS AND APPLICATIONS

Two main categories of data files are created by the monitoring system:

- History files (0.5 sec averaged values recorded every 30sec, except wind speed and direction that are 10' average)
- Dynamic files (High sampling frequency at 100 Hz with 60 sec duration)

The History files are created continuously while the Dynamic files are recorded every 2 hours (Automatic) or when particular threshold has been over passed (Alert files) or even at user demand (Request).

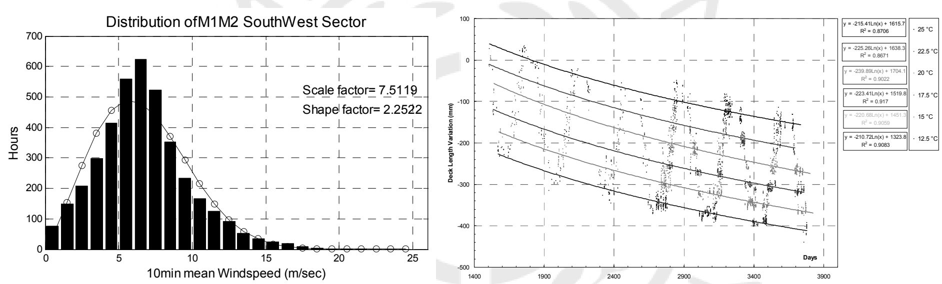

Figure 4. Wind speed distribution and deck shortening calculation (History files)

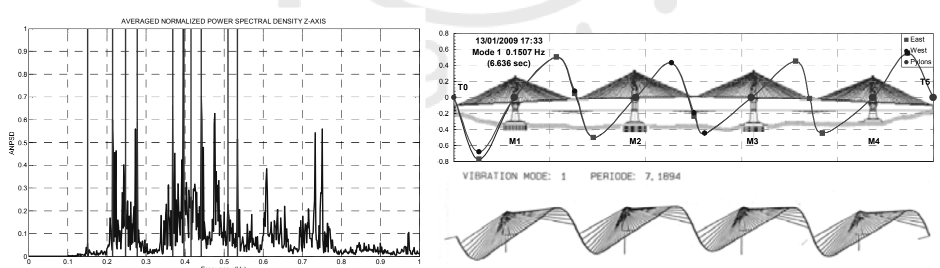

Figure 5. Identification of participating deck modes and respective shape [1]

All types of files (History/Automatic/Alert/Request) are very useful in order to understand the actual bridge response. Each of them can be used for different analysis purposes. In particular the History files are very useful in:

- Characterization of Environmental conditions, (wind, temperature)

- Estimation of deck creep and shrinkage
- Evaluation of static impact of wind loads
- Identification of potential loss of cable load from overall force distribution.

On the other hand dynamic files are used for calculating the dynamic parameters of the structure as well as to measure the response under particular loading conditions such as strong wind events, earthquakes and traffic.

4 AUTOMATIC PROCESS (SMART MONITORING)

Besides the analysis of the acquired data, it is essential for a structural monitoring system to automatically identify and adjust accordingly the data recording parameters, in order to answer particular demands. Moreover, a smart automated alert management can significantly decrease the, otherwise vast, volume of the recorded data. This can accelerate the required processing time and allow more elaborate analyses to be performed.

The structural monitoring system of Rion Antirion Bridge incorporates special modules that can automatically identify and perform special actions for earthquake (seismic mode) and strong wind events (wind mode).

During an earthquake event the following actions are automatically performed:

- Earthquake alert declaration in case that more than 3 channels, from different sensors (that were set as alert declarers), exceed specific threshold (5% of g) within a reasonable time window.
- Classification of earthquake intensity through the response of particular sensors (that were set as response indicators) into 3 different cases.
- Real time transmission of relevant information on control room for safe traffic management
- Notification of event via different means (email/SMS/phone message) of selected persons
- Processing of the recorded data and automatic report creation with the structure response measurements.
- Transmission of abovementioned report to dedicated persons.

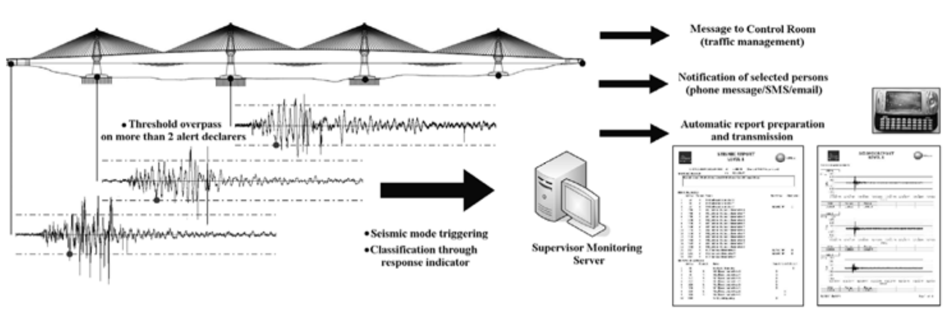

Figure 6. Overview of seismic mode functioning

Seismic mode has also the ability for self diagnosis in case that completion of the above mentioned tasks is prevented for any reason. For example in case of external communication loss, an external server that has been already informed that an earthquake occurs, will inform the dedicated people that the communication with the Bridge site is impossible and will provide the latest update regarding case classification.

The approach of the monitoring system to wind related event is similar with the seismic mode. However, there are some important differences:

- The declaration of a wind related event is based not only the wind intensity (wind speed threshold) but also in the measured response of particular elements (cables for instance). This is due to the fact that for various aerodynamic phenomena, the response of a structure is not proportional with the wind speed.
- Since the duration of a wind related event can be significant longer than an earthquake event (there are already recorded cases that wind speed was above 20 m/sec for more than 48 hours), it is necessary to reduce the acquisition frequency and increase the length of the records (i.e. the deck modal frequencies that can be excited are not above 2 Hz and cable modes with frequencies more than 10 Hz have insignificant contribution to vibration amplitude). This reduction of data volume is necessary for real time automated processing and reporting.

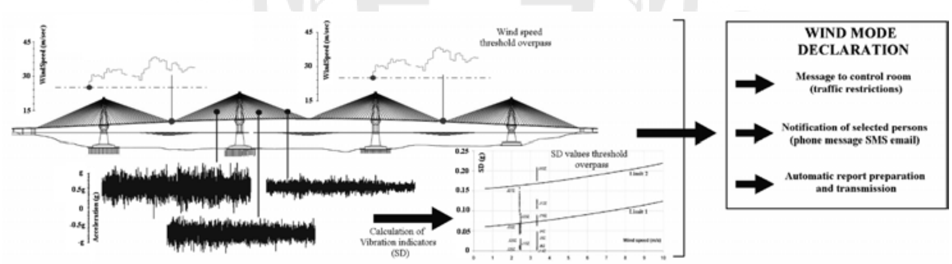

Figure 7. Overview of wind mode functioning

5 MAINTENANCE

The operation of a monitoring system that should provide important and meaningful data anytime this is required, calls for an intense and continuous follow up. The main points for ensuring proper & continuous functioning of Rion Antirion Bridge monitoring system are:

- Persistent follow up of the acquired data.
- Logging each possible malfunction and measurement quality degradation.
- Constant availability of all required spare parts, in site storehouse.
- Immediate notification of experts for troubleshooting and repair.
- Computerized annual maintenance of monitoring system (levels 1 to 3, see

Fig.2) and specialized maintenance every 5 years, including sensors calibration.

It's worth mentioning that during 2010, the total downtime was less than 0.5%.

6 FUTURE ENHANCEMENTS

Additionally to the already mentioned maintenance actions, it is important to proceed with necessary upgrades of the system in order to improve data quality and system robustness. A new architecture of monitoring system is currently under development and will be implemented progressively in the near future. Some critical points are:

- Improvement of data synchronization (less than 1 msec tolerance), through GPS technology.
- Redistribution of computational tasks over different hardware in order to minimize failure risk and increase systems flexibility for additional sensor installation and more elaborate automatic process.
- Enhancement of anti-aliasing policy by incorporating more suitable hardware low pass filters and increase acquisition frequency.

7 CONCLUSIONS

A significant infrastructure such as Rion Antirion Bridge incorporates a structural monitoring system that can give invaluable structural response information for a wide variety of loading cases. It is also required for the safety of the users in case of special events such as Earthquake and wind. The upgrades and the constant maintenance of the system are the key points for high uptime, reliable data acquisition.

ACKNOWLEDGEMENTS

Design, supply and implementation of the system were performed by Advitam.

REFERENCES

[1] H.Wenzel D.Pichler, "Ambient Vibration Monitoring", WILEY publications, 2006.

GEODETIC MONITORING OF BRIDGE OSCILLATIONS

Evangelia Lambrou[1] and George Pantazis[2]

[1,2] National Technical University of Athens, School of Rural and Surveying Engineering, Greece
e-mail: litsal@central.ntua.gr, gpanta@central.ntua.gr

ABSTRACT: A total geodetic methodology is being presented for the simultaneous real-time monitoring of two or more points on a given bridge. The methodology is based on the **synchronization of two high accuracy and dexterous total stations**. The application was carried out on the Halkida Bridge. The geospatial data is presented in time series. In addition, the determination of the main frequency of oscillation was calculated by using the FFT analysis.

KEY WORDS: Bridge; total station; synchronization; simultaneous real-time monitoring; Halkida; oscillation

1 INTRODUCTION

The gigantic technical and industrial structures that have been built in recent decades such as big bridges, silos and dams need continuous monitoring of their dynamic behavior during their operation.

The monitoring of the dynamic oscillation and the deformation of any certain bridge, constitute today one of the most interesting subjects of study. Through these studies, external factors and their influence on the operation of a bridge have become familiar to scientists and have given them the insight for better constructions. The goal of a ″bridge's monitoring″ is for the determination of:

- The bearing ability of a bridge's body
- The deformations and the payload of specific cross sections
- The resilience of the construction materials
- The change of the temperature or the augmentation of the humidity

The monitoring of these phenomena may be carried-out simply by using systems of geotechnical instruments. The measurements made by geotechnical instruments are quite accurate of the order of ±0.1mm and their measurements are direct and continuous. But these measurements are uncorrelated to each other, as they don't refer to the same reference system and provide only quantity information. Furthermore, their credibility depends on the proper operation of the instruments.

Today, this type of monitoring can be totally supported by using geodetic instrumentation and methodology. The evolution of the geodetic total stations and GPS receivers has maximized their contribution to bridge deformation and oscillation monitoring with adequate accuracy.
The main advantages of using the geodetic methods are as follows:

- The measurements are correlated to each other.
- The coordinates of the selected points are referred to a unique reference system.
- The use of a network adjustment.
- The determination of the absolute and relative movements between the selected points.
- The evaluation of the results is carried out for a specific confidence level, according to the user.
- There are qualitative and quantitative results.
- The geodetic measurements can also be adjusted with the geotechnical ones in an entire adjustment.

2 GEODETIC MONITORING METHODS

The geodetic methods that are used for monitoring purposes, utilize conventional (terrestrial) or satellite instrumentation. These methods are applied by establishing continuous and/or repeated measurements at regular time intervals of a 3D network.

This monitoring is realized by using robotic total stations [5], [7] or receivers of the satellite positioning system. The points of the network are established on the bridge's body and on the surrounding area of any stable ground.

Special care must be paid to the means used for the establishment of a network points. The selection of these points must ensure their stability at the place set, in time and the unique set up of the instrument. Also, the unique sighting of the targets at every campaign of the measurements is very important. As the final uncertainty of the calculated coordinates and the calculated displacements mainly depends on the above mentioned parameters, therefore, special designed constructions are used:

- pillars with a metal head on their top, which bears the appropriate screw for the placement of the selected instruments (photo 1a)
- Permanent plates in the ground with mobile poles to support the instruments (photo 1c).
- Permanent plates, with the appropriate projection screw, which can be placed on vertical walls of a bridge's body (photo 1b).
- Mini reflectors, which have been permanently positioned on the bridge's body for accurate targeting and distance measurements (photo 1d).

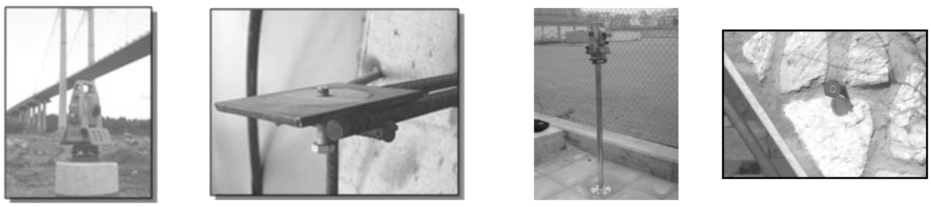

(a) (b) (c) (d)

Photo 1. Means for realization of the network's points

Once the appropriate adjustment of the network has been achieved, either by using terrestrial or satellite measurements, the coordinates of the network's points are calculated as well as their uncertainties for every campaign of measurement. Moreover, the absolute and relative displacement of each point is computed for a selected confidence level. Thus, the simultaneous 4D (3D and time) determination of the change of position of each point is feasible by an accuracy, which fluctuates between a few mm to a few centimetres. Additionally, the time series of the oscillation of each point can be drawn.

As far as the advanced modern total stations are concerned, those are used in these applications:

- They have servo electric or piezoelectric movement. They can turn from phase I to phase II in about 2 sec. That means that they can monitor a target with an angular speed of 200m/sec at 100m.
- They can automatically recognize a target without human assistance (ATR). Thus, they can take the measurement, by self targeting and without the need of an observer. Hence, eliminating the systematic error that is caused by a human's sighting.
- They can lock on a target and take a measurement at specific time interval as the user defines. The maximum operation frequency is 10Hz depending on the environmental conditions as the mean operation frequency is about 4Hz.
- Their angle measurement accuracy reaches ±0.5″, their distance measurement accuracy ±0.6mm±1ppm and they reach an accuracy of ±3mm when tracking a target. Thus, the uncertainty of the determined coordinates of each point can be of the order of few millimeters.
- Results can be sent in real time to a connected PC at the field or to the office PC, as they support internet connection.
- They register simultaneously the 4^{th} dimension, which is the time of the observation, by an accuracy of ±0.01sec or more. The registered time used could be set at any given time or at the original Universal Coordinated Time (UTC) [10] as the GPS receiver registers. This possibility is available thanks to the credible embodied chronometer that they have. In addition, their operation in Windows CE interface permits their synchronization to the UTC time, directly via internet connection, by using the appropriate time server.

Otherwise, the ActiveSync software is used on a PC in order to communicate with the total station. During this communication the PC time is transferred to the total station. The time of the PC could be set at any given time or the PC could be pre- synchronized via the internet by using a worldwide time server [12], which has an accuracy of ±0.001sec.

A total station connection to a PC could be carried out, either by a USB cable or a wireless connection by Bluetooth. The synchronization of the total station with the UTC time is essential and important as, in this way, measurements and results can be compared with others, which could be gathered simultaneously by GPS or by using geotechnical instruments.

As far as the GPS receivers that are used for these applications are concerned:

- They must be double frequency receivers for more accurate results.
- An advanced choke ring antenna must be used.
- They have the opportunity to register measurements in high frequencies 10 - 20Hz [8]. This helps the monitoring of bridges as well as springy constructions, antennas and high buildings such as sky scrapers.
- The accuracy of the calculated coordinates is of the order of some centimeters.

A great disadvantage of using a GPS in such monitoring tasks is that the bridge is a very unfriendly environment for GPS antennas. Many multipaths in the GPS signal are caused, due to the metal structure of the bridge's body, the movement of the vehicles, the passing of the pedestrians, the reflection of the water's surface, the weight of the antenna and its own oscillations caused due to the wind. All the above mentioned parameters cause an error which can reach 10cm, even if choke ring antennas are used [6].

The above instrumentation can be also used together. The measurements can be adjusted together for several phases.

As both kinds of instruments and methods provide the monitoring in 4 dimensions, the automatic measurements of at least 4Hz and the independence of the measurement from the observer and his/her personal errors then the major benefits of the use of a total station vice GPS are:

- It provides more accurate results so the network is more sensitive to the determination of movements or oscillations.
- It provides reliable measurements as it is influenced at a minimum by the environment.
- It allows for the possibility to install the network's point on any given position on the bridge's body, even on ″difficult positions″, where a GPS's antenna cannot be placed. Such as:
    - where there is no sky view and the satellite signal is relatively impossible or problematic.
    - where The GPS's antenna receives many multipath signals due to the above mentioned parameters.

There have been many applications made worldwide for a bridge's monitoring. As in the case of the old bridge of Arta in 1983, in Greece, by using terrestrial methods, the Humber Bridge [1], the suspension of the Forth Road Bridge in Scotland, [4] by using GPS receivers, the Halkida Cable Bridge in Greece, by using both a total station and a GPS receiver [2], [9] and the Gorgopotamos Bridge in Greece [3].

3 SIMULTANEOUS AND REAL TIME MONITORING BY USING TOTAL STATIONS

The aim of the proposed methodology is the monitoring possibility of a bridge oscillations at two difficult and yet different positions on its body, by using total stations during continuous traffic. The main purpose is for the position of each target to be registered in space and time and to be comparable to each other.

Two instruments should be used, a-priori synchronized to each other and/or with the universal time UTC. They will monitor simultaneously two different targets (reflectors), which have been mounted on specified positions on the bridge's body. Thus, the oscillation time series for each target can be drawn. The comparison of the corresponding time series of each target will give the differential oscillation between the points at the same time.

An experiment of this kind was carried out on Halkida's cable-stayed high Bridge, in Greece. A permanent network was established in the surrounding area for the bridge's monitoring. The network consisted of 6 beton pillars, which were installed in the surrounding area and about 50 retro reflectors, which were stabilized on specified positions on the bridge's body.

Two advanced total stations were used. The Trimble VX and the Topcon IS. Both provided angular accuracy of ±1″ or ±0.3mgon as their distance measurement accuracy was ±3mm±2ppm and ±2mm±2ppm, respectively. They operated in Windows CE interface and they registered their measurements automatically by frequency of 1Hz and 4Hz, respectively.

Prior to their use, both instruments were connected to a PC and they were simultaneously synchronized to the UTC time, using the same server.

However, a few days earlier the drift of their time keepers had been calculated for some days. It was found that their clocks had a delay, which was less than a second within the two-day time period that they were checked. So, from this it was gathered that if they were synchronized just before the measurements, then the time correction for the following few hours would be insignificant. The measurements were registered by 1Hz frequency for 15 minutes for each experiment.

Two different experiments were carried out. In the first one we had to verify the simultaneous of the registration and the instruments' credibility. Thus, both instruments were monitoring the same omni direction prism, which was situated at the middle of the bridge, between the two main pillars of the bridge (fig. 1).

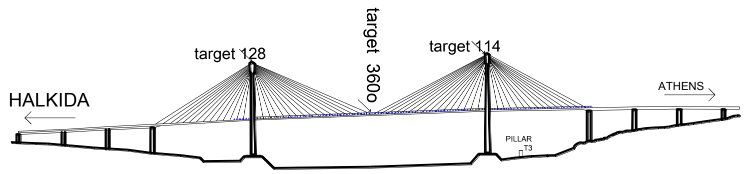

Figure 1. The Halkida bridge and the monitoring locations

Figures 2, 3 illustrate the time series for the y and z coordinates, respectively. The fine line is the registration of the VX station as the bold one is the registration of the IS. The diagrams show that both instruments give the same result at the same time. Some small differences that appeared were within the expected uncertainty of the measurements.

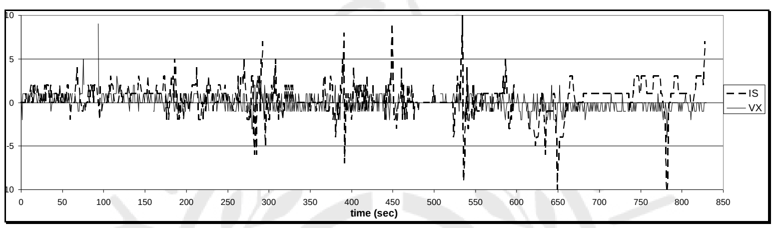

Figure 2. Time series of the cross-section displacement

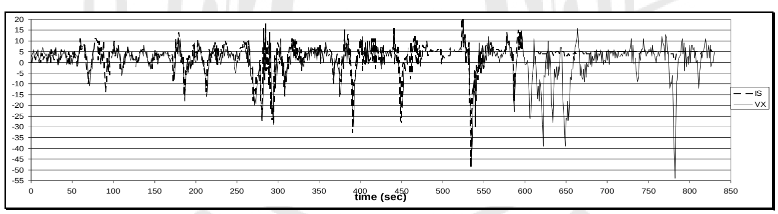

Figure 3. Time series of the vertical displacement

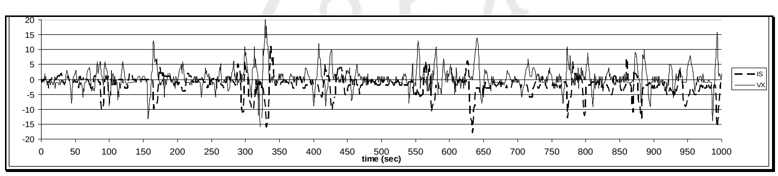

Figure 4. Time series of the cross-section displacement

In the second experiment each total station monitored a different target. The reflector-targets were situated at the highest point of the two main pillars of the bridge (fig.1). The goal was to observe the oscillation frequency differences between these points caused by the same traffic. Figures 4, 5 illustrate the time series.

The coordinates of the points were calculated by the total station software in real-time and the time series were drawn-up by a laptop, which was connected to the station. The accuracy of the coordinates was estimated at ±3mm.

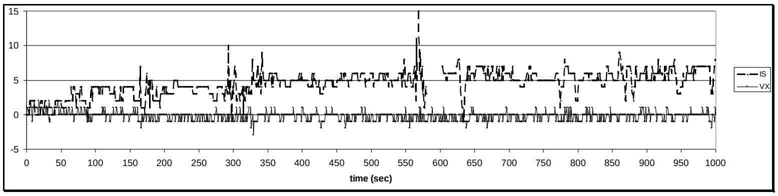

Figure 5. Time series of the vertical displacement

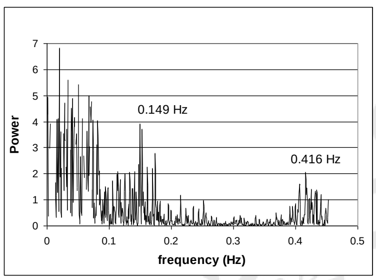

Figure 6. Spectral analysis of vertical displacement for VX (first experiment)

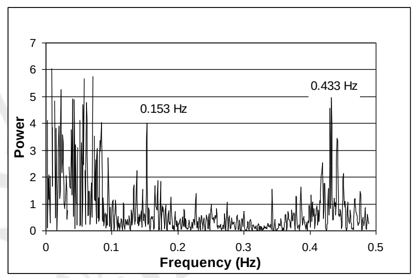

Figure 7. Spectral analysis of vertical displacement for IS (first experiment)

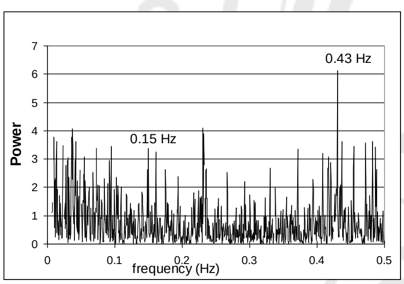

Figure 8. Spectral analysis of vertical displacement for VX (second experiment)

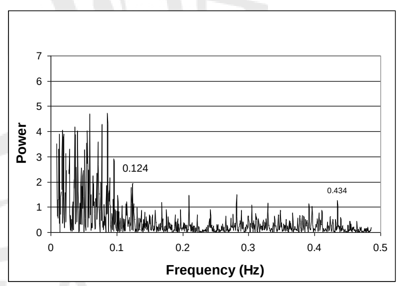

Figure 9. Spectral analysis of vertical displacement for IS (second experiment)

Additionally, a spectral analysis FFT was carried out where the frequencies of the oscillations were calculated. Figures 6, 7, 8 and 9 present the frequencies of the vertical direction in both experiments. The main frequency that was calculated for each case using the Lomb method [11], was about 0.4Hz. This is within the bridge's construction study.

4 CONCLUSIONS

The bridge's oscillation monitoring is of great importance for the scientific community. The GPS monitoring doesn't prove to be adequate, due to the random errors, which are increased by the environment and the existing materials. The advanced total stations seem to be an alternative solution to this problem as they provide considerable accuracy. Although their registration frequency is smaller than the GPS receivers their results have credibility.

The experiments that were carried-out show that the main frequency of a bridge's oscillation can be calculated even with registrations of 1Hz frequency. It is reminded that today, the registration can be achieved with 7-10Hz by newer total stations. Furthermore, the registration of an accurate time as well as the opportunity of synchronization to the UTC time, gives scientists the possibility to combine their measurements with a GPS's measurements or a geotechnical instruments data. It is also worth mentioning, how remarkable it is that we now have the opportunity to monitor targets in difficult or covered points.

Finally, the establishment of such targets is cheaper than the establishment of GPS antennas, not to mention more easily attainable and safer as the weather conditions don't influence them. It could be then concluded, that the use of an advanced total station in the monitoring of a bridge is more advantageous than that of a GPS. The disadvantage of the slow registration (1-4Hz) that these total stations provide today is expected to be surmounted in the years to come, making them more robust.

REFERENCES

[1] Ashkenazi V, and Roberts G, ″Experimental monitoring of the Humber bridge using GPS″, Civil Engineering, 120, pp 177-182, 1997.

[2] Lekidis V, Tsakiri M, Makra K, Karakostas C, Klimis N, Sous I, ″Evaluation of dynamic response and local soil effects of the Evripos cable-stayed bridge using multi-sensor monitoring systems", Engineering Geology, Vol. 9, pp. 43-59, 2005.

[3] Psimoulis P, ″ Documentation of the potential of GPS and RTS to measure oscillations of rigid structures″, Doctoral Thesis (In Greek), 2009.

[4] Brown CJ, Roberts GW, Atkins C, Meng X, Colford B, ″Deflection and frequency responses of the Forth Road Bridge measure by GPS″, *Proc. Of Int. Conf. by the Institution of Civil Engineers*, ICE, 479-486, 2007.

[5] Gikas V, Daskalakis S, ″Full scale validation of tracking total stations using a long stroke elctrodynamic shaker″, *Proc. of the 13th FIG Congress*, Munich 2006.

[6] Ogundipe O, Roberts G, ″Antenna Selection for Bridge Deformation Monitoring – Comparison of Multipath Mitigation Characteristics for Three Types of Antennas″ *Proc. of* FIG Working Week 2011, Marrakech 3-4 May 2011

[7] Palazzo D, Friedmann R, Nadal C, Filho M, Veiga L, Faggion P, ″Dynamic Monitoring of Structures Using a Robotic Total Station″, *Proc., XXIII FIG Congress*, Munich, Germany, 2006

[8] Roberts G, Brown C, Meng X, ″Deflection Monitoring of the Forth Road Bridge by GPS″, *Proc. 18th International Technical Meeting of the Satellite Division of The Institute of Navigation*, Long Beach, CA, pp. 1403-1413, 2005.

[9] Tsakiri M, Lekidis V, Stewart M, Karabelas J, ″Testing procedures for the monitoring of seismic induced vibrations on a cable-stayed highway bridge″, *Proc. 11th FIG Symposium on Deformation Measurements*, Santorini, Greece, 2003.

[10] Zogg H, Lienhart W, Nindl D, ″Leica TS30 White Paper″, Leica Geosystems, 2009

[11] Lomb NR. Least-squares frequency analysis of unequally spaced data. Astrophys Space Sci, 1976

[12] National Institute of Times and Technology, http://www.nist.gov/pml/div688/grp40/its.cfm

DAMAGE IDENTIFICATION IN BRIDGES USING EMPIRICAL MODE DECOMPOSITION OF THE ACCELERATION RESPONSE TO RANDOM TRAFFIC

Jill Meredith[1] and Arturo González[2]

[1,2] University College Dublin, School of Civil Engineering, Dublin
e-mail: jill.meredith@ucdconnect.ie, arturo.gonzalez@ucd.ie

ABSTRACT: Recent studies have shown that Empirical Mode Decomposition can be used to detect and locate multiple damages when applied to the acceleration response of a beam model subject to the crossing of a constant load. This paper further examines the technique using simulations of random traffic with varying velocity and magnitude of the traffic loads.

KEY WORDS: Damage detection; Empirical mode decomposition; Signal decomposition; Vibration-based analysis.

1 INTRODUCTION

In bridge health monitoring, the need for damage detection methods that can be applied to complex structures has led to extensive research in global detection methods which examine changes in the measured vibration response of the structure. Time series analysis is receiving increased attention in the field as it permits vibration signals, from structures, to be decomposed into fundamental basis functions that are used to characterise the vibration response. Recently, a new time-series analysis method, Empirical Mode Decomposition (EMD), has been developed to analyse nonlinear and non-stationary data.

EMD is a signal processing method which decomposes any time series data into a set of simple oscillatory functions, defined as Intrinsic Mode Functions (IMFs), by a procedure known as the sifting process [1]. An IMF must satisfy two conditions: (1) Within the data range, the number of extrema and the number of zero crossings are equal or differ by one only; and (2) the envelope defined by the local maxima and the envelope defined by the local minima are symmetric with respect to the mean.

In 1998, Huang et al [1] proposed detecting damage in a structure by applying an intermittency frequency to the IMF's. The intermittency frequency should be smaller than the frequency of discontinuity but larger than the highest structural frequency appearing in the measurement. The basic concept of this approach is that a sudden loss of stiffness in a structural member will cause a discontinuity in the measured response that can then be detected through a distinctive spike in the filtered IMF. The damage location can then be determined by the time occurrence of the observed spike.

This method has since undergone research to establish its true effectiveness in this area. Xu & Chen [2] conducted experiments, on the use of EMD, using a three storey steel frame building model which was welded to a base plate and bolted to a shaking table. A sudden change of structural stiffness was simulated and signals were acquired using accelerometers. The measured structural response time history was processed to obtain the first IMF component using the EMD approach with intermittency check. This component was then used to identify the damage time instant and damage location of the building. Xu & Chen concluded that the EMD approach can accurately identify the damage time instant by observing the occurrence time of the damage spike in the first IMF component of the acceleration response. They found it to be a useful tool for damage detection in real structures in the sense that it is a signal based and model free method, requiring no prior knowledge on the structure.

Yang et al [3] performed a similar study employing a four-storey ASCE benchmark building. They also found that they could detect exact damage locations. They noted that the magnitude of the spikes identifying the damage depends on the external loads, the damage location and the severity of damage.

Recently, Meredith et al [4] used EMD to detect multiple damage locations in the acceleration response of a beam model subject to the crossing of a load. This investigation concluded that EMD could be used to detect damage from the accelerations of a structure subject to a moving load. It was found that high levels of noise and a long beam length introduced some small inaccuracies, however an increase in observation points could overcome this. This paper further develops this research using simulations based on large samples of moving loads generated stochastically. Velocity and magnitude of the moving loads are generated by applying random sampling to statistics from real Weigh-In-Motion data. The aim of this preliminary analysis is to check if the response of a structure to everyday traffic (as opposed to the use of a calibrated load of known characteristics) can be used as a tool to identify damage using EMD. For this purpose, the sensitivity of the EMD approach to detect sections with different levels of damage is tested using unknown speeds of traffic for different characteristics of the traffic fleet.

2 TESTING ARRANGEMENT

2.1 Beam model

The response of a one dimensional simply supported finite element beam model subject to a moving load is simulated using Matlab 7, as described by Hester et al [5]. A crack is modelled as a reduction in stiffness of the beam in the area of the crack with the assumption that the crack does not affect the mass of the structure. The severity or depth of the crack is described by the variable δ which is the ratio of the crack height to the beam depth. The area of influence of this stiffness reduction is approximated with a triangular shape which extends 0.5d either side of the crack.

For testing purposes, the beam is assumed to be made of material with a modulus of elasticity of 34 GPa and a density of 2400 kg/m^3. The beam cross-section is uniform of width 0.5 m, depth 1 m and span length of 10 m. The crack is assumed to be located at a distance of 7 m from the first support in all simulations. Acceleration signals are obtained at the midspan of the beam, at a frequency of 10 kHz as the loads travel across the structure.

2.2 Characteristics of the sample of moving loads

In generating load flow simulations for testing, the random variables defining magnitude and velocity of the load are adopted from real traffic. An effective procedure for collecting real time traffic records is termed weigh-in-motion (WIM) [6]. WIM data which was collected for over half a million trucks from a site in Netherlands is used here to obtain the magnitude and velocity of moving loads involved in the simulation. For the purposes of this study only trucks with 2 axles are considered and data is cleansed so that only velocities between 10 and 35 m/s are included. The resulting data contains approximately 130,000 trucks. Both velocity and gross vehicle weight of the trucks are normally distributed with a mean of 23.92 m/s and 10209 kg and a standard deviation of 1.78 m/s and 3572.8 kg respectively.

2.3 Testing procedure and signal processing

Testing is carried out for 1, 100 and 250 runs of single loads crossing the beam, where weight and velocity of each load is randomly sampled from the distributions provided in Section 2.2. The acceleration signal is obtained for each run and EMD is carried out on it. A highpass filter is then applied to the first IMF which removes the highest natural frequency of the beam present in the simulated response and leaves the frequencies of any discontinuities.

For explanatory purpose, *Fig.1* and *Fig.2* show the acceleration signal from a beam model with just one load crossing before and after undergoing processing. The beam is modelled with a crack of $\delta = 0.3$ at 7 m from the first support with a load of 96 kN travelling at 25 m/s over it.

The original signal and the first IMF are given in *Figs.1(a)* and *1(b)* respectively. For a velocity of 25 m/s, the damage spike should occur at 0.28 s. It can be seen from the filtered IMF (*Fig. 2(a)*) that the method clearly allows damage to be located at that point in time. *Fig.2(b)* shows a close up of the damage spikes in this location. The damage spikes, located at the nodes, spread 0.5 m either side of the damage as this is how the area of influence of damage has been modelled. At the damage location (i.e., 0.28 s), there is no peak due to the fact that the elements either side of the node at this point have the same properties, therefore the filtering process does not detect any discontinuity between these. A small peak will also occur at the sensor location (i.e., 0.2 s), however, as this is known a priori, it can be easily eliminated as a possible source of damage.

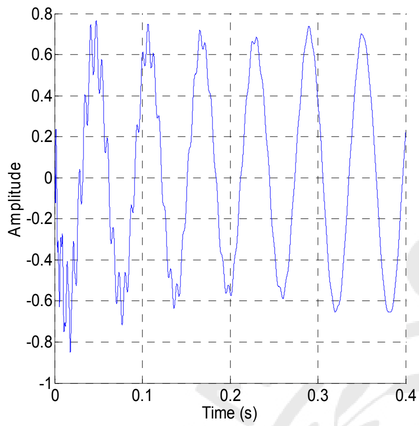

Figure 1(a). Original Acceleration Response

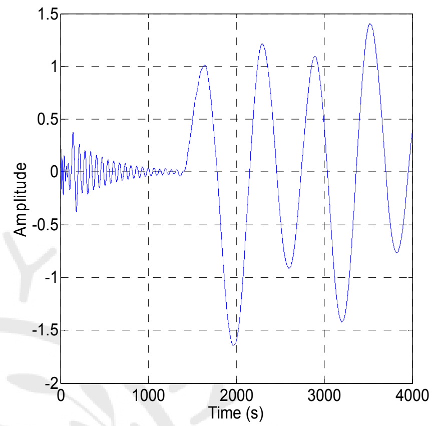

Figure 1(b). First IMF of signal in Fig.1(a)

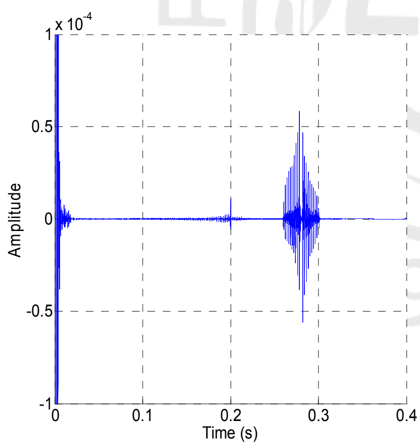

Figure 2(a). Signal after applying high-pass filter to Fig.1(b)

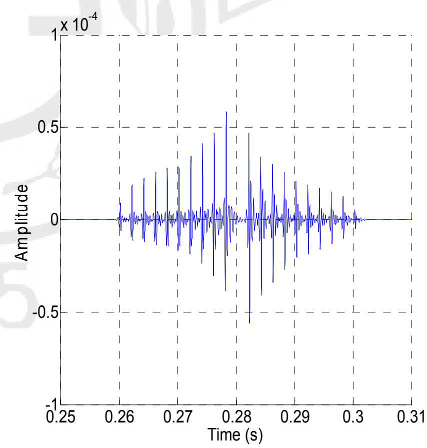

Figure 2(b). Close up of Fig.2(a) showing damage location

It should also be noted that there is a transient at the beginning of the filtered signal (*Fig. 2(a)*), which can be expected as a result of the filtering process. I.e. the filter encounters a change in frequency at the start up of the signal, which is greater than the cut-off frequency, leading to large initial spiking.

3 TESTING RESULTS AND DISCUSSION

Tests were carried out using 1, 100 and 250 runs of loads randomly sampled according to the statistical distributions defined in Section 2.2. *Fig.3* shows the results for 100 runs of load with damage of δ = 0.3.

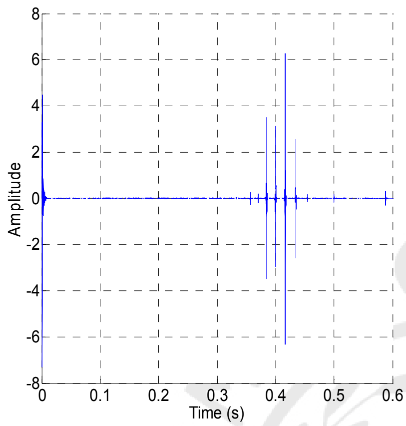

Figure 3(a). IMF 1 after filtering

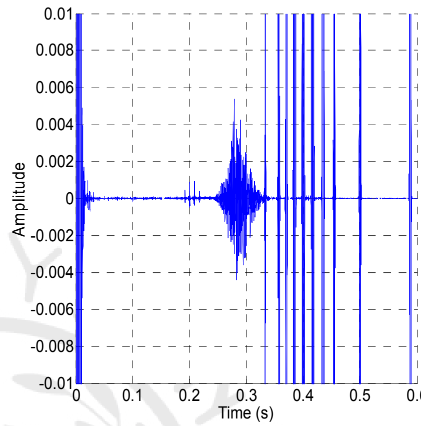

Figure 3(b). Close up of Fig.3(a)

The mean velocity for this random sample of 100 runs is 24.26 m/s, and it can be associated to sensor and damage locations at 0.206 s (5 m from support) and 0.2885 s (7 m from support) respectively. The initial start-up spike and the exit spikes of the different loads are visible in *Fig.3(a)*, however, the damage is not. A close up of the signal is shown in *Fig.3(b)*, here the damage can be clearly seen with the maximum damage spike occurring at 0.2783 s (6.75 m from support). In this instant, therefore, the method is accurate to within 0.25 m given the assumed variability in speed. This displays the capabilities of the method to capture the damaged location, however, the spikes caused by the exiting of the loads from the beam can make the results unclear when shown in this manner. To more clearly show the occurrence of the damage spike, a 3D histogram is used in *Fig.4*. To create the histogram, the maximum spike value, and the time associated with it, is taken for every 10 data points. To allow results to be seen clearly the initial start up spiking and all zero spike amplitude values are removed from the data. The histogram shows the time occurrence on the x-axis, the spike amplitude on the y-axis and the number of spikes on the z-axis. This type of representation places the large damage spikes from the exit spiking to the rear of the histogram and keeps the relatively smaller spiking from the damage at the front.

To calculate spiking locations there are two possible methods. The first method is to assume there is an axle detector system on site that can provide the mean velocity. It is then simply a matter of multiplying the time location of the spike by the velocity to establish its location on the beam. For this data, as previously mentioned, the mean velocity is 24.26 m/s, this places the sensor and damage spikes at 5.01 m (0.2067 s) and 6.92 m (0.2852 s) respectively which compares well with their exact locations of 5 m and 7 m.

The second method of locating the spikes is based on the histogram results only. The exiting spike, which extends to the rear of the histogram, is located and the beam length (10 m) is then divided by its time occurrence giving the mean load velocity. *Fig.4* shows an exit spike at 0.4086 s which gives a mean velocity of 24.47 m/s. The latter places the sensor and damage spikes at 5.06 m (0.2067 s) and 6.98 m (0.2928 s) respectively which again compares well with the exact locations.

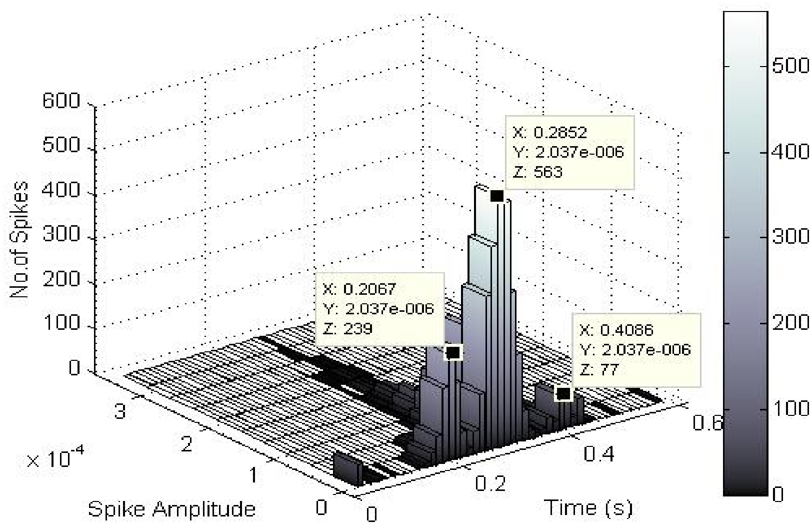

Figure 4. 100 runs of randomly sampled load on a beam with damage of δ = 0.3

As the second method relies only on results and no prior knowledge is required, this is the one applied. Overall the representation of the results in *Fig. 4* is clearer and easier to interpret than those obtained from *Fig. 3*.

To show the sensitivity of this method to small levels of damage, *Fig.5* shows results for 100 load runs across a beam with damage of δ = 0.05 (i.e. a crack depth of 50 mm). Using the mean velocity of 24.54 m/s, calculated from the exit spike at 0.4178 s, the sensor and damage spikes occur at 5.07 m and 7.15 m. As can be seen from these histograms the results of this method are accurate to within 0.15 m of the damage location in spite of the variability in speed and magnitude of the load. Testing was also carried out to determine the effect the number of runs has on determining the location of damage. *Fig.6* shows the results for 250 load runs with a beam damage value of δ = 0.3. In this case the mean velocity is 24.7 m/s, calculated from the exit spike at 0.4047 s, and the sensor and damage spikes occur at 5.0 m and 7.0 m exactly. Damage is still easily determined in these results and in fact testing shows that an increase in the number of runs improves the clarity of the results.

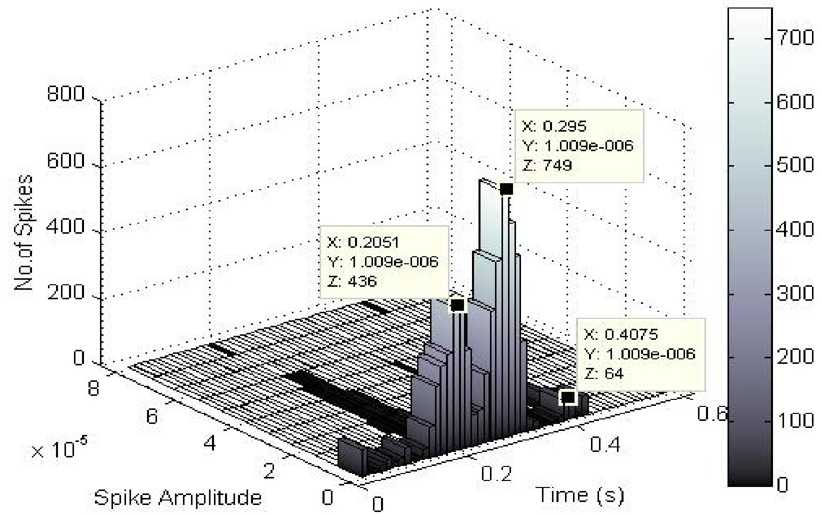

Figure 5. 100 runs of randomly sampled loads on a beam with damage of δ = 0.05

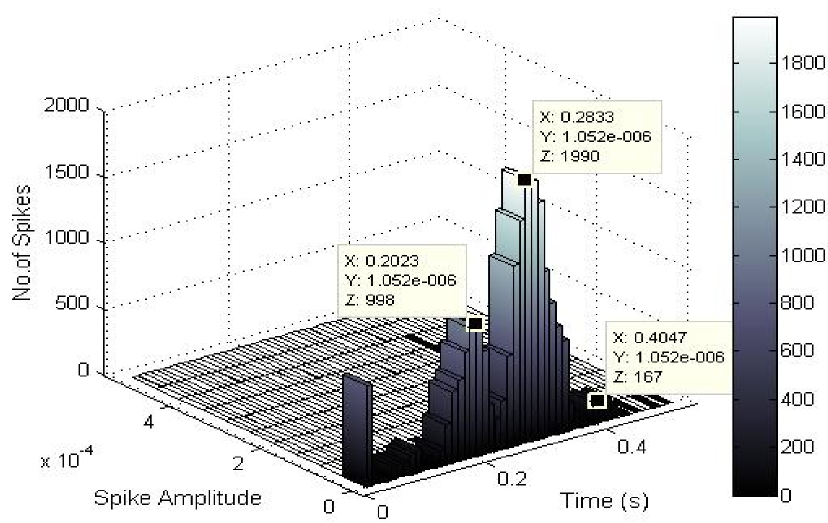

Figure 6. 250 runs of randomly sampled loads on a beam with damage of δ = 0.3

4 CONCLUSIONS

In view of long-term health monitoring requirements of structures, such as bridges, it is desirable that the damage detection techniques employ operating loads, such as vehicular loads, as excitation sources, which do not require controlled vibration conditions, a perfect knowledge of the excitation source or closure of the structure. This paper has proposed a health monitoring technique with the potential to be used with everyday traffic, and to identify and locate damage with minimal use of resources. The approach does not require a mathematical model of the response of the structure, any knowledge of the structure in the undamaged state or detailed information on the properties of the crossing loads.

Preliminary testing of the technique has been carried out here on a simple numerical model of multiple loads moving over a damaged beam. It was found that the method is capable of detecting damage as small as 5% of the beam depth and locating it to within 0.15 m of its exact location. It was also found that an increase in the number of load crossings will improve the accuracy of the results. This approach is shown to be a promising tool for damage detection of real structures with relatively low-costs and simple implementation.

ACKNOWLEDGMENTS

The authors wish to thank David Hester, a researcher within the UCD School of Architecture, Landscape and Civil Engineering, for his help with the simulation model employed in the paper. The authors also wish to acknowledge the Irish Research Council for Science, Engineering and Technology (IRCSET) for their financial support towards this investigation.

REFERENCES

[1] Huang, N.E, Shen, S, Long, S, Wu, M, Shih, H, Zheng, Q, Yen, N, Tung, C, Liu, H, "The empirical mode decomposition and the Hilbert spectrum for nonlinear and non-stationary time series analysis", *Proc. R. Soc. London, Ser. A*, Vol. 454, pp. 903-995, 1998

[2] Xu, Y.L, Chen, J, "Structural Damage Detection using Empirical Mode Decomposition: Experimental Investigation", Journal of Engineering Mechanics, Vol. 130, No. 11, pp. 1279-1288, 2004.

[3] Yang, J.N, Lei, Y, Lin, S, Huang, N, "Hilbert-Huang Based Approach for Structural Damage Detection", Journal of Engineering Mechanics, Vol. 130, No.1, pp.85-95, 2004.

[4] Meredith, J, González, A, Hester, D, "Empirical mode decomposition of the acceleration response of a prismatic beam subject to a moving load to identify multiple damage locations", *Proc. Intl. Conference on Structural Engineering Dynamics*, 20-22 June, Portugal, 2011.

[5] Hester, D, González, A, Rowley, C, "Aspects of dynamic responses of bridges to moving loads due to cracking", *Bridge and Infrastructure Research in Ireland*, pp.111-119, Galway, 2008.

[6] O'Connor, A.J, O'Brien, E.J, "Traffic Load Modelling and Factors Influencing the Accuracy of Predicted Extremes", Canadian Journal of Civil Engineering, Vol. 32, pp. 270-278, 2005.

IBSBI 2011, October 13-15, 2011, Athens, Greece

BRIDGE HEALTH MONITORING TECHNIQUES
Integrating Vibration Measurements and Physics-based Models

Dimitra-Christina Papadioti[1], Costas Papadimitriou[2]
and Panagiotis Panetsos[3]

[1,2] University of Thessaly, Dept. of Mechanical Engineering, Greece
[3] Egnatia Odos S.A., Capital Maintenance Department, Greece
e-mail: dxpapadioti@uth.gr, costasp@uth.gr, ppane@egnatia.gr

ABSTRACT: A structural health monitoring (SHM) system, integrating vibration measurements and physics-based finite element (FE) models, is reviewed and the importance of FE model updating techniques is emphasized. Novel methods to speed up computations in SHM systems are presented, including the integration of component mode synthesis techniques into existing state-of-the-art FE model updating methods. The developed methodology is illustrated using selected applications from instrumented bridges of the Egnatia Odos motorway.

KEY WORDS: Structural monitoring; Structural identification; Model updating; Damage detection; Bayesian inference.

1 INTRODUCTION

Vibration measurements from bridges can be used to understand the dynamic behavior of the various bridge components (superstructure, soil, bearings, dampers) and their interaction under actual operational conditions, estimate the dynamic characteristics of bridges, assess the mechanisms activated under the different vibration levels experienced by the bridge, validate or improve modeling procedures, select the most appropriate models for the bridge components, calibrate the parameters of the selected finite element (FE) models, assess structural damage (detect, identify location and severity of damage), quantify and propagate uncertainties in structural performance predictions, estimate damage accumulation due to fatigue in the entire body of steel bridges [1], as well as predict the remaining lifetime of bridge components under uncertainty. An effective bridge monitoring system requires the development of computationally efficient techniques and specialized software that integrates information from physics-based mathematical models of bridge components with the information collected from vibration measurements under various operational conditions, including normal operation under the action of everyday traffic loads, wind loads and environmental effects (e.g. temperature), as well as sudden extreme events such as moderate to strong earthquakes or strong winds.

This work reviews structural health monitoring techniques based on FE models. It concentrates on FE model updating techniques for damage detection, localization and severity. Novel algorithms to speed up computations in SHM systems are presented that integrate component mode synthesis (CMS) techniques with existing state-of-the-art FE model updating methods.

2 HEALTH MONITORING TECHNIQUES

2.1 Overview

Successful health monitoring of structural systems depends to a large extent on the integration of cost-effective intelligent sensing techniques, accurate physics-based computational models simulating structural behaviour, effective system identification methods, sophisticated health diagnosis algorithms, as well as decision-making expert systems to guide management in planning optimal cost-effective strategies for system maintenance, inspection and repair/replacement. Structural integrity assessment of highway bridges can in principle be accomplished using continuous structural monitoring based on vibration measurements. Taking advantage of modern technological capabilities, vibration data can be obtained remotely, allowing for a near real-time assessment of the bridge condition. Using these measurements, it is possible to identify the dynamic modal characteristics of the bridge and update a theoretical FE model. The results from the identification and updating procedures are useful to examine structural integrity after severe loading events (strong winds and earthquakes), as well as bridge condition deterioration due to long-term corrosion, fatigue and water scouring.

Algorithms and graphical user interface (GUI) software has been developed for monitoring the condition of bridges [2]. The bridge SHM system combines information from FE structural models representing the behaviour of bridges and vibration measurements recorded using an array of sensors. It incorporates algorithms related to (1) modal identification from ambient and earthquake-induced vibrations, (2) finite element model validation and updating based on identified modal properties, and (3) structural damage detection and identification based on finite element model updating.

2.2 Identification of modal models

Experimental modal identification algorithms for bridges process either ambient or earthquake-induced vibrations in order to identify the modal characteristics. In the SHM system, the modal characteristics are used as damage detection indices. Also, they are used to validate and update FE models and to identify the location and severity of damage. A brief overview of modal identification methods is given in [2-3]. Recent efforts have been concentrated on developing algorithms and GUI software for automated modal identification based on ambient vibrations with minimum user interference (e.g. [4-5]). As part of the proposed bridge monitoring system, GUI software has also been developed from the University of Thessaly group for computing the modal properties by processing either ambient or earthquake acceleration recordings [2].

2.3 Finite element model validation and updating

FE model updating methods based on modal data are used to develop high fidelity models so that predictions are consistent with measured data. The need for model updating arises because there are always assumptions and numerical errors associated with the process of constructing a theoretical model of a structure and predicting its response using the underlined model. Moreover, model updating methodologies are useful in predicting the structural damage by continually updating the FE models using vibration data [6-8]. Such updated models obtained periodically throughout the lifetime of the structure can be further used to update the response predictions and lifetime structural reliability based on available data [9]. Graphical user interface software has been developed from the University of Thessaly group as part of the bridge monitoring system for automating the FE model updating process using various modal-based model updating methodologies [10]. The software interfaces with the commercial COMSOL Multiphysics [11] software that provides the necessary finite element modeling tools.

2.4 Damage identification/localization

A framework for damage identification has been introduced in [8] and has been applied to bridge SHM in [12]. The damage detection algorithm is based on reconciling FE models with data collected before and after damage using a Bayesian methodology for selecting a model class from a family of competitive parameterized model classes. The Bayesian methodology is outlined in [8,12] based on measured modal characteristics. The structural damage identification is accomplished by associating each parameterized model class in the family to a damage pattern in the structure, indicative of the location of damage. Using the Bayesian model selection framework, the probable damage locations are ranked according to the posterior probabilities of the corresponding model classes. The severity of damage is then inferred from the posterior probability of the model parameters derived for the most probable model class. Based on asymptotic approximations, the damage diagnosis involves solving a series of FE model updating problems for each model class in the family.

The effectiveness of the methodology depends on several factors, including (a) model classes and parameterization (number and type of parameters) that are introduced to simulate the possible damage scenarios, (b) type, location and magnitude of damage or damages in relation to the sensor network configuration and (c) model and measurement errors in relation to the magnitude of damage. At least one member in the family of model classes should contain the actual damage scenario, otherwise the damage prediction from the methodology is ineffective. Measurements should contain adequate information for simultaneously identifying all model classes introduced for monitoring possible damage scenarios. Damages of small magnitude in relation to model error and measurement noise may be hidden and difficult to be identified. Damage predictions can be improved by introducing high fidelity finite element model classes and estimation algorithms that provide more accurate values of the modal characteristics.

3 EFFICIENT COMPUTATIONAL TECHNIQUES

3.1 Computational requirements for FE model updating and SHM

Finite element (FE) model updating techniques based on modal measurements are often formulated as single or multi-objective optimization problems. The objectives are related to the modal residuals that measure the discrepancies between the measured and the FE model predicted modal characteristics (modal frequencies and mode shapes). Non-gradient and gradient-based optimization algorithms are used to compute the optimal solutions based on the measured data. These iterative algorithms require repeated solutions of the FE model for various values of the model parameters. Gradient-based optimization algorithms also require repeated computation of the gradients of the modal characteristics (frequencies and mode shapes) involved in the residuals. For high fidelity FE models with very high number of degrees of freedom, of the order of millions, repeated solutions of the modal characteristics and the gradients of the FE models are computationally very demanding. Dynamic reduction techniques can be incorporated in the finite element model updating formulation to alleviate the computational burden. In particular, component mode synthesis methods (CMS) [13] can be used to substantially reduce the number of generalized coordinates by several orders of magnitude.

3.2 Integration with CMS methods

CMS methods are well suited methods for substantially reducing the number of generalized coordinates and consequently the computational effort required for solving iteratively the single- and multi-objective optimization problems. CMS techniques divide the structure into sub-structural components with mass and stiffness matrices that are reduced using fixed-interface and constrained modes. Exploiting certain parameterization schemes often encountered in FE model updating, it can be shown that CMS allows the repeated computations to be carried out efficiently in a significantly reduced space of generalized coordinates [14], avoiding the repeated solution of the fixed-interface and constrained modes and the assembling of reduced system matrices for each function evaluation involved in the iterative process.

Specifically, for structural components behaving linearly, an efficient model updating technique arises for component mass and stiffness matrices that depend linearly on only one of the free model parameters to be updated. In this case the reduced mass and stiffness matrices of a component also depends linearly on the free model parameter, allowing significant computational savings to be achieved during optimization by avoiding the repeated computation of the fixed-interface and constrained modes of each component during the iterative process [14]. Using the resulting linear representation of the assembled mass and stiffness matrices of the reduced system in terms of the model parameters, computationally efficient algorithms [15] can be used to further reduce the computational cost involved in estimating the gradients and Hessians of the objective functions representing the modal residuals

4 APPLICATIONS

4.1 Health monitoring of Egnatia Odos Motorway bridges

A SHM system has been implemented on ten Egnatia Odos motorway bridges, instrumented by accelerometer networks and continuousely monitored for structural evaluation and maintenance purposes by the Bridge Maintenance Unit of Egnatia Odos S.A. These bridges include from East to West: Γ2 Kavala bridge, Γ9 and Γ10 Polymylos bridges, Γ1, Γ7, Γ8 bridges in Malakasi A-C motorway section, Metsovo bridge, T9 Peristeri bridge, Γ4 Krystallopigi Bridge and Mesovouni bridge. Recently, detailed high fidelity FE models based on solid tetrahedral elements have been developed for five of these bridges in an effort to improve the modelling of the bridges and the reliability of the SHM system. Bridge soil-foundation-structure interaction has been included in the modelling. In addition, nonlinearities manifested in structural components, such as bearings and dampers, under larger amplitude response can also be incorporated in the modelling. The sources of complexities in the FE modelling are the nonlinearities, activated under moderate and strong earthquake excitations, and the very large number of DOFs, of the order of hundred of thousands or even millions, due to the high fidelity FE models required for reliable SHM results. The CMS technique is a computationally efficient tool to handle these linear and nonlinear models for finite element model updating and SHM by reducing the large number of DOFs to a very small number.

4.2 FE model updating and SHM of Metsovo bridge

An application on the Metsovo bridge shown in Figure 1 is used to demonstrate the computational efficiency and accuracy of the reduced models in CMS-based FE model updating and SHM methodologies. The Metsovo bridge is the highest reinforced concrete bridge of Egnatia Motorway, with the height of the taller pier M2 equal to 110m. The total length of the bridge is 537m. The bridge has 4 spans, of length 44,78m, 117,87m, 235,00m, 140,00m and three piers of which pier M1, 45m high, supports the boxbeam superstructure through pot bearings (movable in both horizontal directions), while M2 and M3 piers (110m and 35m, respectively) connect monolithically to the superstructure and are founded on huge circular Ø12,0m rock sockets in the steep slopes of the Metsovitikos river, in a depth of 25m and 15m, respectively.

The commercial software package COMSOL Multiphysics [11] is used for developing the FE models of the bridge. The models were constructed based on the design plans, the geometric details and the material properties of the structure. Soil structure interaction is neglected in the present analyses. If needed, the soil can also be modeled by FEs or simplified spring models and be included as an extra component on the FE modeling. Detailed FE models for the bridge are created using three-dimensional tetrahedron solid FE to model the whole structure. An extra coarse mesh and quadratic Lagrange elements are chosen to predict the lowest 20 modal frequencies and mode shapes of the bridge. The selected size of the elements in the extra coarse mesh is the maximum possible one that can be considered, corresponding to the order of the thickness of the deck cross-section. The selected FE model, shown in Figure 2, has 563,586 DOFs. For demonstration purposes, the bridge is divided into fifteen physical components shown in Figure 3. Nine components are related to the four spans of the bridge, three components relate to the three piers, while the last three components relate to the head of the piers. The components associated with the piers also include the foundation of each pier. The retained modes per component and interface are based on the value of the component fixed-interface modal frequencies and interface constrained modal frequencies. Modes with modal frequencies less than $\rho\omega_c$ are retained, where ω_c is the cut off frequency selected to be the 20th modal frequency for the whole structure that is of interest in our present application. The number of internal and

Figure 1. Metsovo bridge

Figure 2. FE model (563,586 DOFs)

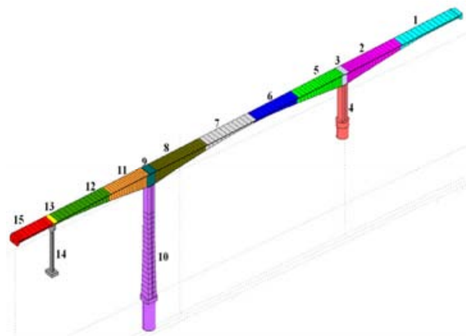

Figure 3. Substructuring (15 Components)

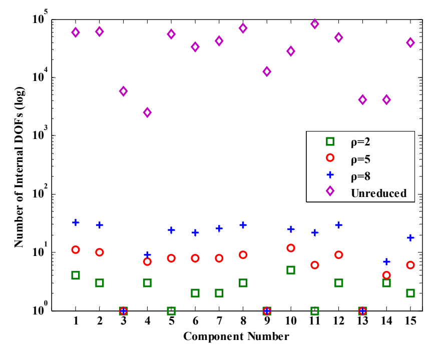

Figure 4. Number of GC per component

boundary DOFs along with the number of retained modes per component for three representative values of ρ=8, 5 and 2 are shown in Figure 4.

The finite element model is parameterized using seven parameters. The first four parameters θ_1 to θ_4 account for the stiffness of the four deck components, while the next three parameters θ_5 to θ_7 account for the stiff\ness of the piers of the bridge. The parameters scale the nominal values of the properties that they model so that the nominal finite element model corresponds to values of $\theta_1 = \cdots = \theta_7 = 1$. The model updating is performed using 10 measured modes. Measured modal frequencies and mode shapes are simulated from the nominal FE model and are used for FE model updating. In order to examine the computational efficiency and the effectiveness of the proposed reduction techniques, results for the retained number of generalized coordinates and the achieved error between the estimated optimal model parameters and the exact values of the model parameters are given in Table 1. It is clear that extremely accurate results can be achieved by reducing the number of DOFs by more than three and even four orders of magnitude.

Table 1. Generalized coordinates (GC) and error in parameter estimates

	Reduction in Internal DOFs only	Error (%)	Reduction in Internal & Boundary DOFS	Error (%)
Full Model	563,586	0.00	563,586	0.00
Retained ρ=8	8,325	0.00	360	0.00
Retained ρ=5	8,150	0.10	155	0.10
Retained ρ=2	8,084	1.00	66	1.00

5 CONCLUSIONS

The proposed CMS techniques allow one to efficiently handle detailed linear and nonlinear high fidelity computational models of bridge components and thus improve damage identification capabilities in FE model-based SHM methodologies. The SHM framework can be used by highway managing authorities as part of an intelligent bridge management system to provide information useful for bridge monitoring and integrity assessment.

ACKNOWLEDGMENTS

This research was co-funded by the European Union (European Social Fund) and the Greek Ministry of Education, Lifelong Learning and Religious Affairs in the context of «Hrakleitos II» of the Operational Programme «Education and Lifelong Learning » (NSRF 2007-2013).

REFERENCES

[1] Papadimitriou, C, Fritzen, CP, Kraemer, P, Ntotsios, E, "Fatigue Predictions in Entire Body of Metallic Structures from a Limited Number of Vibration Measurements using Kalman Filtering." Structural Control and Health Monitoring, n/a. doi: 10.1002/stc.395, 2010.

[2] Ntotsios, E, "Structural Identification of Complex Structures based on Vibration Measurements", *Ph.D. Thesis*, Dept. of Mechanical Eng., Univ. of Thessaly, 2009.

[3] Ntotsios, E, Karakostas, Ch, Lekidis, V, Panetsos, P, Nikolaou, G, Papadimitriou, C, Salonikos, T, "Structural Identification of Egnatia Odos Bridges based on Ambient and Earthquake Induced Vibrations", Bull. of Earthquake Eng., Vol. 7, No. 2, pp. 485-501, 2009.

[4] Verboven, P, Cauberghe, B, Parloo, E, Vanlanduit, S, Guillaume, P, "User-assisting Tools for a Fast Frequency-Domain Modal Parameter Estimation Method", Mechanical Systems and Signal Processing, Vol. 18, No. 4, pp. 759–780, 2004.

[5] Peeters, B, Van Den Branden, B, Laquiere, A, De Roeck, G, "Output-only modal analysis: development of a GUI for Matlab", *Proceedings of IMAC 17*, Kissimmee, FL, USA, pp. 1049-1055, 1999.

[6] Teughels, A, De Roeck, G, "Damage Detection and Parameter Identification by Finite Element Model Updating", Archives of Computational Methods in Engineering, Vol. 12, No. 2, pp. 123-164, 2005.

[7] Fritzen, CP, Jennewein, D, Kiefer, T, "Damage Detection based on Model Updating Methods", Mechanical Systems and Signal Processing, Vol. 12, No. 1, pp. 163-186, 1998.

[8] Papadimitriou, C, "Bayesian inference applied to structural model updating and damage detection", *9th ASCE Joint Specialty Conference on Probabilistic Mechanics and Structural Reliability*, Albuquerque, New Mexico, 2004.

[9] Papadimitriou, C, Beck, JL, Katafygiotis, LS, "Updating Robust Reliability Using Structural Test Data", Probabilistic Engineering Mechanics, Vol. 16, No. 2, pp. 103-113, 2001.

[10] Christodoulou, K, Papadimitriou, C, "Structural Identification based on Optimally Weighted Modal Residuals", Mechanical Systems and Signal Processing, Vol. 21, pp. 4-23, 2007.

[11] COMSOL AB, *COMSOL Multiphysics User's Guide*, 2005 [http://www.comsol.com/].

[12] Ntotsios, E, Papadimitriou, C, Panetsos, P, Karaiskos, G, Perros, K, Perdikaris, PC, "Bridge Health Monitoring System based on Vibration Measurements", Bulletin of Earthquake Engineering, Vol. 7, No. 2, pp. 469-483, 2009.

[13] Craig Jr, RR, Bampton, MCC, "Coupling of Substructures for Dynamic Analysis, AIAA Journal, Vol. 6, No. 7, pp. 678–685, 1965.

[14] Papadioti, DC, Papadimitriou, C, "Finite element model validation and predictions using dynamic reduction techniques", *COMPDYN 2011*, M. Papadrakakis, M. Fragiadakis, V. Plevris (eds.), Corfu, Greece, 2011.

[15] Ntotsios, E, Papadimitriou, C, "Multi-objective optimization algorithms for finite element model updating", *ISMA2008*, Leuven, pp. 1895-1909, 2008.

BRIDGE-VEHICLE INTERACTION ANALYSIS BASED ON MICROWAVE RADAR INTERFEROMETRY
An Experimental Investigation of Evripos Cable-Stayed Bridge

Vassilis Gikas[1], Stamatis Daskalakis[2], Thanassis Mpimis[3]

[1,2,3] National Technical University of Athens, School of Rural and Surveying Engineering, Greece
e-mail: vgikas@central.ntua.gr, stamdask@gmail.com, ampimis@central.ntua.gr

ABSTRACT: This paper examines the use of microwave radar interferometry technology to study the dynamic response of Evripos cable-stayed bridge (Greece) due to vehicular traffic. Analysis of the results provides detailed displacement time-histories and resonance frequencies obtained for the deck and the towers associated with individual heavy vehicle traffic events.

KEY WORDS: Bridge vehicle interaction; Displacement; Radar; Interferometry.

1 INTRODUCTION

Enhanced by the rapid expansion of bridge systems and the fast increase of both ordinary and exceptional traffic loads, research on the dynamic response of bridges under moving vehicles has been booming in the past two decades [1]. Traditionally, monitoring the dynamic response of bridges caused by vehicular traffic was performed using networks of accelerometers and more recently fiber-optic sensors [2, 3, 4, 5]. Also, in the last fifteen years extensive research has been undertaken in the use of Global Positioning System (GPS) which has led to the development of rather integrated and automated monitoring systems [4, 6]. In fact, some very recent configurations employ GPS antennas attached on the top of towers or even directly on the suspension cables [6]. Such systems, notwithstanding they are accurate and reliable they need to be placed in close contact to the structure; besides, they measure the impact response of the structure at a limited number of points. In addition to these methods, other approaches based on optical / digital close-photogrammetric principles have been recently deployed [7]. These systems can operate remotely; however, scale and atmospheric effects might constrain their use depending on the specific geometry characteristics of a structure.

In this paper we present a new measurement technique and a system which rely on the microwave interferrometric principle. The proposed method allows ultra-high accuracy displacement measurements in real-time, at long sensing distances and a high sampling rate. In this article, the method is used to study the dynamic behavior of Evripos cable-stayed bridge (Greece) due to heavy vehicle traffic.

2 MICROWAVE RADAR INTERFEROMETRY

2.1 Background and Principles of Operation

The working principle of ground-based microwave radar systems relies on the interferometric technique. This technique allows the computation of object displacement using the phase variation information measured by a radar sensor from repeated electromagnetic pulse transmissions [8]. Originally, the method was applied to map terrain elevation movements of large areas using imagery collected over time by radar systems placed onboard aircraft or satellite platforms. The same principle has recently applied in ground-based radar systems to measure the displacements of structures and physical processes [8].

A key feature of these systems is the very high (<1 m) range resolution for any observation distance lying within the operational limits of the sensor. This is important as it allows performing high resolution displacement measurements at both short and long operating distances. To achieve such a high distance resolution the system used in this paper (IBIS-S) employs a special wave transmission technique known as Stepped Frequency - Continuous Wave (SF-CW) technique. According to this approach the radar sensor emits a series of long duration electromagnetic waves at different frequencies [8]. Notably, in a similar manner to satellite interferometry, ground-based systems can measure displacements in the sensor viewing direction (radial displacements). Therefore, in order to produce projected displacements the geometric layout that defines an observation scenario should be resolved and taken into account.

2.2 IBIS-S Radar System

The IBIS-S system (Image By Interferometric Survey) is a coherent microwave radar system produced by IDS SpA capable to measure remotely dynamic displacements with high sampling frequency (up to 200 Hz) and ultra-high accuracy (up to 1/100 mm) [8, 9]. Its performance depends on the configuration used (type of antennas) and operational conditions (such as observation geometry setup and reflectivity of illuminated object). In contrast, the impact of atmospheric conditions on measurements is minimal due to the dynamic nature of observations. Also, the short observation times (usually 10-30 min) and the moderate (up to 500 m) distances involved render the system practically invulnerable to atmospheric influences. Nevertheless, in case the system is operated in static mode then, atmospheric conditions will affect raw measurements. This mode of operation is however beyond the scope of this paper.

The IBIS-S system allows direct, real time measurement of displacements in practically all whether conditions with no need to access the test site. The system has been designed to reach a range resolution of 0.75 m independently of observation distance thanks to SF-CW electromagnetic wave propagation technique.

3 TEST SITE AND FIELD MEASUREMENTS

3.1 Description of Evripos Cable-Stated Bridge

The Evripos cable-stated bridge is located nearby the town of Chalkis in Central Greece. It is a concrete made roadway bridge that crosses Evripos channel between the island of Evia and the mainland of Greece. The bridge is formed by a central span of 215 m and two back spans of 90 m each. The total bridge length is 695 m. Its deck is 12.6 m wide and only 0.45 m thick – probably, the thinnest concrete bridge deck in Europe. The deck is suspended from 72 pairs of cables, arranged in a semi-fan and connected to two H-shaped concrete towers of a total height 90 m.

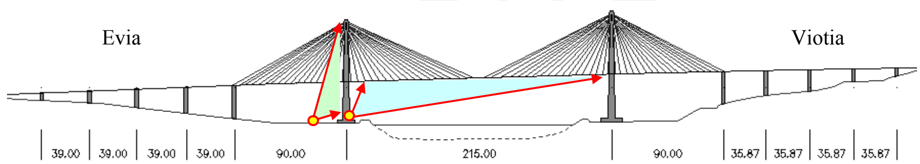

Figure 1. Interferometric Radar observation geometry scenarios

3.2 Experimental Scenarios and Data Collection

In order to study the dynamic behaviour of Evripos bridge a number of sets of measurements were undertaken implementing various observation scenarios. This study shows the results obtained from the displacement analysis of the recordings of the bridge deck and the towers that relate to a number of selected individual heavy vehicle traffic events. More specifically, two experimental scenarios are considered (*Fig. 1*).

The first observation scenario includes monitoring the bridge deck for a total time period spanning 84 min of continuous measurements. The focus in the analysis of this test relies on the kinematics of the mid-span of the bridge for a number of heavy vehicle traffic events of various characteristics. In this working scenario the radar sensor was setup as shown in *Fig. 2* so that, the central span of the bridge was within the field of view of the instrument. The aim of the second experiment is to study the displacement and spectral frequency characteristics of a limited number of points lying at the upper part of the towers caused due to individual heavy truck vehicles crossing the bridge. For this purpose the radar sensor was setup at a close distance from the basement of the tower, facing upwards. A dataset of 22 min of continuous observations was acquired.

Figure 2. IBIS-S sensor setup during the bridge deck monitoring scenario

In order to identify and classify individual traffic events in the radar measurements and to assist interpretation of the results obtained, the structure was video recorded for the whole duration of the experiments. A high resolution video camera was setup to operate from a suitably selected location depending on the observation scenario. Also, a total station survey was undertaken to obtain some critical dimensions of the structure and to reconstruct the observation geometry between the IBIS-S sensor and the structure. This information is necessary during data analysis in order to reduce the observed displacements into their projected (horizontal and vertical) equivalents.

4 DATA ANALYSIS AND DISCUSSION

4.1 Dynamic Behavior of the Deck

This experimental scenario examines the deflection response of the mid-span cross-section of the bridge against individual (i.e. only a single heavy vehicle crossing the bridge at a time) heavy vehicle traffic events. The central cross-section is located at 105.7 m from each of the towers and corresponds to radar range bin 111. *Fig. 3* shows the vertical displacements observed at the middle of central span for a small (160 sec) subset of data. As can be seen from this plot there exists a number of distinctly peak settlement values ranging from 10 mm to 50 mm that appear to be associated with individual traffic events. This observation is fully justified by examining this diagram in combination with *Table 1*. This Table contains a summary record (based on the video camera information) of all heavy vehicle events observed for the same time interval shown in *Fig. 3*. Cross-examination of the video camera time recordings against the peak displacement times (observed by the radar sensor) reveals an agreement of the order of 1 sec (which equals the resolution of video camera clock). Interestingly, the magnitude of midpoint settlements shows a perfect agreement with type (and thus to a certain extend weight) of passing vehicles – for instance, the displacement caused by a small truck (event no 7) is observed to be seven times less (~ 7 mm) compared to the displacement (~ 50 mm) caused by a very heavy truck (event no 1). Obviously, based on this dataset alone, is not easy to reach concrete conclusions about the displacement effects that certain types of vehicles shall impose on the bridge. This is because no information about the actual weight (tare and payload) of passing trucks is available; besides, this test was undertaken under normal traffic conditions and therefore, passenger vehicle traffic shall influence end-results.

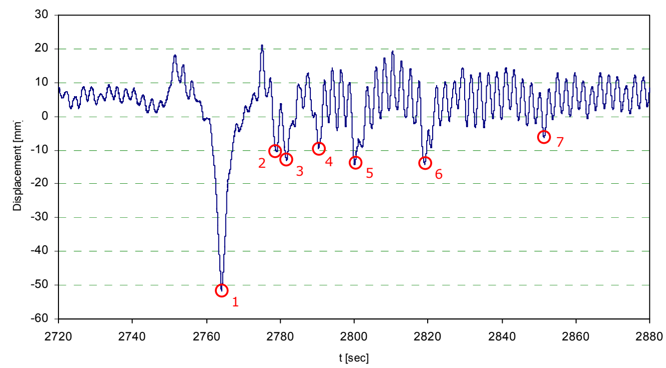

Figure 3. Vertical displacements at the middle of central span for the sample period of Table 1

Table 1. Time information and classification of heavy vehicle traffic events (E: Evia, V: Viotia)

Event No	t [sec]	vehicle type	direction
1	2763	Very heavy truck	E → V
2	2777	Heavy truck	E → V
3	2781	Pullman	V → E
4	2789	Heavy truck	E → V
5	2800	Tow truck	E → V
6	2818	Heavy truck	V → E
7	2850	Truck	E → V

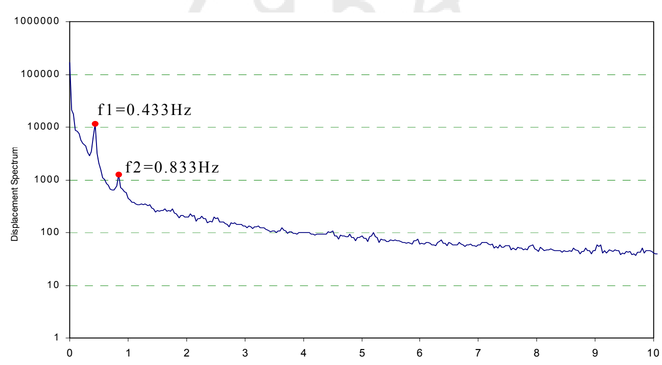

Figure 4. Frequency response of mid-span cross-section (D= 0+105.7 m)

Contrary to displacement computations, frequency analysis is independent of actual weight load. *Fig. 4* shows the frequency analysis response of the mid-span cross-section obtained from the processing of the entire dataset (i.e. 84 min). This diagram reveals a vibration pattern in which two dominant oscillation frequencies (f_1= 0.433 Hz, f_2= 0.833 Hz) clearly prevail.

Table 2. Video snapshots, direction of travel and tower displacements for two traffic events

event	t [sec]	vehicle	direction	width [mm]	Video capture
1	768	Very heavy truck	E → V	7.5	
2	897	Very heavy truck	V → E	7.3	

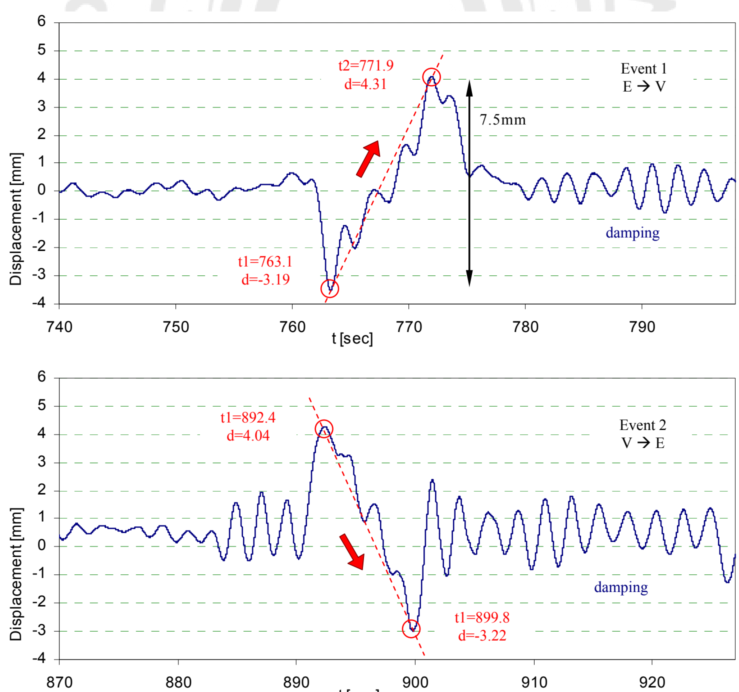

Figure 5. Horizontal displacements observed at tower (H= +72.2 m) for the scenarios of Table 2

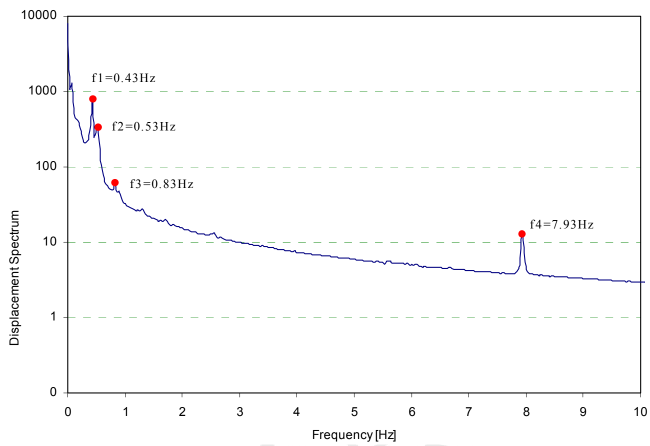

Figure 6. Frequency response of tower (H=+72.2 m)

4.2 Dynamic Behavior of the Towers

This second experimental test aims to assess the kinematics of the bridge towers due to individual (i.e. only a single heavy vehicle crossing the bridge at a time) traffic events. For this purpose heavy vehicle traffic was classified into categories according to axle number and direction of travel. In this study, two characteristic examples of very heavy truck vehicles traveling at opposite directions are considered. *Table 2* contains summary information of both traffic events. More specifically, it contains direction of travel and time information that relates to the time instant that both vehicles pass through the tower located on the Evia island side. Also, it reports the maximum absolute horizontal displacement observed for each case, at a tower level +72.2 m above the basement (range bin 82). Notably, displacement values of 7.5 mm and 7.3 mm are observed respectively. However, examination of the time series displacements for the two events leads into some very interesting conclusions. *Fig. 5* shows the horizontal displacements observed for the time intervals required each of the vehicles to cross the bridge from lateral span to lateral span. From the analysis of this plot two points are immediately evident.

Firstly, a linearly increasing or decreasing displacement pattern is observed depending on the direction of travel. Secondly, the midpoint time (defined as the middle time between peak to peak displacements) computed for both traffic events coincides with the video camera time recordings for which both vehicles traveled through the tower (see *Table 2*). This observation reveals clearly an ideal symmetric behavior in the dynamic displacements observed on the tower as a function of the vehicle location from the tower – suggesting that the tower is consistently yields towards the side of the moving vehicle. The final point to make from *Fig. 5*, relates to the displacement pattern observed just before the vehicle enters and after it leaves the part of deck which restricted by the outer cable locations attached to the tower (i.e. semi-fan span distance). More specifically, note the displacement pattern in the top plot of *Fig. 5* for the time intervals δt1 [755-765] sec and δt2 [775-790] sec. During time interval δt1 the vehicle travels on the approach span from Evia to Viotia and thus, no significant movements are observed. In contrast, during time interval δt2 the vehicle travels on the mid-span (towards Viotia) and thus, some residual movements are still evident. Finally, in a similar manner to Section 4.1, *Fig. 6* depicts the frequency response of the same point (+72.2 m / range bin 82) computed using all available observations (i.e. 22 min). This plot suggests that the tower exhibits a complex vibration pattern in which four primary oscillation frequencies are evident. Interestingly, harmonic frequencies f_1 and f_3 coincide with those observed for the deck analysis.

5 CONCLUSIONS

In this paper a microwave remote sensing technique was applied to measure the dynamic deflections of Evripos cable-stayed bridge caused by individual traffic events. Analysis of the results revealed maximum settlements and horizontal displacements at the mid-span cross-section and towers of the order 50 mm and 7.5 mm respectively. Frequency analysis exhibits a composite vibration pattern characterized by two and four dominant frequencies for the deck and towers respectively.

REFERENCES

[1] Yang, YB, Yau, JD, Wu, YS, *Vehicle-Bridge Interaction Dynamics - With Applications to High-Speed Railways*, World Scientific, 2004.

[2] Erol, B, “Evaluation of High-Precision Sensors in Structural Monitoring”, Sensors, Vol. 10 No. 12, pp. 10803-10827, 2010.

[3] Jingnan, L, “Progress in Deformation Monitoring for Dams, Bridges and Power Lines”, Annals of GIS, 1947-5691, Vol. 16, No. 2, pp. 81-90, 2010.

[4] Yigit, CO, Li, X, Inal, C, Ge, L, Yetkim, M, “Preliminary Evaluation of Precise Inclination Sensor and GPS for Monitoring Full-Scale Dynamic Response of a Tall Reinforce Concrete Building”, Journal of Applied Geodesy, Vol. 4, pp. 103-113, 2010.

[5] Radulescu, ATG, Radulescu, GMT, Radulescu, VMG, “Geometric Structural Monitoring in Kinematic Regime - Dynamic Surveying as Means to Assure a Structure Safety”, *Proc. FIG Congress 2010,* Sydney, Australia, April 11-16, 2010.

[6] Roberts, GW, Brown, CJ, Ogundipe, O, “Monitoring the Severn Suspension Bridge by GNSS”, *Proc. FIG Working Week*, Morocco, 18-22 May, 2011.

[7] Jiang, R, Jauregui, D, “Development of a Digital Close-Range Photogrammetric Bridge Deflection Measurement System”, Measurement, Vol. 43, No. 10, pp. 1431-1438, 2010.

[8] Gentile, C, “Radar-based Measurement of Deflections on Bridges and Large Structures: Advances, Limitations and Possible Applications”, *Proc. IV ECCOMAS Thematic Conference on Smart Structures and Materials*, 2009.

[9] Rödelsperger, S, Läufer, G, Gerstenecker, C, Becker, M, “Monitoring of displacements with ground-based microwave interferometry: IBIS-S and IBIS-L”, Journal of Applied Geodesy Vol. 4, pp. 41-54, 2010.

USING ROBOTIC THEODOLITES (RTS) IN STRUCTURAL HEALTH MONITORING

The Gorgopotamos Railway Bridge as a case study

Panos Psimoulis[1,2] , Elina Kokkinou[2], Nikitas Bazeos[2], Stathis Stiros[2] and Dimitris Karabalis[2]

[1]currently Post-Doc Fellow in Geodesy and Geodynamic Lab., ETH Zurich
[2]University of Patras, Dept. of Civil Engineering, Greece
e-mail: panospsimoulis@ethz.ch; elinakokkinou@hotmail.com; bazeos@upatras.gr; stiros@upatras.gr; karabali@upatras.gr

ABSTRACT: The deflections of the middle of a 30-m long span of the historical Gorgopotamos Bridge in central Greece were measured using RTS. Statistically significant deflections of the order of ±6-7mm, above the noise level of ±2mm were found only for the vertical axis, and they were analysed in semi-static and dynamic components, consistent with those derived from FEM analysis. RTS measurements permit a self-assessment of their accuracy and are likely to represent a powerful tool in structural health monitoring.

KEY WORDS: Railway Bridge; RTS; Deflection; Monitoring; Measurements.

1 INTRODUCTION

The measurement of the dynamic displacements of bridges is necessary for their design, operation and the evaluation of their structural health and of their post-repair performance [1],[2],[3],[4]. Still, this is a quite difficult task, for till recently no instruments permitting accurate measurements of displacements relative to a coordinate system independent of the bridge were available, as is the case with geodetic techniques. Only in the last decade GPS has been used to measure displacements of flexible bridges [5] and more recently of stiff bridges [6].

The Robotic theodolite (RTS) is another geodetic instrument that permits to measure displacements relative to a fixed coordinate system, and its major advantage is that it can be used in areas of limited or of no view of satellites.

In this article we show that RTS can be used not only for monitoring of displacements of long, cable stayed bridges [5], but also of short-span, stiff bridges. As an example we present a summary of measurements of the displacements of the Gorgopotamos Bridge in central Greece, excited by passing trains. The importance of this study is threefold. First, this is a historical bridge, destroyed and repaired twice, and its dynamic characteristics are really unknown. Second, its openings are up to around 30m, and hence it represents a very unfavorable case, practically testing the limits of application of the RTS. Third, we present a methodology which is not limited to certain measurements, but also permits assessment of their accuracy.

2 THE GORGOPOTAMOS RAILWAY BRIDGE

The Gorgopotamos Railway Bridge is located about 150km northwest of Athens, in central Greece, and was constructed in 1905. The bridge was destroyed and rebuilt twice during Second World War (Fig.1). The first destruction was in 1942 and after its reconstruction in 1943, it was destroyed again in 1944. The bridge was reconstructed again in 1948 and since then is still in use.

The bridge has total length of 211m and 32m maximum height. It is curved in plan, consisting of seven sub-linear spans of approximate length of ~30m, which are supported by six pylons. The bridge is a composite structure with a truss deck, two steel pylons (M_1, M_2) and four masonry pylons (M_3-M_6); see Figure 1.

It is obvious that due to the partial reconstruction, the dynamic characteristics of the bridge differ from the initial design. There is however evidence of significant oscillations of the bridge during the passage of trains, which are forced to reduced speed.

3 RTS- PRINCIPLES AND MEASUREMENT PROCESS

RTS is the evolution of the common total station. The instrument emits a ray which is reflected on a reflector fixed on the specific point is received back and analysed, and the instantaneous coordinates of the reflector are computed in a pre-defined coordinate system. RTS is also equipped with a servo-mechanism and an automatic target recognition device, permitting to lock on a specific

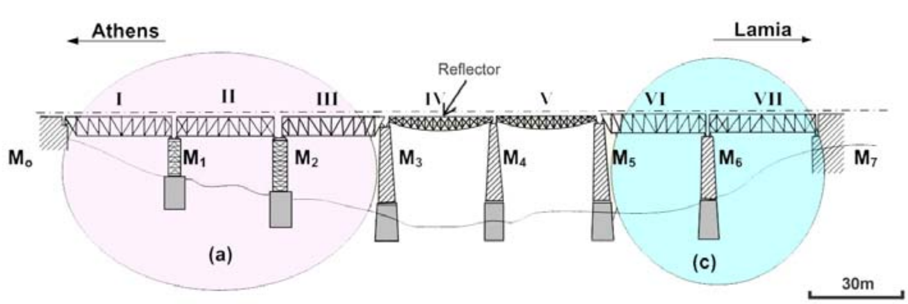

Figure 1. The Gorgopotamos Railway Bridge with area a and c indicating the destroyed parts of the Bridge in 1942 and 1944, respectively. Also the reflector position discussed in this article is indicated.

target, follow its movement and record its coordinates with a rate up to 10 Hz.

Basic requirements for accurate measurements are the visibility of the reflector, the absence of perturbations of the atmosphere along the raypath and the use of a high-quality prismatic reflector.

4 METHODOLOGY

The aim of this study was to estimate the deflection of the bridge caused by the passing trains. For this reason were focused on the midspan of an opening where the greatest displacements were expected.

The measurements were made before, during and after the passing trains. The measurement noise (uncertainty) was estimated based on the measurements of the intervals before and after the train passage, corresponding to intervals of no bridge excitation. Measurements during passing trains, corresponding to the train excitation intervals, were compared with the measurement noise, and if the signal of the excitation interval was larger than the noise, measurements corresponded to real displacements.

5 FIELD MEASUREMENTS

Our study was focused on measurements of the displacements of point R_3 at the midspan between pylons M_2-M_3 where maximum displacements was expected. This point was marked by a high-accuracy prismatic AGA-type reflector, fixed on the metallic bridge handrail. A Leica TCA 1201 RTS was set on stable ground at a distance of circa 150m from the reflectors, at a point permitting unobstructed view of the reflectors (Fig.2). Details on the use and the limitations of this instrument, and the solutions adopted to obtain high-accuracy data, useful for structural analysis are described in [7] and [8].

Independent dating of the excitation intervals using GPS as chronographs were also used.

Measurements during several trains of different type (passenger or freight), with different velocity and load were made. In this study we focus on the recordings of a 7-wagon freight train.

6 DATA ANALYSIS

Using a common linear transformation [7],[9] the recorded coordinates relative to a rather arbitrary system were transformed into coordinates in a system with the y-axis tangent to the railway at the observation point and x-axis normal to it. Then the mean value of the recordings from the intervals before and after the passing train was subtracted from each instantaneous coordinate. Thus three time series describing the apparent displacements along the longitudinal, lateral and vertical were obtained.

The next step was the determination of the interval of the passing train by combining the records of the chronographer, the GPS records and the RTS records. It was identified the time the train entered and left the bridge (solid lines, Fig.3) and the time interval the train was passing in front of the targets (dotted lines, Fig.3).

Figure 2. The Gorgopotamos Railway Bridge and in the foreground the RTS used for the measurements focusing on reflector R_3. An inset shows the prismatic reflector and on top of it the antenna of a GPS, used as a chronograph.

The measurement noise was estimated based on the data from the intervals before and after the passing train corresponding to no excitation interval. The data formed zones of amplitude ±1mm expressing the noise level of measurements. This amplitude was smaller than that defined from experiments, ±2mm [8], which, was however adopted as a pessimistic estimate.

Apparent displacements during the excitation interval were smaller than this value for the longitudinal and lateral axes, and hence expressed only measurement noise. On the contrary, those corresponding to the vertical axis were reaching to 6-7mm and hence they reflected real displacement of the bridge due to the train excitation.

7 ANALYSIS OF DEFLECTIONS

The vertical deflections of bridge during its excitation by the passing train were decomposed into a high-period and a low-period component, corresponding to semi-static and dynamic displacements [6],[7]. For the decomposition a moving

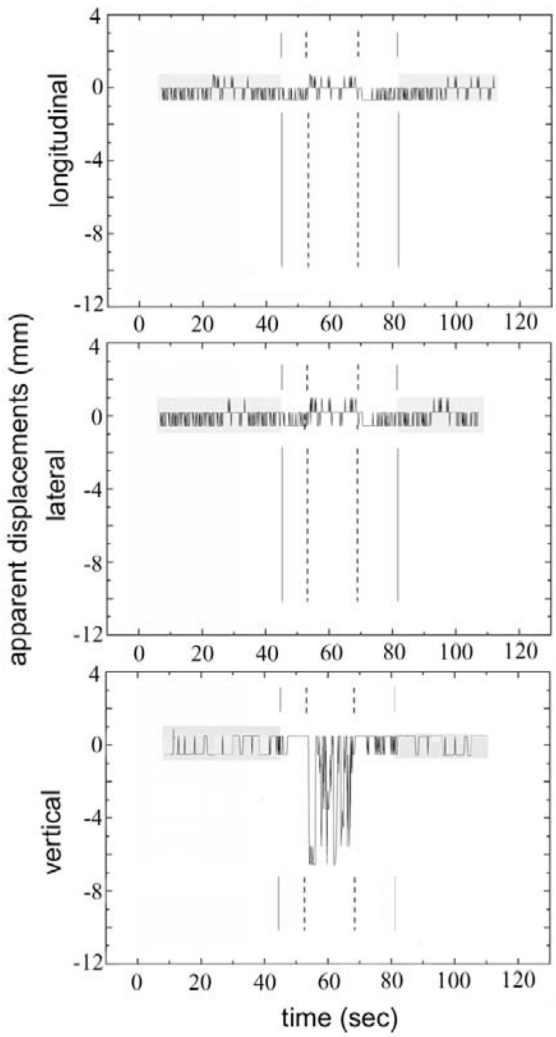

Figure 3. The time series of longitudinal, lateral and vertical axes corresponding to the excitation of the bridge by a 7-wagon passing passenger train. The vertical solid vertical lines define the interval of the passage on the bridge and the dotted ones the interval during which the train was passing in front of the current reflector. Grey zones indicate measurement noise, of maximum amplitude ±1mm. Only the time series of vertical axis reveals real displacement, larger than the noise, reaching up to 6-7mm.

average filter with step 21 and overlap 20 was used; a simple but efficient technique, as is analyzed elsewhere. Results are shown in Figure 4.

The high-period component has a trapezoid pattern representing a mean semi-static displacement of 3mm (horizontal dotted line). On the other hand the low- period component has a wave-form pattern, corresponding to an oscillation with mean amplitude ±4mm and very much consistent with that derived for other train bridges on the basis of FEM analysis [10].

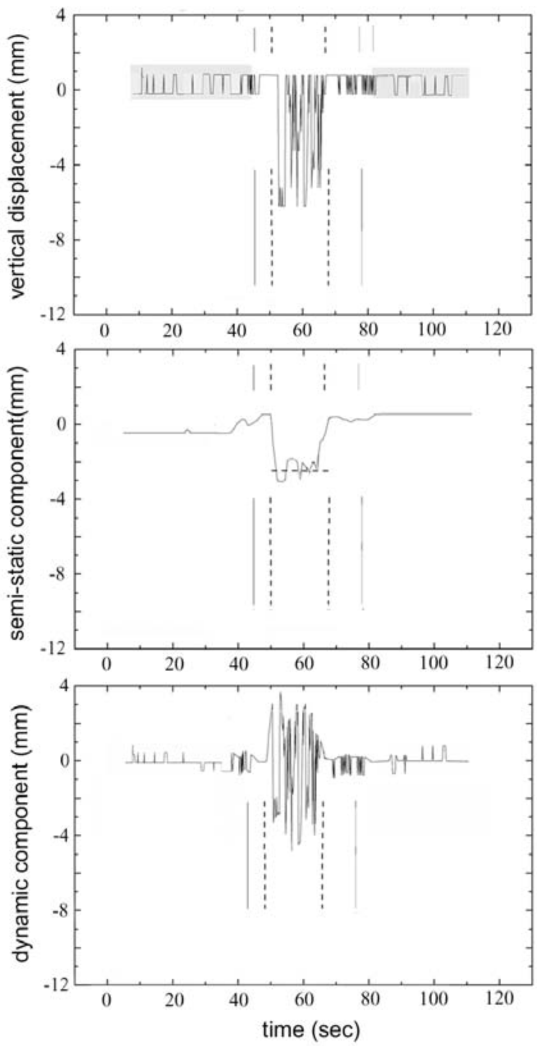

Figure 4. Decomposition of the apparent vertical displacements (top) into high (middle) and low-period components, corresponding to semi-static and dynamic displacements.

8 CONCLUSIONS

The output of this study is that RTS permitted to record the deflections of the midspan of a 30m long opening of the historical Gorgopotamos bridge when excited by a passing train. It was found that only the vertical deflections were significant (up to ±6-7mm), above the measurement noise (±1-2mm). The latter was defined by a comparison of recorded apparent displacements before, during and after the train passage, and experimental data, and indicates that the proposed method cannot only permit the measurement of small-amplitude deflections, but also an assessment of their accuracy.

Obtained results are consistent with FEM modeled deflections of bridges and indicate that RTS is a powerful in structural health monitoring.

ACKNOWLEDGMENTS

We are indebted to OSE SA, the Greek Railroad Company and especially to Mrs D. Spyropoulou, Mr. K. Tzanakakis and Mr. S. Kariotis for granting permission to study the Gorgopotamos Railway Bridge and for field support. Partial financial support through a research grant by the Greek Secretariat for Research and Technology (GGET) is acknowledged.

REFERENCES

[1] Borzi, B., Calvi, G.M., Elnashai, A.S., Faccioli, E., Bommer, J., «Inelastic spectra for displacement-based seismic design», Soil *Dynamics and Earthquake Engineering*, Vol. 21, 47-61, 2001

[2] Kim, H.S., Chun, Y.S., «Structural damage assessment of building structures using dynamic experimental data», *Structural Design of Tall and Special Buildings*, Vol. 13, 1-8, 2004

[3] Karavasilis, , T.L., Bazeos, N., Beskos, D.E. (2006). «Maximum displacement profiles for the performance based seismic design of plane steel moment resisting frames», *Engineering Structures*, 28(1), 9-22.

[4] Asimakopoulos, A.V., Karabalis, D.L. and Beskos D.E., «Inclusion of P-Δ effect in displacement-based seismic design of steel moment resisting frames», *Earthquake Engineering and Structural Dynamics,* Vol. 36, 2171-2188, 2007

[5] Lekidis V, Tsakiri M, Makra K, Karakostas C, Klimis N, Sous I., «Evaluation of dynamic response and local soil effects of the Evripos cable-stayed bridge using multi-sensor monitoring systems», *Engineering Geology*, Vol. 79, 43-59, 2005

[6] Moschas, F, Stiros, S., «Measurement of the dynamic displacements and of the modal frequencies of a short-span pedestrian bridge using GPS and an accelerometer». *Engineering Structures*, Vol. 33, 10-17, 2011

[7] Psimoulis, P. and Stiros, S., «Measurement of deflections and of oscillation frequencies of engineering structures using Robotic Theodolites (RTS)», *Engineering Structures*, Vol. 29, No. 12, 3312-3324, 2007

[8] Stiros, S. and Psimoulis, P., «Identification of near-shore wave characteristics using Robotic Total Station (RTS)», *Journal of Surveying Engineering* ASCE, Vol 136, No 4, 172-179, 2010

[9] Psimoulis, P.A. and Stiros, S., «Experimental assessment of the accuracy of GPS and RTS for the determination of the parameters of oscillation of major structures», *Computer-Aided Civil and Infrastructure Engineering*, Vol. 23, No. 5, 389-403, 2008

[10] Xia, H., and Zhang, N., «Dynamic analysis of railway bridge under high-speed trains», *Computers and Structures*, Vol. 83, 1891-1901, 2005

TOPIC 5

Long Span Bridges

Computational Techniques

A SIMPLIFIED ANALYSIS OF THE BEHAVIOR OF SUSPENSION BRIDGES UNDER LIVE LOAD

Leonidas T. Stavridis

National Technical University of Athens, Dept. of Civil Engineering, Greece
e-mail : stavrel@central.ntua.gr

ABSTRACT: The maximum response of the cable and the stiffening girder due to live load are determined, by means of an analytic procedure, considering the girder hinged at its ends. The problem of interaction between the cable and the stiffening girder is examined through the analogy to a fictitious tensioned beam under transverse load, whereby a closed –form solution is achieved by means of a simple quadratic equation. The behavior of the whole system is governed by four simple dimensionless parameters.

KEY WORDS: Suspension bridge; Stiffening girder; Static Analysis; Design.

1 INTRODUCTION

The present paper aims to provide a simple tool for the analysis of a suspension bridge on a purely analytical base, in order to determine the response of the cable and the girder under the action of the live load.

It is shown that the behavior of the whole system is governed by four dimensionless design parameters, The determination of the maximum static response of the system under the most unfavorable location of the live load for each specific case, is made possible using only the above four parameters, through a direct procedure easily programmable in a personal computer.

2 ANALYSIS

The earth anchored structural system is depicted in Fig.1, with one main span of length L and two equal side spans of length L_s . It is assumed, that the cable overrides the top of the towers without friction. The last assumption permits one to ignore in this context the influence of the deformation of the towers on the system's response.

The horizontal component H_g of the cable tensile force is appropriately calibrated with respect to the desired sag f , so that for the existing dead load g the deck takes an absolutely horizontal position. The same conditions also hold for the side spans of length L_s and cable sag f_s . According to the previous assumption it will be :

$$H_g = g*L^2/(8*f) = g*L_s^2/(8*f_s) \tag{1}$$

and consequently, as the two cable parts exhibit the same curvature, it must hold:

$$f_s = L \cdot \beta^2 \cdot \lambda \tag{2}$$

where $\beta = L_s / L$ and $\lambda = f / L$ (3)

The action of an additional live load p on the girder tends to deform the cable and this additional cable deflection η will be imposed exactly the same on the stiffening girder, due to the assumed inextensibility of the hangers. The resulting increase in cable force will be represented by its horizontal component H_p . The purpose of the analysis consists in determining both these quantities.
The girder is subjected to a total load $q(x)$, consisting of the permanent load g , a live load p acting on a specified length and the actions $q_c(x)$ of the hangers directed upwards which, due to the small distances of the hangers, can be considered as continuously distributed. It is :

$$q(x) = - q_c(x) + g + p \tag{4}$$

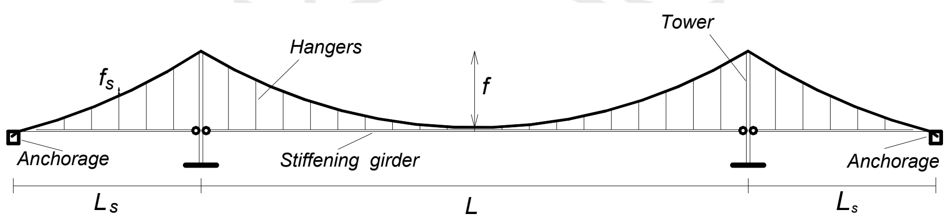

Figure 1. Structural layout

If the new cable geometry is described by $z(x)$, with :

$$z(x) = y(x) + \eta(x) \tag{5}$$

and $y(x)$ representing the initial cable profile, it may be written :

$$q_c(x) = -\frac{d^2 z}{dx^2}(H_g + H_p) \tag{6}$$

with $(H_g + H_p)$ representing the horizontal component of its total axial force.
According to the classical beam equation it may be obtained:

$$EI\frac{d^4\eta}{dx^4} - \frac{d^2\eta}{dx^2}(H_g + H_p) = p - \frac{H_p}{R} \tag{7}$$

where R represents the cable curvature under the load g

This equation may be recognized as the equation of a fictitious simple beam, having a transverse load $(p - H_p/R)$ and subjected to an axial tensile load $(H_g + H_p)$, according to the second order theory of beams [1] (Fig.3).

The deflection $\eta(x)$ of a simple beam due to a transverse load q and subjected to a tensile force H, is obtained from the following expression [2] :

$$\eta(x) = \frac{q}{H}\left[\frac{\cosh(k \cdot L/2 - k \cdot x)}{k^2 \cdot \cosh(k \cdot L/2)} - \frac{1}{k^2} + \frac{x \cdot (L - x)}{2}\right] \tag{8}$$

with
$$k = \sqrt{\frac{H}{EI}} \tag{9}$$

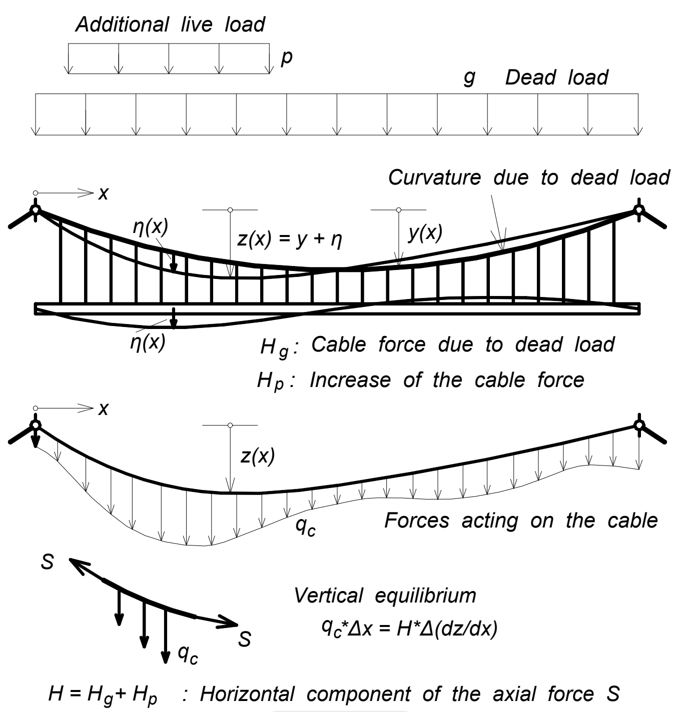

Figure 2. Cable deformation under direct action of live load

For the two-hinged stiffening girder, the deflection function $\eta(x)$ in Eq. (9) can be approximated quite satisfactorily for practical purposes, according to an established result of the second order theory of beams [3], from the relation

$$\eta = W_1 \cdot \frac{1}{1 + \frac{H_g + H_p}{P_{cr}}} \tag{10}$$

where W_1 represents the (first order) deflection line of the simply supported beam under the load $(p - H_p/R)$ and P_{cr} its buckling load, equal to $(\pi^2\, EI/L^2)$.

Now, the increase H_p of the cable force H_g of a cable fixed at its ends for ratios λ between 1/8 and 1/12, is related to its additional deflection η through the relation [4] :

$$\frac{H_p}{A_c E_c} * L_c = \frac{g}{H_g} \int_0^L \eta dx \tag{11}$$

where the length L_c is given from the expression :

$$L_c = L * \left[1 + 8 * \lambda^2\right] \tag{12}$$

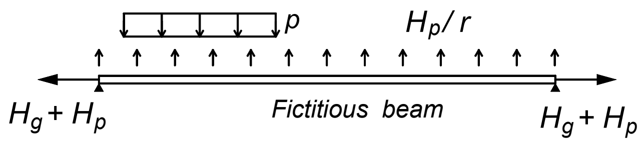

Figure 3. Acting forces on the fictitious beam

The unknown magnitude H_p can be determined from the condition that the deflection curve *η(x)* according to Eq. (10) – or, more strictly, according to Eq. (8) - must also satisfy the "cable equation" (11).

Two loading configurations for the live load *p* have to be taken into account, namely one acting on the left half of the girder span and the second one extending over the whole span. The first loading yields the maximum deflection and subsequently the most unfavorable girder bending, whereas the second one yields the maximum value of cable force. It may be written:

$$W_1(x) = \frac{(p^* - H_p / R) * L^4}{24 * EI} \left[\left(\frac{x}{L}\right)^4 - 2 * \left(\frac{x}{L}\right)^3 + \left(\frac{x}{L}\right) \right] \tag{13}$$

with p^* equal either to *p*/*2* for the partial loading of the left half of the span, or to *p* for the loading of the whole span. Substituting into Eq. (11) is obtained :

$$\frac{H_p}{A_c E_c} * L_c = \frac{g}{H_g} \left[\frac{(p^* - H_p / R) * L^5}{120 * EI} \frac{1}{1 + \frac{H_g + H_p}{P_{cr}}} \right] \tag{14}$$

Introducing the following dimensionless parameters

$$G = \frac{H_g * L^2}{E \cdot I} \quad , \quad \gamma = \frac{p^*}{g} \quad , \quad \varepsilon = \frac{H_g}{A_c \cdot E_c} \quad , \quad Z = \frac{H_p}{H_g} \tag{15}$$

the following algebraic equation for the unknown *Z* is obtained :

$$Z^2 + (\frac{\pi^2}{G} + \omega + 1) * Z - \gamma * \omega = 0 \tag{16}$$

where $$\omega = \frac{8 \cdot \pi^2}{15 * \varepsilon} \cdot \frac{1}{1/\lambda^2 + 8} \tag{17}$$

On the other side, substituting into Eq.(11) the exact expression of $\eta(x)$ from Eq.(8), performing the indicated integrations and considering the above introduced parameters, the following equation is obtained

$$Z \cdot \varepsilon \cdot (1 + 8 \cdot \lambda^2) = 64 \cdot \lambda^2 \cdot \frac{\gamma - Z}{Z + 1} \cdot \left[\frac{2 \cdot \sinh(D/2)}{D^3 \cdot \cosh(D/2)} - \frac{1}{D^2} + \frac{1}{12} \right] \tag{18}$$

with $$D = \sqrt{G * (Z + 1)} \tag{19}$$

It is found that the value of Z obtained from Eq.(16) differs from the exact solution of the above not directly solvable equation (18) by less than 1‰, a fact which allows to consider the former value as the proper solution of the problem.

3 DETERMINATION OF MAXIMUM RESPONSE

In order to obtain the maximum values of the response, the following loading patterns have to be considered:

1. For the maximum values of the cable force H_p, the live load p extends over the whole length of the girder.
2. For the maximum span bending moment M_{max}, as well the maximum deflection η_{max}, the live load p extends over the left (or the right) half of the central span.

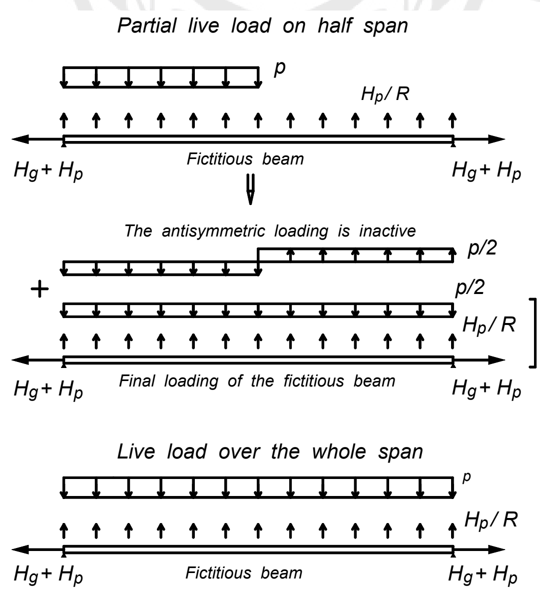

Figure 4. Characteristic positions of live load on the fictitious beam

The last two quantities, approximately located at the quarter of the span, can be directly determined according to the exact expression (8). Of course this procedure must be based on a value of Z which is determined for the specific location of the live load p, by taking into account the half value of it as previously stated.

Splitting the considered loading into a symmetric and an antisymmetric part as previously examined (Fig. 4), it is noted that the antisymmetric loading develops no additional cable force and the beam behaves like a simply supported one having the half span and subjected to the half live load. Then, by superposing the relevant quantities at the quarter and at the middle of the span in the full and the half length beam respectively, the following expressions are obtained:

$$\frac{M_{max}}{M_g^0} = -\frac{8\cdot(\gamma - Z)}{D^2}\cdot\left[\frac{\cosh(D/4)}{\cosh(D/2)} - 1\right] - \frac{8\cdot\gamma}{D^2}\cdot\left[\frac{1}{\cosh(D/4)} - 1\right] \tag{20}$$

and

$$\frac{\eta_{max}}{L} = \frac{8\cdot\lambda\cdot(\gamma - Z)}{(Z+1)\cdot D^2}\cdot\left[\frac{\cosh(D/4)}{\cosh(D/2)} + \frac{3\cdot D^2}{32} - 1\right] + \frac{8\cdot\lambda\cdot\gamma}{(Z+1)\cdot D^2}\cdot\left[\frac{1}{\cosh(D/4)} + \frac{D^2}{32} - 1\right] \tag{21}$$

where
$$M_g^0 = \frac{g\cdot L^2}{8} \tag{22}$$

represents the bending moment of the freely supported beam of length L under the dead load g.

4 PARAMETRIC STUDY

On the basis of the above relations and for the constant values of $\lambda = 0.1$ and $\varepsilon = 0.002$ which represent logical design decisions, the diagrams showing the variation of the ratios (H_p / H_g) , (M_{max} / M_g^0) and (η_{max} / L) are first determined (Figs.5 to 7).

The ratio (H_p / H_g) is independant of the stiffness factor G, depending only on the loading ratio γ .

The ratio (M_{max} / M_g^0) is very little influenced from the parameter γ , as long the values of G are greater than 450. The ratio (η_{max} / L) is practically unaffected by values of G greater than 300.

From the Fig.7 it may be readily certified that for very long spans, the stiffening contribution of the girder becomes negligible, while for moderate spans this contribution is clear as may be seen from the left portion of the curves. Moreover from the same diagrams it may be concluded that increasing the dead load leads to an increase of the structure's stiffness.

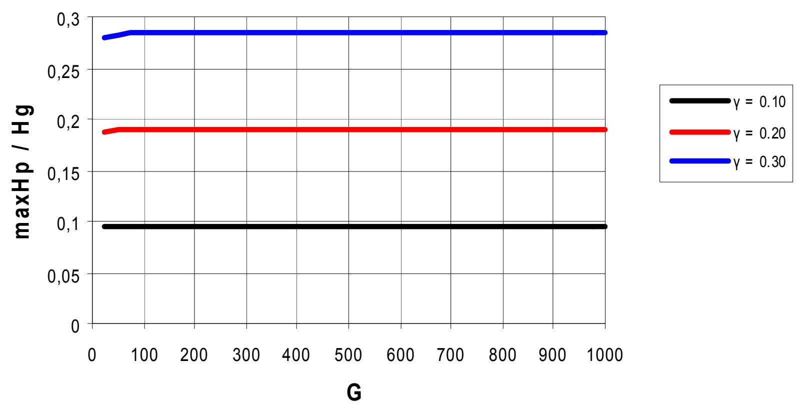

Figure 5. Maximum cable force H_p

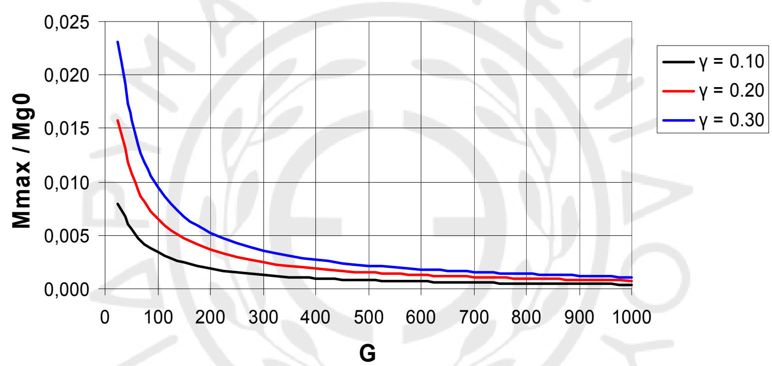

Figure 6. Maximum span bending moment

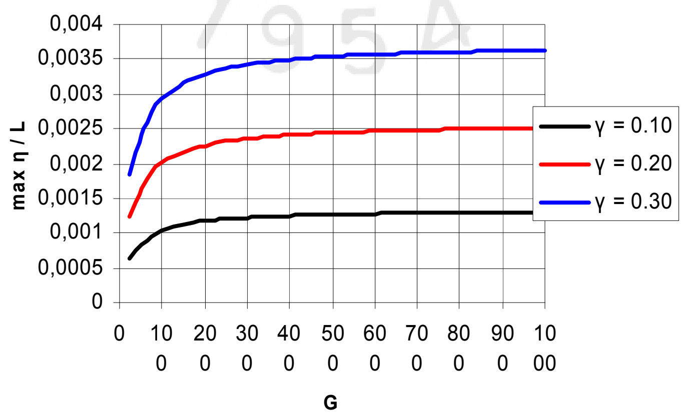

Figure 7. Maximum deflection

5 CONCLUSIONS

The problem of evaluating the static response of a suspension bridge with hinged stiffening girder, under the additional action of the live load can be tackled directly with a minimum computing effort. It is shown that the response is totally determined on the basis of four dimensionless parameters. The procedure followed permits the establishment of diagrams which show the influence of the above design parameters on the response and moreover they allow very quick its quantitative assessment.

REFERENCES

[1] Stavridis L. (2010), "*Structural systems : behaviour and design*" , Thomas Telford ICE Publishing, London

[2] Timoshenko S. (1956), "*Strength of materials Part II*", D. Van Nostrand Company Inc., New York.

[3] Roik K. (1983), "*Steel Structures*" (in German) , Wilhelm Ernst & Sohn, Berlin

[4] Timoshenko S. (1943). "Theory of Suspension Bridges", *J. Franklin Inst*., 235(3), 231-238; 235(4), 327-349.

STAY CABLES' RAIN-WIND INDUCED VIBRATIONS
Response Characteristics, Exciting Mechanisms, and Modelling

Dimitrios Sophianopoulos, Theodore Konstantakopoulos

University of Thessaly, Dept. of Civil Engineering, Greece
e-mail: dimsof@civ.uth.gr, tkonstadak@civ.uth.gr

ABSTRACT: The strongly nonlinear phenomenon of rain-wind induced vibrations of stay cables is discussed, focusing on issues related to their exciting mechanisms, the cable response characteristics and the adequate modeling. Numerical results obtained are compared to wind-tunnel test data as well as to full scale measurements on cable-stayed bridges.

KEY WORDS: Rain-wind induced vibrations, stay cables, bridges.

1 INTRODUCTION

Large amplitude Rain-Wind-Induced-Vibrations (RWIV) of stay cables are a challenging problem in the design of cable-stayed bridges. Such phenomena were first observed on the Meikonishi bridge in Nagoya, Japan [1] and also later on other such bridges, as for instance on the fully steel Erasmus bridge in Rotterdam, the Netherlands (1996) and the Second Severn Crossing, connecting England and Wales [3]. It was found that the cables, which were stable under wind action only, were oscillating under a combined influence of rain and wind, leading to large amplitude motions, even for light-to-moderate simultaneous rain and wind action. The frequency of the observed vibrations was much lower than the critical one of the vortex-induced vibrations, while it was also perceived that the cable oscillations took place in the vertical plane mostly in single mode; for increasing cable length however, higher modes (up to the 4^{th}) appeared. Most importantly, during the oscillations a water rivulet appeared on the lower surface of the cable, which was characterized by a leeward shift and vibrated in circumferential directions [1,8,10].

More detailed field measurements – observations, as well as wind-tunnel tests, which were realized at a later time, showed that there were in fact two rivulets formed: one on the upper cable surface and another on the lower surface. This formation and corresponding motion is illustrated in the contents of Photo 1, courtesy of wind tunnel tests conducted in the Hong-Kong Polytechnic Institute, simulating wind-rain action on a cylinder.

Both rivulets were oscillating in circumferential direction at the same frequency as that of the cable, with their point of formation depending on the wind velocity. Their presence and movement alter significantly and in a random manner on the cross-sectional profile of the cable, as acted upon by wind, and hence complicate interaction occurs.

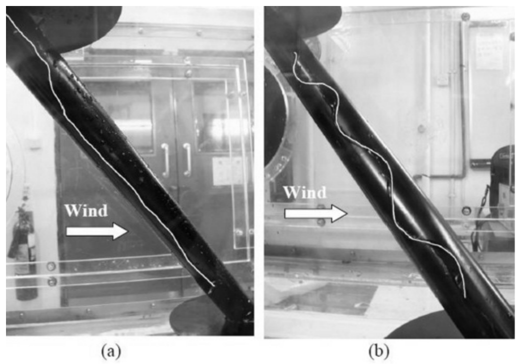

Photo 1. Water rivulets (white curves) on cylinder surface: (a) leeward and (b) windward rivulet

Measurements of the aerodynamic forces as the rivulets formed separately showed the negligible role of the lower rivulet (a fact still not accepted by all relevant studies), and it is generally believed that that the upper rivulet is dominant in inducing cable dynamics, and it is postulated that the instability phenomena observed are ought to either the point of formation or the oscillation of this rivulet itself [2,4]. Moreover, further studies have also indicated that there might be an additional factor triggering the RWIV, namely an axial flow generated at the near wake of the inclined cable and associated with 3D-flow characteristics.

Since the first observation of the foregoing phenomenon, numerous attempts, for modeling these extremely nonlinear (and quite stochastic in nature) vibrations have been made, and reported in the literature. These range from simplified one and two degree of freedom systems of standing and moving rivulets on an idealized cylinder to sophisticates simulations. The latter are based on strip-theory or on approaches coupling unsteady aerodynamics to thin-film models based on lubrication theory for the rain water. None of these however have yet gained any general justification, since to a smaller or larger extent they cannot predict the majority of measured RWIV on either real structures or wind tests.

To this end, and since the exciting mechanisms of RWIV of stay-cables is still under debate in the Engineering Community, the present work aims to clarify all the aforementioned issues by (a) offering an overview of existing scientific knowledge regarding various response characteristics and underlying exciting mechanisms and (b) summarizing the most important models proposed.

The references given at the end of this work are kept to a strict minimum and are only indicative (note that a vast literature is related to the subject), while a strong effort has also been undergone by the authors to keep theoretical analyses and quantitative results as short as possible.

2 RAIN-WIND-INDUCED-VIBRATIONS OF STAY- CABLES

2.1 Major response characteristics and basic principles

These along with the fundamental mechanism of RWIV of stay-cables were thoroughly investigated by Matsumoto et al [2], via a series of wind tunnel tests. Their results indicated that rain-wind-induced vibrations of cables can be classified in three types, i.e.

1) the "galloping type", which includes both divergent galloping and velocity restricted galloping, related to a negative slope of the lift force caused by an "upper water rivulet" and/or "axial flow",
2) the vortex-shedding type with long period and
3) their mixed type.

In particular, it was found that this velocity-restricted response caused by vortex-shedding is excited by the three-dimensionality of conventional Karman vortex shedding along the cable axis. More details concerning the test setup and the whole galloping-based analysis can be found in the contents of the paper cited above. These general characteristics are closely related with the basic principles governing these oscillations [4], which are summarized in what follows:

a) The effective cross-section of the cables during motion is permanently changing. (At this point it should be noted that other studies, mainly of the Japanese School [1, 2] and others not cited herein, explain that the motion of the rivulet leads to *a periodic change of cable cross-section* for the flow).
b) The shape of the cross-section made of the cable and the rivulets depends on the adhesion, on the wind forces and on the momentary acceleration of the cross - section. Because of this dependency the frequency of the variation of the shape is the same with the frequency of its oscillation,
c) As a consequence of the momentary accelerations, the rivulets oscillate on the surface of the cable in the circumferential direction,
d) If the resulting wind force, which acts on the entire cross – section, is oscillating in the same frequency and with the same sign as the oscillation velocity, positive work is produced and the vibrating system receives an energy input, and large amplitudes occur. Their magnitude depends on the structural damping and on the retaining elastic forces due to second-order effects, and
e) The exciting frequency is conditioned by the motion and is identical to the natural frequency. Hence, the rain-wind-induced vibrations are *a self-excited oscillation* that may occur over a wide range of frequencies.

Moreover, in a very interesting work concerning the phenomenology, the mechanical modeling and the numerical simulation of RWIV [13], it was deduced that the major reason, that these vibrations are not fully understood and satisfyingly determined, is that the flow around an inclined cable with rivulets is very complex and the cable aerodynamics of these phenomena depend on various parameters like the inclinations and the diameters of the cable, the geometrical shape and the position of the rivulet as well as the velocity and the angle of the incidence of the flow.

In general, strongly nonlinear multi - parametric dynamic instability phenomena characterize the response of stay – cables under simultaneous rain and wind action [10], and their analysis and simulation is extremely complicated.

2.2 Exciting mechanisms

In accordance with the contents of the previous sub-section, various different approaches – fluid mechanical phenomena are discussed in the literature, in an attempt to identify, describe and validate the exciting mechanisms of RWIV.

According to [1], the instability does not seem to be caused by vortex induced vibrations, because the Strouhal number, the amplitudes and the frequency differ from those of RWIV, while standard galloping effects are also not suitable, since the surface of the cylindrical cable is too smooth without any rigid edge. Wake galloping can be excluded too, because the distance between stay-cables are in most cases very large. It was also concluded, by the above study (and others of similar content) that the dimensions of the rivulets forming on the cable surface are negligible compared to the cable cross-section dimensions, and therefor RWIV are unlikely to be generated by the change of the effective cross – section.

Besides of the explanation of RWIV as a special kind of galloping, many scientists (for instance [2]) discuss that rain-wind-induced vibrations represent a new type of instability phenomena. The excitation mechanism described is caused by the three-dimensionality of Karman vortex shedding, while it was deduced that the oscillations are additionally enhanced by the axial flow in the wake of the cable and by the geometrical shape of the upper rivulet.

On the other hand, as also mentioned earlier, it was assumed [4] that, as a result of the rivulet motion, the effective cross – section undergoes a permanent change and as a result of wind tunnel tests three different excitation mechanisms were reported, parallel and perpendicular to the wind directions in dependence of the rivulet motion at the cable surface. These mechanisms are depicted in Figure 1.

Another possible mechanism of excitation was derived by Seidel and Dinkler [13], based on the phenomena of the Prandtl tripwire, considering the rivulets as a movable disturbance. Following this approach the occurrence of the lower and upper limit of the critical velocity may be explained and all kinds of observable vibrations can be described.

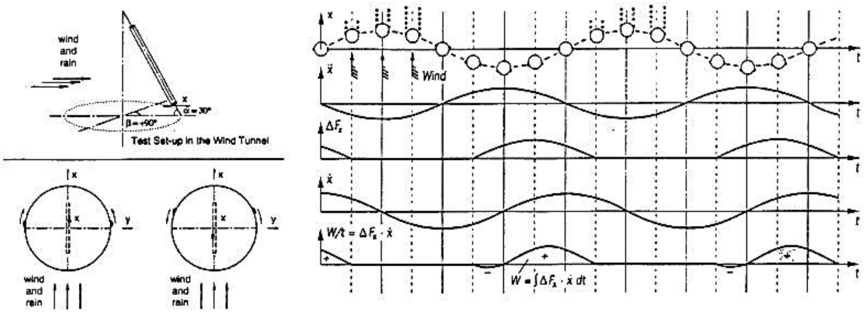

(a)

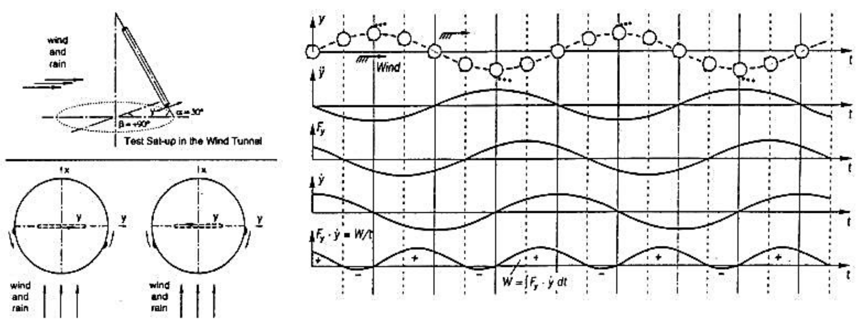

(b)

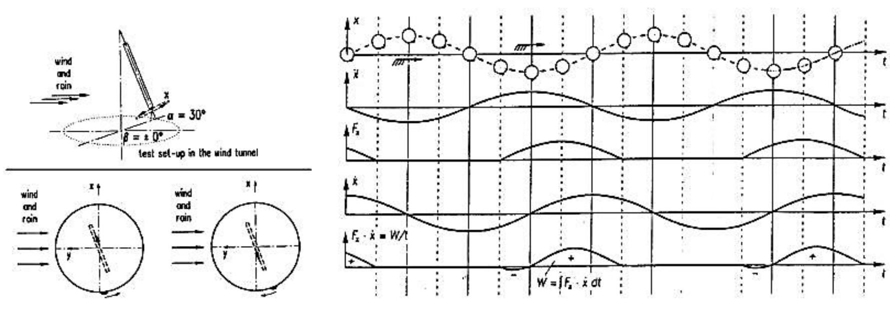

(c)

Figure 1. Exciting mechanisms of RWIV [Verbiede and Ruscheweyh 1998]: (a) Vibration in the wind direction, symmetrical motion of the rivulets on the cross section, (b) Vibration in the cross-wind direction, antimetrical motion of the rivulets on the cross section, (c) Vibration predominantly in the cross-wind direction, mainly caused by the motion of a rivulet at the underside of the cable.

2.3 Modelling

A variety of different mechanical models have been proposed in the literature for simulating RWIV. These may be divided into two main types, namely simplified discrete ones, with one or two degrees of freedom, and sophisticated ones based on strip and lubrication theory. Among the former, the most significant recent ones, to the authors' opinion, are, in chronological order of appearance, the following:

- Stochastic model by Cao et al. 2003 [5, 11]

In this spring-dashpot model, shown in Figure 2, a single rivulet moving on the upper of a cable, under the influence of the wind, gravitational and friction forces is considered.

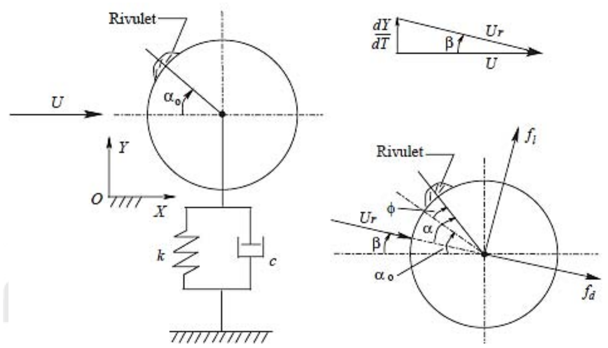

Figure 2. Stochastic mechanical model of Cao et al. 2003

The motion is described by the response of a band-pass filter. If φ(t) is the fluctuation angle describing the motion of the rivulet on the cable perimeter, and after determining the lift and drag forces on the model, a stochastic process is adopted for φ, while the static angle α_0 of the rivulet is taken as a function of the mean wind speed U, as reported by wind tunnel tests. Results based on linearized aerodynamic forces showed that a stochastic resonant phenomenon can be induced depending on the location of the rivulet, while also a stationary stochastic state regarding the cable may also be observed.

- Single-degree-of-freedom models [7-10]

Several simplified 1-DOF models have been reported, with each of them possessing some merit, but none capable of fully modeling RWIV of stay-cables. Three representative such models are shown in Figure 3, while others also exist, not discussed herein for reason given earlier as well as for brevity.

Detailed features of each individual model can be found in the full length papers cited above, but it should be noted that assumptions related to each model restrict their wider applicability and hence only limited wind tunnel test results and real measurements are captured by their response.

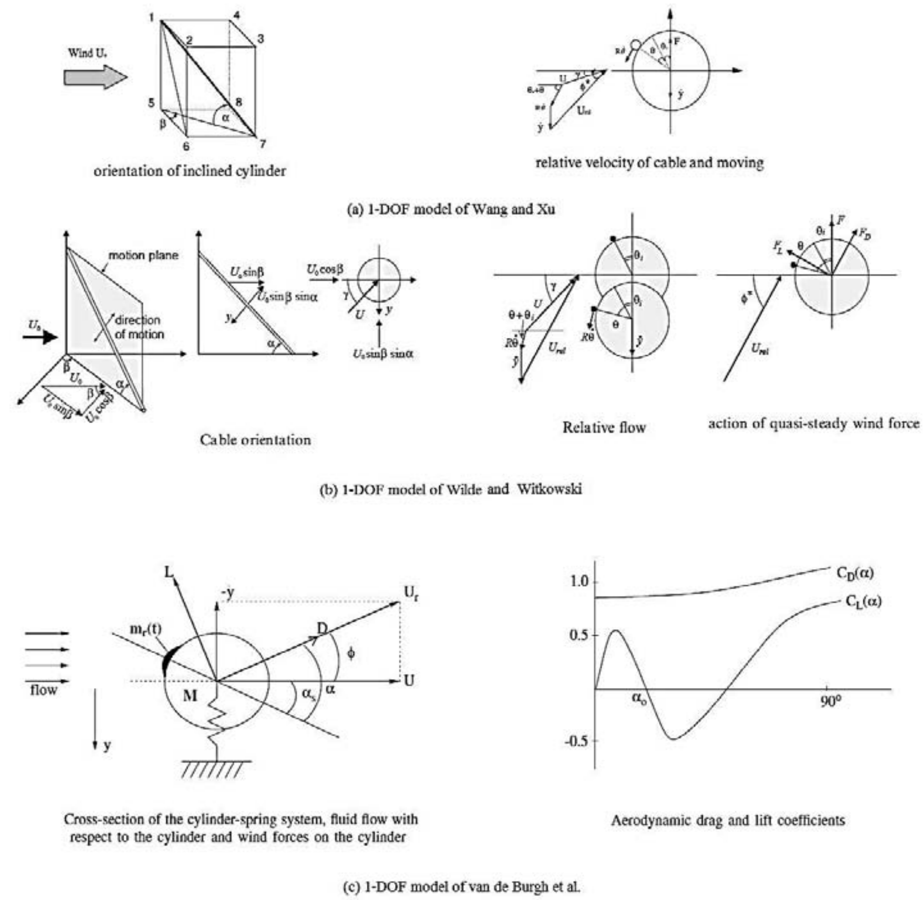

Figure 3. Single-degree-of-freedom models

The second kind of models, the sophisticated ones [6, 14], are more precise by nature, but based on very complicated theories that cannot be easily understood and their results still remain controversial. Further discussion relies far beyond the scopes of the present work.

3 CONCLUSIONS

According to the above overview it is clear that the problem of rain-wind-induced vibration of stay cables remains an open scientific issue, since neither the exciting mechanisms are fully explored nor adequate modeling has been achieved till now. The authors believe that the stochastic nature of these oscillations should be tackled accordingly, but further theoretical research is required, accompanied by large scale experiments and consistent in-situ measurements on cable-stayed bridges worldwide.

REFERENCES

[1] Hikami, Y., Shiraishi, N., “Rain-wind-induced vibrations of cables in cable stayed bridges”, Journal of Wind Engineering and Industrial Aerodynamics, Vol. 29, Nos. 1-3, pp. 409-418, 1988.

[2] Matsumoto, M., Siatoh, T, Kitazawa, M, Shirato, H and Nishizaki, T, “Response characteristics of rain-wind induced vibration of stay-cables of cable-stayed bridges”, Journal of Wind Engineering and Industrial Aerodynamics, Vol. 57, Nos. 2-3, pp. 323-333, 1995.

[3] Macdonald, JHG, Dagless, EL, Thomas, BT, Taylor, CA, “Dynamic measurements of the Second Severn Crossing”, Proceedings of the Institution of Civil Engineers – Transport, Vol. 123, No. 4, pp. 241-248, 1997.

[4] Verwiebe, C, Ruschweyh, H, “Recent research results concerning the exciting mechanisms of rain-wind-induced vibrations”, Journal of Wind Engineering and Industrial Aerodynamics, Vols. 74-76, pp. 1005-1013, 1998.

[5] Cao, DQ, Tucker RW, Wang C, “A stochastic approach to cable dynamics with moving rivulets”, Journal of Sound and Vibration, Vol. 268, No. 2 pp. 291-304, 2003.

[6] Per, U, Nahrath, N, “Modeling of rain-wind induced vibrations”, Wind and Structures, Vol. 6, No. 1, pp. 41-52, 2003.

[7] Wang, L, Xu, YL, “Wind-rain-induced vibration of cable: An analytical model (1)”, International Journal of Solids and Structures, Vol. 40, No. 5, pp. 1265-1280, 2003.

[8] Wilde, K, Witkowski, W, “Simple model of rain-wind-induced vibrations of stayed cables”, Journal of Wind Engineering and Industrial Aerodynamics, Vol. 91, No. 7, pp. 873-891, 2003.

[9] Xu, YL, Wang, LY, “Analytical study of wind-rain-induced cable vibration: SDOF model”, Journal of Wind Engineering and Industrial Aerodynamics, Vol. 91, Nos. 1-2, pp. 27-40, 2003.

[10] Ibrahim, RA, “Nonlinear vibrations of suspended cables – Part III: Random excitation and interaction with fluid flow”, Applied Mechanics Reviews, Vol. 57, No. 6, pp. 515-549, 2004.

[11] Burton, D, Cao, DQ, Tucker, RW, Wang, C, “On the stability of stay cables under light wind and rain conditions”, Journal of Sound and Vibration, Vol. 279, Nos. 1-2, pp. 89-117, 2005.

[12] van der Burgh, AHP, Hartono, Abramian, AK, “A new model for the study of rain-wind-induced vibrations of a simple oscillator”, International Journal of Non-Linear Mechanics, Vol. 41, No. 3, pp. 345-358, 2006.

[13] Seidel, C, Dinkler, D, “Rain-wind induced vibrations – phenomenology, mechanical modelling and numerical analysis”, Computers and Structures, Vol. 84, Nos. 24-25, pp. 1584-1595, 2006.

[14] Taylor, IJ, Robertson, AC, Wilson, SK, Duffy Ma, BR, Sullivan, JM, “New developments in rain-wind-induced vibrations of cables”, Proceedings of the Institution of Civil Engineers – Structures and Buildings, Vol. 163, No. 2, pp. 73-86, 2010.

DYNAMIC ANALYSIS OF LONG SPAN CABLE-STAYED BRIDGES UNDER THE ACTION OF MOVING LOADS

Domenico Bruno[1], Fabrizio Greco[1], Paolo Lonetti[1], Arturo Pascuzzo[1]

[1] University of Calabria, Dept. of Structural Engineering, Italy
e-mail: d.bruno@unical.it, f.greco@unical.it, lonetti@unical.it, arturo_pascuzzo@hotmail.com

ABSTRACT: The main aim of the paper is to investigate the dynamic behavior of cable stayed bridge under the action of moving loads. The basic formulation is developed by using a finite element approach, in which a refined schematization is adopted to analyze the interaction behavior between cable system and moving loads. The cable system is analyzed by using a geometric nonlinear formulation, in which the local vibrations of the stays are taken into account, accurately. Moreover, the analysis focuses attention on the influence of the inertial characteristics of the moving loads, by accounting for the coupling effects arising from the interaction between bridge deformations and moving system parameters. Results are presented with respect to eccentric loading which introduces both flexural and torsional deformation modes. Sensitivity analyses have been proposed in terms of dynamic impact factors, emphasizing the effects produced by the external mass of the moving system and the influence of both "A" and "H" shaped tower typologies on the dynamic bridge behavior.

KEY WORDS: Dynamic amplification factor, Cable stayed bridges, Finite element method, Nonlinear cable formulation.

1 INTRODUCTION

During the last decades, with new developments on the field of high performance materials and construction techniques, cable supported bridges have received much attention and many applications have been proposed to overcome increasing spans. However, new structural problems related to bridge deformability arise due to extreme loading conditions. As a matter of fact, long span bridges are widely subjected to highway or railway loads, which are, frequently, comparable with that involved by the self-weight ones [1]. Therefore, such external excitations are able to affect the bridge behavior and, consequently, to produce significant dynamic amplification effects in both displacement and stress bridge variables. Moreover, due to new developments in the rapid transportation systems, the allowable speed range is significantly increased. As a consequence, non standard excitation modes determine extreme loading conditions, which, strongly, influence dynamic bridge behavior. At this aim, different investigations are needed to describe the interaction behavior between external moving system and bridge vibrations and, consequently, to accurately estimate dynamic impact factors of typical design bridge variables.

The extension of the moving load problem for cable supported bridges with long spans requires a consistent approach to fully analyze bridge cinematic behavior and train-girder interaction. Dynamic response of cable supported bridges produced by wind or seismic excitations have been, sufficiently, analyzed by means of different approaches in the context of either analytical or numerical methods. However, the references dealing with the dynamic response of cable supported bridges in the frameworks of moving loads are relatively few. For cable stayed systems, the effects produced by moving vehicles or railway loads have been analyzed, in terms of dynamic amplification factors related to both displacement or stress variables, with respect to bridges of reduced span only [2-5]. In the framework of long span bridges, the bridge modeling is frequently based on continuum approaches, where the stays spacing is usually small in comparison to the bridge main span [6].

In the proposed work, the dynamic behavior of long span bridges is analyzed by using a generalized formulation based on the finite element method, in which both in plane and out-of plane deformation modes have been accounted for. Cable-stayed bridges based on both "H" and "A" shaped typologies with a double layer of stays have been considered. A parametric study in a dimensionless context has been analyzed by means of numerical results, in terms of typical kinematic and stress bridge variables for both in plane and eccentric loading conditions. In particular, results are proposed to investigate the effects of moving system description with reference to non-standard forces due to Coriolis and centripetal accelerations, which are usually neglected in conventional dynamic analyses. Finally, the influence on dynamic bridge behavior of pylon typology with reference to both "A" and "H" shapes has been analyzed and comparisons in terms of both moving loads and tower characteristics have been proposed.

2 THEORECTICAL FORMULATION

2.1 Cable formulation

To accurately simulate the realistic behavior of cable structures, the cable element presented in this paper is based on a 3D nonlinear geometric truss formulation. In particular, every single cable of the suspension system is simulated with n truss elements, which are connected each other and to the corresponding ends to the girder profile and the top tower cross section. The theoretical formulation is consistent to large deformation theory based on the Green-Lagrange's strain measure and the second Piola-Kirchhoff stress [7], whereas the material behavior is assumed to be linearly elastic. With reference to the structural scheme reported in Fig. 1, the weak form can be derived by using the principle of d'Alembert as follows:

$$\sum_c \int \sigma_n \delta\varepsilon_n dV_0 + \sum_c \int \mu_c \ddot{\underset{\sim}{u}} \delta \underset{\sim}{u} dV_0 = \sum_c \int \underset{\sim}{g}_c \delta \underset{\sim}{u} dV_0 + \sum_c \underset{\sim}{F} \delta \underset{\sim}{u} dV_0 \quad (1)$$

where $\sum_c(\cdot)$ involves a summation over the elements introduced to discretize the geometry of the cable, the dot represents the time derivative with respect to the time, $\underset{\sim}{u}$ is the displacement vector, μ_c is the mass per unit volume cable density, $\underset{\sim}{g}_c$ is the selfweight loads of the cable and $\underset{\sim}{F}$ is reaction force vector.

2.2 Initial configuration under dead loads

In order to analyze the actual behavior of the cable system the initial configuration in terms of stresses and strains should be determined. In particular, the prestressing forces of the cable system are solved with respect to the end step of the balanced cantilever construction, in which only central segment of the deck is left. The values of the cable tensions are obtained enforcing the deck, during the application of the dead loads, to stay in the undeformed configuration, by means of the following conditions [1]:

$$\underset{\sim}{u}_z^G + \underset{\sim}{C} \cdot \underset{\sim}{X} = 0 \quad (2)$$

where $\underset{\sim}{u}_z^G$ is a vector containing the self weight displacements in absence of the prestressing forces, $\underset{\sim}{X}$ is the prestressing force vector, $\underset{\sim}{C}$ is the flexibility matrix of the structure. It is worth noting that since, the structure is characterized by a nonlinear behavior, Eq.(2) corresponds to a nonlinear equation system, whose solution requires a numerical procedure to be calculated.

2.3 Girder formulation

The girder and tower are described by 3D geometric nonlinear beam elements, based on a Euler-Bernoulli (EB) formulation and a Green-Lagrange's strain assumption. The girder is connected with the cable elements at the end points of the cross-section on the *yz* plane and at the top cross section of the towers, based on "H" or "A" shaped typologies. With reference to Fig.1, the displacements of the cross-section are expressed by the following relationships:

$$\overline{u}_x = u_x - \vartheta_z y, \quad \overline{u}_y = u_y, \quad \overline{u}_z = u_z + \vartheta_x y \quad (3)$$

where (u_x, u_y, u_z) and $(\theta_x, \theta_y, \theta_z)$ are the displacements and rotation fields of the centroid axis of the girder with respect to the global reference system, respectively.

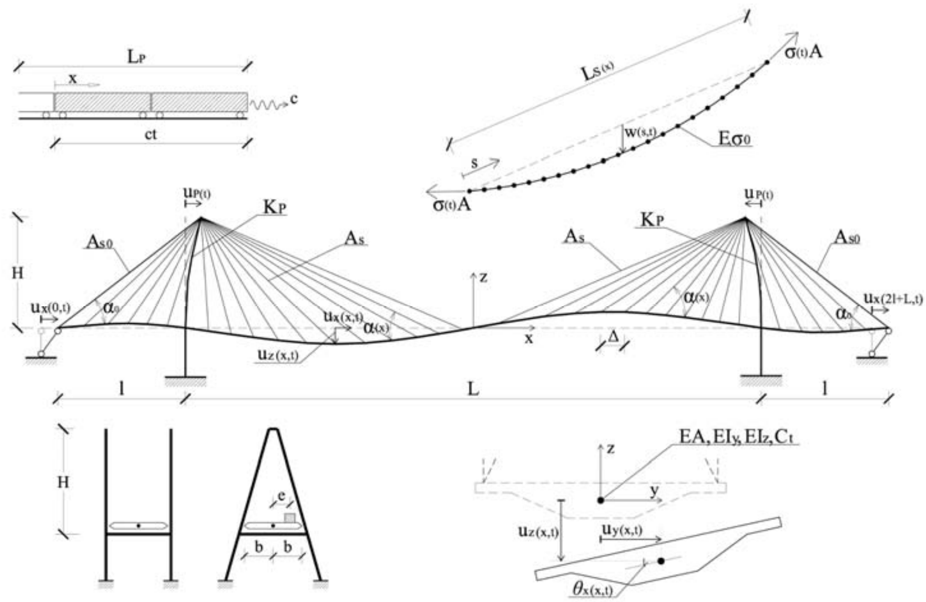

Figure 1. Structural model of the bridge

The external loads are assumed to proceed, with constant speed c from left to right along the bridge development and are considered to be perfectly connected to the girder profile. Consequently, the moving system is identified, kinematically, in terms of girder vertical displacements and thus no frictional effects have been considered between moving loads and girder. However, the interaction between moving loads and bridge motion has been considered introducing non standard contributions arising from Coriolis and centripetal inertial forces, which are, mainly, produced by the coupling behavior between moving system and bridge deformations. In particular, with respect to a fixed reference system, velocity and acceleration functions of the moving system have been evaluated by means of a eulerian description, as:

$$\dot{\bar{u}}_z = \frac{\partial \bar{u}_z}{\partial t} + \frac{\partial \bar{u}_z}{\partial x} c, \qquad \ddot{\bar{u}}_z = \frac{\partial^2 \bar{u}_z}{\partial t^2} + \frac{\partial^2 \bar{u}_z}{\partial x \partial t} 2c + \frac{\partial^2 \bar{u}_z}{\partial x^2} c^2, \quad \text{with } c = \frac{\partial x}{\partial t} \tag{4}$$

Moreover, the moving system is supposed to be described by equivalent distributed loads and masses acting over the girder profile. With respect to a moving reference system, from the left end of the bridge, and to an eccentricity distance e of the moving load with respect to the centroid of the cross section, the mass and loading functions during the external load advance can be written by the following expressions:

$$\rho = \lambda \overline{H}\left(x_1 + L_p - ct\right)\overline{H}\left(ct - x_1\right), \tag{5}$$

$$f = p\overline{H}\left(ct - X\right)\overline{H}\left(X + L_p - ct\right), \tag{6}$$

$$\rho_0 = \lambda_0 \overline{H}\left(x_1 + L_p - ct\right)\overline{H}\left(ct - x_1\right), \tag{7}$$

$$m = p \cdot e\ \overline{H}\left(ct - x_1\right)\overline{H}\left(x_1 + L_p - ct\right), \tag{8}$$

where $\overline{H}(\cdot)$ is the Heaviside function, L_p is the length of the moving loads, x_1 is the referential coordinate located at the left end girder cross section, (λ, p) are the per unit length mass and self weight loads, respectively, and λ_0 represents the torsional distributed polar mass moment produced by the external loading.

The dynamic equilibrium equations have been derived in explicit form, consistently with a variational approach, in which both internal and external works are evaluated by means of the following relationship:

$$\begin{aligned}
&\sum_c \int \left(N\delta\varepsilon_n + M_x\delta\chi_x + M_y\delta\chi_y + M_t\delta\theta_x\right)dL + \sum_c \int \mu \ddot{\underset{\sim}{u}}\delta \underset{\sim}{u} dL + \\
&\sum_c \int \mu_0 \ddot{\underset{\sim}{u}}\delta \underset{\sim}{u} dL = \sum_c \int \underset{\sim}{g}_G \delta \underset{\sim}{u} dL + \sum_c \underset{\sim}{F}\delta \underset{\sim}{u} dL + \\
&+\sum_c \int \rho\left(\ddot{\overline{u}}_z + 2c\dot{\overline{u}}_z + c^2\overline{u''}_z\right)\delta\overline{u}_z dL + \sum_c \int \dot{\rho}\dot{\overline{u}}_z \delta\overline{u}_z dL
\end{aligned} \tag{9}$$

where (N, M_x, M_y, M_t) are the internal stress resultants, $(\varepsilon_n, \chi_x, \chi_y, \theta)$ are the corresponding generalized beam strains, (μ, μ_0) are mass moment and polar mass moment of the girder, $\underset{\sim}{g}_c$ is the self weight load of the girder and $\underset{\sim}{F}$ is reaction force vector.

3 FINITE ELEMENT IMPLEMENTATION

Governing equations given by Eq.(1) and Eq.(9) introduce a non linear set of equations, which have been solved numerically, using a user customized finite element program, i.e. COMSOL Multiphysics TM version 4.1 [8]. Finite element expressions are written starting from the weak form, introducing isoparametric shape functions (ζ_i, ξ_i) to represent cable and girder variables as:

$$\underset{\sim}{u}_C(r,t) = \sum_{i=1}^{n} \zeta_i(\underset{\sim}{r})\underset{\sim}{u}_{iC}(t),\ \ \underset{\sim}{u}_G(r,t) = \sum_{i=1}^{n} \xi_i(\underset{\sim}{r})\underset{\sim}{u}_{iG}(t), \tag{10}$$

where n represents the number of nodes of the master finite element. In particular, Lagrange interpolation functions are adopted to analyze the behavior of the cable system, whereas for girder elements based on EB formulation Hermit cubic interpolation functions are employed. Substituting Eq.(10) in the governing equations, given by Eq.(1) and Eq.(9), the following discrete equilibrium equations are obtained:

$$\sum_{i=1}^{n}\left[\underset{\sim}{M}_i+\underset{\sim}{N}_i^1\right]\ddot{\underset{\sim}{U}}_i+\sum_{i=1}^{n}\underset{\sim}{N}_i^2\underset{\sim}{U}_i+\sum_{i=1}^{n}\left(\underset{\sim}{K}_i+\underset{\sim}{N}_i^3\right)\underset{\sim}{U}_i=\sum_{i=1}^{n}\underset{\sim}{P}_i \tag{11}$$

where $\underset{\sim}{M}_i$ is the mass matrix, $\underset{\sim}{K}$ is the stiffness matrix, $\underset{\sim}{P}_i$ is the external load vector and $\left(\underset{\sim}{N}_i^1,\underset{\sim}{N}_i^2,\ \underset{\sim}{N}_i^3\right)$ are non-standard matrix obtained from the coupling effects produced by the interaction forces between moving loads and bridge motion. In order to solve the nonlinear algebraic equations an implicit time integration scheme based on a variable step-size backward differentiation formula (BDF) is adopted. Moreover, during the time integration, due to the fast speeds of the moving loads, a small time step size is utilized, which typically, no more than 1/10 of the fundamental period of vibration of the structure.

4 RESULTS AND CONCLUSIONS

The bridge and moving loads dimensioning has been opportunely selected consistently to typical values utilized in several bridge applications and mainly derived from both structural and economical reasons. As a result, the dimensionless parameters related to aspect ratio, pylon stiffness, allowable cable stress, moving loads characteristics are assumed equal to the following representative values [1,6]:

$$\begin{gathered}\frac{L}{2H}=2.5,\ \frac{1}{H}=5/3,\ \frac{\mathrm{K_p}}{\mathrm{g}}=50,\zeta=\frac{\lambda}{\mu}=1,\ \zeta_0=\frac{\mu_0}{\mu b^2}=1.16,\tau_0=\frac{\lambda_0}{\lambda e^2}=1,\\ \varepsilon_{Fy,z}=\left(\frac{4I_{y,z}\sigma_g}{H^3 g}\right)^{1/4}=0.2,0.48,\ \varepsilon_\omega=\left(\frac{C_t\sigma_g}{Eb^2Hg}\right)^{1/2}=0.15,\\ \varepsilon_A=\left(\frac{A\sigma_g}{Hg}\right)=54.5,\ a=\left(\frac{\gamma^2H^2E}{12\sigma_g^3}\right)=0.1,\vartheta=c\left(\frac{\mu\sigma_g}{EgH}\right)^{1/2}\end{gathered} \tag{12}$$

where σ_g is the design stress under selfweight loads, γ is the stays specific weight, C_t torsional girder stiffness, b is half girder width.

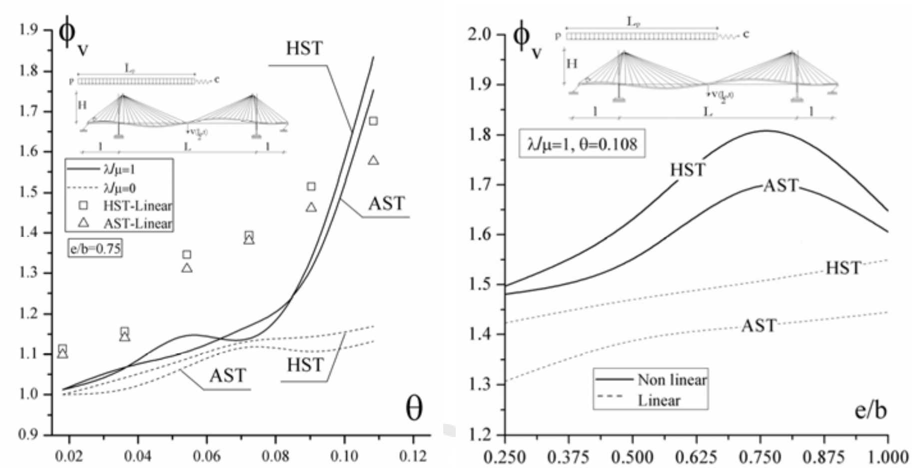

Figures 2-3. Dynamic amplification factors of the vertical midspan displacement for AST and HST: influence of the speed and the cable formulation (Fig. 2) and eccentricity of the moving loads (Fig.3)

In order to evaluate the influence of both mass schematization and tower typology, in Fig.s 2-3, the actual solution has been compared with a corresponding one, in which the external mass is assumed to be completely neglected, (i.e. λ/μ =0). The results point out different predictions for high range of speed parameters, where it has been proved that non-standard terms in the acceleration function provide notable amplifications in the bridge variables. Comparisons in terms of cable formulation based on secant Dishinger assumption are also reported.

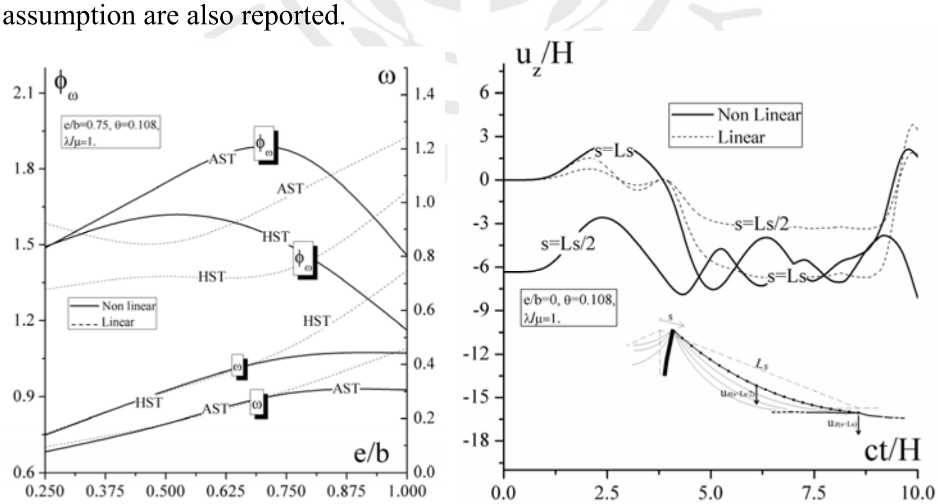

Figures 4-5. Midspan torsional rotation dynamic amplification factors and maximum displacement vs normalize eccentricity of the moving loads (e/b) for AST-HST (4). Time history of the vertical displacement of the longest stay (5)

In Fig.s 3-4, the effects of the eccentricity of the moving system for both A-shaped tower (AST) or H-shaped tower (HST) is investigated. In particular, comparisons to emphasize the prediction of the dynamic amplification factor and the maximum value of the torsional rotation, assuming different formulations in the prediction of cable suspension system behavior are developed. Finally, in Fig.5, time histories of the vertical displacements related to different cross-sections of the longest cable of the suspension system are reported. The results show how the cable elements are subjected during the moving load application to an oscillating behavior in the vertical displacements, leading to local vibration effects along longitudinal axis of the stay.

CONCLUSIONS

Long span bridges under moving loads have been analyzed for both flexural and torsional deformation modes, in terms of dynamic impact factors for typical kinematic and stress variables of the bridge. The effects of the inertial description of the moving system on the dynamic bridge behavior have been investigated, by means of a parametric study developed in terms of both moving loads and bridge characteristics. The analyses show how the actual behavior of the bridges is quite influenced by mass description of the moving loads or the formulation adopted to analyze cable vibrations of the suspension system.

REFERENCES

[1] Gimsing, NJ, *Cable supported bridges: concepts and design*. John Wiley & Sons Ltd, 1997.
[2] Au, FTK, Wang, JJ, Cheung, YK, “Impact study of cable-stayed bridge under railway traffic using various models”, Journal of Sound and Vibration, Vol.240, No. 3, pp. 447-465, 2001.
[3] Yang, F, Fonder, GA, “Dynamic Response of Cable-Stayed Bridges under Moving Loads”, J Eng.ng Mech, Vol. 124, No.7, 741-747, 1998
[4] Yau, JD, Yang, YB, Vibration reduction for cable-stayed traveled by high-speed trains. Finite Elements in Analysis and Design. Vol. 40, pp.341–359, 2004.
[5] Huang, D, Wang, TL, “Impact analysis of cable stayed bridges”, Computer and Structures. Vol. 43, No.5, pp.897-908, 1992.
[6] Bruno, D, Greco, F, Lonetti, P, “Impact analysis of cable stayed bridges”, Enginnering Structures, Vol. 30, pp.1160-1177, 2008.
[7] Crisfield, MA, Non-linear finite element analysis of solids and structures, Vol.1, John Wiley & Sons Ltd, 2000.
[8] Comsol, Reference Manual, Stockholm, Comsol AB, 2007.

DESIGN OF LONG - SPAN BRIDGES WITH CONVENTIONAL REINFORCED CONCRETE DECKS

Ioannis A. Tegos[1] and Stergios A. Mitoulis[2]

[1,2] Aristotle University of Thessaloniki, Dept. of Civil Engineering, Greece
e-mail: itegos@civil.auth.gr, mitoulis@civil.auth.gr

ABSTRACT: This paper investigates the applicability of conventionally reinforced concrete decks in long-span bridges, i.e. in bridge decks without prestressing tendons. A bridge actually built almost a decade ago by the Egnatia Highway SA, which lies along the Northern Part of Greece, was used as the benchmark bridge for the investigation. The analysis and design of the real bridge was performed according to the codes existing during the bridge final design. The bridge was re-designed according to Eurocodes utilizing a conventionally reinforced concrete deck by adopting Eurocode's class D. The study verified that the concrete sections with only ordinary strength steel can be utilized in bridges with span lengths up to 46 m.

KEY WORDS: Bridge; Exposure Class D; Eurocode; Ordinary Strength Steel; RC deck.

1 INTRODUCTION

Integral abutment and integral pier bridges are jointless bridge structures, whose deck is rigidly connected to both the abutments and the piers. They improve aesthetics and earthquake resistance towards the traditional systems with expansion joints, which permit thermal expansion and contraction, creep, and shrinkage. The increased cost of maintenance or replacement [1] of these faulty expansion joints, along with the initial cost of their design, manufacture, and installation, led to the advancement of the case for integral abutment bridges, which are compatible with conventionally reinforced concrete decks.

The final design of bridges takes into account the influence of the bridge classification, as defined by the exposure classes A, B, C and D of Eurocode 2 Part 2 [2]. Bridge design and is strongly related to the classification used during analysis as it reflects on the bridge structural cost and the long-term condition, namely the durability, of the bridge.

The use of ordinary steel for reinforcement for the design of long span bridges, without prestressing tendons, which leads to the compulsory adoption of an exposure class A or B, was also studied, in terms of constructability and cost-effectiveness. An investigation was conducted in order to identify the applicability of conventionally reinforced concrete decks in long-span bridges, i.e. in long bridge deck spans without using prestressing tendons. The selection of the bridge exposure class is strongly affected by the serviceability needs of the deck that is related to the allowance for deck cracking or not. It is noted that the erection of bridges with conventionally reinforced decks, i.e. without prestressing, longer than 20m is a relatively demanding construction. This is due to the fact that the ratio of the longitudinal reinforcement at splices results high and additionally the depth of the deck cross section, which is needed in order to control the deck's deflection, is typically large.

2 DESCRIPTION OF THE BENCHMARK BRIDGE GENERAL

The investigation utilised an as-built bridge as benchmark. The bridge of Kleidi-Kouloura belongs to Egnatia Motorway that runs across Northern Greece. It is a cast-in-situ structure with a total of three spans and a total length equal to 135.8 m. Figure 1 illustrates the longitudinal section of the bridge and the cross sections of the box-girder deck, the pier and its foundation. The deck of the bridge has a constant height of 2.18 m, while prestressing consists of tendons 20x19T15 (20 tendons of 19 wires with diameter 15mm each) with a parabolic geometry. The bridge has a seat-type abutment on which the deck is supported through two sliding bearings, while is rigidly connected to the piers. The clearance between the deck slab and the backwall is bridged by an expansion joint with a movement capacity of ±100 mm. The bridge has an agle of skew equal to 63.4°, as shown in Figure 2.

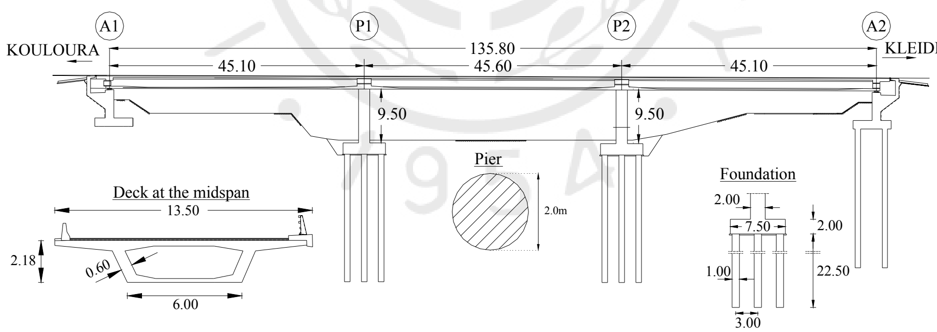

Figure 1. Geometric layout of Kleidi-Kouloura Bridge.

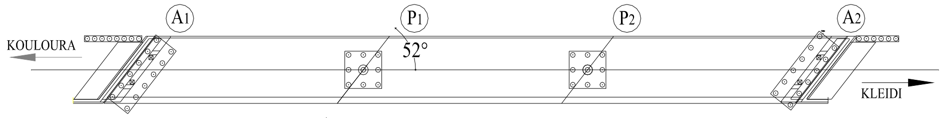

Figure 2. Plan view of Kleidi-Kouloura Bridge.

3 DECK DESIGN WITH ORDINARY STRENGTH STEEL

The last decade an intense effort and research was conducted to utilize ordinary strength steel in bridge decks. This is due to the need for rigid deck to abutment and deck to pier connections that allow the dissipation of part of the induced seismic energy through hysteretic behavior of the abutments and the piers. Design of conventionally reinforced bridge decks also eliminates the disturbance caused by the prestressing tendons during construction. In this framework an investigation was conducted to identify the constructability of long spans, up to 46.0 m, by utilising only ordinary strength steel, i.e. without prestressing tendons. In order to achieve such a design alternative, the cross section of the bridge deck was selected to be a void-slab, as shown in Fig. 5.

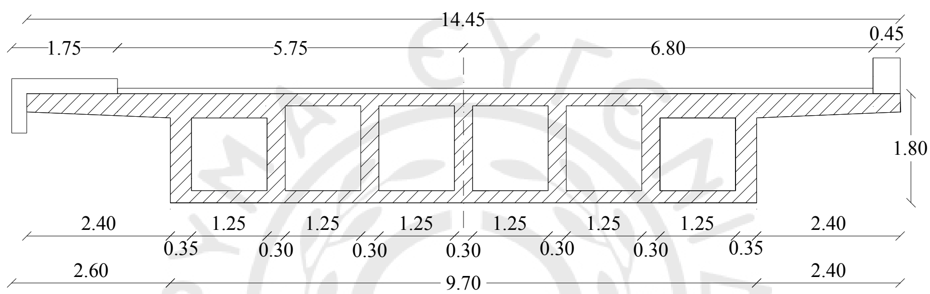

Figure 3. Cross section of the void-slab deck at the mid-span.

The use of conventional strength steel reinforcement for the erection of long span bridge spans is restrained due to the reasons underlined in the introduction. However, the preliminary design of the reinforced concrete deck that was attempted in this study was based on the codes' prescriptions [2] [3]. The selection of the void-slab bridge gave an acceptable longitudinal reinforcement ratio at splices, as shown in Figure 6 and 7. The scaling and the layout of the reinforcement with bars of 14.0m long, as shown in figures 8 and 9, and the use of bundled bars was found to facilitate the cast of concrete. The shear action was receiver by appropriate ratio of shear reinforcement. The control of the deflection was achieved by the resulting hyperstatic bridge system.

4 THE BRIDGE DECK

The bridge deck is connected rigidly to the piers. The cross section of the deck is solid over the piers, which means that is has no voids. Solid deck sections extend to a distance equal to 2·d=2·1.75 =3.50 m at both sides of the piers, where d is the depth of the deck's cross section. The cross section of the deck is also solid over the abutments and extends to a distance equal to 1.5·d=2.65 m from the support. The reason why the deck cross section was designed to be solid over the supports (i.e. abutments and piers) is that the punching shear loading of the deck, due to the concentrated loads, was found to be more critical than the corresponding shear loading. This is due to the fact that the piers' diameter that is 2.0 m, is smaller than 3.5 times the depth of the deck's cross section, which is equal to 3.5·d = 3.5·d = 6.15 m. Additionally, the typical favorable influence of prestressing is not developed, due to the fact that only ordinary strength reinforcement bars were used for the deck.

5 MODELING

Modeling of the deck of the bridge was attempted by shell elements of SAP 2000 [4].

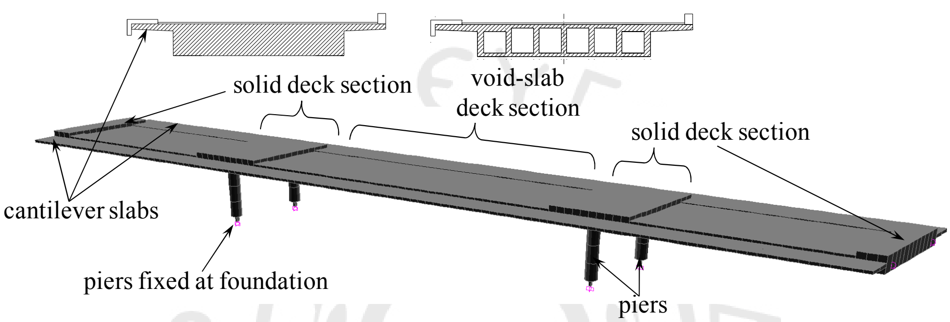

Figure 4. The model of the bridge with the shell elements.

6 BENDING DEFLECTION AT MID - SPAN

The calculation of the deck's vertical deflection was performed assuming that the bridge deck is cracked, i.e. the effective stiffness of the deck was calculated. It was found that the high ratio of the longitudinal reinforcement is favorable for the stiffness of the long span of the deck. The stiffness of the deck is equal to $K_{II,eff} = 0.69 \cdot E_{cm} \cdot J_c$. The deflection of the deck was then calculated equal to 170 mm namely equal to L/264=45.6m/264, which is acceptable.

7 DESIGN OF THE BRIDGE DECK

The deck belongs to class D according to Eurocode 2 Part 2 [2] in both the longitudinal and the transverse direction. Table 1 shows the bending moments and the total reinforcement requirement of the deck against the ultimate limit state loading.

Table 1. The bending moments and the longitudinal reinforcement at the mid-span and at the support.

	Bending Moment (MN·m)	Longitudinal reinforcement area (cm^2)
Central span	61.88	882.34
Support	-65.50	970.26

8 REINFORCEMENT SCALING AND LAYOUT

The reinforcement of the bridge deck was designed in a manner to avoid longitudinal reinforcement splicing at deck flanges that are in tension, i.e. splicing of the reinforcement bars is avoided were the bending moments are positive at the spans and negative at the supports.

Single or bundled bars appropriately scaled were utilised under the following concept:

(a) The reinforcement laps were set in a manner that the maximum length of the reinforcement bars, that is 14.0m, is a multiple of the required lap lengths of the Ø20mm bars. This was achieved by determining the maximum allowed ratio of the longitudinal reinforcements, which is the upper bound set by the code [5] and is related to the reinforcement to concrete bond conditions, the diameter of the bar and the grain size, which is the nominal maximum aggregate size. Then the **n** parameter was defined, which was the integer part of the maximum bar length (14.0m) divided by the required lap length. Then, **n** groups of bars were utilised, which were set in the transverse direction of the deck cross section according to Figures 5 to 8. For example the in case of Ø20 reinforcement bars and for a maximum grain size 16 mm, groups of 20 bars, from which 19 are effective as shown in Figure 5, can be utilised, according to Figures 5 and 6, for the bottom flange of the deck, where the bond conditions are good. For a slight over-reinforcing of the deck, i.e. the use of a longitudinal reinforcement ratio only 5.3% greater than the one allowed by Eurocode 2 Part 1 [5], it was found that reinforcement splices can be avoided.

8.1 Single bar reinforcement

Single bars can be used for the reinforcement of the top flange of the deck, i.e. at deck's supports, where the bonding conditions are unfavorable and hence the reinforcement lap lengths are large.

The groups of bars consist of 14 reinforcement bars, from which 13 are effective, Figures 5 to 8. This led to a 7.7% overdesign. It is noted though that this over-reinforcing is much smaller than the one that would be needed in case the code's splices were applied.

8.2 Bundled bars

(b) The use of bundled bars according to Eurocode 2 [5] and EKOS 2000 section 17.12 [6] is deemed to be a design alternative in case of more demanding deck reinforcements. The spacing between the bar bundles and the lap lengths are determined by the equivalent diameter $Ø_n$ of the bundled bars. Figures 9 to 12 illustrate the reinforcement scaling and layout in case bundled bars 2Ø20 are used for the reinforcement of the deck at the mid-span and at the supports.

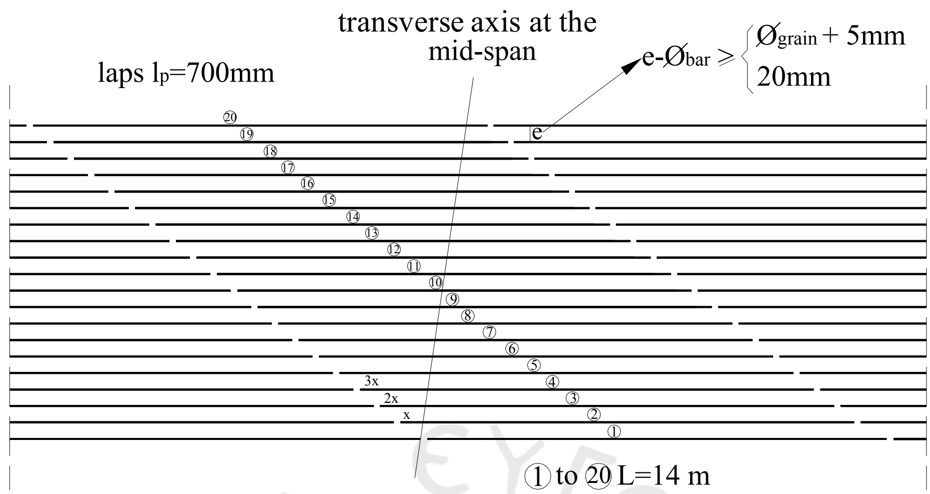

Figure 5. Reinforcement scaling with single bars Ø20 of the deck at the mid-span (the scale is distorted) (where **x** is the reinforcement lap and **e** is the spacing of the bars).

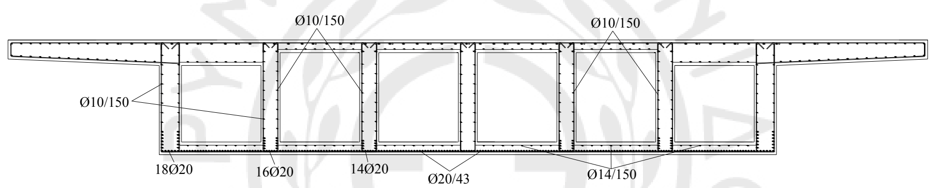

Figure 6. Cross section of the deck with the single-bar reinforcement layout at the mid-span.

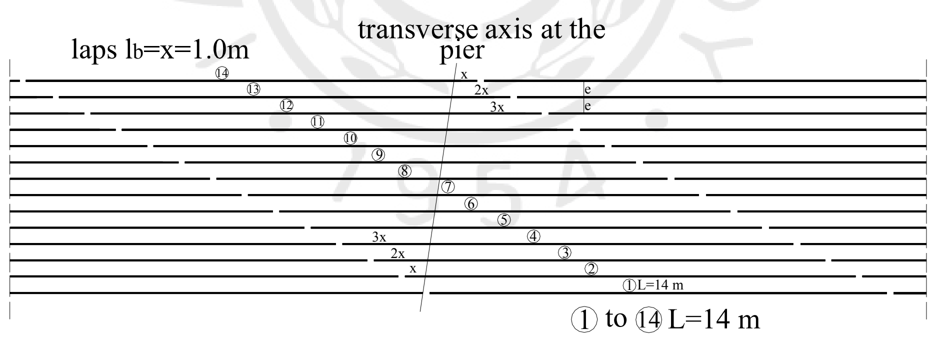

Figure 7. Reinforcement scaling with single bars Ø20 of the deck at the support (the scale is distorted), (where **x** is the reinforcement lap and **e** is the spacing of the bars).

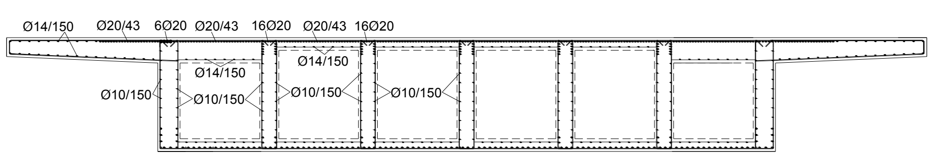

Figure 8. Cross section of the deck with the single-bar reinforcement layout at the support.

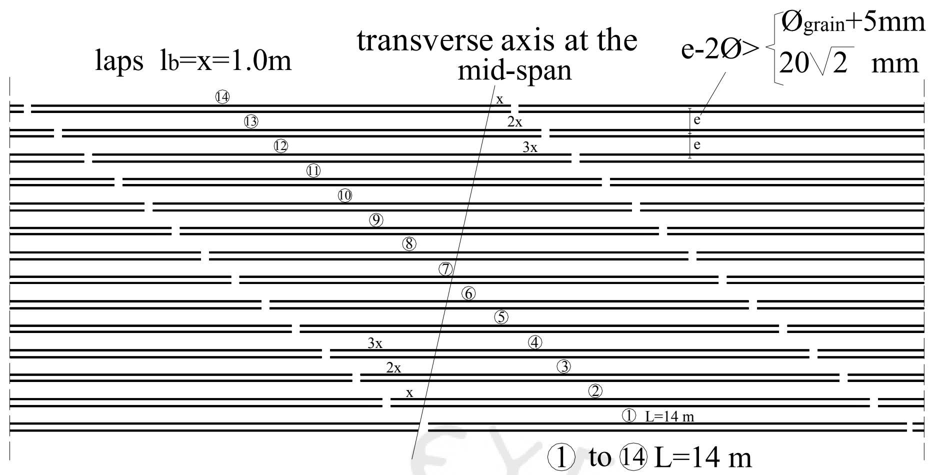

Figure 9. Reinforcement scaling with bundled bars 2Ø20 of the deck at the mid-span (the scale is distorted) (where **x** is the reinforcement lap and **e** is the spacing of the bundled bars).

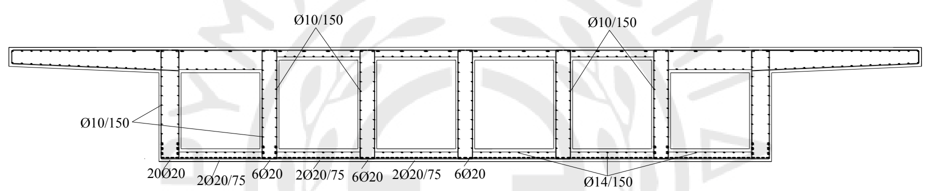

Figure 10. Cross section of the deck with the bundled bar reinforcement layout at the mid-span.

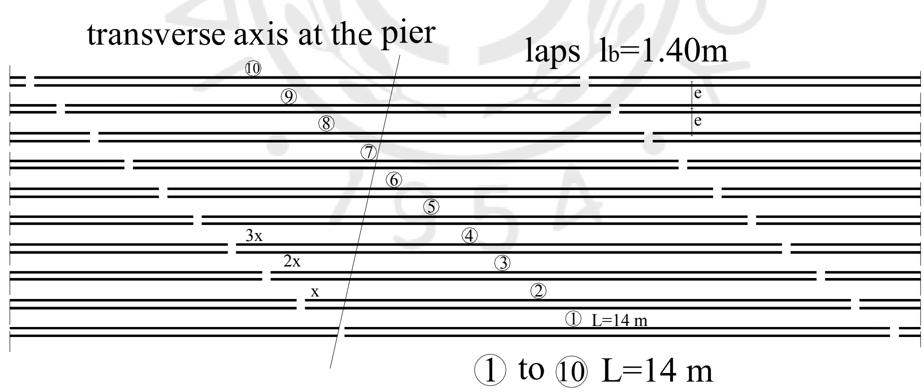

Figure 11. Reinforcement scaling with bundled bars 2Ø20 of the deck at the support.

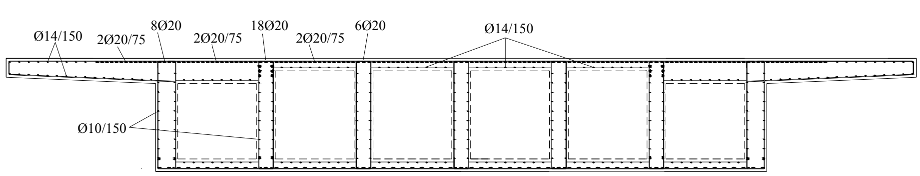

Figure 12. Cross section of the deck with the bundled bar reinforcement layout at the support.

9 CONCLUSIONS

The applicability of conventionally reinforced concrete decks in long-span bridges, i.e. in bridge decks without using prestressing tendons, was studied utilising a benchmark bridge actually built along the Egnatia Highway. The study came up to the following conclusions:

- The deck of the bridge can be reinforced with bundled bars. It was found that 14x2Ø20 and 10x2Ø20 were found to be adequate for the deck's mid-span and supports correspondingly. The checks showed that concrete with a maximum grain size 31 mm can be used. The over-reinforcing steel is up to 8 % at the mid-span and 11 % at the support.
- An alternative reinforcement layout is the use of bar groups of 20 bars and 14 bars for the deck's mid-span and support respectively. In that case concrete with a maximum grain size 16 mm can be used, while the over-reinforcing steel is up to 5 % and 8 % for the deck's mid-span and supports correspondingly.
- As far as its concerns the deflection of the deck it was found that the deck's deformation is acceptable, despite the fact that no prestressing was utilised and due to the use of high longitudinal reinforcement ratios.
- The use of more steel bars aiming at avoiding reinforcement splices, was up to 11%. The last overuse of steel was found to be less than the corresponding overuse that would be needed in the conventional design case with reinforcement splices.
- This paper shed light on the reinforced bridge and showed that the use of only ordinary strength steel can be a design alternative for long span bridges.

REFERENCES

[1] Mitoulis SA, Tegos IA, Stylianidis K-C., "Cost-effectiveness related to the earthquake resisting system of multi-span bridges", *Engineering Structures*, Vol. 32, Isuue 9, pp. 2658-2671, 2010.
[2] EN 1992-2 Eurocode 2: Design of concrete structures-Part 2: Bridges, 2004.
[3] DIN-Fachbericht 102, Betonbrücken, DIN Deutsches Institut fuer Normung e.V, 2003.
[4] Computers and Structures INC. SAP 2000. Nonlinear Ver. 11.0.4. *User's Reference Manual*, Berkeley, California; 2002.
[5] EN 1992-1 Eurocode 2 - Part 1: Design of concrete building and civil engineering structures, 2004.
[6] Ministry of Environment, Land Planning and Public Works of Greece. Greek code for the design of reinforced concrete structures, (EKOS-2000), Athens, (In Greek), 2000.

MAIN GATEWAY "SHEIKH ZAYED" BRIDGE, ABU DHABI, UAE

Costas Constantoulakis[1] and Georgios Nikolopoulos[2]

[1,2] Archirodon Construction Overseas
e-mail: constant@archirodon.net, gnikolopo@archirodon.net

ABSTRACT: The paper provides an outline of the architecturally unique structure, which is presented along with the major material quantities associated with the construction. The reader is guided through the challenges involved with the design, detailing and construction of the bridge, and the imposing in size and sophistication temporary works involved. The paper concludes with a description of the construction operations that led to the successful completion of the project.

KEY WORDS: Abu Dhabi; Bridge; Construction.

1 INTRODUCTION

Sheikh Zayed Bridge (SZB) was envisaged to be the new main crossing to the island city of Abu Dhabi, capital of the Emirate of Abu Dhabi and the UAE and at the same time, a timeless "landmark" project to highlight the rising economic status and power of the Emirate.

Photo 1. View of the underside of the bridge

The architectural design was entrusted to architect Zaha Hadid, world-renowned for her groundbreaking and prominent designs. Its characteristic feature is a continuous synthesis of wavy piers and arches intended to simulate the shape of the windswept sand dunes that form the quintessence of the Emirate’s desert landscape. The structure is integrated with two independent bridge decks with no visible underlying supports, presenting an uninterrupted constant side-view, further embellished by two external open cells, as shown in *Photo 1*.

The challenge of bringing this innovative idea to life was attained by Archirodon Construction (Overseas) Co SA (ARCO), based on the structural design and construction supervision of High Point Rendel (HPR).

2 DESCRIPTION

The completed bridge is of a total length of 842m, divided into 11 spans of lengths ranging from 60m to 160m, as shown in *Figure 1*. The bridge comprises 4 massive reinforced concrete piers and three steel arches supported by them, that combine to form a continuous support system for the two road decks. The 1st (western) arch provides two points of support along the underside of the bridge, while the 2 longest spans are suspended from the remaining 2 arches by multi-strand hangers. The road decks are provided with 6 additional points of support at the piers, plus the 2 abutments and 2 land-piers at the western approach spans of the structure.

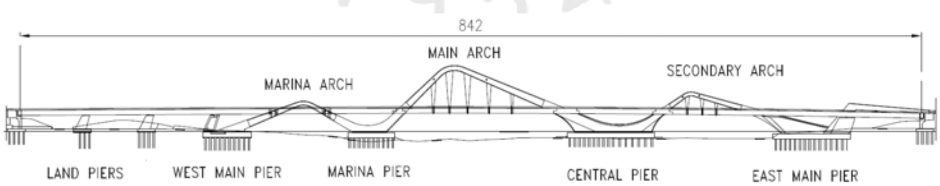

Figure 1. Bridge Elevation

The cross-sections of the 2 independent, cast in situ, post-tensioned concrete decks are typically 23.7m wide and comprise 3 closed and 2 open cells, adequate to accommodate a 5-lane carriageway plus emergency lane and pedestrian walkway each.

The bridge piers and abutments were constructed on massive 16.000 m³ pile-caps supported by 670, 1.5m diameter, cast-in-situ concrete piles, 20 to 25m long.

To provide indication as to the sheer magnitude of the project, the major quantities associated with the construction of the SZB are summarized below:

• Concrete, 40 MPa and 50 MPa	250,000 m^3
• Post-tensioning strands	5,000 T
• Reinforcement	50,000 T
• Structural steel - Permanent Works	12,000 T
• Structural steel - Temporary Works	22,000 T

3 PROJECT CHALLENGES

The flagship nature of the project, its sheer size and geometric complexity, along with the need to successfully complete the bridge without compromising the aesthetic elegance and clarity of the design, brought ARCO ahead of addressing and overcoming substantial engineering challenges, such as:

- The detailing, fabrication, transportation, handling, erection and welding-to-position of the steel arches, comprising a total of 22 segments weighing between 350T and 650T each.
- Construction of the 4 main piers, all inclined and curved in space, situated partially or fully on the waterway.
- The construction of the heavy bridge decks, 70% of which had to be executed above water.
- Abidance with the contractual requirement to guarantee that no part of the structure shall be subject to stresses above the design-specified envelope, both during construction and service of the bridge.
- The very severe design parameters (wind & earthquake) that had to be adopted for the design of the permanent as well as temporary works.

To successfully address the aforementioned challenges, ARCO decided to invest on well-winnowed engineering experience to constitute the core of its construction planning and operations, by:

- Assembling a strong in-house Engineering Department, consisting of Temporary Works (TW), Permanent Works (PW) and Construction Methods (CM) Sections. This department was entrusted with the conceptual, preliminary and final design and detailing of all temporary works along with the in-house development of detailed construction methods, with the exception of the final design of the arches erection performed by VSL-Singapore Technical Office. The department also performed extensive work for the detailing of permanent works, including full 3D modeling of concrete components, post tensioning geometries, and steel reinforcement layouts, especially in congested areas of the works (steel content reaching 500-600kg/m³ in some places). This effort resulted to the in-house production of over 16,000 detailed construction drawings.

- Acquiring the services of Buckland & Taylor of Vancouver-Canada, a world-leading Bridge Engineering Consultancy, throughout the construction period to perform:
  a) Independent checking and certification of all TW designs.
  b) Independent checking, verification and certification of conformity to stress specifications, which extended to the review and evolution of the PW design with the aid of an integral 3D model of the PW and TW, including time effects.
  c) Construction analysis based on the aforementioned model including construction stage analyses to define pre-cambering requirements for the structural components as well as other useful information (such as support reactions on the arches temporary support structures to be corroborated against site measurements to verify the analyses etc).

4 TEMPORARY WORKS

In total approximately 22,000T of steel were used for the temporary works of the SZB project. Temporary structures were designed in-house, approved by the Independent Engineer, fabricated (~30% in-house), erected and lowered several times before eventually being decommissioned. The lack of standardization of the bridge components resulted to a quantity-of-temporary-steel/concrete ratio of 88 kg/m^3, which seems overwhelming compared to the 17 kg/m^3, recently used by ARCO in the construction of a similar size, concrete-deck, cable-stayed bridge.

4.1 Deck and Piers

A heavy shoring system founded on 762x16mm driven, steel tubular piles was implemented for the construction of the bridge decks and piers.

The falsework for the construction of the piers was typically arranged on a 5m x 5m grid, formed by 500mm diameter circular steel columns (reaching heights up to 20m) and heavy H sections serving as primary and secondary beams.

The falsework used for construction of the decks, comprised 2 steel box-girders per deck supported by steel circular columns. The box-girders were spaced 12m apart, and spanned 20m to 25m, serving as primary beams, these 4m-long formwork modules were placed consisting of transverse lattice girders at 2m centers, steel purlins and plywood skin as shown in *Photo 2 and Figure 2*. To accelerate construction, the initially developed system good for a 160m-long twin deck was used in spans 1 – 2 – 3, 9 – 10, 11, 7 and a second system was fabricated, to be used in spans 4 – 5 – 6 and 8. The second system was fabricated mainly from re-used sections from the decommissioning of the pier scaffolding, and comprised 3 heavy trusses acting as main longitudinal support beams and HEA500 beams at 2m centers acting as cross members.

Photo 2. Falsework for construction of deck

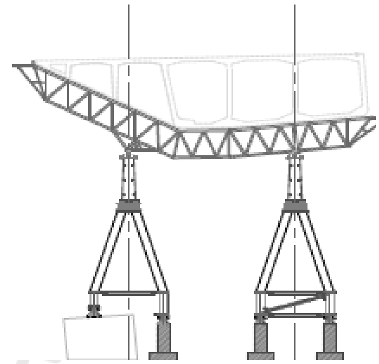

Figure 2. Diagram showing falsework

4.2 Arches

A unique and innovative scheme of TW was developed for the erection of the steel arches, consisting of:

- Four-legged towers 5m x 5m in plan, reaching heights up to 60m and positioned on a 40m x 32m grid, shown in *Photo 3 and Figure 3*.
- 2 main longitudinal box-beams, spanning 40m and cantilevering 14m.
- 2 transverse crane beams moving longitudinally, spaced 6m apart and spanning 32m.
- Transverse twin lattice beams acting as supports to the arches using lockable hydraulic jacks of 600T capacity and equipped with load-monitoring sensors linked to a data-logger.
- A turntable rotating 360° by means of 4m-long stroke double-acting hydraulic jacks over an orthogonal frame, moving transversely, bearing the lifting system that comprised 4 strand jacks of 330T capacity
- The "rotator", a special device used to rotate the steel segments from the "outer web down" position (as fabricated and transported) to the "bottom flange down" position, suitable for erection.
- A clamping system consisting of up to 120 Macalloy bars, 30mm in diameter and heavy shear plates, to hold the segments firmly together during welding operations.

All temporary works components were fabricated under strict quality control. Upon completion, all elements were load-tested and certified by a reputable third-party organization.

In addition to the aforementioned TWs, ARCO mobilized and used a large number of heavy marine and land equipment, such as (heavy floating cranes, barges, tug boats, land cranes, tower cranes, piling equipment, special trailers etc).

Photo 3. Temporary works for the erection

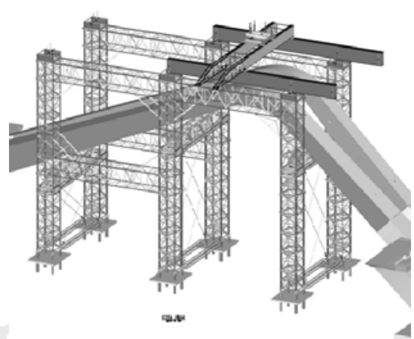

Figure 3. 3-D Model of TW

5 CONSTRUCTION

5.1 Foundations and Piers

The 4 Marine piers and their pile-caps were constructed within double walled cofferdams, which also provided working and storage space *Photo 4*. 2 temporary bridges provided access to the Marina and Central Piers.

The construction of the pile-caps, ranging in volume from 9,000m^3 to 16,000m^3, was divided in pouring stages of up to roughly 3,000m^3. An in-depth analysis was performed ahead of casting, to ensure thermal cracking is avoided. After casting, each component was covered with insulating blankets, and the temperature was monitored with the use of appropriate thermo-couplers and data collection-recording system, until cooling down (approximately 2 weeks).

Photo 4. Construction of Piers

Similarly the construction of the piers was divided in castings of up to 1,000m^3, (usually 300m^3 to 600m^3). This called for accurate detailing of the steel reinforcement adapted to the predefined construction joints. Due to difficulty of access to the inner chambers of the piers, we opted for extensive use of sacrificial formwork (precast concrete panels).

The main difficulties encountered during the construction piers, was the total lack of repetition, accessing and working in very steep areas, and the incredible congestion of reinforcing steel and PT ducts, which necessitated the use of self-compacting concrete, which in turn required the use of waterproof shutters in certain areas.

5.2 Bridge Deck

Construction of the twin road decks was simultaneous with each deck section constructed in two stages. The first stage included the casting of the bottom slab, all webs and the top slab of the 2 open outer cells, with pours of up to ~1000 m^3, a laborious albeit delicate exercise due to the sensitivity of the mix requiring operational precision to a meticulously planned construction methodology. The second stage of deck construction would commence upon striking of the webs' shutters, and see the remaining part of the top slab cast on a light custom made formwork.

5.3 Arches

Fabrication of the 3 steel arches was subcontracted in March 2004, to STPI, Thailand with the target completion date set at the end of 2005. The materials used in the fabrication were purchased by ARCO and hence issued to the fabricator. The geometry and complex detailing of the arches, constituted their fabrication an onerous and time consuming operation which led ARCO at the beginning of 2006, under the pressure of the minimal progress noted in the fabrication line, to decide upon a split of the arches fabrication to two fronts. A second fabricator (company Fabtech), based in the industrial area of Jebel-Ali, was employed to carry out the fabrication of the secondary arch.

The erection of the Main and Secondary Arches was performed using the purpose-designed-and-built systems described previously. The arch segments were fabricated in the "outer web down" position, to permit match trial at the fabrication shop. They were hence transported on special multi-wheel trailers to the dock and loaded on special marine vessels equipped with 2x600T cranes. Upon arrival at the port of Abu Dhabi, they were transferred to the contractor's barges and towed to site. With the aid of the aforementioned handling and erection systems they were placed on the "rotator" unit to be brought "bottom flange down", their intended position for erection. The segments were subsequently lifted, tilted vertically and finally moved to their intended position.

All lifting operations, linear and rotational, were meticulously pre-engineered and modeled in a 3D environment. Each element was joined to the previously installed one, and rested on a support truss placed near the free end incorporating a pair of 600T hydraulic jacks with load monitoring sensors, to be used for adjusting the new segment to its intended place for fixing. With the segment in place, clamping of the back joint was done while the load was still held by the lifting gear. Once the clamping was complete, the load was released from the lifting jacks for welding operations at the joint to commence. Welding would take 3 to 7 days (24-h shifts) depending on segment sizes and plate thicknesses (up to 100mm). The loads on the support jacks were constantly monitored to confirm their compliance with the design requirements, which was mostly the case, as it was only very seldom that adjustments had to be made. Marina arches were erected with the aid of a 1,500T crawler-crane, working on a backfill cofferdam.

Following the completion of all welding operations, the bolted joints of the arches to the piers were injected with epoxy grout and the bolts (Macalloy bars) were re-stressed to their design-required forces.

The arms supporting the Marina arches were fitted with 5m-long heavy steel jackets, connected to the concrete by a multitude of shear studs. Marina arch presented the additional difficulty of having to be welded to the aforementioned steel jackets on both sides, within only a few millimeters of tolerance. Very precise surveying and execution of fabrication and erection, resulted to the successful placement and welding of the segments without the need for field corrections.

6 CONCLUSION

The involvement and dedication of top-range Engineers and staff combined with the extensive and meticulously planned engineering efforts enabled the successful completion of this extremely complex and demanding project, in full compliance with the strict structural and geometrical requirements, and without the occurrence of any significant accidents or temporary works failure.

NONLINEAR MODELLING OF THE STATIC RESPONSE OF LONG-SPAN CABLE STAYED BRIDGES

D. Bruno[1], F. Greco[1*], P. Lonetti[1], E. Bianchi[1]

[1] Department of Structural Engineering, University of Calabria, Cosenza, Italy
e-mail: d.bruno@unical.it; f.greco@unical.it, lonetti@unical.it

ABSTRACT: This work proposes a numerical investigation on the nonlinear static behavior of self-anchored long span cable-stayed bridges with a fan-shaped arrangement of stays, taking into account the coupled effects of the nonlinear response of the single stay and the instability effect of the axial compression in the girder.

KEY WORDS: Geometrical nonlinearities, nonlinear stay's behavior, numerical model.

1 INTRODUCTION

Due to the notable progress in structural engineering, material and construction technologies, cable-stayed bridges have become an efficient solution for long span crossing [1-3]. A standard analysis, based on linear assumptions and on the Dischinger's fictitious tangent modulus, may introduce several inaccuracies for long span bridge for which the main girder has the tendency to become more slender and lighter. As a consequence, a nonlinear analysis taking into account for both material and geometrical nonlinear effects must be adopted. Nonlinear effects may arise from different sources, including the sag effect due to the self-weight of the cable stays, changes in the geometrical configurations the due to large deformations, constitutive behavior of the structural components, the coupling between torsion and bending of the girder. Previous contributions to the study on the nonlinear behavior of cable-stayed bridges are given in [4-6], including one or more of these sources of nonlinearities and focusing essentially on a plane model. This contribution proposes a numerical investigation on the nonlinear static behavior of long span cable-stayed bridges with a fan-shaped arrangement of stays, by considering the nonlinear behavior of the single stay in coupling with the instability effect of the axial compression in the girder. The analysis is carried out by numerically solving the nonlinear problem both with reference to a continuous model, assuming a continuous distribution of the stay stiffness along the girder, and to a discrete finite element model, corresponding to the actual stays spacing. In the former case the nonlinear differential problem is numerically integrated, in order to obtain simplified solutions able to capture the main non linear effects on the static response. In the latter one, a nonlinear finite element model is adopted to accurately determine the influence of nonlinear effects and to assess the limit of validity of the former one.

2 STATIC BEHAVIOR OF LONG - SPAN CABLE STAYED BRIDGES

2.1 Continuous model

In this section a continuous model for the analysis of the static response of cable stayed bridges is presented based on a diffuse stays arrangement ($\Delta/L << 1$) according to the modern tendency in the design of long span cable stayed bridges to adopt a small spacing between the stays. An approximate but simple analysis able to investigate on the main aspects of the nonlinear behavior of bridge is thus carried out . Nonlinear effects may arise from different sources, including the sag effect due to the self-weight of the cable stays, changes in the geometrical configurations the due to large deformations, constitutive behavior of the structural components. In particular, the proposed model is able to predict the static behavior of cable stayed bridges taking into account the nonlinear behavior of the single stay, adopting the Dischinger's fictitious secant modulus for the cables to model the stays nonlinear behavior and taking into account the instability effect due to the axial compression in the girder. The analyzed bridge scheme is illustrated in the fig. 1. The stays are fan shaped with constant spacing Δ. The girder is supported by stays joining at the tower tops. The two lateral stays, called anchor stays, assure the bridge equilibrium and are anchored by means of two vertical supports; the girder is not horizontally constrained.

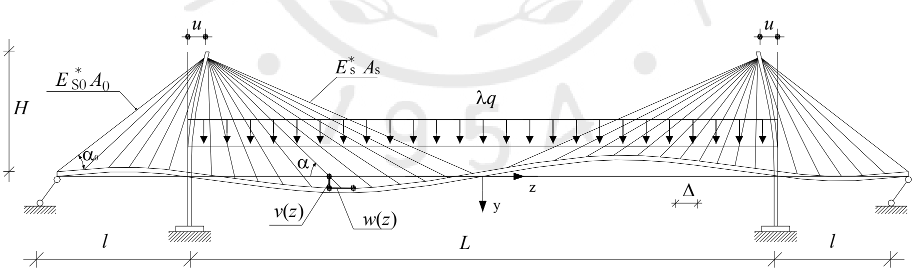

Figure 1. The long-span cable stayed bridge structural scheme.

It is assumed that the erection method is such that the deck's final configuration is practically straight and free from bending moments. In such circumstances stresses produced by dead loads are evaluated from the statically determinate scheme where hinges are placed at the nodes. The aim of this work is to analyze the bridge static response when live load λp increasing with the parameter λ are applied, starting from the straight equilibrium configuration of the bridge's deck corresponding to the application of the dead load g and cables pre-stress. The cable stayed bridge deformation is defined by the following displacement parameters:

- The function *v(z)* which represents the girder's vertical displacements;
- The girder's horizontal displacement *w(z)*;
- The pylon tops horizontal elastic displacement *u*.

As a matter of fact, the horizontal equilibrium of the bridge requires shear forces to be the same at the pylon top sections and this ensures that displacements of the pylon tops will always be opposite.

The vertical and horizontal equilibrium equations for the girder respectively are:

$$EIv^{IV}+\left[\left(N^g+\Delta N(w)\right)v'\right]'-q_V=\lambda p\,,\; EAw^{II}+q_0=0\,, \tag{1}$$

where EI is the girder flexural stiffness, N^g represents the axial force in the girder due to the dead load g

$$N^g(z)=gH/2\left[\left(L/(2H)\right)^2-\left(z/H\pm L/(2H)\right)^2\right], \tag{2}$$

$\Delta N(w)=EAw'$ indicates the axial force increment in the girder due to live loads, E and A are respectively the Young modulus and the cross section area for the girder, q_v denotes the vertical component of the stays-girder interaction:

$$q_V=E_S^*A_S/(H\Delta)\left[-vsin^3\alpha+(u\mp w)sin^2\alpha\cos\alpha\right], \tag{3}$$

and q_o is the horizontal component of the stays-girder interaction

$$q_O=E_S^*A_S/(H\Delta)\left[\mp vsen^2\alpha\cos\alpha-(\mp u+w)sen\alpha\cos^2\alpha\right], \tag{4}$$

In the above equations the + or - sign applies respectively to the left or right part of the bridge. In eqn (4) E^*_S represents the Dischinger's secant modulus for the cables:

$$E_s^*=E\left[1+\frac{\gamma^2El_0^2}{12\sigma_g^{\;3}}\frac{1+\left(\sigma_g+E_s^*\Delta\varepsilon\right)/\sigma_g}{2\left(\left(\sigma_g+E_s^*\Delta\varepsilon\right)/\sigma_g\right)^2}\right]^{-1}, \tag{5}$$

where σ_g is the initial stress in the cables under the dead loads g, E is the Young modulus, l_0 is the horizontal projection of the stay length, γ is the specific weight and $\Delta\varepsilon$ represents the axial strain in the cables produced by the additional displacements v, w and u. Usually the stays cross section area A_s is designed so as dead loads produce constant tension in all stays and this together with the assumed initially straight configuration of bridge deck under dead loads, leads to $A_S = g\Delta/(\sigma_g sin\alpha)$ in which σ_g is defined as a function of the allowable stress σ_a as $\sigma_g = g\sigma_a/(p+g)$ by assuming that the stress increment in the stays are proportional to the design live loads p. For the anchor stays the cross sectional geometric area A_0 is designed in such a way that the allowable stress σ_a is obtained for live loads p applied to the central span only, leading to:

$$A_0 = gl / 2\sigma_{g0}\left[1+\left(l / H\right)^2\right]^{1/2}\left[\left(L / (2l)\right)^2 - 1\right]. \tag{6}$$

where the initial tension σ_{g0} in the anchor stays is equal to:

$$\sigma_{g0} = \sigma_a\left[1+\frac{p}{g}\frac{\left(L / (2l)\right)^2}{\left(L / (2l)\right)^2 - 1}\right]^{-1}. \tag{7}$$

The horizontal equilibrium equations for the pylons, involving the effects of the stays-girder interaction, should lead to integral equations. In order to write the horizontal equilibrium equation for the left pylon in a differential form, a fictitious rigid beam is considered on which the horizontal component of the stays-girder interaction is applied only for the left part of the bridge. The towers stiffness is distributed on the fictitious rigid beam for the entire span of the bridge. Consequently, the horizontal left pylon equilibrium equation assumes the following expression:

$$EA_t u^{II} - q_0' - Ku / \left(L + 2l\right) = 0, \tag{8}$$

where A_t and K are respectively the fictitious beam cross-section (assumed theoretically infinite) and the pylon tops flexural stiffness. The horizontal component of the stays-girder interaction q_0' assumes the expression given by eqn (4) for the left side of the bridge (z ˛0) whereas it vanishes on the right one (z>0).

Solutions for the differential equations (1) and (9) are obtained imposing the appropriate boundary conditions. With reference to the girder vertical equilibrium the associated boundary conditions require that the girder vertical displacement and the curvature vanish at both $z= -L/2-l$ and $z= L/2+$l.

The two boundary conditions associated with the horizontal equilibrium of the left pylon impose that at the left edge of the fictitious rigid beam $EA_t u^I$ is equal to the horizontal component of the anchor stay axial force S_0:

$$S_0 = -(w-u)E^*_{so}A_0 / H \; sen\alpha_o \cos^2\alpha_o \,, \tag{9}$$

whereas at the right edge $EA_t u^I$ vanishes. In eqn (12) E^*_{s0} represents the Dischinger's secant modulus for the anchor cable adopting eqn(8) for σ_{g0}.

The boundary condition related to the horizontal equilibrium of the girder, require that the internal axial force is equal to the horizontal component of the anchor stays axial forces, namely

$$w'(-L/2-l) = (w-u)E^*_{so}A_o / (EAH) sen\alpha_o \cos^2\alpha_o \,, \tag{10}$$

$$w'(L/2+l) = -(w+u)E^*_{so}A_o / (EAH) sen\alpha_o \cos^2\alpha_o \,. \tag{11}$$

In order to analyze the main parameters governing the differential problem the above equations are rewritten in a dimensionless form. To this end dimensionless quantities are introduced:

$$\xi = \frac{z}{H};\ V = \frac{v}{H};\ U = \frac{u}{H};\ W = \frac{w}{H};\ a = \frac{\gamma^2 E H^2}{12{\sigma_g}^3};\ \ \varepsilon = \sqrt[4]{\frac{4I\sigma_g}{H^3 g}}\ . \tag{12}$$

The boundary value problem, governing the equilibrium of the long-span cable stayed bridge, can be reformulated as a non-linear system of first order ordinary differential equations subject to boundary conditions only at two-points. This transformation technique causes an increase of the variables number. The unknown variables, defined in the dimensionless integration domain [$-r_1$-r_2, r_1+r_2], are [V, V^I, V^{II}, V^{III}, V^{IV}, U, U^I, W, W^I]. The reformulated boundary value problem assumes the form:

$$\boldsymbol{y}'(\xi) = \boldsymbol{g}(\boldsymbol{y},\xi),\quad -r_1\text{-}r_2 \le \xi \le r_1 + r_2 \tag{13}$$

where $\boldsymbol{y}$=[y_1, y_2, y_3, y_4, y_5, y_6, y_7, y_8] is a vector of the unknown functions of the problem (collecting displacement parameters and their derivatives). $\boldsymbol{g}$ is an opportune vector function.

In equation (13) the prime denotes differentiation with respect to ξ. Equation (13) is subjected to the two-point linear boundary conditions:

$$\boldsymbol{B}_0\boldsymbol{y}(0)+\boldsymbol{B}_1\boldsymbol{y}(1)=\boldsymbol{c} \tag{14}$$

where $\boldsymbol{B}_0$ and $\boldsymbol{B}_1$ are opportune matrices containing coefficients of boundary and matching conditions and $\boldsymbol{c}$ is an opportune known vector. The boundary value problem has been solved by means of an iterative collocation method implemented in MATLAB which provides a *C1*-continuous solution by using a cubic collocation polynomial on each subinterval of the mesh. Starting from an initial guess for the solution and the mesh, at each iteration the method adapts the mesh to obtain a sufficiently accurate numerical solution. In the numerical computations the cross section area of the fictitious beam has been assumed equal to $A_t = A\ 10^3$.

2.2 DISCRETE MODEL

In the present subsection a discrete model is examined with reference to the actual stays spacing, taking into account the geometric nonlinear effects for the cable system under general load conditions, in order to obtain more accurate results and to assess the limit of validity of the continuous model.

This discrete model has been studied by means a displacement-type finite element (FE) approximation, implemented in the commercial software COMSOL MULTIPHYSICS™. In order to reduce the computational effort in the numerical calculations, a simplified three dimensional finite element model has been developed, by using beam and spring elements to model the bridge deck and the pylons, respectively. In detail, the deck is replaced by a longitudinal spline with equivalent sectional and material properties; on the other hand axial inextensibility for pylons was supposed, whereas their flexural stiffness in both principal directions is taken into account by using linear spring elements having equal values of the stiffness constant. Moreover, the equilibrium equation of a girder element has been derived through the application of the virtual work principle, accounting for the instabilizing effect produced by the axial compression force N_e corresponding to the total applied load $g + \lambda p$; to this end the following weak contribution was added:

$$-\int_L N\theta\delta\theta \, dL \tag{15}$$

where N is the axial force, θ denotes the bending rotation and L is the element length.

The cable system is modeled according to the Multi Element Cable System (MECS) approach, where each cable is discretized using multiple truss element. The stiffness reduction caused by sagging is accounted for by allowing the cable to deform under applied loads.

The constraint condition between the girder and the stays is modeled with offset rigid links to accommodate cable anchor points, by means of the extrusion coupling variable methodology (see [x] for additional details). Briefly, once the displacement field of the 3D beam (u,v, w, θ_x, θ_y, θ_z) is linearly extruded from the source domain (the stiffening girder) to the destination ones (the lines which contain anchor points), prescribed displacements are imposed as constraint on the destination domains, by means of the following constraint equations:

$$\bar{u}^{(l)} = u + \theta_z b;\ \bar{v}^{(l)} = v;\ \bar{w}^{(l)} = w + \theta_x b;\ \bar{u}^{(r)} = u - \theta_z b;\ \bar{v}^{(r)} = v;\ \bar{w}^{(r)} = w - \theta_x b \tag{16}$$

where $\bar{u}^{(l)}, \bar{v}^{(l)}, \bar{w}^{(l)}$ and $\bar{u}^{(r)}, \bar{v}^{(r)}, \bar{w}^{(r)}$ are the prescribed displacements on left and right anchor point, respectively. A regular mesh is used to obtain the discrete model: each cable stay is divided in twenty linear truss elements, whereas 350 beam elements are used for the stiffening girder.

The bucking and post-bucking behaviors have been investigated by using nonlinear analyses taking into account large deformation but small strain with linear stress-strain relationship and a solution strategy has been adopted, based on the damped Newton method. A suitable modeling technique in this case, where the relationship between applied loads and displacements is highly nonlinear, is to use an algebraic equation that controls the applied live loads λp so that the lateral midspan deflection δ_l reaches the prescribed increments. The ODE interface in COMSOL MULTIPHYSICS™ is useful for entering this coupled algebraic equation, written as follows $\delta_l(\lambda) = \bar{\delta}_l^{(i)}$ here $\bar{\delta}_l^{(i)}$ is the desired vertical displacement stepped up by employing a parametric solver.

3 RESULTS

Here numerical results for both the continuous model and the discrete one are presented. The case of uniform load applied on the central span is considered to examine the instabilizing effect produced by the axial force in the girder for increasing live loads λp. The following dimensionless parameters are used:

$$\frac{L}{2H}=2.5,\frac{l}{H}=5/3,\frac{b}{H}=0.1,\frac{\Delta}{L}=1/105,\frac{\sigma_a}{E}=7200/2.1\times10^6,\frac{K}{g}=50 \quad (17)$$

whereas the material properties assume the values that concern the usual case of steel girders and towers. The value of the dead load g is equal to 300,000 N/m, and the ratio between live load p and dead load g adopted to determine the stays cross section as shown in section 2, is assumed $p/g = 0.5 \div 1$.

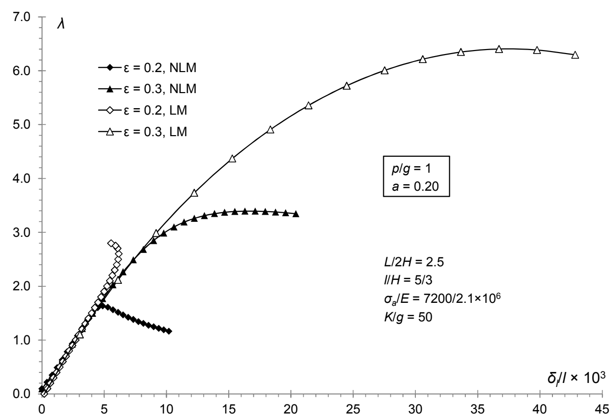

Figure 3. Plot of δ_l (lateral midspan deflection) versus the load parameter λ for different values of ε in both the cases of nonlinear (NLM) and linear (LM) discrete model.

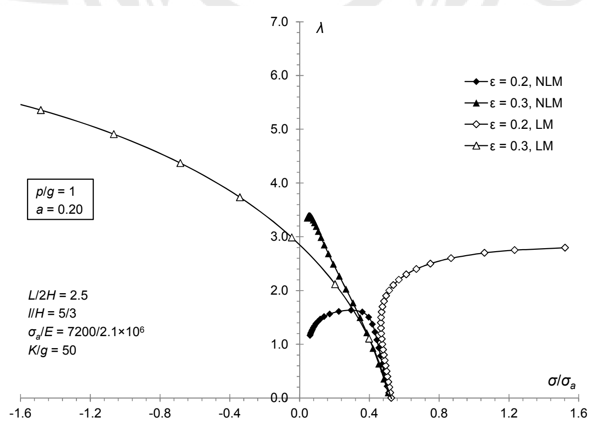

Figure 4. Plot of σ (lateral span central stays stress) versus the load parameter λ for different values of ε in both the cases of nonlinear (NLM) and linear (LM) discrete model.

The other parameters ε and a, respectively representing a measure of the relative stiffness between the girder and stays and the stay deformability, are used to define the bridge geometry. A parametric analysis is carried out by adopting the following values for the above quantities: $\varepsilon = 0.2 \div 0.3$ and $a = 0.10 \div 0.20$. Figures 3 and 4, referred to the discrete model, shows the typical snapping behavior occurring for high values of λ for which the instabilizing effect of the axial compression in the girder is coupled with the softening behavior of stays response in the lateral span. These figures also show results obtained by neglecting geometric nonlinearities of stays due to dead load (LM).

Finally, table 1 shows the influence of bridge parameters on the maximum load increment λ_{max} for both the continuous and discrete model. The influence of stays geometric nonlinearities is also pointed out.

Table 1. Influence of the stiffness parameter ε on the maximum load capacity λ_{max} in both the cases of nonlinear (NLM) and linear (LM) approaches and for both continuous (C) and discrete (D) models.

		λ_{max}							
	a / ε	0.10				0.20			
		NLM (C)	NLM (D)	LM (C)	LM (D)	NLM (C)	NLM (D)	LM (C)	LM (D)
$p/g = 0.5$	0.2	2.39	2.58	4.11	3.96	2.18	2.37	4.11	3.90
	0.3	5.30	5.57	9.69	9.50	5.35	5.39	9.69	9.42
$p/g = 1$	0.2	1.61	1.74	2.88	2.81	1.48	1.63	2.88	2.78
	0.3	3.44	3.49	6.53	6.44	3.32	3.39	6.53	6.41

4 CONCLUSIONS

Results show that the simplified continuous model is able to capture with a reasonable accuracy the nonlinear bridge behavior when the stay spacing is relatively small. Moreover, numerical computations show the strong influence of the nonlinear stays response on the stability behavior of the bridge under dead loading on the central span. As a matter of fact, neglecting the nonlinear stays response leads to a notable overestimation of the actual loading carrying capacity of the bridge.

REFERENCES

[1] Gimsing, NJ. “Cable supported bridges: Concepts and design”, John Wiley & Sons, 1983.
[2] Leonhardt, F, Zellner, W, “Past, present and future of cable-stayed bridges”, Proceedings of the Seminar of Cable- Stayed Bridges, Recent Developments and Their Future, Yokohama, Japan, pp. 1–33, 10–11 December 1991.
[3] Troitsky, MS, “Cable-stayed bridge-theory and design”, London: Crosby Lockwood Staples, 1977.
[4] Bruno, D, Grimaldi, A, “Nonlinear behavior of long- span cable-stayed bridges”, Meccanica, 20, 303-313, 1985.
[5] Adeli, H, Zhang, J, “Fully nonlinear analysis of composite girder cable-stayed bridges” Comput Struct, 54(2), pp.267–77, 1995.
[6] Wang, PH, Lin, HT, Tang, TY, “Study on nonlinear analysis of a highly redundant cable-stayed bridge”, Comput Struct, 80(2), pp.165–82, 2002.
[7] COMSOL AB. Structural Mechanics Module User’s Guide. September 2008.

EVALUATION OF THE LOAD CARRYING CAPACITY OF A BRIDGE SYSTEM UNDER EXTERNAL PRESTRESSING

Leonidas Stavridis, Konstantinos Spiliopoulos and Aikaterini Ioannidou

National Technical University of Athens, Dept. of Civil Engineering, Greece
e-mail: stavrel@central.ntua.gr, kvspilio@central.ntua.gr, kioanni@yahoo.com

ABSTRACT: In this paper a simply-supported concrete bridge system with a given external prestressing layout is examined. A sophisticated step-by-step computer package is used to calculate the load carrying capacity of the system. In this way one may achieve the best possible choice of the initially adopted geometrical data, with reference to the ultimate load of the system.

KEY WORDS: Concrete bridge; External cable; Prestressing; Ultimate load.

1 INTRODUCTION

Solid slab bridges have traditionally been economical only for spans of up to about 25 meters in length. One possibility for increasing the economical span range of slab bridges is the use of external prestressing [1]. In this way one may avoid the troublesome bottom slab and webs of a box girder by providing external tendons which play the role of maintaining the lever arm for flexural resistance at midspan. A further benefit from the use of external tendons is that they are at all times accessible for inspection, maintenance and if required replacement.

The structural system proposed in this study consists of a simply-supported solid slab with external tendons underneath. Structural steel posts provided at two locations at the third points of the span deviate the external tendons and transfer the vertical component of their tensile force to the slab.

Whereas an analytical model assuming linear elastic behaviour is usually sufficient for the design of slab bridges, this assumption is not valid for the externally prestressed slabs. The calculations required to verify the safety (and serviceability) will be correspondingly more complex and will require consideration of both geometric and material nonlinearities.

Regarding safety requirements, a simplified approach for the determination of the basic design parameters of the system is presented first. This approach is then checked using a well established software package (ATENA [2]). This finite element program takes into account a realistic concrete behaviour, following the evolution of the cracks that appear during the incremental application of the loading.

2 DESCRIPTION OF THE GEOMETRICAL DATA OF THE BRIDGE

The bridge consists of a slab of *6m* width and *30m* length and having a thickness of *50 cm*. The external prestressing system consists of a pair of cables of a cross-section $A_s=3210mm^2$, each of them lying in a vertical plane. The cables, having a horizontal segment at a distance of *1.75m* from the bottom of the slab, as shown in Fig.1 are anchored at the two ends of the bridge, providing, in addition, a vertical support to the slab with the aid of two steel posts located at the third points of the span with a distance of *3m* between their planes (Fig.1).

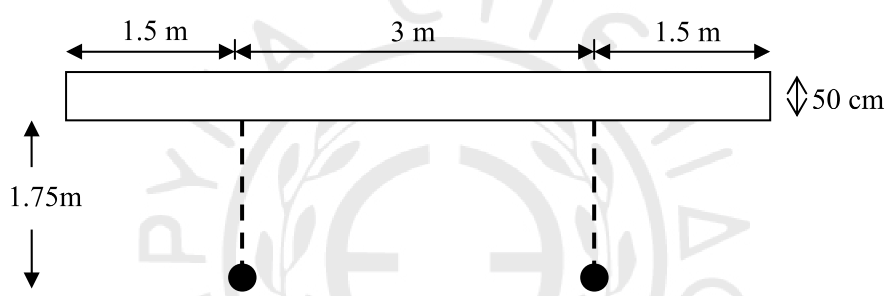

Figure 1. Section layout of the bridge system

An internal prestressing is also provided in the slab with parabolic cables along its span, with a total cross-sectional area of A_p= 6465 mm^2.

The above geometrical data have been chosen from a preliminary simplified overall strength requirement based on the static theorem of plasticity supposing a nominal live load of 4.2 kN/m^2. Assuming a safety factor of 1.3 for the dead load and 1.5 for live load, an ultimate load of 133.5 kN/m for the bridge is prescribed, which implies a required bending moment capacity at midspan of $133.5\text{x}30^2/8=15018$ kNm.

Denoting by M_{pl} the bending resistance of the slab and assuming that the external cable will reach its yield strength then at mid-span the following equation must hold [3]

$$M_{pl} + A_s \times f_{sy} \times h \geq 15018 \quad (1)$$

where h represents an estimated lever arm of the external cable force (Fig.2). Based on the above equation the required bending resistance of the slab M_{pl} should be greater than 4746 kNm.

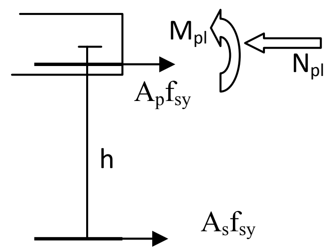

Figure 2. Internal forces at midspan

It should be pointed out that the bending resistance of the slab cross-section M_{pl} depends not only on the internal prestressing cross-sectional area A_p but also on the externally acting compressive force $N_{pl} = A_s f_{sy}$. These two entities constitute a pair on the interaction diagram of the ultimate resistance of the slab's section. This diagram may be seen in Fig. 3. According to this diagram, a value of M_{pl} equal to 4814 kNm is deduced, which obviously satisfies the above Eq. (1).

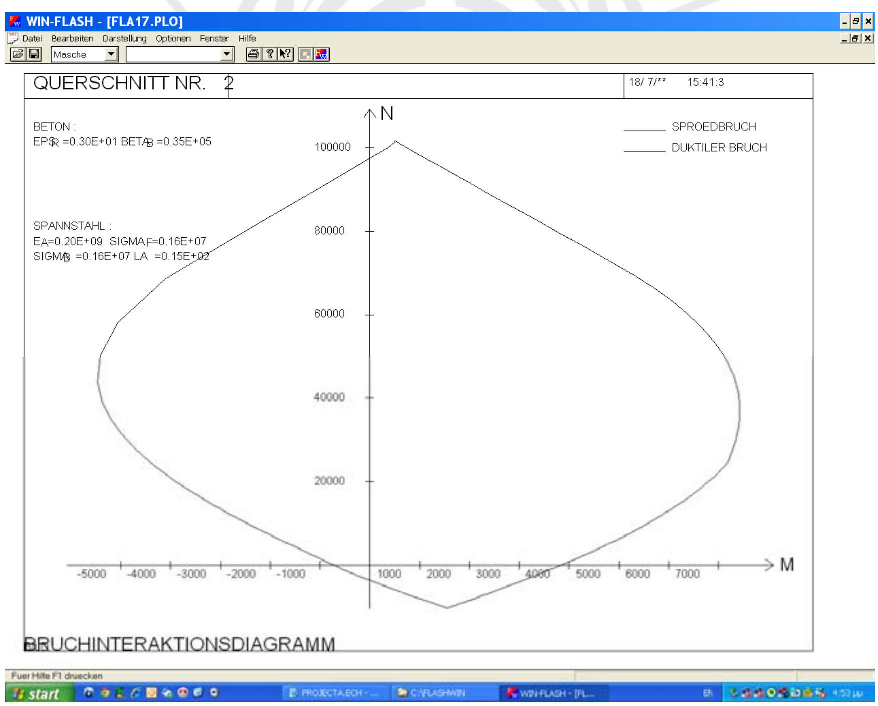

Figure 3. Interaction diagram

3 FINITE ELEMENT FORMULATION

3.1 General considerations

The nonlinear finite element ATENA [2] is used to perform a more realistic analysis. The main characteristics of the assumed concrete behavior are:

- Non-linear behavior in compression including hardening and softening
- Fracture of concrete in tension based on nonlinear fracture mechanics
- Biaxial strength failure criterion
- Reduction of compressive strength after cracking
- Tension stiffening effect
- Reduction of the shear stiffness after cracking (variable shear retention)
- Two different crack models: fixed crack direction and rotated crack direction

Perfect bond between concrete and reinforcement is assumed within the smeared crack concept. No bond slip can be directly modeled except for the one included inherently in the tension stiffening. However, on a macro-level a relative slip displacement of reinforcement with respect to concrete over a certain distance can arise, if concrete is cracked or crushed. This corresponds to a real mechanism of bond failure in case of the bars with ribs.

The reinforcement in both forms, smeared and discrete, is in the uniaxial stress state and its constitutive law is a multi-linear stress-strain diagram.

The material matrix is derived using the nonlinear elastic approach. In this approach the elastic constants are derived from a stress-strain function called here the equivalent uniaxial law. This approach is similar to the nonlinear hypoelastic constitutive model, except that different laws may be used here for loading and unloading. The detailed treatment of the theoretical background of this subject can be found, for example, in [4]. This approach can be also regarded as an isotropic damage model, with the unloading modulus representing the damage modulus.

3.2 Stress – strain relations for concrete – Equivalent uniaxial law

The nonlinear behavior of concrete in the biaxial stress state is described by means of the so-called effective stress σ_c^{ef} , and the equivalent uniaxial strain ε^{eq} . The effective stress is in most cases a principal stress.

The equivalent uniaxial strain is introduced in order to eliminate the Poisson's effect in the plane stress state.

$$\varepsilon^{eq} = \frac{\sigma_{ci}}{E_{ci}} \tag{2}$$

The equivalent uniaxial strain can be considered as the strain, that would be produced by the stress σ_{ci} in a uniaxial test with modulus E_{ci} associated with the direction i . Within this assumption, the nonlinearity representing damage is caused only by the governing stress σ_{ci}. Details can be found in [4]. The complete equivalent uniaxial stress-strain diagram for concrete is shown in Fig. 4.

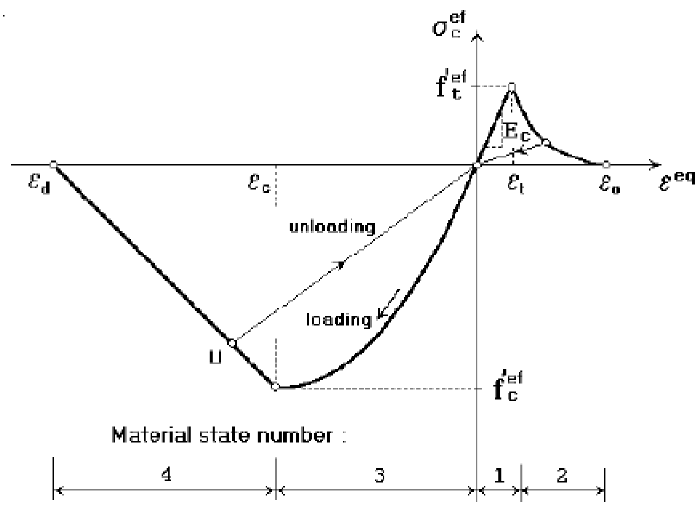

Figure 4. Uniaxial stress-strain law for concrete

The numbers of the diagram parts in Fig. 4 (material state numbers) are used in the results of the analysis to indicate the state of damage of concrete.

Unloading is a linear function to the origin. An example of the unloading point *U* is shown in Fig. 4. Thus, the relation between stress σ_c^{ef} and strain ε^{eq} is not unique and depends on a load history. A change from loading to unloading occurs, when the increment of the effective strain changes the sign. If subsequent reloading occurs the linear unloading path is followed until the last loading point U is reached again. Then, the loading function is resumed.

The peak values of stress in compression and in tension are calculated according to the biaxial stress state. Thus, the equivalent uniaxial stress-strain law reflects the biaxial stress state.

3.3 Tension after cracking

Two types of formulations are used for the crack opening:

- A fictitious crack model based on a crack-opening law and fracture energy. This formulation is suitable for modeling of crack propagation in concrete. It is used in combination with the crack band.
- A stress-strain relation in a material point. This formulation is not suitable for normal cases of crack propagation in concrete and should be used only in some special cases.

Alternative softening models of either exponential or linear type are shown in Figs. 5-7.

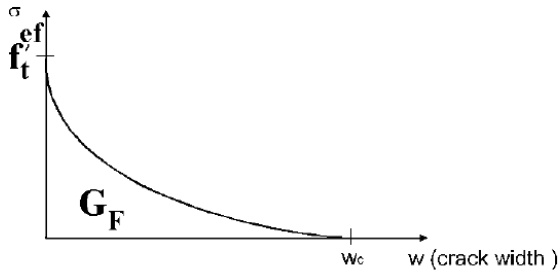

Figure 5. Exponential crack opening law

This function of crack opening was derived experimentally by [5].

$$\frac{\sigma}{f_t^{'ef}} = \left\{1 + \left(c_1 \frac{w}{w_c}\right)^3\right\} \exp\left(-c_2 \frac{w}{w_c}\right) - \frac{w}{w_c}\left(1 + c_1^3\right)\exp\left(-c_2\right) \qquad (3)$$

$$w_c = 5.14 \frac{G_f}{f_t^{'ef}}$$

where: w is the crack opening, derived from strains according to the crack band theory [6]

w_c is the crack opening after the complete release of stress

σ is the normal stress in the crack (crack cohesion)

$c_1 = 3$ and $c_2 = 6.93$ are constants

G_f is the fracture energy

$f_t^{'ef}$ is the effective tensile strength

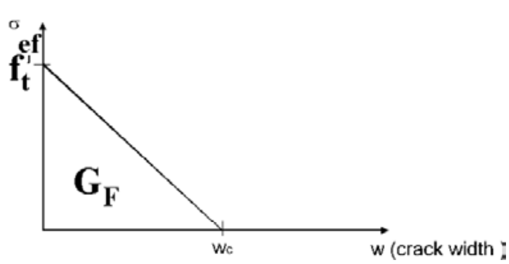

Figure 6. Linear crack opening law

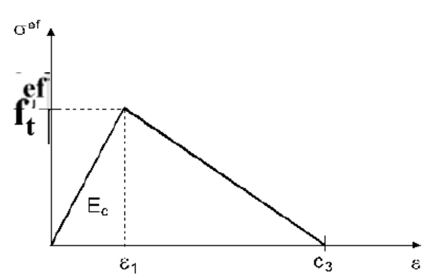

Figure 7. Linear softening based on strain

3.4 Two models of smeared cracks

The smeared crack approach for modeling of the cracks is adopted in the program. Two options are available for crack models: the fixed and the rotated crack model. In both models the crack is formed when the principal stress exceeds the tensile strength. Thus the initial isotropic material becomes orthotropic.

- Fixed crack model: In this crack model [7], the crack direction is the principal stress direction when the crack initiates (Fig. 8). With further loading this direction is fixed and is the material axis of orthotropy.
- Rotated crack model: In the rotated crack model ([8], [9]), the direction of the principal stress coincides with the direction of the principal strain. Thus, no shear strain occurs on the crack plane and only two normal stress components must be defined, as shown in Fig. 9.

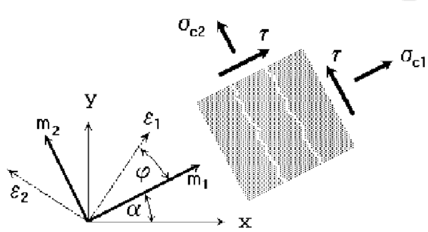

Figure 8. Fixed crack model

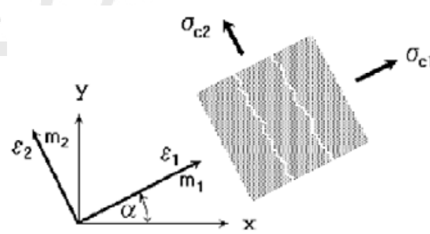

Figure 9. Rotated crack model

4 LOAD CARRYING CAPACITY OF THE PROPOSED BRIDGE SYSTEM UNDER EXTERNAL PRESTRESSING

The simply supported-prestressed concrete bridge considered in section 2 was analyzed with the ATENA 2D program, whose basic features were described above. A longitudinal section of the bridge together with the two types of tendons may be seen in Fig. 10 as plotted by the program.

Figure 10. Prestressed concrete bridge with external cable

4.1 Analysis

At the top surface of the slab, an increasing uniform load is applied in steps of 1.00 kN/m. The solution method is the Arc-Length method. The behaviour of the system is monitored through a load-displacement curve.

After 197 steps of analysis, the value of the collapse load is q = 121.90 kN/m. One may see that this is quite close to the design target of 133.5 kN/m set in section 2. The cracks due to flexure (Fig.11) are approximately 3.00mm.

Both cables have almost reached the yield strength (1600 MPa) (Fig.11).

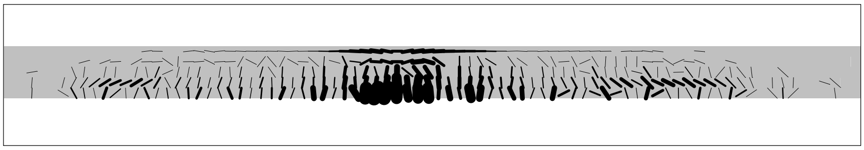

Figure 11. Cracks in the middle sections, due to flexure of the bridge

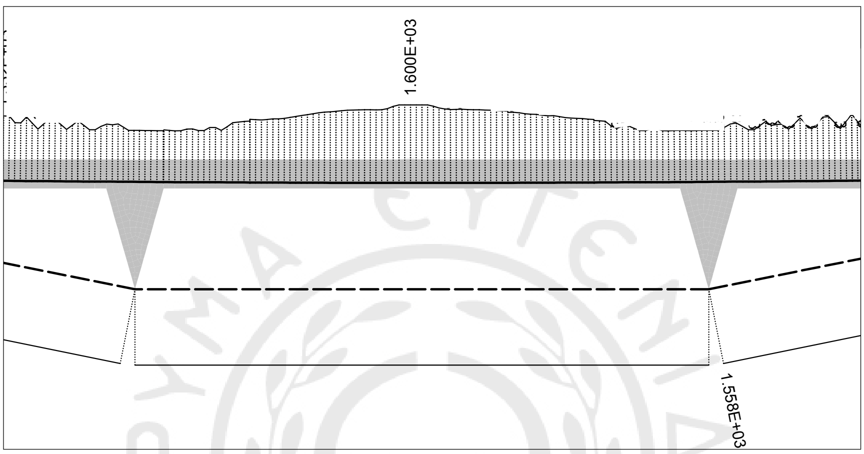

Figure 12. Final stress σ_x in the two cables

5 CONCLUSIONS

The preliminary estimation shows a satisfactory agreement with the more sophisticated finite element results which, of course, is more representative of the real behaviour of the structure.

REFERENCES

[1] Menn, C., Govreau, P., "Scale Model Study of an Externally Prestressed Concrete Slab Bridge", Proc. Intl. Conference on Cable Stayed Bridges, Bangkok, 1987.
[2] ATENA, Nonlinear Analysis Software, Cervenka Consultants, 2009.
[3] Stavridis, L., *Structural Systems: Behaviour and Design* , Thomas Telford, London 2010.
[4] Chen, W. F., Saleeb, A. F., "Constitutive Equations for Engineering Materials", *John Willey & Sons*, ISBN 0-471-09149-9, 1982.
[5] Hordijk, D.A., "Local Approach to Fatigue of Concrete", *Doctor dissertation, Delft University of Technology,* Netherlands, ISBN 90/9004519-8, 1991.
[6] Bažant, Z. P., Oh, B. H., "Crack Band Theory for Fracture of Concrete", *Materials and Structures, Rilem,* Vol. 16, 155-177, 1983.
[7] Červenka, V., "Constitutive Model for Cracked Reinforced Concrete", *Journal ACI*, Proc. V.82, Nov-Dec., No.6, pp.877-882, 1985.
[8] Vecchio, F. J., Collins, M. P., "Modified Compression-Field Theory for Reinforced Concrete Beams Subjected to Shear", *Journal ACI*, Proc. V.83, Mar-Apr., No.2, pp.219-231, 1986.
[9] Crisfield, M. A., Wills, J., "The Analysis of Reinforced Concrete Panels Using Different Concrete Models", *Jnl. of Eng. Mech.,* ASCE, Vol. 115, March, No.3, pp.578-597, 1989.

TOPIC 6

Geotechnical Problems

Soil-Structure Interaction

Fabrication and Construction

STRUCTURAL CHARACTERIZATION OF EXISTING BRIDGES FOR SEISMIC VULNERABILITY ANALYSIS

Mariella Mancini[1], Giovanni Fabbrocino[1]

[1] Structural and Geotechnical Dynamics Lab. StreGa,Department SAVA University of Molise, Italy
e-mail: mariella.mancini@unimol.it, giovanni.fabbrocino@unimol.it,

ABSTRACT: Safety of existing constructions is a very relevant problem, especially in areas exposed to seismic risk. This applies not only to buildings, but also to infrastructures. Transportation systems functionality is however strictly dependent upon performances of bridges and viaducts. The present paper deals with seismic vulnerability of existing bridges, with specific reference to the structural characterization in view of quantitative assessment of real performances. The topic is well documented as the analysis of single structures, but some issues related to management of road networks are not well developed from a structural and seismic point of view. Actually, available Bridge Management Systems (BMS) are often well defined, but cover basically qualitative aspects of the problem. The approach to the assessment of a relevant number of bridges at regional level is described and some interesting aspects related to the integration of traditional BMS data and information required by structural vulnerability analysis are discussed. Procedures for the definition of specific structural conditions indexes are described and discussed.

KEYWORDS: Maintenance; existing bridges, seismic performances.

1 INTRODUCTION

Safety of existing constructions is a very relevant problem, especially in areas exposed to natural hazards, like earthquakes [1]. This applies not only to buildings, but also to infrastructures, like road and railway transportation systems, whose functionality depends on structural performances of bridges and viaducts, as well as related geotechnical structures.

In the last decades, attention of relevant Authorities, stakeholders and professional personnel involved in transportation systems management has been mainly paid to develop rational methods able to guide maintenance and ensure serviceability both of structural and non-structural components [2].

Actually, available Bridge Management Systems (BMS) are often well defined [3, 4, 5, 6], but cover basically qualitative aspects of the problem, while quantitative aspects related to structural components and detailing is generally incomplete. Effects of earthquakes occurred in some European countries and especially in Italy in the last years modified the perception of the risk, so that a number of actions aimed at assessing the structural and seismic performance of infrastructure more in detail [7, 8, 9].

It is easy to recognize that information needed for seismic vulnerability evaluation of existing bridges are quite complex and need to be calibrated depending on the scope of the analysis. In the present paper, the problem of the structural characterization of existing bridges at regional scale is addressed. In particular, the integration between available information on existing bridges and outcomes of field surveys and tests is addressed. The aim of the work is the definition of a rational tool able to support the structural maintenance of bridges at regional scale and provide criteria for the prioritization of interventions once vulnerability classification are available. It represents one of the outcomes of a large activity aimed at the seismic vulnerability evaluation of a number of bridges belonging to a relevant road network in central Italy [10, 11].

2 KNOWLEDGE LEVELS IN EXISTING BRIDGES

Seismic codes issued in early 2000s, recommend a distinct approach between the assessment of existing construction and their structural upgrading and the design of new constructions. This concept is present in many National and International codes, mainly with reference to existing buildings [12, 13].

As bridges and infrastructures are considered, formal documents do not still exist, even if guidelines and code chapters proposal are available [9]. The main difference between new and existing constructions is represented by the sources of uncertainties in determining the structural modeling and mechanical material parameters.

Mean values of mechanical parameters are recommended in combination with confidence factors (CF) dependent upon the knowledge levels (KL). Knowledge levels achievement are strictly related to the number of tests and the accuracy and extension of inspections performed on the construction. Table 1 illustrates the three levels of inspections related to code KL's, namely, *limited* (KL1), *normal* (KL2) and *full* (KL3) and extends the recommendation provided for bridges [9] on the analogy with EC8 Part 3 for buildings [12]. N_{tot} in Table 1 represent the number of piles present in the bridge of interest.

Table 1. Recommended minimum requirements for each level of inspection

	Structural detailing inspection	Testing of materials	
		Concrete samples	Rebar samples
Limited	20% $N_{tot}\geq2$	20% $N_{tot}\geq2$	20% $N_{tot}\geq2$
Extended	40% $N_{tot}\geq3$	40% $N_{tot}\geq3$	40% $N_{tot}\geq3$
Comprehensive	60% $N_{tot}\geq4$	60% $N_{tot}\geq4$	60% $N_{tot}\geq4$

A careful review of code provisions and proposed guidelines shows that some aspects that are not fully established and that a certain margin of interpretation exists. This applies particularly to the design of the knowledge path and to the spatial configuration, as well as to the outcome of the test results. Moreover, the approach seems to fit requirements for detailed analysis of single structures, but cannot be easily used to large numbers of bridges belonging to road networks at regional scale.

3 STRUCTURAL CONDITION ASSESSEMENT

The brief discussion of KLs required by seismic codes for the assessment of existing bridges points out the relevant role of some components of the bridge system. They are actually a sub-set of all components considered in maintenance and management of road networks. In fact, bridges age, deterioration caused by heavy traffic and critical environment conditions result in a higher frequency of repairs and can impact a reduced load carrying capacity. This circumstance leads to take decisions on maintenance works generally based on inspections and engineering judgment, but also to collect a relevant amount of information and data that need to be integrated in the seismic vulnerability assessment process.

Degradation and maintenance process are critical for the definition of reliable tools to support inspections for KL achievement as well as to support decisions for seismic upgrading of vulnerable constructions.

As a result, a review of available Bridge Management Systems (BMS) appeared the basic step for the definition of a dataset able to describe the status of the bridge from a seismic standpoint and the components to be assessed and tracked during the service life of the structure. In this sense, a similar process seems to fit the requirements of the design of structural health monitoring systems and perform an integration between safety demand for users and an integrated sustainability of constructions.

Table 2 represents the basic matrix that links the different class of elements that play a role in the development of the seismic performance of the bridge and the defects that can be observed. Each defect can be associated to a weight W, variable 1 to 5, depending on its impact on seismic and structural performances [4]. Some aspects that lead to the definition of the weight W are here reported:

- Defect develops and constitute a risk (risk present);
- Defect can affect the load capacity (risk potential);
- Defect can trigger other malfunctions and/or damage to surrounding areas (induced risk);
- Defect can trigger relevant economic losses due to repairing and upgrading (economic risk).

It is worth noting that each class of elements can be influenced the class of elements considered, so it’s possible that the same degradation has different weight in each structural class.

Table 2. Summary of relevant components and related defects

Defects \ Component	Deck	Girder	Diaphragm	Pier cap	Pier	Abutment
No damage	0	0	0	0	0	0
Damp patch	1	1	1	1	1	1
Deteriorated concrete/crawl	2	2	2	3	4	3
Corroded/deformed longitudinal bars	5	5	4	5	5	5
Longitudinal cracks	2	2	2	2	-	2
Transverse cracks	5	-	-	-	2	-
Cracks at the beam to slab connection	2	3	-	-	-	-
Transverse/diagonal cracks	-	5	5	5	3	5
Confinement bars exposed/corroded	-	5	-	5	5	5
Longitudinal/diagonal cracks	-	-	-	-	5	-
Cracks at the pier cap connection	-	-	-	-	2	-
Cracks at the beam to diaphragm connection	-	3	-	-	-	-
Head beam bars exposed/corroded	-	5	-	-	-	-
Damage induced by supports defects	-	-	-	3	-	-
Defects in neoprene supports	-	-	-	3	-	-
Out of plumb	-	-	-	-	-	5

Table 3. Severity, Diffusion and Extension Levels and their quantitative formulation

Severity Level	ID.	Short–term consequences	S
L	Low	No	1
M	Medium	Functional	2
H	High	Structural	5
Diffusion Level	ID.	Frequency of occurrence	F
F1	Limited	Minor	1
F2	Medium	Moderate	2
F3	Extended	Extreme	3
Extension Level	ID.	Extension of defect	E
E1	Limited	Minor	1
E2	Medium	Moderate	2
E3	Extended	Extreme	3

The level of reliability of the data is obviously related to the number of the class elements directly investigated. As a consequence, the KL defined according to Code provisions or according to the available data can be expressed as the ratio between the number of inspected elements, N_{insp}, and the total number of elements, N_{max}, present in the bridge:

$$k = \frac{N_{Insp}}{N_{\max}} \tag{1}$$

Similarly, the severity level of each kind of degradation, its diffusion along the bridge and its local extension have to be estimated and a parametric representation is needed [5]. Severity Level can be estimated depending on its short-time consequences. It is high if the damage can progress in a structural failure, average if the damage can lead to functional failure, low if the probability of damage is negligible resulting in no short-term consequences. The Diffusion Level can be associated to the frequency of occurrence of the anomaly. If the phenomenon is limited, confined in a few locations and no more than 25% of the extension of the damage elements, medium if it affects an area between 25% and 75%, widespread almost the entire class of observed elements exhibits the degradation of interest. The Level of Extension refers to the area of each element affected by each anomaly. Table 3 summarizes the above mentioned levels for the anomaly definition and provide their quantitative evaluation given by the parameter S. The latter is one of the factors needed for the calculation of the Element Structural Condition Index (ESCI). It can be defined for each element class, as the sum of Level of Severity, Spread and Extension, increased of the assigned weight, for all the damaged observed:

$$ESCI = \sum_{1}^{i} (W_i \cdot S_i \cdot F_i \cdot E_i) \tag{2}$$

The ESCI can be associated only of the elements directly observed on site, whose number can change between a bridge and another in the same stock.

An homogenization of the indexes can be based on the introduction of the reliability of the information depending on the level of knowledge KL.

In fact, since a number of elements cannot be inspected or their data are not available at the moment of the assessment, the frequency of observation can be used to weight the ESCI index based on the inspected elements using the factor FO given by the ratio:

$$FO = \frac{1}{k} \tag{3}$$

where k depend on Knowledge Level achieved.
A Global Structural Condition Index can be expressed by the equation:

$$GSCI = ESCI \cdot IF \cdot AF \cdot FO \tag{4}$$

It is based on ESCI index, but it is corrected taking into account the rank of the structural class within the bridge – via the IF, Importance Factor, of the structural class – and the age of the bridge using the Age Factor AF [3]. Table 4 reports the selection criteria adopted for AF and IF factors.

Table 4. Importance Factor and Bridge Age Factor

Elements	IF	Bridge age	AF
Deck	0,8	Before 1900	1,05
Beam	1	1900-1940	1,00
Intermediate diaphragm	0,7	1941-1965	0,97
Pier cap	0,9	1965-1980	0,95
Pier	1	1981-2005	0,90
Abutment	0,8	2005 and later	0,85

For each class of elements of the viaduct, is estimated both the ISCE and GSCI. After the evaluation of the GSCI for the different classes of elements, it can be used both for the single structure or the entire stock. If a single structure is concerned, it is possible to assess the maintenance state of each class of elements and the presence of localized problems. Then, maintenance can be carried out for selected classes of elements and developing phenomena requiring restoration interventions can be identified. If the management of the road network is of interest, the approach allows the comparison of the states of the different classes of structures and a global ranking of the structures. The indexes calculated, can be normalized using the absolute maximum value to facilitate the comparison, as part of the same opera, and other same classes indices the case of classification of a population of bridges. Therefore, the relevant indexes turn in:

$$\overline{ESCI} = \frac{ESCI}{ESCI_{MAX}} \cdot 100 \quad ; \quad \overline{GSCI} = \frac{GSCI}{GSCI_{MAX}} \cdot 100 \qquad (6)$$

3.1 Structural condition indexes relevant ranges

The framework presented in the previous sections leads to identify the main issues related to the maintenance level and the structural characterization of different bridge components. It provides a quantitative formulation of the observed deterioration states and is strictly dependent upon reliability of information. Combined evaluation of number of deterioration, the sum and average of severity provide an outlook on the nature of ESCI and GSCI parameters. Relation between the above mentioned estimates of the bridge condition is able to mark the nature of structural degradation. Moderate and spread damage, as well as active critical mechanisms with short-term effects can be identified. This information is certainly of interest for effective management of the infrastructure stock, for management of economic and technical resources, and planning of assessment and retrofitting. ESCI is able to describe the condition of each bridge class of components and is related only to inspections outcomes. Then, maintenance can be carried out for selected classes of elements and developing phenomena requiring maintenance and upgrading interventions can be identified as well. Moreover, ESCI makes possible a direct comparison between the maintenance needs of the elements in the same viaduct. For each elements class, ranges of intervention priority classification depends of number of damage found. ESCI values greater than 50 are not usual, as shown by a number of simulations carried out on a relevant number of real cases. In fact, a careful review of the defects catalog, and the possibility of high diffusion and extension, ESCI high values correspond to a so level of deterioration and damage that are not compatible with a safe service of the structure.

Table 5. ESCI relevant ranges and performance thresholds.

Number of damage observed	ESCI	Consequences
1-2	0< ESCI <5	No effects
	5≤ ESCI <15	Functional
	ESCI >15	Structural
3-4	0< ESCI	No effects
	10≤ ESCI <25	Functional
	ESCI >25	Structural
>5	0< ESCI <15	No effects
	15≤ ESCI <30	Functional
	ESCI >30	Structural

GSCI can be used to compare at a higher level the structure and take account all the main features and defects of the bridge within a stock. When the single structure is concerned, it is possible to assess the maintenance state of each class of elements and the presence of localized problems. If the management of the road network is of interest, the approach allows the comparison of the states of the different classes of structures and a global ranking of the structures.

A summary of typical ESCI ranges are reported in Table 5 depending on the number of relevant observed deterioration phenomena, so that typical performance thresholds can be derived.

4 CONCLUSIONS

Safety of existing constructions is a very relevant problem, especially in areas exposed to seismic risk. This applies not only to buildings, but also to infrastructures. Transportation systems functionality is however strictly dependent upon performances of bridges and viaducts. The present paper deals with seismic vulnerability of existing bridges, with specific reference to the structural characterization in view of quantitative assessment of real performances. The topic is well documented as the analysis of single structures, but some issues related to management of road networks are not well developed from a structural and seismic point of view. A procedure able to provide quantitative comparative data for networks at regional scale has been presented.

Outcomes of the work can be used for structural management of the network, as well as a support to the design of inspections and tests for structural characterization of existing bridges.

REFERENCES

[1] *fib* Bulletin n° 39. (2007). Seismic bridge design and retrofit - structural solutions State-of-art report ISBN 978-2-88394-079-6.

[2] Godart, B., Vassie, P.R., (2001)– "Deliverable D13 – Bridge Management System: extended review of existing systems and outline framework for a European project", Bridge Management in Europe (BRIME),4th Framework Programme European Commision DG VII.

[3] Franchetti, P., Pellegrino, C., Soffiato, A., Modena, C. (2003) - "La manutenzione programmata di ponti e viadotti: criteri per la valutazione dell'efficienza in servizio", XIII National Conference SIIV (Italian Society Road Infrastructures), Padua, Italy.

[4] Martinello, S. (2005) - "Dalla valutazione numerica dello stato di degrado dei ponti al collaudo", Proceedings of the Conference "New trends in bridge and viaducts design". Edited by M. Arici and E. Siviero, Taormina, Italy.

[5] Montepara A., Merusi F., Giuliani F.. (2008). Sviluppo di una nuova metodologia per la valutazione delle priorità di intervento di manutenzione di ponti e viadotti", XIII National Conference SIIV (Italian Society Road Infrastructures), Enna, Italy.

[6] Campitelli, P., (2004) - "Pianificazione della manutenzione strutturale di ponti, ottimizzazione della modellazione numerica", Tesi di Dottorato di Ricerca in Ingegneria Civile, Università degli studi di Parma.

[7] Boni M.P., Cividini A., Pergalani F., Petrini V., "Valutazione speditiva della vulnerabilità sismica di ponti, opere di sostegno, gallerie", XIII Convegno Anidis, 28 giugno- 2 Luglio 2009 Bologna.

[8] Bordot F., Zonta D., Zandonini R., "La vulnerabilità sismica della provincia autonoma di Trento", XIII Convegno Anidis, 28 giugno- 2 Luglio 2009 Bologna

[9] Pinto P.E., Mancini G. 2009. Seismic assessment and retrofit of existing bridges. Proc. of RELUIS-DPC 2005-2008 final Conference. Naples, Italy. Research Line 3, Existing bridges – Final report. http://www.reluis.it/doc/pdf/Atti_ConvegnoFinale_Reluis_Linea_III.pdf.

[10] Di Carluccio A., Fabbrocino G., Santucci de Magistris F., Todisco F., Fabbrocino S. 2009. Approccio metodologico alla valutazione di vulnerabilità per infrastrutture distribuite: aspetti geologici e geotecnici. Atti del XIII Convegno Nazionale "L'ingegneria sismica in Italia", Bologna.

[11] Fabbrocino G., Di Carluccio A., Mancini M., "Valutazione dello stato di fatto in prospettiva sismica delle opere d'arte infrastrutturale", XIII Convegno Anidis, 28 giugno- 2 Luglio 2009 Bologna.

[12] CEN (2005) "Eurocode 8 Part 3: Assessment and retrofitting of existing structures" European Committee for Standardization, Brussels, Belgium.

[13] NTC. 2008. Norme tecniche per le costruzioni, D.M. 14/01/2008, Gazzetta Ufficiale n. 29 del 04.02.2008, Suppl. Ord. n.30, 2008.

EARTHQUAKE RESISTING FOUNDATION OF A LONG BRIDGE ON A COVERED RIVER BED

Eleni Zygouri[1], Dimitris Bairaktaris[2]

[1,2] D. Bairaktaris and As/tes Structural Design Office Ltd – Athens – Greece ,
e-mail: baisteng@otenet.gr

ABSTRACT: The V-shaped piers of a long bridge are founded on the existing structure of the covered bed of Kifissos river in Faliron seashore. The vertical and the longitudinal horizontal reactions of the piers are transferred directly on the strengthened through penetrating piles central pier wall of the bed. The transversal reactions are transferred on pairs of piles outside the abutment walls through horizontal beams over the cover slab.

KEY WORDS: Bridge; Piles; Soil – structure interaction.

Photo 1. General View

1 INTRODUCTION

The flyover bridge of the Kifissos Avenue along and over the open bed of the homonyme river terminates at Faliro seashore with an overpass at the crossing of the two maritime avenues Makariou and Posidonos and at the area of the Olympic installations (Ph.1). This terminating part of the flyover consists of a straight segment of 223 m total length along and over the covered bed of the river and a semicircular segment of 162 m total length, surrounding the parking area of the Olympic installations.

At the end of this part the flyover continues with three separated curved branches connecting the Kifissos Avenue with the terrestrial traffic network. (Fig.1)

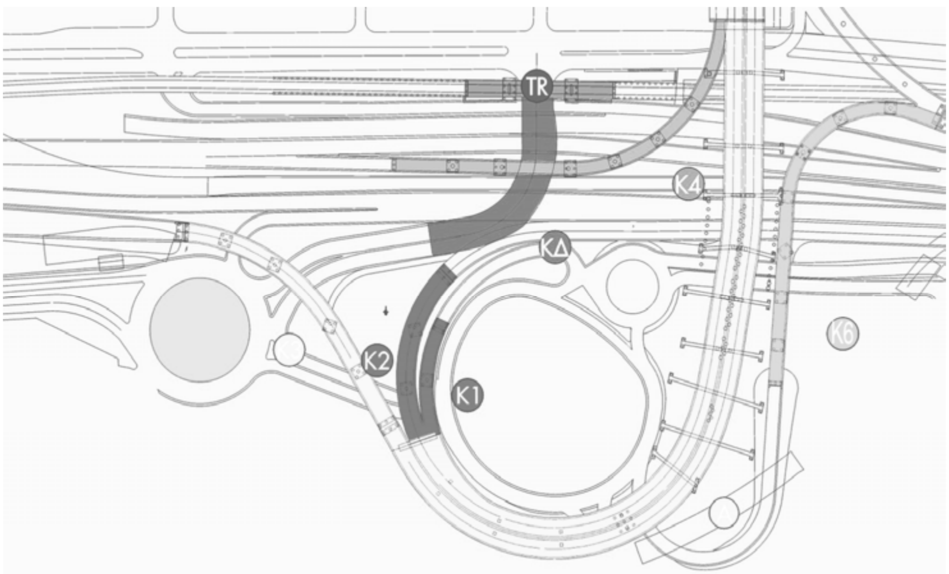

Figure 1. Plan View

The subject of this presentation consists to the earthquake resisting foundation of the piers supporting the straight segment of the flyover deck along and over the existing covered bed of the Kifissos river. The deck structure is a prestressed continuous hollow slab with 9 spans of variable length from 20,00 m to 35,60 m. The overall width of the deck is 20 m and the thickness 1.50 m with longitudinal circular voids of 0.90 m diameter at a spacing of 1.30 m.

The deck is supported on V shaped piers through elastomeric bearings equipped with stoppers and founded on the central pier wall of the covered bed.

The piers of the second semicircular segment of the deck are of the same shape and are founded on pile caps connecting the heads of nine bored concrete piles.

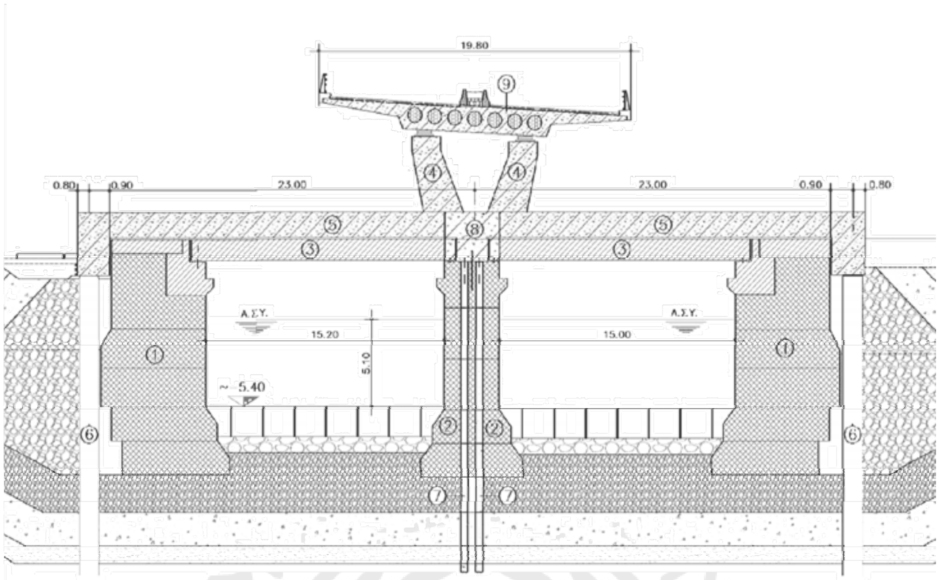

1. ABUTMENT OF EXISTING COVERED BED.
2. PIER OF EXISTING COVERED BED.
3. DECK SLAB OF EXISTING COVERED BED.
4. PIER OF NEW BRIDGE.
5. CONNECTING BEAM TRANSFERING HORIZONTAL FORCES.
6. BORED PILES RESISTING HORIZONTALLY
7. PILES Φ50, L=35 m, 4 Tubes a Manchettes, PENETRATING THE EXISTING PIER
8. LINEAR PILECAP OF PILES Φ50.
9. NEW BRIDGE PRESTRESSED DECK.

Figure 2. Typical cross section

2 SOIL CONDITIONS

According to the Geotechnical Investigation Report the Soil of foundation consists of the following layers with the corresponding geotechnical characteristics.

- Layer 1: Recent artificial loose deposits of 3.70 to 4.00 m thickness having E_s=30 MPa
- Layer 2: Silty sand to sandy silt until a depth of 19.00 to 23.00 m
  having γ=20 κN/m^3, c=0, φ=34^o, E_s=19 MPa
- Layer 3: Sand , clay until a depth of 30.00 m
  having γ=20 κN/m^3, c_u=0,11, φ_u=0, E_s=18 MPa

- Bottom layer of marl with inclusions of conglomerate having E_s=60 MPa

3 THE KIFISSOS RIVER COVERED BED STRUCTURE

The covered bed of the river under the bridge has a total width of 46 m and contains two side abutment walls of 6 m thickness consisting of columns of lean concrete blocks and a central pier wall with 4 m thickness, forming two separate channels each one with 15 m free width.

At a length of 160 m the central pier consists of a reinforced concrete wall supported on bored concrete piles of 1.80 m diameter in a zigzag placing at a spacing of 2.30 m along the axis of the bridge. The rest part of the central pier consists of columns of lean concrete blocks founded on sanitary soil layers. The free height of the channels is 8.50 m. The bottom is covered by lean concrete blocks of 1.80 m thickness.

The channels are covered by reinforced concrete slabs of 1.20 m thickness and 15 m free span simply supported on the side abutments and on the central pier wall. (Fig.2)

4 THE SYSTEM OF FOUNDATION

The V-shaped piers of the bridge are supported on the central pier wall of the covered bed and transfer on it the vertical and the horizontal reactions and moments in the longitudinal direction due to the imposed thermal, shrinkage and creep displacements and to braking and seismic actions.

The bearing capacity required for these reactions is available only in the first part of the central pier consisting of a thick reinforced concrete wall supported on bored piles.

The rest part consisting of overlaid lean concrete blocks founded on sanitary soil layers does not offer the required bearing capacity.

This part is strengthened with soldier piles in a zigzag arrangement penetrating the pier, the underlying soil layers and based on the bedrock of marl.

The head of the piles are connected with a reinforced concrete cap beam along and over the central pier wall.

The diameter of the piles is 0.50 m and contains peripheral longitudinal and transversal reinforcement, a central core of structural steel and four “tubes a manchette” in the perimeter for the injection of cement grouting under high pressure, in order to be obtained better homogeneity of the concrete mass and better friction resistance of the interface between pile and soil.

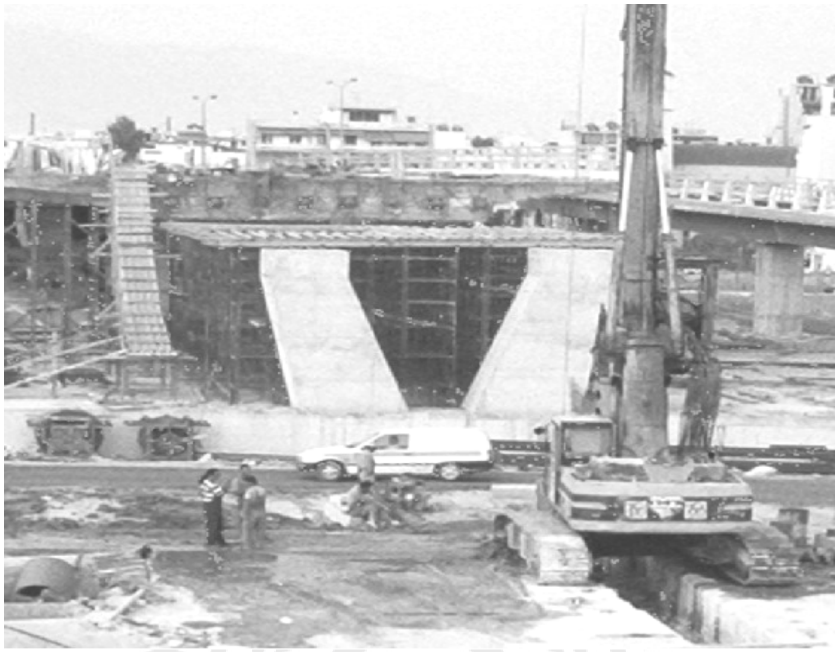

Figure 4. Installation of piles Φ 50

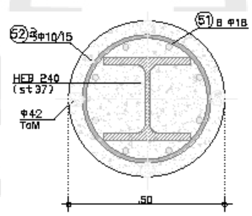

Figure 5. Piles cross section

5 DESIGN METHODOLOGY

The analysis of the bridge have been performed separately for the overall superstructure and for the system of foundation of each one isolated pier. In the analysis space model of the superstructure the deck is represented by a mesh of thick plate finite elements, the elastomeric bearings by short shear beam elements and the piers by 3D-beam elements rigid end jointed on the structure of the foundation. (Fig. 4)

For the seismic action the spectral analysis method is applied based on the response spectrum provided by the EAK 2000 for the ground acceleration 0.16g which is specified for the region of the bridge. The seismic displacements and the internal forces result from the superposition of the response of the first 24 eigenmodes according to the SRSS method.

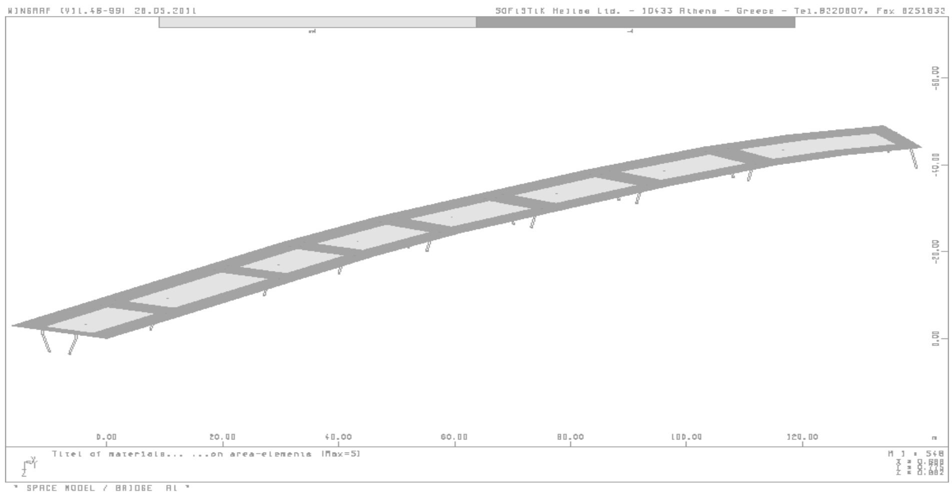

Figure 4. Analysis model of the upperstructure

In the analysis space model of the system of foundation for each one pier the corresponding part of the central pier wall is represented by a mesh of thick shell finite elements, the horizontal connecting beam and the piles by 3D-beam elements and the horizontal resistance of the soil on the piles by horizontal linear springs with constant corresponding to the modulus of subgrade reaction of the penetrated soil layers. On the model are applied the transversal support reactions of the piers for the normal operating and for the seismic actions. The omission in the model of the side abutment walls and of the cover slab of the river bed is considered to affect the analysis results at the safe side. (Fig. 5)

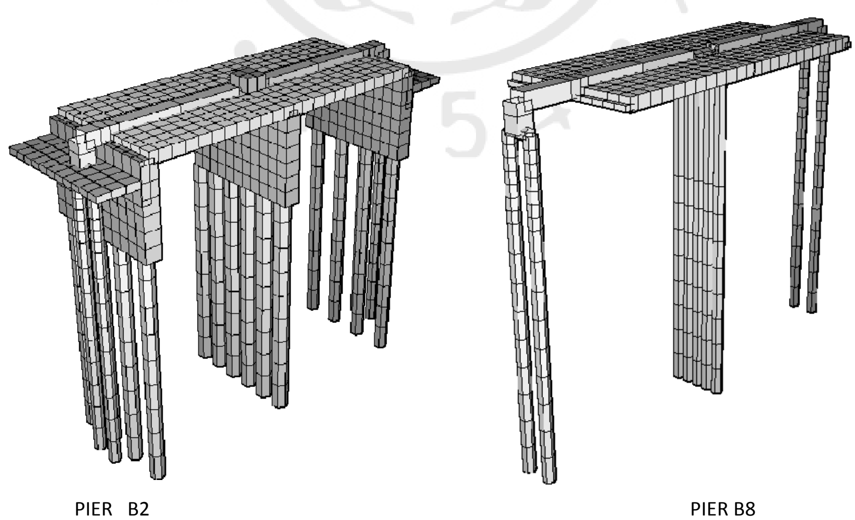

Figure 5. Analysis models of the foundations

6 CONCLUSIONS

The necessity for the application of the above system of foundation was imposed from the fact that the construction of the bridge had to be executed exclusively over and outside the existing covered bed of the river, avoiding any intervention in its interior, because at the same time an independed contract for the cleaning of the covered channels from accumulated muddy deposits was in progress. By this way both contracts have been successfully realized according to the prescribed time schedule, insuring for the bridge foundation conditions with the required safety.

ACKNOWLEDGEMENTS

The authors are thankfull for their contribution to the integration of the project to the civil engineers of Y.PE.HO.DE. ans the Contractor MOCHLOS S.A. .

REFERENCES

[1] Leonhardt F, *"Vorlesungen uber Massivbau, 6. Teil, Grundlagen des Massivbruckenbaues"*, Springer – Verlag, Berlin/Heidelberg 1979
[2] Clough R.W. – Penzien J, *"Dynamics of Structures"* Mc Graw – Hill Book Co, 2. Edition, Singapore, 1993.
[3] Bathe K.J, *"Finite Element Procedures in Engineering Analysis"*, Prentice Hall, Inc, New Jersey, 1982.
[4] Xanthakos P, *"Bridge Substructure and Foundation Design"*, Prentice – Hall PTR, New Jersey, 1995.
[5] Tomlinson M.J, *"Pile Design and Construction Practice"*, Cement and Concrete Association, London 1977.
[6] Poulos H.G, Davis E.H, *"Pile Foundation Analysis and Design"* John Wiley & Sons, Inc. New York, 1980.

SOME NEW THOUGHTS ON THE PERFORMANCE-BASED DESIGN OF CAISSON SUPPORTED BRIDGES

Nikos Gerolymos, Athanasios Zafeirakos and George Gazetas

National Technical University of Athens, School of Civil Engineering, Greece
e-mail: gerolymos@gmail.com, azafeirakos@yahoo.com, gazetas@ath.forthnet.gr

ABSTRACT: The present paper examines the seismic performance of caisson foundations under a new design philosophy, where soil "failure" is allowed to protect the superstructure. To investigate the effectiveness of such an approach, a caisson–column supported bridge structure is used as an example. Two alternatives are compared: one complying with conventional capacity design, with *over-designed* foundation so that the soil is marginally plastified; the other following the new design philosophy, with *under-designed* foundation, "inviting" the plastic "hinge" into the soil. Key performance measures of the systems are then compared, such as: accelerations, spectral response, displacements, pier base rotations and settlements. It is shown that separation of the caisson from the supporting soil and extensive soil plastification contribute beneficially to the seismic performance of both the foundation and the superstructure.

KEY WORDS: Bridge piers, Caisson foundations; Seismic soil-structure interaction; Soil capacity mobilization; performance measure parameters

1 INTRODUCTION

Caisson foundations deeply embedded in soft soil have been widely used to support major structures, especially bridges. Despite their large dimensions, caissons have been shown *not* to be immune to seismic loading as it was believed for many years, as was confirmed in the Kobe (1995).

Interestingly, although the lateral and seismic response of deep foundations has been of considerable interest for many years leading to the development of a number of methods of varying degrees of accuracy, efficiency and sophistication, only few of them are *devoted* to caissons. Instead, the methods of solution developed for (rigid) embedded foundation and for (flexible) piles have been frequently.

This paper aims to shed some light in the seismic design of caisson foundations under the prism of performance based design, which in geotechnical earthquake engineering has, until recently, received little attention. More specifically, a *new seismic design philosophy* is applied, in which yielding of the soil-foundation system is "utilised" to *protect the superstructure* - exactly the opposite of conventional capacity design (in which plastic "hinging" is restricted to the superstructure, thus underestimating the effect of soil and foundation). Fig. 1 schematically illustrates the difference between conventional design and the new concept, providing the basic idea of plastic “hinging” in the superstructure and the foundation respectively.

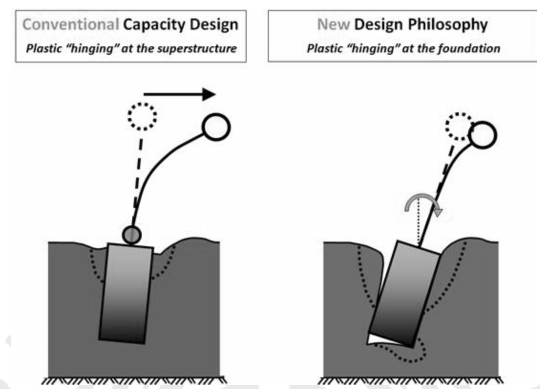

Figure 1. Conventional capacity design (plastic “hinging” in the superstructure) compared with the new design philosophy (plastic “hinging” below ground)

To unravel the effectiveness of the new design philosophy (compared to conventional capacity design), a simple but realistic bridge structure founded on caisson foundation is used as an example. Two configurations are analysed and compared: (*a*) the first comprises a 8 m pier founded on a rigid cubic caisson, and (*b*) the second consists of a 33 m pier founded on a similar caisson, corresponding to a conventionally and an *un*-conventionally designed system respectively. Both systems are subjected to an artificial acceleration time history imposed at the base. This artificial seismic excitation is appropriately calibrated in a way that the spectral acceleration of a 1-DOF oscillator placed at the surface remains constant for a wide range of frequencies, practically unaffected by the dynamic characteristics of the soil-structure system (e.g. effective fundamental period). The analysis methodology will be explained thoroughly in the sequel.

Evidently, it is shown that allowing plastic hinging at the foundation restricts the loading transmitted onto the superstructure, but without avoiding the increase of earthquake-induced foundation settlements and rotations. Overall, however, the new design approach provides substantially larger safety margins.

It should be noted at this point that the results presented herein can be seen as a first demonstration of the potential advantages of the new concept. To become applicable in practice, the new design philosophy will have to be extensively verified analytically and experimentally (shaking table and centrifuge testing), something which is the scope of the EU-funded project "*DARE*" (*Soil-Foundation-Structure Systems Beyond Conventional Seismic "Failure" Thresholds*).

2 PROBLEM DEFINITION AND ANALYSIS METHODOLOGY

2.1 Problem Definition and Model Description

A bridge pier is founded through a rigid cubic caisson of side h = 10 m in a 20 m thick 2-layer cohesive soil stratum. The soils are saturated with S_u = 65 kPa at the upper 6 m and S_u = 130 kPa at the lower 14 m. The two alternative design approaches, conventional and un-conventional, are represented by two different column heights. In both cases the concentrated mass of the deck, M, is 2700 Mg, corresponds to a static factor of safety in both systems FS_V = 5. The design spectral acceleration is chosen S_a = 0.6 g.

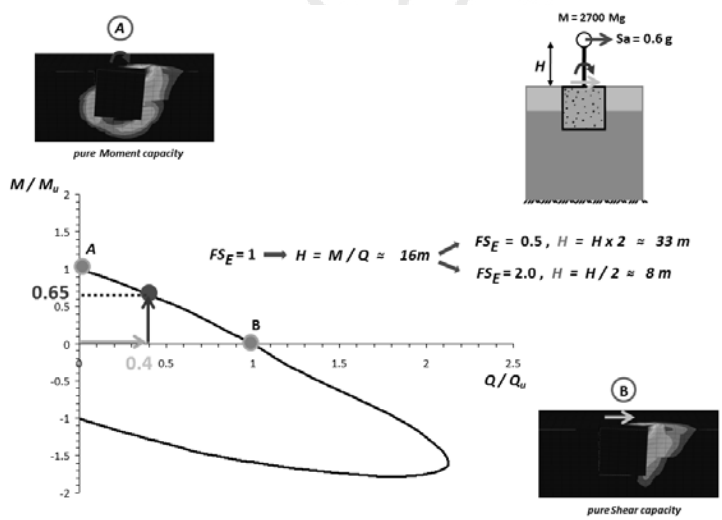

Figure 2. Failure envelope of the soil–caisson configuration and calculation process of the alternatives' column heights.

The problem is analysed with the use of the advanced Finite Element code ABAQUS. Both caisson and soil are modeled with 3-D elements, elastic for the former and nonlinear for the latter. The mass-and-column superstructures are modeled as single degree of freedom oscillators. The caisson is connected to the soil with special contact surfaces, allowing for realistic simulation of possible detachment and sliding at the soil-caisson interfaces. The column heights associated with the two alternative design approaches, are calculated as illustrated in Fig. 2:

- For a specific vertical force at the head of the caisson, the moment (M)−horizontal load (Q) interaction diagram is produced, corresponding to the failure envelope (in $M-Q$ space). Since $M = Q \cdot H$, the interaction the between M and Q may also be interpreted as the lever arm height above the pier base (H) that leads to failure for a given Q. Furthermore, each point on failure envelope corresponds to a safety factor for seismic loading FS_E = 1.0. In Fig.3 the results are presented normalized with respect to the pure moment capacity Mu (with no horizontal loading) and the pure horizontal capacity Qu (with no moment loading) of the caisson−soil system.

- Given the mass of deck, M = 2700 Mg, and the design spectral acceleration, S_a = 0.6 g, the pseudo-static pier base shear force, $Q = M \cdot S_a$, is calculated, leading, in our case, to a ratio of $Q/Q_u = 0.4$.
- Having calculated Q/Q_u, the respective moment, M, at failure is extracted, $M / M_u = 0.65$, resulting further in a pier height H = 16 m (for a FS_E = 1.0).
- Given the pier height for FS_E = 1.0, a shorter pier, H = 8 m, is designed in compliance with conventional capacity design, resulting from a FS_E = 2.0 and a taller pier, H = 33 m, is considered in the spirit of the new philosophy, designed with a FS_E = 0.5 (lower than 1.0 − under-designed pier). In fact, as it will be shown below, the *under-designed* system will not allow the design seismic action to develop. Hence, FS_E does not really have a physical meaning in this case; it is just an *apparent* temporary factor of safety.

The pier is modeled with 3-D linear elastic beam elements having properties of concrete. The cross-section of the pier is calculated so that the elastic (fixed-base) vibration period T_{st} = 0.6 sec, for both cases, deliberately larger than the first natural period, T = 0.41 sec, of the soil profile used in the analysis. In this way spurious oscillations at the boundaries of the model are limited as a result of a destructive interference (existence of a cut-off period for radiation damping equal to the first natural period of the soil profile) of the outward spreading waves (Gerolymos and Gazetas 2006, Gerolymos et al. 2008). This results in a solid cylindrical section with a diameter of d = 3 m for the conventionally designed pier (H = 8 m) and a hollow section of d = 8.5 m and thickness t = 1.5 m for the un-conventionally designed pier (H = 33 m). Fig. 3 illustrates the geometric configuration of both systems.

2.2 Methodology

The seismic performance of the two alternatives is investigated through nonlinear time-history analysis. It should be highlighted that in most published earthquake response analyses the examined systems are subjected to a variety of seismic motions to capture the interplay between the exciting dynamic characteristics (e.g. dominant periods, frequency content, PGAs, sequence of pulses) and the vibrational characteristics (natural, T_{st}, and effective fundamental period, T_s) of the structures. This paper, however, follows a methodology in which both systems are subjected to an appropriately calibrated seismic motion, so that their effective fundamental periods T_s fall within a

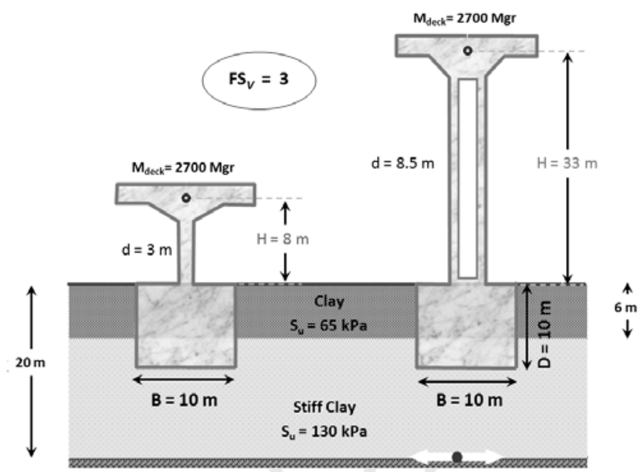

Figure 3. Schematic illustration of the conventional and un-conventional system.

plateau of constant spectral accelerations, thus eliminating the aforementioned interactions. Having, in this way, removed any bias of the response mechanisms on the dynamic properties, we may focus on the main question posed in this study, whether plastic mobilization of soil is beneficial or detrimental, and compare the two alternatives on a "*fair*" basis. The procedure consists of the following steps:

1) A real accelerogram (also denoted as "natural" record) is selected as seismic excitation for both systems. In this paper the one recorded at Sakarya during 1999 Turkey earthquake is used.
2) The "natural" record is then used as base excitation in a one-dimensional wave propagation analysis of the 2-layer soil profile and the free-field (top of soil profile) acceleration time-history along with the respective response spectrum are derived. This spectrum is then compared with an artificial *target response spectrum*, which, in our case, resembles a typical code design spectrum, having a plateau in S_a = 0.6 g for a wide range of periods (0.2 to 1.6 sec; it will be shown that the effective periods T_s of both over and *under-designed* systems fall into this specific range).
3) Within a heuristic optimization procedure (trial and error technique), the base excitation is back-calculated by deconvoluting the calculated free-field motion, until the response spectrum matches the *target*. Upon matching, the new modified motion is used as the base seismic motion for the 3-D analyses of both systems.

3 ANALYSIS: RESULTS AND DISCUSSION

The comparison of the performance of the two design alternatives subjected to the artificial accelerogram is presented in Figs. 4–7, in terms of acceleration and displacement time–histories, deck "*floor*" response spectra, pier base moment–rotation and settlement–rotation. The acceleration time–histories calculated at the deck are presented in Fig. 4a. Even though both systems were subjected to a design spectral acceleration of S_a = 0.6 g (Fig. 4c), the response of the *under-designed* (H = 33 m) system is significantly smaller, reaching a maximum of a = 0.3 g, in accord with the design seismic factor of safety FS_E = 0.5, than for the *over-designed* (H = 8 m, FS_E = 2.0) where the full seismic action is developed (a = 0.6 g). This is the first evidence that mobilization of soil capacity hinders the development of the design seismic action, which is further demonstrated in the substantial decrease in the "*floor*" spectral accelerations at the mass of the superstructure (i.e., the accelerations of the computed motion of the superstructure mass) in the *under-designed* case, as depicted in Fig. 4b.

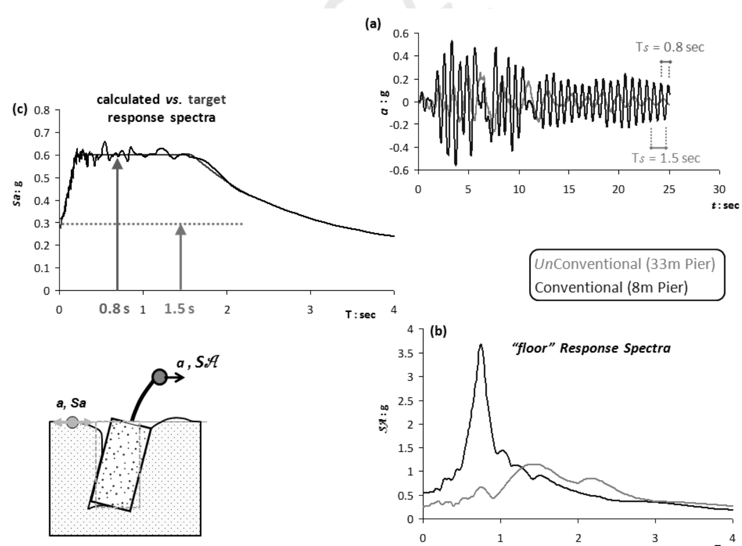

Figure 4. Comparison of the response of the two alternatives subjected to the artificial accelerogram. (a) Acceleration time–histories at the deck mass, with the respective effective periods T_s. (b) Response spectra of the motion of the mass. (c) Computed free-field and target response spectra used for the dynamic analyses.

The effective periods due to soil–structure–interaction effects, T_s, of the alternatives were derived from the free oscillations at the end of each shaking, resulting in T_s = 0.8 sec for the *over-designed* and T_s = 1.5 sec for the *under-designed* system (Fig. 4a), both falling within the range of the target spectrum plateau, S_a = 0.6 g. The main prerequisite for the validity of our methodology is thus met.The time histories of deck horizontal displacement, i.e. the *drift*, for the two alternatives are compared in Fig. 5. As graphically illustrated in the adjacent sketch notation, the *drift* has two components (see also Priestley et al.

1996): (i) the "*rigid drift*" $U_{rigid} = \theta H$, i.e. the displacement due to motion of the caisson as a rigid body, and (ii) the "*flexural drift*", i.e. the structural displacement due to flexural distortion of the pier column. Both U_{rigid} and U_{flex} are presented normalized with the respective maximum total displacement, U_{total_max}. This way, the contribution of pier flexural distortion and caisson rotation to the final result of interest (i.e. the total drift) can be inferred.

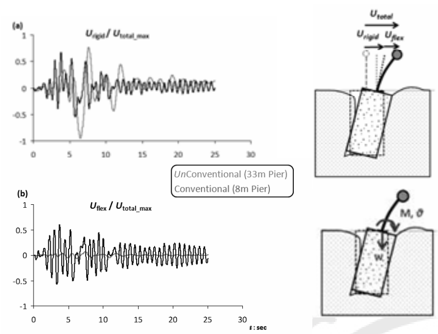

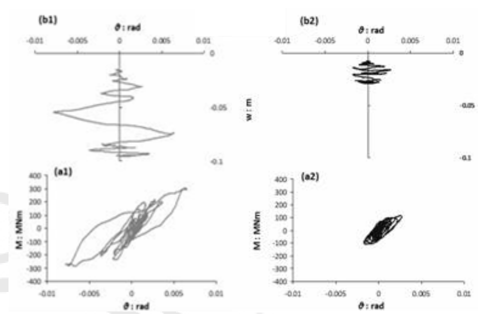

Figure 5. (Left): Comparison of the response of the two alternatives. (a) Time–histories of the "rigid–body" drifts normalized with the respective maximum total drift . (b) Time–histories of the flexural drifts normalized with the respective maximum total drift.

Figure 6 (Right): Comparison of the response of the two alternatives in terms of Overturning moment–rotation (M–θ), (b1), (b2)and settlement–rotation (w–θ), (a1), (a2) at the head of the caisson.

As might have been expected, for the conventional design (*over-designed foundation*) the drift is mainly due to pier distortion U_{flex}, and thus increased structural distress. Exactly the opposite is observed for the *under-designed* foundation of the new design philosophy: the *drift* is mainly due to foundation rotation U_{rigid}, causing less seismic loading on the pier but increased total displacements due to soil yielding. Nevertheless, the total residual displacement for the new concept might be slightly larger, but quite tolerable: $U_{residual} \approx 5$ cm (compared to ≈ 0.5 cm for the conventional). In a nutshell, choosing to design a bridge pier *unconventionally* could substantially reduce the cost but would also demand appropriate provisions to accommodate for the increased seismic displacements.

In Fig. 6a the comparison is portrayed in terms of the foundation experienced moment–rotation (*M–θ*). As expected, while the conventionally designed foundation experiences limited inelasticity (Fig. 6a2), the *under-designed* foundation (new design philosophy) behaves strongly inelastic (Fig. 6a1). Since both piers were modeled for elastic behavior, the main difference between the two alternatives lies in the mechanism of energy dissipation due to soil yielding. However, energy dissipation is not attainable at zero cost: in our case the cost is the increase of foundation settlement. Fig. 6b compares the settlement–rotation (*w–θ*) response for the two alternatives.

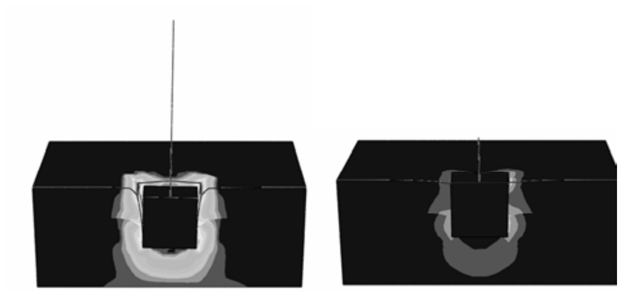

Figure 7. Contours of plastic shear strain at the end of shaking for both alternatives (deformation scale factor = 20).

The conventionally designed system is subjected to a practically elastic settlement $w \approx 3$ cm (Fig. 6b2). In marked contrast, the *under-designed* system of the new philosophy experiences larger but quite tolerable dynamic settlement: $w \approx 10$ cm (Fig. 6b1). Moreover, despite the excessive soil plastification, not only the structure does not collapse, but the residual (permanent) rotation is rather limited (as already attested by the residual deck drift), providing further evidence that mobilisation of soil capacity failure acts as a "*safety valve*" for the superstructure. Fig. 7 compares the response of the two alternatives in terms of plastic shear strain contours at the end of the shaking. In the conventionally designed system there is very little inelastic action in the soil, concentrated mainly at the top and bottom of the caisson. In contrast, the new design scheme experiences rather extended "plastic hinging" in the form of mobilization of passive–type soil failure in front and back of the caisson accompanied by gap formation and sliding in the sides.

REFERENCES

[1] Anastasopoulos I, Gazetas G, Loli M, Apostolou M, Gerolymos N, "Soil failure can be used for seismic protection of structures", *Bull Earthq Eng* 6(4):705–722, pp. 309-326, 2010.

[2] Gerolymos N, Gazetas G, "Winkler model for lateral response of rigid caisson foundations in linear soil", *Soil Dyn Earthquake Eng* 26(5):347–361, 2006.

[3] Gerolymos N, Gazetas G, "Static and dynamic response of massive caisson foundations with soil and interface nonlinearities - Validation and results", *Soil Dyn Earthquake Eng* 26 (5), pp. 377-394, 2006.

[4] Gerolymos N, Gazetas G, Tazoh T, "Seismic response of yielding pile in non-linear soil", In: *Proc. 1st Greece–Japanworkshop*, seismic design, observation, and retrofit of foundations, Athens, 11–12 October, pp 25–36, 2005.

[5] Gerolymos N, Giannakou A, Anastasopoulos I, Gazetas G, "Evidence of beneficial role of inclined piles: observations and numerical results". *Bull Earthq Eng* 6(4):705–722 Special Issue: Integrated approach to fault rupture- and soil-foundation interaction, 2008.

[6] Giannakou A, Gerolymos N, Gazetas G, Tazoh T, Anastasopoulos I, "Seismic Behavior of Batter Piles: Elastic Response", Journal of Geotechnical and Geoenvironmental Engineering, ASCE, 136, No.9, 1187-1199, 2010.

[7] Priestley MJN, Seible F, Calvi GM, "Seismic design and retrofit of bridges", Wiley, New York, 1996.

INSTABILITY PROBLEMS FOR HIGH PIERS

Elisabeth Karatzas[1], Velvet Karatzas[2] and George Karidis[3]

[1,2] University of East London, Dept. of Civil Engineering, United Kingdom
[3] Imperial College London, Dept. of Civil Engineering
e-mail: ikara@tee.gr

ABSTRACT: For structures with compression members whose slenderness ratio (λ)≤25 one can check their stability for static loads using first order theory in a very simple and safe way by using $P_{critical\ joint\ load}$. $P_{critical\ joint\ load}$ is defined as the maximum axial load a joint can take before it fails. Furthermore, by defining a proper spring constant ratio for the upper structure in relation to the base spring constant, $P_{critical\ joint\ load}$ may be affected thus, the possible failure of the structure might also be affected.

KEY WORDS: instability; piers; $P_{critical\ joint\ load}$; spring rotational constants

1 INTRODUCTION

In general, the piers of bridges are usually tall structures with very strong columns and foundations. Thus, one can claim that for these columns-foundations EI→∞. These piers can be considered to behave as a two member structural model that may fail due to axial loads for one of the three following reasons:

a) Due to buckling (Euler's cases) when λ>25 according to EC2
b) Due to material failure (squashing) when λ<25 according to EC2 and/or
c) Due to the surpassing of $P_{critical\ joint\ load}$

where $P_{\boldsymbol{critical\ joint\ load}}$ is the maximum axial load that a joint can bear before it fails.

The aim of this paper is to investigate the behaviour of piers whose λ≤25 with the help of the $P_{critical\ joint\ load}$ term and with the help of the spring rotational constants. In the paper "*Instability Problems-Investigation of $P_{critical\ joint\ load}$ under moment lods*"[1] $P_{critical\ joint\ load}$ was derived from the investigation of the differential equation $y'' = -\frac{M}{EI}$ for λ≤25 which means that $EI \to \infty$. Now, one may say that $P_{critical\ joint\ load}$ is an extension of Euler's equation although they differ significantly. The differences lie in the assumptions made. Euler assumes ideal slender sections with a specific *EI* value that deform while their support restraints remain still. On the contrary, with the $P_{critical\ joint\ load}$ equation, $EI \rightarrow \infty$ and the support restraints are also forced to rotate thus, the members with their base rotate as a whole.

2 STRUCTURAL ANALYSIS

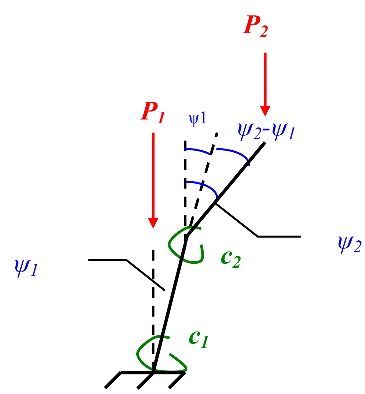

Figure 1. Two member structural model.

Considering Fig. 1 above, the following equations are derived:

$$P_2 \cdot h_2 \sin(\psi_2) = c_2 \cdot (\psi_2 - \psi_1) \tag{1}$$

$$(P_1 + P_2) \cdot h_1 \cdot \sin(\psi_1) + c_2 \cdot (\psi_2 - \psi_1) = c_1 \cdot \psi_1 \tag{2}$$

due to very small rotational angles, the following is true:

$$c_2 \cdot \psi_1 + \psi_2 \cdot (P_2 \cdot h_2 - c_2) = 0 \tag{3}$$

$$\left[(P_1 + P_2) \cdot h_1 + c_2 - c_1\right] \cdot \psi_1 + c_2 \cdot \psi_2 = 0 \tag{4}$$

Now, if one sets:

$$P = P_2 = \alpha_1 \cdot P_1 \tag{5}$$

and

$$h = h_2 = \alpha_2 \cdot h_1 \tag{6}$$

and

$$c = c_2 = \alpha_3 \cdot c_1 \tag{7}$$

$P_{critical\ joint\ load}$ is calculated using the matrix below:

$$\begin{vmatrix} c \cdots\cdots\cdots\cdots\cdots\cdots\cdots\cdots\cdots\cdot P\cdot h - c \\ (P+\frac{P}{\alpha_1})\cdot\frac{h}{\alpha_2} - c - \frac{c}{\alpha_3}\cdots\cdots\cdots\cdot c \end{vmatrix} = 0 \tag{8}$$

Solving matrix (8) above, the following equation is derived:

$$P^2 \cdot h^2 \cdot (\frac{\alpha_1 + 1}{\alpha_1\alpha_2}) - P \cdot h \cdot c \cdot (\frac{\alpha_3 + 1}{\alpha_3} + \frac{\alpha_1 + 1}{\alpha_1 \cdot \alpha_2}) + \frac{c}{\alpha_3}^{2} = 0 \tag{9}$$

The solutions of the quadratic Eq. (9) are known. Fig. 2 below shows two possible solutions of quadratic Eq. (9), in other words, two possible failures of a two member model.

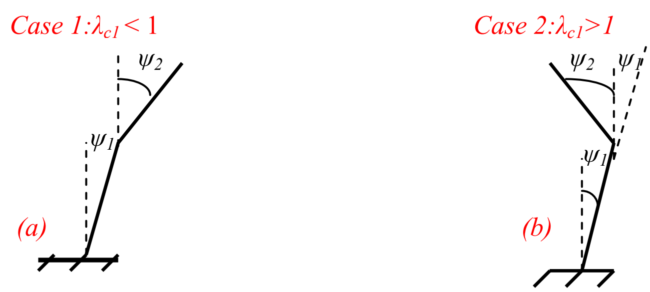

Figure 2. Possible failures of a two-member model.

3 INVESTIGATION OF QUADRATIC EQUATION (9)

If one adds Eq. (3) and Eq. (4) which apply for very small angles the following equation is derived:

$$P_{\text{joint load}} = \frac{c_1\left(1 + \frac{1}{\alpha_2}\right)}{h_{\text{total}}\left(\frac{\psi_2}{\psi_1} + \left(\frac{1}{\alpha_1} + 1\right)\cdot\frac{1}{\alpha_2}\right)} \tag{10}$$

When the denominator of Eq. (10) gives the maximum value then the minimum $P_{joint\ load}$ is derived. This is succeeded when $\frac{\psi_2}{\psi_1} \geq 1$. Using Eq. (3) and Eq. (4) one can calculate the ratio ψ_2/ψ_1 because $P_{critical\ joint\ load}$ is the so-called "branching load" of stability. However, one cannot calculate the values of ψ_2 and ψ_1 individually without using second order theory.

Next, the following tables are presented where $P_{critical\ joint\ load}$ is derived in function of c_1/h_2, c_2/h_2, and c_1/h_{total}. Note the values of α_1 and α_2 are constant and refer to the example that follows while the values of α_3 vary.

Table 1. $P_{critical\ joint\ load}$ results for area of soft sub-level

$\boldsymbol{\alpha_1}$ = 5,45 α_2 = 4		$\boldsymbol{P}_{critical\ joint\ load}$	$\boldsymbol{P}_{critical\ joint\ load}$	$\boldsymbol{P}_{critical\ joint\ load}$	$\boldsymbol{\psi_2}$ and $\boldsymbol{\psi_1}$
$c_2 = c_1$	α_3=1	0,461 c_1/h_2	0,461 c_2/h_2	0,613 c_1/h_{total}	ψ_2=1,855ψ_1
$c_2 = 2c_1$	α_3=2	0,586 c_1/h_2	0,293 c_2/h_2	0,779 c_1/h_{total}	ψ_2=1,414ψ_1
c_2=2,66c_1	α_3=2,66	0,6248 c_1/h_2	0,235 c_2/h_2	0,831 c_1/h_{total}	ψ_2=1,307ψ_1
c_2=3c_1	α_3=3	0,6395 c_1/h_2	0,213 c_2/h_2	0,850 c_1/h_{total}	ψ_2=1,271ψ_1
c_2=4c_1	α_3=4	0,668 c_1/h_2	0,167 c_2/h_2	0,888 c_1/h_{total}	ψ_2=1,200ψ_1
c_2=5c_1	α_3=5	0,687 c_1/h_2	0,1334 c_2/h_2	0,914 c_1/h_{total}	ψ_2=1,160ψ_1
c_2=7,52c_1	α_3=7,52	0,7144 c_1/h_2	0,095 c_2/h_2	0,950 c_1/h_{total}	ψ_2=1,105ψ_1
c_2=10c_1	α_3=10	0,728 c_1/h_2	0,0728 c_2/h_2	0,968 c_1/h_{total}	ψ_2=1,070ψ_1
c_2=20c_1	α_3=20	0,748 c_1/h_2	0,0374 c_2/h_2	0,995 c_1/h_{total}	ψ_2=1,039ψ_1
c_2=100c_1	α_3=100	0,7676 c_1/h_2	0,007676 c_2/h_2	1,020 c_1/h_{total}	ψ_2=1,0077ψ_1
c_2=1000c_1	α_3=1000	0,77186c_1/h_2	0,000771 c_2/h_2	1,026 c_1/h_{total}	ψ_2=1,00077ψ_1

Table 2. $P_{critical\ joint\ load}$ results for area of soft upper-structure

$\boldsymbol{\alpha_1}$ = 5,45 α_2 = 4		$\boldsymbol{P}_{critical\ joint\ load}$	$\boldsymbol{P}_{critical\ joint\ load}$	$\boldsymbol{P}_{critical\ joint\ load}$	$\boldsymbol{\psi_2}$ and $\boldsymbol{\psi_1}$
c_2=c_1	α_3=1	0,461 c_1/h_2	0,461 c_2/h_2	0,613 c_1/h_{total}	ψ_2=1,855ψ_1
c_2=0,5c_1	α_3=0,5	0,322 c_1/h_2	0,644 c_2/h_2	0,428 c_1/h_{total}	ψ_2=2,897ψ_1
c_2=0,33c_1	α_3=0,33	0,245 c_1/h_2	0,742 c_2/h_2	0,326 c_1/h_{total}	ψ_2=3,88ψ_1
c_2=0,25c_1	α_3=0,25	0,19375 c_1/h_2	0,775 c_2/h_2	0,257 c_2/h_2	ψ_2=4,447ψ_1
c_2=0,2c_1	α_3=0,20	0,16476 c_1/h_2	0,8238 c_2/h_2	0,219 c_2/h_2	ψ_2=5,6769ψ_1
c_2=0,1c_1	α_3=0,10	0,09048 c_1/h_2	0,9048 c_2/h_2	0,120 c_2/h_2	ψ_2=10,434ψ_1
c_2=0,05c_1	α_3=0,05	0,0475 c_1/h_2	0,95 c_2/h_2	0,063 c_2/h_2	ψ_2=20ψ_1
c_2=0,01c_1	α_3=0,01	0,0099 c_1/h_2	0,990 c_2/h_2	0,0132 c_2/h_2	ψ_2=100ψ_1

From Table 1 it is derived that the greater the c_2/c_1 ratio, the smaller the difference between the rotational angles, and $\Delta\psi$ tends to zero. In other words, the two-member model tends to behave as a one-member model and thus, the value of $P_{critical\ joint\ load}$ increases. From Table 2 it is derived that as c_2/c_1 decreases, $P_{critical\ joint\ load}$ also decreases.

4 EXAMPLE

In the 7th Annual Congress of Geotechnics 2010 that took place in Volos, Greece, the paper with title "*Experimental Validation of Bridge Pier Seismic Design Employing Soil Ductility*"[2] was presented. The paper shows the behaviour and the points of failure of the two piers with their foundations that were tested in different experiments that took place in the Greek Metsovio University (see Fig. 3 below). Now, the authors of this paper will use the paper mentioned above as well as the book called "*Statik und Stabilitat der Baukonstruktionen*"[3] in order to explain why these piers failed in the way they did using the term $P_{critical\ joint\ load}$.

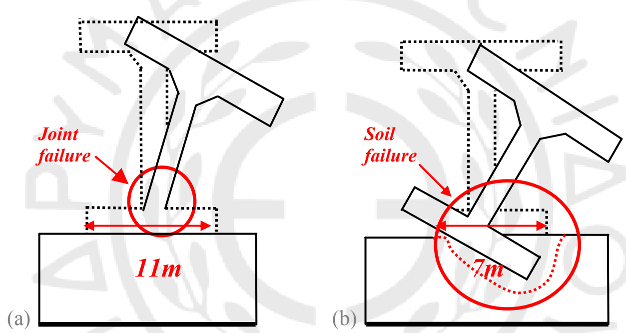

Figure 3. Piers and their foundations with their points of failure.

Thus, using the data of the experiments and the methodology in the book mentioned above, the following is derived for the 11m foundation (see Fig. 3a):

$$\alpha_3 = \frac{c_2}{c_1} = \frac{24{,}75 \cdot 10^{12}}{9{,}29 \cdot 10^{12}} = 2{,}66 \qquad (11)$$

and for the 7m foundation (see Fig. 3b):

$$\alpha_3 = \frac{c_2}{c_1} = \frac{15{,}75 \cdot 10^{12}}{2{,}095 \cdot 10^{12}} = 7{,}52 \qquad (12)$$

Substituting these values into Eq. (9), the following results are derived and presented in a table format below as well as in Fig. 4:

Table 3. Results derived using Eq. (9)

	c_2/c_1	α_3	$P_{critical\ joint\ load}$	ψ_2/ψ_1
11m foundation	2,66	2,66	$0{,}831c_1/h_{total}$	$\psi_{2\alpha}/\psi_{1\alpha}=1{,}307$
7m foundation	7,52	7,52	$0{,}95c_1/h_{total}$	$\Psi_{2\beta}/\psi_{1\beta}=1{,}105$

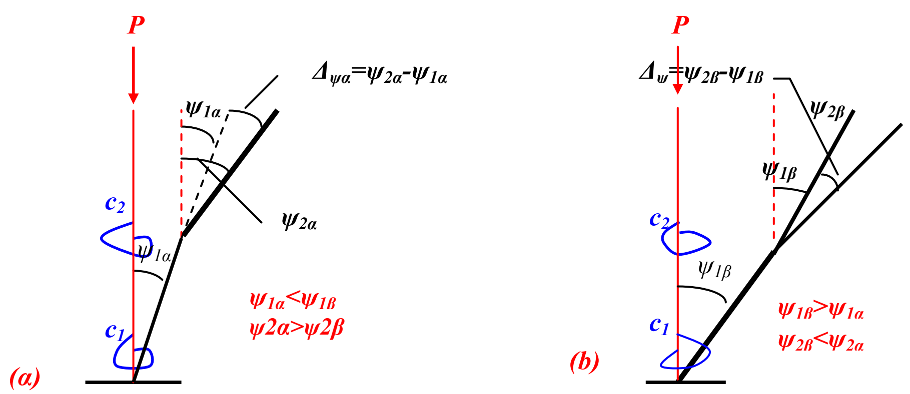

Figure 4. Rotational angles for a structural two-member model.

The difference of the rotational angles of the two-member model is that for the 11m pier-foundation:

$$\Delta_{\psi_\alpha}=\psi_{2\alpha}-\psi_{1\alpha}=(1{,}307-1{,}00)\psi_{1,\alpha}=0{,}307\psi_{1\alpha} \tag{13}$$

and for the 7m pier-foundation:

$$\Delta_{\psi_\beta}=\psi_{2,\beta}-\psi_{1\beta}=(1{,}105-1{,}00)\psi_{1\beta}=0{,}105\psi_{1,\beta} \tag{14}$$

When $\Delta_{\psi\alpha}=0{,}307\psi_{1\alpha}$ there is concrete fracture failure at the joint between first and second member see Fig. (3a). Now, if one wishes to succeed concrete fracture failure in Fig. (3b) as well then the following must hold:

$$0{,}307_{\psi_{1,\alpha}}=0{,}105_{\psi_{1,\beta}} \tag{15}$$

or

$$\psi_{1\beta}=2{,}9238\psi_{1\alpha} \tag{16}$$

However, while $\psi_{1\beta}$ is getting larger in order to succeed concrete fracture failure, soil failure may occur first (depending on the soil type), as it happened in the experiments that took place in the Greek Metsovio University.

If soil failure does not occur first, then concrete fracture failure will occur because:

$$\Delta_{\psi\beta} = \psi_{2,\beta} - \psi_{1\beta} = (1{,}105 - 1{,}00)\psi_{1\beta} = 2{,}9238 \times 0{,}105_{\psi 1\alpha} = 0{,}307_{\psi 1,\alpha} \quad (17)$$

The above calculations explain the results of the experiments that took place in the Greek Metsovio University.

5 CONCLUSIONS

The absolute magnitude of $P_{critical\ joint\ load}$ of a structure where $\lambda \leq 25$ is a function of P, h, and the ratio c_2/c_1 where c_2 is the spring rotational constant of the second member and c_1 is the spring rotational constant of the first member (foundation).

In cases where the structures have $\lambda \leq 25$ two kinds of failures are observed: a) failure in the structure itself, and b) soil failure. Moreover, in the case of failure in the structure itself two kinds of failures are observed depending on the c_2/c_1 ratio:

Case 1a: small rotational angle ψ_1 and big rotational angle ψ_2 is observed in structures with soft upper-structures when $c_2 < c_1$ as shown in Fig. (4a).

Case 1b: Big rotational angle ψ_1 and small rotational angle ψ_2 is observed when $c_2 >> c_1$. This indicates that there is a strong upper-structure and a soft sub-structure as shown in Fig. (4b).

Between the possible cases of failure denoted above as cases 1a and 1b, it is possible for soil failure to occur before failure occurs in the structure itself. This may happen when angle ψ_1 surpasses the allowable endurance angle of the soil as shown in the experiments that took place in the Greek Metsovio University. When $c_1 << c_2$, then $P_{critical\ joint\ load}$ is maximum. In other words, the two member model behaves as a one member model. On the contrary if $c_1 > c_2$ it means that there is a soft upper-structure and $P_{critical\ joint\ load}$ is small.

The knowledge of $P_{critical\ joint\ load}$ for structures with compression members whose $\lambda \leq 25$, is absolutely necessary because it provides a better understanding/evalution of the structures and their behaviour. In other words, a better compatibility is succeeded between upper-structure (pier) and sub-structure (foundation).

Finally, in this paper, it is shown in a very simple and comprehensible manner how to calculate the stability of structures when $\lambda \leq 25$.

REFERENCES

[1] Velvet Karatzas, Elisabeth Karatzas, "*Instability Problems-Investigation of $P_{critical\ joint\ load}$ under moment lods*", Washington, 3rd international fib 2010.

[2] Drosos, Georgarakos, Anastasopoulos, and Gazetas, "*Experimental Validation of Bridge Pier Seismic Design Employing Soil Ductility",*7th Annual Congress of Geotechnics, Volos-Greece, October 2010.
[3] Petersen, "Statik und Stabilitat der Baukonstruktionen", Vieweg, pp. 910- 912, 1982.

SEISMIC BEHAVIOR OF LONG BRIDGES WITH SLENDER ABUTMENTS

Eleni Zygouri[1], Dimitris Bairaktaris[2]

[1,2] D. Bairaktaris and As/tes Structural Design Office Ltd – Athens – Greece ,
e-mail: baisteng@otenet.gr

ABSTRACT: Slender abutments of long bridges subjected the earth pressures from the backfill maintain at the top a permanent contact with the ends of the deck adapted to the contraction displacements. In case of earthquake action the resistance of the backfill is activated resulting to the reduction of the displacements and of the seismic actions on the piers and their foundation.

KEY WORDS: Bridge; Earthquake response; Soil – structure interaction.

1 INTRODUCTION

For the attainment of the required structural resistance of long bridges against earthquake actions the following three alterative design choices are offered.

a. The provision of elastoplastic behavior through the formation of plastic hinges developing limited plastic rotation mainly at the bottom cross section of the piers. The reduced elastoplastic stiffness corresponding to a higher value of the predominant eigenperiod and the increased hysteretic dumping ratio imply lower response of the structure to the seismic action. Disadvantages of this design choice are the extensive horizontal displacements and the eventual plastic hinge formation at the totality of the piers resulting to a kinematical mechanism, a fact not excluding a total failure of the structure. Anyway the necessity arises for the detection of the plastic hinges under the soil covering the bottom part of the pier and for the corresponding repair.

b. The application of seismic isolation devices. Simple elastometalic bearings at the supports of the deck on the piers and abutments cause higher flexibility of the structure in the horizontal direction and thus a higher value of the predominant eigenperiod. By using more sophisticated seismic isolation devices, which offer moreover and an increased dumping ratio, as par example elastomeric bearings with ductile metal core, friction pendulum bearings or hydraulic viscous dampers, a further lowering of the response is obtained. The relatively high cost of the devices, the necessity for long term inspection and maintenance and the extensive horizontal displacements are some of the disadvantages which have to be taken into account for this choice.

c. The activation of the horizontal resistance of the compacted backfill behind the abutments aiming at the reduction of the horizontal displacements in the longitudinal direction and consequently to less horizontal forces and bending moments of the piers. This design choice presupposes the permanent or the occasional connection between the top of the abutments and the ends of the deck structure. For bridges of short length, where the longitudinal contraction of the deck due to the thermal, creep and shrinkage effects is limited, this permanent connection is possible and widely applied. But for bridges of long length, for which an extensive contraction of the deck is expected, a permanent connection with the stiff structure of the abutments will cause extensive tensile stresses not acceptable for the concrete structure of the deck. For that case solutions providing an occasional connection activated by a sudden stimulation in case of an earthquake event have been proposed, par example by using strong hydraulic dampers in the longitudinal direction. The high cost of the corresponding devices, the required strong supporting substructure at the abutments and the necessity for long term inspection and maintenance are factors which have to be taken into account for this choice.
For this last case a proposal for an extremely simple and economical system providing a permanent connection of the ends of the deck with the top of the abutments of long bridges, without unfavorable effects for the structure, is presented in the sequence in detail.

2 THE SLENDER ABUTMENT METHOD (SAM)

For the bridges of a long length where extensive contraction at the longitudinal direction due to thermal, shrinkage and creep effects is expected, the traditional formation provides the deck to be supported on the abutments through sliding bearings permitting the foreseen horizontal displacements. In that case the abutment acts as a vertical cantilever loaded by the horizontal earth pressures of the backfill and by the horizontal reactions of the bearings. High values of bending moments and shear forces are developed for this actions imposing an increased thickness and thus a considerable stiffness for the abutment. The stiffness is furthermore increased through the rigid connection of the wall supporting the deck with the wing walls enclosing the backfill at the two sides. Under this form the abutments constitute members operating independently of the rest structure of the bridge and do not contribute to its resistance against the seismic actions.

An abutment with permanent simple contact of the top at the end of the deck does not act as a free vertical cantilever and operates under the form of a single span vertical wall rigidly or elastically jointed at the bottom and pin jointed at the top. The bending moments and the shear forces developed due to the earth pressures of the backfill and the contraction displacement of the top have values much lower than those corresponding to the free cantilever. For these values a small thickness of the wall can be applied and an increased flexibility to be obtained which, under the action of the earthpressure of the backfill, developes a flexure adapted to the contraction displacement and imposes the permanent contact of the top of the abutment to the deck. Under this form the considerable horizontal resistance of the backfill is activated and contributes significantly to the total resistance of the bridge against the seismic actions with consequence lower values for the horizontal displacements of the deck and the top of the piers. The limited displacements permit to consider their behavior as elastic during the earthquake motion avoiding the undesirable effects of the elastoplastic one.

Criterion of sufficient flexibility of the abutment to insure its permanent contact to the deck is the value of its top horizontal deflection considered as a free cantilever, to be greater than the foreseen contraction displacement at the end points of the deck. For this estimation the stage II stiffness can be used with the long term values of the Young' s modulus for the concrete, since this is in accordance with the long term action of the creep and shrinkage. Moreover a significant part of the creep and shrinkage contraction is developed during the erection and before the completion of the deck of a long bridge, so that they can not be taken into account to the contraction displacements affecting the behavior of the abutment.

3 CONSTRUCTION PROVISIONS

The following simple construction provisions are necessary in order the structural system of the bridge to operate according to the slender abutment concept. (Fig. 1)

The wall of the abutment supporting the bridge have to be separated from the wing walls at the two sides by vertical free joints along its total height, although both are based on a common fundament.

For the bearings at the abutments the capacity for sliding in not necessary and this is limited to permit the rotation at the end point of the deck.

In order a sufficient contact surface to be obtained between the deck and the abutment adapted to the value of the end rotation the lower part of the end cross sections of the beams or the slab is formed with a convex cylindrical scheme to be in contact with a similar concave cylindrical surface at the bottom of the breast wall of the abutment. For expected significant end rotation of the beams is suggested both surfaces to be equipped with a layer of elastomeric material covered by a PTFE film reducing the friction resistance to the rotation.

A temporary horizontal steel beam below the level of the bearings in contact with the front surface of the abutment and fastened at the two sides on the wing walls permits the depositing and compaction of the backfill before the erection of the deck.

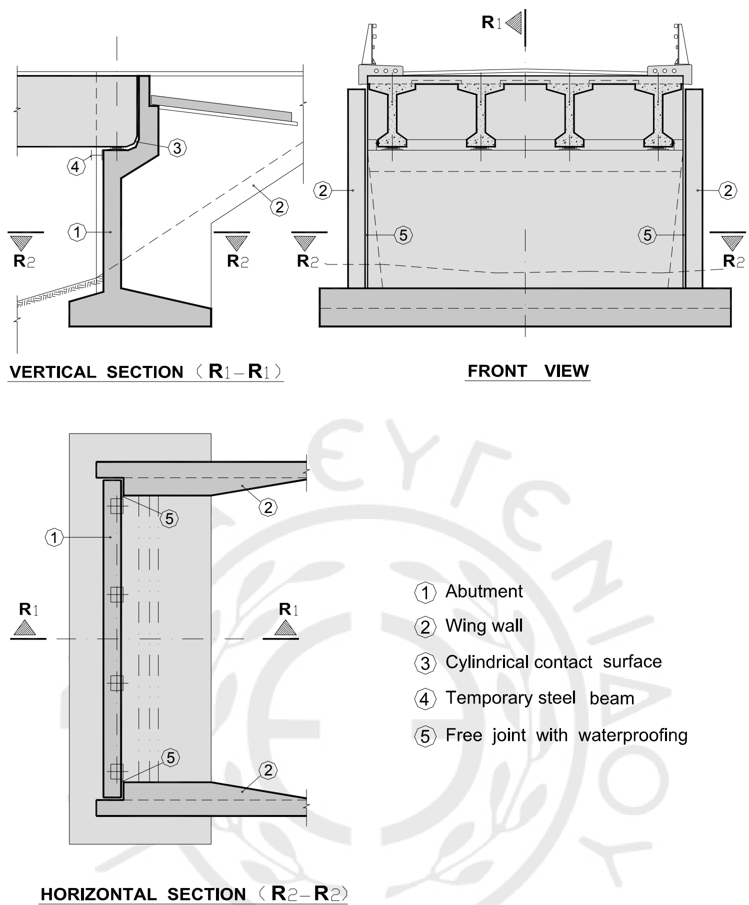

Figure 1. Geometry of slender abutment

A granular material for the backfill with specified grade of compaction have to be provided.

A part of the upper asphalt layer of the paving behind the abutments have possibly to be replaced some time after the completion of the bridge so that cracks due to the movements of the backfill to be canceled.

4 COMPARATIVE PRESENTATION OF APPLICATION EXAMPLES

The advantageous effect of the proposed design concept of the slender abutments is verified through the analysis of a four span long bridge, of 144 m total length to earthquake action. (Fig 2). The spans are 31,35 – 40,70 – 40,70 – 31,35 m, the width of the deck 20 m and consists of 7 precast and prestressed beams of 2,00 m height bearing the slab of 0.20 m thickness. (Fig 3)

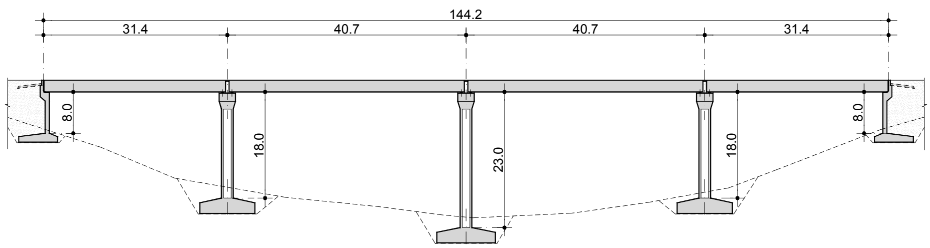

Figure 2. Longitudinal section

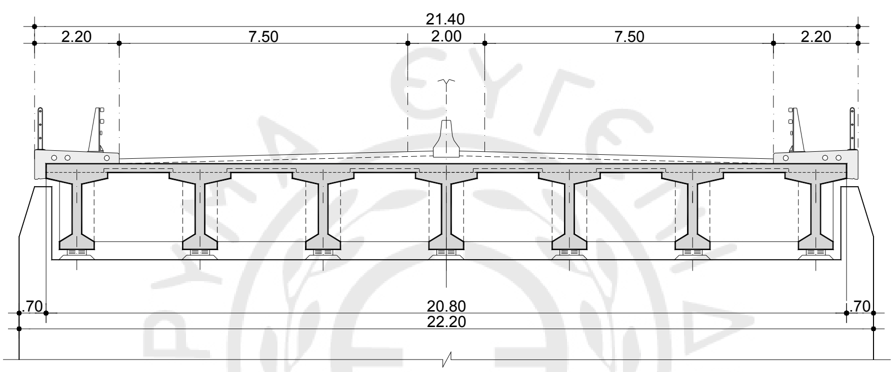

Figure 3. Typical cross section

The piers are reinforced concrete three column frames with columns of rectangular hollow cross section considered as rigid jointed on the foundation with total height 18 – 24 – 18 m, while the height of the abutments is 8 m. The beams are supported on the piers and abutments through elastomeric bearings. The analysis is executed on a space finite element model of the structure where the slab and the abutments are represented by Kirkchoff plane finite elements, the piers by 3-D beam elements, the elastomeric bearings with shear beam elements and the soil behind the abutments by linear horizontal springs with constants corresponding to the modulus of subgrage reaction (Fig. 4). On the model are applied the dead and the live loads, the prestressing, the imposed deformations and the earthquake actions in the longitudinal direction for a seismic ground acceleration 0,24 g applied on the structure and the soil behing the abutments. A dynamic spectral analysis is applied where the displacements and the internal forces of the structural members result from the superposition of the response of the 24 first eigenmodes, according to the SRSS method, for elastic behavior of the system.

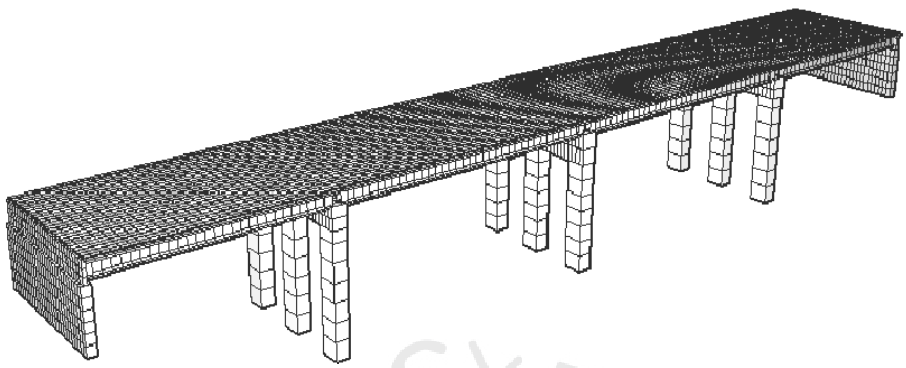

Figure 4. F.E. Model of analysis

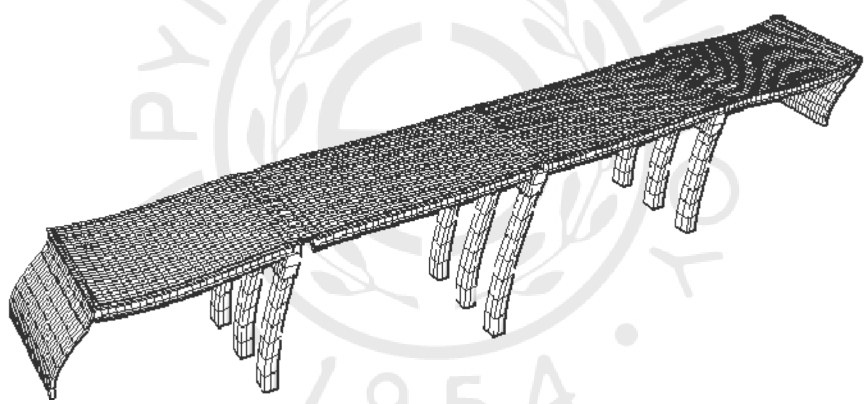

Figure 5. Deformed shape of the structure (case 2)

The analysis is executed for two cases:

Case 1, without end contact of the deck to the top of the abutments and with sliding bearings of 80 mm thickness at the piers and 100 mm thickness at the abutments.

Case 2, providing slender abutments of 0.50 m thickness with permanent end contact of the deck to their top, represented in the analysis model by pin joints. Sliding bearings of 50 mm thickness are provided only at the piers.

Results of the analysis for both cases concerning critical locations of the structure are presented in Table 1, permitting the comparison between them.

Table 1. Comparative Analysis Results

	CASE 1 **Stiff Abutments**	**CASE 2** **Slender Abutments**
Predominant Eigenperiod (sec)	1,17	0,57
Seismic Displacement of Deck (mm)	142	58
ABUTMENTS		
Thickness (m)	1,50	0,50
Bottom Bending Moment (kNm/m)	3450	850
COLUMNS OF PIERS		
Hollow Cross Section (m)	2,80 x 2,20 x 0,35	2,80 x 2,00 x 0,30
Top Displacement δ_x (mm)	97	57
	B2, B4 / B3	B2, B4 / B3
Axial Force N (kN)	-7650 / -8400	-8330 / 8900
Shear Force V (kN)	1850 / 1870	1230 / 950
Bending Moment max M (kNm)	30400 / 29700	17930 / 15930
FOUNDATION OF COLUMNS		
Number of bored piles (Premissible load 3500 kN for earthquake action)	9	5

5 CONCLUSIONS

From the analysis results presented in Table 1 becomes evident that the horizontal displacements and the internal forces of the piers developed for the earthquake action in the case where the slender abutments method is applied have values equal to 50-60% of those corresponding to the usually applied system of stiff abutments with sliding bearings. The corresponding values for the abutments are much lower.

This advandageous result is obtained exclusively by a passive system of low cost not requiring long term inspection and maintenance, something not avoided in the case of seismic isolation or hydraulic shock absorbtion systems using high cost sophisticated devices. Moreover expansion joints of the paving over the abutments with negligible opening are required.

Considering the analysis procedure have to be noted that better approximation to the actual conditions would result by representing in the analysis model the backfill behind the abutments at a length three times the height through massive solid finite elements subjected the ground acceleration, instead of the linear horizontal springs and the additional seismic earthpressure, which in the example are introduced with values specified by the codes. This improvement of the analysis is expected that implies even better results for the slender abutments method, taking into consideration that the provisions of the codes point usually at the safe side.

REFERENCES

[1] Veletsos A.S., Nair V.V., "Seismic interaction of structures on hysteretic foundations", Journal of Structural Engineering, ASCE 101 (1), pp. 109-129, 1975.

[2] Mylonakis G., Gazetas G, "Seismic soil-structure interaction: beneficial or detrimental?", Journal of Earthquake Engineering, 4(3), pp 277-301, 2000.

[3] Kramer, S. *"Geotechnical Earthquake Engineering"* , Prentice Hall, Inc, New Jersey, 1996.

[4] Skinner, R.I., Robinson, W.H. and Mc Verry, G.H. *"An Introduction to Seismic Isolation"*, John Wiley & Sons, Inc, New York, 1993.

[5] Farzad, N. and Kelly, J.T. , *"Design of Seismic Isolated Structures"*, John Wiley & Sons, New York, 1999.

BRIDGE PIER FOUNDED ON PILE-GROUP: DUCTILE DESIGN AGAINST FAULTING

A. Tsatsis[1], R. Kourkoulis[1], I. Anastasopoulos[1], G. Gazetas[1]

[1] National Technical University of Athens, School of Civil Engineering, Greece
e-mail: ag_tsa@yahoo.gr, rallisko@yahoo.com, ianast@civil.ntua.gr, gazetas@ath.forthnet.gr

ABSTRACT: This paper explores the feasibility of ductility design for bridge pile group foundations subjected to tectonic deformation. Its potential effectiveness is investigated utilizing a typical bridge structure as an illustrative example. It is shown that allowing plastic hinging at the piles can be an effective way of obtaining vertical offsets of greater magnitude. The penalty to pay is larger rotation at pier base due to pile yielding.

KEY WORDS: Soil-structure interaction; foundation; faulting; ductility.

1 INTRODUCTION

In many large magnitude earthquakes the causative fault rupture may extend all the way to the ground surface. Structures on top of the resulting surface fault scarp may undergo significant differential displacements that could lead to foundation and/or superstructure distress. Thus, seismic codes have invariably prohibited construction in the "immediate vicinity" of active faults. However, this demand is not very easy to comply with, especially for long structures such as bridges.

Modern seismic codes do not prohibit construction of structures near active seismic faults, but only after a special study is conducted, typically assuming elastic foundation response. Such requirement may be quite reasonable, since any damage to the foundation is typically difficult to discover and even more difficult to repair. However, such a requirement is particularly stringent and overly conservative in the case of piled foundations subjected to faulting-induced deformation.

To begin with, experience has shown that demanding elastic pile response in such an adverse case of loading leads to excessive levels of reinforcement that may be costly and even difficult (if not impossible) to construct. Most importantly, the hazard associated with a structure being subjected to faulting has a relatively low probability of occurrence, compared to strong seismic shaking.

First of all, experience has shown that the probability of a fault rupture outcropping all the way to the ground surface is relatively low. Even in such a case, the probability of a structure being "hit" by the rupture is substantially lower compared to shaking. As schematically illustrated in Figure 1, in a crudely simplified manner, in the worst case scenario (i.e., if the fault outcrops at the ground surface throughout its entire length) the area affected by the fault rupture will be a narrow zone (no more than 100 m wide) along the fault outbreak. For example, for a fault of length L = 30 km, an area $E_{rupt} \approx 0.1$ x 30 km = 3 km^2 will be affected. In stark contrast, the area that will be affected by the vibratory component of the earthquake will be substantially larger : an eclipse covering an area $E_{vib} \approx 1500$ km^2. Evidently, if ductility design is acceptable for the shaking component of the earthquake, it is more than reasonable to be at least acceptable for the faulting-induced deformation component.

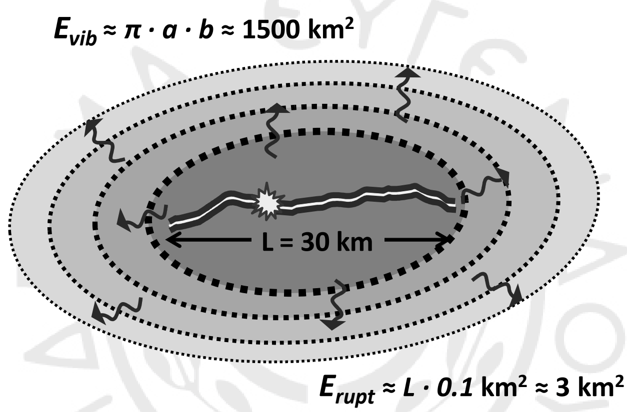

Figure 1. Schematic illustration of the areal effect of the two components of earthquake, fault rupturing and seismic oscillation.

This paper explores the feasibility of ductility design for bridge pilegroup foundations subjected to tectonic deformation. Its potential effectiveness is investigated utilizing a typical bridge structure as an illustrative example. The selected bridge structure is part of a new highway in Southern Greece, running through an area full of active seismic faults.

As shown in Figure 2, the bridge is 75 m long, with 3 simply supported decks on elastomeric bearings, having piers of height H = 8 m. The foundation system is rather typical as well, consisting of 2 x 4 pilegroups with piles of diameter d = 1.2 m and length L =18 m.

Although piled foundations have been shown to be quite vulnerable to faulting induced deformation (Anastasopoulos et al., 2008; Gazetas et al., 2008), they still remain the most preferred solution for bridges combining transmitting superstructure loads to healthier soil strata, decrease of settlement and dynamic rotations.

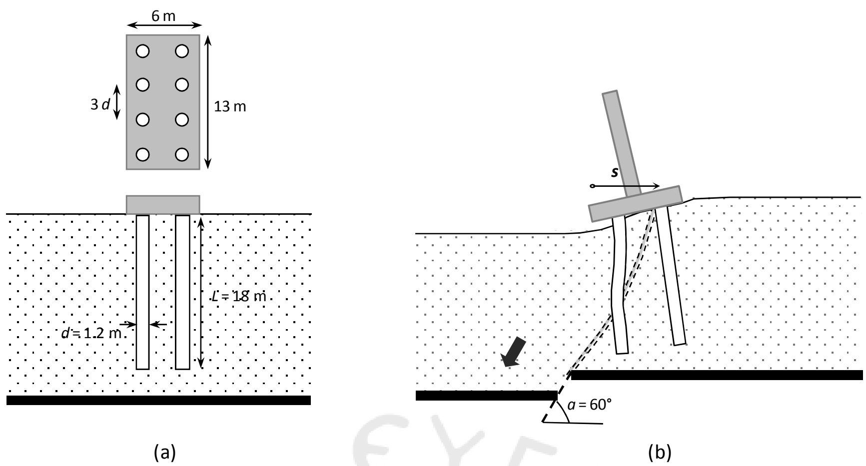

Figure 2. Schematic illustration of : (a) the piled foundation, and (b) the problem explored herein.

2 FINITE ELEMENT MODELING

To realistically simulate the response of the piles, 3D finite element modeling is required. The analysis is conducted employing the FE code ABAQUS. Figure 4 illustrates the geometry and the main features of the FE mesh. Half of the model was simulated, taking advantage of symmetry conditions.

The piles are modelled with beam elements circumscribed by 8-noded hexahedral "dummy" elements (i.e. of zero mass and stiffness). The central beam elements are rigidly connected to the appropriate circumferential element nodes of the same height. The non-linearity of the piles is introduced through moment-curvature relations, computed through cross-section analysis using XTRACT. The pile cap is modelled with hexahedral brick elements, assuming elastic reinforced concrete response (E = 25 GPa). An appropriate interface was used to model the contact between the pile and the surrounding soil, to realistically simulate sliding and detachment between the piles or the pile cap and the corresponding soil.

The soil is modelled with hexahedral brick-type elements of dimension d_{FE} = 1 m, with the mesh refined closer to the piles (d_{FE} = 0.3 m). The non-linear behaviour of the soil is modelled with an elastoplastic constitutive model with strain softening (Anastasopoulos et al., 2007). The Mohr–Coulomb failure criterion is used to define failure accompanied by an isotropic strain softening law, which degrades the friction (φ) and dilation (ψ) linearly with the increase of plastic octahedral shear strain γ^{pl}_{oct}. The soil material utilized in the analyses is idealized dense sand with the following material properties: $\varphi_p = 45^o$, $\varphi_{res} = 30^o$, $\psi_p = 15^o$, and $E = 4000 \div 84000$ kPa. The dip angle of the fault plane was set to $a = 60^o$, while the maximum fault offset at the bedrock was set to h_{max} = 1 m.

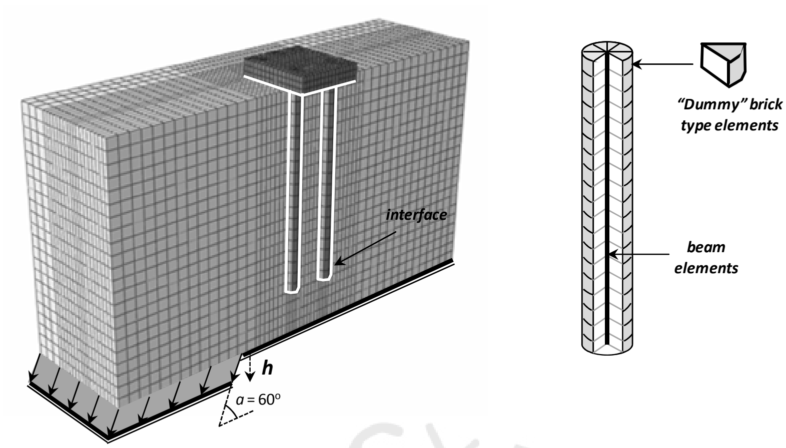

Figure 3. Outline of finite element model employed for the analysis of the pilegroup.

3 ELASTIC ANALYSIS

To argue for the irrationality of demanding elastic response of the foundation in such an adverse case of loading such as tectonic deformation, an example is presented in this section. To that end, the piled foundation of the selected typical bridge is analyzed, subjected to a bedrock offset of merely h = 10 cm. The piles are assumed linear elastic.

First, fault rupture propagation through free field is analyzed. Then, knowing the exact location of fault rupture emergence, the foundation is subjected to fault rupturing at various distances s from its hanging-wall (left) edge. The worst case scenario, both in terms of displacement/rotation and pile distress, corresponds to s = 8 m in this specific case.

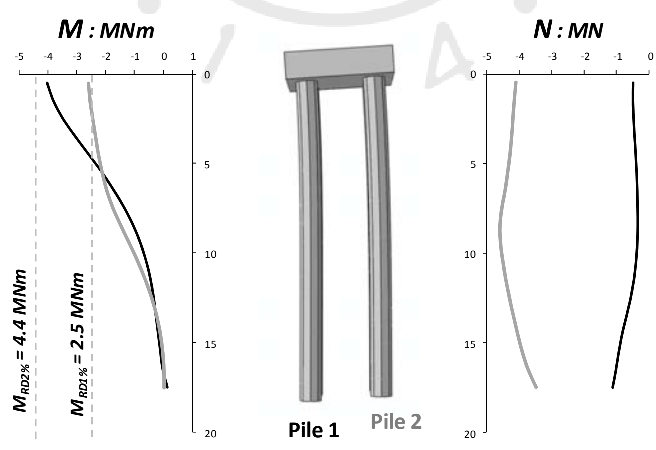

Figure 4. Example of elastic pilegroup analysis : the stressing due to a fault offset h of merely 10 cm cannot be undertaken using reasonable reinforcement ratios (1 to 2%).

Figure 4 depicts the distribution with depth of pile bending moments M and axial forces N. Even a fault offset h of merely 10 cm, the developing M can only be undertaken with a rather "heavy" reinforcement ratio of the order of 4%. With more realistic reinforcement rations (1% to 2% at most, resulting to ultimate moment capacity M_{ult} = 2500 kNm and M_{ult} = 4400 kNm, respectively), the piles would unavoidably yield developing plastic hinges. In conclusion, very "heavy" reinforcement ratios are required to undertake elastically even minor bedrock offsets of the order of few centimeters. Such reinforcing can be unreasonably expensive and most of the times very difficult to realize.

4 NON LINEAR ANALYSIS

4.1 The effect of longitudinal reinforcement ratio

Allowing plastic hinging at the foundation may lead to a significant increase of the dislocation the piles may sustain. To that end, the nonlinearity of the piles is introduced in the analysis. Figure 5 depicts the moment curvature curves of the pile for two characteristic cases of reinforcement ratio: a lower bound of 1% corresponding to the current code of practice, and an upper bound of 4% (corresponding to the maximum reinforcement that may be installed in a pile). As depicted in Figure 5, ultimate capacity and ductility capacity are two contradicting concepts. As expected, the increase of the reinforcement ratio from 1% to 4% leads to a (3 times) larger bending moment capacity of the pile. However, this also results to a decreasing of its ductility capacity (by a factor of 2 in this particular case).

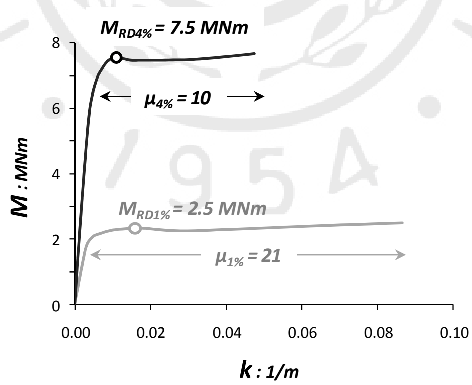

Figure 5. Moment curvature relations for the d = 1.2 m piles, as calculated through XTRACT.

Figure 6 compares the two reinforcement ratios in terms of ductility demand over ductility capacity $\mu_{demand}/\mu_{capacity}$ with respect to the imposed bedrock offset h and fault outcropping location s. When $\mu_{demand}/\mu_{capacity}$ exceeds 1, the pile has reached its ultimate bending capacity, plastic hinges have developed, and the response is nonlinear. Pile failure is reached when the ductility capacity is exhausted, meaning that the pile has not only developed plastic hinges, but has suffered significant damage being essentially destroyed.

Evidently, the performance of the heavily reinforced piles is favorable. The lightly reinforced piles fail at h = 45 cm, while those the heavily reinforced can endure vertical bedrock offset of the order of h = 70 cm. In both cases, however, exploiting the plastic region of the piles increases spectacularly the levels of bedrock offset the piles may endure (compared to the elastic analysis).

The advantageous performance of the heavily reinforced piles though is not concentrated only on enlarging the ultimate bedrock offset. Not only there are fewer lines above the failure line in the case of heavy reinforced piles, but the width of the zone where the piles fail is substantially narrower. In other words, not only a greater bedrock offset is needed to lead the heavily reinforced piles to failure, but the fault has to outcrop at a very specific location, minimizing substantially the possibility of failure due to tectonic deformation.

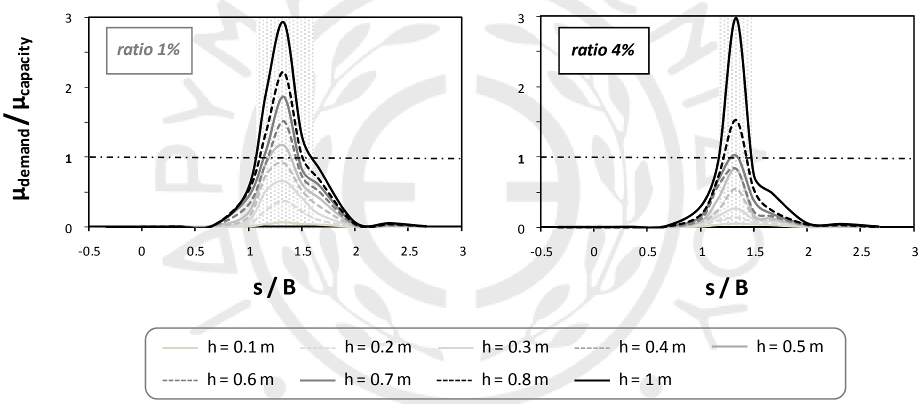

Figure 6. Evolution of ductility demand to ductility capacity with respect to the fault outcropping location *s*, and the fault offset *h*.

4.2 Consequences to the superstructure

Allowing the formation of plastic hinges at the foundation level seems to be a quite effective way to obtain larger values of vertical bedrock offset, that could not be obtained otherwise, and therefore increase the design margins. However, there is always a price to pay. Exploiting the ductile response of the foundation unavoidably generates adverse consequences to the superstructure. Pile yielding inevitably leads to an increase of the rotation they develop due to rupture imposed bending.

Figure 7 compares the two reinforcement ratios (1% and 4%) in terms of pilecap rotation θ with respect to the normalized outcrop distance s/B for two representative levels of bedrock fault offset, h = 30 cm and h = 50 cm. The increase of θ is directly associated with the level of pile yielding. For h = 30 cm (Figure 7a), the heavily reinforced pilegroup (4%) develops almost half the rotation of the lightly reinforced system (1%). Observe that there is practically no difference between the heavily reinforced and the elastic pilegroup. For h = 50 cm, the differences between the "heavily" and the "lightly" reinforced system becomes larger, since, now, both pilegroups have entered their plastic region and behave nonlinearly.

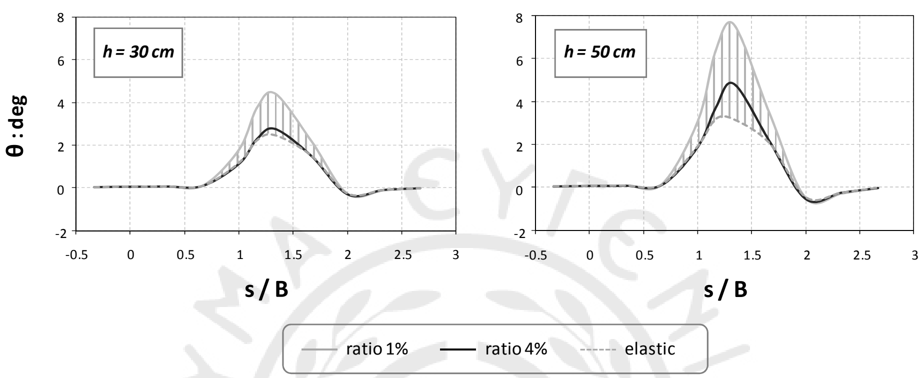

Figure 7. Rotation at the pier base with respect to the normalized fault outcrop location *s/B* , for h = 30 cm and 50 cm. Pile yielding leads to an increase of pier rotation, that has to be taken into account.

In summary, the increase of pier rotation due to pile yielding may be significant. Although it may decrease with heavier reinforcement, it may still be substantial, and has to be taken into account in design.

5 CONCLUSIONS

The key conclusions can be summarized as follows:

a) The demand for elastic response of a piled foundation of a bridge pier against large tectonic deformation is unreasonably conservative and sometimes even meaningless. It is shown that even a minor bedrock offset of a few centimetres may cause pile yielding. With elastic design, this unavoidably leads to a requirement for excessive reinforcement that can be, apart from expensive, impossible to construct.
b) Allowing plastic hinging at the piles can be an effective way of obtaining vertical offsets of greater magnitude and therefore increasing the design margins.
c) Heavier reinforcement may lead to a more favourable performance. In spite of reducing the ductility capacity, the increased bending moment capacity results to large deformation margins before the exhaustion of the ductility capacity. Apart from the increase of fault offset they can sustain, using larger

reinforcement ratios leads to decrease of the width of the area where the piles are really rupture sensitive.

d) Although the adoption of a ductile pilegroup design can be an effective means to design for larger fault offsets, it is unavoidably associated with an increase in pier rotation. This is something that has to be taken into account in design, in order to avoid falling of a deck.

ACKNOWLEDGMENTS

The research presented in this paper was funded by the European Research Council (ERC) Programme *"IDEAS, Support for Frontier Research – Advanced Grant"*, under Contract number ERC–2008–AdG 228254–DARE.

REFERENCES

[1] Anastasopoulos, I., Gazetas, G., Drosos, V., Georgarakos, P., Kourkoulis, R., (2008d). "Design of bridges against large tectonic deformations." Earthquake Engineering and Engineering Vibrations, Vol. 7, No. 4. (1 December 2008), pp. 345 - 368.

[2] Anastasopoulos, I., Gazetas, G., (2007). "Foundation-structure systems over a rupturing normal fault: Part II. Analysis of the Kocaeli case histories." Bulletin of Earthquake Engineering, 5 (3), pp. 277-301.

[3] Anastasopoulos, I., Gerolymos, N., Gazetas, G., Bransby, M.F., (2008a). "Simplified approach for design of raft foundations against fault rupture. Part I: Free□field." Earthquake Engineering and Engineering Vibration, 7 (2), pp. 147-163

[4] Anastasopoulos, I., Gerolymos, N., Gazetas, G., Bransby, M.F., (2008b). "Simplified approach for design of raft foundations against fault rupture. Part II: Soil-structure interaction." Earthquake Engineering and Engineering Vibration, 7 (2), pp. 165-179.

[5] Bransby, F., Davies, M.C.R., El Nahas, A., Nagaoka S., (2008). "Centrifuge modelling of normal fault□foundation interaction." Bulletin of Earthquake Engineering, Special Issue: Integrated approach to fault rupture and soil-foundation interaction, 6(4), pp. 607-628.

[6] Faccioli, E., Anastasopoulos, I., Gazetas G., Callerio, A., Paolucci, R., (2008)."Fault rupture-foundation interaction: selected case histories." Bulletin of Earthquake Engineering, Special Issue: Integrated approach to fault rupture and soil-foundation interaction, 6(4), pp. 557-583.

[7] Gazetas G., Pecker, A., Faccioli, E., Paolucci, R., Anastasopoulos, I., (2008)."Preliminary design recommendations for dip-slip fault-foundation interaction." Bulletin of Earthquake Engineering, Special Issue: Integrated approach to fault rupture- and soil foundation interaction, Vol. 6, no. 4, pp. 677-687.

[8] Pamuk A, Kalkan E, Ling HI (2005). "Structural and geotechnical impacts of surface rupture on highway structures during recent earthquakes in Turkey." Soil Dyn Earthq Eng, Vol. 25, pp. 581-589.

[9] Chang K-C., Chang, D-W., Tsai, M-H., Sung, Y-C., (2000)." Seismic performance of highway bridges." Earthquake Engineering and Engineering Seismology, 2(1), pp. 55-77.

[10] Kawashima, K. (2001). "Damage of Bridges Resulting from Fault Rupture in The 1999 Kocaeli and Duzce, Turkey Earthquakes and The 1999 Chi-Chi, Taiwan Earthquake." Workshop on Seismic Fault-Induced Failures-Possible Remedies for Damage to Urban Facilities, University of Tokyo Press, pp. 171-190.

GENERALISED FRAGILITY CURVES FOR STRAIGHT BRIDGES, FOR ARBITRARY ANGLE OF INCIDENCE OF THE SEISMIC ACTION, INCLUDING SOIL-BRIDGE INTERACTION

Ioannis Moschonas[1], Andreas Kappos[2] and Anastasios Sextos[3]

[1,2,3] Aristotle University of Thessaloniki, Dept. of Civil Engineering, Greece
e-mail: imoschon@civil.auth.gr, ajkap@civil.auth.gr, asextos@civil.auth.gr

ABSTRACT: An analytical procedure is presented for the derivation of fragility curves for bridges subjected to seismic action at any angle of incidence, based on an extended version of static nonlinear analysis. The procedure is applied to a straight bridge taking also into account soil-bridge interaction, to assess its effect on bridge response and fragility.

KEY WORDS: Angle of incidence; Bridges; Fragility; Soil-Bridge Interaction; Vulnerability.

1 INTRODUCTION

The effect of the angle of incidence of the incoming seismic waves on the response and the fragility of bridges was investigated by the authors [1, 2]; to this purpose the static nonlinear analysis procedure was extended to account for the angle of incidence effect and a previously proposed analytical methodology for the derivation of fragility curves in the principal bridge directions [3] was also adopted to this general case. The new procedure was then applied to both a straight bridge [1] and a skew bridge [2].

A crucial parameter that affects bridge response is the dynamic interaction between the bridge and the supporting ground, in particular at the abutment-backfill-embankment interface, subsequent to the closure of the longitudinal gap between the deck and the abutment backwall. In previous works soil-bridge interaction effects for seismic action acting along the principal bridge directions was investigated both with regard to bridge response [4-6] and bridge fragility [3]. The effect of the angle of incidence was also investigated, but only for the response of a curved bridge using dynamic analysis [7]. Hence, a next step is the investigation of soil-bridge interaction effects on bridge response using *static* nonlinear analysis, extended for the case of arbitrary angle of incidence of the seismic action, and the derivation of fragility curves for this general case, which is the subject of the present work.

2 METHODOLOGY FOR THE DERIVATION OF GENERALISED FRAGILITY CURVES

The proposed methodology for the derivation of generalised fragility curves for arbitrary angle of incidence of the seismic action is summarised below; a more detailed description can be found elsewhere [2].

At first, the earthquake motion is analysed into its principal components [two horizontal (major and minor) and one vertical]. In the general case the two horizontal components are considered as acting simultaneously (dual-component seismic action) while in the simpler case, only the major horizontal component is taken into account (single-component seismic action). Then they are used to derive the horizontal earthquake components E_x and E_y acting along the longitudinal and the transverse bridge direction, respectively. These components are then used for the derivation of pushover curves for each predefined angle of incidence of the seismic action (e.g. from 0° to 180° at 15° increments), applying the proposed procedure [2], wherein the interaction between biaxial moment and axial force at critical pier sections or biaxial shear force and axial force at bearings (wherever present) is also taken into account.

Then, damage states are defined firstly in a qualitative manner, e.g. using definitions provided in HAZUS [8], and are then quantified using bridge deck displacement along the earthquake direction, δ_{ξ}, separately for damage developed at the bridge, $\delta_{\xi,DSi,Br}$, and the abutment-backfill-foundation (ABF) system, $\delta_{\xi,DSi,ab}$,. The minimum of these two values is the final median threshold value of displacement for each damage state, $\delta_{\xi,DSi}$. Finally, generalised fragility curves are derived, i.e. fragility curves for each angle of incidence of the earthquake. The probability of exceedance P_f of a damage state is firstly expressed as a function of δ_{ξ}. Then, the evolution of damage diagram (the primary vulnerability curve) is plotted using the target displacement along the earthquake direction for increasing earthquake intensity levels expressed by the peak ground acceleration, A_g, which is then used in combination with $\delta_{\xi,DSi}$ to derive the corresponding median threshold value $A_{g,DSi}$. Assumimg the probability density function as lognormal, the probability of exceedance of a certain damage state P_f can be found from the cumulative probability function of the lognormal distribution. For the total lognormal standard deviation (total uncertainty) a value of 0.6 is adopted in line with similar studies [8].

3 SOIL-BRIDGE INTERACTION

3.1 Modelling of the abutment-backfill-foundation (ABF) system

The ABF system was modelled by Sextos et al. [9, 10] in 3D space using the ABAQUS software [11]. The backfill, the embankment and the foundation soil were modelled using tetrahedral solid elements, while brick elements were used to model abutments and pile groups. A dense finite element grid was set up for the areas of stress concentration and/or abrupt geometry change, i.e. in the vicinity of the abutment, backfill, and pile groups. Then, pushover analysis was performed separately for the two principal bridge directions leading to the corresponding idealised, bilinear pushover curves (Fig. 1); it has to be noted that this bilinearisation involves a significant degree of subjectiveness. Having obtained the abutment-embankment stiffness for various levels of earthquake intensity, and assuming (for simplicity) that the dynamic and the static stiffness of the particular system do not differ substantially [12] the bi-linear curve obtained through nonlinear static analysis was used for defining the hysteresis loop required for dynamic analysis. The damping of the ABF system was also derived according to the literature [12].

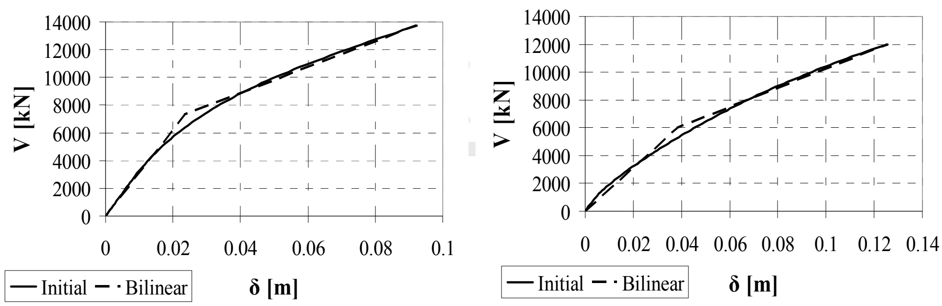

a. Longitudinal direction *b.* Transverse direction

Figure 1. Pushover curves of the abutment-backfill-foundation system [9, 10].

3.2 Modelling of pier foundations

Soil-bridge interaction at the pier foundation base [10] was taken into account by considering the pile-to-pile interaction and forming the corresponding 6DOF dynamic impedance matrices with the use of the computer code ASING [13]. For the case of nonlinear static analysis only the stiffness matrix is considered.

4 APPLICATION TO A STRAIGHT BRIDGE

4.1 Description and modelling of the selected bridge

The selected bridge (Fig. 2) is an overpass crossing the Egnatia Odos motorway in Northern Greece. It is a 3-span bridge (L=71.2m) with a continuous deck consisting of an 11m wide prestressed tee-section with two cylindrical voids (D=1.10m). The two piers M1 and M2 (h=8.5m D=1.7m) are monolithically connected to the deck. The deck movement at the abutments is free up to 0.12m when the longitudinal gap is designed to close and the ABF system is activated. In the transverse direction the deck movement is restrained by stoppers without any gap. The foundation of the bridge consists of 2×2 pile groups with pile lengths of 32m in pier M1 and 28m in pier M2, respectively.

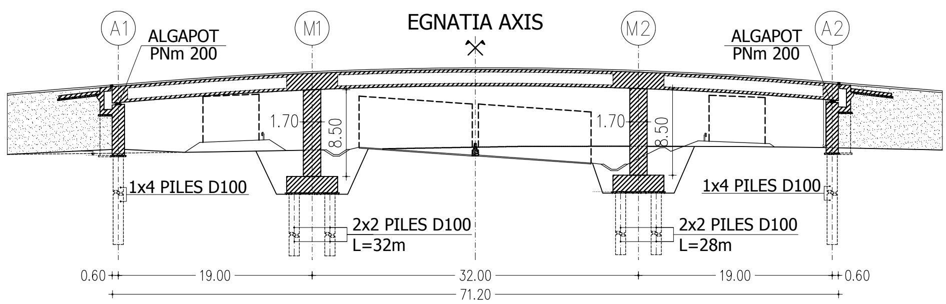

Figure 2. Elevation view of the selected overpass bridge (Pedini bridge)

The bridge is analysed using the SAP2000 software [14]. The deck and the two piers are modelled using frame elements. As explained previously, the ABF system is modelled implicitly in a series system with the 0.12m gap while the 6×6 dynamic impedance matrices at the pier-foundation level are modelled as 6DOF springs and dashpots ('SBI' case in Table 1). In addition, another bridge model is created where soil-bridge interaction is ignored ('Non-SBI' case). In this model the ABF system is not modelled in the longitudinal direction, while in the transverse direction only its initial (elastic) stiffness is considered, i.e. it is modelled as a linear spring. The modal characteristics of the longitudinal and the transverse prevailing mode for both the SBI and the Non-SBI models are given in Table 1. It is seen that in the longitudinal direction, consideration of foundation compliance (SBI case) results into a 10% increase in the fundamental period because piers dominate the bridge's longitudinal response. In the transverse direction the corresponding increase is only 0.8% because the significant transverse stiffness of the almost fully restrained bridge deck, due to the also significant stiffness of the ABF system, dominates the bridge response. In contrast, the mass activated in each direction remains practically unaffected.

Table 1. Modal characteristics of the Pedini bridge

Prevailing Mode	SBI case		Non-SBI case	
	T [sec]	ε [%]	T [sec]	ε [%]
Longitudinal	0.82	99.4	0.73	99.8
Transverse	0.73	91.5	0.72	91.2

4.2 Evaluation against dynamic analysis results

At first, the proposed methodology for the derivation of pushover curves for various angles of incidence is evaluated against the more accurate inelastic dynamic analysis. Due to space limitations only the SBI case is evaluated here; the Non-SBI case has already been evaluated in [1]. The seismic action is modelled using the major horizontal component (single-component seismic action) of the Thessaloniki earthquake described in Table 2. The selection of a single record is justified on the grounds that the uncertainty due to the seismic action is assumed as part of the total uncertainty which is set to 0.6 (see §2).

Table 2. Characteristics of selected ground motion

Place	Station	Date	Time	M	R [km]	Components	A_g [g]
Thessaloniki	City Hotel	20/06/78	08:03:21	6.1	29	N-S	0.139
						E-W	0.146

For the evaluation, the 'dynamic pushover curves' using the maximum displacement and the corresponding simultaneous shear force [δ_{max}–$V_b(t_{max})$] are derived from response-history analysis and are then plotted on the same diagram (Fig. 3) with the corresponding δ_{max}–V_b points derived using the quadrilinear pushover curve for the longitudinal direction and the equal displacement approximation, and the pushover curve itself. From Fig. 3 it is observed that over the entire displacement range, the δ_{max}–$V_b(t_{max})$ points lie closely to the quadrilinear pushover curve, with an exception in the range after yielding of the ABF system where a small difference (10%) is observed. This matching is expected because both the bilinear (Fig. 4a) and the quadrilinear (Fig. 4b) pushover curves prior and subsequent to the activation of the ABF system, respectively, are the envelopes of the corresponding $\delta(t)$-$V_b(t)$ diagrams.

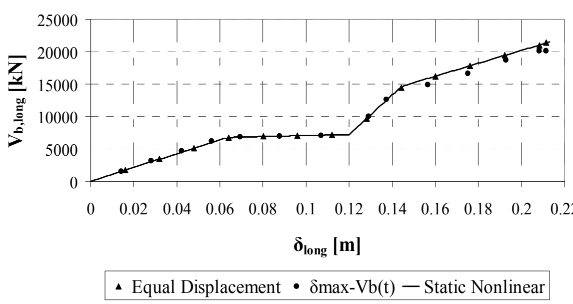

Figure 3. Dynamic and static pushover curves in longitudinal bridge direction – SBI case – Thessaloniki earthquake – Single-component seismic action

Comparing the δ_{max}–$V_b(t_{max})$ points with the corresponding δ_{max}–V_b points, it is observed that until the ABF system is activated, the equal displacement rule leads to 13% larger displacements, mainly because the seismic input energy in dynamic analysis is smaller than the corresponding one in static analysis due to the modelling of radiation damping. After the ABF system is activated, the difference between the equal displacement approximation and the dynamic response is reduced to 5%. Since the aforementioned differences are reasonably small, the use of the equal displacement rule to estimate the target displacement over the whole range of displacements is deemed to be justified.

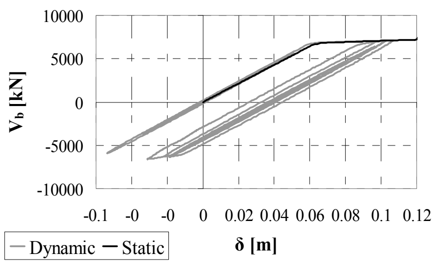

a. Bilinear pushover curves

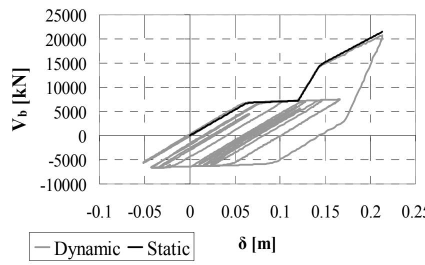

b. Quadrilinear pushover curves

Figure 4. $\delta(t)$-$V_b(t)$ diagrams and the corresponding envelope functions (pushover curves)

4.3 Effect of soil-bridge interaction on bridge response and fragility

The proposed methodology for the derivation of pushover curves for various angles of incidence is applied here for 7 angles of incidence from 0° to 90° (step of 15°). Target displacements are estimated using the equal displacement approximation, which was found (§4.2) to be valid for the entire range of bridge displacements. From the derived pushover curves (Fig. 5) it is observed that starting from the case of longitudinal excitation (α=0°) the shape of pushover curves remains quadrilinear up to the angle of 45°, which implies that bridge response is substantially affected by the activation of the abutment-backfill system. Regarding bridge failure, it is seen that the critical excitation direction is the longitudinal one (α=0°, $A_{g,u}$=1.32g), i.e. where the effect of the activation of the ABF system is maximised. The least critical direction is at an angle of α=60° (A_{gu}=2.27g), i.e. when the response in the transverse direction starts to become dominant; it is important that $\alpha=90^o$ is *not* the least critical direction.

Although generalised fragility curves were then derived for the overpass bridge for all damage states described in [1, 2], for both SBI and Non-SBI cases, only those for the last damage state (DS4: failure/collapse) are shown in Fig. 6 due to space limitations. At first, it is observed that when soil-bridge interaction is accounted for, the most and least critical directions match the ones revealed by the individual pushover analyses (Fig. 5), a fact that is anticipated since DS4 is defined on the basis of the ultimate bridge displacement. Comparing the median threshold values of A_g for the critical and the least critical direction between the SBI and the Non-SBI case, it is also observed that consideration of soil-bridge interaction leads to a significant decrease in the threshold values, from 20% (in the least critical direction, α=60°) to 36 % (in the most critical direction, α=0°).

Finally, in the SBI case, the bridge fragility is found to be significantly affected by the angle of incidence of the seismic action given that the difference in median threshold values of A_g between the critical and the least critical direction is approximately 70%, whereas if soil-bridge interaction is neglected this difference becomes 40%.

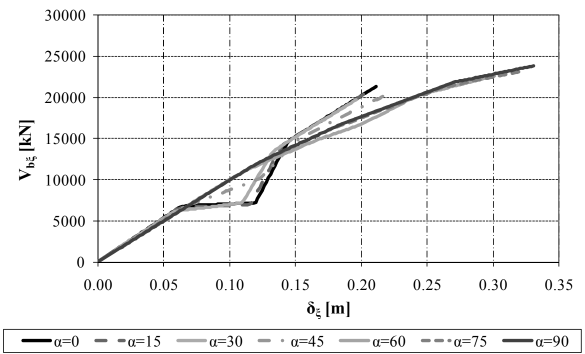

Figure 5. Pushover curves for Pedini bridge, for various angles of incidence

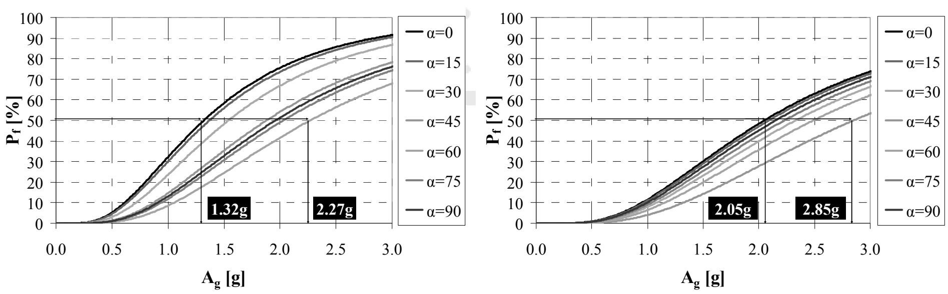

a. SBI case *b.* Non-SBI case

Figure 6. Generalised fragility curves for Pedini bridge – DS4: Failure/Collapse

5 CONCLUSIONS

In the paper a methodology for the derivation of generalised bridge fragility curves for arbitrary angle of incidence of the seismic action proposed by the authors is extended to include the effect of soil-bridge interaction, and is applied to a straight overpass bridge.

The case-study shows first that soil-bridge interaction results only to a small increase (10%) in the period of vibration in the longitudinal direction while it has negligible effect (0.8%) in the transverse direction. The proposed methodology for the derivation of pushover curves for arbitrary angle of incidence of the seismic action was evaluated against dynamic inelastic analysis and it was found that both the bilinear and the quadrilinear forms of pushover curves envelope the corresponding dynamic response (dynamic pushover curves) and that the equal displacement approximation is a valid assumption, also in the case where the soil-bridge interaction is taken into account, at least for the specific case studied.

From the derived pushover and generalised fragility curves for arbitrary angle of incidence of the seismic action, it is also found that the activation of the abutment-backfill-foundation system dominates the bridge response up to an angle of incidence of 45°. Regarding bridge failure, referring either to its seismic response or its fragility, the critical direction is the longitudinal one while the least critical is found to be for a 60° angle, i.e. not a principal direction. It was also interesting to observe that consideration of soil-bridge interaction increases the predicted fragility of the bridge (lower damage thresholds, up to 36%) as well as the effect of varying angle of incidence (70% difference between critical and least critical direction, compared to 40% in the case that interaction is neglected).

REFERENCES

[1] Moschonas, IF, Kappos, AJ, "Generalised fragility curves for bridges, for arbitrary angle of incidence", *CD-ROM Proc. COMPDYN 2009*, Paper No. 186, Rhodes, 2009.
[2] Moschonas, IF, Kappos, AJ, "Generalised fragility curves for bearing-supported skew bridges, for arbitrary angle of incidence of the seismic action", *CD-ROM Proc. COMPDYN 2011*, Paper No. 377, Corfu, 2011.
[3] Moschonas, IF, Kappos, AJ, Panetsos, P, Papadopoulos, V, Makarios, T, Thanopoulos, P, "Seismic fragility curves for greek bridges: methodology and case studies", Bulletin of Earthquake Engineering, Vol. 7, No. 2, pp. 439-468, 2009.
[4] Kappos, AJ, Manolis, GD, Moschonas, IF, "Seismic assessment and design of R/C bridges with irregular configuration, including SSI effects", Engineering Structures, Vol. 24, No. 10, pp. 1337-1348, 2002.
[5] Kappos, AJ, Potikas, P, Sextos, AG, "Seismic assessment of an overpass bridge accounting for non-linear material and soil response and varying boundary conditions", *CD-ROM Proc. COMPDYN 2007*, Paper No. 1580, Rethymno, 2007.
[6] Kappos, AJ, Sextos, AG, "Effect of foundation type and compliance on seismic response of RC bridges", Journal of Bridge Engineering, ASCE, Vol. 6, No. 2, pp.120-130, 2001.
[7] Taskari, ON, Sextos, AG, Kappos, AJ "3D Finite Element Modelling of a Highway Bridge Considering the Effect of Soil and Foundation", *CD-ROM Proc. 6th GRACM International Congress on Computational Mechanics*, Thessaloniki, 2008.
[8] FEMA-NIBS, *Multi-Hazard Loss Estimation Methodology - HAZUS-MH MR4: Earthquake Model Technical Manual*, Federal Emergency Management Agency (under a contract with the National Institute of Building Sciences), Washington, D.C., 2003.
[9] Sextos, AG, Mackie, KR, Stojadinović, B, Taskari, O, "Simplified P-y Relationships for modelling embankment-abutment Systems of Typical California Bridges", *CD-ROM Proc. 14th World Conference on Earthquake Engineering*, Paper No. 05-02-0032, Beijing, 2008.
[10] Sextos, AG, Taskari, O, "Comparative Assessment of Advanced Computational Tools for Embankment-Abutment-Bridge Superstructure Interaction", *CD-ROM Proc. 14th World Conference on Earthquake Engineering*, Paper No. 05-02-0031, Beijing, 2008.
[11] ABAQUS/PRE, *User's Manual*, Hibbit, Karlsson and Sorensen Inc., 2004.
[12] Zhang, J, Makris, N, "Kinematic response functions and dynamic stiffnesses of bridge embankments", Earthquake Engineering & Structural Dynamics, Vol. 31, No. 11, pp. 1933-1966, 2002.
[13] Sextos, AG, Pitilakis, KD, Kappos, AJ, "Inelastic dynamic analysis of RC bridges accounting for spatial variability of ground motion, site effects and soil-structure interaction phenomena. Part 1: Methodology and analytical tools", Earthquake Engineering & Structural Dynamics, Vol. 32, No. 4, pp. 607-627, 2003.
[14] CSI, CSI Analysis Reference Manual for SAP2000®, ETABS®, and SAFE®, Computers & Structures Inc., Berkeley, California, 2009.

BRIDGE OF DREAMS
A cable stayed Pedestrian Bridge in Athens

Phaedon Karydakis [a],

[a] Ph.Karydakis and Associates, structural design office, Athens, Greece
e-mail: karmad44@otenet.gr

ABSTRACT: A cable stayed composite pedestrian bridge is constructed over a main avenue in the Athens area. The composite bridge has an overall length of 60.0 m, with a clear span of 32 m, above one of the main roads in Athens and is 4.0 m wide.

The bridge is cable stayed, suspended from two pylons, diagonally positioned, on each side of the deck. The bridge is reached through a set of ramps and escalators on each side and four elevators, housed within the pylons.

The main beam is a box girder, z shaped along the length of the bridge, with transverse I shaped girders. The cables inclined in both directions, form the shape of children rope pulling, a popular game with the school. To avoid thermal distortion, because of the asymmetric positioning of the suspension towers, there is a longitudinal joint, close to the centre of the span.

The two parts are connected with a stainless steel axis, in a cylindrical socket, that allows only longitudinal movements, while restraining relative rotations and movements in the transverse direction. The torsional rotation is restrained by a sliding bolt.

The cables are suspended on the composite main pylons and anchored through the internal structural system of the façade, to the pile cups.
Each pylon is supported by six concrete prestressed piles.

KEY WORDS: Cable stayed composite pedestrian bridge

1 INTRODUCTION

In December 2009, a 15 year old boy was killed by a speeding car, while crossing the road, for his school annual Xmas dance. A few days later, his classmates organized a demonstration, demanding the right to a safer life. They asked for a pedestrian bridge, with the motto “bridge our dreams”.

Almost instantly, a group of engineers was mobilized, mainly graduates from the same school, the necessary funds were donated and the bridge of children – bridge of dreams was designed, totally on volunteer work and funding. After many beurocratic and other problems, nearly two years after the incident, the erection is under way.

2 THE DESIGN

2.1 The design prerequisites

The bridge is located in the urban area of Athens, crossing over the main highway that leads to Athens overcrowded northern suburbs and the Olympic Stadium Complex. Although an urban avenue, because of high traffic loads, with the assistance of traffic police, during rush hours high priority is given to road traffic, transforming the road to a high speed one. Meanwhile the area is filled with schools and thousands of students have to cross the road at the specific point.

Before the Olympic Games, there were plans for submerging the road, but the project was cancelled for lack of funding.

The major task was to design a bridge that would, above all, appeal to the pedestrians, especially young school children, to use.

The bridge should fit well within the urban order of magnitude, but on the other hand should be an area landmark, a memorial to the lost child and a symbol to the joint effort to preserve the most precious possession, life.

Figure 1. Bridge of dreams

2.2 The basic design principles

After many alternative solutions, the final design was based on the following principles:

The bridge level should be as low as possible, over the necessary highway gabarit, to minimize climbing effort, with ramp-stairs, to make access appealing.

Twin elevators on each side insure that the bridge can be used by disabled persons and single escalators upwards ease access. The ramp stairs (not simple ramps due to lack of space) make the transportation of bicycles easy.

The bridge should be transparent but innovative, so to become a symbol and landmark without imposing itself over the surrounding buildings.

2.3 The design

Following the above design principles a cable stayed, composite bridge was designed, suspended from two composite pylons that also house the elevator shafts. The bridge has an overall length of 76.0 m, a free span of 31.5 m and is 4.00 m wide.

The bridge deck has a minimum clearance of 5.15 m over the highway, has an overall deck thickness of 75 cm and is supported by 16 fully locked galvanized cables, with a diameter of 33 mm, 8 on each side of the bridge,.

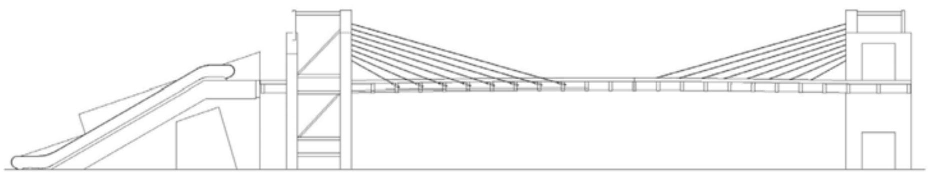

Figure 2. Bridge of dreams – view of the structural system

2.4 The structural elements

The principle structural elements are two composite pylons, anti symmetrically positioned along the bridge deck, the composite deck, the supporting cables, the central joint and the stairs and escalators leading to the deck.

The composite pylons, house the elevators, support the bridge deck and anchor the prestressed cables. The anchor loads of the cables are transferred through the steel bracings in front of the glass façade of the pylons to the pile caps and to the ground anchoring system, which is provided through twelve in situ casted piles, six for each pylon. The piles that are under constant tension are postensioned to control concrete cracking and reinforcement corrosion.

The composite deck is formed by a Z-shaped in plan torsion tube, in the form of a two cell box girder that runs along the bridge and transverse variable height I-beam cross girders spaced every 1.5 m.

The concrete slab is casted in situ, on a high bond trapezoidal steel sheet and relative shear studs to provide composite action of the deck and a horizontal diaphragm.

The cables are positioned anti symmetrically on each side of the bridge, inclined in both directions, between the top of the pylons and the external side of the main z-shaped box girder and anchored on the composite pylons head, through a system of specially designed anchor heads that house the postensioning and cable stress monitoring system and the lighting elements for the cables.

Because of the antisymetric shape of the structure, axial forces introduced in the deck from temperature differences and shrinkage would cause significant structural distortion, bending moments along the vertical axis of the deck and torsion of the pylons. In order to avoid this unfavourable structural condition, a joint is designed close to the center of the deck that allows only longitudinal sliding, between the two parts of the bridge. With the use of a sliding cylindrical axis in the center of the main box girder and an additional smaller one close to the end of the joint transverse beam, bending and torsional moments and shear forces are transferred through the two parts of the bridge, resulting in a continuous structure without expansion consequences.

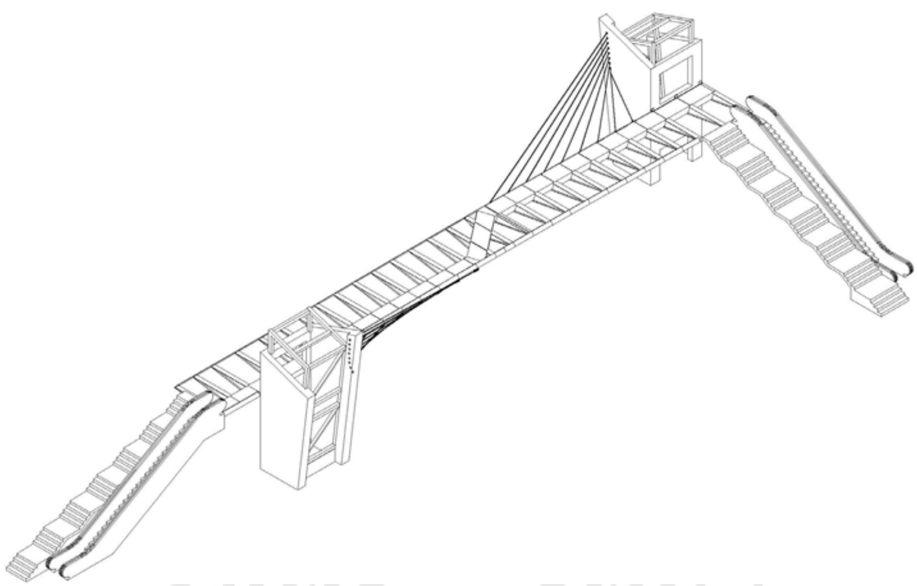

Figure 3. Bridge of dreams – the structural system – axonometric view

The pylons are composite, but the steel part including the cable anchoring are initially freestanding, so as to be erected with steel construction accuracy, calibrated into the correct position and then casted in concrete.

In this way tolerances can be minimized and most parts of the bridge prefabricated.

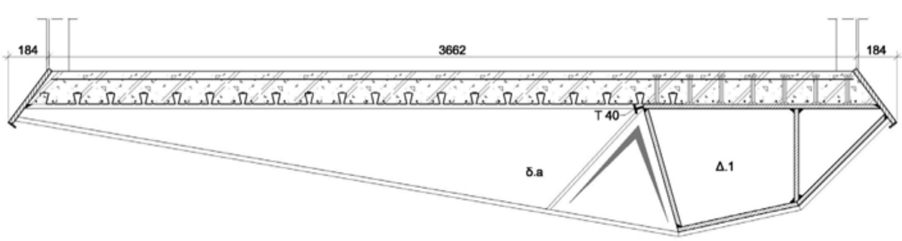

Figure 4. Bridge of dreams – typical crossection of the bridge deck

2.5 The architectural symbolism

The z-shape of the main beam and of the cable anchoring system in the façade, symbolizes the first letter of the Greek word «ζωή», which means life. The inclination of the pylons and the cables in both directions resemble boys involved in the game of rope pulling, a popular game in this school.

3 THE ANALYSIS

The bridge was analyzed by different models of varying accuracy.
In the final analytical model, non linear analysis was used, with surface finite elements for the pylons, deck beams and concrete slabs and cable elements for the cables.

All construction phases and dynamic loading for the wind, earthquake and the dynamic impact from people walking on the bridge deck were considered.

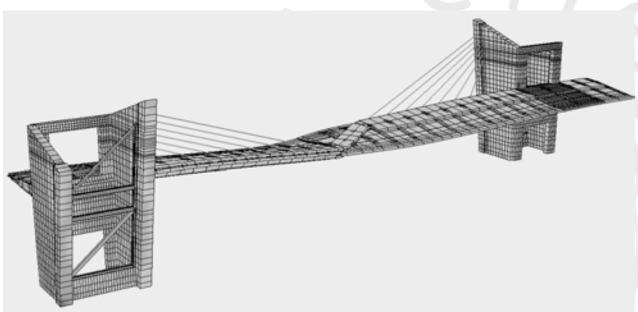

Figure 5. The full mathematical model of the bridge

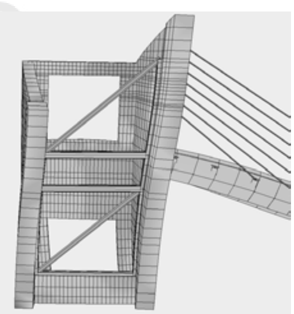

Figure 6. Deformed pylon

Displacements were calculated and compensated through initial counter displacements, in the construction drawings, so that after the tensioning of the cables, and casting the concrete part of the deck, the deck geometry will be the desired one.

4 THE ERECTION

Because of the high significance of the highway to Athens traffic, during erection the minimum possible traffic disturbance should occur.

The bridge will be delivered to the site, as a finished steel structure in two parts. All steel items, including the high bond trapezoidal steel sheet and the railing will be preassembled.

One temporary middle support will be positioned in the existing walkway between the lanes of different directions and the two parts of the bridge will be lifted in place, one by one, connected to the main pylons, temporarily resting on the middle support.

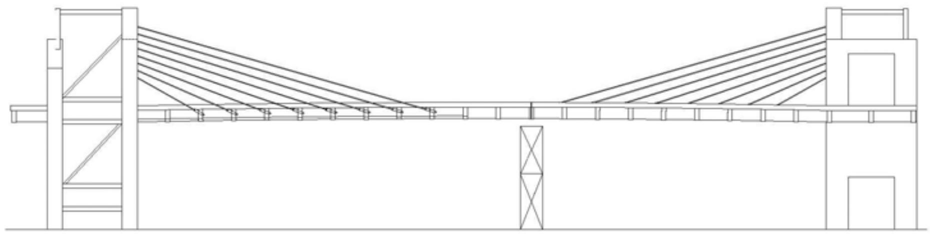

Figure 7. Bridge of dreams – erection sequence

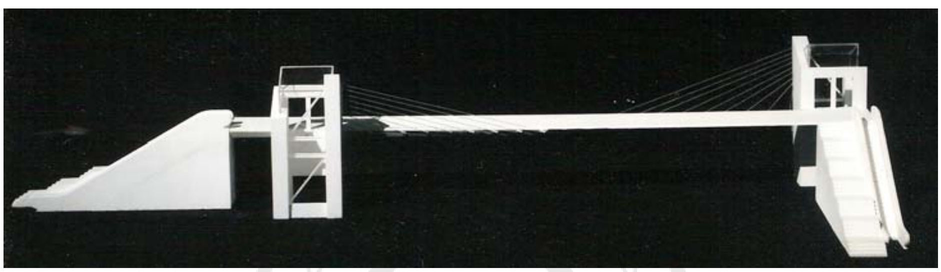

Figure 8. Bridge of dreams - The architectural model

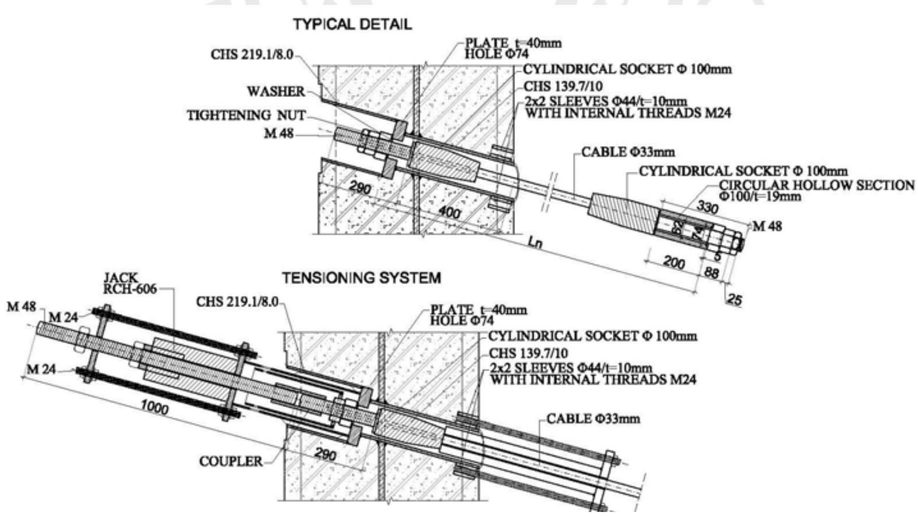

Figure 9. Cable anchors and tensioning equipment.

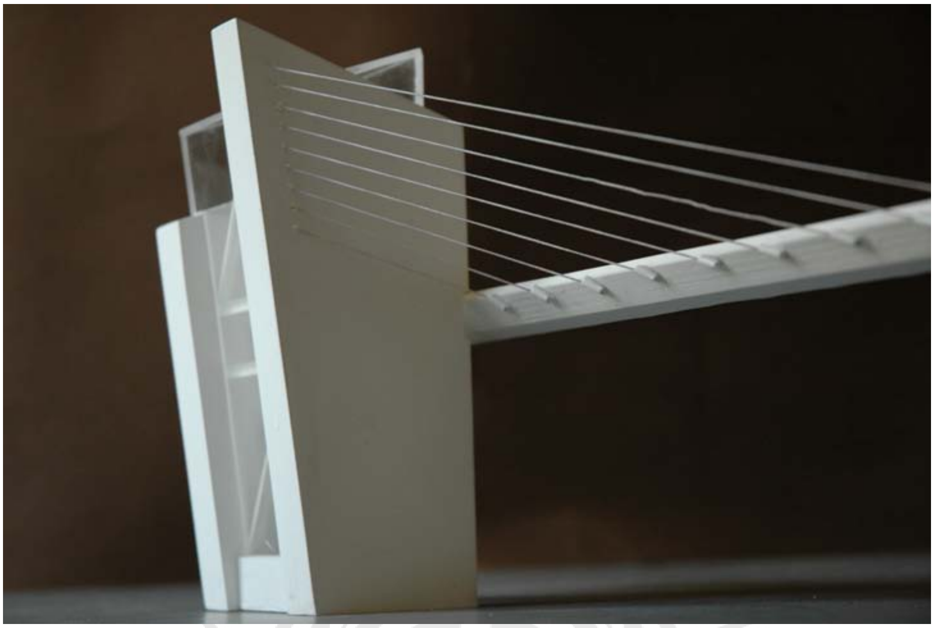

Figure 10. Bridge of dreams – picture of the model with the inclined pylons and the cables, anti symmetrically positioned

After jacking the two pieces in the middle joint, to acquire the intended co-linearity along the longitudinal axis, the central sliding joint will be moved to its position and locked into place.

Then the cables will be placed and tensioned. After the tensioning of the cables, the temporary middle support will be removed and the concrete deck casted. For the positioning anchoring and monitoring the supporting cables, special equipment has been designed and constructed.

The bridge will be monitored by the Steel Structures Laboratory of the NTUA. The monitoring includes, load cells positioned at the anchoring system of the cables, strain gauges at critical points of the steel columns of the composite pylons and the main box girder, thermometers and extension meters at the joints.

The deflection along the length of the bridge will be monitored with a laser measuring system.

ACKNOWLEDGMENTS

The bridge is dedicated to the memory of Solon Ph. Karydakis, whose unfortunate loss was the inspiration for the "bridge of dreams", the dreams of the school children, the lost dreams of Solon.

The realization of the project started after the mobilization of the school children demanding the construction of the footbridge.

A. Samaras and associates SA were responsible for the architectural design, with the participation of professor S. Pollalis.

Ph. Karydakis and associates Ltd were responsible for the structural design.

The whole project was organized and executed by the Hellenic American Educational Foundation, assisted by a great number of volunteers.

Funding was provided by G. Prokopiou family and many donors from the construction industry.

MODULAR SCAFFOLDING SYSTEMS FOR BRIDGES

Panagiotis Xinos[1]

[1] Wilhelm Layher GmbH & Co KG, Responsible for Greece, Greece
e-mail: panagiotis.xinos@layher.com

ABSTRACT: With advanced modular scaffolding systems, construction of scaffolding on or underneath bridges can be done quickly, economically and safely. With its unique connection technology, the Allround System of Layher has become a synonym for modular scaffolding worldwide.

KEY WORDS: Temporary Bridge; Modular Scaffolding System; Allround; TG 60; Layher; Shoring

1 INTRODUCTION

The Layher Allround System is a very flexible modular scaffolding system developed in 1974. The comprehensive product range and continual new developments allow an unlimited spectrum of uses, and the precision and weight optimization of all components ensure time savings and safe handling.

2 THE ALLROUND NODE CONNECTION TECHNOLOGY

When using traditional tubes and couplers it is not possible to transfer the loads in one plane. Because of the geometry of the connection elements (couplers) there is always an offset in vertical and horizontal direction (Figure 1). This will cause additional undesirably bending moments in the tubes and reduces the bearing capacity as well as the stiffness of the construction.

In contrast to tube and couplers the modular Layher Allround System can transfer all loads in one plane (Figure 2). The axes of all ledgers connected to such an Allround connection point in the form of a rosette (Figure 3) have the same point of intersection. That means that there is no offset (except for diagonals) and hence no undesirable bending moment in the connection when transferring axial loads.

Also a great flexibility is given because of the possibility to connect ledgers with angles (Figure 4). Since there are no screws the connection method is unbeatably fast.

Figure 1. Node connection with tubes and couplers

Figure 2. Allround node connection

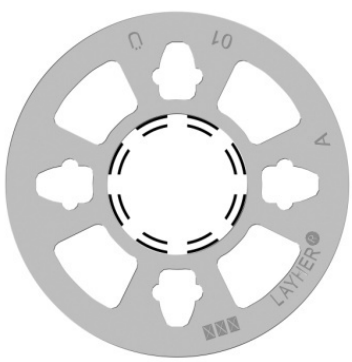

Figure 3. Allround Rosette (top view)

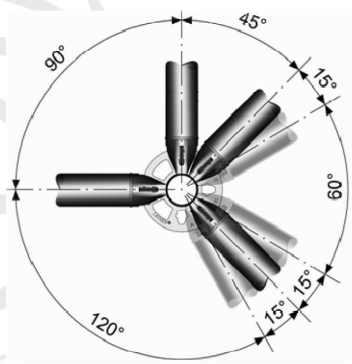

Figure 4. Possible angles at the holes

3 ALLROUND FRAMES FOR SHORING

3.1 Use of frames instead of single elements

Over the years Layher developed many additional parts based on this ingenious Allround system to create more possibilities in scaffolding and to build these safer, stronger and more economic.

One of these developments is the TG 60 frame. High grade steel in combination with a short vertical buckling length of 1 m makes the TG 60 frame very strong in comparison to single Allround components with standards and ledgers in vertical distance of 2 m height (Figure 5 and 6). As a result less material is needed for shoring and thus the costs for rental and assembly is reduced.

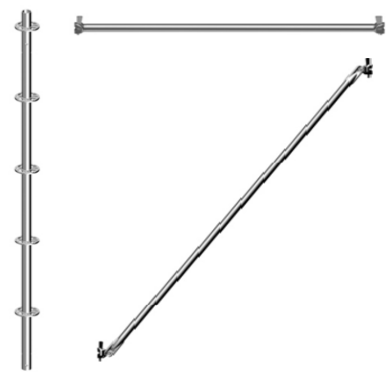

Figure 5. Single Allround components (standard, ledger and diagonal)

Figure 6. TG 60 frame for shoring with integrated Allround Rosettes

3.2 TG 60 Project Jyväskylä

The big advantage in bearing capacity of TG 60 frames was used at a bridge project in Jyväskylä (Finland). The cross section of the bridge including the shoring is shown in Figure 7.

The bridge section consists of a concrete plate with thickness 25 to 35 cm and two big integrated concrete webs with 1.40 m height. So the vertical loads due to self weight of concrete were not uniformly distributed. Regarding the influence width for each support point in combination with the loads according to [1] (self-weight, formwork and working operation) on top the vertical loads shown in Figure 8 were acting.

It is obvious that under the big webs higher loads are acting in comparison to the thin concrete plate. Loads up to 65 kN at head jack means that usual Allround with ledger distance of 2.00 m is not sufficient. Regarding the self weight of scaffold and the laterally wind loads the maximum axial forces increase up to approximately 90 kN at bottom of the scaffold for second-order theory (Figure 9).

For such big loads it is necessary to work with the strong TG 60 frames. The utilization of the frames is round about 86%. For the rest of the scaffold it is possible to use regular Allround material, the maximum axial force is 42.7 kN what meets the bearing capacity of the standards with ledgers in the distance of 2.00 m.

Due to the combination of TG 60 and regular Allround it was possible to optimize the material and reduce the time for erection and dismantling. The shoring for this bridge was also possible without using any tubes and couplers because the grid was totally planned in system bay length.

For the important lateral bracing the usual Allround diagonals were used. A big global stiffness was reached to transfer the horizontal loads safely to the ground.

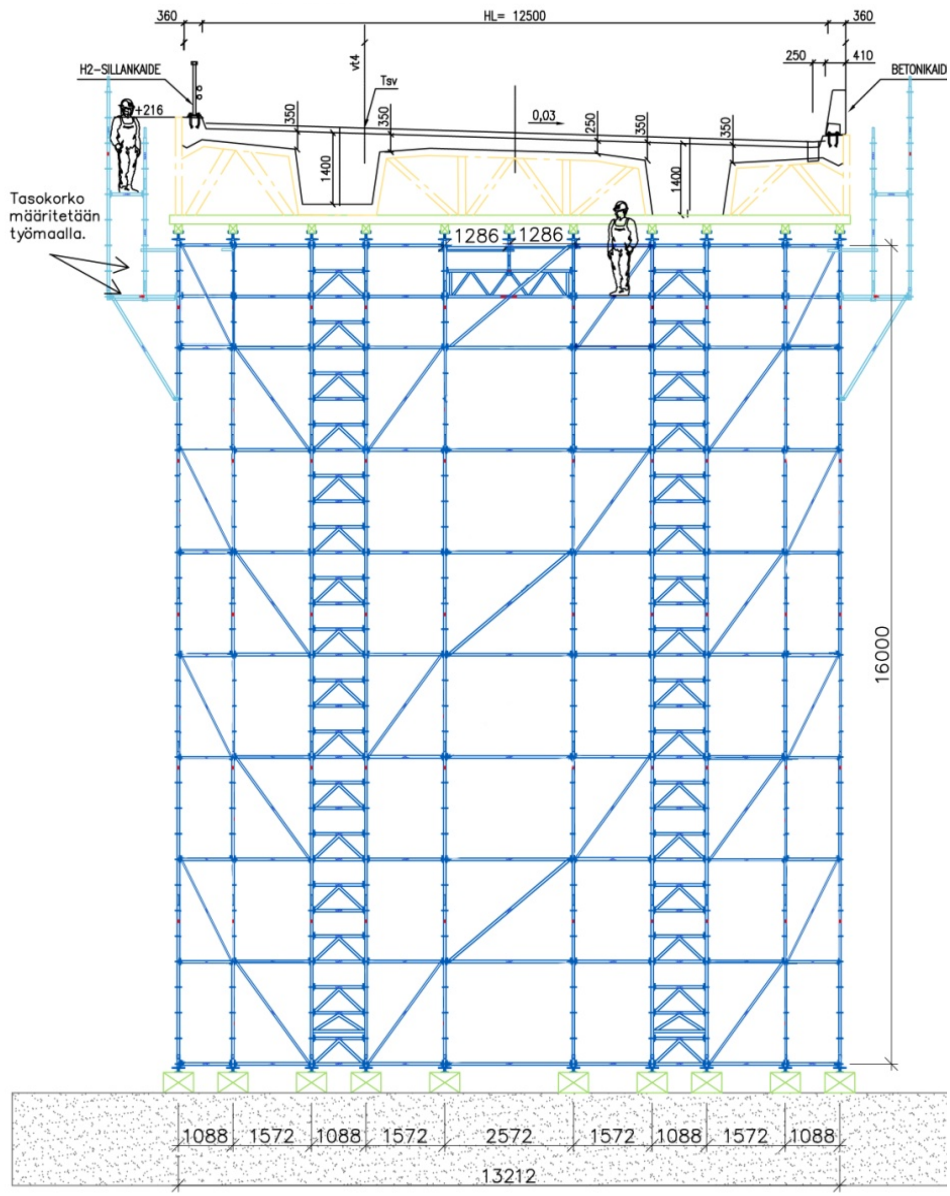

Figure 7. Cross section of the bridge in Jyväskylä (Finland)

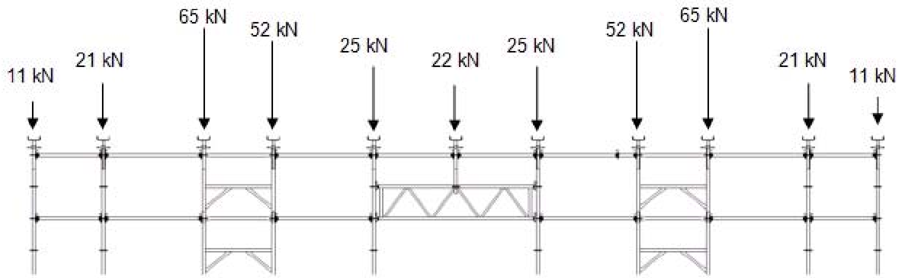

Figure 8. Acting vertical loads (design values) at the head jacks of the scaffold

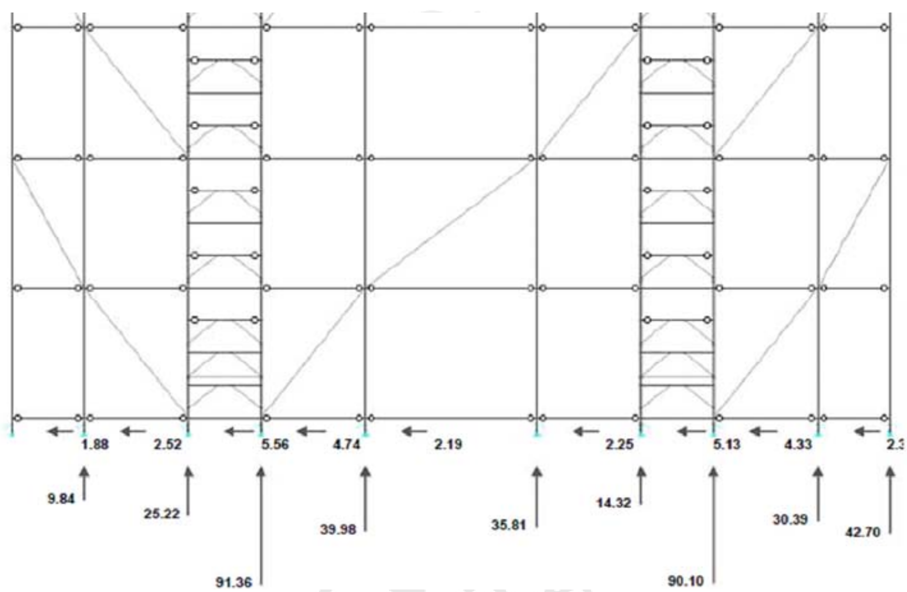

Figure 9. Static system and support loads (design values) of determining loading case combination for second-order theory

4 ALLROUND BRIDGING SYSTEM

During renovation or repair of existing bridges often a separate temporary bridge for pedestrians must be installed. For this use the Layher Allround Bridging System (short: AR-BRS) was developed also based on the ingenious Allround system. It is a separate strong modular truss system (Figure 10) which is adapted to the Allround scaffold by the use of wedge heads. The weight of the truss is only 60 kg per meter and can be assembled by hand. The bearing capacity of the truss depends on the bearing capacity of the single components. In Figure 11 the cross sections and the steel grades are shown. The chord can be used as tension and compression member and has a bearing capacity of $F_d = 235$ kN (design value). The post can carry a compression force of $N_d = 191$ kN and the diagonal tension rod can carry up to $Z_d = 190$ kN (only tension). Resulting from this the truss with a lever arm of 2.74 m (vertical distance of axis from chord to chord) has a bearing capacity of $M_d = 2.74$ m * 235 kN = 644 kNm for the bending moment. The bearing capacity for shear forces depends on the inclination of the diagonal rod. With the geometry of the system lines the maximum shear force is calculated according to equation (1).

$$Q_d = Z_d * \frac{2.74}{\sqrt{2.74^2 + 2.07^2}} = Z_d * 0.798 = 190\text{kN} * 0.798 = 151.6\text{kN} \qquad (1)$$

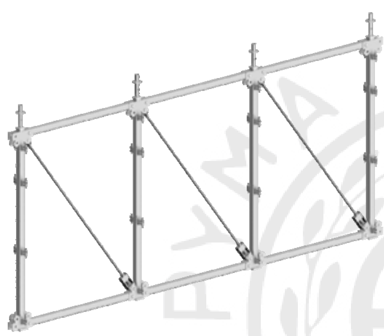

Figure 10. Allround Bridging System (modular truss system)

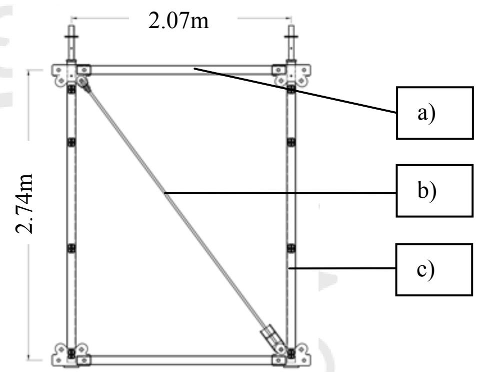

Figure 11. System sizes and static values of cross sections:

a) Chord 80x80x4mm (A=11.8cm²)
Grade S 355, E=210000 N/mm²

b) Diagonal rod D=20mm (A=3.14cm²)
Grade St 750/875, E=205000 N/mm²

c) Post 80x80x4mm (A=11.8cm²)
Grade S 355, E=210000 N/mm²

Because the chord can carry tension and compression forces the AR-BRS can be used as single span beam, continuous beam or even as cantilever beam. If there are alternating shear forces in the system it is possible to make a cross bracing with the diagonal rods. Furthermore it is possible to adjust the length of the diagonals in an easy way by turning a nut. So an existing deflection can be removed or in the run up to the use a camber can be given to the bridging system.

A pedestrian bridge consists mostly of an inner Allround scaffold (Figure 12 part d)) and two outer load bearing trusses (Figure 12 parts e)). The Allround scaffold is a non-bearing part of the bridge for vertical loads but it has to stiffen the trusses in cross direction and must carry all the horizontal loads (e.g. lateral wind loads). Bridges with spans up to 30 m are possible depending on the width of bridge, the live load and finally the lateral wind loads. For long span bridges (e.g. more than 25 m) in public use a dynamic check is very important because the natural frequency is going down close to the frequency of the pedestrians steps (approximately 2 Hz).

Short bridges (up to 20 m) are very stiff that means the natural frequency is far away from the critical frequency of the pedestrians. In Figure 13 such a long span bridge is shown. To reduce the dynamic sensibility the stiffness of the construction must be increased. This was reached with the installation of additional ropes (at the third points in horizontal direction and close to the support structure in vertical direction).

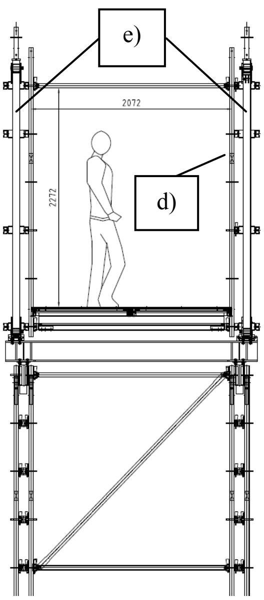

Figure 12. Cross section of a temporary pedestrian bridge at the support element

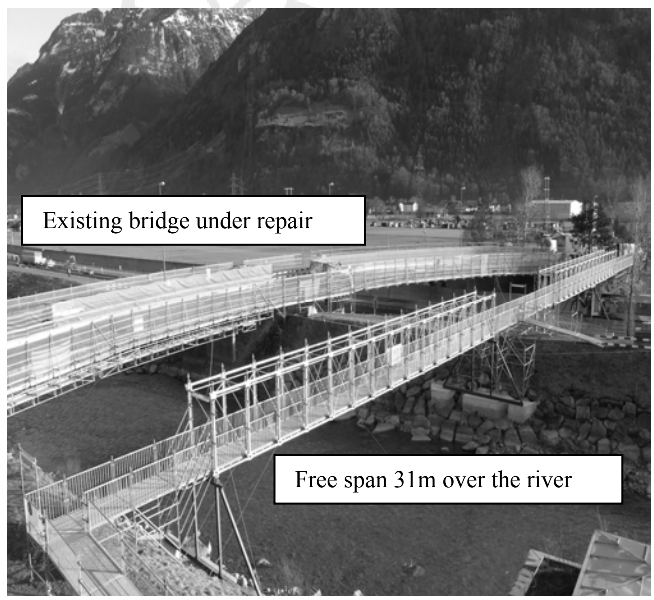

Figure 13. Use of the Layher Allround Bridging System as a temporary bridge for pedestrians during the repair of an existing bridge beside

5 CONCLUSIONS

Advanced modular scaffolding systems are superior to traditional ways of scaffolding regarding structure, speed, flexibility and safety.

The use of frames instead of single parts makes the system even more efficient in assembly and increases the bearing capacity.

The AR-BRS from Layher can be used in several fields of scaffolding. To build bridges with scaffolding material was the primary idea behind this development. Thanks to the modular construction and full compatibility to Allround it is now also possible to build other constructions with big spans or to carry high loads. Use as support structure for roofs, as holding girder for façade scaffolds or even for use as span over for stages in the event sector. With the Layher Allround Bridging System a milestone in scaffolding is reached which opens more possibilities and finally creates more economic solutions

ACKNOWLEDGMENT

I would like to express my gratitude to Mr. Roland Hassert, Product Developer at Wilhelm Layher GmbH, Germany for the technical support provided for this paper.

REFERENCES

[1] DIN EN 12812:2008-12, German Standard for shoring – requirements and design

RAILWAY ARCH STEEL BRIDGE OF 110M SPAN

Nestoras Loukatos[1], Neonellis Tzanetos[1], Evagelos Xypolitidis[1] and Ilias Kritikos[1]

[1] N.Loukatos & Associates SA, Greece
e-mail: info@stand.gr

ABSTRACT: The article presents the as built design and the erection of the single line railway bridge over a landslide area at the West Ring Road Aigaleo in Athens. It is the longest railway arch bridge that has ever been constructed in Greece (110m). At the two ends there are composite box girder access bridges that are also among the first applications of such kind in Greece [1].

KEY WORDS: ARCH BRIDGE; BRIDGE ERECTION; IBSBI 2011; RAILWAY BRIDGE; STEEL BRIDGE.

1 INTRODUCTION

At start, at the area of the construction the train was planed to pass on an embankment without the necessity of a bridge. However, the activation of a landslide that started on May 1990 and continued widening with more incidents despite the stabilization works, required the change of the alignment passing through the toe of the landslide's area and the replacement of the embankment with an arch bridge.

Photo 1. Photorealistic illustration

Photo 2. Bridge after erection

The whole project consists of the following consecutive parts :

- The first part is a 50m two-span composite box girder access bridge from the abutment A1 to the pier M2.
- The middle part is an 110m arch bridge which skips the landslide area from

the pier M2 to the pier M3.
- The last part is a 110m four-span composite box girder bridge from the pier M3 to the abutment A2.

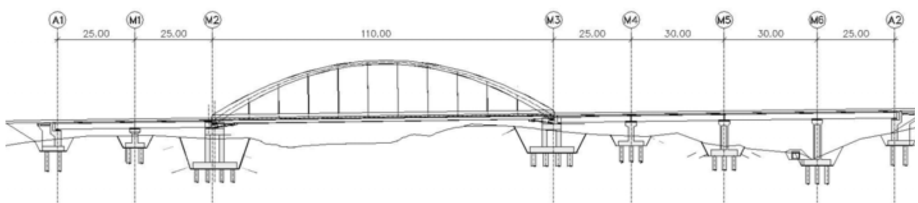

Figure 1. Logitudinal section of bridge

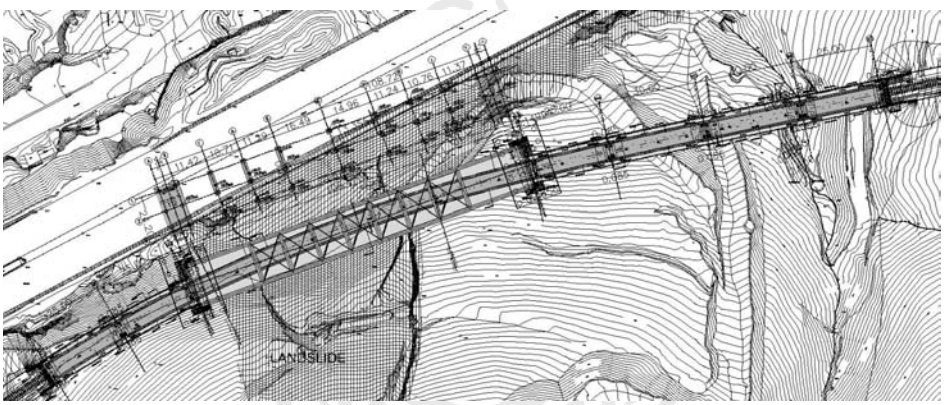

Figure 2. General plan view

2 ACCESS BRIDGES

Certain reasons have made the composite box girder bridge an appropriate solution:

- Big part of the alignment belongs to a curvature (R=450m) which causes torsion and requires a closed cross section with adequate torsional stiffness.
- A faster construction can be achieved by bringing the complete steel part ready and creating the concrete slab with the use of precast concrete slabs instead of formwork.

The bridges are formed as one span simply supported beams of 25m or 30m length. The height of the box is 1900mm and the widths of the upper and bottom flanges are 8600mm and 4000mm. The thickness of the steel parts are 30mm for the bottom flange, 20 to 25mm for the inclined webs and 50mm for the upper steel flanges that have a width of 700mm. A diaphragm is placed at every 4000mm. Moreover longitudinal stiffeners (two at the bottom flange and one at each web) are placed for the control of the plate buckling [2]. The concrete plate (B35) is of uniform thickness 350mm made on precast concrete slabs. The composite function is accomplished via shear studs (Φ22, 175mm, type: Nelson) [3].

All piers are of rectangular section except M5 and M6 which are higher and have hollow sections with dimensions 4.40x2.50m. The piers M1 and M4 that are shorter are of solid type with dimensions 4.40x2.50m.

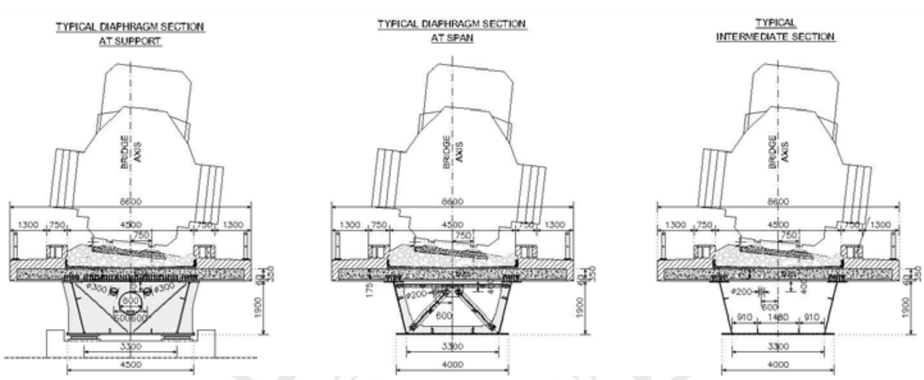

Figure 3. Sections of access bridges

3 ARCH BRIDGE

The length of the bridge is 110m. Concerning the plan view, the biggest part of the dead line belongs to a curve with R=450m, ending at a clothoid. The deck is made of a steel orthotropic plate on main cross girders, acting as a tie with permanent tension stresses, supported by suspension rods (2Φ130 every 9600mm) that are connected to the two parabolic arches. The maximum distance between the tie and the arches is 18m.

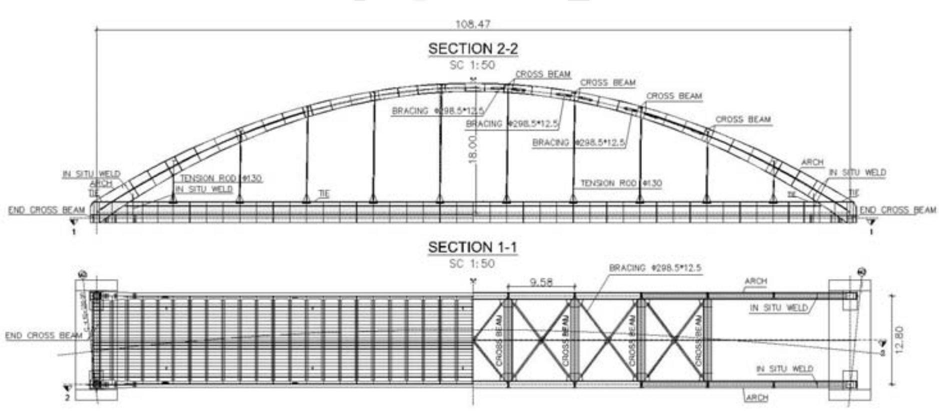

Figure 4. Longitudinal section and plan view of the arch bridge

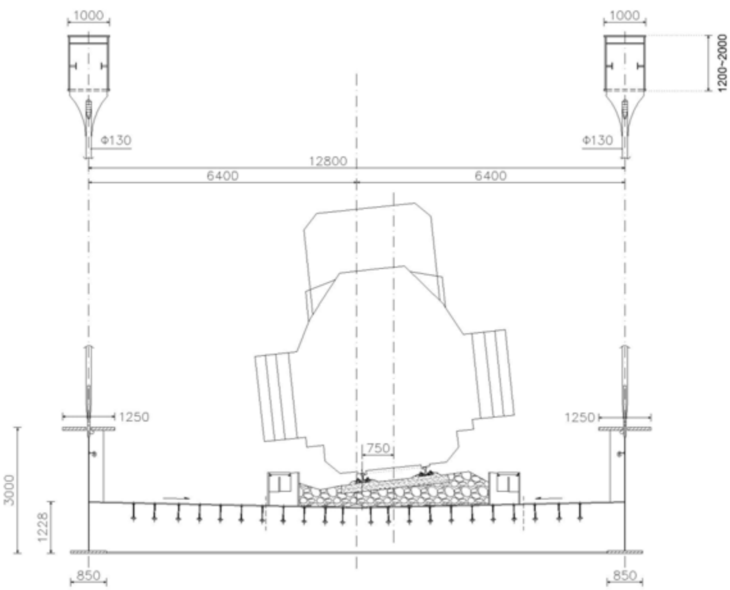

Figure 5. Cross section of the arch bridge

The arch was preferred due to the low height beneath the dead line [4]. Moreover the curved alignment demanded an increased bridge width and the appropriate arches position to equalize their loadings due to the eccentricities. The geometric characteristics of the arches parabola, the variable arches web height and the distance between the arch and the tie were chosen after a wide range of trials to achieve mainly axial loadings of the arches and the decrease of the vertical and horizontal deflections [5].

Finally the distance of the arches' axis was decided 12.80m. Each arch is made of a steel box with constant width 1000mm and a height that varies from 1200mm on top to 2700mm at the two edges. Inside the box, transverse stiffeners are placed at every suspension point and at the thirds between these points. The ties are monolithically connected with the arches at the edges and they are of I-section. The arches are connected with transverse boxes of 1000mm width and height adjusted to the arches height, at the internal suspension points such that a minimum free height of 7500mm is left for the trains crossing. Diagonal bracings of circular hollow section Φ298,5 with 12.5mm thickness are placed between these transverse boxes.

Steel cross beams of inverted I-section are connected to the ties at almost every 2400mm and support the steel orthotropic deck plate of 25mm thickness which has longitudinal stiffeners 325x20mm at every 500mm. The end cross beams are of box type.

The piers M2 and M3 are of multiple box type with plan dimensions

17.30x6.00m. The pier M2 is founded with 24 piles Φ120 of 15m depth and the pier M3 is founded with 24 piles Φ150 of 30m depth.

Four elastomeric bearings are placed between the bridge and the piers. Moreover, four Shock Transmission Units of Maurer (MHD 1000/1000) are placed for the longitudinal decrease of the bridge's seismic and non seismic movements [6]. Those devices act as non-linear viscous dampers during an earthquake. Their small coefficient ($P=Cv^{\alpha}$, C=1000kNs/m, α=0,02) enables their activation even during actions with small velocity as acceleration-braking loads. On the contrary, no reaction occurs for actions with almost zero velocity as thermal movements. At the transverse direction the bridge is restrained with shear keys.

4 WIND LOAD

Computational simulation has been carried out for the realistic estimation of the wind load, using appropriate computational fluid dynamics software, simulating the structure including the ground. From the analyses it has been pointed that there is no hazard for the bridge to get "in phase" due to the wind load and that the expected wind pressures at the various parts would be less than those calculated and used at the design according to EC1.

Photo 3. Wind load simulation 1

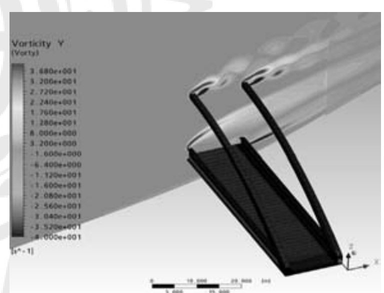

Photo 4. Wind load simulation 2

5 ERECTION OF THE ARCH BRIDGE

5.1 General

The erection of the arch bridge required avoiding the activation of the landslide, keeping the road open, ensuring the access of the bridge during the erection, choosing appropriate dimensions and weight for the various bridge parts depended on the availability of the equipment and designing economical temporary works. These preconditions were satisfied by constructing the bridge 24.2m parallel to its final position and at the same height, on temporary works founded with piles at the landslide's toe. After the construction, a pulling mechanism made the bridge slide to its final position.

Photo 5. Erection

Photo 6. Sliding

5.2 Erection procedure

Two steel 6-column edge pylons (Π2 and Π3) and seven concrete 3-column internal pylons (Γ, Δ, Ε, Ζ, Η, Θ, Ι) were constructed for the erection of the deck. After the completion of the deck, temporary pylons for the erection of the arch have been placed on the deck [7].

The tie girders had come at 6 pieces, supported before their assembly at their ends by the temporary pylons except the biggest parts having a length of 22m that were supported additionally at their middles from the pylons Γ and Θ. The procedure started from the pylon Π3 with the assembling of the two special parts (feet) at the connection of the arch and the tie-girder with the end cross beam. The assembly of the other tie girders with their cross beams followed consecutively from pylon Γ to the pylon Π2. At the end, the assembly of the last two feet at the top of pylon Π3 with the other end cross beam completed the first part of the deck construction. The total deck was completed with the welding of the orthotropic deck on the system of the tie girders and the cross beams.

Each arch had been brought at 5 pieces. That required the construction of four 8-column pylons for the support of the independent parts. Moreover, five internal 4-column pylons had been constructed to support those parts at their middles. All these pylons were constructed at the ground and uplifted and put via cranes on the completed deck. The arches assembly started simultaneously from both edges and finished with the placement of the middle parts. Meanwhile, the permanent steel parts connecting the two arches were placed between the already welded arches.

At the end of the assembly, the bridge was uplifted 50mm by hydraulic jacks that had been placed at Π2 and Π3. The bridge was no longer supported internally beneath the deck. Moreover the differential deflection between the arch and the deck had allowed the removal of the temporary pylons that had been used for the arch erection.

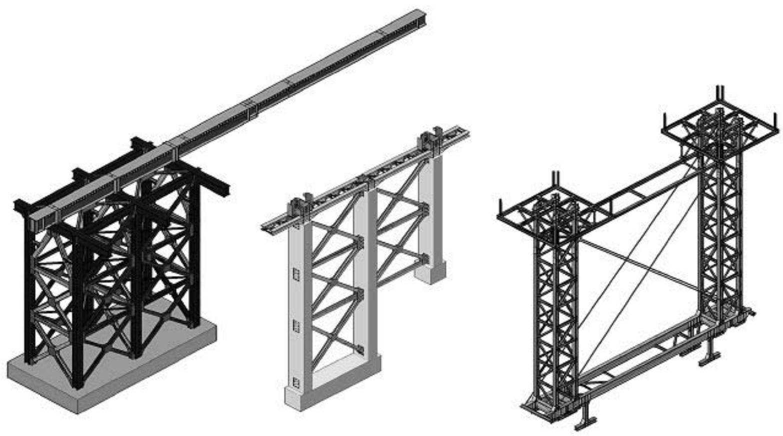

Photo 7. Temporary pylons for the erection of the arch bridge

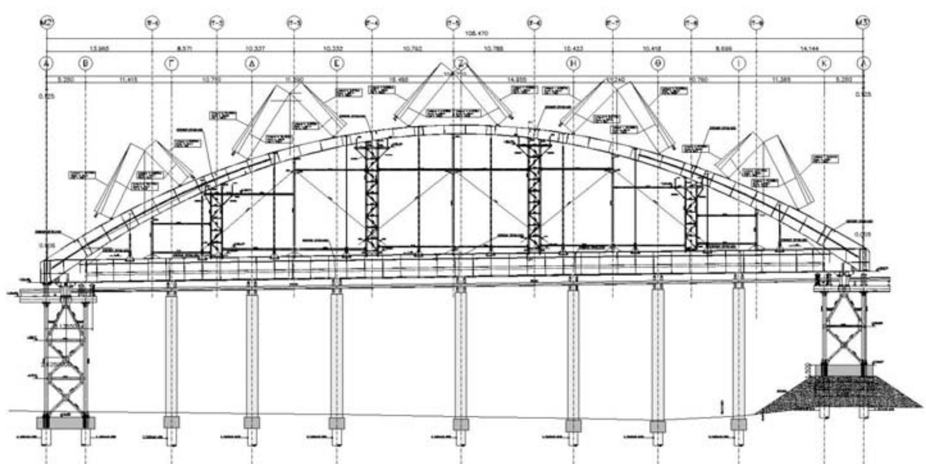

Figure 6. General side view for the temporary structures

5.3 Sliding

On the top of the pylons Π2 and Π3, two sliding beams had been placed from the start, connecting the pylons with the piers M2 and M3. Four "sledges" had been placed between the sliding beams and the bottom of the bridge. Those mechanisms could move through a rail with a PTFE covering. Right after the uplift of 50mm and the removal of every chock from the top of the internal pylons, the load was led to the sledges. 2 pistons were placed at M2 and M3 and pulled the bridge to its final position through steps of approximately 75cm. The pulling machines consisted of two pumps, activating two hydraulic jacks pulling two bars Φ32 connected with pins to the bottom flange of the one tie girder.

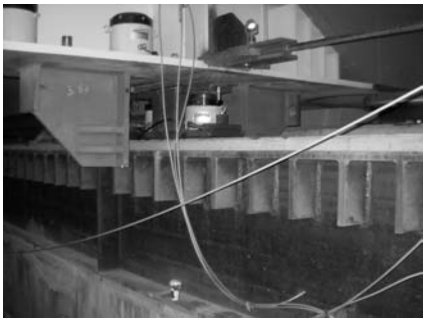

Photo 8. Sledge and pulling bar

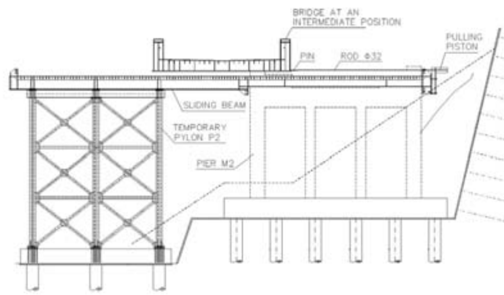

Figure 7. Side view of sliding beam

6 CONCLUSIONS

Concerning the steel structures, the self weight of the arch bridge is 11.5kN/m2 or 146kN/m. The steel temporary structures' weight for the arch bridge's erection was 6kN/m2 or 78kN/m. Finally the steel used for the access bridges is 3.2kN/m2 or 27.4kN/m. The above area (m2) and length (m) quantities correspond to the bridge's plan view and dead line respectively.

In this project, steel and composite steel-concrete type of bridges are used in a bridge of a big main span and many limitations because of the special conditions of the alignment (small available height, curved alignment at plan view, big span, prohibition of access at the landslide area). The use of the arch bridge for the big span and the composite box girder access bridges for the smaller spans with the capability of precast big parts and the great steel's strength, gave us the opportunity to deal satisfactory with the project's particularities.

REFERENCES

[1] N. Loukatos & associates SA, Journal of ACEG (Association of Civil Engineers of Greece), vol 378, pp. 24-34, January 2010

[2] Bauer T., Muller M., Uth H., *Eisenbahnbruckenbau nach DIN-Fachbericht Band 2*, John Wiley & Sons, Inc., Bauerk, 2003.

[3] Vayias Ioannis, *Composite Structures*, Sections Edition, Kleidarithmos, Athens, 1994.

[4] Ermopoulos Ioannis, *Steel and Composite Bridges*, First Edition, Kleidarithmos, Athens, 2000.

[5] Xanthakos P. Petros, *Theory and Design of Bridges*, First Edition, John Wiley & Sons, Inc., New York, 1994.

[6] Greek guidelines for the design of bridges with seismic isolation, Hellenic Ministry of Environment, Country Planning and Public Works , June 2007.

[7] Le Bulletin Ponts Metalliques, no 19

BRIDGE CONSTRUCTION MANAGEMENT
Effective Tools to Control Construction Schedules

Theodoros Tzaveas[1]

[1] Egnatia Odos AE, Works Division, Thessaloniki, Greece
e-mail: theodtzav@egnatia.gr

ABSTRACT: Bridge construction always fits within the critical path of highway projects. Through a case study of a complex balanced cantilever viaduct, this paper identifies the potential use of implementing specific management techniques to effectively manage the construction process and produce forecasting assessments for the project completion date.

KEY WORDS: Bridge construction; Earned Schedule; Construction Management

1 INTRODUCTION

In project management, it is vital to have adequate means of obtaining information about the progress of a project against a baseline and the anticipated outcome of the project. A project has traditionally been viewed as successful if it was completed on time, within budget and with the specified quality. Earned Value (EV) systems, being a standard method of measuring project performance, have been setup to deal with the complex task of controlling and adjusting the baseline project schedule during execution, taking into account project scope, timed delivery and total project budget. Vanhoucke and Vanvoorde [1] state that although EV systems have been proven to provide reliable estimates for the follow-up of cost performance within certain project assumptions, it often fails to predict the total duration of the project. Another question frequently asked is how the project managers handle the effects of re-baselining in making their forecasts.

Lipke [2] proposed the concept of “Earned Schedule" (ES) to address these issues. Rather than just looking at schedule performance using the value of work, earned schedule also looks at when the work was to be completed. ES aims to measure schedule performance using a time-based measure from which time index metrics are derived.

The purpose of the paper is to examine the capability of the methods to represent the schedule performance effectively in a late bridge construction project with inherent complexities and unforeseen events and to adequately forecast the final duration. The three scenarios include the overall time schedule, a re-baselining at early stages and the low-level work breakdown structure (WBS) applied to a single structural element.

2 PROJECT MONITORING TOOLS, EVM VS. ES

Earned Value Management (EVM) uniquely connects cost, schedule and requirements thereby allowing for the creation of numerical project performance indicators and enable managers to express the cost and technical performance of their project in an integrated and understandable way to employees, superiors and customers. However EVM schedule indicators, namely Schedule Performance Index SPI(c) and Schedule Variance Index SV(c) are, contrary to expectation, reported in units of cost rather than time with an irregular behaviour at around 2/3 of the project duration. From this time of uncertainty until project completion, the manager cannot rely on the schedule indicators portion of EVM.

The technique to resolve the problem of the EVM schedule indicators is Earned Schedule (ES). The ES idea is simple: identify the time at which the amount of EV accrued should have been earned [2]. By determining this time, time-based indicators, namely SPI(t) and SV(t) can be formed to provide schedule variance and performance efficiency management information. The computed value of ES describes where the project should be in its schedule performance.

3 THE BRIDGE CONSTRUCTION AND THE MONITORING OF THE CONSTRUCTION SCHEDULE

The case study used in this paper is related to the construction of a complex viaduct which is part of a 37km section from Panagia to Grevena in the western part of the Egnatia Odos motorway with an overall cost of 720.000.000€, crossing a mountainous area with complex geology and severe environmental constraints. This bridge carries the road over a deep valley and a river *(Photo 1)*. At the southern end of the valley the carriageway splits into two separate viaducts, the lengths of which are different due to the prevailing topography.

Photo 1. The 636m Venetikos Bridge

The structure consists of twin segmental box girder viaducts, with integral piers varying in height from 29m to 70m. The overall length is 636m and 531m for the eastbound and westbound structures respectively. The isolated site, with its steep 70m-deep valley, required a bridge solution driven more by construction method than anything else, which is why a balanced cantilever bridge was chosen. Similarly, the position of the river Venetikos in relation to the steep valley slope resulted in spans up to 120m.

3.1 Time Schedule Details

In a bridge of such size and complexity, overall time is mainly determined from the construction equipment (machinery, cranes, and formworks) which is available on the construction site and obviously not all activities start simultaneously. Thus in addition to the scheduling of works for the construction of foundations and pier walls, critical activities for the completion of the bridge are the available number of formwork for the construction of pierheads and cantilevers, and effective use and transfer from pier to pier, which involve logistics and value engineering analysis to optimize the procedure to be finally adopted. A WBS established to make such a complex project more manageable and is formed in such a way to help breakedown the project into manageable chunks that can be effectively estimated and supervised. The overall cost of the bridge budgeted at 19.6 m€. The start date of the construction was the 27th of May 2005, with a planned duration of 129wks. The schedule is characterized by slow early progress, followed by a significant acceleration at a percentage completion of about 10% of works. The actual duration was 145.2 wks.

3.2 Particular aspects of construction

There are several factors affected the schedule performance. Some of them were unforeseen events and others required re-work of several activities. However, most or all of them are common in the construction projects. Variations in the initially assumed geotechnical conditions, under-skilled personnel in demanding activities, late supply and management of equipment were the main aspects influenced the schedule performance.

3.3 Analysis and results

For the analysis of the overall bridge construction schedule, nine control periods were determined taking into account the percentage completion of works and main events along the timeline of the project. Based on the activities' progress and completion dates, the curves of Earned Value (EV) and Planned Value (PV) against costs, are prepared at each control period, followed by the accumulation of all the results representing the overall schedule performance as illustrated in *Fig. 1*.

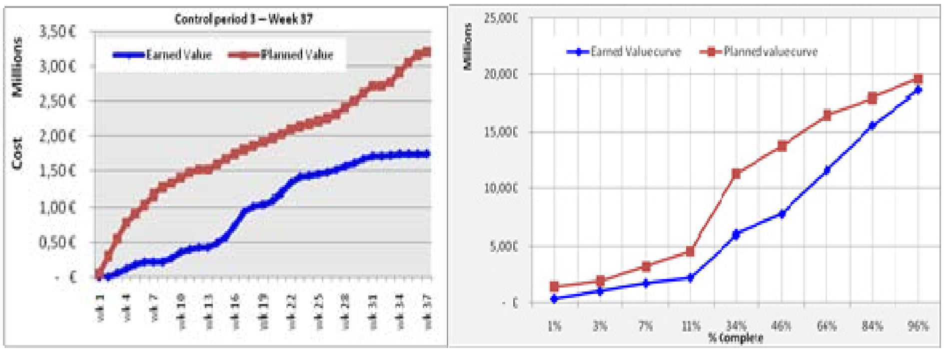

Figure 1. EV, PV curves (a) for specific control period, (b) for the overall duration

Following the principles and techniques of the methodologies the main duration metrics and indices were calculated with both methods. EV metrics were obtained directly from MS-Project where ES values were processed manually. *Fig. 2* portrays the forecasting performance of the two methods, along with the actual duration (top) and baseline duration (bottom) for comparison. It is apparent that Earned Schedule converges faster towards the actual duration but without any remarkable results.

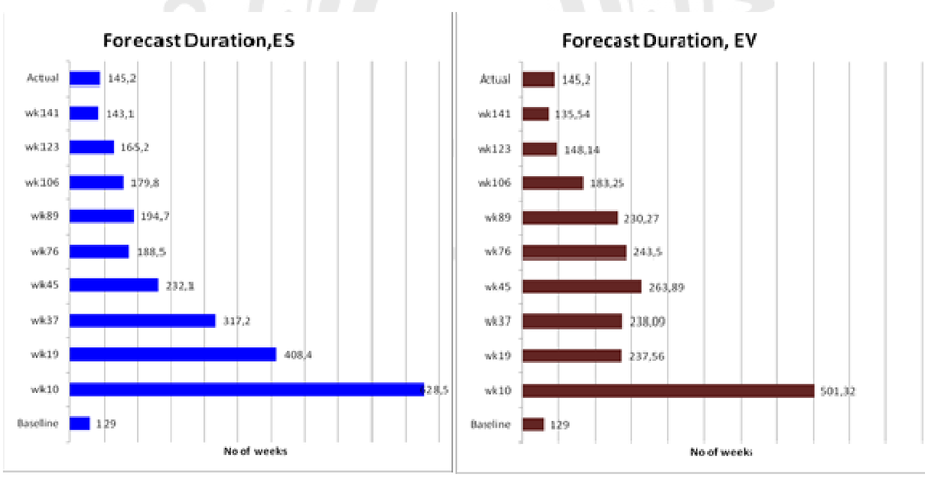

Figure 2. Forecast duration (a) for Earned Schedule, (b) for Earned Value

The schedule performance is illustrated in *Fig. 3* where SPI for both methods is plotted against the percentage of work performed. It is clear, from a value of as low as 0.2, that there is a late start and slow progress at the beginning, up to approximately 1/3 of the work completed, which clearly indicates a problematic project. *Fig. 3b* indicates the “weeks behind” schedule as estimated with the earned schedule for each control period.

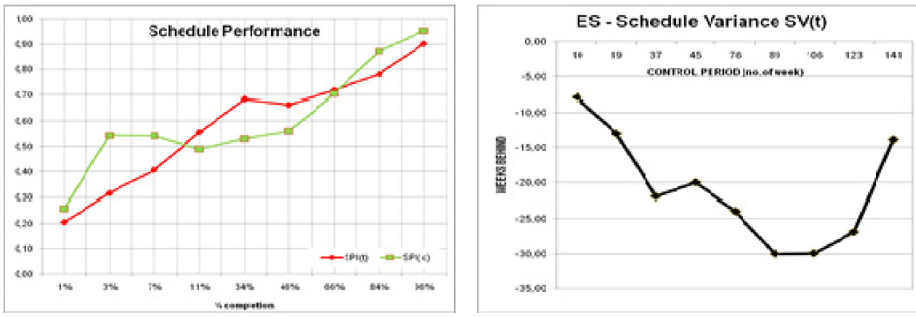

Figure 3. (a) Schedule Performance Index for ES and EV, (b) ES weeks behind

3.4 Re-Baselining

Construction projects have to be performed in complex dynamic environments that are often characterized by uncertainty and risks. The literature contains ample evidence that many construction projects fail to achieve their time, budget and quality goals. As Callahan and Hohns [3] have pointed out, most contractors use a schedule "…as a guide, not a ruler." It is generally understood that the contractor is responsible for scheduling, sequencing and prosecuting the work to comply with the requirements of the contract documents. The project owner will review the contractor's initial schedule "for conformance with the Contract Documents". In the case study the re-baselining deemed necessary after the completion of the foundation works which attributes the higher risk and uncertainty in the original schedule. During this process a revised baseline is set, which purposely involves the Planned Value (PV) of the 3rd control period since it corresponds to approximately 10% of work completion. A recalculation of EV and ES metrics was carried out in order to assess the forecasting result, having recovered the project from a late start. In *Fig.4* the revised baseline is plotted against the original PV and the EV curve.

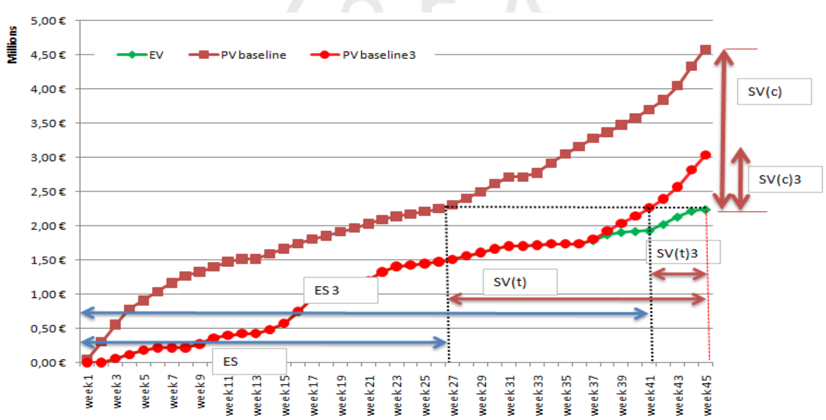

Figure 4. Plotted curves of Earned Value and Planned Value during re-baselining

The values from the analysis and the revised indices are shown in Table 1. It is remarkable how the schedule performance index is improved, with values of 0.7 and 0.9 for EV and ES analysis respectively comparing with original corresponding values of 0.49 and 0.56. What is to be noted is that the forecasting made with ES is 144.7wks and is remarkably close to the actual duration of 145.2wks, whereas EV suggests a value of 189wks.

Table 1. EV & ES metrics – Forecasting of overall duration

EV & ES Metrics	Original Baseline	New Baseline
BCWP, EV(€)	2.239.983,37	2.239.983,37
BCWS, PV(€)	4.582.255,75	3.034.095,15
SV(c) (€)	- 2.342.272,38	- 794.111,78
SPI(c)	0,489	0,7
ES	25,01	40,11
SV(t), (wks)	-19,99	-4,89
SPI(t)	0,56	0,89
Forecasting with ES	232,08	**144,72**
Forecasting with EV	263,80	184,29
Actual	**145,2**	**145,2**

3.5 Pier-Cantilever

A third analysis included the schedule performance of a single structural element which includes the foundation and column of the pier, the pier table and the cantilevers. The pier selected, has all its activities along the critical path of the project. The planned duration was 48,2 weeks. Thirteen control periods were set from the start date to 100% completion of the cantilevers. *Fig. 5* portrays the curves of EV and PV where the recovery of the schedule and acceleration of works at 62% completion, is apparent. Major delays taken place at the intervals of 26-28% and 53-62% of project completion.

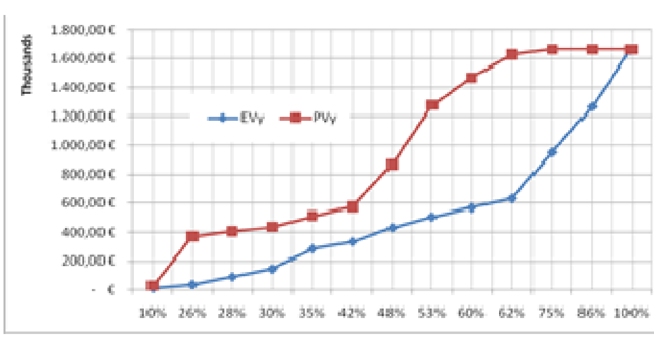

Figure 5. Planned Value vs. Earned Value

Fig. 6 illustrates the schedule performance and the schedule variance calculated with Earned Schedule and *Fig. 7* portrays the project duration forecasting. It is noted that the planned work should have been completed at 62% completion. It is very clear from the first diagram that SPI(c) tends to increase at 2/3 completion in order to receive eventually the value of 1.0, thus not accurately representing the schedule performance. On the contrary SPI (t) follows a smoother trend, with a better representation of the performance reaching a value of 0.8.

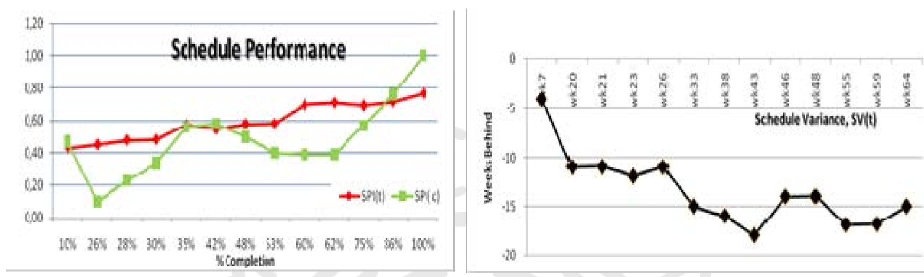

Figure 6. (a) EV & ES Schedule Performance and (b) ES, Schedule Variance

Very good convergence is shown by ES (*Fig.7a*) after the 43rd week which corresponds to the 50% completion at a SPI(t) value of around 0.6. On the contrary convergence with EV (*Fig.7b*) is reached after the 80% completion of works.

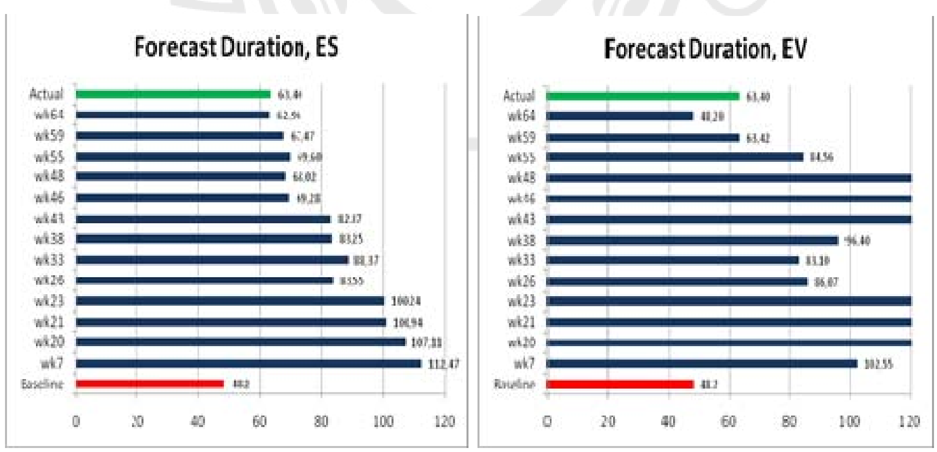

Figure 7. Forecast duration (a) for Earned Schedule, (b) for Earned Value

4 CONCLUSIONS

Highway construction projects are quite uncertain in nature and often are late, exceeding original budget. Although responsibilities of parties and causes of such events are interesting to explore further in a contractual framework, for a client who needs to prioritize work and effectively manage European funding within strict deadlines, the ability to forecast the end date of a project and have progress indicators early in the course of construction is of vital importance. Testing the performance of the techniques on an actual construction project was a challenge as it allows easy comparisons of the forecasting ability and performance indicators analytically obtained, with real values. In this paper the application of the EV and ES methodologies was presented, as specific-duration methods, using EV metrics and evaluate them on real-life construction project data extracted from a complex viaduct in Egnatia Odos highway, using MS-Project. The three analyses carried out reveal the superiority of the ES method showing reliable results during the whole project duration, confirming conclusions previously published in literature related to the weakness of the EV method to produce reliable duration forecasting even at 50% project completion.

The use of EVM or the ES method depending on the need and knowledge of the project manager might lead to similar results for project monitoring in the early and occasionally in middle stages. However this statement can be misleading if a re-baselining is applied at early project stages, and that needs to be handled very carefully. In general, the EV metrics shall be set-up as early warning signals to detect potential problems in an easy and efficient way. The forecasting results and the assessment of schedule performance on the three cases demonstrate that reliable early warning signals are available. We refer to Cooper [4] stating that the use of EVM can be questioned when applied in highly complex projects. Due to the cycles of rework, the accuracy of the EVM metrics can be biased, leading to incorrect management decisions. Therefore further investigation is necessary to this research topic and more data is necessary for assessment and comparison purposes when a complex project also subjects to a vast amount of rework cycles.

REFERENCES

[1] Vandevoorde, S., Vanhoucke, M., *‘A comparison of different project duration forecasting methods using earned value metrics’*, International Journal of Project Management, 24, pp.289-302, 2006.

[2] Lipke, W., *Schedule is different*, The Measurable News, PMI College of Performance Management, pp.9-13, 2003.

[3] Callahan, M. T. and Hohns, H. M., *Construction Schedules: Analysis, Evaluation, and Interpretations of Schedules in Litigation and Dispute Resolution, Second Edition*. John Wiley & Sons, Inc. New York, 1998.

[4] Cooper, K.G., *Your projects real price tag*, Harvard Bus Rev.,pp.13-15, 2003.

AUTHOR INDEX